

Lecture Notes in Civil Engineering

Md. Abdul Mannan
R. Sathyanathan
N. Umamaheswari
Hemant S. Chore *Editors*

Emerging Trends in Composite Structures

Select Proceedings of ICC-IDEA 2023

 Springer

Lecture Notes in Civil Engineering

Volume 387

Series Editors

Marco di Prisco, Politecnico di Milano, Milano, Italy

Sheng-Hong Chen, School of Water Resources and Hydropower Engineering,
Wuhan University, Wuhan, China

Ioannis Vayas, Institute of Steel Structures, National Technical University of
Athens, Athens, Greece

Sanjay Kumar Shukla, School of Engineering, Edith Cowan University, Joondalup,
WA, Australia

Anuj Sharma, Iowa State University, Ames, IA, USA

Nagesh Kumar, Department of Civil Engineering, Indian Institute of Science
Bangalore, Bengaluru, Karnataka, India

Chien Ming Wang, School of Civil Engineering, The University of Queensland,
Brisbane, QLD, Australia

Zhen-Dong Cui, China University of Mining and Technology, Xuzhou, China

Lecture Notes in Civil Engineering (LNCE) publishes the latest developments in Civil Engineering—quickly, informally and in top quality. Though original research reported in proceedings and post-proceedings represents the core of LNCE, edited volumes of exceptionally high quality and interest may also be considered for publication. Volumes published in LNCE embrace all aspects and subfields of, as well as new challenges in, Civil Engineering. Topics in the series include:

- Construction and Structural Mechanics
- Building Materials
- Concrete, Steel and Timber Structures
- Geotechnical Engineering
- Earthquake Engineering
- Coastal Engineering
- Ocean and Offshore Engineering; Ships and Floating Structures
- Hydraulics, Hydrology and Water Resources Engineering
- Environmental Engineering and Sustainability
- Structural Health and Monitoring
- Surveying and Geographical Information Systems
- Indoor Environments
- Transportation and Traffic
- Risk Analysis
- Safety and Security

To submit a proposal or request further information, please contact the appropriate Springer Editor:

- Pierpaolo Riva at pierpaolo.riva@springer.com (Europe and Americas);
- Swati Meherishi at swati.meherishi@springer.com (Asia—except China, Australia, and New Zealand);
- Wayne Hu at wayne.hu@springer.com (China).

All books in the series now indexed by Scopus and EI Compendex database!

Md. Abdul Mannan · R. Sathyanathan ·
N. Umamaheswari · Hemant S. Chore
Editors

Emerging Trends in Composite Structures

Select Proceedings of ICC-IDEA 2023

 Springer

Editors

Md. Abdul Mannan
Universiti Malaysia
Sarawak, Malaysia

N. Umamaheswari
Department of Civil Engineering
SRM Institute of Science and Technology
Chennai, Tamil Nadu, India

R. Sathyanathan
Department of Civil Engineering
SRM Institute of Science and Technology
Chennai, Tamil Nadu, India

Hemant S. Chore
Dr. B. R. Ambedkar National Institute
of Technology Jalandhar
Jalandhar, Punjab, India

ISSN 2366-2557

ISSN 2366-2565 (electronic)

Lecture Notes in Civil Engineering

ISBN 978-981-99-6174-0

ISBN 978-981-99-6175-7 (eBook)

<https://doi.org/10.1007/978-981-99-6175-7>

© The Editor(s) (if applicable) and The Author(s), under exclusive license to Springer Nature Singapore Pte Ltd. 2024

This work is subject to copyright. All rights are solely and exclusively licensed by the Publisher, whether the whole or part of the material is concerned, specifically the rights of translation, reprinting, reuse of illustrations, recitation, broadcasting, reproduction on microfilms or in any other physical way, and transmission or information storage and retrieval, electronic adaptation, computer software, or by similar or dissimilar methodology now known or hereafter developed.

The use of general descriptive names, registered names, trademarks, service marks, etc. in this publication does not imply, even in the absence of a specific statement, that such names are exempt from the relevant protective laws and regulations and therefore free for general use.

The publisher, the authors, and the editors are safe to assume that the advice and information in this book are believed to be true and accurate at the date of publication. Neither the publisher nor the authors or the editors give a warranty, expressed or implied, with respect to the material contained herein or for any errors or omissions that may have been made. The publisher remains neutral with regard to jurisdictional claims in published maps and institutional affiliations.

This Springer imprint is published by the registered company Springer Nature Singapore Pte Ltd.

The registered company address is: 152 Beach Road, #21-01/04 Gateway East, Singapore 189721, Singapore

Paper in this product is recyclable.

Contents

Structural Engineering and Health Monitoring	
Strength of Concrete with Partial Replacement of Aggregate with Granite	3
S. Suresh Babu and T. Abishek	
State-of-the-Art Review on Synthesis and Utilization on Graphene Oxide in Concrete Under Elevated Temperature	13
I. Ramana and N. Parthasarathi	
Analyzing the Characteristics of Self-Compacting, Basalt Fiber, Ultra-High-Performance Concrete Using Nanowaste Product at Both High and Normal Temperature Changes	21
M. K. Muniyasamy and M. Dinesh Kumar	
Experimental Study on Nanomaterials in High-Performance Concrete	31
K. Sathishkumar and L. Krishnaraj	
An Investigation on Behaviour of Non-metallic Arca Fibre-Reinforced Concrete Beam	43
S. Govindasami and K. Sathish	
Replacement of Fine Aggregate with Copper Slag in Concrete: A State-of-the-Art Review	47
V. K. Nithyashree and M. Surendar	
Enhancement of Concrete Strength of Using PPF and Analysis by ANSYS for Strength Comparison	55
Pathapati Rohithkumar, Abishek Rauniar, and V. R. Prasath Kumar	
Microstructural and Plastic Shrinkage Studies on M-Sand and Coconut Shell Used Self-Compacting Concrete	67
S. Prasanth, S. Prakash Chandar, and K. Gunasekaran	

Hybrid Testing Approach for Thermo-Mechanical Testing of Structures Using Impedance Matching	83
T. Jay Vishnu, E. Vinothini, M. S. Aditya, and Mohit Verma	
Study on the Effect of Marble Dust as Partial Replacement to Cement with Steel Fibre in Concrete	91
M. S. Yuvaraj, Manoj Kumar Sah, Shaik Kutagal Md. Jabeer, Thallika Venu Kumar, Marumani Harish, and Bibek Mishra	
State of Art on Enhanced Energy-Efficient Building Through Various Materials and Construction Techniques	99
Thennarasan Latha Abinaya and Balasubramanian Murugesan	
Steel and Composite Structure	
Study on Self-Consolidating Hybrid Fibre-Reinforced Concrete	117
R. Sruthi and K. Suganya Devi	
Effect of High Performance on Glass Fibre-Reinforced Concrete Beams	125
R. Kamalesh and A. Leema Rose	
Investigation on Innovative Cold-Formed Steel Built-Up Columns Using Lipped and Unlipped Channels	131
V. A. Veera Vignaesh, S. T. Dhaarini, and C. Manoj Kumaar	
Strength Study on Engineered Cementitious Composites Using Hybrid Fibres	143
S. Samuel and N. Pannirselvam	
Investigation of Bending Effect on Steel–Concrete–Steel (SCS) Sandwich Composite Sections Considering Width–Thickness Ratio and Global Provisional Codes Validation	153
Wesam Al Agha, Taha Ahmed Ghaleb Mohammed, Mohanad Ali Ishaq Najajra, and Nambiappan Umamaheswari	
Experimental Investigation on Mechanical Properties of Steel Fibre in M50 Grade Concrete	167
S. Prakash Chandar and T. S. Lakshmi	
Analytical Study on the Bending Behavior of the Composite Beam with T-shaped Shear Connector Under Partial Interaction	181
Rakesh Bhatia and R. Ramasubramani	
Planning and Analysis of G+2 Residential Building and Design of Slab and Beam with Sisal Fiber Polymer Reinforcement	193
Phumen Teron, Ningthoujam Khelendra, Shanmuga Raj, and Balasubramanian Murugesan	

Nonlinear Static Analysis Study on Progressive Collapse Behaviour of 2D RC Frame with Different Grades of Steel 201
 P. Jagatheswari and R. Ramasubramani

Behaviour of Steel–Concrete Composite Beams Provided with Headed Stud Shear Connectors 217
 Ammu C. Bose and N. Umamaheswari

Bridge and Tunnel Engineering

Behavior of Double Layer Compound Cold-Formed Steel Columns 231
 V. Hari Krishnan and C. Manoj Kumar

Flexural Behaviour of Cold-Formed Ferritic Stainless Steel Built-Up Joists 241
 C. Manoj Kumar, Dinesh Kumar Marnadu, A. Harikaran, M. Saran Kumar, and Venus David Rayan

Flexural Behaviour of Corrugated Web Beams Using Cold-Formed Steel Sections 253
 C. Manoj Kumar, S. T. Dhaarini, S. Rithish, and A. Thirunavukarasu

Analytical Behavior of Optimum Position of Multi-level Outriggers in RCC Frames 265
 S. Naveen Kumar and K. S. Satyanarayanan

Study on the Shear Behavior of Hybrid Fiber-Reinforced Concrete Beams 277
 M. Bhuvaneshwari and Yaci Joshy

Plastic Shrinkage and Microstructural Analysis of Butyl Rubber in Light-Weight Concrete 287
 S. Prakash Chandar, Vishnu, and P. T. Ravichandran

Numerical Investigation of Encased Composite Beams with Reinforcements Passing Through the Web Openings 305
 L. Vaishnavi and N. Umamaheswari

Study on Behavior of Plastic Road—A Case Study 317
 K. Surya Prakash, T. M. Jeyashree, and M. A. Venkiteswaran

Holonic Construction Scheduling System for Construction Projects Using Python Programming Language 327
 S. Gopinath and Rukhsar

Study of Characteristics of Expansive Soil Stabilized with Tire Derived Aggregate and Fish Scale Powder 337
 D. Gokulkumar, P. T. Ravichandran, and K. Divya Krishnan

Earthquake Engineering

Dynamic Response of Cable-Stayed Bridge Under Seismic Vulnerability Analysis: State of the Art	353
Inamdar Zakeer Ahamed Kadir Ahamed and Rajendra B. Magar	
Complex and Lightweight Tensegrity Structure Under Dynamic and Impact Loads; State of the Art	363
Shaikh Irfan Badiyoddin Shaikh and Rajendra B. Magar	
Demountable Shear Connector in Steel–Concrete Composite Floors: A State-of-the-Art Review	373
G. Suba Sreenidhi and G. Senthil Kumar	
Effect of Steel Fibre and Plastering Sand on GGBS and Silica Fume Based Geo-Polymer Concrete	383
C. Gowthamaraj and G. Vimalanandan	
Shear Resistance Behavior of Partially Sandwich Composite Structures Considering Elements Varying Dimension and Comparison Using Global Provisional Codes	395
Wesam Al Agha, Mohanad Ali Ishaq Najajra, Taha Ahmed Ghaleb Mohammed, and Nambiappan Umamaheswari	
Effect of Bracing Structural System on the Seismic Response of High-Rise Reinforced Concrete Building for Strengthening with Soft Storey	409
Taha Ahmed Ghaleb Mohammed, Mohanad Ali Ishaq Najajra, and Wesam Al Agha	
Experimental Studies on the Flexural Strength Using Bagasse Ash and M-Sand in Concrete	421
S. Sundararaman and S. Azhagarsamy	
Performance-Based Seismic Analysis of RC Multi-storey Framed Building Equipped with Dampers	431
R. Arvind, M. Helen Santhi, G. Malathi, and V. Vasugi	
Numerical Studies on RC Beams Strengthened with an Externally Bonded Aramid FRP Sheets	439
Gurram Kalyani and N. Pannirselvam	
Analysis and Design of G+15 High-Rise Residential Structures with and Without Floating Column in Nepal	449
Nisha Jha, Pratiksha Simkhada, and R. Ramasubramani	

Disaster Management

Inferences on Strength and Ductility of High Performance Concrete Mixed with Steel and Macro-synthetic Fibres 467
 S. Syed Ibrahim and S. Kandasamy

Study the Interaction Behaviour of Integrated Infilled Frames with Interface Materials 479
 S. Jaya Harish, S. Muthu Kumar, and K. S. Satyanarayanan

Experimental Investigation on Lightweight Expanded Clay Aggregate (LECA) as a Coarse Aggregate in Concrete 491
 S. Prakashchandar and R. Senthamilselvi

Experimental Study on Strengthening of Damaged Steel Flexural Members Using CFRP Composite Wraps 507
 G. Arun Kumar, S. A. Vengadesh Subramanian, and N. Umamaheswari

Strengthening of Structures Using FRP Composites Fibres 519
 D. Murugan and N. Pannirselvam

The Behavior of RC Beam with an Opening Filled with the Hollow Square Section Under Static Loading 527
 P. Gokul and L. Sabarigirivasan

Application of Data Mining Techniques and Hedonic Pricing Methods to Determine the Real Estate Land Prices in the Chengalpattu District 541
 K. Mahima Christin, M. B. Sridhar, B. Divya, and R. Sathyanathan

Optimization of Inventory Control Management to Impact on the Profitability of Construction Projects 551
 S. Sarath Babu and A. Arokia Prakash

Developing Management Information System for Construction Equipment Maintenance 563
 B. Indhu and J. Ajay

Research Advancements in the Study of Microbiology of Aerosols 575
 Rajitha J. Rajan and Sathyanathan Rangarajan

Coastal and Harbour Engineering

Behaviour of Quartz Powder-Based Fibre-Reinforced Concrete 585
 P. Kaviya and A. Sattainathan Sharma

Investigations on Ambient Cured Alkali-Activated One-Part Geopolymer Concrete 595
 F. Stellamary and T. Ch. Madhavi

Experimental Investigation on the Incorporation of Reed Plant Ash in Concrete	603
P. Eshanthini, K. Sarayu, and K. Srishanth	
Study on the Bonding Behavior of Hybrid Fiber-Reinforced Concrete Using Ramie and Glass Fibers	613
S. Torhffi David, R. Ramasubramani, and P. T. Ravichandran	
Study on Effectiveness of Reinforced Concrete Beam Strengthening with Carbon Fibre-Reinforced Polymer	623
Taha Ahmed Ghaleb Mohammed, Mohanad Ali Ishaq Najajra, and Wesam Al Agha	
Comparative Study on Structural Performance Between Reinforced Concrete Beam and Ferro-Cement Laminate Strengthening	635
Mohanad Ali Ishaq Najajra, Taha Ahmed Ghaleb Mohammed, and Wesam Al Agha	
Experimental Investigation on Chemically Treated Hooked End Steel Fiber Embedded in Rubberized Concrete	649
K. Thiagarajan and N. Umamaheswari	
Study on Mechanical Properties of Polymer Fiber-Reinforced Nano-Concrete Under Elevated Temperature	663
S. Hariharan and S. Karthiga	
Planning, Analysis and Design of Vented Drainage Canal Across River Ganga in Falta, West Bengal	675
Vishnu Vardhan Reddy, Avinash Pandey, Siddharatha Sarkar, Balasubramanian Murugesan, and Monisha Ravi	
Study on the Improvement of Properties of Expansive Soil Using Seashell Powder	687
V. Janani, Jigisha Yadav, and P. T. Ravichandran	

About the Editors

Dr. Md. Abdul Mannan is working currently as a professor in the Faculty of Engineering at the University of Malaysia Sarawak (UNIMAS). He graduated B.Sc. (Civil) from Raishashi University, M.Sc. (Civil) from University Kebangsaan Malaysia, and Ph.D. (Civil) from University Malaysia Sabah. His areas of research interest are advance concrete technology, integrated design project, reinforced concrete design, strength of materials, engineering mathematics, highway engineering, engineering mechanics, structural steel design, structural analysis, etc. He has published around 50 research papers in national/international journals.

Dr. R. Sathyanathan is currently working as an associate professor in the Department of Civil Engineering, College of Engineering and Technology, SRM Institute of Science and Technology, Kattankulathur, India. He obtained his B.E. (Civil) from Government College of Technology, Coimbatore, and M.E. (Irrigation Engineering Management) from the Center for Water Resources, College of Engineering, Anna University, Chennai and Ph.D. from SRM University, Kattankulathur. He has 22 years of professional experience in academics. His areas of research interest include coastal hydrodynamics, watershed management, meteorological data analysis, GIS and remote sensing applications in water resources and environmental engineering. He has published around 50 papers in national/international journals and six chapters. Apart from his academic pursuits, he devotes himself to mentoring and advising students who are enthusiastic about pursuing careers in different domains of civil engineering research. He actively reviews paper for many international journals published in the field of Water Resources Engineering.

Dr. N. Umamaheswari is currently working as a professor at the Department of Civil Engineering, College of Engineering and Technology, SRM Institute of Science and Technology, Kattankulathur, India. She obtained her B.E. (Civil) and M.E. (Structures) degrees from Madurai Kamaraj University, Madurai, and Ph.D. from SRM University, Kattankulathur. She is having 30 years of professional experience of which 26 years are in academics. Her area of research interest includes steel-concrete composite structures, steel structures, finite element analysis, and fracture mechanics.

She has published around 60 papers in national/international journals and conferences, received four grants for organizing/attending international/national programs from Government of India and SRM IST, executed one in-house project, received a patent grant, visited UK and Japan, performed collaborative research with foreign experts, organized/chaired international conferences, and authored a book.

Dr. Hemant S. Chore is working currently as an associate professor and the head in the Department of Civil Engineering at Dr. B. R. Ambedkar National Institute of Technology Jalandhar (Punjab), India. Prior to joining NIT Jalandhar in 2018, he was working as a professor in the Department of Civil Engineering at Datta Meghe College of Engineering, New Mumbai, affiliated with the University of Mumbai for 24 years. He has got rich experience in the field of academics and research. His area of research interest includes soil-structure interaction, pavement analysis and design, structural engineering, and utilization of waste materials in geotechnical and highway construction. He has guided 08 Ph.D.s till now with 09 more candidates pursuing their Ph.D.s under his supervision. He has guided more than 50 M.Tech. candidates for their Dissertations. He has got more than 60 research publications in refereed journals and more than 200 papers in the proceedings of national and international conferences.

Structural Engineering and Health Monitoring

Strength of Concrete with Partial Replacement of Aggregate with Granite



S. Suresh Babu and T. Abishek

1 Introduction

Rapid expansion can be seen in the building trades. On the other hand, the world's supply of raw materials required to make concrete is dwindling, while industrial waste is rising. So, these countries are exploring alternatives to cement in order to meet demand. The purpose of this research was to find a way to partially substitute fine aggregate with granite quarry refuse. Compressive strength more than 200Mpa is characteristic of the igneous rock family of which granite is a member because it is created by the crystallisation of magma. Granite powder can be used as a partial replacement for fine aggregates since its physical properties are similar to those of natural river sand. Using granite demolition debris has various benefits, including lowering construction costs and easing the environmental crisis. Due to its high silica and feldspar content, granite powder is a potential material. As a result of silica, cement-like pozzolanic behaviour is seen. It also aids in forming a consistent blend by binding the basic materials together. The pozzolanic quality is claimed to increase concrete's durability. Granite powder is useful for packing and filling the matrix of concrete because of its small particle size. Cement, coarse aggregate, fine aggregate, water, and admixtures (if any) make-up the matrix of a concrete slab. The goal of the task is to adjust the granite powder content by switching out the coarse aggregate. The performance characteristics of concrete can be altered by the addition of granite powder. Concrete's workability, compressive strength, and split tensile strength have all been compared to standard concrete since they contribute to a building's stability. It is hoped that the findings would aid in solving the issues of granite quarry solid waste management and a lack of available natural sand. High performance concrete was studied by Kanmalai Williams et al. (2008) [6], who reported on the impact of using

S. S. Babu · T. Abishek (✉)

Department of Civil Engineering, SRM Valliammai Engineering College Kattankulathur,
Chennai 603203, India

e-mail: tabishek046@gmail.com

granite powder as a partial replacement of fine aggregate. According to the findings, adding more granite powder lowers the material's compressive strength. Dr. Flexi Kala (2013) [3] found that using small amounts of granite powder to partially replace sand in concrete with admixtures improved the material's durability and strength. The weight percentages of granite powder and the other admixtures were 0, 25, 50, 75, and 100. Not only did the concrete have a larger plastic strain value, but the drying shrinkage strains were also greater than normal concrete's. According to a 2013 study by M. VijayaLakshmi et al., [4] adding granite powder to concrete not only increases its mechanical characteristics but also its pozzolanic property by efficiently filling the concrete matrix. When compared to the strength of the control mixture and higher, which decreased significantly when granite powder was replaced by sand at a rate of more than 15%. An extensive experimental research on compressive strength, split tensile strength, and comparison with regular concrete was given by A. Arivumangai et al. in 2014 [5]. The use of granite powder in concrete was shown to increase both its strength and its durability. Granite powder was investigated by Makarla Susmitha Kumari et al. (2018) [9] as a potential fine aggregate replacement. The amounts of granite powder applied ranged from 10 to 25 per cent. In addition, 20% fly ash can be substituted for cement in any percentage of granite powder. The revealed results were encouraging for using fly ash to replace 20% of the cement and granite powder to replace 20% of the fine aggregate. Concrete with 60% sand replacement, as suggested by Yuvraj Patil et al. (2018) [11], has high compressive strength. Kavya B R et al. (2019) [10] showed what would happen if fine aggregate was replaced with varying percentages of granite slurry (10%, 15%, 20%, 25%, and 30%) found that the concrete containing 20% granite slurry performed relatively well. According to Grzegorz Prokopski et al. (2020) [12], the average density of concrete increases when granite powder is used as a partial replacement for sand because the microstructure of the cement matrix is compacted. Concrete with granite powder added to it is the subject of an attempt by Danish Shaikh et al. (2021) [8]. Using granite powder as a partial replacement for sand in the concrete matrix was found to be successful, as evidenced by the test results.

2 Research Significance

From the literature study, it is known that the granite powder is one of the promising materials for replacing fine aggregate. Studies revealed the technogenic materials can be used as fillers, which also solves the environmental problem to a certain extent. However, optimizing the percentage of granite powder to replace fine aggregate is an important consideration to obtain high concrete strength. The aim is to optimize the percentage of granite powder in concrete and to determine the physical properties of concrete. Thus, this research was conducted to experiment the potential use of granite powder as a replacement for fine aggregate together with admixtures.

3 Experimental Programme

3.1 Materials

Portland Pozzolana Cement, a type of cement. In this research, fly ash served as the foundation. Fly ash can make-up anywhere from 15 to 35% of Portland Pozzolana Cement by weight. Components Necessary for Portland Pozzolana Cement conforms to the requirements of IS 1489:2015, parts 1 and 2 [15, 16]. Table 1 lists the cement's physical qualities, whereas table 2 lists its chemical properties.

Nearly 60%–75% of the total volume of concrete is occupied by aggregate. Coarse aggregate is the larger variety, whereas fine aggregate is the smaller. The coarse aggregate employed in this investigation was an everyday blue metal with a nominal size of 20 mm. To make practical concrete, proper gradation of aggregates is the most crucial factor. The coarse aggregates for the course have been sieved. Table 3 provides the percentages passing via various sieve sizes as specified by IS 2386(1):1963 [1]. The characteristics of coarse aggregate that meet the requirements of IS 2386(3):1963 [13] are given in Table 4.

Table 1 Physical properties of cement

Properties	Experimental value	Values as per IS 1489: 2015
Specific gravity	3.13	3.15
Finesses (blaine) m ² /kg	356	300 (minimum)
Normal consistency (%)	30	-
Initial setting time (min)	56	30(minimum)
final setting time (min)	245	600(maximum)
Soundness(le chatelier expansion (mm)	3	10(maximum)
Compressive strength (MPa)	16	16(minimum)
A) 3 days	25	22(minimum)
B) 7 days	34	33(minimum)
C) 28 days		

Table 2 Chemical properties of cement

composition	Experimental value	Values as per IS 1489: 2015
Insoluble residue (%)	2.3	3 (maximum)
Magnesia (%)	1.65	6 (maximum)
Sulphuric anhydride (SO ₃) (%)	2.6	3.5(maximum)
Loss of ignition, (%)	3.06	5(maximum)
Chloride content, (%)	0.06	0.1(maximum)
Sodium oxide (Na ₂ O + 0.658 K ₂ O) (%)	0.1	0.6(maximum)

Table 3 Sieve analysis of coarse aggregate

Sieve size (mm)	% passing
25	100
20	96
16	85
12.5	62
10	24
6.3	01
4.75	00

Table 4 Properties of coarse aggregate

Properties	Experimental value	Values as per IS 2386(3):1963
Specific gravity	2.67	2.6–2.9
Bulk density kg/m ³	1790	-
Water absorption (%)	1.35	Less than 2
Fineness modulus	6.85	6.75–8
Impact value (%)	19	10–20(strong)
Crushing test	12.5	-
<i>Flakiness test</i>	20.1	-
<i>Elongation test</i>	26	-

Fine aggregate used to meet zone II grading requirements is often natural river sand. The qualities of granite powder that was obtained from a crushing unit were investigated. The particle size distribution curves of river sand and granite powder are shown in Fig. 1. The characteristics of river sand and granite powder are given in Table 5. The chemical make-up of river sand and granite powder is given in Table 6.

Water: IS 3025–1988 [17] and IS 456–2000 [14] compliant drinking water were used in this study.

Additive chemistry: The local superplasticizer (conplast SP-430) was employed at a concentration of 1% to attain the appropriate workability. Table 7 gives some of the characteristics of superplasticizers.

3.2 Mix Combination and Casting

In the present investigation, four mix combination of granite powder was involved. The percentage replacement of granite powder (20%, 25%, 30%) is given in Table 8, which was compared to the conventional concrete mix. In the laboratory, the cement, coarse aggregate, fine aggregate, and granite powder were initially mixed to form

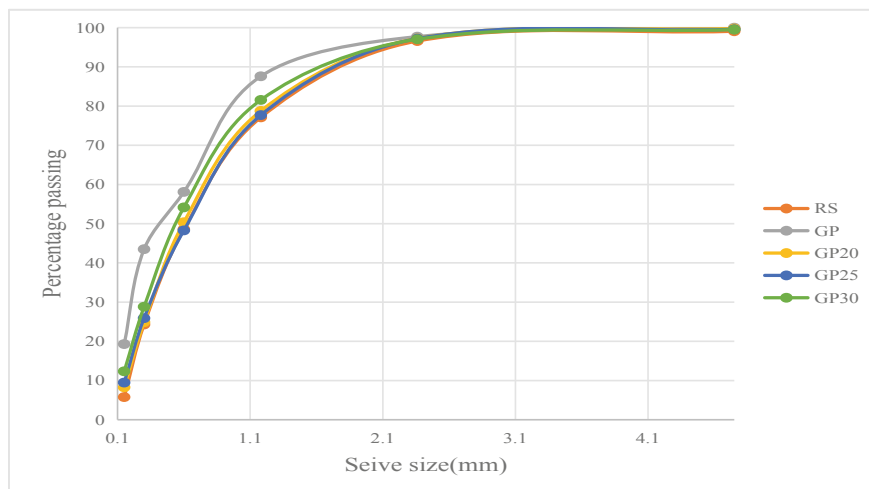


Fig. 1 Particle size distribution curve of river sand and granite powder

Table 5 Physical properties of river sand and granite powder

Properties	Experimental value		Values as per IS 2386(3): 1963
	River sand	Granite powder	
Specific gravity	2.668	2.653	2.65–2.67
Bulk density kg/m^3	1602	1598	-
Water absorption (%)	3.2	5.4	2–6
Fineness modulus	2.5	3.8	2–4

Table 6 Chemical composition of river sand and granite powder

Composition	River sand (%)	Granite powder(%)
SiO_2	73.46	74.39
AL_2O_3	10.78	13.5
Fe_2O_3	3.38	0.86
MnO	0.09	0.02
MgO	1.33	0.38
CaO	3.58	0.41
Na_2O	2.25	4.16
K_2O	2.06	4.79
TiO_2	0.45	0.17
P_2O_5	0.08	0.02

Table 7 Properties of superplasticizers

Properties	Values
Brand	Conplast SP-430
Specific gravity	1.2
Density kg/m ³	1260
Colour	blue
Base chemical	SNFC

Table 8 Percentage replacement of granite powder

Specimen designation	FA%	GP%
CC	100	0
20GP	80	20
25GP	75	25
30GP	70	30

homogeneous mixture. Then, the liquid components were added to the dry mix and continued the mixing for another 4 min.

Cubes of size 150 mm x 150 mm x 150 mm and cylinder of diameter 150 mm and length 300 mm were casted for each mix to determine the hardened properties of concrete. For each mix proportion, minimum of three cube and three cylinder were casted to obtain the average test results.

4 Results and Discussion

Workability: The test results shown in Fig. 2 explain the effect of GP on the workability as per is code IS 1199–1959 [18]. The workability of concrete decreases with increase of GP. Lowest workability was observed for the substitution of 30% GP (30GP). This is because workability and water demand depends on the partials size and shape of the materials added. From Fig. 1, it is clear that particle size of GP is finer then river sand. The uneven and angular texture of GP is the reason behind the decrease of workability.

Compaction Factor: The test was conducted as per IS 1199–1959 [18]. The mix 30GP shows the highest compaction factor when compared to other mix as shown in Fig. 3. The smaller size of GP has effectively contributed to the packing and filling of concrete matrix which in turn showed a gradual increase in the compaction factor from CC to 30GP.

Compression Strength: The compressive strength of different mix proportion having 20%, 25%, 30% GP as a replacement to river sand is tested at ages of 7, 14, 28, and 56 days. The compression test results are shown in Fig. 4; from the graph, it is clear that the compression strength of 25GP is maximum when compared to the other mix (Fig. 5 and Fig. 6).

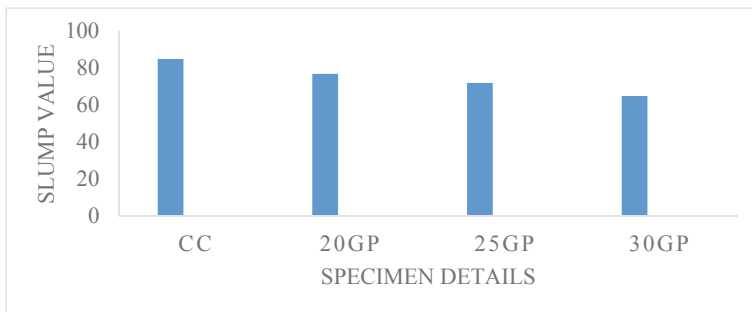


Fig. 2 Slump value

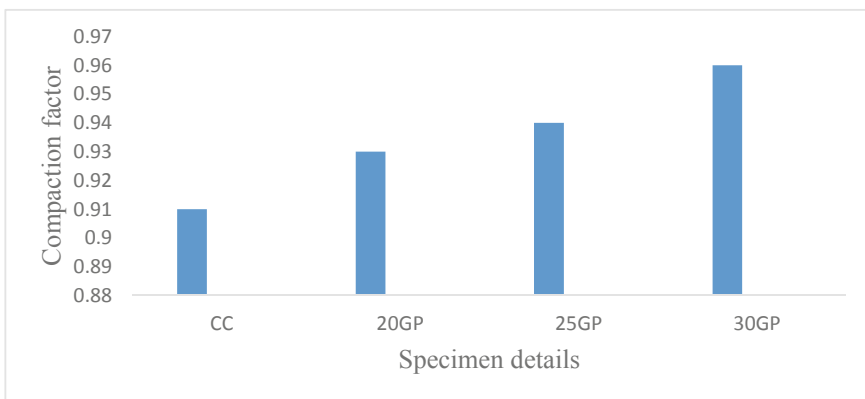


Fig. 3 Compaction factor



Fig. 4 Casting of cube and cylinder

Fig. 5 Testing of cube and cylinder

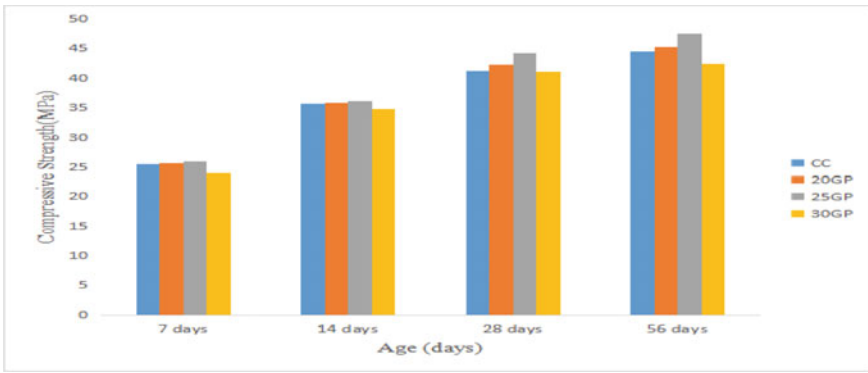


Fig. 6 Compression test

Cylinder specimens were examined for split tensile strength at 20%, 25%, and 30% GP and 7, 14, 28, and 56 days. Figure 7 displays that the tensile strength increased up to a 25% replacement rate, and then suddenly dropped for the 30GP blend. The results indicate that the best tensile strength was achieved with a 25% GP substitution.

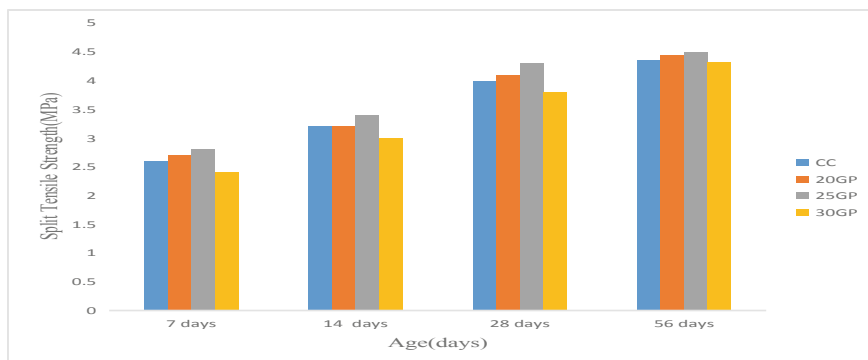


Fig. 7 Split tensile test

5 Conclusion

Concrete qualities like workability, compressive strength, and split tensile strength are investigated in a research of concrete made with GP as a partial replacement to river sand. When added to concrete, GP improves the material's mechanical qualities, as was observed empirically. When compared to the other mix proportions and across all ages of curing, concrete with 25% GP (25GP) had the strongest strength of the four studied. Based on these findings, it can be concluded that GP can be used to partially replace river sand to produce concrete with increased strength while also reducing environmental impact.

References

1. IS 2386(Part 1):1963. Methods of test for aggregates for concrete: Part 1 Particle size and shape. New Delhi: Bureau of Indian Standards.
2. IS 10262:2009. Guidelines for concrete mix proportioning. New Delhi: Bureau of Indian Standards.
3. Dr.T.Felix Kala, "Effect of Granite Powder on Strength Properties of Concrete", International Journal of Engineering and Science Vol.2, Issue 12 May 2013.
4. M. Vijayalakshmi, A.S.S. Sekarb, G. Ganesh prabhu, "Strength and durability properties of concrete made with granite industry waste". Construction and Building Materials 46 (2013) .
5. A. Arivumangai, T. Felixkala, "Strength and Durability Properties of Granite Powder Concrete" Journal of Civil Engineering Research 2014.
6. Kanmalai WC, Partheeban P, Felix KT (2008) Mechanical properties of high performance concrete Incorporating granite powder as fine aggregate. International Journal on Design and Manufacturing Technologies 2(1):67-73
7. T. Felixkala, P. Partheeban, 'Granite powder concrete' Indian Journal of Science and Technology vol.3, No.3 (Mar 2010) ISSN: 0974-6846.
8. Shaikh D, Patel T, Shaikh M, Qazi T, Mahajan M (2021) Partial Replacement of Fine Aggregate with Granite Fines. International Journal of Recent Advances in Multidisciplinary Topics 2(4):110-112

9. Makarla Susmitha Kumari, Rajendra Prasad Singh, W Sai Deepak, "A Study on Performance of Granite Powder in Concrete", *International Journal for Research in Applied Science & Engineering Technology*, Volume 6, Issue IV, pp 3518–3522, April 2018.
10. Kavya BR, Chandrashekar AR (2019) AN EXPERIMENTAL STUDY ON PARTIAL REPLACEMENT OF FINE AGGREGATE WITH GRANITE SLURRY AND CEMENT WITH GGBS. *International Research Journal of Engineering and Technology* 06(07):1842–1847
11. Yuvraj Patil, Anand R Chavan, Umarfarook H. Momin, Harshada P Kadam, Sanjay N Patil, "Studying the compressive strength of concrete with Granite as partial replacement to sand", *International Research Journal of Engineering and Technology*, Volume: 05, Issue: 04, pp 4339–4342, Apr-2018
12. Prokopskia G, Marchukb V, Hutsa A (2020) "The effect of using granite dust as a component of concrete mixture. *Case Studies in Construction Materials (Elsevier)* 13:1–7
13. IS 2386(Part 3):1963. Methods of test for aggregates for concrete: Part 3 Specific Gravity, Density, Voids, Absorption and Bulking. New Delhi: Bureau of Indian Standards.
14. IS 456:2000. Code of Practice for Plain and Reinforced Concrete. New Delhi: Bureau of Indian Standards.
15. IS 1489(Part 1):2015. Specification for Portland-Pozzolana cement: Part 1 Fly Ash Based. New Delhi: Bureau of Indian Standards.
16. IS 1489(Part 2):2015. Specification for Portland-Pozzolana cement: Part 2 Calcined Clay Based. New Delhi: Bureau of Indian Standards.
17. IS 3025:1988. Methods of Sampling and Test (Physical and Chemical) For Water and Wastewater. New Delhi: Bureau of Indian Standards.
18. IS 1199:1959. Methods of Sampling, Testing and Analysis for Fresh concrete. New Delhi: Bureau of Indian Standards.

State-of-the-Art Review on Synthesis and Utilization on Graphene Oxide in Concrete Under Elevated Temperature



I. Ramana and N. Parthasarathi

1 Introduction

From previous stage to till now, OPC plays an important role in the construction industry. The output of cement fabrication has surpassed 3.6 billion tones globally in order to satisfy human kind need for the urbanization which concern building framework for the economically developing nations like India and China [1]. It is well known the concrete is strong in compression but same time, there is a weak in tension. Concrete has a huge applications in bridges, roads, buildings, etc. Concrete plays a major role in building infrastructure and building construction. Because of the presence of fragile nature in concrete, there is a formation of cracks, low tensile strength, the capacity of strain is very low when compared to other materials [2]. To overcome this disadvantages, lots of efforts were made to increase the concrete strength with the help of fibre, admixture, waste materials, etc. At present, fibre-reinforced concrete (FRP) plays a major role in civil research since 1960. FRP helps to reduce the formation of cracks in micro level but it lacks to reduce the crack formation in nano level. The introduction of nanomaterials in cement provides more opportunities to improve the strength of the concrete [3]. The word “nanotechnology” was coined by Nobel prize winner Richard P. Feynman in 1959. The word nanotechnology differs from field to field. But nanotechnology is generally defined as observing, controlling and reconstructing the matter in the order of nanometer to provide the nanotechnology with new properties and functions [4]. The utilization of nanotechnology in concrete on a trading scale is producing limited amount and some of them were introduced in the market. The advantages of using nanotechnology in concrete are used to produce more durable and strongest material when compared to the conventional material. Nanotechnology in concrete is using appropriate methods,

I. Ramana · N. Parthasarathi (✉)

Department of Civil Engineering, Faculty of Engineering and Technology, SRM Institute of Science and Technology, Kattankulathur, Tamil Nadu 603203, India

e-mail: parthasn@srmist.edu.in

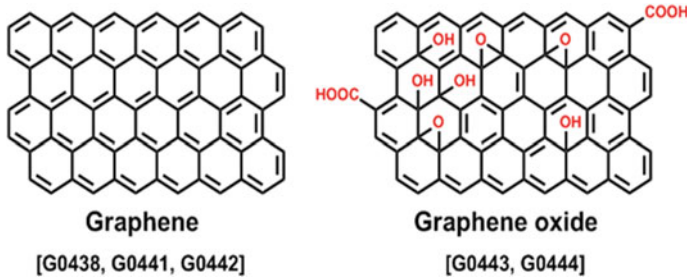
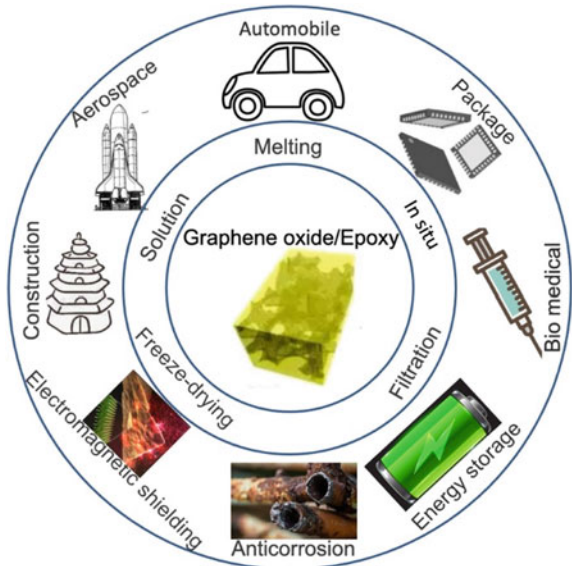


Fig. 1 Structural components of graphene and graphene oxide [6]

and the nano-sized particles are incorporated into concrete. The main advantage of utilizing nanomaterials is to attain flexural and compressive strength in earlier stage when it is in volume ratio to high surface and it also improves the pore structure in concrete. Graphene oxide is one of the types of nanoparticles [5]. In spite of being the nanoparticles used in many other field, the application of graphene oxide in civil engineering is growing rapidly nowadays. Graphene oxide is the derivative of graphene is made up of single layer of carbon atom thick. The incorporation of graphene oxide gives us to achieve good compressive, tensile strength and also it has strong durability. Graphene has an extra hydroxyl group consists of same hexagonal network of carbon. Graphene oxide is seen in four various forms such as powder, ribbon, flakes and sheets (Fig. 1).

Recent developments have sparked new innovations for enhancing the characteristics of traditional material [7]. Over the last few decades, there has been a focus on developing the characteristics of Ordinary Portland Cement (OPC) by incorporating various nanomaterials. The adsorption quality of the graphene oxide and cement modifying cement properties with GO reduces fluidity while greatly increasing mechanical characteristics [8]. Notably, the development of mechanical characteristics in cement with the addition of developed graphene oxide dispersion gathered the mechanism of C-S-H and acts as a bridge towards attractive forces. According to the researches, the establishment of graphene oxide aggregates will capture water free by reducing the workability [9]. By the mechanism of van der Waals forces between GO sheets cause cement flakes to influence one another, the physical relationship between GO and cement flakes partly explains the decreased the efficiency of cement mixture [10]. There are significant variations in the rate of increase as well as the better dosage of GO among these reports. Some experiments with GO suspensions mixed directly with cement have been found that gathered GO spread instead of GO nanosheets contributed to improvements in mechanical durability [11] (Fig. 2).

Fig. 2 Applications of graphene oxide [12]



2 Graphene Oxide

Graphene oxide is the major type of nanoparticles. It is the derivative form of graphene. In the recent years, the nanotechnology has developed by researchers by doing many research. Graphene oxide is used in all fields like medicine, chemical, biotechnology, etc. [13]. Nowadays, the implementation of graphene oxide in construction industry is developing more. Graphene is a single layer of carbon atoms which is formed by the oxidation of graphite. Graphene oxide is available radially and it is cheap when compared to other nanomaterials. Many research scholars have paid the attention towards the graphene because of its excellent chemical, electrical, mechanical and thermal characteristics. Currently, the perfect material for graphene is graphene oxide [14]. Graphene oxide is made up of additional hydroxyl group fix towards the carbon network of same hexagonal group. Graphene oxide is a single layered nanomaterial which is composed of oxygenated graphene sheets with hydroxyl (OH) and epoxy (O) at their basal planes and carboxyl (COOH) and carbonyl (CaO) on the edge of the sheet. As a result of the existence of these active groups, the van der Waals force between graphene oxide particles will change, aiding dispersion and reactivity [15]. The sonication process damages the outside of the graphene oxide due to this damage the size reduced from micro to nano level. If the oxygen group is removed in the graphene oxide, it will be reduced then it is known as the reduced graphene oxide. In the recent years, the graphene oxide has the pioneering studies for their better performance and increased durability and mechanical characteristics. Graphene oxide is one of emerging technologies identified by the researchers to control the process of cement hydration. Graphene oxide (GO) is readily and

uniformly scattered in water than graphene. Graphene oxide is an encouraging 2D nanomaterial's result of chemical exfoliation of graphite, which has a homogeneous and stable dispersion in water [16]. Graphene oxide also has the intention towards the appearance in the nanosheets form which can be studied using Hummer method. Graphene oxide nanosheets have a significant impact for bringing the modification of cement. When compared to other material, graphene and its derivatives has high elastic modulus and strength. Graphene oxide also lays the foundation for introducing the new techniques which is hydrophilic nanocomposites [17]. Because of its cement composites applications and better qualities, graphene oxide is used for allowing the functionalization process.

3 Composition of Graphene Oxide

Composition of graphene oxide was first discovered by British scientist B.C. Brodie in the year of 1859 was investigated under flake graphite [18]. Graphene oxide consists of two main process they are one is TOP-DOWN PROCESS which involves the reduction of larger structure into smaller structure. The second process involves the BOTTOM UP PROCESS, and it is also known as molecular nanotechnology that describes the method of assembly or self-assembly which is used to create materials from the atom or molecular components [19]. Among this two process, the top down process is mostly used in nanotechnology. Graphene oxide is produced mainly by two methods they are modified hummers and off man method, and these two methods are used for improvement and for safety purposes. When compared to off man method, hummers method is mostly used due to this natural and more safety purposes. If there is any changes that happened in the hammers method, then it is known as modified hammers Method. The exact definition for this method used for this is standardization [20]. When carbon agent is mixed with solvent, potassium permanganate is produced. After that when the potassium permanganate is mixed with hydrogen peroxide, if there is any metal ions present in this solution can be removed; as a result, the yellow brown liquid and yellow bubbling liquid are produced [21]. The shape and size of the graphene oxide was produced by using hammers method. Other researchers use thermal treatment or exposure to strong oxidizers to expand graphite, which increases the carbon source's interlayer spacing and allows to facilitate the graphene oxide layer delamination [22] (Fig. 3).

4 Effect of Elevated Temperature on Mechanical Properties

Compressive strength, tensile strength, elastic modulus and stress-strain response in compression are the mechanical qualities of major interest in fire-resistant design [23]. In comparison, different properties of concrete at elevated temperatures are mostly used for research. The elevated temperature for mechanical properties tests

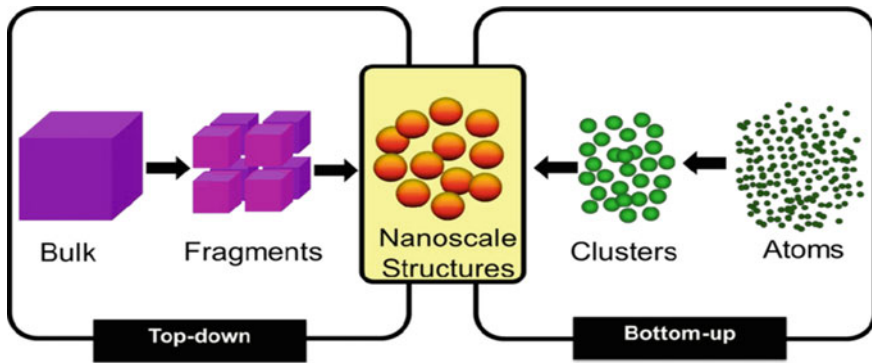


Fig. 3 Process of graphene oxide [13]

is often performed on concrete specimens commonly in cubes and cylinders with varying diameters [24].

5 Compressive Strength

The ratio of fluctuation for concrete at increased temperatures, that consist of boundaries (of the shaded region) indicating variation in reported test data across the range. The fluctuation of compressive strength as determined by Euro code is also represented in these data. The employment of distinct binders in HSC generates a superior and compact microstructure that consist of low calcium hydroxide, produce valuable influence on compressive strength at room temperature. Binders that are used to produce the better results for increasing compressive strength, which is due to a dense microstructure [25]. Because of a scarcity of standardized testing methodologies for conducting property tests, different testing settings and test procedures are used which is the another major reason because of the large diversity in the elevated temperature for the strength properties of concrete [26].

6 Tensile Strength

Because tensile strength of concrete is substantially less than the compressive strength, at room and elevated temperatures, it is typically neglected in strength estimations. However, from the standpoint of fire resistance, it is a significant quality, because cracking often caused by tensile strains, and structural damage of the member under tension because the microcracking advancement is a common cause. Concrete tensile strength can be rather high. More important in cases of fire- concrete spalling triggered on the members under fire conditions [27]. As a result, knowledge of

the HSC tensile strength varies with temperature, which is critical for forecasting. Spalling caused by fire in HSC members.

7 Conclusion

The outcome of the recent status of graphene oxide production in cement composites and the developments is discussed. Graphene oxide has the capacity to create novel high performance in cement characteristics long lasting. Improved microstructural, mechanical and durability characteristics of Go is unique and it has the possibilities of bringing new developments in upcoming years. Studies reveals that the little amount of Go is enough to raise the mechanical performance of concrete. However, because of the various properties of go, as well as the complexity of cement, there is significant discrepancy in these results. The majority of current studies is focused on the graphene oxide applications in mortar or cement paste. The use of cement paste, particularly UHSC with a low w/c, has received little attention. There is slightly less details available on the durability connected characteristics of cement composites carrying graphene oxide then there is on the mechanical properties. As a result, more in-depth studies on the durability of GO reinforced cement composites are required. The combination of GO and other materials can not only improve the mechanical and durability of cement, but also add smart properties and multi functionality, such as EMI shielding, efficacy, thermal and electrical conductivity are the factors to be considered in graphene oxide. It is to be appraisal for the application of graphene oxide merge with other material will permit to use in cement-based materials. The reinforcing mechanism of graphene oxide is widely accepted. As a result, GO influence on cement composites is still being researched in the construction field because of the appealing applications. The main challenges were connected with dispersion difficulties, as well as a negative effect on workability and fluidity properties at higher dosages. This comprehensive review further our current research understanding progress on the use of GO as a nanoreinforcement is used in cement-based materials, and it provides useful information for future research priorities. The standards of nanomaterials include graphene oxide, carbon nanotubes, nanotitanium oxide, nanosilica and the mixing of slurry. Nanomaterials are taken more consideration. Because of the strong van der Waal forces that attract particles at the small-scale level, agglomeration of nanomaterials is a frequent issue. Ultra sonication is the process which is used for mechanical separation and admixture to prevent cluster in the cement matrix are required for properly dispersed nanomaterial. Cement pastes lose their ability to be worked easily when nanomaterials are added, which may be due to the permeation of free water. Because of their high reactivity, nanomaterials might hasten the hydration of cement by giving the C-S-H gel places to attach. The primary motivation for using nanomaterials is the seeding of C-S-H gel onto their large surface. Nanomaterials have the ability to refine pores which is highly desired because it increases strength and durability. The addition of nanomaterials consistently results in development in compressive, flexural and tensile

strengths, fracture toughness and other properties. GO seems to be the best candidate among the nanofillers mentioned so far for enhancing the characteristics of cement-based composite. Similar to CNTs, 2D nanosheet can reinforce the fragile cement matrix. The oxygen groups are also preferred for cement unique dispersion, C–S–H nucleation and microstructure densification. When adding nanomaterials to cement, admixtures are crucial in maintaining the cement's workability. An intriguing area for research is the durability of nanomaterial consist of concrete and cement matrix. It is important to examine how such composites behave when subjected to degradation processes like decarbonation, acid resistance and sulphate resistance.

References

1. Qin H, Wei W, Hang Hu Y (2017) Synergistic effect of graphene-oxide-doping and microwave-curing on mechanical strength of cement. *J Phys Chem Solids* 103(November):67–72. <https://doi.org/10.1016/j.jpcs.2016.12.009>
2. Yang H, Cui H, Tang W, Li Z, Han N, Xing F (2017) A critical review on research progress of graphene/cement based composites. *Compos Part A Appl Sci Manuf* 102:273–296. <https://doi.org/10.1016/j.compositesa.2017.07.019>
3. Anu Ma Ealias S, Saravanakumar MP (2017) A review on the classification, characterisation, synthesis of nanoparticles and their application. *IOP Conf Ser Mater Sci Eng* 263(3). <https://doi.org/10.1088/1757-899X/263/3/032019>
4. Shamsaei E, de Souza FB, Yao X, Benhelal E, Akbari A, Duan W (2018) Graphene-based nanosheets for stronger and more durable concrete: a review. *Constr Build Mater* 183:642–660. <https://doi.org/10.1016/j.conbuildmat.2018.06.201>
5. Liu C et al (2020) Application of nanomaterials in ultra-high performance concrete: a review. *Nanotechnol Rev* 9(1):1427–1444. <https://doi.org/10.1515/ntrev-2020-0107>
6. Hanus MJ, Harris AT (2013) Nanotechnology innovations for the construction industry. *Prog Mater Sci* 58(7):1056–1102. <https://doi.org/10.1016/j.pmatsci.2013.04.001>
7. Zheng W et al (2019) Enhancing chloride ion penetration resistance into concrete by using graphene oxide reinforced waterborne epoxy coating. *Prog Org Coatings* 138(July):2020. <https://doi.org/10.1016/j.porgcoat.2019.105389>
8. Khurana I, Saxena A, Bharti, Khurana JM, Rai PK (2017) Removal of dyes using graphene-based composites: a review. *Water Air Soil Pollut* 228(5). <https://doi.org/10.1007/s11270-017-3361-1>
9. Kawashima S, Hou P, Corr DJ, Shah SP (2013) Modification of cement-based materials with nanoparticles. *Cem Concr Compos* 36(1):8–15. <https://doi.org/10.1016/j.cemconcomp.2012.06.012>
10. Smith AT, LaChance AM, Zeng S, Liu B, Sun L (2019) Synthesis, properties, and applications of graphene oxide/reduced graphene oxide and their nanocomposites. *Nano Mater Sci* 1(1):31–47. <https://doi.org/10.1016/j.nanoms.2019.02.004>
11. Devi SC, Khan RA (2018) Effect of graphene oxide on mechanical and durability performance of concrete. *J Build Eng* 27(November):101007. <https://doi.org/10.1016/j.jobe.2019.101007>
12. Sokolnikov AU (2017) Applications of graphene. *Graphene Defense Secur*, pp 197–259. <https://doi.org/10.1201/9781315120379-9>
13. Chen J, Yao B, Li C, Shi G (2013) An improved Hummers method for eco-friendly synthesis of graphene oxide. *Carbon NY* 64(1):225–229. <https://doi.org/10.1016/j.carbon.2013.07.055>
14. Zaaba NI, Foo KL, Hashim U, Tan SJ, Liu W, Voon CH (2017) Synthesis of graphene oxide using modified hummers method: solvent influence. *Procedia Eng* 184:469–477. <https://doi.org/10.1016/j.proeng.2017.04.118>

15. Qureshi T, Panesar DK (2019) A comparison of graphene oxide, reduced graphene oxide and pure graphene: early age properties of cement composites, May, 2019
16. Chuah S, Pan Z, Sanjayan JG, Wang CM, Duan WH (2014) Nano reinforced cement and concrete composites and new perspective from graphene oxide. *Constr Build Mater* 73:113–124. <https://doi.org/10.1016/j.conbuildmat.2014.09.040>
17. Jayakaran P, Nirmala GS, Govindarajan L (2019) Qualitative and quantitative analysis of graphene-based adsorbents in wastewater treatment. *Int J Chem Eng* 2019. <https://doi.org/10.1155/2019/9872502>
18. Bautista-Gutierrez KP, Herrera-May AL, Santamaría-López JM, Honorato-Moreno A, Zamora-Castro SA (2019) Recent progress in nanomaterials for modern concrete infrastructure: advantages and challenges. *Mater (Basel)* 12(21):1–41. <https://doi.org/10.3390/ma12213548>
19. Huang XM, Liu LZ, Zhou S, Zhao JJ (2020) Physical properties and device applications of graphene oxide. *Front Phys* 15(3). <https://doi.org/10.1007/s11467-019-0937-9>
20. Pan Z et al (2015) Mechanical properties and microstructure of a graphene oxide-cement composite. *Cem Concr Compos* 58:140–147. <https://doi.org/10.1016/j.cemconcomp.2015.02.001>
21. Liu Y et al (2020) Enhancing ultra-early strength of sulphoaluminate cement-based materials by incorporating graphene oxide. *Nanotechnol Rev* 9(1):17–27. <https://doi.org/10.1515/ntrev-2020-0002>
22. Chen X, Zhang Y, Li S, Geng Y, Hou D (2021) Influence of a new type of graphene oxide/silane composite emulsion on the permeability resistance of damaged concrete. *Coatings* 11(2):1–14. <https://doi.org/10.3390/coatings11020208>
23. Głowacki M, Kowalski R (2020) An experimental approach to the estimation of stiffness changes in RC elements exposed to bending and high temperature. *Eng Struct* 217(September 2019):110720. <https://doi.org/10.1016/j.engstruct.2020.110720>
24. Parthasarathi N, Saraf DS, Prakash M, Satyanarayanan KS (2019) Analytical and experimental study of the reinforced concrete specimen under elevated temperature. *Mater Today Proc* 14:195–201. <https://doi.org/10.1016/j.matpr.2019.04.138>
25. Yazıcıoğlu S, Tuğla R, Ay S, Demirel B (2018) Effect of high temperature on compressive strength of concrete prepared using different types of aggregates. *Lect Notes Civ Eng* 6(Isbs 2017):425–434. https://doi.org/10.1007/978-3-319-63709-9_34
26. Arioz O (2007) Effects of elevated temperatures on properties of concrete. *Fire Saf J* 42(8):516–522. <https://doi.org/10.1016/j.firesaf.2007.01.003>
27. Abed F, Turkey Beddu SB, Najah Ahmed A, Al-Hubboubi S (2021) WITHDRAWN: a review—behaviour of geopolymer concrete to high temperature. *Mater Today Proc*. <https://doi.org/10.1016/j.matpr.2021.05.489>

Analyzing the Characteristics of Self-Compacting, Basalt Fiber, Ultra-High-Performance Concrete Using Nanowaste Product at Both High and Normal Temperature Changes



M. K. Muniyasamy and M. Dinesh Kumar

1 Introduction

In terms of mechanical qualities and construction longevity for the past 30 years, ultra-high-performance concrete (UHPC), a cement-based composites, is the most revolutionary product in concrete technology [1]. It is a “next” material that may offer a practical way to increase the sustainable development of structures and other infrastructure elements [2]. UHPC is a favored material in several nations, including the Netherland, Indonesia, France, Slovenian, German, England, and Japan [3–7] for repairing intricate architectural elements and structures. Because there is less moisture in UHPC than there is in binders, flowability is more crucial than strength [8–12]. The environmental impact of excessive cement use is significantly increased (UHPC has a nearly four-fold greater average global warming potential than regular concrete, for example). To lessen the impact on the environment caused by the cement content of UHPC composition, more research is still required [13–15].

Due to the CO₂ emissions of cement, which range from 0.8 to 1.3 tonnes per tonne depending on the type of fuel used and from 100 to 150 KWT per tonne [16], there is an urgent need to employ an alternative to cement to make concrete. Using pozzolanic materials in place of cement is the trend lately to reduce CO₂ emissions [17, 18]. Since many years ago, concrete has made considerable use of silica-rich agricultural metabolic end such sugar cane bottom ash (NSCBA), nanotextile stalk ash (NCSA), and nanorice stalk ash (NRSA). The strain that conventional concrete production places on the ecosystem is significantly lessened by the use of agricultural waste to make concrete.

M. K. Muniyasamy (✉) · M. Dinesh Kumar
Department of Civil Engineering, Saveetha School of Engineering, Saveetha Institute of Medical and Technical Sciences, Chennai, Tamil Nadu, India
e-mail: muniyasamymk9060.sse@saveetha.com

Sugar Cane Bagasse (SCB), a primary biomass metabolic end fuel made from the waste, tops, and needles of the stem of the plant, is the fibrous fluid residue that is taken during sugar cane milling [19]. Productivity and waste from sugarcane plants reached 655 million tonnes in 2015. Burn bagasse has the benefit of producing energy, but it also produces ash from filters and fly ash from cogeneration [20, 21]. Brazil, China, and the European Union (EU) are regarded as the three top exporters of sugar biomasses.

Numerous research on the effectiveness of bagasse on concrete and mortar, including various temperatures and in severe environments, including concrete powder [22–24]. The covering on rice grains or seeds is called rice husk. When the paddies are being ground, they are generated in large quantities. Researchers are currently interested in this because during the heating phase of production, rice husk produces around 50 percentage carbon and waste material and 50 percentage of SiO_2 [25, 26]. In the years 2017 to 2018, 115 million wheat stalks were generated globally, based on the Agriculture Department of the United States [27].

It is difficult to create basalt fiber-reinforced, self-compacting concrete with ultra-high performance and exceptional qualities. Investigating the results of exposing eco-friendly nanomaterial with sustainable qualities to high temperatures is also necessary. As a result, three mixes were conducted each of the three nanowaste materials, NSCBA, NCSA, and NRSA, using three of the ten combinations as the reference mix. On the best samples, microstructure analysis was conducted.

2 Materials and Methods

- Concrete features were examined using to make nano-sized particles, all agricultural wastes from Egyptian farms were collected, rinsed with tap water, dried, and burned at 600–800 °C for amorphous silica [28–30]. The components utilized in this investigation have all undergone chemical analysis.
- In order to create a mixes that adheres and combines ultra-high compressive strength and fresh SCC properties, the experimental program was developed on the foundation of reference mixes that the authors discovered via a series of trials. Nine mixtures are presented in Table 2 that are intended to the same amount of 1079 kg/m³ of binder.
- The following steps must be followed in order to prepare a cementitious materials as workability in addition to UHPC characteristics as resilience. First, the overall average (sand and limestones) must be mixed for two minutes.
- In this study, three aspects of recently placed samples assessed. These parameters are evaluated using slump flow, V-funnel, and L-box equipment in accordance with EN-12350 parts 8, 9, and 10. The flowability features of SCC were described using fresh state properties of concrete. Fresh SCC length was measured in two directions, and slump flow size was calculated as the mean size (Sf). Using the L-box test, which involved allowing new SCC in the horizontal box to flow through the bars to the horizontal box, maximum passing capacity of fresh concrete was

evaluated. To assess the passage capacity of SCC, the aspect ratio (h_2/h_1) (PA ratio) was calculated after the mixed flow ceased.

- Twelve mixes were separated into four groups for scanning electron microscopy (SEM), with references mix in different ratios being the blends with the best load when different additives and organics additions were made at room temperature of 25 C. Its same four combinations was picked to be examined after being subjected to a 300 °C temperature increase. The very same four mixtures were then evaluated after being exposed to 600 °C. After 28 days of compressive strength testing, specimens with dimensions of 10 10 10 mm were chosen from conventional concrete cores.
- To investigate the impact of nanoparticles on extremely high efficiency self-compacting concrete including basalt fiber, a 3000 KN ELE digital machine was employed. The curing days of all samples were evaluated for mechanical qualities including mechanical properties using cubes measuring 100 mm by 100 mm by 100 mm, cylinders measuring 100 mm by 200 mm, and beams measuring 10 mm by 100 mm by 500 mm, respectively.

3 Results and Discussion

3.1 Fresh State Properties

Flow table test To guarantee that the SCC workability demands are implemented, numerous trials are set up and tested [31], and it illustrates the importance of utilizing nanoparticles in place of low reduction cement to reduce the flow property class from to SF2. That is in agreement with other research [32]. For sample 2, introducing nanocotton stalk ash resulted in a significant reduction in flowability when compared to the control mix and nanosugar cane bagasse: 720, 730, and 680 mm at 1.5, 2.5, and 3.5% dosages, namely M1 to M5 in Table 1. This functional benefit from nanoparticles absorbing energy more quickly than cement, reducing workability while maintaining SF2 category. The porous diameter of the company’s wetness after treatment both contributed to a little decrease in stream diameter of other mixes [33, 34]. The mix ratio 1:1.5:3 and M25 grade of concrete was used.

Table 1 Fresh state properties

Sample name	Flow table	V-funnel test (Time (s))	L-box test H_2/H_1
M1	102	8	0.97
M2	105	6	0.95
M3	110	7	0.9
M4	75	5	0.92
M5	95	6	0.86

Table 2 Compressive strength test

Sample name	Compressive strength (MPa)
M1	122.5
M2	131.25
M3	134.08
M4	144.98
M5	122.9

V-funnel test. The V-funnel time is given in Table 1, and all mixes met the SCC criteria of sample 1 and sample 2 as opposed. With basalt fibers present, which assure great flowability, its initial time, which is extremely low before adding minerals. However, adding nanomaterials, good time management is vital because they are more finely ground than cement [35–37].

L-box test. Increased partially replacing ration reduced development in Table 1. This is caused by the inclusion of rise straws with big linked pores, an excellent mechanical area, tiny size bits, and a hexagonal structure [16, 38].

3.2 Hardened State Properties

Compressive strength. Investigations were done into the compressive (Table 2) of reference samples other mixes at heated and increased temperatures of 400 °C. Ref mix measured 125 MPa at room temperature. When samples were added, the strength increased by 16%, and the maximum strength was attained at 4% NSCBA. The increased strength is a result of NSCBA's high catalytic activity, refined pores, and surface area. Nanoparticles have a super action index, as evidenced by prior research that showed surface areas produced heavy indices of 65% to 100%, respectively [22]. The cementitious reaction of aluminosilicate created by burning procedure interacts with calcium hydroxide generated by hydration process at M9 (NRSA3), producing additional C-S-H gel. Additionally, rice husk straw exhibits internal curing properties and pozzolanic reactions [38–40]. Additionally, the inner RSA structure helps to maintain the curing process when the matrices humidity drops.

Split tensile test Under typical circumstances, organic addition enhances the tensile strength of UHPBF-SCC by 5.6–14.1%. Due to its large reinforcing impact and usefulness as a gauge of toughness and tensile, the addition of basalt fibers plays a crucial role in strength properties [41, 42]. The results that have been presented show improved performance of the concrete and promise for UHPC with compressive characteristics that incorporate mechanically generated of 10 mixtures with various nanodoses is given in Table 3.

Flexural strength test Under typical circumstances, the inclusion for flexure strength in Table 4. Owing to its qualities as a considerable reinforcing indication

Table 3 Split tensile test

Sample name	Split tensile test (MPa)
M1	14.26
M2	15.11
M3	14.96
M4	13.25
M5	11.25

Table 4 Flexural tensile test

Sample name	Flexural tensile test (MPa)
M1	28.55
M2	31.25
M3	30.3
M4	29.66
M5	29.10

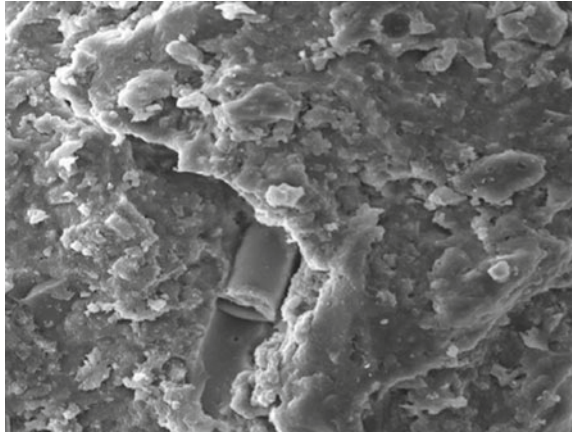
for target strength, introducing basalt fibers [43]. The addition of NRSA to basalt fibers significantly increased flexure strength by 11–28%. The outcomes that have been introduced show improved concrete durability with concrete features, loading generated eco-friendly waste of products as self-sustaining concrete, and meeting specifications in relation to concrete needs and management superintendents [44, 45].

3.3 *Microstructure Analysis*

SEM analysis. Mixtures are chosen as mixtures with the best strength based on their mechanical damage. The connection between the matrix's constituent parts and the additional fiber makes a tightly coupled matrix visible. Since a fresh conversion of CH crystals also speeds up the hydration process, nanoparticle encourages the ongoing synthesis of CSH gels, which overlap with better microstructure in Fig. 1. The addition of nanoparticles reinforced with amorphous silica speeds up the hydration process by promoting the continuous production of CSH gels, which overlap with improved microstructure in Fig. 1 [46].

Ettringite's complete disintegration as well as CH crystal decomposition, that coincides with CSH hydrates, are responsible for this outcome. Additionally, this reaction decreases the ITZ between gels, creating weak zones, which makes it possible for the zones to merge. In parallel, the pores widen. Small gaps are created when water evaporates at cold temperatures; these voids grow at extreme temps [47]. EDX results speak to the role of nanomaterials, particularly those composed of water-wet silica types, in improving the nanostructure [48].

Fig. 1 SEM analysis



XRD analysis. When nanoagriculture wastes are reinforced with such a significant amount of silica at ideal mixtures with a strong compressive strength, high intensity peak of C-S-H presented in 2 theta value of 28.6 is seen. Comparing nanoparticles to reference mixes, low calcium hydroxide peaks are found at 18.7 in Fig. 2.

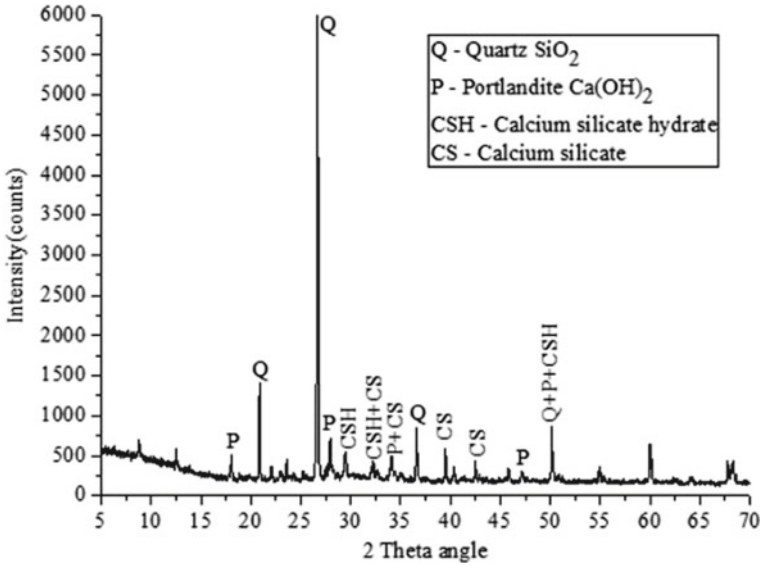


Fig. 2 XRD analysis

4 Conclusions

This study examines how three agricultural wastes influence the efficiency of a basalt fiber identity concrete that has been designed to be extremely efficient. Apart from the structural analysis, the characteristics and strengthening capabilities under high temperature circumstances were examined. The following findings are drawn upon the study's completion:

- In addition to UHPBF-SCC characteristics with improved in 25% in fresh state and hardened state properties, self-compacting concrete characteristics obtained.
- Composite material and the use of nanoagriculture waste products reduce the flowability by reducing flow dimension, lengthening, and lowering H_2/H_1 .
- Using basalt fibers enhances tensile strength and flexural modulus with values of much more than 12.5% and 15%, respectively.
- Fibers added to biodegradable nanoconcrete enhance the material's ability to withstand high heats.
- At 300 °C, ettringite disintegration, capillary absorption, and water absorption reduced the capacity of the concrete; continually, pore growth and further crack propagation occurred at 600 °C.

References

1. Akeed MH, Qaidi S, Ahmed HU, Faraj RH, Mohammed AS, Emad W, Tayeh BA, Azevedo ARG (2022) Ultra-high-performance fiber-reinforced concrete. Part I: developments, principles, raw materials, Case Stud Constr Mater 17:e01290, <https://doi.org/10.1016/j.cscm.2022.e01290>
2. Amin M, Zeyad AM, Tayeh BA, Saad Agwa I (2022) Effect of ferrosilicon and silica fume on mechanical, durability, and microstructure characteristics of ultra high performance concrete, Constr Build Mater 320:126233, <https://doi.org/10.1016/j.conbuildmat.2021.126233>
3. Chen Y, Yu R, Wang X, Chen J, Shui Z (2018) Evaluation and optimization of ultra-high performance concrete (UHPC) subjected to harsh ocean environment: towards an application of layered double hydroxides (LDHs). Constr Build Mater 177:51–62. <https://doi.org/10.1016/j.conbuildmat.2018.03.210>
4. Zhou M, Lu W, Song J, Lee GC (2018) Application of ultra-high performance concrete in bridge engineering. Constr Build Mater 186:1256–1267. <https://doi.org/10.1016/j.conbuildmat.2018.08.036>
5. Azmee NM, Shafiq N (2018) Ultra-high performance concrete: from fundamental to applications. Case Stud Constr Mater 9:e00197. <https://doi.org/10.1016/j.cscm.2018.e00197>
6. Udi UJ, Almeshal I, Megat Johari MA, Mohd Zahid MZA, Hassan MH, Musa KA, Albijawi M, Abu Bakar BH (2022) Efficiency of high performance fiber reinforced cementitious composites as a retrofit material for fire-damaged concrete. Mater Today Proc 61:477–486. <https://doi.org/10.1016/j.matpr.2021.12.278>
7. Khan M, Lao J, Dai J-G (2022) Comparative study of advanced computational techniques for estimating the compressive strength of UHPC. J Asian Concr Fed 8:51–68. <https://doi.org/10.18702/acf.2022.6.8.1.51>
8. López Boadella I, López Gayarre F, Suárez González J, Gómez-Soberón J, López-Colina Pérez C, Serrano López M, de Brito J (2019) The influence of granite cutting waste on the

- properties of ultra-high performance concrete. *Mater (Basel)* 12:634. <https://doi.org/10.3390/ma12040634>
9. Yu R, Spiesz P, Brouwers HJH (2014) Effect of nano-silica on the hydration and microstructure development of Ultra-High Performance Concrete (UHPC) with a low binder amount. *Constr Build Mater* 65:140–150. <https://doi.org/10.1016/j.conbuildmat.2014.04.063>
 10. Arora A, Aguayo M, Hansen H, Castro C, Federspiel E, Mobasher B, Neithalath N (2018) Microstructural packing- and rheology-based binder selection and characterization for Ultra-high Performance Concrete (UHPC). *Cem Concr Res* 103:179–190. <https://doi.org/10.1016/j.cemconres.2017.10.013>
 11. Arora A, Yao Y, Mobasher B, Neithalath N (2019) Fundamental insights into the compressive and flexural response of binder- and aggregate-optimized ultra-high performance concrete (UHPC). *Cem Concr Compos* 98:1–13. <https://doi.org/10.1016/j.cemconcomp.2019.01.015>
 12. Shi Y, Long G, Zen X, Xie Y, Shang T (2021) Design of binder system of eco-efficient UHPC based on physical packing and chemical effect optimization. *Constr Build Mater* 274:121382. <https://doi.org/10.1016/j.conbuildmat.2020.121382>
 13. Wang X, Wu D, Geng Q, Hou D, Wang M, Li L, Wang P, Chen D, Sun Z (2021) Characterization of sustainable ultra-high performance concrete (UHPC) including expanded perlite. *Constr Build Mater* 303:124245. <https://doi.org/10.1016/j.conbuildmat.2021.124245>
 14. Mostafa SA, Ahmed N, Almeshal I, Tayeh BA, Elgamal MS (2022) Experimental study and theoretical prediction of mechanical properties of ultra-high performance concrete incorporated with nanorice husk ash burning at different temperature treatments. *Environ Sci Pollut Res*. <https://doi.org/10.1007/s11356-022-20779-w>
 15. Abadel A, Abbas H, Almusallam T, Alshaikh IMH, Khawaji M, Alghamdi H, Salah AA (2022) Experimental study of shear behavior of CFRP strengthened ultrahigh performance fiber-reinforced concrete deep beams. *Case Stud Constr Mater* 16:e01103. <https://doi.org/10.1016/j.cscm.2022.e01103>
 16. Wang J, Xiao J, Zhang Z, Han K, Hu X, Jiang F (2021) Action mechanism of rice husk ash and the effect on main performances of cement-based materials: a review. *Constr Build Mater* 288:123068. <https://doi.org/10.1016/j.conbuildmat.2021.123068>
 17. Thomas BS, Yang J, Mo KH, Abdalla JA, Hawileh RA, Ariyachandra E (2021) Biomass ashes from agricultural wastes as supplementary cementitious materials or aggregate replacement in cement/geopolymer concrete: a comprehensive review. *J Build Eng* 40:102332. <https://doi.org/10.1016/j.jobe.2021.102332>
 18. Faried AS, Mostafa SA, Tayeh BA, Tawfik TA (2021) Mechanical and durability properties of ultra-high performance concrete incorporated with various nano waste materials under different curing conditions. *J Build Eng* 43:102569. <https://doi.org/10.1016/j.jobe.2021.102569>
 19. Quintero JA, Rincón LE, Cardona CA (2011) Production of bioethanol from agroindustrial residues as feedstocks. In: *Biofuels*. Elsevier, pp 251–285. <https://doi.org/10.1016/B978-0-12-385099-7.00011-5>
 20. da J, Andrade Neto S, de França MJS, de Amorim Júnior NS, Ribeiro DV (2021) Effects of adding sugarcane bagasse ash on the properties and durability of concrete. *Constr Build Mater* 266:120959. <https://doi.org/10.1016/j.conbuildmat.2020.120959>
 21. Cordeiro GC, Filho RDT, de Almeida RS (2011) Influence of ultrafine wet grinding on pozzolanic activity of submicrometre sugar cane bagasse ash. *Adv Appl Ceram* 110:453–456. <https://doi.org/10.1179/1743676111Y.0000000050>
 22. Minnu SN, Bahurudeen A, Athira G (2021) Comparison of sugarcane bagasse ash with fly ash and slag: an approach towards industrial acceptance of sugar industry waste in cleaner production of cement. *J Clean Prod* 285:124836. <https://doi.org/10.1016/j.jclepro.2020.124836>
 23. Moretti JP, Nunes S, Sales A (2018) Self-compacting concrete incorporating sugarcane bagasse ash. *Constr Build Mater* 172:635–649. <https://doi.org/10.1016/j.conbuildmat.2018.03.277>
 24. Sebastin S, Priya AK, Karthick A, Sathyamurthy R, Ghosh A (2020) Agro waste sugarcane bagasse as a cementitious material for reactive powder concrete. *Clean Technol* 2:476–491. <https://doi.org/10.3390/cleantechnol2040030>

25. Chen R, Congress SSC, Cai G, Duan W, Liu S (2021) Sustainable utilization of biomass waste-rice husk ash as a new solidified material of soil in geotechnical engineering: a review. *Constr Build Mater* 292:123219. <https://doi.org/10.1016/j.conbuildmat.2021.123219>
26. Kang S-H, Hong S-G, Moon J (2019) The use of rice husk ash as reactive filler in ultra-high performance concrete. *Cem Concr Res* 115:389–400. <https://doi.org/10.1016/j.cemconres.2018.09.004>
27. Shah SAY, Zeeshan M, Farooq MZ, Ahmed N, Iqbal N (2019) Co-pyrolysis of cotton stalk and waste tire with a focus on liquid yield quantity and quality. *Renew Energy* 130:238–244. <https://doi.org/10.1016/j.renene.2018.06.045>
28. Zhou B, Wang L, Ma G, Zhao X, Zhao X (2020) Preparation and properties of bio-geopolymer composites with waste cotton stalk materials. *J Clean Prod* 245:118842. <https://doi.org/10.1016/j.jclepro.2019.118842>
29. Amin M, Zeyad AM, Tayeh BA, Saad Agwa I (2021) Effects of nano cotton stalk and palm leaf ashes on ultrahigh-performance concrete properties incorporating recycled concrete aggregates. *Constr Build Mater* 302:124196. <https://doi.org/10.1016/j.conbuildmat.2021.124196>
30. Agwa IS, Omar OM, Tayeh BA, Abdelsalam BA (2020) Effects of using rice straw and cotton stalk ashes on the properties of lightweight self-compacting concrete. *Constr Build Mater* 235:117541. <https://doi.org/10.1016/j.conbuildmat.2019.117541>
31. Faried AS, Mostafa SA, Tayeh BA, Tawfik TA (2021) The effect of using nano rice husk ash of different burning degrees on ultra-high-performance concrete properties. *Constr Build Mater* 290:123279. <https://doi.org/10.1016/j.conbuildmat.2021.123279>
32. Ribeiro B, Yamamoto T, Yamashiki Y (2020) A study on the reduction in hydration heat and thermal strain of concrete with addition of sugarcane bagasse fiber. *Materials* 13:3005. <https://doi.org/10.3390/ma13133005>
33. Almeshal I, Abu Bakar BH, Tayeh BA (2022) Behaviour of reinforced concrete walls under fire: a review. *Fire Technol*. <https://doi.org/10.1007/s10694-022-01240-3>
34. Khan M, Cao M, Chaopeng X, Ali M (2022) Experimental and analytical study of hybrid fiber reinforced concrete prepared with basalt fiber under high temperature. *Fire Mater* 46:205–226. <https://doi.org/10.1002/fam.2968>
35. Karimipour A, Ghalehnovi M, de Brito J, Attari M (2020) The effect of polypropylene fibres on the compressive strength, impact and heat resistance of selfcompacting concrete. *Structures* 25:72–87. <https://doi.org/10.1016/j.istruc.2020.02.022>
36. Algin Z, Ozen M (2018) The properties of chopped basalt fibre reinforced self-compacting concrete. *Constr Build Mater* 186:678–685. <https://doi.org/10.1016/j.conbuildmat.2018.07.089>
37. El-Sayed AA, Fathy IN, Tayeh BA, Almeshal I (2022) Using artificial neural networks for predicting mechanical and radiation shielding properties of different nano-concretes exposed to elevated temperature. *Constr Build Mater* 324:126663. <https://doi.org/10.1016/j.conbuildmat.2022.126663>
38. Ali N, Canpolat O, Aygörmez Y, Al-Mashhadani MM (2020) Evaluation of the 12–24 mm basalt fibers and boron waste on reinforced metakaolin-based geopolymer. *Constr Build Mater* 251:118976. <https://doi.org/10.1016/j.conbuildmat.2020.118976>
39. Branston J, Das S, Kenno SY, Taylor C (2016) Mechanical behaviour of basalt fibre reinforced concrete. *Constr Build Mater* 124:878–886. <https://doi.org/10.1016/j.conbuildmat.2016.08.009>
40. Chidighikaobi PC (2019) Thermal effect on the flexural strength of expanded clay lightweight basalt fiber reinforced concrete. *Mater Today Proc* 19:2467–2470. <https://doi.org/10.1016/j.matpr.2019.08.110>
41. Ramesh B, Gokulnath V, Ranjith Kumar M (2020) Detailed study on flexural strength of polypropylene fiber reinforced self-compacting concrete. *Mater Today Proc* 22:1054–1058. <https://doi.org/10.1016/j.matpr.2019.11.292>
42. Alireza R, Arefeh S (2020) Durability of ultra-high-performance self-compacting concrete with hybrid fibers. *Mag Concr Res* 9:1–11

43. Khan M, Cao M, Xie C, Ali M (2022) Effectiveness of hybrid steel-basalt fiber reinforced concrete under compression. *Case Stud Constr Mater* 16:e00941. <https://doi.org/10.1016/j.cscm.2022.e00941>
44. Aisheh YIA, Atrushi DS, Akeed MH, Qaidi S, Tayeh BA (2022) Influence of steel fibers and microsilica on the mechanical properties of ultra-high-performance geopolymer concrete (UHP-GPC). *Case Stud Constr Mater* 17:e01245. <https://doi.org/10.1016/j.cscm.2022.e01245>
45. Cui S, Xu X, Yan X, Chen Z, Hu C, Liu Z (2020) Experimental study on the interfacial bond between short cut basalt fiber bundles and cement matrix. *Constr Build Mater* 256:119353. <https://doi.org/10.1016/j.conbuildmat.2020.119353>
46. Aisheh YIA, Atrushi DS, Akeed MH, Qaidi S, Tayeh BA (2022) Influence of polypropylene and steel fibers on the mechanical properties of ultra-high-performance fiber-reinforced geopolymer concrete. *Case Stud Constr Mater* 17:e01234. <https://doi.org/10.1016/j.cscm.2022.e01234>
47. Elsayed M, Tayeh BA, Elmaaty MA, Aldahshoory Y (2022) Behaviour of RC columns strengthened with ultra-high performance fiber reinforced concrete (UHPFRC) under eccentric loading. *J Build Eng* 47:103857. <https://doi.org/10.1016/j.jobe.2021.103857>
48. Zhang H, Ji S, Wang L, Jin C, Liu X, Li X (2022) Study on dynamic splitting tensile damage characteristics of basalt fiber reinforced concrete based on AE and DSCM. *J Build Eng* 57:104905. <https://doi.org/10.1016/j.jobe.2022.104905>
49. Choudhary R, Gupta R, Nagar R (2020) Impact on fresh, mechanical, and microstructural properties of high strength self-compacting concrete by marble cutting slurry waste, fly ash, and silica fume. *Constr Build Mater* 239:117888. <https://doi.org/10.1016/j.conbuildmat.2019.117888>
50. Raju RA, Lim S, Akiyama M, Kageyama T (2020) Effects of concrete flow on the distribution and orientation of fibers and flexural behavior of steel fiber-reinforced self-compacting concrete beams. *Constr Build Mater* 262:119963. <https://doi.org/10.1016/j.conbuildmat.2020.119963>
51. Sanjeev J, Sai Nitesh KJN (2020) Study on the effect of steel and glass fibers on fresh and hardened properties of vibrated concrete and self-compacting concrete. *Mater Today Proc* 27:1559–1568. <https://doi.org/10.1016/j.matpr.2020.03.208>

Experimental Study on Nanomaterials in High-Performance Concrete



K. Sathishkumar and L. Krishnaraj

1 Introduction

In the course of the past few years, the use of nanomaterials in high-performance concrete has gained significant attention from researchers and the construction industry. Nanomaterials, which are materials with dimensions on the nanometer scale, have unique properties that make them ideal for enhancing concrete's mechanical characteristics and durability [1]. High-performance concrete (HPC) is a type of concrete that is specially designed to exhibit exceptional strength, durability, and long-term performance. It is typically used in construction projects, where high strength and durability are required, such as high-rise buildings, bridges, and dams. However, even with its superior performance characteristics, HPC still has room for improvement in terms of durability and strength. One way to improve the properties of HPC is by incorporating nanomaterials into the mix [2]. The addition of nanomaterials has been shown to improve the strength and durability of concrete, as well as its resilience to environmental impacts such as corrosion, freeze–thaw cycles, and chemical attack. Nanomaterials can also reduce the porosity of the concrete, which can increase its resistance to water penetration and reduce the likelihood of cracking.

There are several types of nanomaterials that have been studied for use in concrete, including nanoparticles, nanofibers, and nanotubes. Nanoparticles are particles with a size of less than 100 nm and can be made from a variety of materials such as silica, titanium dioxide, and carbon. Nanofibers and nanotubes, on the other hand, are long, thin structures with a diameter on the nanometer scale, and are typically made from materials such as carbon or polymer [3]. The use of nanomaterials in concrete is still a relatively new field of research, and much is still unknown about how these materials interact with the cement matrix and affect the properties of the resulting

K. Sathishkumar · L. Krishnaraj (✉)

Department of Civil Engineering, Faculty of Engineering and Technology, SRM Institute of Science and Technology, Kattankulathur, Tamil Nadu 603203, India

e-mail: krishnal@srmist.edu.in

concrete. This experimental study aims to fill this knowledge gap by investigating the effects of incorporating various types and amounts of nanomaterials into high-performance concrete. The investigation will center on determining the mechanical properties of concrete, such as flexural strength, tensile strength, and compressive strength. Tensile strength refers to the greatest tensile stress that a material can endure before breaking, whereas compressive strength refers to the maximum compressive stress of which a material is capable of withstanding before failing. Flexural strength is a measure of a material's capacity to endure bending. The investigation will look at the concrete's lifespan as well as its mechanical properties. Durability is an essential factor in long-term concrete performance and is often determined by resistance to climatic conditions such as freeze–thaw cycles and chemical attack [4].

To conduct the study, a series of laboratory experiments will be carried out using different combinations of nanomaterials and concrete mixtures. The nanomaterials will be added to the concrete mix in varying amounts, and the resulting concrete samples will be tested under different conditions to evaluate their performance. Materials are subjected to compressive strength testing, tensile strength tests, flexural strength tests, and durability tests. The findings of this work are anticipated to offer light on the methods by which nanoparticles improve the properties of concrete [5]. This knowledge can be used to boost HPC performance by maximizing the use of nanomaterials in certain applications. The findings of the study could have a significant impact on the construction sector, as the use of nanoparticles in concrete could lead to the development of more durable and sustainable constructions. To summarize, the experimental study of nanoparticles in high-performance concrete is an important step toward understanding the potential benefits of using these materials in construction.

By investigating the effects of various types and quantities of nanomaterials, this study gain insights into their potential applications and contributions to the field of concrete [6].

2 Literature Review

High-performance concrete (HPC) is a widely used material in construction projects that require high strength and durability, but there is still room for improvement. Adding nanomaterials to HPC has shown promising results in significantly enhancing its mechanical properties and durability. This review aims to evaluate the current state of knowledge regarding the use of nanomaterials in HPC and identify gaps in existing research.

The review searched various online databases for peer-reviewed articles in English published between 2000 and 2022. A total of 72 articles were included, which showed that the addition of nanoparticles, nanofibers, and nanotubes to HPC can significantly enhance its mechanical properties and durability. Nanoparticles were the most studied type of nanomaterial, and they were found to increase the compressive, tensile, and flexural strength of HPC by filling the pores in the cement matrix, leading to a denser

and more compact structure. Nanofibers and nanotubes were also found to improve the tensile strength of HPC by bridging the cracks in the cement matrix, resulting in a more ductile and tough structure.

The review also highlighted the importance of several factors, such as the type and number of nanomaterials used, the mixing method, and the curing conditions, on the effects of nanomaterials on HPC. Optimal conditions for incorporating nanomaterials into HPC are still under investigation, and further research is required to determine the best conditions for each type of nanomaterial. This systematic literature review indicates that the addition of nanomaterials to HPC has the potential to significantly improve its mechanical properties and durability, leading to the development of more durable and sustainable structures in the construction industry. However, more research is needed to optimize the use of nanomaterials in HPC.

The basic idea behind concrete technologies of high-strength or high-performance concrete is significantly derived from the meticulously chosen components and mix ratios, which may be closely designed to have preliminary improvement of properties like high strength and low porosity. For more than three decades, construction projects all over the world have relied on concrete with compressive strengths ranging from 40 to 140 MPa. This results in high early strength, a reduction in column size, the creation of long-span superstructures, and an increase in the structure's durability. The manufacturing of high-strength concrete typically involves using a low w/c ratio, which results in the material having poor workability and an inability to spread through formwork corners without the intervention of external forces.

Sand, cement, water-binder-type super plasticizer sand-binder ratio, and seed admixture are considerations. Fibers add strength and reduce cracking to concrete. 1% fiber improved strength and durability. Water vaporization and water inward migration generate a moisture clog, raising pore pressure and causing critical stresses and spalling. Thinner concrete constructions using high-performance cementitious pointing mortar. Eliminating heavy raw materials like natural aggregates and using low-density porous elements reduces concrete weight.

3 Methodology and Materials

3.1 Methodology

Before beginning the process of designing the concrete mix, a comprehensive review of the relevant literature is carried out. Assemble all the components required to produce concrete having a compressive strength that varies between sixty to one hundred megapascals.

Experiments are carried out to determine whether the proposed strength can be achieved by casting the material into cubes and cylinders. The fourth and final test is an assessment of the subject's physical strength, which can be taken in the interval of 3, 7, and 28 days. When the appropriate ratios for the ingredients that go into the

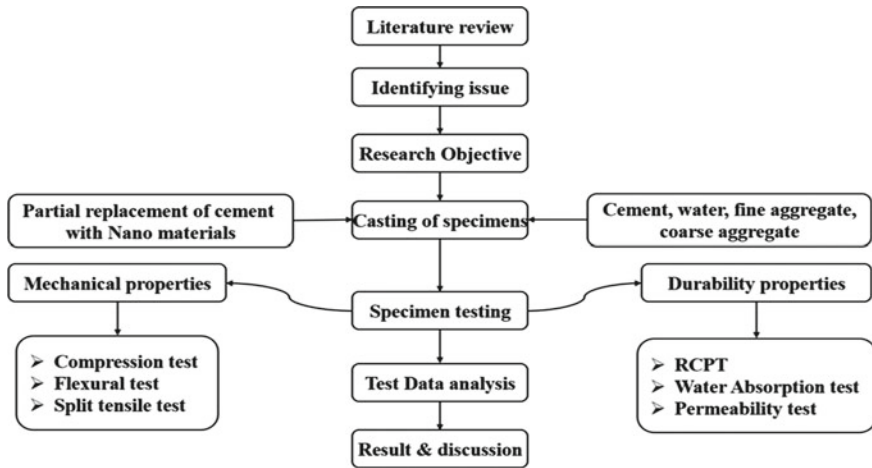


Fig. 1 Research methodology

concrete to achieve the desired level of strength have been determined, the concrete is then used to cast cubes, cylinders, and beams in order to evaluate its compressive and tensile strengths.

This is done so that the desired level of strength can be achieved. The results that were obtained can be compared with the results that can be found in the existing body of research, and by the compressive strength of the materials, new equations can be proposed for determining tensile strength. The methodology represents at the Fig. 1.

3.2 Materials

It is probable that the nanomaterials may decrease the porosity of the cement, which will lead to a transition zone that is denser. Additionally, the use of nanoparticles in reinforced cement may make it feasible to construct high-strength concrete structures that are also more durable. This, in turn, will lead to a decrease in the amount of maintenance that is required or the need for early replacement the incorporation of nanoparticles into concrete results in an overall improvement to the material's mechanical properties as well as its durability. The workability, air content, and setting times of concrete may all be affected differently depending on several different circumstances. The usage of dispersion is necessary to make advantage of the one-of-a-kind reactivity that nanoparticles possess. In this experiment, the following materials are to be used Ordinary Portland cement (Grade 53), coarse aggregate, water, M sand, nanoclay, and silica fume.

Nanoclay is formed of natural, deteriorated phyllosilicates. Nanoclay is processed for several uses. Water between layers may inflate or shrink them. Nanoclay's water

absorption can create stable gels. Nanoclay may transform desert sand into farmland. This page explains nanoclay and silicon and ferrosilicon fume silica. Concrete uses silica dust. Pozzolan reacts. Strong silica-fume cement. Silica fume is used by admixture providers. Finish and cure silica-fume concrete carefully. Electric furnaces produce silicon and alloys. Raw materials include quartz, coal, and woodchips. Furnace smoke is sold as silica fumes instead of landfilled. This is a concrete additive.

3.3 Preparation of Materials and Testing Procedure

Material selection and preparation: Cement: Type I Ordinary Portland Cement, Coarse Aggregate: Crushed granite with a maximum size of 20 mm, Fine Aggregate: Natural River sand with a fineness modulus of 2.6, Nanoclay: Commercial grade nanoclay with a particle size of fewer than 100 nm, Mix Design: The mix design will be based on the ACI method, with a target compressive strength of 60 MPa. The water-to-cement ratio will be kept constant at 0.35 for all mixes. The percentage of nanoclay added will be 10%, 15%, and 20% by weight of the cement. Mixing: The mixing will be done using a pan mixer. The dry materials (cement, aggregates, and nanoclay) will be mixed for two minutes. Then, the water will be added, and mixing will continue for an additional four minutes. Casting: The concrete will be cast into 100 mm cubes. A total of 27 cubes will be cast, with 9 cubes for each percentage of nanoclay added. The casting will be done in three batches of 9 cubes each. Curing: The cubes will be demolded after 24 h and cured in water at a temperature of 23 ± 2 °C for 28 days. The water will be changed every seven days to maintain the pH level and prevent algae growth. Testing: The mechanical properties of the concrete will be evaluated using a compression testing machine, flexural testing machine, and splitting tensile testing machine according to ASTM standards. The durability properties of the concrete will be evaluated using the water absorption test and freeze–thaw test. The tests will be conducted on the 28th day of curing. The Data Analysis: The data obtained from the tests will be analyzed using statistical software, and the results will be presented in tables and graphs. In conclusion, this procedure and methods aim to investigate the potential of using nanoclay to enhance the mechanical and durability properties of high-performance concrete. Table 1 gives the chemical properties of nanoclay. The results of this experimental study could have significant implications for the construction industry, particularly in developing more sustainable and durable structures.

Table 1 Chemical properties of nanoclay

Chemical composition	Nanoclay (%)
Dialuminum dioxide	6.0 ± 1.0
SiO ₂	45 ± 2.0
Na ₂ O	0.6 ± 0.2
Fe ₂ O ₃	0.5 ± 0.2
TiO ₂	0.05 ± 0.02
CaO ₂	1.0 ± 0.1
MgO	1.3 ± 0.1
AO ₂	1.0 ± 0.1
Loss on ignition	40 ± 2.0

4 Results

4.1 Raw Material Characterization

Table 1 displays the physical properties and chemical compositions of nanoclay (NC), silica fume (SF), and OPC. The sizes and forms of NC and SF particles were also studied, with NC having a lower average diameter than SF powder. The chemical compositions of SF and NC acquired from EDX analysis are given in Table 2. NC included 65.93% CaO, 3.35% SO₃, 15.81% K₂O, and 5.82% P₂O₅, whereas SF contained 10.6% CaO, 63.34% SiO₂, 15.36% K₂O, and 3.16% Na₂O. XRD analysis was used to determine the mineral phases in NC and SF, and Table 4 provides the dominating chemicals, reference COD, and score in NC. Table 1 also includes the main compounds, reference COD, and SF score. NC comprises P₂O₅ in the chemical formula Ca₄ K₂(P₁₀O₃₀)(H₂O)₁₆, as well as a SO₃ component in the chemical formula K₂Ca₅(SO₄)₆(H₂O) in addition to CaO, the most abundant constituent in this type of ash. The presence of P₂O₅ in alternative cement components may contribute to delayed setting time and lower compressive strength in young concrete. P₂O₅ impurities also inhibit cement particle disintegration, slow the hydration reaction of C₄A₃S, and delay the formation of ettringite. Increasing the rate of cement substitution with NC resulted in increased ettringite formation, according to SEM pictures. An XRD examination of geigerite with the chemical formula K₂Ca₅(SO₄)₆(H₂O) revealed that NC contained 3.35% SO₃ by mass. The increased SO₃ content generated by replacing cement with NC resulted in a drop in compressive strength in the first two days as well as a delay in the development of ettringite, which may result in weak resistance in subsequent testing.

Table 2 Physical properties of nanoclay

Color	White
Surface area	65 m ³ /g
Appearance (form)	Powder
Diameter	30–70 nm
Length	1–3 μm
Vent volume	1.26–1.34 ml/gm
pH	4.5–7

4.2 Slump Test

In all combinations, the slump value and the activity of SF and NC were clearly connected. For SF and NC mass percentage combinations, slump values ranged from 113 to 132 mm, and declined as SF concentration increased. Slump test values of 128, 125, and 123 mm were reported for RS-containing mixes with replacement ratios of 10%, 20%, and 30% of the cement mass, respectively. For the reference combination, the slump test value was 132 mm. Slump test values were lower when NC was used as a cement alternative to the RS10% combination. These values ranged from 125 to 122 to 119 to 117 mm NC was added to cement at a rate of 2.5%, 5%, 7.5%, and 10%, respectively. In contrast, the slump value for the mixture including NC and RS10% was 128 mm. This low slump can be attributed to the mixes' high specific surface areas, which are approximately six times that of the cement mix, as well as their irregular shapes. This result is consistent with previous research. Furthermore, as the SF and NC contents increased, so did the binder's specific surface area and volume fraction, owing to the mortar's high surface area, large amount of adsorbed water, and decreased amount of free water.

4.3 Compressive Strength of Nanoclay

Figure 2 and Table 3 display the results indicating that replacing a portion of cement with clay residues, such as NC, yields superior compressive strength compared to 90 days later, the reference combination. However, as compared to the reference mixture, there was a slight loss in compressive strength after 7 days. The results show that NC can be utilized to replace up to 30% of the cement mass, with a slightly higher compressive strength at 90 days than the control mixture. Nonetheless, the performance of NC-based concrete is comparable in terms of reduced compressive strength at early ages (7 days), which is a common occurrence for many supplementary cementitious materials and can be attributed to the dilution effect generated by cement content reduction and the delayed onset of pozzolanic reaction for most supplementary cement materials. The letter NC is included. At 7 days, the compressive strength of NC10-NC0, NC20-NC0, and NC30-NC0 was roughly 2%, 1%, and

5% lower than the control combination, respectively. The compressive strength of the NC-based concrete increased with age, as evidenced by the fact that at 90 days, NC10-NC0, NC20-NC0, and NC30-NC0 had 5%, 8%, and 1% higher compressive strengths, respectively.

A few factors could have led to the rise in compressive strength. The high fineness of NC contributes to the increased efficacy of pozzolanic materials by functioning as a filler material and reacting with $Ca(OH)_2$, both of which result in improved concrete strength and properties. The fineness increases NC activity and fills the majority of very fine pores. The XRD analysis revealed that NC contains a large

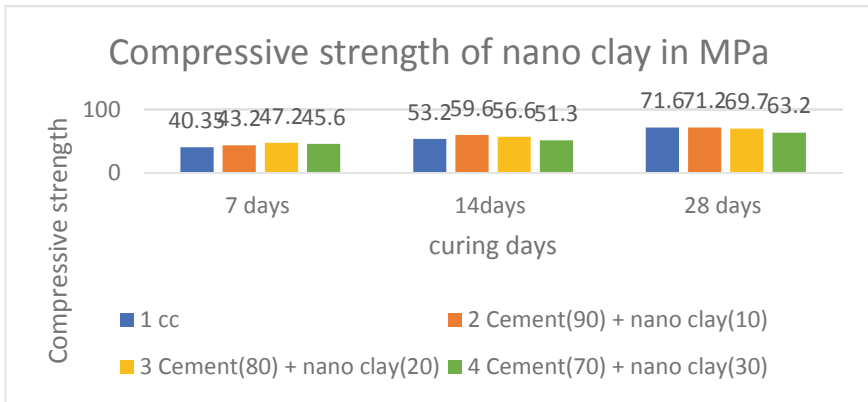


Fig. 2 Displays the compressive strength that replacing a portion of cement with clay residues

Table 3 Compressive strength analysis of NC concrete

S. No.	Mix type	Compressive strength (MPa)		
		7 days	14 days	28 days
1	cc	40.35	53.2	71.6
2	Cement (90) + nanoclay(10%)	43.2	59.6	71.2
3	Cement (80) + nanoclay(20%)	47.2	56.6	69.7
4	Cement (70) + nanoclay(30%)	45.6	51.3	63.2

Table 4 Splitting tensile strength analysis of NC concrete

S. No.	Mix type	Splitting tensile strength (MPa)		
		7 days	14 days	28 days
1	cc	6.4	6.5	7.1
2	Cement (90) + nanoclay(10%)	6.3	6.6	7.2
3	Cement (80) + nanoclay(20%)	6.5	6.8	7.3
4	Cement (70) + nanoclay(30%)	6.6	6.9	7.4

amount of active silica, which reacts with cement products like $\text{Ca}(\text{OH})_2$ to generate additional CSH gel at later ages. Compressive strength decreased with increasing NC substitution ratios (7 and 10%) with RSA at all ages (7, 28, and 90 days) compared to the reference blend. The decrease in compressive strength could be attributable to a reduction in cement content and workability.

Hydrated cement contains calcium hydroxide. Nonetheless, according to the research, this situation is allowable.

4.4 Splitting Tensile Strength

Table 4 displays at 28 days, the split tensile strength test results for HSC samples with NC and SF. The findings show that SF, up to 20% of the cement mass, can be utilized as a partial replacement for cement to obtain higher split tensile strength than the control mixture. The pozzolanic activity and microfilming capabilities of RSA are responsible for the increase in split tensile strength. The high SiO_2 concentration of RSA combines with cement hydration byproducts ($\text{Ca}(\text{OH})_2$) to form extra C–S–H, reducing concrete porosity and improving the microstructure of the interfacial transition zone, and thereby raising the paste matrix's split tensile strength. However, increasing the cement mass replacement rate to 30% reduces the split tensile strength marginally due to a large amount of accessible silica reacting with all of the produced.

The range of properties in various AWA types is a crucial factor in improving concrete qualities. As a result, sesame waste ash can be blended with SF, NC, and cement to provide highly effective cementitious materials for HSC production. Split tensile strength is improved by using SF and NC as partial replacements for cement in HSC. Compressive strength improves by 5% and 8% when 10% and 20% SF are mixed with 5% NC, respectively, as compared to the reference combination. As the NC ratio increases, the split tensile strength of HSC falls. At 28 days, split tensile strengths of HSCs containing 20% SF mixed with 0%, 2.5%, 5%, 7.5%, and 10% NC were 7.1, 7.2, 7.3, 6.7, and 6.3 MPa, respectively. The chemical composition of the ash, which comprises 65% CaO, has a positive effect on HSC strength. Because the chemical compositions of SF and NC are combined, synergistic interactions occur, increasing the strength of HSC. Furthermore, due to its vast surface area, NC has the ability to spread widely throughout the cement matrix, filling microscopic pores.

5 Discussion

The studies reviewed in the literature show that the addition of nanomaterials, particularly nanoparticles, can significantly improve the mechanical properties and durability of HPC. The improvements in mechanical properties include increased compressive, tensile, and flexural strength, while the improvements in durability

include increased resistance to freeze–thaw cycles and chemical attack. The improvements in strength and durability can be attributed to the ability of nanoparticles to fill the pores in the cement matrix, creating a denser and more compact structure. The nanoparticles also help bridge the cracks that occur in the concrete, leading to a more ductile and tough structure. In addition to nanoparticles, nanofibers and nanotubes have also been studied for use in HPC [7]. While they are not as commonly studied as nanoparticles, the studies have shown that the addition of nanofibers and nanotubes can improve the mechanical properties of HPC, particularly its tensile strength. The improvements in strength are attributed to the ability of these materials to bridge the cracks in the cement matrix and create a more ductile structure.

One of the main challenges is the lack of standardization in the testing methods and procedures used to evaluate the mechanical properties and durability of HPC. This makes it difficult to compare the results obtained from different studies. Another challenge is the potential toxicity of some nanomaterials, which can pose a risk to human health and the environment. The safe handling and disposal of these materials need to be carefully considered [8].

The optimal conditions for incorporating nanomaterials into HPC also need to be investigated further. The studies reviewed in the literature show that the effectiveness of nanomaterials depends on several factors, such as the type and number of nanomaterials used, the method of mixing, and the curing conditions [9]. The optimal conditions for each type of nanomaterial need to be determined to ensure their maximum effectiveness. The experimental studies conducted on the use of nanomaterials in HPC have shown that these materials can significantly improve the mechanical properties and durability of concrete. Nanoparticles, nanofibers, and nanotubes have all been studied for use in HPC, with nanoparticles being the most studied. The improvements in strength and durability are attributed to the ability of nanomaterials to fill the pores in the cement matrix, bridge the cracks, and create a denser and more compact structure [10].

Despite the potential benefits of incorporating nanomaterials in HPC, there are several challenges that need to be addressed, such as standardization in testing methods and procedures, potential toxicity, and optimal conditions for incorporation. Further research is needed to address these challenges and to determine the most effective and sustainable methods for incorporating nanomaterials into HPC. Overall, the findings of the reviewed literature have important implications for the construction industry, as the use of nanomaterials in HPC could lead to the development of more durable and sustainable structures [11].

6 Conclusion

- Because of the favorable chemical compositions of oxides that have the potential to improve the qualities of cement paste, NC and SF can be used as supplementary cement ingredients. CaO and SiO₂ are the most abundant oxides in NC and SF, accounting for 65.93% and 10.60%, respectively, and 0.17% and 63.87%. K₂O

is the most abundant major oxide, accounting for 15.81% of NC and 15.36% of SF, respectively.

- As shown by TGA/DTA, heat treatment of NSSA and RSA at 700 °C efficiently eliminates carbon and unburned organic residues and resulting in better ash characteristics. XRD examination shows that the mineral composition stays unchanged.
- Slump test results were decreased due to the increased surface area of NC and SF. As the cement replacement rate increases, the findings of the slump tests are regressed. Slump reduction of 14% is attained by replacing 30% of the cement with a combination of 10% NC and 20% SF.
- When RSA is used as a partial cement substitution at 20%, the compressive strength for HSC is higher than the reference combination. However, a replacement rate more than 20% has a negative impact on the compressive strength of HSC. In contrast, incorporating NC at 2.5% and 5% as a partial replacement in combination with optimal SF substitution (20%) results in the maximum compressive strengths of 88.9 and 90.7 MPa at 28 days.

When compared to control concrete, mixing NC with SF to make HSC yields higher tensile, flexural, and modulus of elasticity values. The RS20-NS5 mixture has the highest tensile strength, flexural strength, and modulus of elasticity of all the mixes tested, measuring 7.3, 10.7, and 38,600 MPa, respectively.

Traditional vs. high-performance concrete hydration and durability. Nanoclay absorbs water when used in cement. Clay-building. High-performance concrete utilizes nanoclay's catalyst, nanofillers, reactive pozzolanas, nanoreinforcements, and counterbalance. Nanoclay enhances mechanical and microstructure performance but decreases water permeability.

Nanoclay enhances concrete's strength, permeability, chemical resistance, and absorption. Nanoclay strengthens concrete. Nanoclay reduces bleeding and segregation. More-fibred concrete transmits nonlinear lighter. For better performance and economical optical fibers used, and also light-transmitting concrete has less compressive strength. Fibers are permeable in concrete. Light-transmitting concrete is hence weaker. Expanding the contact surface may improve optical fiber interaction with light-transmitting concrete.

References

1. Qu X, Zhao X (2017) Previous and present investigations on the components, microstructure and main properties of autoclaved aerated concrete—a review. *Constr Build Mater* 135:505–516. <https://doi.org/10.1016/j.conbuildmat.2016.12.208>
2. Wu L, Mei M, Li Z, Liu S, Wang X (2022) Case studies in construction materials study on photocatalytic and mechanical properties of TiO₂ modified pervious concrete. *Case Stud Constr Mater* 17(August):e01606. <https://doi.org/10.1016/j.cscm.2022.e01606>
3. Güneysi E, Khoshnaw G, Ipek S (2014) Abrasion and freezing—thawing resistance of pervious concretes containing waste rubbers 73:19–24. <https://doi.org/10.1016/j.conbuildmat.2014.09.047>

4. Zhang H et al (2022) Analyzing the pore structure of pervious concrete based on the deep learning framework of Mask R-CNN. *Constr Build Mater* 318(November):125987. <https://doi.org/10.1016/j.conbuildmat.2021.125987>
5. Singh A, Sampath PV, Biligiri KP (2020) A review of sustainable pervious concrete systems: emphasis on clogging, material characterization, and environmental aspects. *Constr Build Mater* 261:120491. <https://doi.org/10.1016/j.conbuildmat.2020.120491>
6. Hussin H, Osama A, El-Dorghamy A, Adbellatif MM (2021) Towards an integrated mobility system: The first and last mile solutions in developing countries; the case study of newcairo. *Tranp Res Interdiscip Perspect* 12
7. Zhong R, Wille K (2016) Compression response of normal and high strength pervious concrete. *Constr Build Mater* 109:177–187. <https://doi.org/10.1016/j.conbuildmat.2016.01.051>
8. Joshi T, Dave U (2022) Case studies in construction materials construction of pervious concrete pavement stretch, Ahmedabad, India—case study. *Case Stud Constr Mater* 16:e00622. <https://doi.org/10.1016/j.cscm.2021.e00622>
9. Chen X et al (2020) Design of a chitosan modifying alkali-activated slag pervious concrete with the function of water purification. *Constr Build Mater* 251:118979. <https://doi.org/10.1016/j.conbuildmat.2020.118979>
10. Uddin MJ, Smith KJ, Hargis CW (2021) Development of pervious oyster shell habitat (POSH) concrete for reef restoration and living shorelines. *Constr Build Mater* 295:123685. <https://doi.org/10.1016/j.conbuildmat.2021.123685>
11. Wu S, Wu Q, Shan J, Cai X, Su X, Sun X (2023) Effect of morphological characteristics of aggregate on the performance of pervious concrete (a) (b) (c). *Constr Build Mater* 367(November):130219. <https://doi.org/10.1016/j.conbuildmat.2022.130219>

An Investigation on Behaviour of Non-metallic Areca Fibre-Reinforced Concrete Beam



S. Govindasami and K. Sathish

1 Introduction

Natural fibre materials shall be used as reinforcing materials because of those materials have sufficient stiffness and are renewable. This research focused towards reducing the quantity of steel by introducing natural fibres in concrete for increasing the stiffness of structural members as a sustainable construction technology based on the following investigations which were carried out on introducing fibre in concrete as reinforcement. Researchers investigated jute and coir concrete [1], hybrid fibre-reinforced columns and beams [2], composites with chemically treated fibres [3], geopolymer column beam as fibre-reinforced structural member [4], tensile strength of synthetic fibre concrete [5], compared fibre-reinforced beams with conventional reinforcement [6], glass fibre polymer beams [7], strength of areca fibre concrete [8], mechanical properties of areca sheath fibre concrete [9], areca fibre as an effective reinforcing material [10], effect of chemical treatment on areca fibre composites [11] and strength properties of areca fibre-reinforced concrete [12].

2 Materials and Methods

It was preferred to prepare concrete of M30. The dried areca empty fruits were soaked in de-ionized water for five days for paving the way to the fibre to come out easily from the fruit. Sieves were used to remove broken fibres and impurities. The cube specimens of concrete were casted with areca fibre. To test the split tensile strength of areca fibre, cylindrical specimens of size 100 mm diameter and 200 mm height

S. Govindasami (✉) · K. Sathish
Vel Tech High Tech Dr. Rangarajan Dr. Sakunthala Engineering College (Autonomous), Avadi,
Chennai 600062, India
e-mail: drsgovindasami@gmail.com

were casted. Beam specimens were casted with the size of $100 \times 100 \times 700$ mm on testing the flexural strength of concrete.

3 Results and Discussions

Table 1 reveals that there is an increase of compressive strength from 42.92 N/mm^2 to 46.45 N/mm^2 by adding the areca fibre from 0.25% to 0.75%, respectively. It shows 15.60% increase with the conventional concrete's compressive strength. Further, while increasing the quantity of areca fibre from 0.75 to 1.0%, the compressive strength of areca fibre concrete decreased from 46.45 to 45.11%. Similar results were obtained by the researchers on their investigations [12].

It is observed from Table 2 that there is an increase of split tensile strength from 5.53 N/mm^2 to 6.01 N/mm^2 by adding the areca fibre from 0.25% to 0.75%, respectively. It shows 42.08% increase with the conventional concrete's split tensile strength. Further, while increasing the quantity of areca fibre from 0.75 to 1.0%, the split tensile strength of areca fibre concrete decreased from 42.08 to 30.97%.

Flexural strength of areca fibre concrete is presented in Table 3 and the results show that there is an increase of flexural strength from 6.11 N/mm^2 to 6.73 N/mm^2

Table 1 Compressive strength of areca fibre concrete at 7 days and 28 days

Volume fraction (%)	Compressive strength of areca fibre concrete (N/mm^2)		Percentage increase with conventional concrete		Percentage decrease with conventional concrete	
	7 days	28 days	7 days	28 days	7 days	28 days
0	28.67	40.18	–	–	–	–
0.25	25.50	42.92	–	6.82	11.06	–
0.50	30.22	47.93	5.4	19.29	–	–
0.75	31.89	46.45	11.23	15.60	–	–
1.0	29.15	45.11	2.67	12.27	–	–

Table 2 Split tensile strength of areca fibre concrete at 7 days and 28 days

Volume fraction (%)	Split tensile strength of areca fibre concrete (N/mm^2)		Percentage increase with conventional concrete	
	7 days	28 days	7 days	28 days
0	2.97	4.23	–	–
0.25	3.54	5.53	19.20	30.73
0.50	3.7	5.97	24.58	41.13
0.75	3.3	6.01	11.11	42.08
1.0	3.0	5.54	1.01	30.97

Table 3 Flexural strength of areca fibre concrete without steel rods at 7 days and 28 days

Volume fraction (%)	Flexural strength of areca fibre concrete (N/mm ²)		Percentage increase with conventional concrete	
	7 days	28 days	7 days	28 days
0	4.43	5.63	–	–
0.25	4.65	6.11	5	8.53
0.50	4.87	6.38	10.1	13.32
0.75	5.02	6.24	13.32	10.83
1.0	5.14	6.73	16.02	19.54

Table 4 Flexural strength of areca fibre with steel rod concrete at 7 days and 28 days

Volume fraction (%)	Flexural strength of areca fibre concrete with steel rod (N/mm ²)	Percentage increase with conventional concrete
	28 days	28 days
0	6.3	–
0.25	7.83	24.29
0.50	8.97	42.38
0.75	10.03	59.21
1.0	9.10	44.44

by adding the areca fibre from 0.25% to 1.0%, respectively. It shows 19.54% increase with the conventional concrete's flexural strength. Similar results were obtained by the researchers on their investigations [7].

Table 4 gives the results of flexural strength of areca fibre concrete with steel rod. There is an increase of flexural strength from 7.83 N/mm² to 10.03 N/mm² by adding the areca fibre from 0.25% to 0.75%, respectively. It shows 59.21% increase with the conventional concrete's flexural strength. Further, while increasing the quantity of areca fibre from 0.75 to 1.0%, the flexural strength of areca fibre concrete with steel rod decreased from 59.21 to 44.44%.

4 Conclusions

Adding of areca fibre in concrete was investigated with the percentage of increase of compressive strength, split tensile strength and flexural strength with steel rod. It is concluded that adding of areca fibre up to 0.75% in concrete is economical on the behaviour of compressive strength and split tensile strength. But the flexural strength of areca fibre concrete without steel rods is increasing from 6.11 N/mm² to 6.73 N/mm² by adding the areca fibre from 0.25% to 1.0%, respectively. So, it is recommended to increase the quantity of areca fibre more than 1.0%. Further,

maximum flexural strength of areca fibre concrete with steel rod achieved as 10.03 N/mm² by adding the areca fibre of 0.75%.

References

1. Tariq KA, Ahmad J, Husnain SA, Ijaz MS (2023) Influence on compressive and tensile strength properties of fiber-reinforced concrete using polypropylene, jute, and coir fiber. *J the Mech Behav Mater*. <https://doi.org/10.1515/jmbm-2022-0263>
2. Hait P, Mitra R, Farsangi N (2022) Experimental investigations of resilient hybrid fibre reinforced SCC beam-column subassemblies under cyclic loadings. *Structures* 41:389–403
3. Pankaj, Jawalkar C, Kant S (2022) Study on mechanical properties and delamination factor evaluation of chemically treated nettle fiber reinforced polymer composites. *J Nat Fibres*. <https://doi.org/10.1080/15440478.2022.2135053>
4. Kumar VS, Ganesan N, Indira PV, Murali G, Vatin NI (2022) Behaviour of hybrid fibre-reinforced ternary blend geopolymer concrete beam-column joints under reverse cyclic loading. *Polymers*. <https://doi.org/10.3390/polym14112239>
5. Blazy J, Drobiec Ł, Wolka P (2021) Flexural tensile strength of concrete with synthetic fibers. *Materials* 14(16). <https://doi.org/10.3390/ma14164428>
6. Folino PP, Ripani M, Xargay H, Rocca N (2020) Comprehensive analysis of fiber reinforced concrete beams with conventional reinforcement. *Eng Struct*. <https://doi.org/10.1016/j.engstruct.2019.109862>
7. Yuan JS, Gao D, Zhu H, Chen G, Zhao L (2020) Flexural behavior of reinforced concrete beams reinforced with glass fiber reinforced polymer rectangular tubes. *Front Mater*. <https://doi.org/10.3389/finats.2020.577299>
8. Aishwarya G, Dinesh T, Andrews N, Sreelekshmi VS, Resmi V (2019) Study of strength of concrete using areca fiber and tile powder as additives. *Int Res J Eng Technol* 6(4):4016–4019
9. Jothibasu S, Mohanamurugan S, Vijay R, Lenin Singaravelu D, Vinod A, Sanjay MR (2018) Investigation on the mechanical behavior of areca sheath fibers/jute fibers/glass fabrics reinforced hybrid composite for light weight applications. *J Ind Text*. <https://doi.org/10.1177/1528083718804207>
10. Desai RH, Krishnamurthy L, Shridhar TN (2016) Effectiveness of Areca (Betel) fiber as a reinforcing material in eco-friendly composites. A review. *Indian J Adv Chem Sci* 81:27–33
11. Dhanalakshmi S, Ramadevi P, Basavaraju B (2016) A study of the effect of chemical treatments on areca fiber reinforced polypropylene composite properties. *Sci Eng Compos Mater*. <https://doi.org/10.1515/secm-2015-0292>
12. Kumar A, Anoop Kishan K, Divakar L, Sudheer (2015) Study on compressive strength of concrete using areca fibre as reinforcement. *Int J Eng Trends Technol* 24(3):121–124

Replacement of Fine Aggregate with Copper Slag in Concrete: A State-of-the-Art Review



V. K. Nithyashree and M. Surendar

1 Introduction

Self-compacting concrete (SCC), a novel type of concrete, was introduced by the construction industry in 1988 in response to the needs of extensive infrastructure and development projects requiring thick reinforcement. By using CSC, formwork in tight places and around large bracing can be filled without the use of external vibrators or energy sources. Due to its weight and high mortar content, it may softly circulate, ensuring homogeneity and avoiding segregation and bleeding. However, one of the drawbacks of SCC is that it costs more money, especially because superplasticizers and a lot of cement are used. In order to solve this problem and increase sustainability while overcoming SCC limitations, additional cements are being used as reasonably priced cement substitutes.

Sustainability is the ability of concrete to withstand physical, chemical, and biological harm. As a result of the environment, chemical attack can take many different forms, including sulphate attack, acid attack, carbonation, alkaline silica aggregate reaction, and others. Abrasion, impact, frost damage, overloading of concrete structures, as well as natural disasters like earthquakes, floods, and fires, can all cause physical disintegration. Bacteria, moss, lichen, marine boron, shells, and sponges all contribute to biological harm. Due to the fact that chemical assaults are mostly to blame for the fundamental deterioration of concrete structures, researchers are faced with the essential challenge of finding solutions to sustainability issues.

Demand for building supplies including cement, fine aggregates, and coarse aggregates has significantly increased as a result of urbanisation. To meet the demands of the building industry, over 48.3 billion tonnes of construction aggregates were produced globally in 2015. These resources are already few, though, and future

V. K. Nithyashree (✉) · M. Surendar
Civil Engineering Department, Easwari Engineering College (Autonomous), Chennai, India
e-mail: nithya19899@gmail.com

generations won't be able to meet their needs only with the help of these restricted natural resources. This has a negative impact on the construction sector.

The process of mining and producing the materials required in building consumes a lot of energy and has a big environmental impact. Furthermore, the demand for fine aggregates has increased due to the building industry's rapid expansion in developing nations like China and India. The combined effect of these variables has rendered the building business increasingly unsustainable, necessitating a quick search for workable alternatives that can help the sector survive.

Even though a wide range of industrial raw materials are produced in significant quantities, many nations face significant hurdles due to the limited availability and utilisation of these minerals as fine aggregates. Due to the accumulation of waste, large expanses of land become occupied. Construction uses manmade aggregates or industrial waste to address this issue and lessen its reliance on finite natural resources. Natural resource conservation and resource consumption reduction are made possible by this strategy.

Even though a wide range of industrial raw materials are produced in significant quantities, many nations face significant hurdles due to the limited availability and utilisation of these minerals as fine aggregates. Due to the accumulation of waste, large expanses of land become occupied. Construction uses manmade aggregates or industrial waste to address this issue and lessen its reliance on finite natural resources. Natural resource conservation and resource consumption reduction are made possible by this strategy.

2 Literature Review

- (1) According to Rajamane and colleagues the study, it is both practical and sustainable to produce geopolymer mortar using copper slag pellets for high temperature applications. Copper slag mortar's compression resistance at room temperature is comparable to that of mortars with river sand as the primary material. Additionally, the compressive strength of the copper slag mortars improves as the ratio of binder to copper slag rises, a trend that is not seen in river sand samples. The study discovered that copper slag mortars have more residual resilience at high temperatures than river sand-based mortars in terms of thermal stability.
- (2) According to Rajeeth et al. the study, the digressive value of fresh concrete increases as the proportion of copper slag in concrete decreases. According to the study, concrete made using 40% copper slag instead of M-sand (manufactured sand) had the highest compressive strength, which was around 10% greater than concrete made with M-sand. This makes us think that copper slag-infused concrete has stronger qualities than regular concrete. Concrete containing 40% copper slag demonstrated a compressive strength that was 26% higher than concrete made with M-sand, indicating enhanced durability and resistance to chemical assault.

- (3) Farshad Ameri and colleagues the study found that the optimum performance in terms of fire resistance was obtained when 20% copper slag (CS) was added to alkali-activated slag (AAS) composites in place of some of the river sand. Additionally, the incorporation of CS into AAS composites presents a chance to create new building materials that are more effective and environmentally benign. The higher fire resistance of AAS with CS composites, which shows that they can tolerate high temperatures more effectively than traditional materials, is highlighted in the study in particular. The performance of the materials can be increased by substituting CS for river sand in AAS composites, and the environmental impact can be diminished by reusing waste products.
- (4) According to Akit Negi and colleagues the study, concrete's performance and qualities are strongly influenced by the amount of copper slag that is contained in it. A better workability and strength of concrete can result from the copper slag's favourable properties, which include a homogeneous and lustrous surface texture, less moisture absorption, and increased compressive strength. A fractional tensile test revealed that copper slag-infused concrete in the Beas River has higher tensile strength compared to conventional concrete. This increase in density can help concrete become stronger and more durable overall, making it an attractive option for a range of building applications.
- (5) Yasser Sharif et al. This study's goals were to solve environmental issues with waste concrete slurry (WCS) and look into solutions to build using concrete more affordably while protecting natural resources. 11 SCC blends with various ratios of WCS as coarse aggregates were evaluated for freshness and curing qualities using a variety of tests and criteria. The SCC mixtures examined performed well in sagging tests (class SF2), funnel tests (classes VF1 and VF2), and L-box testing (class PA2) in accordance with the 2005 EFNARC recommendations.
- (6) Priyavarshiny et al. A range of sectors can profit from the technical and environmental advantages of using copper slag in concrete. Additionally, it has been demonstrated by compressive strength tests that adding more copper slag (up to 40%) and additives such *Bacillus subtilis* (at a dosage of 180 ml) will improve the compressive strength of concrete. Copper slag is a viable choice for sustainable building practises because industries can profit technically and environmentally from using it in the manufacturing of concrete.
- (7) Abhishek Maharishi and colleagues The results of the study indicate that substituting copper slag (CS) for fine natural aggregate (FNA) can greatly increase concrete's strength and durability by up to 40%. For concrete with exceptional strength and durability attributes, CS up to 40% FNA is advised. At 28 days, the concrete mixture with 40% CS (CS-40) exhibited the highest compression resistance, 13% more so than the CS-0 control mixture. The improvement in cohesion and stress distribution in the concrete matrix, made possible by the increase in compression strength and angular form of CS particles, is responsible for this gain in strength.

- (8) Nikita Gupta et al. Due to its glassy structure and limited water absorption capabilities, copper slag added to self-compacting concrete (SCC) produced favourable fresh qualities. The CSH gel layers accumulated in SCC mixtures containing 10–30% copper slag, resulting in a more dense microstructure and higher resistance. The presence of voids, porosity, and microcracks in SCC mixes made with 50% and 60% copper slag, on the other hand, may have contributed to the minor reduction in strength. SCC's strength qualities were improved overall by the addition of copper slag, with the best results being shown at lower copper slag concentrations.
- (9) Ali Rezaei Lori and colleagues Evaluation of the effects of employing copper slag as an aggregate in pervious concrete was the study's main objective. The mechanical and hydraulic properties of the pervious concrete were examined in order to determine the impacts of the substitution of copper slag. The amount of copper slag aggregate had an effect on the location and size of pores in the pervious concrete, according to a study on pore size distribution. In conclusion, pervious concrete's density, permeability, and porosity were all raised by adding copper slag as an aggregate. This implies that use copper
- (10) Ravitheja et al. The experimental results show that adding copper slag instead of river sand reduces the compressive strength of concrete. However, by substituting copper slag for up to 40% of the natural river sand, the concrete's compressive strength was increased. Flexural strength improved with the addition of 40% copper slag; however, as copper slag concentration was elevated further, flexural strength declined. Additionally, when 1% nanosilica was added to combinations containing 100% copper slag, the filling of holes and capillary channels, the enhancement of the concrete's mechanical and durability properties, and the rise in density all showed promise. It is crucial to carefully consider the ideal copper slag addition and content. Vijayaraghava et al. (2017) Through an examination of the usage of alternate cementitious materials, in particular copper slag, iron slag, and recycled concrete aggregates, the study sought to address the demand for sustainable practises in the building sector. The study's goal was to advance knowledge of sustainable construction techniques and offer useful data for potential applications in the sector by examining the effects of these components on concrete characteristics.
- (11) Dos Anjos et al. [6] The study found that utilising copper slag in place of fine aggregate does not significantly reduce concrete's tensile strength until copper slag content exceeds 50%. Additionally, employing copper slag in place of fine aggregate provides a sustainable waste management solution because it is a by-product of the copper industry. Overall, adding copper slag to concrete has the potential to enhance a variety of characteristics and provide a more eco-friendly building material.
- (12) Rahul Sharma et al. [13] The experiment tested the durability of self-compacting concrete (SCC) using copper slag (CS) as the fine aggregate. The VS2 category was satisfied by the T500 time, which evaluates how long it takes concrete to reach 500 Pa.s of viscosity. This suggests that the T500 time is the ideal viscosity for SCC. After the initial curing period, the mix with

20% CS produced the highest compressive strength across the different CS replacement levels. But as the CS replacement level crossed the 60% mark, the compressive strength started to decline. It is vital to consider the level of CS replacement since too much replacement could lead to a loss in strength as a result of an increase in the amount of free water in the mixture.

- (13) Janakiramaiah and colleagues The use of copper slag in concrete offers numerous technical and environmental benefits in a variety of industries. When up to 10% of copper slag is added to the fine aggregate, the concrete's compressive and split tensile strengths are also boosted. Additionally, substituting copper slag for overall, copper slag is a useful substitute material in the building industry due to the technical advantages, cost savings, and environmental advantages it offers when used in concrete.
- (14) Chithra and colleagues The study's findings support the notion that adding nanosilica to cement pastes, mortars, and concrete mixtures that replace copper slag for fine aggregate has a number of advantages. In particular, the use of nanosilica enhances homogeneity, speeds up hydration, reduces setting time, boosts compressive strength, and reduces sorptivity and water absorption values. In cement mortars that substitute 40% copper slag for fine aggregate, using nanosilica up to 2% results in better compressive strength and decreased water absorption and sorptivity values.
- (15) Jayaprakash and colleagues The results of the compression tests showed that the concrete was stronger when up to 40% copper slag by weight was added to the fine aggregate. No matter what percentage of fine aggregate was replaced with copper slag, the concrete's flexural strength was always higher than the control mix.
- (16) Mithun and colleagues Compressive strength tests indicated that neither the ordinary Portland Cement Concrete (OPCC) mix nor the Alkali Activated Slag Concrete (AASC) mix made up of sand and copper slag (CS) showed any symptoms of deterioration after being subjected to 10% Na₂SO₄ solutions for a year. The strength increases in sand and CS mixes were a little bit higher when comparing AASC mixes to OPCC mixtures. In contrast, when subjected to a 10% MgSO₄ solution over the course of a year, AASC mixes with particles exhibited a faster rate of strength depreciation than OPCC mixes.
- (17) According to Ravisankar et al. the results of the study show that substituting some of the sand in ultra-high-performance concrete (UHPC) with copper slag provides a variety of benefits. First, the angular shape and rough texture of copper slag particles promote better interlocking, improving workability and reducing segregation in the concrete mix. In addition to providing technological advantages, using copper slag in UHPC reduces the quantity of waste that would otherwise be disposed of in landfills.
- (18) Alinda Dey and colleagues This investigation provides strong evidence that copper slag can be used as an important and valuable replacement material to address environmental issues and enhance the tensile strength and durability of prospective projects. The corpus of research supports the idea that some of

the coarse and fine particles in concrete mixtures can be replaced with copper slag to improve the overall qualities of concrete.

- (19) Ramzi Taha and colleagues All of the copper slag-containing mixtures demonstrated compressive strengths in cement mortars that were equal to or greater than the combination used as a control, which contained no copper slag. In particular, mortars with a 50% substitution of copper slag showed a remarkable increase in compressive strength of over 70% when compared to the control mixture. When copper slag is substituted for sand, the concrete gains around 5% more density. The compressive, tensile, and flexural strengths of the concrete were comparable to the control mix when up to 50% of the sand was replaced with copper slag. These findings lead to the suggestion that in situ copper slag might be utilised in concrete.

3 Conclusion

The study's findings suggest that it is safe to add copper slag to concrete mixtures. According to the study, copper slag can be added to self-consolidating concrete (SCC) to boost its strength and workability. Notably, the compressive strength data showed statistically significant increases at both 28 and 90 days of curing. This shows that copper slag can significantly boost SCC performance. The findings of this study are important for both SCC researchers and the copper industry. It provides evidence of the benefits and viability of including copper slag into SCC mixtures, which can help produce more ecologically friendly and high-performing concrete products. In conclusion, the study reveals that incorporating copper slag into.

1. Copper slag substitution raised SCC's compressive strength by up to 30% at all curing ages. Beyond that, the strength decreased somewhat but remained equivalent to the strength of control concrete.
2. Split tensile strength was increased by up to 60% in SCC mixtures including copper slag. The angular edges of the copper slag grains improved the cohesion of the concrete matrix, which boosted strength.
3. During a SEM analysis, the surface morphology of SCC mixes with 100% sand showed ettringite development, microcracks, and voids. Ettringite developed, as evidenced by the presence of aluminium and sulphur in an SCC mixture without copper slag under EDS testing. CSH gel layers accumulate in SCC combinations with copper slag concentrations ranging from 10 to 30%. The concrete matrix's microstructure thickened, strengthening it.
4. SCC combinations with more than 30% copper slag experienced a minor loss in strength. According to SEM analyses, ettringite crystals were discovered in a mixture of SCC that comprised 40% copper slag. It was discovered that voids, porosity, and microcracks were present in SCC combinations containing 50 and 60% copper slag, respectively.

SSC combinations exhibited remarkable fresh characteristics as a result of the glassy structure and reduced water absorption of copper slag grains.

References

1. Gesoglu M, Guneyisi E, Ozbay E (2009) Properties of SCCs made with binary, ternary, and quaternary cementitious blends of fly ash, blast furnace slag, and silica fume. *Constr Build Mater* 23(5):1847–1854
2. Shi C, Meyer C, Behnood A (2009) Utilization of copper slag in cement and concrete—a review. *Resour Conserv Recy* 52:1115–1120
3. Al-Jabri KS, Hisada M, Al-Oraimi SK (2009) Copper slag as sand replacement for high performance concrete. *Cem Concr Compos* 31(7):483–488. <https://doi.org/10.1016/j.cemconcomp.2009.04.007>
4. Wu W, Zhang W, Ma G (2010) Optimum content of copper slag as a fine aggregate in high strength concrete. *Mater Des* 31(6):2878–2883
5. Brindha D, Nagan S (2011) Durability studies on copper slag admixed concrete. *Asian J Civil Eng (Building and Housing)* 12(5):563–578
6. Dos Anjos MAG, Sales ATC (2017) Blasted copper slag as fine aggregate in Portland cement concrete. *J Environ Manage*. <https://doi.org/10.1016/j.jenvman.2017.03.032>
7. Arivalagan S (2013) Experimental study on the flexural behaviour of reinforced concrete beams as replacement of copper slag as fine aggregate. *J Civil Eng Urbanism* 3(4):176–182
8. Al-Jabri KS, Al-Saidy AH, Taha R (2011) Effect of copper slag as a fine aggregate on the properties of cement mortars and concrete. *J Construct Build Mater* 25(2):933–938
9. Meenakshi SS, Illangovan R (2011) Performance of copper slag and ferrous slag as partial replacement of sand in concrete. *Int J Civil Struct Engg* 1(4):918–927
10. Babu KM, Ravitheja A (2019) Effect of copper slag as fine aggregate replacement in high strength concrete. *Mater Today Proc* 19:409–414
11. Nair AS, Sreemahadevan Pillai PR (2018) The effect of GGBFS and copper slag on strength of self compacting concrete: an experimental study. *Int J Eng Adv Technol* 7(4):47–53
12. Elangovan R, Venkatesh Babu DL, Venkatasubramani R (2015) Studies on high strength self-compacting concrete with copper slag. *Int J Appl Eng Res* 10(10):26879–26896
13. Sharma R, Khan RA (2017) Fresh and mechanical properties of self compacting concrete containing copper slag as fine aggregates. *J Mater Eng Struct* 4(1):25–36
14. Sharma R, Khan RA (2017) Durability assessment of self-compacting concrete incorporating copper slag as fine aggregates. *Constr Build Mater* 155:617–629
15. Gong W, Ueda T (2018) Properties of self-compacting concrete containing copper slag aggregate after heating up to 400 C. *Struct Concr* 19(6):1873–1880
16. Veerajju M, Arunchaitanya S (2018) Experimental study on high strength self—compaction concrete by using fly ash as a partial replacement of cement and copper slag with fine aggregate. *Int J Innov Technol Explor Eng* 7(8):13–19
17. Rex Dhivakar Arockia Raj J, Arunachalam K, Mohandas K (2018) Self-compacting concrete with copper slag as partial substitute for sand. *J Comput Theor Nanosci* 15(3):977–981
18. Arunchaitanya S, Arunakanthi E (2019) Usage of mineral admixtures in self-compacting concrete—a review. *Int J Innov Technol Explor Eng* 8(3):58–62
19. BIS (2013) Ordinary portland cement 43 grade -specification. BIS 8112, New Delhi 2013, India
20. Afshoon I, Sharifi Y (2014) Ground copper slag as a supplementary cementing material and its influence on the fresh properties of self-consolidating concrete, IES. *J Part A: Civ Struct Eng* 7(4):229–242

Enhancement of Concrete Strength of Using PPF and Analysis by ANSYS for Strength Comparison



Pathapati Rohithkumar, Abishek Rauniyar, and V. R. Prasath Kumar

1 Introduction

The construction and engineering industries are constantly exploring new ways to improve the strength and durability of building materials [1]. One promising development in this area is the use of polypropylene fibers as reinforcing agents in concrete. These synthetic fibers offer several advantages over traditional steel reinforcement, including high tensile strength, chemical resistance, and a lower cost [2]. The goal of this research is to investigate the mechanical properties of polypropylene fibers and optimize their use in enhancing the strength of concrete. The research will involve a series of experiments to determine the optimal fiber length, diameter, and volume fraction that would provide maximum strength to concrete [3]. The experiments will examine the impact of these variables on the mechanical properties of concrete under various conditions, such as compressive, tensile, and flexural strength [4]. Statistical methods, such as regression analysis and ANOVA, will be used to analyze the results [5] of the experiments and determine the most effective combination of fiber properties for use in concrete. The findings of this research will have significant implications for the construction industry, as they will contribute to a better understanding of the mechanical properties of polypropylene fibers and lead to the development of stronger and more durable concrete structures [6].

Furthermore, the optimization of fiber properties will reduce the number of fibers used, thus lowering costs and minimizing environmental impact [7]. Polypropylene fibers have the potential to revolutionize the construction industry by providing a more sustainable and cost-effective alternative to traditional steel reinforcement. In addition to examining the mechanical properties of polypropylene fibers, this research will also investigate their impact on other properties of concrete, such as workability

P. Rohithkumar · A. Rauniyar · V. R. Prasath Kumar (✉)
Department of Civil Engineering, Faculty of Engineering and Technology, SRM Institute of Science and Technology, Kattankulathur, Tamil Nadu 603203, India
e-mail: prasathv@srmist.edu.in

and durability. The workability of concrete affects its ability to be poured, placed, and compacted into forms, while durability refers to its ability to withstand long-term exposure to environmental conditions [8]. The findings of this research will provide valuable insights into the overall performance of concrete reinforced with polypropylene fibers, which will have important implications for the development of new construction materials and techniques [9]. Overall, this research is of great significance for the construction and engineering industries, as it has the potential to contribute to the development of stronger, more durable, and more sustainable building materials.

2 Literature Review

The purpose of the literature review is to provide a comprehensive overview of the current state of research on the mechanical properties of polypropylene artificial fibers and their optimization for enhanced strength concrete based on the results of the literature review. Moreover, the review would identify gaps in existing research and make recommendations for future research in this area [10–16]. By reviewing the scientific literature, they will be able to gain a deeper understanding of the current state of research on the mechanical properties of polypropylene artificial fibers and how they may be optimized for concrete with enhanced strength. By reviewing these materials and their potential applications for the construction industry [17], a foundation will be laid for future research in this area, advancing our understanding of these materials and their potential uses. Moreover, the review will provide a valuable resource for researchers, practitioners, and policymakers in the construction and engineering industries, which will aid in the development of new and innovative building materials and techniques [18]. In conclusion, a systematic literature review of the mechanical properties of polypropylene artificial fibers, polymer waste materials, and their optimization for enhanced strength concrete would provide a comprehensive and up-to-date overview of the current state of research in this field [19]. The review would provide valuable insights into the potential applications of these materials in the construction industry and help to inform the development of new and innovative building materials and techniques [20].

3 Methodology and Materials

3.1 Methodology

To assess the existing research in this area and identify gaps in our knowledge, a systematic literature review would be conducted as first step in the methodology as shown in Fig. 1.

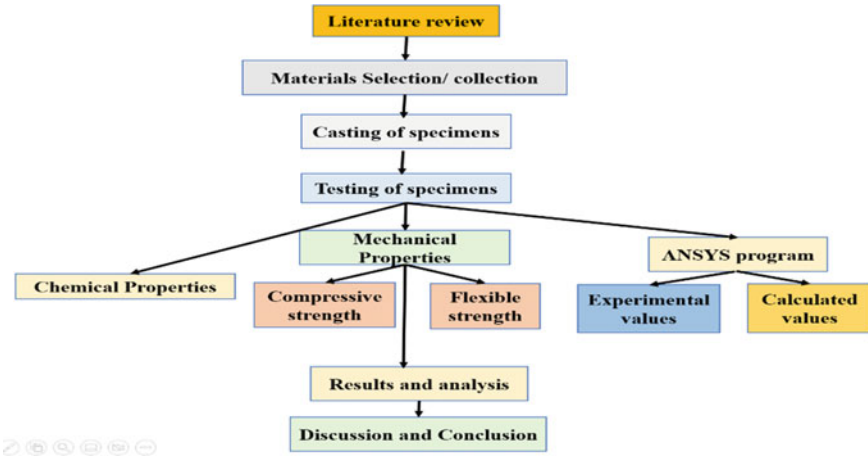


Fig. 1 Research methodology

An experimental study would then be conducted to investigate the mechanical properties of polypropylene fibers as well as their influence on concrete’s mechanical properties. As part of the experimental procedures, concrete specimens containing varying concentrations of polypropylene fibers will be prepared and tested under various mechanical conditions. The experimental results will be complemented by numerical simulations, using numerical simulations, concrete specimens would be modeled using finite element methods, and various loading conditions would then be applied. To validate the mathematical model and gain a better understanding of how concrete reinforced with polypropylene fibers behaves, the numerical simulations would be compared with the experimental results.

3.2 Material

High Performance Concrete. High performance concrete is more durable and stronger than conventional concrete. It depends on qualities of normal concrete available at a given period and place. In industrial countries high performance concrete for 28 days compressive strength of 70 to 80N/mm², factor of durability 80%, and water content less than 0.35 [21, 22]. **Ordinary Portland cement (Grade 53).** IS established this grade in 1987; commercial production began in 1991. Modern cement factories’ better technology made this grade possible in the nation. OPC 53 Grade cement must meet BIS standard IS:12,269–1987 with a 28-day strength of 53 MPa or 530 kg/sqcm [18]. **Coarse aggregate and Fine aggregate.** Concrete utilizes sand, gravel, and crushed stone. Coarse may be generated by blasting or crushing quarries [23]. Manufactured sand replaces river sand. River sand is limited

due to the fast-growing construction industry. Due to less river sand, more artificial sand is needed. M-availability Advantages include sand and transportation costs [24]. **Casting of Specimens.** Weighed the materials accurately and mixed them thoroughly for three minutes using a digital mixing machine. Natural fibers were mechanically sprinkled inside the mixer after the concrete ingredients had been thoroughly mixed. The specimens were prepared using permanent steel molds for compressive, tensile, and flexure tests [25]. **Properties of Polypropylene Fiber.** Fibers made from polypropylene contain crystalline and non-crystalline regions. However, if the force is larger than 0.75%, spherulites may become highly oriented and are converted to microfibrils. Fibers with anisotropic properties are formed by these highly anisotropic microfibrillar structures [27].

3.3 *Methods and Preparation of Materials*

The approach involved blending polyester resin, silica sand with a grain size of 250 μm , and recycled polymers derived from PET beverage bottles, TV carcasses (polycarbonate waste), and tire rubber from automotive recycling centers. To initiate the polymerization process, a 1 mL dosage of methyl ethyl ketone peroxide (MEKP) was introduced as an initiator to the pre-accelerated resin, as depicted in Fig. 3. To assess the workability of the samples, a slump test was conducted, as depicted in Fig. 2. To modify the mortars and replaced a portion of the silica sand with varying concentrations (ranging from 1 to 3% by weight) of polycarbonate, tire rubber, and PET particles, as indicated in Table 2. The preparation of the samples involved utilizing a wooden mold to create and compact polymer mortar specimens measuring 150 \times 150 \times 150 mm. For each type of concrete, a total of nine specimens were produced. The specimens were originally recommended to be cured at room temperature for 24 h. However, found that a post-curing process at 35 $^{\circ}\text{C}$ for two hours was more convenient to ensure full polymerization (Fig. 4).

Fig. 2 Slump test



Fig. 3 Mixing materials**Fig. 4** Casting specimens

3.4 Model Based on Finite Elements (ANSYS)

For the simulation of polymer concrete, ANSYS 16.0 was used as a commercial finite element package. The Newton–Raphson method is used by ANSYS to solve nonlinear problems, where the total load is divided into increments of load until the solution is converged. The finite element SOLID186 is recommended by ANSYS for modeling materials such as concrete. Observe that this element has a quadratic displacement behavior that corresponds to a higher order 3-D 20-node. A node of the element has three degrees of freedom, so it consists of 20 nodes. There is a wide range of properties that the element can support, including plasticity, hyper-elasticity, creep, stress stiffening, large deflections, and large strains. Various strain hardening yield stress–strain curves were used to model polymer mortar. All materials were calibrated using testing data, and the parameters adopted were validated using these data.

4 Results and Analysis

4.1 Compressive Strength

The data in the graph presents the compression strength values of polymer mortars with polypropylene artificial fibers. In this study, silica sand, polyester resin, and various polymer wastes, including PET, polycarbonate, and tire rubber particles, were used to prepare the mortars. The PET-based polymer mortars showed the highest compression strength values, followed by those with polypropylene artificial fibers and polycarbonate-based mortars. The mortars with tire rubber particles showed the lowest strength values. Specifically, the highest pressure was achieved with polymer mortar containing 1 wt.% of PET particles, with a value of 78 MPa, representing an improvement of up to 20% compared to the control mortar. The compatibility of the polyester resin and waste PET is believed to account for this increase in strength. In contrast, the compressive strength values of the polypropylene artificial fiber and polycarbonate mortar were like those of the control mortar, indicating that both materials have comparable mechanical properties. It is noteworthy that the literature indicates that polycarbonate resins have lower moduli of elasticity and compressive strength than polyester resins. Table 1 represents the compressive strength analysis of mortar, and Fig. 5 shows the effective and changing values of compressive strength.

Table 1 Compressive strength analysis

Mix type	Mix composition	Compressive strength in MPa		
		7 days	14 days	28 days
Polymer waste mortar	PET-based mortar	62	68	79
	Polyester resin	60	63	69
	Polycarbonate	61	66	71

Table 2 Comparison of experimental and calculated results for compressive test

Polymer mortar	Compressive strength (MPa)	
	Experimental	Calculated
Control	66	67.3
PET-based mortar	79	80.3
Polyester resin	69	71.3
Polycarbonate	71	73.3

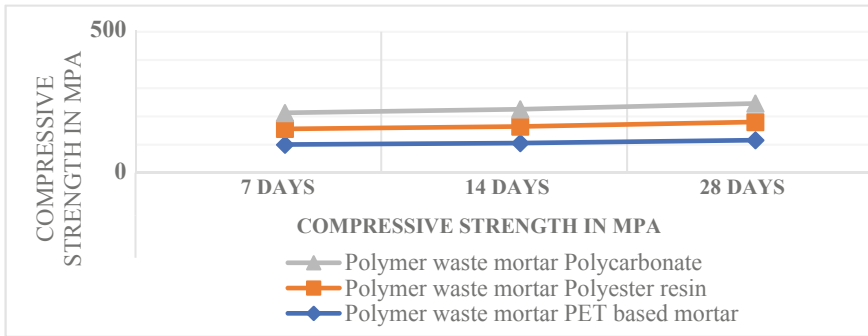


Fig. 5 Following graph shows the compression strength for all mix types

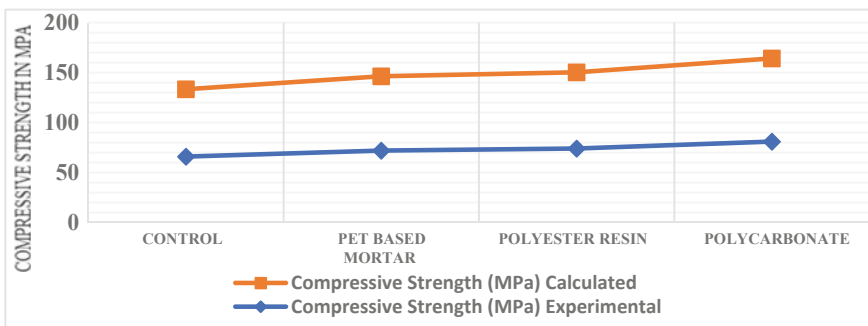


Fig. 6 Graphical representation of comparison of experimental and calculated results for compressive test

4.2 Compressive Strain at Ultimate Strength

A graph showing the compressive strain at ultimate strength values can be seen in Fig. 6, and Table 2 shows comparison of experimental and calculated results for the compressive test. When waste PET (up to 20%) or polycarbonate particles (up to 11%) are added to the control mortar, deformation increases significantly. Conversely, tires rubber particles resulted in a reduction of deformation values by 20%.

4.3 Flexural Strength

The compression strength values of polymer mortar specimens with polypropylene artificial fiber are shown in Fig. 7 and Table 3. The highest compressive strength was obtained for the PET-based polymer mortar, followed by polycarbonate-based mortar and tire-based mortar, and finally, the polypropylene artificial fiber. Adding

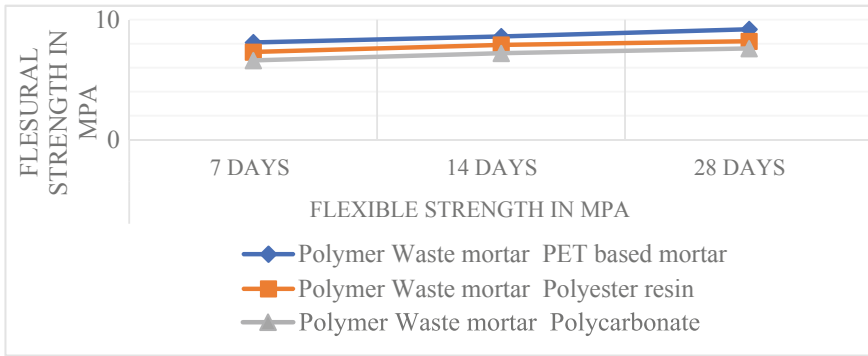


Fig. 7 Graphical representation of flexible strength analysis

Table 3 Flexural strength analysis

Mix type	Mix composition	Flexible strength in MPa	
		7 days	14 days
Polymer waste mortar	PET-based mortar	8.1	8.6
	Polyester resin	7.3	7.9
	Polycarbonate	6.6	7.2

1 wt.% of PET particles to the polymer mortar resulted in a 20% improvement in compression strength compared to the control mortar. The compatibility of polyester resin and waste PET is responsible for this increment. However, both polypropylene artificial fiber and polycarbonate-based mortar showed similar behavior to the control mortar, indicating that they have similar mechanical properties. Literature suggests that polycarbonate resins have lower modulus of elasticity and compressive strength than polyester resins.

As the concentration of waste polycarbonate or tire rubber particles increases, flexural strength values increase, whereas they decrease with an increase in waste PET concentration. The roughness of the matrix facilitates mechanical anchoring between its polymer particles and PET particles, resulting in slight increases in flexural strength values for particles with a size less than 20 mm. However, particles with rough, fibrillated elements, detached particles, and some cavities, as observed in waste polycarbonate, reduce flexural strength values due to the generation of empty spaces resulting in mechanical testing failures. Tire rubber particles exhibit a higher level of roughness, resulting in similar flexural strength values to those observed in the control mortar. Both experimental and calculated load–displacement curves for polymer mortar specimens were generated using ANSYS, with a good agreement between the experimental and calculated values. ANSYS is thus an appropriate tool for obtaining calculated data.

Table 4 Displacement at ultimate flexural strength

Polymer mortar	Flexural load (kN)		Displacement at ultimate
	Experimental	Calculated	Experimental
Control	7.76	8.13	0.63
PET	9.00	9.48	0.86
Polycarbonate	6.44	6.79	0.89
Polyester resin	6.52	6.84	0.83

4.4 Displacement at Ultimate Flexural Strength

As shown in Table 4, the displacement at ultimate flexural strength values represents the maximum displacement. Higher particle concentrations result in gradually increasing values for polymer mortar with PET particles but decrease for polymer mortar with polycarbonate or tire rubber. Polymer mortar with 3 weights produced the highest value. As compared to the control mortar, there has been an improvement of 45% in the percentage of PET particles. When PET particles are subjected to flexural loads, they produce more ductile polymer mortars.

5 Discussion

Using polypropylene artificial fiber and polymer mortar with polycarbonate for enhancing concrete strength is an investigation that provides valuable insight into its potential use as a reinforcement for concrete [28]. Based on the results of the tensile tests, it was determined that polypropylene fibers were both strong and elongating, making them a suitable substance for use as fibers in concrete reinforcement. A strong, flexible reinforcement network can be created within a concrete matrix using polypropylene fibers and polymer mortar with polycarbonate [2], resulting in improved mechanical properties. Concrete mixtures reinforced with fibers performed significantly better in tests compared to unreinforced concrete mixtures. It has been found that both polypropylene fibers and polymer mortar with polycarbonate significantly increase the resistance of concrete to compressive and tensile stresses when used in conjunction with the fibers in concrete beams reinforced with the fibers. A more uniform distribution of forces may have been achieved due to fiber's ability to transmit stress between matrix and aggregate. The result is that the concrete structure will be less prone to cracking and will have improved durability [29]. According to the study, the optimization algorithm provided important insights into the most appropriate fiber parameters to maximize concrete strength improvements. Based on the algorithm, fiber volume fraction and length were found to be the optimal fiber parameters. Polypropylene fibers can enhance concrete's strength in a variety of ways, which is important for the construction industry. More sustainable building material can also be developed because of the study's results. Among the widely

used construction materials, concrete contributes a substantial amount to greenhouse gas emissions. A concrete mixture reinforced with polypropylene fibers and polymer mortar containing polycarbonate can reduce carbon dioxide emissions during production by reducing the amount of cement required. Concrete structures reinforced with polypropylene fibers can also be less likely to require maintenance and repair over the lifespan of the structure because of their improved strength and durability. As a result, maintenance and repair activities can reduce emissions.

The findings of this study provide a solid basis for future research in this area. Based on the results of this study, it appears that synthetic fibers made from polypropylene are capable of significantly strengthening concrete, making them an interesting reinforcement material for the construction industry. Further research is required to evaluate the long-term performance, as well as the potential reduction of greenhouse gas emissions in the construction industry, of polypropylene fibers and polymer mortar with polycarbonate.

6 Conclusion

This study examines the influence of various waste polymer materials, including PET, polycarbonate, and tire rubber, on the compressive and flexural properties of polymer mortars made up of a variety of polymer materials. Using a polymer mortar that contained these waste particles as compared to a control mortar that did not contain any waste particles, the researchers compared the mechanical properties of the two types. There was also a study examined the relationship between the morphology and crystallinity of the waste particles as well as the mechanical properties obtained as a result of the investigation. According to the study, adding one pound to the product resulted in an increase of 1. Upon compressive loading of polymer mortars with PET particles, the mortars had the highest modulus of elasticity, as well as the highest deformation when subjected to compression loads, as well as the highest compressive and flexural strength. There is a high degree of crystallinity in the PET particles and a roughness characteristic linked to these results. Compared to the control mortar, a mortar that contained polycarbonate or tire rubber particles resulted in lower mechanical properties such as compressive strength, flexural strength, and modulus of elasticity than a mortar containing only polycarbonate or tire rubber particles. There was also a simulation method employed in this study, which results in higher agreement with the experimental data than the finite element analysis. As a result of these findings, the researchers believe that their next step is to modify the waste particles by chemical treatment or coating them with silanes in order to improve the interaction between the waste particles and the matrix and increase mechanical properties of the polymer mortars.

References

1. Qu X, Zhao X (2017) Previous and present investigations on the components, microstructure and main properties of autoclaved aerated concrete—a review. *Constr Build Mater* 135:505–516. <https://doi.org/10.1016/j.conbuildmat.2016.12.208>
2. Wu L, Mei M, Li Z, Liu S, Wang X (2022) Case studies in construction materials study on photocatalytic and mechanical properties of TiO₂ modified pervious concrete. *Case Stud Constr Mater* 17:e01606. <https://doi.org/10.1016/j.cscm.2022.e01606>
3. Güneysi E, Khoshnaw G, Ipek S (2014) Abrasion and freezing—thawing resistance of pervious concretes containing waste rubbers. 73:19–24. <https://doi.org/10.1016/j.conbuildmat.2014.09.047>
4. Zhang H et al. (2022) Analyzing the pore structure of pervious concrete based on the deep learning framework of Mask R-CNN. *Constr Build Mater* 318:125987. <https://doi.org/10.1016/j.conbuildmat.2021.125987>
5. Wang Z, Zou D, Liu T, Zhou A, Shen M (2020) A novel method to predict the mesostructure and performance of pervious concrete. *Constr Build Mater* 263:120117. <https://doi.org/10.1016/j.conbuildmat.2020.120117>
6. Singh A, Sampath PV, Biligiri KP (2020) A review of sustainable pervious concrete systems : emphasis on clogging, material characterization, and environmental aspects. *Constr Build Mater* 261:120491. <https://doi.org/10.1016/j.conbuildmat.2020.120491>
7. Raul F, Merten M, Vanessa F, Lunkes H (2022) Clogging and maintenance evaluation of pervious concrete pavements with recycled concrete aggregate. vol 342. <https://doi.org/10.1016/j.conbuildmat.2022.127939>
8. Khankhaje E, Rafieizonooz M, Razman M, Mirza J (2017) ScienceDirect comparing the effects of oil palm kernel shell and cockle shell on properties of pervious concrete pavement. *Int J Pavement Res Technol* 10(5):383–392. <https://doi.org/10.1016/j.ijprt.2017.05.003>
9. Lederle R, Shepard T, De La V, Meza V (2020) Comparison of methods for measuring infiltration rate of pervious concrete. *Constr Build Mater* 244:118339. <https://doi.org/10.1016/j.conbuildmat.2020.118339>
10. Abdelhady A, Hui L, Zhang H (2021) Comprehensive study to accurately predict the water permeability of pervious concrete using constant head method. *Constr Build Mater* 308:125046. <https://doi.org/10.1016/j.conbuildmat.2021.125046>
11. Zhong R, Wille K (2016) Compression response of normal and high strength pervious concrete. *Constr Build Mater* 109:177–187. <https://doi.org/10.1016/j.conbuildmat.2016.01.051>
12. Joshi T, Dave U (2022) Case studies in construction materials construction of pervious concrete pavement stretch, Ahmedabad, India—case study. *Case Stud Constr Mater* 16:e00622. <https://doi.org/10.1016/j.cscm.2021.e00622>
13. Chen X et al (2020) Design of a chitosan modifying alkali-activated slag pervious concrete with the function of water purification. *Constr Build Mater* 251:118979. <https://doi.org/10.1016/j.conbuildmat.2020.118979>
14. Uddin MJ, Smith KJ, Hargis CW (2021) Development of pervious oyster shell habitat (POSH) concrete for reef restoration and living shorelines. *Constr Build Mater* 295:123685. <https://doi.org/10.1016/j.conbuildmat.2021.123685>
15. Wu S, Wu Q, Shan J, Cai X, Su X, Sun X (2023) Effect of morphological characteristics of aggregate on the performance of pervious concrete (a) (b) (c). *Constr Build Mater* 367:130219. <https://doi.org/10.1016/j.conbuildmat.2022.130219>
16. Braga DS, Santos E, Junior A, De Nazar L, Vieira S (2022) Case studies in construction materials effect of pore characteristics on the sound absorption of pervious concretes. 17. <https://doi.org/10.1016/j.cscm.2022.e01302>
17. Akkaya A (2021) Experimental investigation of the use of pervious concrete on high volume roads. 279. <https://doi.org/10.1016/j.conbuildmat.2021.122430>
18. Wang J, Meng Q, Tan K, Santamouris M (2022) Evaporative cooling performance estimation of pervious pavement based on evaporation resistance. *Build Environ* 217:09083. <https://doi.org/10.1016/j.buildenv.2022.109083>

19. Adil G, Kevern JT, Mann D (2020) Influence of silica fume on mechanical and durability of pervious concrete. *Constr Build Mater* 247:118453. <https://doi.org/10.1016/j.conbuildmat.2020.118453>
20. He S, Jiao C, Li S (2023) Investigation of mechanical strength and permeability characteristics of pervious concrete mixed with coral aggregate and seawater. *Constr Build Mater* 363:129508. <https://doi.org/10.1016/j.conbuildmat.2022.129508>
21. Barnhouse PW, Iii WVS (2016) Material characterization and hydraulic conductivity modeling of macroporous recycled-aggregate pervious concrete. *Constr Build Mater* 110:89–97. <https://doi.org/10.1016/j.conbuildmat.2016.02.014>
22. Viana S, Magalhães S, Elizabeth M (2021) Case studies in construction materials mechanical behavior and water in filtration of pervious concrete incorporating recycled asphalt pavement aggregate. 14. <https://doi.org/10.1016/j.cscm.2020.e00473>
23. Zhang Q, Feng X, Chen X, Lu K (2020) Mix design for recycled aggregate pervious concrete based on response surface methodology. 259. <https://doi.org/10.1016/j.conbuildmat.2020.119776>
24. Huang W, Wang H (2022) Multi-aspect engineering properties and sustainability impacts of geopolymer pervious concrete. *Compos Part B* 242:110035. <https://doi.org/10.1016/j.compositesb.2022.110035>
25. Tahiri I, Dangla P, Vandamme M, Huy Q (2022) Cement and concrete research numerical investigation of salt-frost damage of pervious concrete at the scale of a few aggregates. *Cem Concr Res* 162:106971. <https://doi.org/10.1016/j.cemconres.2022.106971>
26. Dutra P et al. (2022) Performance evaluation of pervious concrete pavements with recycled concrete aggregate. vol 315, no. September 2021. <https://doi.org/10.1016/j.conbuildmat.2021.125384>
27. Zaetang Y, Sata V, Wongs A, Chindaprasirt P (2016) Properties of pervious concrete containing recycled concrete block aggregate and recycled concrete aggregate. *Constr Build Mater* 111:15–21. <https://doi.org/10.1016/j.conbuildmat.2016.02.060>
28. Seifeddine K, Amziane S, Toussaint E (2022) Thermal behavior of pervious concrete in dry conditions. *Constr Build Mater* 345:128300. <https://doi.org/10.1016/j.conbuildmat.2022.128300>
29. Afa T, Author T, By-nc-nd CC (2021) Case studies in construction materials. 14. <https://doi.org/10.1016/j.cscm.2021.e00502>
30. Khankhaje E, Razman M, Mirza J, Warid M (2017) Properties of quiet pervious concrete containing oil palm kernel shell and cockleshell. *Appl Acoust* 122:113–120. <https://doi.org/10.1016/j.apacoust.2017.02.014>
31. Khankhaje E, Razman M, Mirza J, Warid M, Rafieizonooz M (2016) Properties of sustainable lightweight pervious concrete containing oil palm kernel shell as coarse aggregate. *Constr Build Mater* 126:1054–1065. <https://doi.org/10.1016/j.conbuildmat.2016.09.010>
32. Öz HÖ (2018) Properties of pervious concretes partially incorporating acidic pumice as coarse aggregate. 166:601–609. <https://doi.org/10.1016/j.conbuildmat.2018.02.010>
33. Zhang G, Wang S, Wang B, Zhao Y, Kang M, Wang P (2020) Properties of pervious concrete with steel slag as aggregates and different mineral admixtures as binders. *Constr Build Mater* 257:119543. <https://doi.org/10.1016/j.conbuildmat.2020.119543>
34. El-hassan H, Kianmehr P, Zouaoui S (2019) Properties of pervious concrete incorporating recycled concrete aggregates and slag. *Constr Build Mater* 212:164–175. <https://doi.org/10.1016/j.conbuildmat.2019.03.325>

Microstructural and Plastic Shrinkage Studies on M-Sand and Coconut Shell Used Self-Compacting Concrete



S. Prasanth, S. Prakash Chandar, and K. Gunasekaran

1 Introduction

Concrete is a manmade substance of cement, aggregates, and water bonded together as a single material. After water, concrete is the second most widely used material in the world. It is also the most often used building material globally [1]. Due to its versatility and durability, self-compacting concrete (SCC), which came after concrete, became more popular. Since this concrete is so easily flowable, complete compaction can be achieved without the use of vibration. It has a number of advantages, including low labor costs, reduced noise pollution, quick casting times, well-finished surfaces, design flexibility, simple placement in out-of-reach places, and a uniform concrete matrix free of honeycombing [2]. SCC is, therefore, highly sought in the heavy construction sector. Ecological imbalance results from the diminution of natural resources brought on by using natural aggregates [3, 4]. As a result, in an effort to protect the environment, people are using a variety of aggregates made from waste generated by various domestic, industrial, and agricultural sources. Coconut shell (CS) is the agricultural wastes utilized as coarse aggregate in the making of concrete [5]. In addition, people are looking for alternatives for river sand since it is not widely accessible everywhere in the world. One of the materials used as a substitute for river sand by many studies is M-sand [6, 7]. According to the literature, M-sand has been used very rarely used in the production of SCC. This study recommended using M-sand as the fine aggregate and CS as the coarse aggregate when making concrete. Volume changes in fresh concrete are common. One of the most detrimental characteristics of concrete that affect its durability is the occurrence of volume change. The volume deviation in concrete leads to cracks formation of surface of the concrete. The volume modification brought on by concrete innate

S. Prasanth (✉) · S. Prakash Chandar · K. Gunasekaran
Department of Civil Engineering, Faculty of Engineering and Technology, SRM Institute of Science and Technology, Kattankulathur, Tamil Nadu 603203, India
e-mail: ps8471@srmist.edu.in

characteristics is called plastic shrinkage. The presence of cracks in concrete is one of the least appealing flaws. One significant factor that contributes to concrete cracking is contraction. Manufacturing concrete that does not shrink and crack is challenging. The only factors that must be considered are quantity, the width of crack, and length of crack propagation. This study evaluated the plastic shrinkage behavior and microstructural properties of SCC manufactured with a combination of CS and M-sand.

2 Materials Used

53 grade ordinary Portland cement was utilized according to Indian Standard 12,269:2013 [8]. The coarse aggregate of size 10 mm and fine aggregate of less than 4.75 mm were used. River sand and M-sand confirmed to zone-III grade according to IS 383:2016[9]. Figure 1 shows the M-sand sample. A superplasticizer, Conplast SP430 was used as a water-reducing admixture in accordance with IS 9103:1999 [10]. In this investigation, the coarse aggregate was replaced with waste CS gathered from a local market. The raw CS was crushed to the desired size using a coconut shell crusher machine located in SRMIST. The crushed CS is shown in Fig. 2.

2.1 Mix Proportion

For this investigation, three SCC mixes were prepared according on the already designed mix proportion by the earlier study [11]. Table 1 displays the mix proportion of three SCC mixes. In the case of SCCSCM, M-sand was used as a replacement for 25, 50, 75, and 100% of the river sand.

Fig. 1 M-sand sample



Fig. 2 Crushed coconut shell**Table 1** Mix proportion

Mix	Proportion	Cement content (kg/m ³)	Water–cement ratio
SCCC	1:2.22:3.66	320	0.55
SCCSC	1:1.47:0.65	510	0.42
SCCSCM	1:1.60:0.65	510	0.42

3 Experimental Investigation

The following experiments examined the SCCSC, including workability, plastic shrinkage, and microstructural study.

3.1 Workability Test

The slump flow, T500, and V-funnel experiment were used to study the filling capacity behavior of all compounds in accordance with the standard set by EFNARC (2005) [12]. The L-box experiment was performed to determine the SCC ability of passing through reinforcement bars. The slump flow is divided into three categories such as SF1, SF2, and SF3, by EFNARC 2005. According to the designations SF1, SF2, and SF3, the slump flow ranges are 550–650 mm, 660–750 mm, and 760–850 mm, respectively. The passing ability is divided into two categories: PA1 and PA2. PA1 stands for 0.8 with two rebars, while PA2 stands for 0.8 with three rebars. The GTM screen stability test was performed to measure SCC stability. According to EFNARC 2005 guidelines, a segregation ratio between 5 and 15% of the sample weight is satisfactory.

Fig. 3 Screeding



Fig. 4 Bull float application



Fig. 5 Trowelling



Fig. 6 Air circulation through fan



Fig. 7 Plastic shrinkage crack

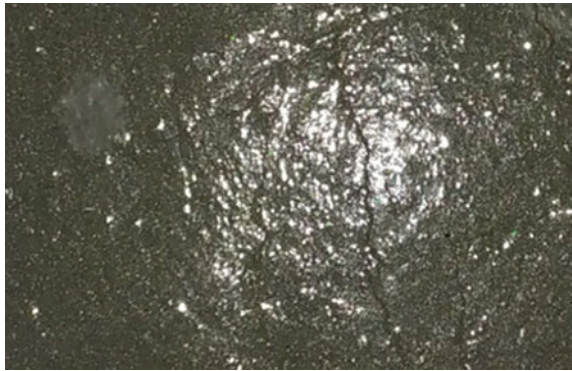


Fig. 8 Crack length measurement



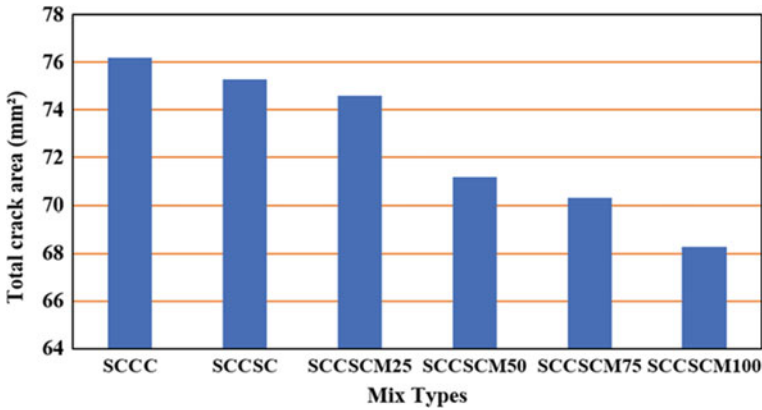


Fig. 9 Plastic shrinkage crack test result

3.2 Plastic Shrinkage

The plastic shrinkage test was carried out on a slab of size $533 \times 838 \times 40$ mm suggested by the previous study [13–15]. The required size of slab mold was cast with fresh-state concrete with proper tamping to expel the air voids in the fresh concrete. After that, aluminum straight-edge floating was used to remove the air voids in the concrete; this method was applied to the surface of the slabs to ensure that the water bleeding had vanished entirely. Bull floating and trowelling was used to make a smooth and dense surface, which helps to spot elimination on the slab surface. It was observed that the atmospheric temperature ranged between $27^{\circ} + 2^{\circ}\text{C}$ and $27^{\circ} - 2^{\circ}\text{C}$, with the relative humidity ranging between 42 and 88%, during the experiment. The cast slab is exposed to atmospheric conditions, which helps to evaporate excess accumulated surface water. Air circulation was done with the help of a pedestal fan. The fan was turned off and removed when the complete air circulation was done. The width of the plastic shrinkage crack was observed using a handheld microscope with an ocular magnification of $40\times$ and a sensitivity of 0.01 mm. Then, the length of the shrinkage crack was observed with the help of scale and thread. This procedure was done as many cracks formed in the slab as possible. The average crack width was multiplied by its length; the average crack area was observed. The crack measurement procedures are displayed (Figs. 3, 4, 5, 6, 7, 8, 9).

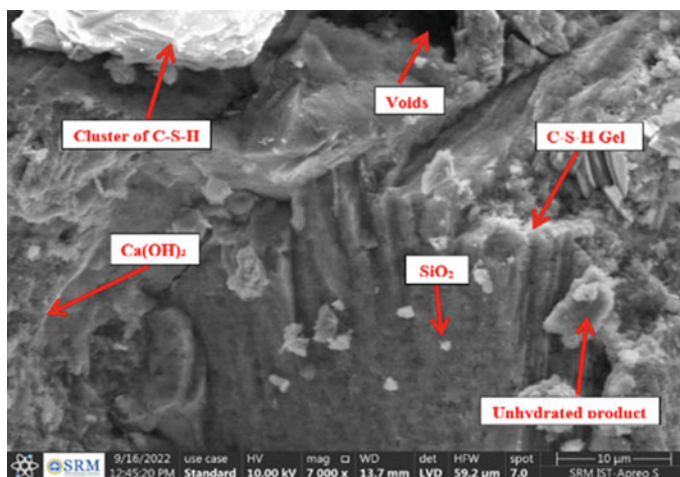


Fig. 10 SEM image of SCCC

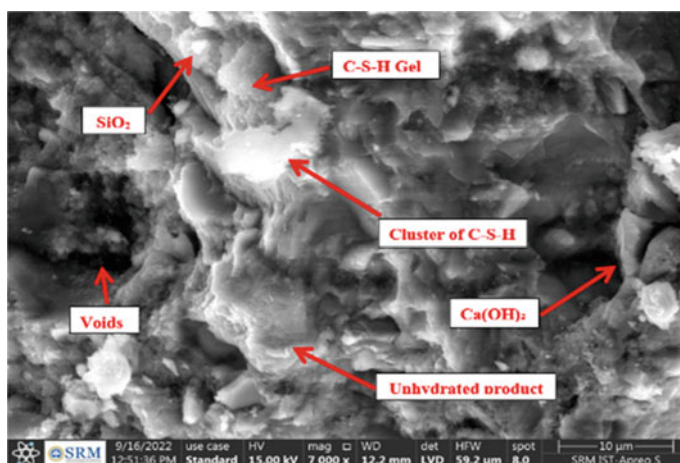


Fig. 11 SEM image of SCCSC

4 Results and Discussion

4.1 Slump Flow

The test findings of slump flow for all the mix proportions are displayed in Table 2. The slump flow diameter for all the mixes ranged between 702 and 748 mm. As per EFNARC guidelines, these slump flow values satisfied the SCC flow requirements and fall under SF2 slump flow class (660–750 mm). The maximum flowing ability

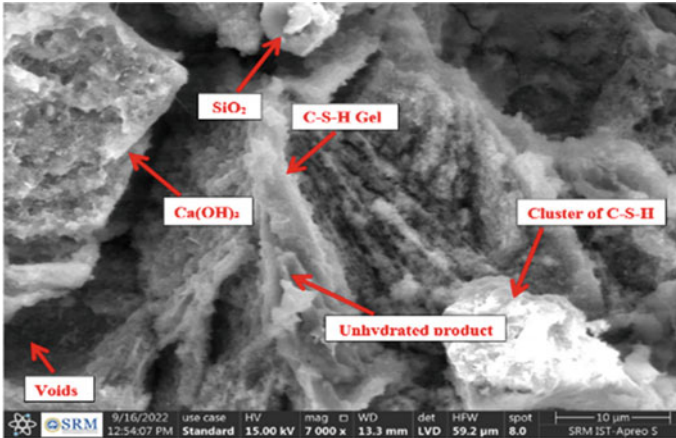


Fig. 12 SEM image of SCCSCM25

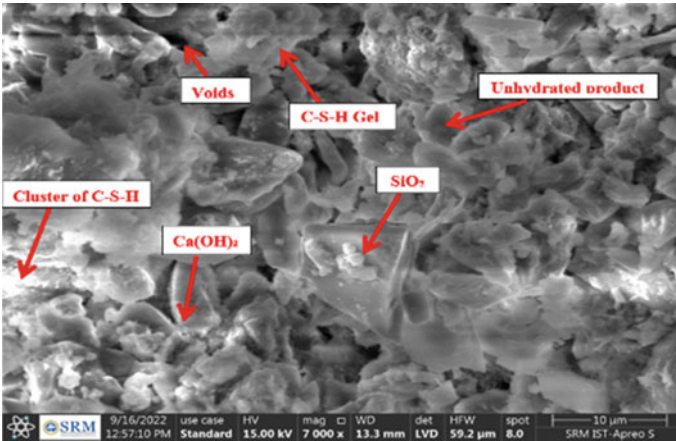


Fig. 13 SEM image of SCCSCM50

of the slump was achieved for the mix SCCSCM100. This enhancement of flow properties happened due to replacing of M-sand and the use of superplasticizer (SP) in SCCSC.

4.2 T500 Test

The T500 time experiment was also performed to evaluate the filling ability of SCC. The test outcomes of SCCSC with varying combinations of M-sand are depicted in

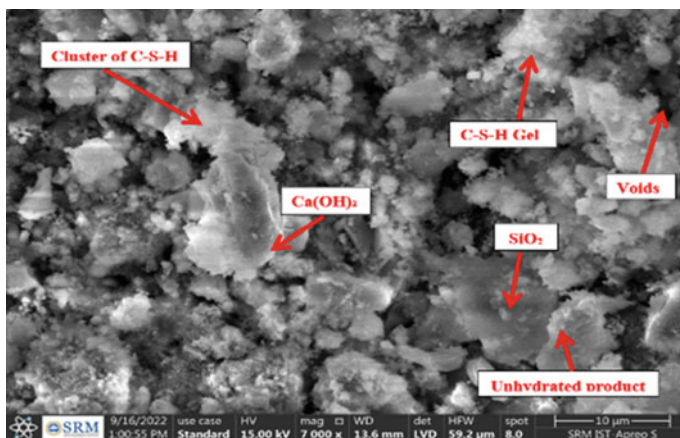


Fig. 14 SEM image of SCCSCM75

Fig. 15 SEM image of SCCSCM100

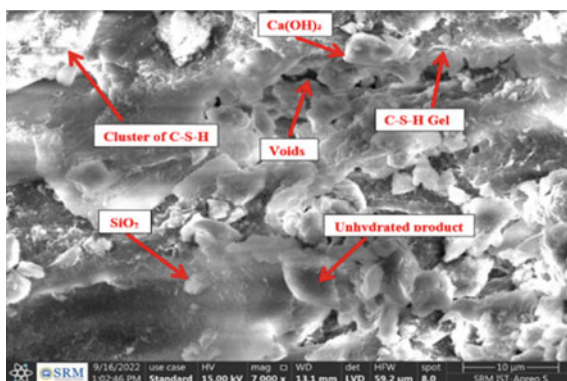


Table 2 Rheological properties of different mixes used

Mix ID	Slump flow (mm)	T-500 (sec)	V-funnel (sec)	PA	SR (%)	Fresh concrete density (kg/m ³)
SCCC	702	6.45	9.82	0.93	5.58	2440
SCCSC	715	4.59	8.64	0.95	3.36	2070
SCCSCM25	721	4.77	8.41	0.87	3.52	2080
SCCSCM50	729	4.73	8.29	0.88	3.55	2090
SCCSCM75	732	4.81	8.17	0.94	3.76	2095
SCCSCM100	748	4.92	8.93	0.96	3.92	2105

Table 2. The T500 time flow of all the compound ranged from 6.45 s to 4.92 s which falls under VS2 class according to EFNARC. The replacement of M-sand in SCCSC increased the flow diameter steadily.

4.3 V-Funnel Test

V-funnel experiment also identifies the viscosity and filling capacity of the SCC. Table 2 shows the V-funnel test outcomes. According to EFNARC guidelines, the V-funnel time of all mixtures was within the VS2 class (8–12 s) which satisfied the flow requirements of SCC. The mix SCCSCM 100 exhibits deferred flow time when compared to SCCSC mixes. It is possible that this is due to the SP dosage and the addition of M-sand to composite, both of which rise the flowability of SCC.

4.4 L-Box Test

The L-box experiment evaluated the passing capacity of all the mixes. Table 2 presents the experiment outcomes of all the mixes. EFNARC guidelines recommend that the ability to pass value be equal to or greater than 0.8 to ensure that the SCC will not be blocked during the placement process. The L-box passing capacity outcomes for all mixes varied from 0.88 to 0.96, which is fell within the limits. The test findings indicated that the mix SCCSCM100 achieved more viscous at higher levels of M-sand substitution.

4.5 GTM Screen Stability Test

The GTM screen stability experiment was employed to assess the mixture stability. Table 2 shows the test findings of all the mixes. The outcome demonstrated 100% M-sand replacement enhanced the stability and segregation resistance (less than 15%) of all the mixes. The developed mixes can be concluded from all of these that they satisfy and confirm the requirements of say, SCC.

4.6 Plastic Shrinkage

The plastic shrinkage experiment was performed to observe the width, length of the crack, area of the crack, and the number of cracks and crack area percentage. The experimental test results of all the mixes blended with various proportions of M-sand replacement were displayed in Table 3 and depicted in Fig. 9. The formation of cracks

Table 3 Plastic shrinkage test

Mix types	Number of cracks	Crack width (mm)		Crack length (mm)		Total crack area (mm ²)	% Crack area in terms of R-sand
		Minimum	Maximum	Minimum	Maximum		
SCCC	10	0.1	0.7	15	46	76.20	100
SCCSC	9	0.1	0.8	20	52	75.3	98.81
SCCSCM25	10	0.1	0.9	17	48	74.60	97.9
SCCSCM50	8	0.1	0.7	18	50	71.17	93.3
SCCSCM75	9	0.1	0.7	15	50	70.30	92.2
SCCSCM100	7	0.1	0.5	14	46	68.27	89.5

number and crack area identified in SCCSCM 100 was 7 and 68.27 mm², which is 22.22 and 9.34% lower than SCCSC. According to test results, 100% replacement of M-sand instead of natural sand and 100% replacement of CS in place of conventional coarse aggregate reduced the total shrinkage crack area. It has been observed that the CS fibrous nature was controlled and prevented the development of shrinkage cracks. The same declining trend was followed in previous studies [13–15].

4.7 Scanning Electron Microscope (SEM) Analysis

The SEM picture of all the mixture blended with various combinations of M-sand is displayed in Figs. 10, 11, 12, 13, 14 and 15. The internal microstructure of all the mixes was analyzed and compared with SCCSC. The captured SEM images visualized the formation and distribution of hydration products of the mix. The SEM images visualized the development of calcium silica hydrated (C–S–H) gel, portlandite (Ca (OH)₂), quartz (SiO₂), and ettringite. When M-sand is used as a 100% substitution for natural sand in concrete production, SEM images demonstrate that the hydration products are consistently finer and more quietly packed, resulting in denser concrete with greater strength. These formations of elements were one of the reasons for the strength performance of the mix. The incorporation of M-sand in place of river sand has enhanced strength and altered the distribution of minerals.

4.8 X-Ray Diffraction (XRD)

The XRD analysis of all the mixes with various combinations of M-sand in SCCSC is shown in Figs. 16, 17, 18, 19, 20 and 21. The XRD patterns analysis was taken

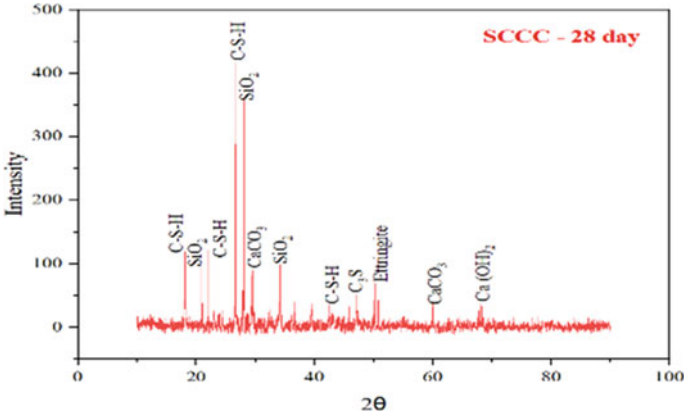


Fig. 16 XRD image of SCCC

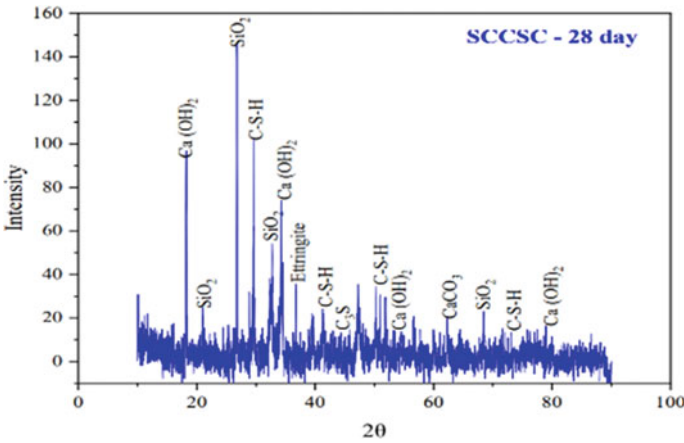


Fig. 17 XRD image of SCCSC

to detect the crystalline phase of the mixture. The crystalline phases identified in the mixes are calcium silica hydrated (C–S–H) gel, quartz (SiO₂), portlandite (Ca (OH)₂), calcite (CaCO₃), and ettringite. The C–S–Hand SiO₂ are the major crystalline phases in all the mixtures.

5 Conclusions

This study examined the effects of M-sand on self-compacting concrete. Based on the findings of the study, it is possible to draw the following specific conclusions:

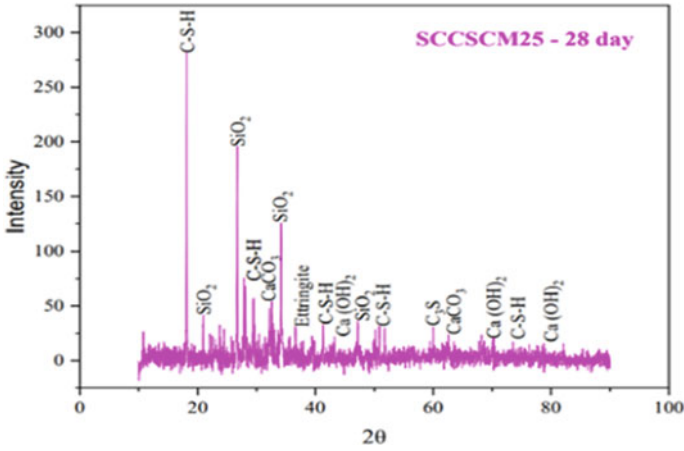


Fig. 18 XRD image of SCCSCM25

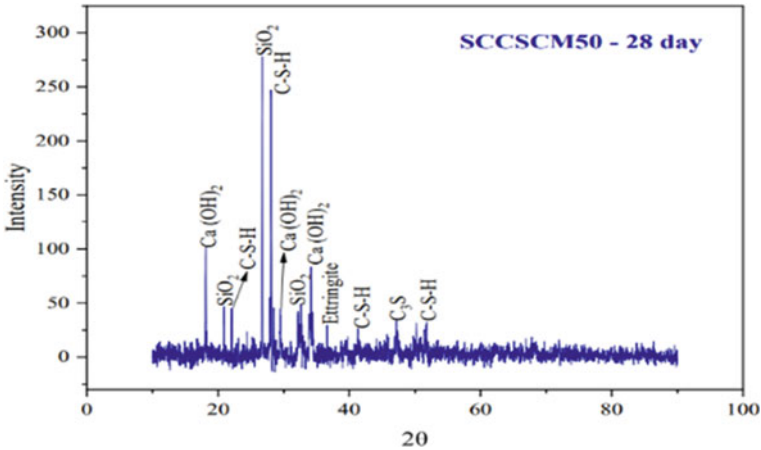


Fig. 19 XRD image of SCCSCM50

1. Using coconut shell and M-sand with superplasticizer in SCC enhances the rheological properties significantly when the replacement rate increases.
2. According to the results of the plastic shrinkage tests, the overall crack area decreases as the proportion of M-sand raises. It can be advised to substitute M-sand for river sand to lower the plastic shrinkage crack area compared to conventional concrete because the usage of M-sand in SCCSC reduces shrinkage overall.
3. The SEM micrograph confirms that CS and M-sand impact the microstructure of mixes, which visualizes the formation of hydration products. Adding M-sand improves the integrity of SCC mixes by densifying the pore structure.

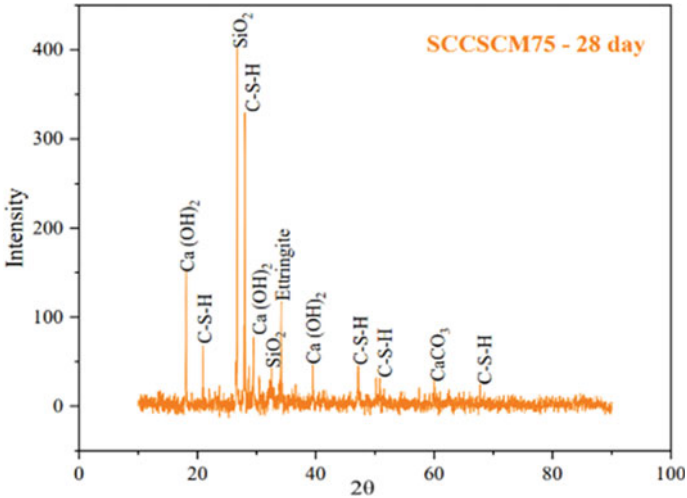


Fig. 20 XRD image of SCCSCM75

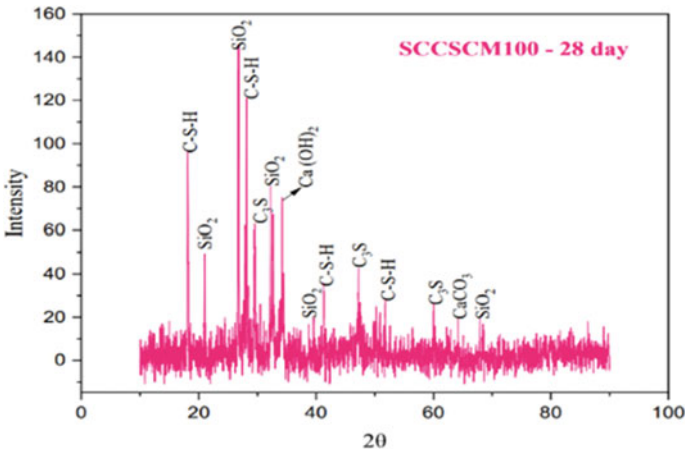


Fig. 21 XRD image of SCCSCM100

4. XRD phase analysis pattern identifies the crystalline phases formed in SCC mixes. Calcium silica hydrated (C-S-H) gel, quartz (SiO₂) is the prominent peak identified in all the mixes.

Further investigations are being conducted to evaluate its durability and structural element behavior for its appropriateness in practical implementations.

References

1. Dey S, Kumar VVP, Goud KR, Basha SKJ (2021) State of art review on self-compacting concrete using mineral admixtures. *J Build Pathol Rehab* 6:1–23. <https://doi.org/10.1007/s41024-021-00110-9>
2. Palanisamy C, Velusamy S, Krishnaswami N, Manickam K, Rathinasamy L, Anna malai I (2022) Experimental investigation on self-compacting concrete with waste marble and granite as fine aggregate. *Mater Today Proc* 65:1900–1907. <https://doi.org/10.1016/j.matpr.2022.05.159>
3. Jiang Y, Zhang S (2022) Experimental and analytical study on the mechanical properties of rubberized self-compacting concrete. *Constr Build Mater* 329:127177. <https://doi.org/10.1016/j.conbuildmat.2022.127177>
4. Meena RV, Jain JK, Beniwal AS, Chouhan HS (2022) Sustainable self-compacting concrete containing waste ceramic tile aggregates: fresh, mechanical, durability, and microstructural properties. *J Build Eng* 57:104941. <https://doi.org/10.1016/j.jobe.2022.104941>
5. Bari H, Salam MA, Safiuddin M (2021) Fresh and hardened properties of brick aggregate concrete including coconut shell as a partial replacement of coarse aggregate. *Constr Build Mater* 297:123745. <https://doi.org/10.1016/j.conbuildmat.2021.123745>
6. Gokulnath V, Ramesh B, Raghuraman R (2020) Study on the effect of M-sand in self-compacting concrete with addition of steel fibers. *Mater Today Proc* 22:843–846. <https://doi.org/10.1016/j.matpr.2019.11.029>
7. Suriya D, Chandar SP, Ravichandran PT (2023) Impact of M-sand on rheological, mechanical, and microstructural properties of self-compacting concrete
8. IS-12269: (2013) Ordinary portland cement, 53 grade—Specification, Bureau of Indian Standards, New Delhi, pp 17
9. IS383 (2016) Coarse and fine aggregate for concrete, Indian Standard Code. Third edit, pp 1–17
10. IS 9103 (1999) Specification for Concrete Admixtures, Bureau of Indian Standards, New Dehli, pp 1–22
11. Ramasubramani R, Gunasekaran K (2022) Sustainable replacement materials for concrete production from renewable resources and waste on interfacial bond properties, innovative infrastructure. *Solutions* 7:1–9. <https://doi.org/10.1007/s41062-022-00869>
12. EFNARC (2005) The European guidelines for self-compacting concrete. vol 63. <http://www.efnarc.org/pdf/SCCGuidelinesMay2005.pdf>
13. Gunasekaran K, Annadurai R, Kumar PS (2013) Plastic shrinkage and deflection characteristics of coconut shell concrete slab. *Constr Build Mater* 43:203–207. <https://doi.org/10.1016/j.conbuildmat.2013.02.019>
14. Ramasubramani R, Gunasekaran K (2022) Study on plastic shrinkage of coconut shell concrete slab made with M-sand, innovative infrastructure. *Solutions* 7:1–8. <https://doi.org/10.1007/s41062-021-00614-w>
15. Prakash Chandar S, Gunasekaran K (2019) Study on the effect of quarry dust on plastic shrinkage in concrete slab made with the waste coconut shell as aggregate. *J Green Eng* 9:282–290

Hybrid Testing Approach for Thermo-Mechanical Testing of Structures Using Impedance Matching



T. Jay Vishnu, E. Vinothini, M. S. Aditya, and Mohit Verma

1 Introduction

With the advancement in the performance-design methodologies, architects are coming with the structures with unique design and functionalities. The current trends demand these structures to be resilient with respect to the fire hazard, while fulfilling the performance objectives. There is a need for a method that can emulate more realistic hazard conditions for demonstrating the safety and compliance of the structure with the target performance objectives. This will help the engineering community to take necessary actions to prevent the collapse of the structure at the time of hazard. The numerical models capable of capturing the behavior of the structure at an elevated temperature will help in the devising appropriate measures to ensure the safety of the structure. However, these models will still need validation with the experimental data for different building materials and structural systems. The cost associated with the experiments to capture the behavior of full-scale structure at elevated temperature is huge. The testing procedure that is widely used to study the behavior of a structure at an elevated temperature is standard heat resistance testing. These tests are mostly carried out on a single element of the building like a beam or a column subjected to standard heat loading prescribed by ASTM E119 [1]. The major drawback of this testing method is that it does not consider the interaction of the test specimen with the surrounding environment [2, 3]. Conventionally, passive boundary conditions like (pinned, roller, hinged, etc.) are provided to represent idealized thermal restraints during the test. However, these restraints are not able to adapt according to the dynamics of the surrounding structure during testing. Also, the standard fire curve does not represent the actual representation of the thermal loading that a structure is subjected to in case of fire. It fails to account for the various factors like type of fuel, its availability, ventilation in the building, etc.

T. J. Vishnu · E. Vinothini · M. S. Aditya · M. Verma (✉)
CSIR-Structural Engineering Research Centre, Taramani, Chennai 600 113, India
e-mail: mohitverma@serc.res.in

The standard testing procedure does not provide understanding of the structural behavior when only a part of the structure is subjected to elevated temperature.

A more realistic representation of the interactions between the test element and the surrounding structure can be achieved by utilizing end restraints that are able to adapt during the test [4, 5]. In this study, the concept of hybrid simulation is extended to thermo-mechanical testing of coaxial bar using active boundary condition. The active boundary condition during testing at elevated temperature is emulated using hybrid testing, as shown in Fig. 1. The complex (physical substructure, PS) part of structure is tested physically. The remaining part is numerically modeled as virtual substructure (VS). The dynamics interactions at the interface of two substructures is emulated using actuators. The actuators are operated in a feedback control loop acts and provide the active boundary condition at the interface of the test specimen. In this paper, the controls for the actuator are designed using impedance matching [6, 7]. Hybrid testing circumvents the need of idealized spring system and other passive boundary condition that were conventionally adopted.

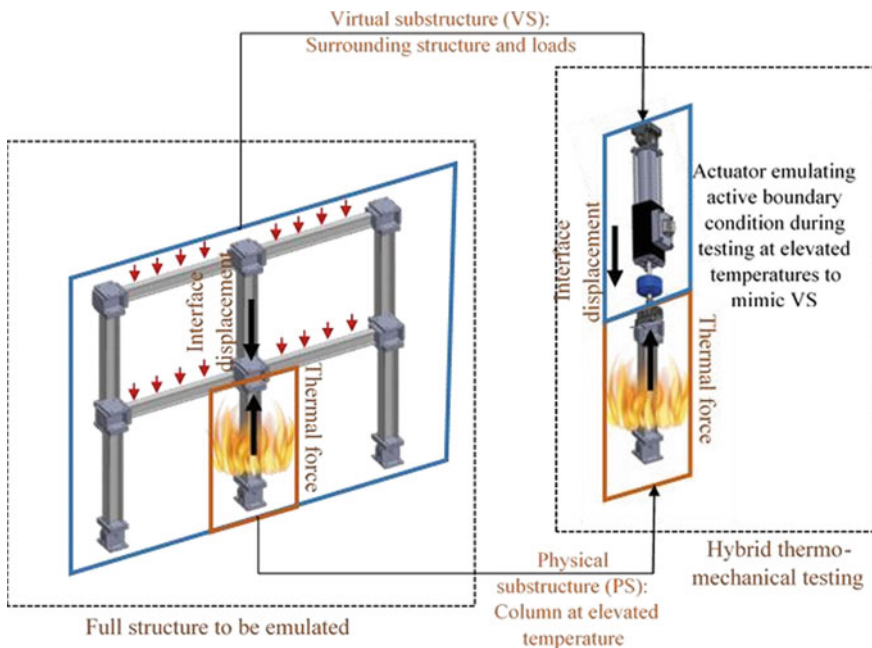


Fig. 1 Schematics of hybrid thermo-mechanical testing of structures

2 Impedance Matching Control Design

Control design for hybrid testing has been a subject of extensive research. The approach that will be adopted is fundamentally different from most techniques presented in the literature and builds on our recent work on impedance matching [8, 9]. The key distinguishing aspects of our approach are that we view control design as a problem of matching the input–output impedances of the actuator with those of the VS. The concept is illustrated in Fig. 2. The control design is decoupled from the dynamics of the PS. This is clear from the fact that the PS does not appear in Fig. 2. Thus, knowledge of PS behavior at elevated temperature is not necessary for control design. This simplifies design of the controller. This is a feedforward strategy. The control components such as delay compensator of conventional approaches do not appear explicitly.

The block diagram for impedance matching is shown in Fig. 3. Impedance matching involves making the shaker behave exactly like a VS. Advantage of this approach is that the control design is independent of PS characteristics. In this case, VS has an input force f , due to thermal effects of PS for which there is a displacement d_V . TS is a controller with electromagnetic shaker as an actuator which gives an output d_T for the same input f . The controller is designed such that the force input from the controller, u , along with the force from PS will result in displacement of shaker to the same value as that of PS. The simplest method of control design is to equate the impedances of VS and TS. The transfer function of controller is then found algebraically using the following equations

$$d_V - d_T = 0 \tag{1}$$

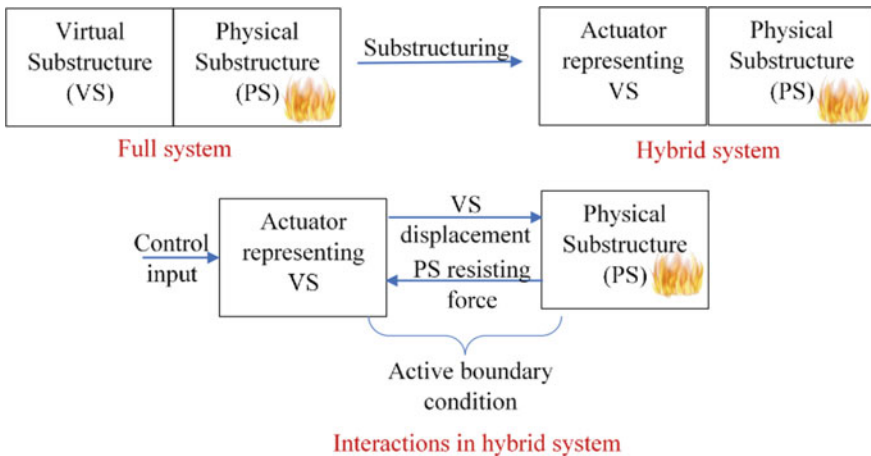


Fig. 2 Conceptual diagram of impedance matching for hybrid thermo-mechanical testing

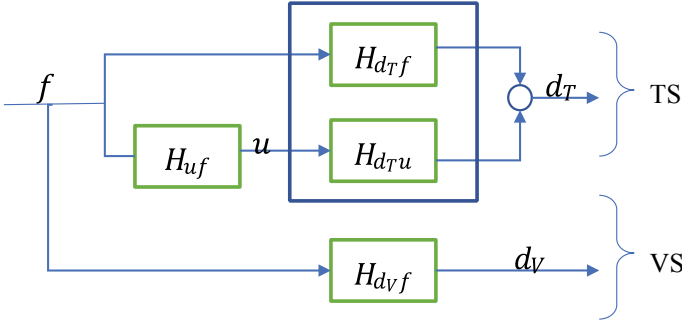


Fig. 3 Block diagram for impedance matching

$$H_{d_v f} \cdot f - (H_{d_r f} \cdot f + H_{d_r u} \cdot u) = 0 \quad (2)$$

$$H_{d_v f} \cdot f = H_{d_r f} \cdot f + H_{d_r u} \cdot H_{u f} \cdot f \quad (3)$$

$$H_{u f} = (H_{d_v f} - H_{d_r f}) \cdot H_{d_r u}^{-1} \quad (4)$$

where the variables and transfer functions are defined in Fig. 3.

3 Transfer System (TS) Dynamics

In hybrid testing, VS is realized physically through the actuators by enabling the transfer of desired output at the interface active boundary to PS. The dynamics of the TS can be studied and incorporated in control design to achieve accurate matching of impedances. In the present study, an electromagnetic shaker is used as a TS. Inside the shaker is a coil that conducts current and is held in a magnetic field. The electromagnetic force F produced by this coil will vary depending on the input current. The presence of the moving coil will also cause the circuit to experience a back electromotive force E_b .

$$F = (Bl)x_c \quad (5)$$

$$E_b = -Bl\dot{x}_a \quad (6)$$

B is the magnetic field intensity, l is the length of the coil, x_c is the current, \dot{x}_a and \ddot{x}_a are the displacement and velocity of the armature. The voltage drop, I , across the armature of the shaker is

$$I = Ri + L\left(\frac{di}{dt}\right) \quad (7)$$

where R is resistance, inductance is L , and rate of change of current is $\frac{di}{dt}$. Using Kirchoff's voltage rule,

$$G_v u + Bl\dot{x}_a = Rx_c + L\dot{x}_c \quad (8)$$

where G_v is the amplifier gain, and u is the control input. The dynamic equilibrium of the shaker can be written as

$$m_a\ddot{x}_a + c_a\dot{x}_a + k_a x_a = Blx_c \quad (9)$$

where m_a , c_a and k_a are the mass, damping, and stiffness of the shaker, respectively. The state space equations of the shaker are given by

$$\begin{bmatrix} \dot{x}_1 \\ \dot{x}_2 \\ \dot{x}_3 \end{bmatrix} = \begin{bmatrix} 0 & 1 & 0 \\ -k_a/m_a & -c_a/m_a & -Bl/m_a \\ 0 & -Bl/L & -R/L \end{bmatrix} \cdot \begin{bmatrix} x_1 \\ x_2 \\ x_3 \end{bmatrix} + \begin{bmatrix} 0 \\ 0 \\ \frac{G_v}{L} \end{bmatrix} u \quad (10)$$

where

$$[x_1, x_2, x_3]' = [x_a, \dot{x}_a, x_c]'$$

4 Application to Coaxial bar

The system to be emulated consists of two coaxial bars restrained at both the ends. It is assumed that one of the bars is subjected to heating, and there no heat transfers between the two bars. A part of coaxial bar which is subjected to thermal loading is taken as PS. An aluminum bar specimen is adopted as PS. The VS is remaining part of coaxial bar, which is a cantilever bar of same size and material as that of PS. The structural partitioning of the system considered is shown in Fig. 4. The VS dynamics are modeled as a single degree of freedom system. During hybrid testing, the dynamics of the VS are mimicked by the electromagnetic shaker.

The properties of the VS and TS are given in Table 1. Based on these properties, the transfer functions shown in Fig. 3 are evaluated as

$$H_{d\tau f} = \frac{0.055866(s + 63.56)}{(s + 40.25)(s + 24.06)(s + 0.6416)} \quad (11)$$

$$H_{d\tau u} = \frac{-185.78}{(s + 40.25)(s + 24.06)(s + 0.6416)} \quad (12)$$

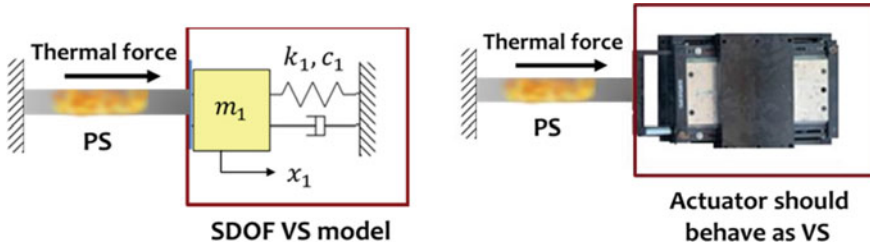


Fig. 4 Pictorial representation of structural partitioning

Table 1 Properties of the VS and the TS adopted in the present study

System	Parameter	Properties
VS	m_1	0.3052 kg
	k_1	1200 N/m
	c_1	0.7671 Ns/m
TS	m_a	17.9 kg
	k_a	175 N/m
	c_a	25 Ns/m
	R	1.5 Ω
	L	0.0236 H
	G_v	4
	Bl	19.62 N/A

$$H_{dvf} = \frac{3.2765}{(s^2 + 2.513s + 3948)} \tag{13}$$

The controller for the hybrid thermo-mechanical testing is evaluated using equation (4) and is given by

$$H_{uf} = \frac{-0.017336(s - 3.174)(s^2 + 68.11s + 1172)}{(s^2 + 2.513s + 3948)} \tag{14}$$

The above controller is non causal and cannot be directly implemented. Therefore, a low-pass filter is added for causal implementation of the evaluated controller (refer [6, 7] for more details). The comparison of the VS dynamics with that of TS with designed controller is shown in Fig. 5. It is found that TS with the designed controller is able to mimic the dynamics of the VS. The designed controller is found to result in stable and accurate representation of the VS dynamics.

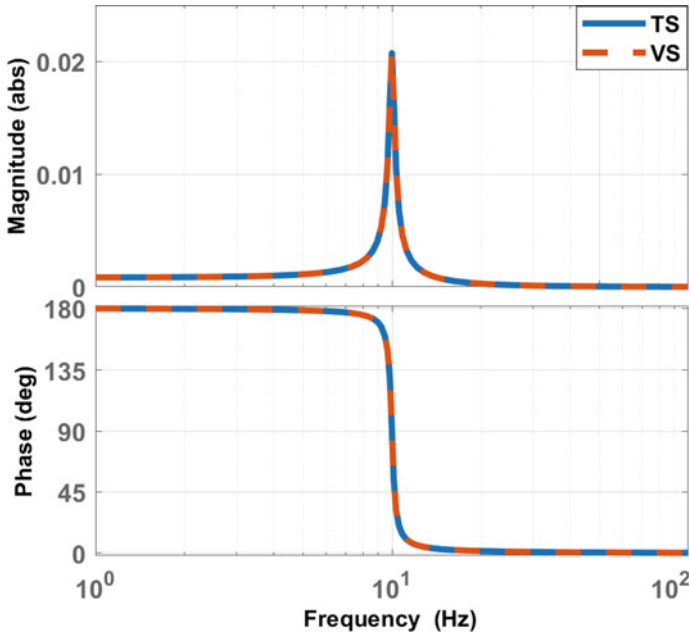


Fig. 5 Comparison of the frequency response of the VS and TS with designed controller

5 Concluding Remarks

Hybrid thermo-mechanical testing provides a cost-effective alternative to full-scale testing structures subjected to elevated temperature. This method captures realistic failure modes of the structure by accounting for its dynamic interaction with the surrounding structure throughout the duration of the test. In this study, impedance matching control design is adopted to ensure that the TS mimics the dynamic behavior of the VS. It is found that TS with the designed controller is able to replicate the dynamics of the VS. Thus, the designed controller is found to result in accurate and stable hybrid testing. The methodology can be extended for studying the thermal vibrations in a space telescope, thermal effects in automotive systems, and even for fire testing of civil structures.

Acknowledgements The project is implemented under CSIR-Fundamental and Innovative Research for Science of Tomorrow (CSIR-FIRST) scheme. Authors acknowledge the funding support from CSIR. The help and support provided by the staff of ASTaR is greatly appreciated.

References

1. ASTM (2019) ASTM E119–16a: standard test methods for fire tests of building construction and materials
2. Grosshandler W (2002) NISTIR 6890–fire resistance determination and performance prediction research needs workshop
3. Gernay T, Gamba A (2018) Progressive collapse triggered by fire induced column loss: detrimental effect of thermal forces. *Eng Struct* 172:483–496
4. Qureshi RK (2021) Evaluation of steel columns under fire: real-time hybrid testing and reliability assessment (Doctoral dissertation, State University of New York at Buffalo)
5. Qureshi RK, Elhami-Khorasani N, Gernay T (2019) Adaption of active boundary conditions in structural fire testing. *J Struct Fire Eng* 10(4):504–528
6. Stefanaki A, Sivaselvan MV (2018) A simple strategy for dynamic substructuring: I. concept and development. *Earthquake Eng Struct Dyn* 47(9):1801–1822
7. Stefanaki A (2017) A simple strategy for dynamic substructuring and its application to soil-foundation-structure interaction (Doctoral dissertation, State University of New York at Buffalo)
8. Verma M, Sivaselvan MV, Rajasankar J (2019) Impedance matching for dynamic substructuring. *Struct Control Health Monit* 26(11):e2402
9. Verma M, Sivaselvan MV (2019) Impedance matching control design for the benchmark problem in real-time hybrid simulation. *Mech Syst Signal Process* 134:106343

Study on the Effect of Marble Dust as Partial Replacement to Cement with Steel Fibre in Concrete



M. S. Yuvaraj, Manoj Kumar Sah, Shaik Kutagal Md. Jabeer, Thallika Venu Kumar, Marumani Harish, and Bibek Mishra

1 Introduction

The versatility of concrete [1] makes it the most commonly utilised building material. Generally, the concrete is a combination of cement, fine, and coarse aggregate. But, due to rapid progress in the construction sector, burden over natural aggregates has increased exponentially [2]. This results in the declination of accessibility towards natural aggregates and leads to quest for possible replacement materials [2].

As one of the most likely consumers of natural resources, the construction industry produces a large amount of solid waste as a by-product of the mineral processing industries, which has a negative impact on the environment and public health [1, 3–5]. Some studies found that “marble dust, a waste powder which is generated from the marble processing units, contains more than 50% of calcium oxide can be used as partial substitute to cement in preparation of concrete [1, 6, 7].” Also another study found that “using marble powder as replacement to cement yields agreeable benefaction to workability of fresh concrete [8].” The engineers can ensure economy in the infrastructure project and limit environmental deterioration by employing this marble dust to produce affordable and sustainable concrete [3]. The effectiveness of employing such a waste product in preserving and enhancing the strength and longevity of concrete has thus been the subject of numerous studies.

As it was evident that the concrete possess low tensile strength capacity, it can get better with addition of steel fibre [9]. Studies found that “the behaviour of concrete with steel fibre depends on the fibre length and percentage fibre addition [10].” Also, the fibre orientation in concrete will have a strong effect on its tensile characteristics [11].

M. S. Yuvaraj (✉) · M. K. Sah · S. K. Md. Jabeer · T. V. Kumar · M. Harish · B. Mishra
Department of Civil Engineering, Mohan Babu University (erstwhile Sree Vidyanikethan
Engineering College), Tirupati 517102, India
e-mail: yuvaraj.mudduluru@gmail.com

The current study’s entire operation was completed in two steps. Marble dust was employed in the first stage as a partial replacement for cement at 10, 20 and 30%. Marble dust was successfully substituted for cement at the ideal ratio. Steel fibre added at 0.5–1.5% [17] in the second stage, following the addition of the ideal amount of marble dust, and the effects on the concrete’s mechanical strength under compression, tension, and flexural were examined.

2 Experimental Study

2.1 Materials

Cement, sand, marble dust, steel fibre [12], and potable water are the materials employed in this investigation (Tables 1, 2, 3 and 4). The sand which was used in the study came from a local riverbed and was zone II-compliant. Both 10 and 20 mm-sized particles make up the coarse aggregate, which comes from a neighbouring granite quarry. The mixture was prepared using potable water.

Table 1 Properties of OPC53 [14, 15]

Property	Values
Fineness	9%
Sp. gr	3.14
Standard consistency	30%
Setting time	30 min

Table 2 Physical properties of FA

Property	Values
Fineness modulus	2.64
Sp. gr	2.65
Bulking	7.69%
Water absorption [13]	1.4%

Table 3 Physical properties of CA

Property	Values
Sp. gr	2.74
Water absorption	0.4%

Table 4 Properties of marble dust

Property	Values
Sp. gr	2.62
Bulk density (kg/m ³)	1140

Table 5 Material quantities for specimen preparation

Specimen	Size (cm)	Vol. (cm ³)	Cement (gm)	FA (gm)	CA (gm)
Cube	15 × 15 × 15	3400	1620	2170	3650
Cylinder	15 × 30	5300	2540	3400	5720
Beam	50 × 10 × 10	5000	2400	3200	5400

2.2 Mix Proportion

Using IS 10262:2009, the ratio of different constituents in the concrete mix for M35 was calculated. The ratio of 1:1.34:2.25 was achieved. For each mix, the ratio, water/cement was held constant, i.e. 0.40.

2.3 Moulding and Curing

Cube specimens of a size of 15 cm cast in order to determine strength of concrete under compressive force. For testing the split tensile strength and flexural strength of concrete, respectively, cylindrical specimens measuring 15 × 30 cm and square prism specimens measuring 50 × 10 × 10 cm were been casted (Tables 5 and 6). After casting, the specimens allowed to sit at room temperature for 24 h to set and harden. The demoulded specimens were thereafter maintained in a tank filled with potable water for curing. The specimens have been dried and evaluated after being cured for 7 and 28 days.

Table 6 Specimen terminology

Specimen	Cement (%)	Marble waste (%)	Steel fibre (%)
M0	100.00	0.00	–
M1	90.00	10.00	–
M2	80.00	20.00	–
M3	70.00	30.00	–
S0	90.00	10.00	0.00
S1	90.00	10.00	0.50
S2	90.00	10.00	1.00
S3	90.00	10.00	1.50

2.4 Specimen Testing

Analogue CTMs with a 2000 kN capacity were used to test the concrete’s strength under compressive load on specimens after 7 and 28 days, and the findings were recorded. Using an analogue UTM with a 600 kN capacity, the concrete specimen’s split tensile and flexure strengths were measured at 7 and 28 days.

3 Results and Discussions

From graph shown in Fig. 1, it was noticed that by increasing marble dust percentage as partial replacement to cement, the strength under compressive load was increased up to 10% replacement and considerable reduction in strength thereafter. Further with addition of steel fibre by keeping marble dust percentage constant at 10%, there is a significant increase in compressive strength throughout as in Fig. 2.

From graph shown in Fig. 3, it was noticed that by increasing marble dust percentage as partial replacement to cement, there was significant increase in split tensile strength up to 10% replacement of cement and reduction in strength thereafter. Further with addition of steel fibre by keeping marble dust percentage constant at 10%, there is a considerable increase in split tensile strength throughout as shown in Fig. 4.

From graph shown in Fig. 5, it was noticed that by increasing marble dust percentage as partial replacement to cement, there was significant increase in bending strength of concrete up to 10% replacement, and it reduced thereafter. Further with addition of steel fibre by keeping marble dust percentage constant at 10%, there is a considerable increase in bending strength throughout as shown in Fig. 6.

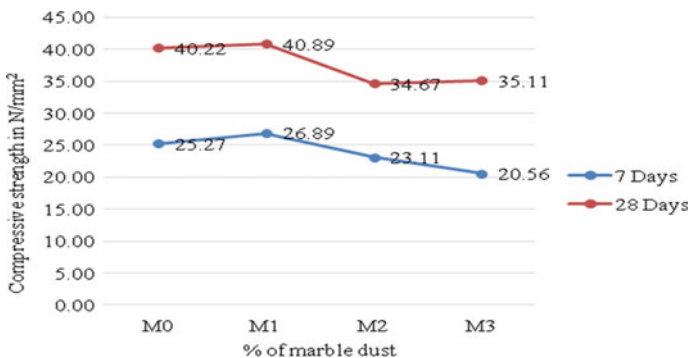


Fig. 1 Compressive strength of concrete with increasing percentage of marble dust

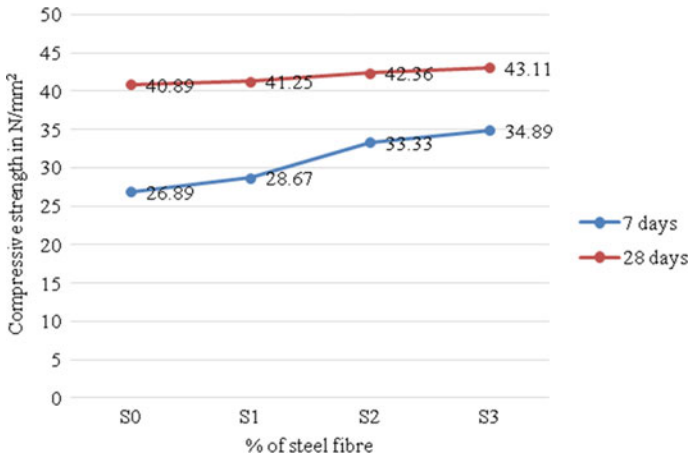


Fig. 2 Strength in compression at 10% marble dust and varying % of steel fibre

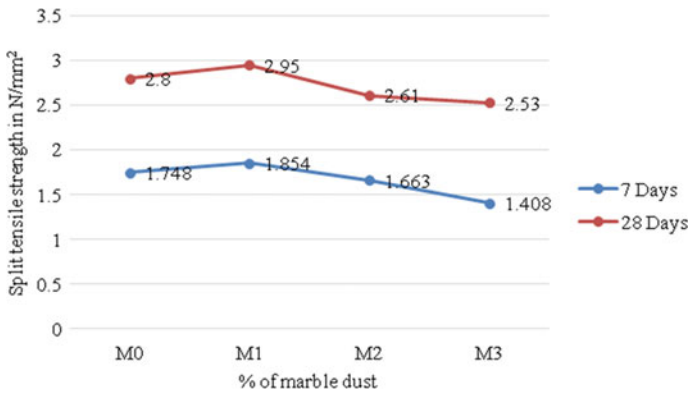


Fig. 3 Splitting tensile strength when marble dust content rises

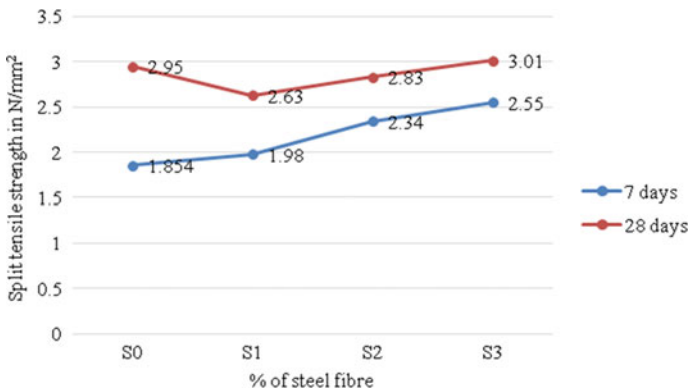


Fig. 4 Split tensile strength at 10% marble dust and varying % of steel fibre

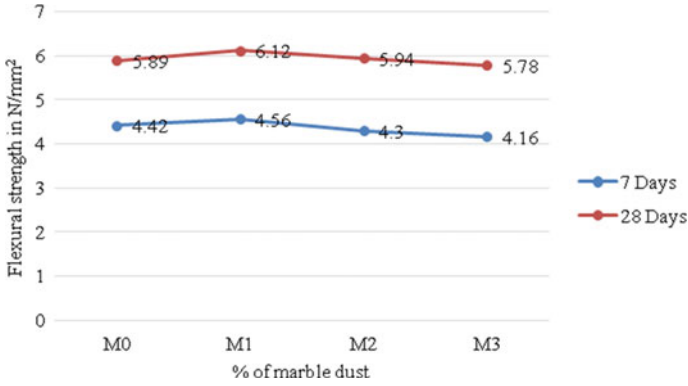


Fig. 5 Flexural strength of concrete as marble dust content increases

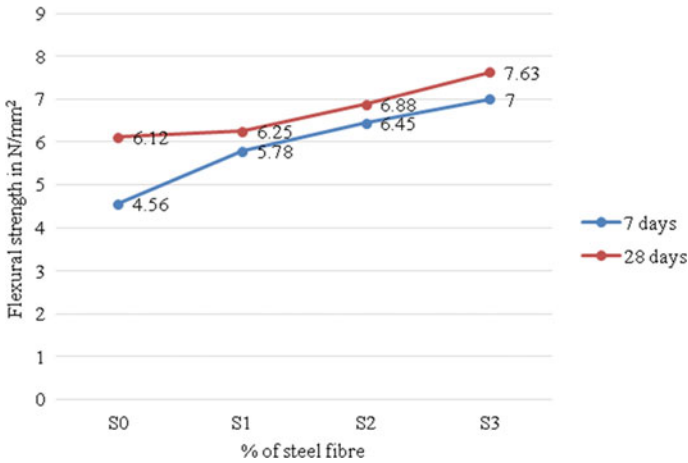


Fig. 6 Flexural strength at 10% marble dust and varying % of steel fibre

4 Conclusions

The conclusions drawn from the study are as follows:

- The value of compressive strength was at its highest (i.e. 40.89 N/mm²) when 10% of the cement was substituted with marble dust powder.
- When marble dust powder was used to replace 10% of the cement, the value of split tensile strength was at its highest (i.e. 2.95 N/mm²).
- The value of flexural strength was at its highest (i.e. 6.12 N/mm²), when cement was partially substituted with marble dust powder by 10%.

- There is a noticeable improvement in the mechanical characteristics of concrete with a 10% marble powder replacement in cement and an increase in the amount of steel fibre.
- In order to reduce environmental harm caused by waste dumping, it is therefore recommendable to use marble waste powder as a partial replacement for cement.

References

1. Kore SD, Vyas AK, Kabeer KI SA (2020) A brief review on sustainable utilisation of marble waste in concrete. *Int J Sustain Eng* 13(4):264–279
2. Omisande LA, Onugba MA (2021) Strength characteristics of concrete produced by replacing fine aggregates with iron filings and marble dust. *Int J Innov Sci Res Technol* 6(3):29–34
3. Ofuyatan OM, Olowofoyeku AM, Obatoki J, Oluwafemi J (2019) Utilization of marble dust powder in concrete. In *IOP Conf Ser: Mater Sci Eng* 640(1):012053
4. Soliman NM (2013) Effect of using marble powder in concrete mixes on the behavior and strength of RC slabs. *Int J Current Eng Technol* 3(5):1863–1870
5. Vaidevi C (2013) Study on marble dust as partial replacement of cement in concrete. *Indian J Eng* 4(9):14–16
6. Sharma S, Pastariya S, Verma GK (2017) Experimental investigation on partial replacement of cement with marble dust powder on properties of concrete. *Int J Softw Hardware Res Eng* 5(9):1–5
7. Kumar R, Kumar SK (2015) Partial replacement of cement with marble dust powder. *Int J Eng Res Appl* 5(8):106–114
8. Yamanel K, Durak U, İlkentapar S, Atabey İİ, Karahan O, Duran C (2019) Influence of waste marble powder as a replacement of cement on the properties of mortar. *Revista de la Construcción. J Construct* 18(2):290–300
9. Song PS, Hwang S (2004) Mechanical properties of high-strength steel fiber-reinforced concrete. *Constr Build Mater* 18(9):669–673
10. Olivito RS, Zuccarello FA (2010) An experimental study on the tensile strength of steel fiber reinforced concrete. *Compos B Eng* 41(3):246–255
11. Laranjeira F, Grünwald S, Walraven J, Blom C, Molins C, Aguado A (2011) Characterization of the orientation profile of steel fiber reinforced concrete. *Mater Struct* 44:1093–1111
12. Xing HG, Xu FG, Zhou JW (2014) Comparative experimental study of mechanical properties of concrete prepared by different fibres. *The IES J Part A: Civil Struct Eng* 7(3):151–162
13. Mohammad SA, Krishna TNC, Saketh T, Ganesh CY, Sathyan D (2023) Fresh and hardened state properties of waste tire fiber and steel fiber reinforced concrete. *Mater Today: Proc* 80:443–448
14. Rama Mohan Rao A, Ramanjaneyulu K (2018) In: *Recent advances in structural engineering*, vol 1. 1st edn. Springer, Singapore
15. Public Resource, <https://law.resource.org/pub/in/bis/S03/Is.12269.1987.pdf>
16. Public Resource (2009). <https://law.resource.org/pub/in/bis/S03/Is.10262.2009.pdf>
17. Science Alert Homepage (2023). <https://scialert.net/>. Last Accessed 12 June 2023

State of Art on Enhanced Energy-Efficient Building Through Various Materials and Construction Techniques



Thennarasan Latha Abinaya and Balasubramanian Murugesan

1 Important Aspects of EE Building

Energy plays a vital role in the construction industry and its entire life cycle [1]. While global energy consumption grows at 2% annually, the demand for energy in India is higher [2]. To ensure the long-term viability of the built environment, energy efficiency is an essential factor [3]. A building design degrades the environment, specifically its exhaustion of air, water, and soil contamination. These grants are related to the material and energy demand of the construction projects [4]. EE strategies need to be analysed to reduce energy consumption [5]. A building that has a comfortable indoor environment and reduced CO₂ emission will lead to negligible damage to the environment [6]. To assess the energy demand of a residential building, there are many factors to be dealt with, such as the material used for wall and roof, building orientation, building location, and zones [7]. In the early investigation, many investigators have adopted agricultural by-products and further industrial waste material for walls and roofing to resolve the thermal comfort and energy efficiency for a specific building [8].

Energy is predominantly utilised in building for lighting, space cooling, air conditioning, etc. [9]. Envelop design optimisation provides a more durable solution for vitality efficiency and the thermal behaviour of the structure [10]. The material alone does not significantly impact energy efficiency; the size of air vents and their shading factor are also important consideration. The orientation of the building has a notable impact on its cooling load [12]. Along these lines, sustainable architecture to achieve

T. L. Abinaya

School of Architecture and Interior Design, Faculty of Engineering and Technology, SRM Institute of Science and Technology, Kattankulathur 603203, Tamil Nadu, India

B. Murugesan (✉)

Department of Civil Engineering, Faculty of Engineering and Technology, SRM Institute of Science and Technology, Kattankulathur 603203, Tamil Nadu, India

e-mail: balasubm1@srmist.edu.in

thermal comfort should think about improving building envelopes through the insulation material [2]. This paper review encompasses the various types of natural fibre and industrial waste used as a building material to resolve the structural envelope's EE and thermal comfort level.

1.1 Identification of Key Factors

This study indicates that there is enough space for a systematic investigation of new research opportunities and priorities on this topic [13]. A search of the Internet literature for works published between the years 2000 to 2020 was carried out. The abstract fields of the following databases were investigated in the Scopus indexed journals with the search terms: “EE materials”, “EE buildings”, and “Construction techniques for EE buildings” for the period from 2000 to 2020. The major keywords found were thermal comfort, energy efficiency, energy conservation, and thermal energy storage [14]. Figure 1 shows the identification of key factors among EE buildings [15]. Thermal comfort is an important factor in achieving the EE building. This resulted in finding out the various journals. The Mendeley software was used to exclude the same findings. As a result, the quantity of articles has decreased. Figure 2 shows the geographical analysis of nations suggests that India and China have done extensive work in EE buildings. The VOSviewer software used for bibliographic analysis for keyword identification and geographical analysis of nations. A large number of natural fibre and industrial waste material publications focusing on mechanical properties were eliminated. Reading through the abstracts, articles relevant to EE materials and construction techniques were identified [16]. The database was created in order to categorise the articles into several categories for study. This article was analysed, and two classification frameworks were created [17]. First, the essential details of the reviewed journal articles were classified as material. The second level of classification was based on EE building construction techniques. This review is also focused on co-fired blended ash, dense concrete, laterite stone, burnt brick, and mud brick to evaluate the EE sustainable walling material and also discussed the construction techniques such as ventilated brick cavity walls, static sunshade technique, staggered stud wall, orientation and massing of the building based on the literature; these techniques were discussed in detail [18].

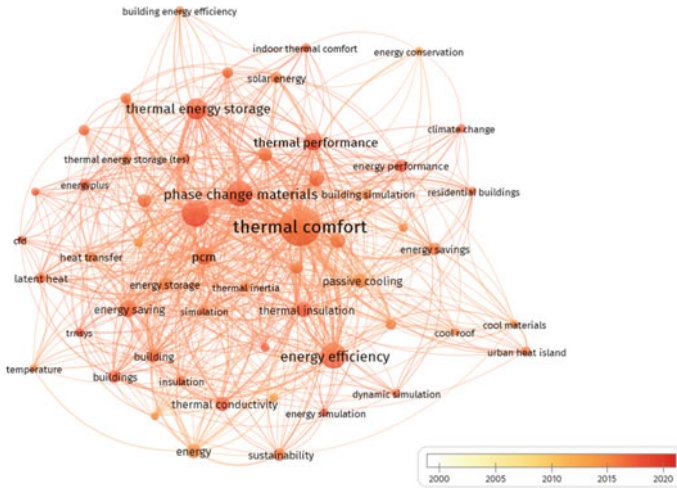


Fig. 1 Bibliographic for keyword identification

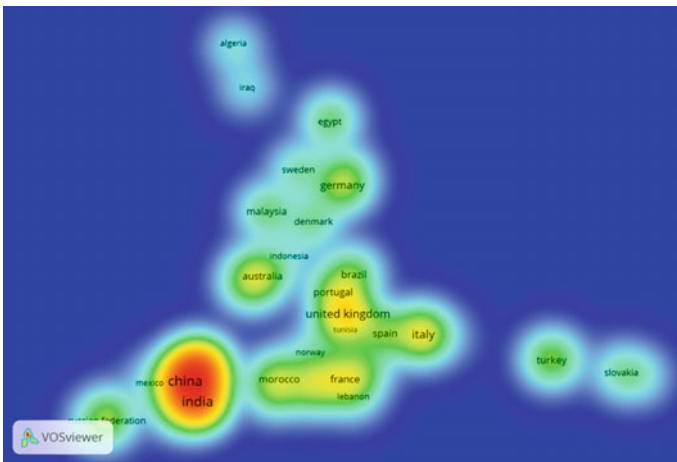


Fig. 2 Geographical of literature review

2 Energy-Efficient Building Materials

2.1 Coconut Fibre as Insulating Material

The coconut fibre is insulated with a wall to reduce the atmospheric condition [19]. Two physical models were developed to analyse the impact of using masonry walls filled with coconut fibre. Coconut fibre could build up the EE of the physical envelope model [20].

The cavity walls are becoming familiar because of their thermal properties, outstanding sound transmission, and resistance to rain penetration [21]. The two identical models were created such as model 1—concrete masonry wall (150 × 200 × 400 mm), model 2—clay masonry wall (100 × 200 × 300 mm). The model has been tested with and without glass fibre and coconut fibre insulation material to improve the thermal efficiency and comfort in private buildings [22].

2.2 Recycled Plastic Aggregate in Concrete

Two identical buildings were planned and constructed with ordinary concrete and recycled mixed plastic concrete [23]. The two buildings were constructed in a south-facing and north-facing. The energy and thermal efficiency of both structures is examined and inspected [24]. The long-term energy investigations and short-term energy investigations were analysed. SUNREL simulation software is the primary simulation tool adopted to forecast energy performance on a yearly premise with different concrete thermal properties [25]. Tracer gas investigation was led for both structures by estimating the net air conversion standard inside and outside air. The blower entryway test was conducted on recycled plastic concrete and normal concrete structures.

2.3 Co-Fired Blended Ash (CBA) Walling Material

CBA blocks were made according to the Indian standards of the developed item were contrasted and the accessible fly ash bricks. The thermal conductivity, durability, and physic-mechanical investigation were conducted on CBA block. CBA was compared with the fly ash brick and found the CBA is 26% lighter in weight when contrasted with the FA bricks [1]. The cooling load of a building reduces 8.3% by utilising CBA bricks. Single storey building was designed and analysed by BIM simulation to minimise the transmission stage of a project, determined the sufficient material combination, and energy consumption house is a high reduction in result [1]. A comparative study was conducted between commercially available fly ash and CBA bricks, including size, density, thermal conductivity, cost, and shrinkage. The BIM tool is used to analyse, demonstrate, and estimate building materials, costs, and vitality requests.

2.4 Aerogel

Aerogel products are an interesting way to replace conventional thermal insulators because their thermal conductivity is very low. Conventional insulation materials

include the production of lightweight mortar, polyurethane, fibreglass, mineral wool, etc., cementing materials based on aerogel have been prepared (Area 2014). The tetraethoxysilane (TEOS) and methytrimethoxysilane (MTMS) precursors are used to prepare the aerogel granules. To develop the cost-effective high thermal insulation product and the aerogel was added to prepare the cement-based composite.

2.5 Preparation of BNT/HE Composite PCM

Preparation of into bentonite (BNT) clay/n-heneicosane (HE) Initial process, in a breaker specific quantity of HE, was situated and it is melted. In that melted, HE was added to BNT clay. Six identical wallboards were employed to prepare the blocks utilising a hardened steel shape with a size of $100 \times 100 \times 100$ (length \times width \times height). BNT powder, water, and HE were responsible for the PCM wallboard mixture [26]. The BNT wallboard was designed using BNT with a limited water volume. At room temperature, the developed BNT and BNT/HE walls board were kept. The two halogen lamps were used to heat the developed cube units 300 W [26]. The heating stage will be ended if the two cubes are raised above the HE melting point. The data logger was used to measure the inside temperature, and during the heating and cooling period, the measured data were loaded to a computer at 30 s intervals.

2.6 Structural Model Using Various Building Materials and Glass Windows

The architecture models were built using various building materials and glass windows. The dimension of the structure model is $5 \times 5 \times 3.2$ m with 0.22 m wall thickness. Eighty structural models were built with different materials (laterite, thick concrete, burn brick, and mud block) and different ventilation glass materials (reflective, green, bronze, and transparent glass). The surface was built with 0.15 m thick, dense concrete, and a roof with a thickness of 0.15 m RCC. The wall is covered by plaster inside and outside of the building model. The thermal analysis of the structure model was carried out using authorised Energy Plus 8.1 simulation software in India's different climatic zone.

3 Energy Efficiency Building Construction Techniques

3.1 Ventilated Brick Cavity Wall

The combined effect of a ventilated block cavity wall with a brick projection was used as EE building elements, sunshade, and hollow roofs. The hollow roof and cavity wall can change the cooling and heating capacity in the building by regulating indoor air temperature and solar heat gain. The cavity walls and designed sunshade can maintain indoor air temperatures low in summer compared to the external temperatures to design a building in the composite climate zone with a hollow roof. The ventilated cavity block walls with a brick projection joined with static sunshade and hollow rooftop were sufficient for long-term indoor temperature regulation. To improve energy requests in a structure area with a cold winter and hot summer, structural components like a sunshade, hollow rooftop, and full-length divider must be appropriately planned.

3.2 Static Sunshade Technique

The static sunshade was designed based on solar geometry, and the effectiveness to regulate sunlight entrance within the structure is the primary priority over seasonal categorisation for a geographic region. The exact static sunshade was designed over the south exterior wall for energy regulation inside the structure. The static sunshade is progressively valuable for energy conservation inside the structure. The static sunshade will serve to cut down the intensity and cooling conditions inside the building.

3.3 Staggered Stud Wall

To improve the EE of residential wall construction, the best option is a staggered stud wall. Enhancing efficiency energy in a residential structure is developing the insulation of the exterior walls of the building. Staggered stud walls improved the energy efficiency up to 58% when related to other conventional walls. The benefits in the EE of the staggered stud wall should be considered related to alternative energy-conserving methodologies such as EE windows and air sealing.

3.4 Orientation and Massing of the Building

The orientation and massing of the building is the initial step in carrying out the high advantage from passive solar systems, and it developed right away in the conceptual stage. To diminish energy load and expand power from the wind and sun, the building should be successfully oriented. The research focused on a detailed examination of the condition data (monthly), passive design approaches, and site characteristics in order to promote the best plan concept for the usage of renewable energy sources. Design determinations carried out in the high initial phase have a considerable impact on vitality utilisation and the inner condition of the structure. EE design is important not just for constructing a better functioning building that uses less energy, but also for promoting awareness of EE design.

4 Analysis on the Energy-Efficient Building Materials

4.1 Coconut Fibre Experimental Methodology

Energy consumption decreased with insulation wall model 1. The coconut and glass fibre [20] insulated model diminished the energy utilisation by 0.66 and 0.58 k W.H. The average energy utilisation for model 1 with different kinds of insulation was recorded at 2-h interims. A model 1.1 no insulation, model 1.2 coconut fibre insulation, model 1.3 fibreglass insulation. Model 1.2 is best performed with coconut fibre during peak hours, and model 1.1 has performed worst. The average energy use for model 2, with the other kind of isolation recorded at an interval of 2 h. Models 2.1 no insulation, model 2.2 coconut fibre insulation, and model 2.3 fibreglass insulation. In most of the testing period, the model without insulation was best in energy consumption. Hence, Model 2.3 was EE and was worked better, following Model 2.2 and Model 2.1. The relative humidity was investigated for models 1.1, 1.2, and 1.3 (without A/C and with A/C) and models 2.1, 2.2, and 2.3 (without A/C and with A/C). For most of the test period, the isolated model's relative humidity was low for a concrete masonry wall. The lascar Easylog USB information loggers and multifunctional small ammeter [22] were installed to monitor the indoor and outdoor air temperature and humidity. Therefore, relative humidity seems to be like positive insulation. During the test period, the clay wall has higher relative humidity, which has a negative effect. The beneficial effect of coconut fibre isolation walls is thermal comfort and energy consumption.

4.2 Energy Analysis on Recycled Plastic Concrete: Experimental Results

The result shows that the proportionate spillage area is 637.5 cm^2 for recycled plastic concrete building and 450 cm^2 for the standard concrete structure has a tighter appearance than the recycled concrete building [25]. The motivation behind this “heating” test was to complete a uniform and constant indoor temperature in two structures. The north and south buildings recorded the indoor temperature of six areas. The north building usually utilises more electric energy than the south building. During the co-heating period, the consistent electricity use in the south building was around 25% lower. Analysis of illumination and daylighting illuminance from natural light and electrical light was measured on the upper floor of the south building using a Licor photometer. Long Term Energy Analysis-to analyse the structure performance with the seasonal variation under typical working conditions. Anticipated Energy performance: The SUNREL programming was used on a yearly premise with different thermal properties of the concrete to predict the energy performance. An 8% lower energy was used to heat plastic isolated concrete structure for the annual charge than a comparable structure with conventional concrete [1].

4.3 Comparative Study: CBA Brick and Fly Ash Brick

This research explores the application of CBA in EE and sustainable wall materials production. The structure model unit was set up as a single story private unit, including 24-h use. The thermal and physical properties of construction material were determined (masonry block, plaster, and slab). The use of CBA bricks in all floor rooms reduced the cooling load compared to the primary case. CBA bricks were discovered 26% lighter in weight when compared fly ash bricks; CBA bricks are stronger than fly ash bricks as a construction material.

4.4 Aerogel-Based Cementitious Material

Aerogel product: The two aerogel granules were prepared by employing tetraethoxysilane (TEOS) and methyltrimethoxysilane (MTMS) prototypes. Aerogel silica was made by catalysed sol–gel process and acid–base process. The first aerogel was developed from MTMS and TEOS in molar apportion corresponding to 0.6. In the initial step: the models were combined with a volume of H_2O and isopropanol by mixing on a magnetic stirrer. To this outcome, an esteemed proportion of 0.1 M hydrochloric corrosive was included, and the arrangement was set at $60 \text{ }^\circ\text{C}$ for 1.5 h. In the second stage: the weighted amount of base NH_4OH (0.5 M) was included dropwise to sol was transferred to silicone moulds and strengthen the structure is

kept for 24 h. The preparation of concrete-based composites by utilising the aerogel will improve practical high warm protection items. The hot-wire technique gives the importance of thermal conductivity, evaluating thermal properties of aerogels concrete materials. This aerogel will enable the production of high thermal insulation products with the use of cement-based composites.

4.5 Laboratory Performance Analysis on BNT/HE

The study of SEM and FT-IR demonstrated that HE was integrated into the BNT pore in remarkable contrast to the components [26]. The DSC study revealed that the 36% HE mixture was 38.3 °C warming and the real temperature was 38.34 °C. The TG study showed exceptional thermal power in the composite PCM. The composite was consistent with long-term thermal strength and chemical stability from the thermal cycling study. Laboratory performance analysis shows the effect of a decrease in the structure's temperature with the composite PCM wallboard BNT/HE [26].

4.6 Thermogravimetric Analysis: Recycled Waste Thermoplastic Block

The block was made using fly ash 15%, cement 15%, waste plastic up to 10%, and sand. The block was cured for 28 days underwater, and the sample was baked and analysed as under compressive strength, water absorption rate, porosity, thermal conductivity, and morphology. Thermogravimetric analysis (TG): thermogravimetric analysis has been used to analyse thermal behaviour. The TG plot indicates mass losses associated with hydrate and carbonate disintegration. The block is observed the compressive strength to be higher than 17Mpa. For EE structure and construction work, the block with thermoplastic waste is quite suitable.

4.7 Analysis of Energy in Five Different Indian Climate Zones for Different Materials in Buildings and Windows

This study used four-building materials: laterite stone, dense concrete, burnt brick, burned brick, and four glass windows, including clear, bronze, green and bronze reflection glasses. Four glass material's spectral optical properties were experimentally measured by Perkin-Elmer lambda 950 wavelengths of 300–2500 nm, respectively. The Design-Builder 4.3.0.039 and Energy Plus 8.1 simulation program conducted thermal analysis were designed with 80 construction models. The thermal simulation was done on summer's peak days in every city in four distinctive climatic

zones. In India, it is discovered that five climatic areas and at 20, 40, 60, 80 and 100% WWR, mud block with bronze-intelligent glass, ventilator glass structures said to be efficient energy, and other concentrated material. The study results allow us to identify the ideal combination of building and glass windows for cooling load reduction in Indian structures in five different climate zones. Summarised properties and samples of various types of insulation materials are shown in Table 1.

5 Analysis on the Constructional Techniques

5.1 Static Sunshade Over a Ventilated Brick Cavity Wall

Four research rooms (3.0 m×4.0 m×3.0 m) of the same orientation were built to study the impact on the internal temperature of a ventilated block wall with a brick projection [27]. A permanent sunshade is horizontally positioned over the south wall and a solid brick-facing wall, 338 mm thick, and RCC 100 mm thick roof. The planned static sunshade over a ventilator for R2, R3, and R4 on the south wall. The three faces (east, west, and south) of R3 and R4 have a ventilated block wall with a block projection. From April 2012 to September 2012, indoor and open-air temperatures were noted every hour. Every hour, the outdoor temperature was differentiated by a worldwide WA700 water-air temperature sensor, aided by WE770 sunlight-focused radiation. All the tests were carried out with the window, and the doors of the four rooms locked. Adequacy with a ventilated block wall with block projection has been set up by looking at rooms R3 and R2, with static sunshade has been examined by different rooms R4 and R2. A planned static sunshade and empty rooftop have been examined by looking at rooms R4 and R1.

5.1.1 Analysis of Thermal Performance

The indoor and outdoor temperature in the four rooms were noted for the initial six months consistently from 2012 April to 2012 September at a one-hour interval throughout the day. The air-conditioned brick wall with brick-projection thermal efficiency research has been conducted by observing normal hourly temperature estimates both inside and outside of rooms R1, R2, R3, and R4. The evaluations of the thermal load levelling (TLL) of the four rooms were determined. The thermal levelling of room R4 over the entire duration of the study was less than R1, R2, and R3. It was shown that ventilated brick wall with brick projection, static sunshade structure, and hollow roof combined resulted in excellent load and thermal comfort. It also helped to lower the indoor temperature during the study period for the hotter part of the day. The impact of EE components is significant for summer cooling and building energy efficiency.

Table 1 Summarised properties and samples of various types of materials

Name	Properties	Inference
Coconut fibre	Thermal conductivity 0.054–0.143W/mK Density 250–380 kg/m ³ Tensile strength 15-327Mpa Water absorption 80–90%	The coconut fibre packed on masonry wall would positively affect thermal comfort and energy consumption
Recycled plastic	Density 0.90–0.91 g/cm ³ Raw density 0.805 g/cm ³ Modulus of elasticity 4100 MPa	Recycled plastic cement with EE structure systems demonstrated to be of huge incentive in bringing down the cooling and warming load of the structure and improving the structure’s comfort level
Co-fired blended ash brick (CBA)	Thermal conductivity 0.55 W/mk Density 1330 kg/m ³	CBA blocks were seen as 26% lighter in weight when compared to FA blocks. CBA blocks diminished 8.3% of the peak cooling load of a structure
Bentonite clay	Thermal conductivity 0.34 W/mK Density 1.8 kg/m ³	The use of the composite PCM created as wallboard in the development of EE structures will open up a new opportunity for HVAC practical purposes in the construction industry [26]
Laterite stone Dense concrete Burnt brick Mud brick	Thermal conductivity 1.3698W/mK Specific heat 1926.1 J/kgK Density 1000 kg/m ³ Thermal conductivity 1.74 W/mK Specific heat 880 J/kgK Density 2410 kg/m ³ Thermal conductivity 0.811W/mK Specific heat 880 J/kgK Density 1820 kg/m ³ Thermal conductivity 0.75W/mK Specific heat 880 J/kgK Density 1731 kg/m ³	The mud brick with glass window reflector buildings is low-heat EE in the studied buildings. According to the study materials, mud brick, burnt brick, laterite, and dense concrete are the choice of materials for the reduction of cooling loads
Recycled waste thermoplastic	Density 0.80–0.91 g/cm ³ Raw density 0.811 g/cm ³ Modulus of elasticity 4500 MPa	The current study results show a clear possibility that bricks with little compromise in mechanical property can contain all types of waste thermoplastics

5.2 Experimental Study on Static Sunshade Design

The polyurethane foam was insulated in three experimental models. The experiment has been brought out for over one year. The exploratory model was balanced with another littler element of the south exterior window and diverse static sunshade, including the proposed sunshade. The model was kept with the same ventilator measurement and sunshade horizontal for a similar examination; sunlit territory and temperature were recorded for six months (December 2002-July 2003). The model measurements were picked according to the experimentation of the period July 2002-December 2002. Furthermore, the analysis has proceeded for the adjusted three models throughout December 2002-July, 2002. Each of the six models was investigated. According to annual requirement, Model 5 with the proposed sunshade indicates improvements in the nature of the area under a sunlight region as well as the average temperature in the cold to low-energy cycle in the summer compared with the M4 model in horizontal M6 sunshade, which is a high area under the sunlight curve, according to the annual requirements. Henceforth, M5 with the proposed static sunshade is more effective regarding model M4 and model M6. Sunlit zone, the rules for selecting the appropriateness of the proposed sunshade over the existing flat sunshade were established, which understudy controls the temperature inside the models

5.3 Experimental Study on a Staggered Stud Wall

Diminishing energy efficiency in traditional houses with wood-framed are thermal bridges a quick way that gives warmth to course through the studs rather than the insulation staggered- stud walls utilise 2×6 base and top plates with 2×4 studs shifting back and forth between sides of divider [28]. It allows sheathing on multiple sides to be added when thermal bridges are dispensed. An exploration study has announced an absence of research facility test information for SS walls utilised as shear walls raising concerns about safety [28]. The motivation behind this exploration was to look at the seismic exhibition of staggered stud dividers and contrast their conduct with comparable regular walls. Monotonous and cyclic laboratory experiments were planned with and without the Gypsum wallboard. The staggered stud was carried out in contrast to traditional walls exceeded 11 mm. In all other tests, the sliding off the base plate was not exceeded 3.3 mm. To remove the noise, the monotonic data were also smoothed. To recognise envelopes around the data utilised the sophisticated algorithm. To compute energy dissipation attributable to hysteresis were additionally utilised the cyclic load deflection. The monotonic curve average has been determined from the proper load–deflection data. The average of the cyclic test was processed by applying two envelopes for every investigation. Identified with conventional walls, the SS wall with a monotonical load had a lesser ductility and deflection. In the monotonic test, the SS wall [29] lost vitality more delicately than

conventional walls. In the cyclic test, the SS wall dissipated more hysteretic energy than conventional walls.

5.4 Building Simulation

This work examines monthly air data, passive design methods, and building components in order to suggest passive solar approaches and select the best plan strategy for the usage of solar power sources. In winter, there are three passive solar techniques utilised to heat the indoor temperature of the building. First simulation: orientation analysis (the solar heat gain from the various directions to the structure is analysed), second simulation: Massing considers, third simulation: Wind for ventilation, fourth simulation: Office space structure decision (It depends on Apachesim's dynamic warm recreation). In the planning stage, the energy efficiency of any structure decision is to be made, especially during the initial stage. The shading method, lighting, IES VE, and wind power can be used to achieve an EE structure to ensure the optimal design. This research was concentrated on the analysis of the monthly site components, passive plan strategies, and climatic information to suggest a passive solar technique to reduce the required complex of energy and choose the excellent planning process for utilisation of sustainable solar sources. For this analysis, IES VE software was used to test a rectangular structure with longer side-oriented north-south and east-west. The second simulation: Massing studies, simulation of passive strategies to direct suitable plan choice for the most EE planning arrangement at every stage. The third simulation: two cases for IES VS performed wind for ventilation simulation: (1) Room with wind tower without the wing-shaped gadget, (2) Room with wind tower with the wing-shaped gadget. It was carried out using the estimation method for IES VE in Macroflow. The fourth simulation: In IES VE simulation was conducted to determine which option will offer more efficiency in energy. It was based on the dynamic thermal simulation by Apachesim. The selection of the perfect massing method in the start time allows the overall performance of the structure to be established with a passive plan.

6 Conclusion

Based on these studies, the use of alternative materials for the development of the building is in a sustainable way. The fundamental target of this review paper is to discuss the literature related to different perspectives of EE materials for construction. The building insulation materials such as coconut fibre determined to have excellent thermal properties, recycled plastic aggregate were designed to provide optimum energy performance and thermal attributes in buildings, CBA brick is an EE building material to gain up sustainable, economic, and ecological interests, aerogel is the cost-effective high thermal insulation material, vacuum insulated panel is considered

a high-performance thermal insulator, and BNT/HE composite PCM that has been created as the wallboard for EE building construction will open up new options for passive photovoltaic, ventilation and air conditioning (HVAC) use in the building sector. Among eighty building models studied in five climatic zones of India, mud brick with bronze-reflective glass window buildings were found to be the most EE in terms of heat gain and recycling waste thermoplastic improve the energy efficiency of construction material. Therefore, to reduce the heat gain through the building wall, the materials and construction methods were most effective, resulting in the building's low indoor temperature. From the literature review, this study focused on the reuse of agricultural waste and industrial waste as a replacement material in the field. Further researcher's focus on the valuable green material for the construction industry. Moreover, it is concluded that other alternative materials are cost-effective and more EE compared to conventional building materials.

References

1. Gavali HR, Ram S, Ralegaonkar RV (2018) Evaluation of energy efficient sustainable walling material. *Thormark*, pp 227–233
2. Roufehaei KM, Hassan A, Bakar A, Tabassi AA (2013) Energy-efficient design for sustainable housing development. *J Clean Prod*
3. Saxena R, Gupta T (2022) Assessment of mechanical, durability and microstructural properties of geopolymer concrete containing ceramic tile waste. *J Mater Cycles Waste Manag* 24(2):725–742
4. Chel A, Kaushik G (2018) Renewable energy technologies for sustainable development of energy efficient building. *Alexandria Eng J* 57(2):655–669
5. Pérez-Lombard L, Ortiz J, Pout C (2008) A review on buildings energy consumption information. *Energy Build* 40(3):394–398
6. Jethy B, Paul S, Kumar S, Adesina A, Mustakim SM (2022) Critical review on the evolution, properties, and utilization of plasticwastes for construction applications. *J Mater Cycles Waste Manag* 24(2):435–451
7. Chen M et al (2019) Recycling of paper sludge powder for achieving sustainable and energy-saving building materials. *Constr Build Mater* 229:116874
8. Masood OAI, Al-Hady MIA, Ali AKM (2017) Applying the principles of green architecture for saving energy in buildings. *Energy Proc* 115:369–382
9. Corinaldesi V, Donnini J, Nardinocchi A (2015) Lightweight plasters containing plastic waste for sustainable and energy-efficient building. *Constr Build Mater* 94:337–345
10. Shaikh PH, Nor NBM, Nallagownden P, Elamvazuthi I, Ibrahim T (2016) Intelligent multi-objective control and management for smart energy efficient buildings. *Int J Electr Power Energy Syst* 74:403–409
11. Transfer M (2022) Compressed earth blocks reinforced with fibers (Doum Palm) and stabilized with lime : manual compaction procedure and influence of addition on mechanical properties. 26:157–177
12. Colorado HA, Saldarriaga L, Rendón J, Correa MA (2022) Polymer composite material fabricated from recycled polyethylene terephthalate (PET) with polyurethane binder for potential noise control applications. *J Mater Cycles Waste Manag* 24(2):466–476
13. Williamson T, Daniel L (2020) Energy and buildings a new adaptive thermal comfort model for homes in temperate climates of Australia. *Energy Build* 210:109728
14. Luo M, Wang Z, Brager G, Cao B, Zhu Y (2018) Indoor climate experience, migration, and thermal comfort expectation in buildings. *Build Environ* 141(March):262–272

15. Bakmohammadi P, Noorzai E (2020) Optimization of the design of the primary school classrooms in terms of energy and daylight performance considering occupant's thermal and visual comfort. *Energy Rep* 6:1590–1607
16. Yuan F et al. (2022) Thermal comfort in hospital buildings—a literature review. 45
17. Du H et al. (2022) Comparison of thermal comfort between radiant and convective systems using field test data from the Chinese thermal comfort database. *Build Environ* 209:108685
18. Somu N, Sriram A, Kowli A, Ramamritham K (2021) A hybrid deep transfer learning strategy for thermal comfort prediction in buildings. *Build Environ* 204:108133
19. Sadeghifam AN, Meynagh MM, Tabatabaee S, Mahdiyar A, Memari A, Ismail S (2019) Assessment of the building components in the energy efficient design of tropical residential buildings: an application of BIM and statistical Taguchi method. *Energy* 188:116080
20. Subramanian GKM, Balasubramanian M, Jeya Kumar AA (2021) A review on the mechanical properties of natural fiber reinforced compressed earth blocks. *J Nat Fibers* 00(00):1–15
21. Chikhi M, Agoudjil B, Boudenne A, Gherabli A (2013) Experimental investigation of new biocomposite with low cost for thermal insulation. *Energy Build* 66:267–273
22. Iwaro J, Mwashia A (2019) Effects of using coconut fiber-insulated masonry walls to achieve energy efficiency and thermal comfort in residential dwellings. *J Archit Eng* 25(1):1–12
23. Siddique R, Khatib J, Kaur I (2008) Use of recycled plastic in concrete : a review. 28:18351852
24. Zhang W, Liu F, Fan R (2018) Electrical power and energy systems improved thermal comfort modeling for smart buildings : a data analytics study. *Electr Power Energy Syst* 103(April):634–643
25. Elzafraney M, Soroushian P, Deru M (2005) Development of energy-efficient concrete buildings. *J Archit Eng* 11(4):122–130
26. Sari A (2017) Thermal energy storage properties and laboratory-scale thermoregulation performance of bentonite/paraffin composite phase change material for energy-efficient buildings. *J Mater Civ Eng* 29(6):1–7
27. Charde M, Gupta R (2013) Effect of energy efficient building elements on summer cooling of buildings. *Energy Build* 67:616–623
28. Rodriguez-Nikl T, Gupta R, Kramer A, Sinha A (2015) Seismic laboratory testing of energy-efficient, staggered-stud, wood-frame shear walls. *J Struct Eng (United States)* 141(3):1–8
29. Leskovar VŽ, Premrov M (2012) Influence of glazing size on energy efficiency of timber-frame buildings. *Constr Build Mater* 30:92–99

Steel and Composite Structure

Study on Self-Consolidating Hybrid Fibre-Reinforced Concrete



R. Sruthi and K. Suganya Devi

1 Introduction

Due to its well-known advantages and properties, including its low cost, extensive availability, and applicability, one of the most often utilized building materials is concrete. Nonetheless concrete is a brittle material with limited tensile strength and low resistance to crack opening and propagation. Compaction by vibration or tamping during casting is a significant factor in the production of conventional concrete structures. This vibration if not done properly will lead to the formation of honeycomb, bug holes, and segregation of aggregates. Self-consolidating concrete can be used to solve this issue by eliminating the need for the vibration of the concrete. Self-consolidating concrete, as opposed to conventional concrete, enhances the efficiency and quality of the concrete while reducing the major problems caused in the construction process. Self-consolidating concrete is acknowledged in the development business because of its different benefits over conventional concrete.

In order to overcome these drawbacks and produce materials with enhanced tensile strength, compressive strength, ductility, toughness, improved durability characteristics, and the prevention of crack initiation and propagation, fibres are incorporated into cementitious concretes. The proportion of fibres used, the properties of the fibre matrix, the volume of fibre inclusion, the fibre geometry, the type of fibres, and the orientation of the fibres in the concrete mixture all have an impact on the fibre's efficiency. There are different types of fibres available in the market to improve the properties of hardened concrete. They may, however, affect the freshened properties of the concrete. Steel, carbon, or polymer make up the majority of the fibres. Researchers have paid the most attention to polypropylene fibres as they are economical, exceptional toughness, and improved resistance to cracking in concrete reinforced with synthetic fibres. However, the properties of concrete are only slightly enhanced by

R. Sruthi (✉) · K. Suganya Devi
Civil Engineering Department, SRM Valliammai Engineering College, Chennai, India
e-mail: sruthiraghu1999@gmail.com

using a single type of fibre for reinforcement. Contrarily, hybrid fibre-reinforced concretes, which are reinforced with different types of carefully chosen fibres, offer improved characteristics.

1.1 Objectives of the Work

The primary objective of this research is to examine the workability characteristics of self-consolidating concrete (SCC) and hybrid fibre-reinforced self-consolidating concrete (HFSCC) by incorporating different percentages of hybrid fibres in both fresh and hardened states. The mechanical properties being investigated encompass compressive strength and split tensile strength. These properties will be evaluated at 7, 14 and 28 days. The results obtained from the tested specimens will be compared to those of the control mixture in order to draw meaningful comparisons.

1.2 Research Significance

- Incorporation of hybrid fibres results in the enhancement of the strength in beams and reduction in workability properties.
- SCC can be used to overcome compaction problems.
- When hybrid fibres, comprising both steel and polypropylene, are utilized, there is an observed increase in the average compressive strength and split tensile strength.

1.3 Material Properties

The several components employed in the experimental examination of concrete, including cement, fine sand, coarse aggregate, super plasticizers, and fibres (steel and polypropylene fibres), are discussed together with the methods used and their properties. The cement used in the concrete mixtures are Portland Pozzolona cement (PPC) [5] with a specific gravity of 3.10 confirmed to the Indian Standard. The river sand are not available easily and economical, and thus, manufactured sand (M sand) conforming to Zone II as per IS: 383–1970 of specific gravity 2.61 was used in the experimental programme. Crushing hard granite stone yields manufactured sand. According to Indian standard specifications, it was tested. Crushed granite coarse material that was accessible locally was utilized. In this project, coarse aggregate with a maximum size of 12.5 mm was used. As a result, testing was conducted in accordance with the instructions provided in the IS Specifications [6]. The test results for cement, aggregates and properties of fibres are given in Tables 1, 2 and 3 respectively.

Table 1 Test of cement

Physical properties	Test method	Result	IS requirements
Consistency	Vicat's apparatus	32%	25–35%
Fineness of cement	Fineness by sieving	4.38%	< 10%
Specific gravity	Density bottle method	3.10	3.0–3.15
Initial setting time	Vicat's apparatus with 1 mm square section needle	34 Min	Not lesser than 30 min
Final setting time	Vicat's apparatus with 1 mm square section with 5 mm dia attached needle	480 Min	Not greater than 600 min

Table 2 Test of aggregates

Physical properties	Coarse aggregates		Fine aggregates	
	Result	IS 2386 (Part 3)-1963 requirements	Result	IS 383–1970 requirements
Moisture content	–	–	3.23%	–
Fineness modulus	–	–	2.75	2.2–3.2
Specific gravity	2.66	2.6–2.85	2.61	2.6–2.8
Impact test	12%	20%	–	–
Water absorption	1.8%	2%	–	–
Angularity number	9.35	–	–	–

Table 3 Properties of fibres

Type of fibres	Steel fibre	Polypropylene fibre
Shape of fibre	Hooked end	Straight
Density (g/cm ³)	7.85	0.91
Tensile strength (MPa)	1100	350
Length	35 mm	12 mm
Diameter	0.550 mm	0.22

1.4 Mix Proportions

The mix design [4] for the SCC was obtained by trial & error method. This was carried out until the required flow was achieved meeting the requirements of EFNARC Guidelines [3]. The concrete mix was designed in accordance with IS 10262–2019 for concrete of the M35 grade. According to EFNARC specifications [3], the total powder content should be 400–600 kg/m³, and the volume percentage of coarse aggregate should be 28–35%. By carrying out fresh property tests of SCC such as the slump cone, L-box, and V-funnel, the workability properties of the fresh

Table 4 Mix proportioning

Materials	Quantity required
Cement	451.25 kg/m ³
Water	156.54 L
Fine aggregate	980.21 kg/m ³
Coarse aggregate	847.57 kg/m ³
Water–cement ratio	0.35
Super plasticizer	5.7 kg/m ³
Steel fibres (%)	0.85
Polypropylene fibres (%)	0.15
Cement	g/m ³

concrete for each mix are investigated for passing ability, filling ability, and segregation resistance. Table 4 contains the final mix which was obtained. S0P0, S0.75P0.15, S0.80P0.15, S0.85P0.15, and S0.90P0.15 indicate the varying percentage of steel(S) and polypropylene (P) fibres.

1.5 Workability of SCC

SCC must meet three criteria: segregation resistance, passage ability, and filling ability. To verify these properties, the following tests are performed. Those are slump flow, which measures flow spread and flow time T500 to access filling ability, V-funnel test, which assesses filling ability and L-box test which assess the passing ability. Testing is done in accordance with EFNARC norms [3]. Steel and polypropylene fibres were mixed with the concrete in varying amounts. The percentage of polypropylene fibres was held constant at 0.15% by volume of concrete, while the percentage of steel fibres was changed from 0.75 to 0.90% to produce the best-performing mix. Slump flow, V-funnel, and L-box were used to determine the influence of hybrid fibres on the flowability of concrete, as illustrated in Fig. 1. Table 5 shows the outcomes of tests on SCC using various mixtures of steel fibre and polypropylene. Addition of 0.90 and 0.15% were not suitable as they did not meet the EFNARC norms [3].



Fig. 1 a V-funnel test; b L-box test

Table 5 Workability of HFSCC

Test	Property	S0P0	S0.75P0.15	S0.80P0.15	S0.85P0.15	S0.90P0.15	Permissible values (EFNARC)
V-funnel	Filling ability	8 s	10 s	10 s	11 s	13 s	6–12 s
L-box	Passing ability	0.83	0.84	0.91	0.96	1.1	0.8–1 (blocking ratio)
Slump flow	Filling ability	715 mm	705 mm	715 mm	690 mm	605 mm	650–800

2 Experimental Study

2.1 Compressive Strength of Cube

A cube-shaped specimen measuring 150 mm in size, made of self-compacting concrete (SCC) and hybrid fibre-reinforced self-compacting concrete (HFSCC), was prepared following the guidelines outlined in the IS 516:2014 standard. After the completion of 7, 14 and 28 days of curing, the samples were allowed to air dry and subjected to testing. To conduct the compression test, the specimen was positioned between two metal plates at the ends of a compression testing machine (CTM) with a capacity of 2000 kN, as illustrated in Fig. 2b. The compression was applied through a hydraulic mechanism. Based on the findings in Table 6, it was determined that adding steel and polypropylene fibres together increased the compressive strength of the HFSCC mix. Maximum compressive strength was attained for the mixture of 0.85% steel and 0.15% polypropylene fibres at 28 days. Compressive strength for S0.85P0.15 mix is found to be better when it is compared to other mixes and is 18.84% higher than the control mix. Steel fibre causes arrestment of cracks and

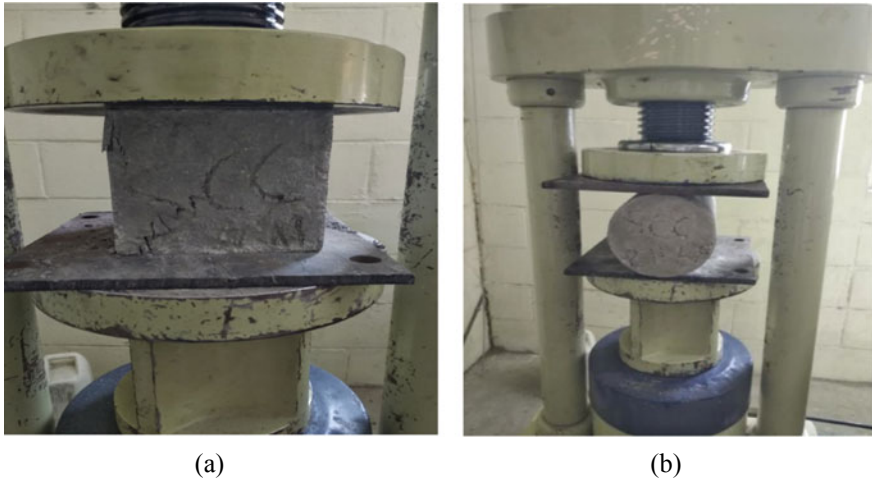


Fig. 2 **a** Compressive strength test; **b** tensile strength test

Table 6 Compressive strength test

HFSCC Mix	Compressive strength (N/mm ²)					
	7th day (N/mm ²)	Increase in strength (%)	14th day (N/mm ²)	Increase in strength (%)	28th day (N/mm ²)	Increase in strength (%)
S0P0	24.8	–	30.43	–	34.5	–
S0.75P0.15	25	0.8	31	1.87	36	4.34
S0.80P0.15	26.5	6.8	31.90	4.83	37.4	8.4
S0.85P0.15	29	16.9	32.5	6.8	41	18.84
S0.90P0.15	25.28	1.93	31.46	3.38	35.5	1.44

contributes to the development of compressive strength. The compressive strength increased up to a steel fibre content of 0.85% before a reduction in strength set in.

2.2 Splitting Tensile Strength of Cylinder

In accordance with IS 5816:1999, 300 × 150 mm SCC and HFSCC cylinders were cast, and samples were air dried and examined after 7, 14 and 28 days of curing. As depicted in Fig. 2b, in a compression testing machine (CTM) of 2000kN, the cylinder was placed between the two end platens and compressed using a hydraulic mechanism. In accordance with the results presented in Table 7, the split tensile strength of the HFSCC mix increased when steel and polypropylene fibres were combined as hybrid fibres. The combination of 0.85% steel and 0.15% polypropylene

Table 7 Tensile strength test

HFSCC mix	Splitting tensile strength (N/mm ²)					
	7th day (N/mm ²)	Increase in strength (%)	14th Day (N/mm ²)	Increase in strength (%)	28th Day (N/mm ²)	Increase in strength (%)
S0P0	1.75	–	2.84	–	3.45	–
S0.75P0.15	1.8	2.7	3.10	9.15	3.89	12.7
S0.80P0.15	2.15	22.8	3.45	21.47	4.4	27.53
S0.85P0.15	2.45	40	3.69	29.92	4.95	43.47
S0.90P0.15	1.96	12	3.5	23.23	4.5	30.43

fibres reached its maximum tensile strength at 28 days. When compared to other mixes, the S0.85P0.15 mix's tensile strength was found to be superior and is 43.47% higher than control mix. The tensile strength improved when steel fibre content was increased up to 0.85%, after which a loss in strength occurred.

3 Conclusion

Literatures were studied, and some of the data were collected from the literature survey. SCC mix containing 0.85% steel and 0.15% polypropylene fibres recorded higher split tensile and compressive strength values. They improve the hardened property of the concrete. Additionally, polypropylene fibre functions as a crack arrester and strengthens the link with cement matrix, while steel fibre increases split tensile strength and compression strength.

Steel fibre additions above 0.85% combined with 0.15% polypropylene fibres reduced the workability of SCC, and the mixture did not meet EFNARC criteria.

When compared to conventional concrete, SCC containing 0.85% steel and 0.15% polypropylene fibres performed most effectively, increasing compressive strength by 18.84% and split tensile strength by 43.47%.

Acknowledgements The authors wish to acknowledge the support of the Laboratory Staff of the Department Of Civil Engineering, SRM Valliammai Engineering College for carrying out the tests.

References

1. Afroughsabet V, Ozbakkaloglu T (2015) Mechanical and durability properties of high strength concrete containing steel and polypropylene fibres. *Construct Build Mater Elsevier*, 94:73–82
2. Anuradha V, Madhavi TC (2022) "Behaviour of self compacting concrete hybrid fibre reinforced hollow beams", *ASCE* (2016). *Structures* 35:990–1001
3. EFNARC (2002) Specifications and guidelines for self compacting concrete

4. IS 10262 (2009) Guidelines for concrete mix design proportioning
5. IS 1489-1 (1991) Specification for Portland pozzolona cement
6. IS 2386-1 (1963) Methods of test for aggregates for concrete
7. IS 456:2000 Indian standard code of practice for plain and reinforced concrete. New Delhi, Bureau of Indian Standards
8. Ismael MA, Hameed YM (2022) Structural behavior of hollow-core reinforced self-compacting concrete beams. *SN Appl Sci* 4:150
9. Murugesan A, Narayanan A (2017) Influence of a longitudinal circular hole on flexural strength of reinforced concrete beams. *Pract Period Struct Des Constr* 22(2):04016021
10. Jabbar S et al. (2016) Effect of an opening on reinforced concrete hollow beam web under torsional, flexural, and cyclic loadings. *ILatin Amer J Solids and Struct* 13:1578–1597
11. Turk K, Bassurucu M, Bitkin RE (2021) Workability, strength and flexural toughness properties of hybrid steel fibre reinforced SCC with high-volume fibre. *Constr Build Mater* 266:120944
12. Mansur MA, Ting SK, Lee S (1983) Torsion tests of R/C beams with large openings. *J Struct Eng* 1780–1791
13. Mansur MA, Tan KH, Lee YF, Lee SL (1991) Piecewise linear behavior of Rc beams with openings. *J Struct Eng* 1607–1621
14. Mansur MA, Tan K, Weng W (2001) Analysis of reinforced concrete beams with circular openings using strut-and-tie model. vol 1. Elsevier, pp 311–318

Effect of High Performance on Glass Fibre-Reinforced Concrete Beams



R. Kamalesh and A. Leema Rose

1 Introduction

High-performance Concrete (HPC) is the name for this new type of concrete. HPC has a very high level of durability, which is achieved by replacing a certain percentage of PPC with other cementitious materials like Silica Fume (SF). Using these replacement materials makes concrete better, both when it is still wet and when it is hard. It is the most versatile building material because it can be mixed with other materials to make up for their weaknesses. This makes the structure stronger and more efficient. Because building materials are always getting better, it is now possible to make different kinds of concrete for a wide range of uses. Adding minerals and chemicals to normal concrete to change its properties has made it possible to make shapes that would have been impossible or very expensive to make with normal concrete alone. It has a high density, a low permeability, a high degree of dimensional stability, a high degree of chemical resistance, and a high modulus of elasticity. It also has a high degree of strength. Normal concrete has low strength and elastic modulus because its structure is very different, especially at the interface between the cement paste and the aggregates, where there is a porous and weak transition zone. Glass fibres are being used in concrete more and more these days. Normal concrete is not very strong and is more likely to crack. Adding glass fibres to concrete gives it a high tensile strength, stops it from cracking, and stops water from leaking out. Also, using glass fibres makes the material stronger and makes it easier to shape. Because building materials are always getting better, it is now possible to make different kinds of concrete for a wide range of uses. Adding minerals and chemicals to normal concrete to change its properties has made it possible to make shapes that would have been impossible or very expensive to make with normal concrete alone.

R. Kamalesh · A. Leema Rose (✉)

Department of Civil Engineering, SRM Valliammai Engineering College, Kattankulathur, Chennai 603203, India

e-mail: Vraleemrose@gmail.com

2 Literature Review

Britto Jeyakumar AMS (2017) [1]. In this chapter, we discuss the experimental results from our investigation into the bending behaviour of beams fabricated from High-performance Concrete (HPC) that partially replaced cement with silica fume and glass fibre. Cement, fine aggregate, coarse aggregate, water, mineral admixtures like Silica Fume (SF), and the Super Plasticizer CONPLAST-430 were used to create HPC in this research. The cement-to-water ratio was decided upon as 0.26. In this experiment, concrete with an average strength of 80 MPa was used. Different combinations were tested by casting cubes, cylinders, and beams of the materials. Seven different mixtures (M1–M7) are cast with varying percentages of SF in the cement (0, 5, 7.5, and 10%), and a second set of specimens is cast with varying percentages of SF and Glass fibre in the cement (0, 5, 7.5, and 10%). Compressive strength, split tensile strength, flexural strength, water absorption, and modulus of elasticity are some of the mechanical properties tested in this way. The findings indicate that concrete made with the most effective replacement for silica fume was 7.5% more cohesive and less likely to separate.

2.1 Objectives of the Study

- To study the effectiveness of strength characteristics on Glass Fibre reinforced concrete.
- To study the ductility behaviour on High-performance Concrete.

2.2 Materials

Portland Pozzolana Cement (PPC) of 53 grades is used as the cement of choice. It was necessary to use coarse aggregate with a nominal maximum size of 20 mm down grade in order to meet the standard set by IS 383–2016. To meet the standards for Zone II, we used a fine aggregate with a fineness modulus of 2.67, which is about the same as medium river sand. Table 1 displays the physical characteristics and sieve analysis of Coarse Aggregate (CA) and Fine Aggregate (FA). The properties of the Silica Fume (SF) and Glass Fibre (GF) used in this study are listed in Table 2.

Table 1 Properties of CA and FA

Properties	CA	FA
Specific gravity	2.89	2.63
Impact test (%)	17	–
Fineness modulus	–	2.68
Water absorption (%)	1.8	–

Table 2 Properties of SF and GF

Properties	SF	GF
Specific gravity	2.2	2.68
Young's modulus (GPa)	–	93.8
Bulk density (kg/m ³)	1450	2.488

Table 3 Compressive strength test

Specimen name	14 days
5SF	34.3
10SF	35
15SF	36.8
0.15GF	37.3

3 Experimental Program

3.1 Mix Combination

The concrete mix were designed as per the requirements of IS 456-2000 and IS 10262-2009. Considering the requirements, concrete mix of grade M40 for reference (RC), concrete with varying percentage of SF and concrete with 0.15% of glass fibre as given in Table 3 was experimented. Water cement ratio of 0.36 was kept constant throughout the investigation.

3.2 Mixing Methods, Casting, and Curing

In case of RC and 0.15SF, cement, aggregate and glass fibre (only for 0.15SF) were mixed dry for two minutes according to IS 456–2000 in order to obtain a homogeneous mix. Then, the water added to the dry mix and continued the mixing for another 4 min. Whereas in case of concrete containing SF, first the GF is soaked for 6 h in the amount of water determined and then it is slowly added to the dry concrete ingredients. The homogeneous mixture is then cast into cubes and cylinders. The nominal dimension of Cube specimen was 150 × 150 × 150 mm and cylinder specimen of

Table 4 Tensile strength test

Specimen name	14 days
5SF	2.6
10SF	2.63
15SF	2.86
0.15GF	3.1

diameter 150 mm and height 300 mm was fixed for each type mix. Specimens were casted and cured for 14 days at normal ambient temperature.

4 Results and Discussion

Compression Testing: The test was as per IS: 516-1959 on cubes shaped specimens cured in batches for 14 days the test results were compared with results of conventional cube of similar size and curing period respectively. Based on the experimental results obtained in this study, the characteristic compressive strength of concrete reached maximum value for 15SF when compared to other concrete mix whilst 0.15GF performed equally with the RF satisfying the requirements. The strength seems to be sensitive to the combination in different proportion of SF and increase in SF content more than 10% to the weight of cement showed a negative result on compression strength.

Split tensile strength: In accordance with IS 5816–1999, the evaluation was carried out on a cylinder with a diameter of 150 mm and a height of 300 mm. The results of different composition of quartz powder are presented in Table 4. Split tensile strength of each specimen with different percentage of silica fume better than that of the conventional concrete. The specimen 15SF with 0.15% glass fibre had the highest splitting tensile strength, by this it is evident that tensile strength of concrete improves effectively by the active influence of adding fibre.

5 Conclusion

In this particular piece of research, the influence that high performance has on beams made of glass fibre reinforced concrete was investigated. The following hypotheses and conclusions are susceptible to being supported by the findings of the experiments.

When compared to conventional concrete, concrete that contains silica fume has a higher compressive strength because it has a more cohesive mix as a result of the addition of silica fume.

Addition of glass fibre in reinforced delays the crack behaviour of concrete. Also, glass fibre, due to its less water absorption capacity improved the workability of fresh concrete.

References

1. Adel A, Azzawi A, Ahmed Sulthan A, Husam KR (2011) Behaviour of high-performance concrete structures. *ARNP J Eng Appl Sci*
2. Apporv S, Yogesh IM, Gourav J (2012) Performance of glass fibre reinforced concrete. *Int J Eng Innov Technol*
3. Barham HM, Aryan FHS, Rabar HF, Hakar HQ, Khaleel HY (2012) Mechanical properties and ductility behavior of ultra high-performance fibre reinforced concrete: effect of low water to binder ratios and micro glass fibres. *Ain Shams Eng J* 12:1557–1567
4. Ibrahim KIM (2016) Mechanical properties of glass fiber reinforced concrete (GFRC). *IOSR J Mech Civil Eng (IOSR-JMCE)*, 2278–1684 13(4):47–50
5. Komal C, Bharti T (2013) Studies of glass fiber reinforced concrete composites. *Int J Struct Civil Eng Res* 2(3):2319–6009
6. Magudeaswaran B, Eswaramoorthi T (2013) Experimental study on durability characteristics of high-performance concrete
7. Nili M, Afrouhsabet V (2010) Combined effect of silica fume and steel fibres on the impact resistance and mechanical properties of concrete. *Int J Impact Eng*
8. Shende A, Pande A, Gulfam Pathan M (2012) Experimental study on steel fibre reinforced concrete for M-40 grade. *Int Refer J Eng Sci*
9. Leema RA, Mohan V et al (2022) Finite element analysis of behavior and ultimate strength of composite column. *Sci Eng Compos Mater* 29:1–7. <https://doi.org/10.1515/secm-2022-0017>
10. Solhmirzaei R, Kodur VKR (2017) Modelling the response of ultra high-performance fibre reinforced concrete beams. *ELSEIVER J*
11. Vaishali GG (2010) An experimental investigation on glass fibre reinforced high performance concrete with silica fume as admixture
12. Vinayagam P (2012) Experimental investigation on high performance concrete using silica fume and super plasticizer
13. Vijayan DS, Revathy J (2016) Flexural response of fibre reinforced polymer laminated prestressed concrete beams. *Indian J Sci Technol*49(42). <https://doi.org/10.17485/ijst/2016/v9i42/101824>
14. Yu R, Spiesz P, Brouwers HJH (2015) Development of high-performance reinforced concrete (UHPRC): towards an efficient utilization of binders and fibres. *ELSEVIER J*
15. IS 383: 2016 Coarse and fine aggregate for concrete—specification
16. IS 10262: 2009 Concrete mix proportioning—guidelines (first revision)
17. IS 1199 (Part 1): 2018 fresh concrete -methods of sampling, testing and analysis part 2 determination of consistency of fresh concrete (first revision)
18. IS: 516—1959 Methods of tests for. strength of concrete
19. IS 456: 2000 Plain and reinforced concrete—code of practice (fourth revision).
20. IS 1489 (Part 1): 1991 Portland-Pozzolana cement specification Part 1 Fly Ash Based.
21. IS 5816: 1999 Splitting tensile strength of concrete—method of test (first revision)

Investigation on Innovative Cold-Formed Steel Built-Up Columns Using Lipped and Unlipped Channels



V. A. Veera Vignaesh, S. T. Dhaarini, and C. Manoj Kumar

1 Introduction

Presently, cold-formed steel (CFS) sections are broadly employed in both commercial and residential structures. Many researchers are coming up with different ideology on built-up sections to provide an economical design for buildings [1–6]. The effective design of compression members for CFS stubs, columns, and beams has been studied with different considerations like with and without stiffeners, varying box sections, fitting screw distance and CFS with lipped and unlipped sections [1, 4, 7–9]. The main advantages of CFS are lightweight, high strength and stiffness, quick and easy erection, uniform quality, more precise details, and cost-effective shipping and handling and they can be manufactured in tiny machine shops and can be fashioned into a wider range of pieces [6, 8–11]. The novelty of work in this paper is a new innovative built-up column consisting of combination of box and I section is developed and connected using screws, while the screw spacing is kept constants for all the heights of the column. The buckling load is used as a design criterion for compression members. The various buckling modes like local, distortional, and global modes decide the ultimate strength of the column. This research aimed at finding the axial load carrying capacity, deformation, and stress distribution in the built-up columns both experimentally by conducting axial compression test and analytically by using Abaqus 4.16 software. Also, the load versus deflection behaviour is compared for all specimens. The experimental and analytical results are compared and validated to derive the suitability of each specimen in the construction industry.

V. A. Veera Vignaesh · S. T. Dhaarini · C. Manoj Kumar (✉)
Department of Civil Engineering, Sathyabama Institute of Science and Technology,
Chennai 600119, India
e-mail: cmanoj1@gmail.com

2 Materials and Test Specimen

2.1 Materials

Cold-rolled sheet of grade IS 513 CR2 of 2 mm thickness is used to build up the columns and Grade M12 screws are fitted vertically throughout the column with equal spacings. Cutting and bending process is carried out in hydraulic machine.

2.2 Test Specimen

For numerical analysis, a total of 18 specimens is analysed using ABAQUS 4.16 software by keeping the cross section dimension and thickness as constant and the height of the column is varied from 300 to 2000 mm by increasing at an interval of 100 mm, whereas for Experimental analysis, 4 specimens of height 300, 500, 1000, and 1500 mm as shown in Fig. 1. are fabricated with cold-rolled sheet of thickness of 2 mm and two plates of size 300×300 mm are placed at top and bottom of each column and CO₂ welding is done. This is done for equal transfer of load throughout the whole column. The cutting and bending process is carried out in hydraulic machine. The sections of arranged by heights as per designed cross section and screws are drilled.

Fig. 1 Fabricated built-up columns of height 300, 500, 1000, and 1500 mm



2.3 Geometrical Properties of Sections

A new innovative built-up column is developed by a combination of box and I section joined using screws consisting of two channel sections with lip joined back-to-back along with the web and two channel sections without lip connected around the outer surface of the flanges of the channel section with lip. The screw spacing is kept constant at 100 mm throughout for all heights of the column. Figures 2 and 3 show the cross section of the column and section of the 1000 mm height column, respectively.

- Thickness of sheet used $t = 2$ mm
- Vertical Screw spacing, $s = 100$ mm
- Slenderness ratio = KL/r
- According to the AISI and AS/NZS,
- Modified slenderness ratio, $(KL/r)_m = \sqrt{(KL/r)_0^2 + (S/r_i)^2}$
- When, $(S/r_i) \leq 0.5 (KL/r)_0$
- $(KL/r)_0$ —Overall slenderness ratio of the built-up column.
- S—Spacing of the intermediate screws
- r—Radius of gyration
- r_i —Minimum radius of gyration of a single angle section
- K—Factor of effective length

Fig. 2 Cross section of the built-up column

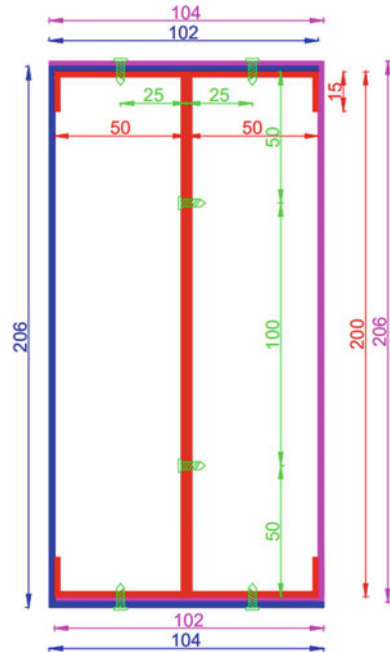
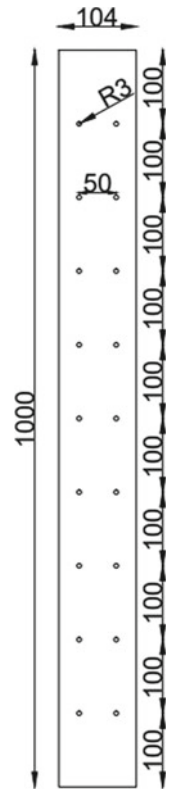


Fig. 3 Longitudinal section of column of height 1000 mm



2.4 Numerical Analysis

The finite element models for the specimen are created and analysed using Abaqus 4.16 software. In finite element analysis, buckling analysis is carried out to study linear behaviour initially. The buckling modes of columns and eigen values are observed. Then using Rik's method, nonlinear behaviour is studied, the curve for load against displacement is obtained for the columns.

2.5 Geometry and Material Property

The three-dimensional geometry of the built-up columns is formed. To account for nonlinearity in material, the values of stresses and strains are assigned to the models. The investigation and validation are carried out using the ABAQUS classic metal plasticity model. To obtain the accuracy of the result, mesh convergence study is performed, hence 10 mm mesh size is applied on all models. The Von Mises yield criterion was used for obtaining the stress-strain curve for the CFS section.

Fig. 4 Geometry and material property

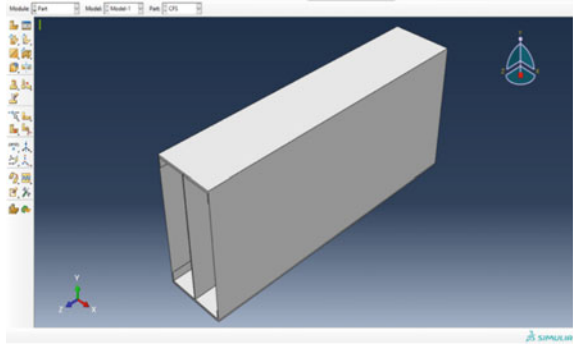
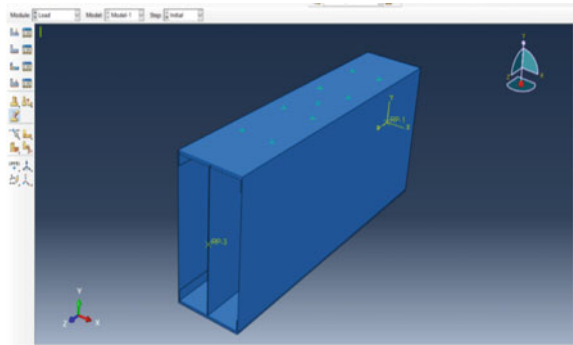


Fig. 5 Boundary condition



The mechanical properties of the section such as Young's modulus of Elasticity as 200,000 MPa, yield strength as 200 MPa, and Poisson's Ratio as 0.3 are assigned. Figure 4 shows the geometry and material property of the FEA model. The boundary conditions as assigned to the model are shown in Fig. 5.

2.6 Experimental Analysis

Axial load test is performed for all the four specimens of heights 300, 500, 1000, and 1500 mm are tested for axial loading and at the mid height two dial gauges are placed and end of the columns to determine the deflection for 300 and 500 mm columns. While for the other specimens of height 1000 and 1500 mm, Linear Variable Differential Transformer (LVDT) is used. The specimen of the height of 300 mm was tested using a compression testing machine (CTM), and the specimen of the height of 500 mm was tested using universal testing machine (UTM). Whereas the other specimens of height 1000 and 1500 mm were tested using column loading machine. The four CFS built-up columns of height 300, 500, 1000, and 1500 mm are fabricated and tested under axial load and results are obtained.

3 Results and Discussions

3.1 Results

From the buckling analysis, the eigen values and the buckling modes are derived based on linear analysis as shown in Fig. 6. The nonlinear analysis is performed to study the load versus deflection pattern by Rik's method. The slenderness ratio, modified slenderness ratio, and axial strength for all 18 columns are obtained from numerical analysis and given in Table 1.

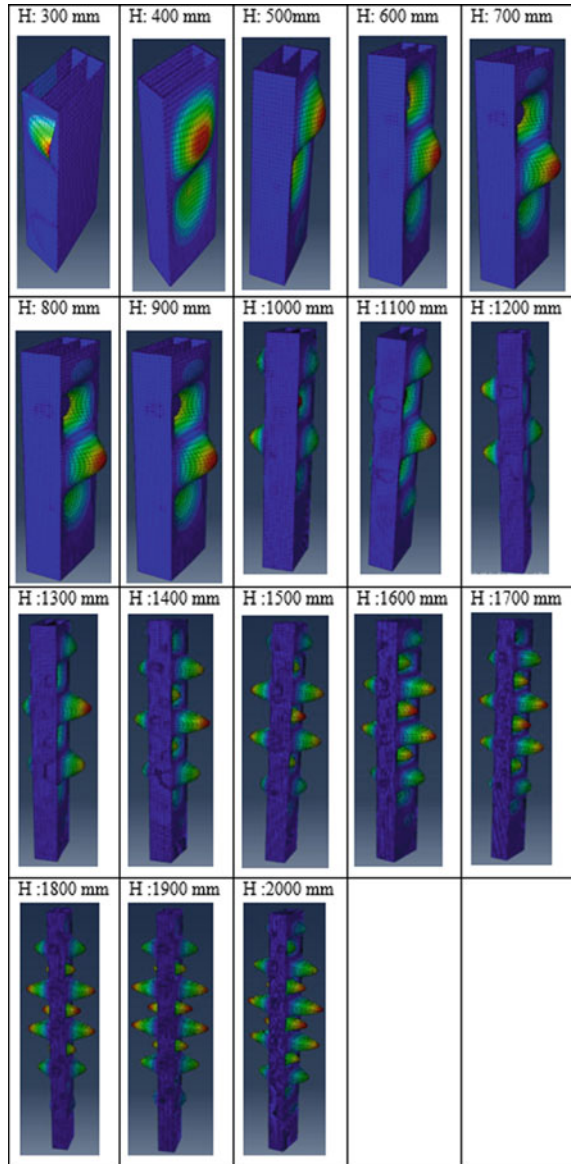
An experimental investigation was carried out for the columns of height 300, 500, 1000, and 1500 mm. As a result of axial load test, the failure pattern of buckling is observed in these columns as shown in Figs. 7, 8, 9, and 10 for the column heights of 300, 500, 1000, and 1500 mm, respectively. Figures 11, 12, 13, and 14 show the curve for axial load (kN) versus deflection (mm) for the column heights of 300, 500, 1000, and 1500 mm, respectively. Also, Table 2 gives the comparison of experimental and FEA load values of the columns, respectively.

3.2 Discussion

In experimental and numerical analysis, the results axial capacity of columns is obtained. The outcome of this work summaries as follows:

- The difference in axial strength outcomes of the experimental and finite element model is about 3% to 6%. From this, the FEA results show good acceptance with the experimental values, and hence FEA from Abaqus 4.16 software is reliable for the determination of axial strength of the column.
- The slenderness ratio of all the columns analysed lies between 8 and 60. The height of the columns was 300 to 2000 mm with 100 mm increment of each column, respectively. Hence, this cross section of the built-up column can be mainly used as a stub column, short column, and intermediate column only.
- As specified in the cross section, the vertical spacing of the screws was 100 mm which did not fail during the experimental testing of the columns.
- The load versus deflection graphs of the columns show that the maximum deflection of experimental investigation is greater than the FEA results. The deflection variation between experimental and FEA is about 50% for 300 mm column, 44% for 500 mm column, 14% for 1000 mm column, and 10% for 1500 mm column. Therefore, for lateral deflection of the column, FEA results are not reliable.
- On increase of column height, the slenderness ratio is increased, and axial strength is decreased.
- In the case of 300 mm column height local buckling occurred at both top and bottom during both the analysis. Since the height is very small, the load was transferred till the bottom.

Fig. 6 Buckling of columns from FEM analysis



- In the case of 500 mm column height, local buckling occurred at only at top during both the analysis.
- In the case of 1000 mm column height, local buckling occurred maximum at top and minimum at intermediate during both the analysis.
- In the case of 1500 mm column height, local buckling occurred minimum at top and maximum at intermediate during both the analysis.

Table 1 Numerical results of CFS built-up columns

Column height (mm)	Slenderness ratio $(\frac{KL}{r})_0$	Modified slenderness ratio $(\frac{KL}{r})_m$	Axial strength, P_{FEA} (kN)
300	8.84	9.35	534.89
400	11.79	12.18	447.12
500	14.74	15.05	388.57
600	17.69	17.95	361.13
700	20.64	20.86	346.62
800	23.59	23.78	341.09
900	26.54	26.71	340.39
1000	29.48	29.64	340.16
1100	32.43	32.58	339.06
1200	35.38	35.51	333.91
1300	38.33	38.45	329.27
1400	41.28	41.39	324.66
1500	44.23	44.33	322.62
1600	47.18	47.28	319.88
1700	50.13	50.22	317.63
1800	53.08	53.16	315.70
1900	56.03	56.11	314.23
2000	58.97	59.05	312.93

Fig. 7 Buckling of 300 mm column



Fig. 8 Buckling of 500 mm column



Fig. 9 Buckling of 1000 mm column

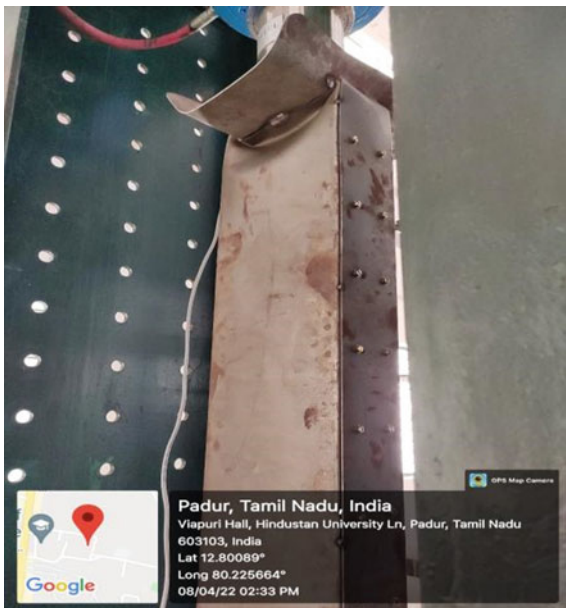


Fig. 10 Buckling of 1500 mm column



Fig. 11 Comparison of experimental and FEA results of 300 mm height column

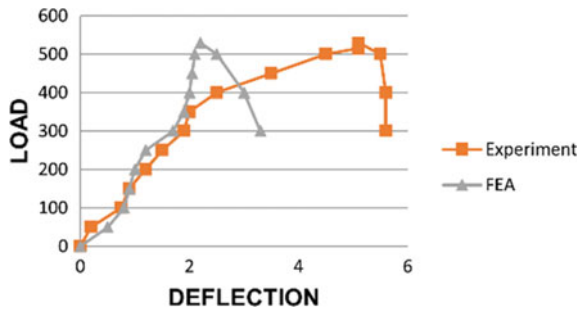
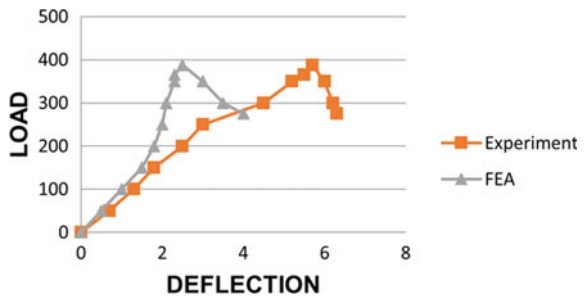


Fig. 12 Comparison of experimental and FEA results of 500 mm height column



- Due to the increase in the slenderness ratio, the change in the failure pattern doesn't seem to improve for all the columns. The failure mode was either local buckling or a combination of local and flexural buckling for all the columns.
- Compared to the previous studies, the axial load capacity of the built-up column has improved without the application of stiffeners.

Fig. 13 Comparison of experimental and FEA results of 1000 mm height column

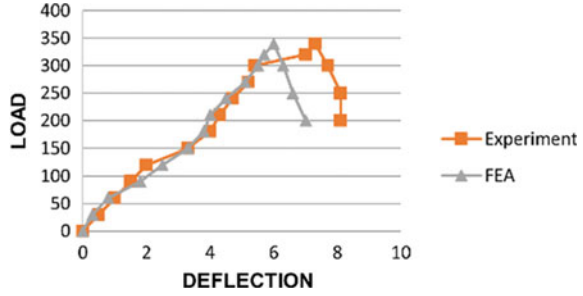


Fig. 14 Comparison of experimental and FEA results of 1500 mm height column

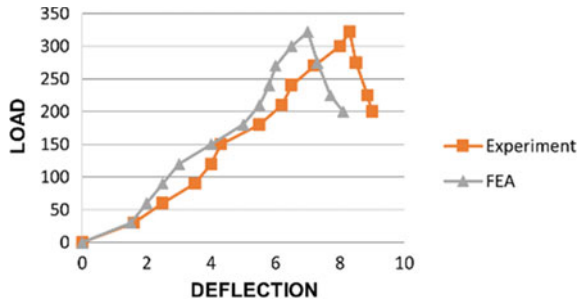


Table 2 Comparison of numerical and experimental load carrying capacities

Height (mm)	FEA load (kN)	Experimental load (kN)
300	534.89	515.5
500	388.57	365
1000	340.16	319
1500	322.62	303

- The performance of this cross section is better when compared to the built-up columns using battens.
- While experimental analysis, on application of load no screw underwent any failure.
- Future study can be performed with varying screw pattern and spacings.
- Further development of this work is to apply the same procedure for long columns and study their axial strength and behaviour.

4 Conclusion

In this research, 4 experimental models and 18 finite element (FE) models of numerical studies were done to understand the axial load carrying capacity and structural behaviour of the designed CFS built-up column with varied heights. The

failure modes, axial load carrying capacity, and load against lateral deflection were discussed. The FE model shows good agreement with the experiment outcomes. Since the modified slenderness ratio of the all the columns falls under 8 to 60, the CFS built-up column can be used as stub columns, short columns, and intermediate columns in construction.

References

1. Beulah Gnana Ananthi G, Ashvini B (2019) Experimental theoretical and numerical studies on cold-formed steel stub channel columns with stiffeners. *Asian J Civil Eng* 20(2):171–185
2. Ananthi GBG, Roy K, Lim JBP (2022) Experimental and numerical study of an innovative 4-channels cold-formed steel built-up column under axial compression. *Steel Compos Struct* 42(4):513–538
3. Nie SF, Zhou TH, Zhang Y, Liu B (2020) Compressive behavior of built-up closed box section columns consisting of two cold-formed steel channels. *Thin-Walled Struct* 151:106762
4. Anbarasu M, Venkatesan M (2018) Behaviour of cold-formed steel built-up I-section columns composed of four U-profiles. *Adv Struct Eng* 22(3):613–625
5. Dar AR, Vijayanand S, Anbarasu M, Dar MA (2022) Cold-formed steel battened built-up columns: experimental behaviour and verification of different design rules developed. *Adv Struct Eng* 25(2):321–335
6. Deepak MS, Shanthi VM (2018) Member distortional buckling behaviour of hybrid double-I-box beams. *Canadian J Civil Eng* 45(8):605–622
7. Deepak MS, Ananthi GBG (2021) Local buckling behaviour and capacities of cold-formed steel Double-I-Box stub and short column sections. *Structures* 34:1761–1784
8. Anbarasu M (2019) Behaviour of cold-formed steel built-up battened columns composed of four lipped angles: tests and numerical validation. *Adv Struct Eng* 23(1):51–64
9. Roy K, Lau HH, Huon Ting TC, Masood T, Kumar A, Lim BJP (2019) Experiments and finite element modelling of screw pattern of self-drilling screw connections for high strength cold-formed steel. *Thin-Wall Struct* 145(3)
10. Roy K, Ting TCH, Lau HH, Lim JBP (2018) Nonlinear behaviour of axially loaded back-to-back built-up cold-formed steel un-lipped channel sections. *Steel Compos Struct* 28(2):233–250
11. Ananthi GBG (2018) A study on cold-formed steel compound angle section subjected to axial compression. *KSCE J Civ Eng* 22(5):1803–1815

Strength Study on Engineered Cementitious Composites Using Hybrid Fibres



S. Samuel and N. Pannirselvam

1 Introduction

Due to its relatively low cost, ability to be cast, ability to be consumed, and ability to be recycled, concrete has become one of the most widely used composite materials. Despite the brittleness of concrete, the cementitious matrix's strength is increased by the random dispersion of short fibres. Fibre reinforced concrete has seen an increase in use over the last few decades [1]. To enhance the material's ability to deflect loads, the concrete's matrix fills macro and micro cracks and restricts the size of crack openings [2]. To create malleable concrete, engineers have turned to engineered cementitious composites (ECC), which rely on short fibre reinforcement. Tension zone strain hardening is possible with ECC. Similarly, high-performance fibre-reinforced cementitious composites (HPFRCCs) include ECC [3]. Because of its ductility, ECC helps to minimise cracking during the loading phase in which it is most effective. In order to account for the randomness of the materials, ECC is based on the principle of reaching substantial ten, and mesoscale modelling techniques have shown a lot of promise in understanding the behaviour of fibre bridging after the development of a fracture [4]. Steel fibres embedded in concrete could be used as an alternative to standard steel bars or welded fabric in some applications. This might turn out to be useful. The concept has been around for quite some time, ever since the first patent application for it was submitted in 1874, although it is only used in a select few situations. Commercial and industrial environments are now the most typical users of steel fibre reinforced concrete for paving and flooring [5]. Over the past decade, the United Kingdom has seen the installation of many millions of square metres of steel fibre reinforced slabs [6].

S. Samuel · N. Pannirselvam (✉)

Department of Civil Engineering, Faculty of Engineering and Technology, SRM Institute of Science and Technology, Kattankulathur, Tamil Nadu 603203, India

e-mail: pannirsn@srmist.edu.in

Polypropylene (PP) fibres, which have unique qualities compared to other synthetic fibres, are a great addition to many different types of construction materials, including concrete [7]. These characteristics strongly suggest that PP fibres be used in the manufacturing process. Fibres made from polypropylene can be spun in either a continuous or discontinuous fashion, and then laid out over a plastic matrix in either of these two configurations. Reinforcing materials frequently include PP fibres [8]. PP fibre is frequently used into the cement matrix to increase the durability of concrete. FRC has a much higher tensile strength than regular concrete and is much less likely to crack. This makes the material last much longer than competing options [9].

This research aims to investigate the mechanical qualities of ECC by subjecting it to some tests, including compression, split tensile, and flexural strength. This is also set up to analyse and investigate ECC's performance in terms of ductility and its long-term durability.

2 Experimental Program

2.1 Materials

According to the requirements of the IS code [11], the cement that was utilised in this investigation was ordinary portland cement of grade 53 MPa. It had a specific gravity of 3.11 and a fineness of 4%. Steel fibres measuring 50 mm in diameter and PP fibres of the same size have been incorporated. In the experiment, fine aggregate (M-sand) and municipal water were both utilised. The incorporation of the superplasticizer 430 has resulted in an increase in the workability of the concrete. In the course of this study, PP fibre and steel fibre were both utilised. (See Fig. 1). In Table 1, you will find a display of the characteristics of the fibres that were measured during the investigation. Table 2 contains a listing of the steel fibre's and the PP fibre's conforming physical properties to ASTM A820 [10].

2.2 Mix Proportions and Procedures

Table 1 contains the results of the research project's trial mixtures, which were used to determine the optimal mix proportions. First, the cement, fine aggregate, and m-sand are mixed together, and then, the fibres are added in the order that is specified for each mix, followed by the water in the ratios that are specified for water to cement, and finally, the superplasticizer is added. After a period of twenty-four hours, the specimens are taken out of the mould and positioned in the curing tank. There, they are kept engrossed in water for a period of twenty-eight days, so that they can cure. During the course of this investigation, a total of six distinct mixtures were utilised in

**Fig. 1** Type of fibres**Table 1** Mix proportions

Mix	Cement	Fine aggregate	HRWRA (%)	W/C	Steel (%)	PPF (%)
A	1	0.5	1	0.3	2	1
B	1	1	0	0.5	2	1
C	1	1.5	1	0.35	2	1
D	1	2	1	0.5	2	1
E	1	2.5	1	0.5	2	1
F	1	3	1	0.5	2	1

Table 2 Physical properties of fibres

Properties	Steel	Polypropylene fibre
Shape of fibre	Hooked end	Straight
Length (mm)	50	60
Diameter (mm)	0.75	0.0038
Aspect ratio (mm)	80	1579
Tensile strength (MPa)	1.225	1600

order to locate the ideal ratio for engineered cementitious composites. The analysis of the specimens allows for the measurement of a variety of mechanical parameters, including tests of compressive, flexural, and split tensile strength.

2.3 Mechanical Properties and Procedure

In order to arrive at an accurate determination of the material's strength, the mechanical properties of the ECC mixture are analysed. The specimens are put through tests of compressive strength, split tensile strength, flexural strength, in that order. After the fine aggregate, cement, and fibres in the water-to-cement ratio have been mixed together, the super plasticizer SP-430 is finally added to the mixture in a proportion that corresponds to the mix proportions for each mix. After that, the mixture is poured into the moulds and allowed to sit for a full day. After a day, they are taken out of the mould and allowed to finish curing. After that, they are subjected to compression, split tensile, density, and flexural strength tests on the 3rd, 7th, and 28th days, respectively. The detailed image of the compression testing machine is illustrated in Fig. 2.

2.3.1 Compressive Strength

In order to evaluate the effectiveness of ECC when combined with hybrid fibres, cubes with dimensions of $100 \times 100 \times 100$ mm were casted with hybrid fibres added to each of the six different mixes before being subjected to compression testing in a machine

Fig. 2 Compression testing machine



[12]. The results have been recorded, and now, they will be compared among the six different mixes in order to determine which one contains the appropriate proportion.

2.3.2 Split Tensile Strength

In order to investigate how well ECC works in conjunction with hybrid fibres and superplasticizer, cylinders measuring (100 × 200 mm) were cast for each of the six different mixtures, and each cylinder was subjected to compression testing using a machine in accordance with the Indian standard code [12]. The results of each test are being recorded, and a comparison of the values will be done in order to determine the appropriate ratio. This test must be done in proper procedure. The load must act equally on either side just like the compression test, so that the value will be correct.

2.3.3 Flexural Strength

The compression testing machine was used to evaluate the results of the flexural strength tests, which were performed on a prism of varying sizes (100 × 100 × 500 mm) that had hybrid fibres added to each of the six different mixes [12]. Each specimen's results will be recorded, and those results will be compared to the values.

2.3.4 Density Test

The bulk density of concrete is defined as the amount of freshly mixed concrete needed to completely fill a given container. Concrete's bulk density is a strong predictor of the material's ability to support structures, allow for the movement of water and solutes, and last for a long time. The volume of concrete that can be produced per cubic metre can be determined with this method [13].

3 Results and Discussions

3.1 Compressive Strength of Concrete

In the compression strength test, the values are recorded all the way up until the point where the test is considered unsuccessful. The results of the test revealed that the compression strength differed between mixtures in accordance with the proportions of the individual components. The results of the test revealed this information to be true. On the basis of the values, we came to the conclusion that the proportion of mix A that included fibre load combined with fine aggregate, cement, water, and superplasticizer was the most effective combination. The values were analysed,

Table 3 Compression test results

Mix ID	Compressive strength (N/mm ²)		
	3 days	7 days	28 days
A	18.00	32.50	39.00
B	10.00	19.50	38.50
C	14.16	28.38	35.40
D	4.00	8.66	28.70
E	8.00	19.34	28.20
F	2.00	16.10	19.80

which led to the discovery of this fact. The desired level of strength was not accomplished because mix B was produced without the utilisation of a superplasticizer. In comparison with the other mixes, the strength of mix A was relatively high due to the proportions of the steel and PPF that were included in that particular mix as well as the ratio of water to cement that was utilised in the formulation of that particular mix. The values of the compressive strength are given in Table 3.

3.2 Split Tensile Test of Concrete

The values were recorded after the specimen was analysed and found to be unsuitable for further testing. The degree to which there was a difference in the values that were obtained from the split tensile test was directly proportional to the proportions of each mix. It was found that mix A was the best mix due to the fibre dosage as well as the proportions of the fine aggregate, cement, water, and superplasticizer that were contained within the mix. Mix B was found to be the worst mix due to the proportions of the fine aggregate, cement, water, and superplasticizer that it contained. The findings of the examinations that were carried out allowed for this conclusion to be drawn. Mix A possessed a potency that was, in contrast to that of the other mixes, to a greater degree elevated. The values of tensile strength are given in Table 4.

Table 4 Split tensile test results

Mix	Split tensile strength (N/mm ²)		
	3 days	7 days	28 days
A	2.10	4.70	5.29
B	1.60	2.90	4.08
C	2.10	4.90	5.40
D	1.60	3.20	4.10
E	1.80	4.30	4.60
F	1.70	3.40	4.10

Table 5 Flexural strength test results

Mix ID	Flexural strength (N/mm ²)		
	3 days	7 days	28 days
A	3.43	5.04	5.77
B	2.32	3.62	5.09
C	2.93	4.64	5.39
D	1.26	2.09	4.62
E	2	3.59	4.63
F	0.79	1.15	3.66

3.3 Flexural Strength of Concrete

During the testing, the specimen was loaded from three different points, and the values were recorded after the specimen failed under the pressure after being subjected to the loading. According to the findings of the experiment, we found that the proportion of the mix A was the most effective when compared to the proportions of the other mixes. This was discovered based on the results of the test. The strength was able to gradually increase at a rate that was predetermined because of the dosage of the fibre content in the mix, the level of the water cement ratio, and the addition of the superplasticizer. The flexural strength values are represented in Table 5.

3.4 Density Test on Concrete

The container that was used for the density test has a capacity of 3 L, and its internal diameter measures 250 mm, while its outer diameter measures 280 mm. The difference between these two diameters is 280 mm. After the mixture has been put into the density jar, the contents of the jar need to be weighed in order to determine the density of the mixture. Mix F was found to have a density that was noticeably higher in comparison with the densities of the other mixes after the results of the measurement were compared to each of them. This was because of the amount of fibre that was utilised in the mixture in conjunction with the proportion of cement to fine aggregate that was utilised. The values that were obtained from the density test that were compared are depicted in a Table 6.

Table 6 Density of concrete

Mix ID	Density (kg/m ³)
A	2076.6
B	2086.6
C	2126.6
D	2173.3
E	2115.3
F	2193.3

4 Conclusion

ECC's mechanical properties and the optimal fibre content for constructing ECC were studied in the current experimental study. This was done, so that we could gain a better understanding of the construction of ECC. Because of the fibre dosage as well as the mix proportions of the cement, fine aggregate, and water, the overall study led us to the conclusion that mix A is the best option for compressive, split tensile, and flexural strength tests. This was determined as a result of the fact that mix A had the proportions of cement, fine aggregate, and water. This verdict was arrived at as a result of the comprehensive research that was conducted. The strength that was achieved was noticeably higher compared to that of the other mixes that were attempted. The graphical representation shows not only the values of each mix but also the value differences that exist between the different mixes. Additional research is being conducted right now with the goal of gaining a deeper comprehension of the microscopic structure of the ECC. Mix F was found to have a density value that was superior to that of the other mixes when they were put through the test. In addition to conducting additional research to identify additional properties, a cost analysis will also be developed at the same time. Subsequent paragraphs, however, are indented.



References

1. Sridhar R (2022) Durability study on engineered cementitious composites with hybrid fibres under sulphate and chloride environments. *Clean Mater* 5:100121, ISSN 2772-3976. <https://doi.org/10.1016/j.clema.2022.100121>
2. Ling-YX, Bo-Tao H, Jian-Cong L, Jian-Guo D (2022) Tailoring strain-hardening behavior of high-strength Engineered Cementitious Composites (ECC) using hybrid silica sand and artificial geopolymer aggregates. *Mater Design* 220:110876, ISSN 0264-1275. <https://doi.org/10.1016/j.matdes.2022.110876>
3. Jun F, Weiwei S, Le C, Bingcheng C, Emran A, Lufei D, Madura P (2022) Engineered cementitious composites using chinese local ingredients: material preparation and numerical investigation. *Case Stud Construct Mater* 16:e00852, ISSN 2214-5095. <https://doi.org/10.1016/j.cscm.2021.e00852>
4. Adeyemi A, Sreekanth D (2021) Development of eco-friendly engineered cementitious composites using glass aggregates: shrinkage properties. *Clean Eng Technol* 5:100299, ISSN 2666-7908. <https://doi.org/10.1016/j.clet.2021.100299>

5. Lili K, Fei W, Yafeng Z, Yanping W, Min W (2022) An exploratory study on using red mud waste as a replacement for fly ash to prepare engineered cementitious composites. *Construct Build Mater* 342:127900, ISSN 0950-0618. <https://doi.org/10.1016/j.conbuildmat.2022.127900>
6. Bashar SM, Veerendrakumar CK, Mohd SL (2018) Optimization of hybrid fibres in engineered cementitious composites. *Construct Build Mater* 190:24–37, ISSN 0950-0618. <https://doi.org/10.1016/j.conbuildmat.2018.08.188>
7. ZhuojunFeng F, Ying WZ, Lili S, Zhong FZ (2022) Optimal design of a low-cost high-performance hybrid fiber engineered cementitious composites. *Construct Build Mater* 345:128372, ISSN 0950–0618. <https://doi.org/10.1016/j.conbuildmat.2022.128372>
8. Bo-Tao H, Ji-Xiang Z, Ke-Fan W, Victor CL, Jian-Guo D (2022) Ultra-high-strength engineered/strain-hardening cementitious composites (ECC/SHCC): material design and effect of fiber hybridization. *Cement Concr Comp* 129:104464, ISSN 0958-9465. <https://doi.org/10.1016/j.cemconcomp.2022.104464>
9. Şukru O, Fuat D (2020) The hybrid effects of PVA fiber and basalt fiber on mechanical performance of cost-effective hybrid cementitious composites. *Construct Build Mater* 263:120564, ISSN 0950-0618. <https://doi.org/10.1016/j.conbuildmat.2020.120564>
10. ASTM A820/A820M—Standard Specification for Steel Fibers for Fiber-Reinforced Concrete
11. IS 12269 (1987): 53 grade ordinary Portland cement
12. IS 516 (1959): Method of Tests for Strength of Concrete
13. IS 1199 (1959): Methods of sampling and analysis of concrete

Investigation of Bending Effect on Steel–Concrete–Steel (SCS) Sandwich Composite Sections Considering Width–Thickness Ratio and Global Provisional Codes Validation



Wesam Al Agha , Taha Ahmed Ghaleb Mohammed ,
Mohamad Ali Ishaq Najajra , and Nambiappan Umamaheswari 

1 Introduction

A novel sandwich structure technique has been developed for submerged-tube tunnels, which involves the integration of two slender steel plates with concrete infill. In recent years, significant research has been conducted on using steel–concrete–steel (SCS) configurations [1]. This study highlights novel aims in SCS sandwich construction and various concrete materials. Specifically, the investigation examines SCS sandwich composite buildings utilising advanced enhanced C-channels bonded to concrete [2]. Specifically, the proposed method involves the creation of steel sandwich composite beams. The structural concrete sandwich (SCS) system

W. Al Agha

Department of Civil Engineering, Delhi Technological University, Delhi 110042, India

W. Al Agha (✉) · N. Umamaheswari

Department of Civil Engineering, Faculty of Engineering and Technology, SRM Institute of Science and Technology, Kattankulathur 603203, Tamil Nadu, India

e-mail: wesamalagha1@gmail.com; wa4977@srmist.edu.in;

wesamalagha_2k21phdce16@dtu.ac.in; wesam.alagha@unich.it

N. Umamaheswari

e-mail: umamahen@srmist.edu.in

W. Al Agha

Department of Engineering and Geology, University G. d'Annunzio of Chieti-Pescara, Viale Pindaro 42, 65127 Pescara, Italy

T. A. G. Mohammed · M. A. I. Najajra

Department of Civil Engineering, Cyprus International University, via Mersin 10 Haspolat, North Cyprus, Turkey

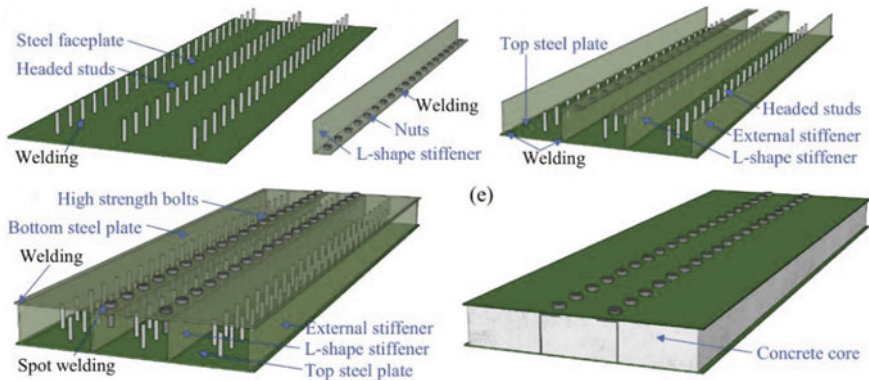


Fig. 1 Typical steel–concrete–steel sandwich element

generally comprises an unreinforced concrete core section framed by two comparatively thin steel plates [3]: the top compression plate and the bottom tension plate. These plates are linked to the concrete infill via welded shear stud connectors, as depicted in Fig. 1.

If plates are tested by flexure, the compression and tension forces are due to their alignment in the bending plane. The utilisation of SCS form construction eliminates the need for additional shear reinforcement. Shear connectors have been delivered for this objective [4]. The utilisation of SCS construction methodology exhibits a high degree of cost-effectiveness. This material exhibits a combination of advantageous properties from both steel and concrete. The material is highly suitable for a diverse range of structures, including but not limited to building cores [5]. The potential failure of conventional reinforced concrete components can be attributed to concrete crushing. Steel yielding can occur due to various factors, including flexure, shear, torsion, or bond failure [3]. Similarly, in SCS components, the collapse can be initiated by any single mode, including tensile yielding of steel, compressive yielding or buckling of steel, the compressive smashing of concrete, the collapse of tension steel, concrete shear failure, or failure of shear connectors. The yielding of steel in tension or compression and the crushing of concrete in compression are determined by the selection of the suitable material and their respective mechanical characteristics. Figure 2 depicts identified failure modes of the SCS component [5].

Chen and Wang [5] presented a study using LS-DYNA in which finite element (FE) simulations were built for the steel–concrete–steel (SCS) sandwich SCSSB-IACs. The FE calculations demonstrated a beneficial correlation with the results obtained from the impact test findings. The present study explored the impact procedure, propagation, and variation in bending and shear force, stress, and strain moments. In addition, finite element (FE) analyses were employed to identify the internal energy histories of the self-compacting steel-slag-based (SCSSB) iron aggregate concrete (IACs). The study's findings revealed that the concrete and bottom face-plate were

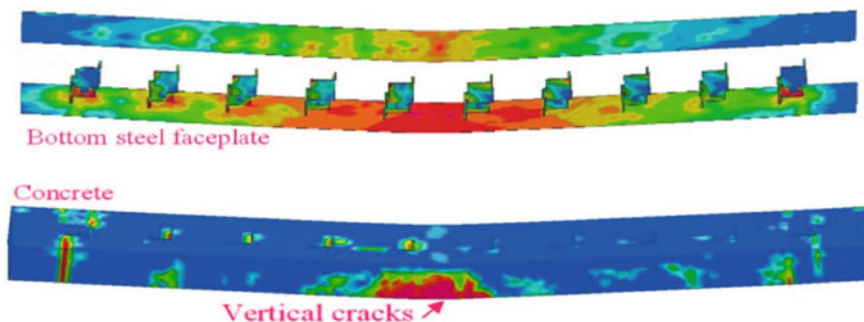


Fig. 2 Failure modes of the SCS sandwich

responsible for absorbing a significant portion of the impact energy. In contrast, a flexural mode primarily characterised the deformation of the SCSSB-IACs.

In summary, exploring the most important effect of using the steel–concrete–steel (SCS) composite in different concrete grades based on bending capacity and local buckling with varying thicknesses of SCS components is significant.

2 Materials and Modelling Setup

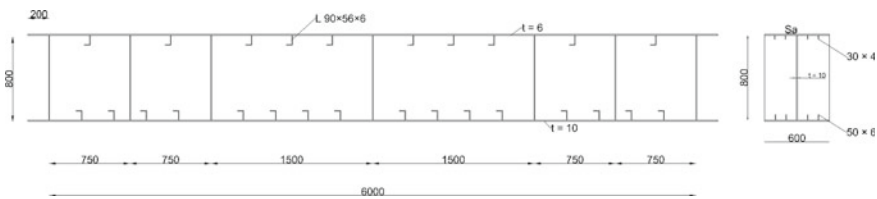
The main objective of this study is to evaluate the structural efficacy of concrete–steel (SCS) beams before and after changing the materials grade of concrete and steel based on Indian standards [6] regarding the bending moment and shear connector characteristics [7]. Moreover, the research necessitates finding and using load–deflection diagrams before and after varying the input of finite element software, Abaqus (6.14). The dimension [7] of steel–concrete–steel composite beam (SCS) is illustrated in Table 1.

The model of all seven beams is made to be the same, as shown in Fig. 3.

The (concrete–steel) specifications has taken based on the relevant study for the validation models and as per Indian standards for the two groups of materials' strength. In the validation models, it was simulated based on the relevant study material for beams (B1, B2, B3, B4, and B5) as the f_{cu} (48.5 MPa) concrete and to be f_{cu} (25.4 MPa) for validation beams (B6 and B7) [7]. The new strength group 1 material, as per Indian standard, has been inserted into the Abaqus to be higher than the validated models of beams where (B1, B2, B3, B4, and B5) as the f_{ck} (53.35 MPa) concrete and f_{ck} (31.6 MPa) for validation beams (B6 and B7) [8]. In contrast, the new strength group 2 material, as per Indian standard, has been included in the Abaqus to be lesser than the validated models of beams where (B1, B2, B3, B4, and B5) as the f_{ck} (38.15 MPa) concrete and higher one by f_{ck} (26.6 MPa) for validation beams (B6 and B7). The same process has been done to define the steel properties of materials of thickness elements in the validation models as thickness 4 equals

Table 1 Dimension of SCS beam

SCS element	Abaqus model (mm)
Length (L)	6400
Width (b)	600
Height (h)	800
Thickness of top flange (t_t)	6
Thickness of bottom flange (t_b)	10
Thickness of axial web (t_{wx})	10
Thickness of transverse web (t_{wy})	L 90 × 56 × 6
Axial ribs in top flange	L 30 × 4
Axial ribs in bottom flange	L 50 × 6
Spacing of shear connector, top flange	375
Spacing of shear connector, bottom flange	500

**Fig. 3** Plan dimension (mm)

to f_u (521 MPa), thickness 6 equals to f_u (536 MPa), and thickness 10 equal to f_u (494 MPa) as f_u the minimum tensile strength [8]. The same insertion is for new strength group 1 material where models are included as thickness 4 equals to f_u (500 MPa), thickness 6 equals to f_u (500 MPa), and thickness 10 equal to f_u (500 MPa). In contrast, the new strength group 2 material, as per Indian standard, has been included in the Abaqus to be lesser than the new strength group 1 material as thickness 4 equals to f_u (450 MPa), thickness 6 equals to f_u (450 MPa), and thickness 10 equal to f_u (450 MPa) [8].

2.1 Numerical Methodology

The model of Abaqus is defined as the anticipated surface at a particular mode resulting from bending capacity using the plastic damage input as part of the analysis of the experimental relevant study. A method for determining the characteristics of a system involves significant model specimens' configuration of a structural SCS framework. The model is varied based on surface factors and the surface's boundary

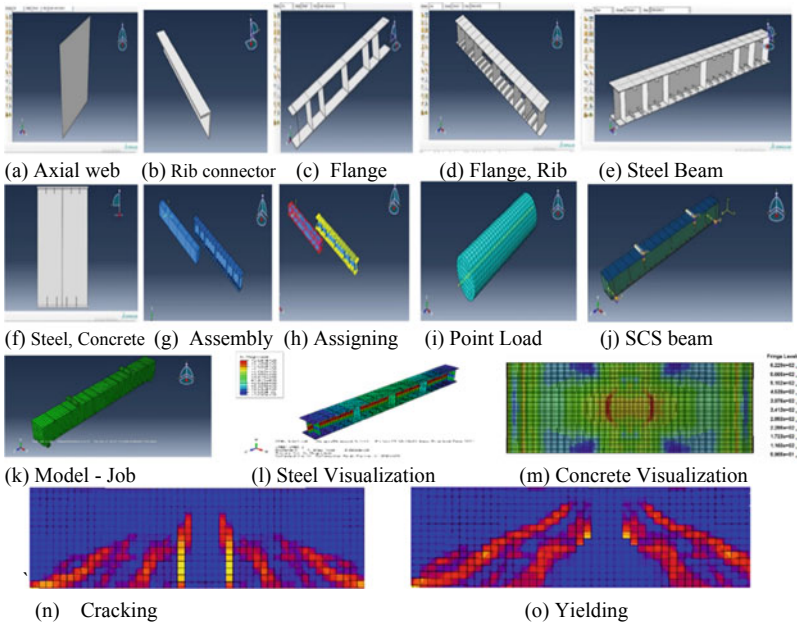


Fig. 4 Numerical modelling steps of SCS beams

conditions. The nodes of interaction have taken points to points interaction, surface-to-points, and surface-to-surface. The steps of modelling for the beams are shown in Fig. 4.

In Fig. 4, the steps of modelling started by defining the elements of steel materials as shown in Fig. 4 (a) axial web; (b) rib connector; (c) top flange and bottom flange with axial web based on dimensions and materials properties. Then, it was linked that all of the steel components were to format the (d) flanges with shear connectors and (e) steel beam with shear connectors, and assign the steel core with concrete as presented in Fig. 4; (f) steel beam with a concrete core. The next step is to release the meshing steps (thick-shell and four-node element) and define load cases as in Fig. 4; (g) assembly of steel model to the concrete core with proper mech increments (100). The most significant step is the interaction between concrete and steel core, as illustrated in Fig. 4. (h) Assigning the points as interaction surface to surface, the following process of loads started as in Fig. 4. (i) Define the point load and duplicate as constraints under the SCS beam at edges. Finally, Fig. 4 (k) starts an analysis of model job to be presented; (l) steel visualisation; (m) concrete visualisation in terms of SCS beams failure as in Fig. 4; (n) cracking behaviour; and (o) yielding behaviour. The same process is followed for SCS validation beams, varying the new material strength groups 1 and 2.

3 Validation of Beams Models as Per Global Codes

This validation's principal objective is determining whether the analysed beam fulfils the minimum structural criteria defined by the international code for the structural specimens. The most significant advantage of utilising this validation results from its capacity to design factors where experimentation is unachievable efficiently. The credibility of this theory is predicated depending on the measure to which the code-based equations concerning the structural behaviour of the beam are integrated with the beam's identified structural performance during assessment. The SCS bending design methodologies were established in the Japanese and European design codes [9–11]. Both design codes use plane section theory and plastic design techniques found in reinforced concrete (RC) structures, with the steel plates regarded as reinforcements as considered the impact of shear. The yield strength (f_{swr}) of the web in the Japanese code is determined through a specific process.

$$f_{swr} = f_{sw} \left(1 - \sigma_w / f_{sw} \right) \quad (1)$$

The parameters “ f_{swr} ” and “ σ_w ” represent the testing yield strength of the web and the shear stress produced by the shear computation, respectively. The European code [9] determines equivalent SCS bending capacity (M_d) and shear capacity (V_d) values as in the equation.

$$\left(\frac{V_d}{V_{pd}} \right)^2 + \left(\frac{M_d}{M_{pd}} \right)^2 \leq 1 \quad (2)$$

V_{pd} represents the shear capacity with zero moments, while M_{pd} indicates the bending capacity in the zero shear force. Despite the boundary condition of zero shears in the pure bending experiments conducted in this study, it is recommended that these techniques be employed in the design process. Additionally [10, 11], the Japanese code proposes taking into account the impact of local buckling by decreasing the compression capacity of the compression flange using the following equation,

$$f_{scr} = \frac{t}{S_a} \sqrt{E_s f_{scr}} \quad (3)$$

The reduced design strength of the compression flange, denoted as f_{scr} , is considered when considering local buckling, which is assumed in contrast to the testing yield strength of the compression flange, represented by f_{scr} . At a given value of $S_a = t$ equal to 1/4 and f_{scr} equal to 400 MPa, as observed in the relevant study, the reduction factor is approximated to 0.56. It had demonstrated that buckling occurred subsequent to the yielding of the specimen and did not significantly impact its bending capacity. European recommendations based on the findings has been indicated that the width–thickness ratio might be calculated for optimal results. It was utilised

conservatively to decrease the design strength. The European code recommends the impact of partial connectivity. The finite element model demonstrates that the transverse webs effectively prevent potential relative collapse between the concrete and steel by providing the shear connections. Consequently, it is recommended that the design of a full shear connection be adopted in practical applications.

4 Results

Twenty-one beams were tested using Abaqus, finite element software, to present the steel–concrete–steel (SCS) sandwich effect compared to varying steel and concrete properties materials. These beams were subjected to load-testing bending failure modes considering local buckling. The seven validated SCS beams with relevant studies have shown lower values than the new strength materials group 1 and higher values than the new strength materials group 2. Furthermore, a series of analyses have been performed to check the composite’s performance. Exploring this SCS composite effect by varying the bottom and top flanges’ thickness is vital. It is significant to investigate the changes in thickness values of the SCS axial web that was studied for all the validation models in contrast to Indian materials of different strengths.

In conclusion, the buckling with varying width–thickness ratios for numerical specimens, the bending capacity, yielding, and ultimate testing were observed, as presented in Tables 2, 3, and 4, where it has δ_t = testing displacement and F_t = testing load. The abbreviation of yt: yielding, dt: detaching, and ut: ultimate are presented with respect the force and displacement.

The comparison between 21 SCS beams might have been observed based on Tables 2, 3, and 4. For instance, in Table 2, the values of validation SCS beams indicate that detaching compared to the yield ratio of displacement varied from 3.0 to 5.1. In contrast to the yield displacement, the ultimate displacement exhibits a range of variability between 3.1 and 7.8. Compared to the detaching case, the ultimate

Table 2 SCS beams results and validation

Testing SCS beams values and validation									
Specimens	δ_{yt} (mm)	F_{yt} (k N)	δ_{dt} (mm)	F_{dt} (k N)	δ_{ut} (mm)	F_{ut} (k N)	δ_{dt}/δ_{yt}	δ_{ut}/δ_{yt}	δ_{ut}/δ_{dt}
Beam 1	33.3	3415	116.8	4409	179.9	4496	3.5	5.4	1.5
Beam 2	29.6	4302	159.2	5706	184.4	4940	5.4	6.2	1.2
Beam 3	22.1	3165	91.6	4380	172.2	4500	4.1	7.8	1.9
Beam 4	30.3	3405	91.0	4496	144.2	4606	3.0	4.8	1.6
Beam 5	34.8	4037	159.5	5245	167.5	5173	4.6	4.8	1.1
Beam 6	24.4	2862	81.4	3789	112.1	3853	3.3	4.6	1.4
Beam 7	32.7	3707	99.6	4754.52	101.3	4664	3.0	3.1	1.0

Table 3 SCS beams results, new strength 1

Testing SCS beams values, new strength 1									
Specimens	δ_{yt} (mm)	F_{yt} (k N)	δ_{dt} (mm)	F_{dt} (k N)	δ_{ut} (mm)	F_{ut} (k N)	δ_{dt}/δ_{yt}	δ_{ut}/δ_{yt}	δ_{ut}/δ_{dt}
Beam 1	21.0	3463	118.1	4609	181.9	4750	5.6	8.6	1.5
Beam 2	29.6	4575	162.4	5827	172.7	5592	5.5	5.8	1.1
Beam 3	14.3	3617	102.3	4435	192.6	4683	7.2	13.5	1.9
Beam 4	22.8	3877	102.0	4471	182.0	4781	4.5	8.0	1.8
Beam 5	25.9	4139	159.2	5367	191.4	5380	6.2	7.4	1.2
Beam 6	11.8	3144	90.3	4063	146.7	4173	7.6	12.4	1.6
Beam 7	18.9	4229	115.5	5008	125.5	5008	6.1	6.6	1.1

Table 4 SCS beams results, new strength 2

Testing SCS beams values, new strength 2									
Specimens	δ_{yt} (mm)	F_{yt} (k N)	δ_{dt} (mm)	F_{dt} (k N)	δ_{ut} (mm)	F_{ut} (k N)	δ_{dt}/δ_{yt}	δ_{ut}/δ_{yt}	δ_{ut}/δ_{dt}
Beam 1	39.0	3391	107.5	4138	150.9	4253	2.8	3.9	1.4
Beam 2	43.4	4093	156.1	4641	165.8	4680	3.6	3.8	1.1
Beam 3	31.2	3228	85.9	3961	168.2	4110	2.8	5.4	2.0
Beam 4	37.4	3613	89.5	4057	168.2	4110	2.4	4.5	1.9
Beam 5	32.7	3539	151.3	4270	183.5	4414	4.6	5.6	1.2
Beam 6	30.2	2883	88.2	3350	123.0	3473	2.9	4.1	1.4
Beam 7	29.4	3131	92.0	3743	49.0	3896	3.1	1.7	0.5

displacement presented a ratio of 1.0 to 1.9. Table 3 presents the ratios alterations for the detaching to yield and ultimate to yield displacement by the ratio (4.5 to 7.6) (5.8 to 13.5), respectively. The ratio of ultimate to detaching displacement varies from 1.1 to 1.9. In conclusion, the comparison of ratio values is summarised in Table 4, which displays the range of test results for the detaching compared to the yield displacement ratio, varying between 2.4 and 4.6. The ultimate compared to yield ratio was from 1.7 to 5.4.

In Fig. 5, (a) represents the SCS beams values from a group of validation models with relevant studies to compare with new strength material in (b,c) SCS beams 1 and 2. It has shown that the group of material 1 exhibited higher values than validation SCS beams. In contrast, new materials SCS beams 2 illustrate lower values than validation SCS values. The same investigation is shown in Fig. 6 in terms of the ultimate load. In Fig. 7, SCS composite effect by varying the bottom (t_b) and top flanges (t_b) thickness is vital. Investigating the changes in thickness values of the SCS axial web (t_w) was significant in terms of validation models and materials properties from Indian standards. The thickness values vary as (5–10–15) mm in the models for the standard beam based on initial dimension simulation. In Fig. 8, it has shown the

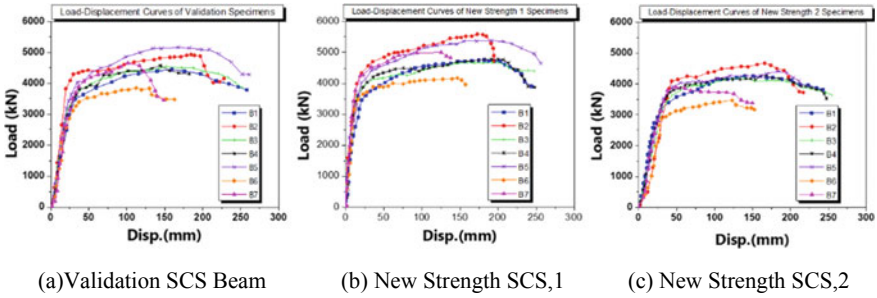


Fig. 5 Comparison of SCS beams, load–displacement

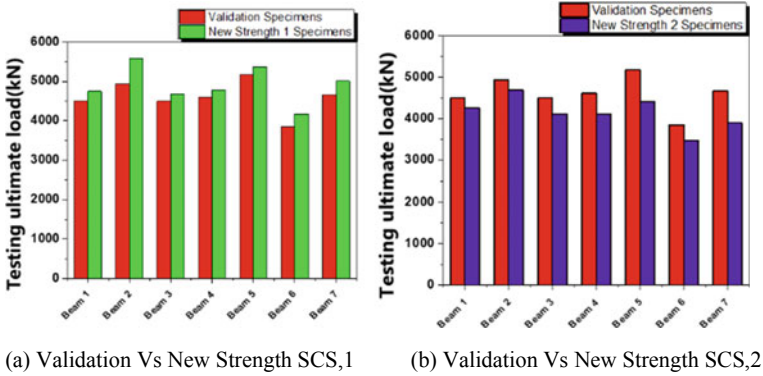


Fig. 6 Comparison of SCS beams, ultimate load

local buckling effect for the ultimate load as varied width–thickness ratio S_d/t by 25 and 41.7 for SCS beams. In Fig. 9, the testing bending capacity illustrated to SCS beams compared to Japanese code, European code, and the proposed approach.

In conclusion, validation specimens verified manually approaching from codes show that the expected ultimate bending capacities of the current design methods and the proposed method are close. The proposed method agrees well with the analytical outputs. It will be safely used in reality without taking into account the material's hardening.

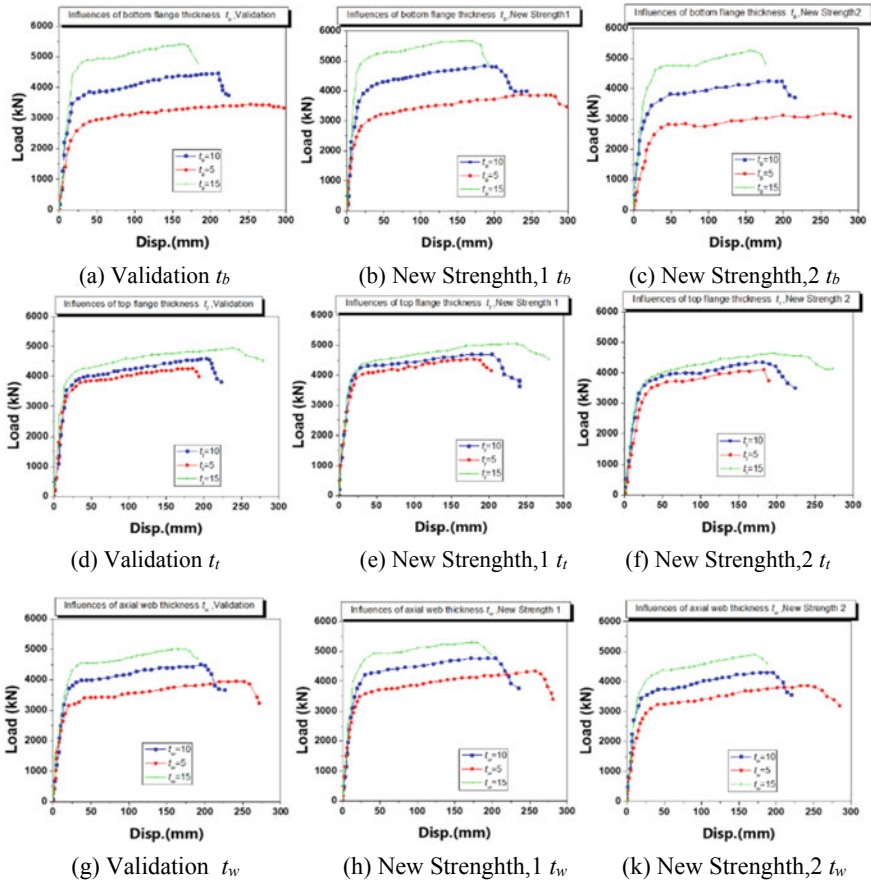


Fig. 7 Comparison of SCS beams, thickness of steel plates

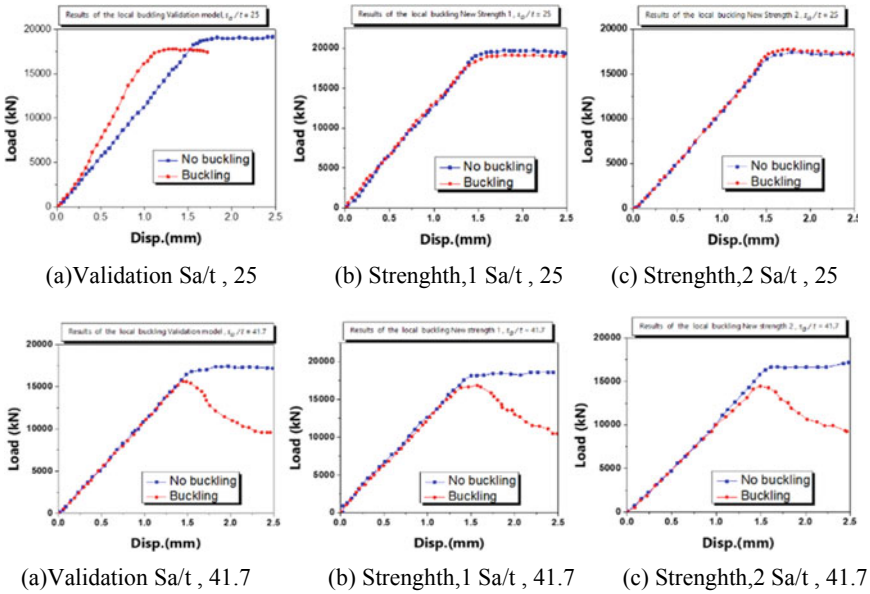


Fig. 8 Comparison of SCS beams, local buckling

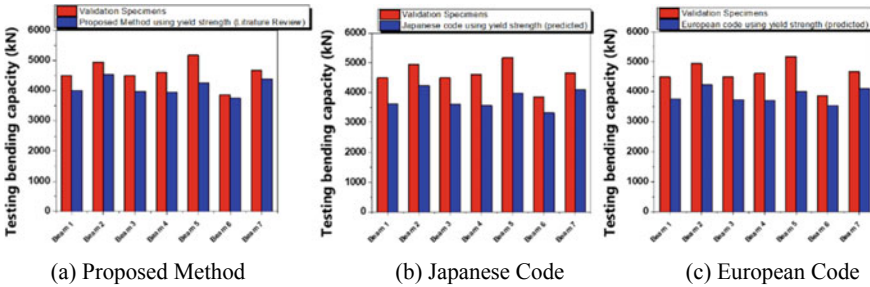


Fig. 9 Comparison of SCS beams, testing bending capacity “Global Code”

5 Conclusion

In this study, twenty-one steel–concrete–steel (SCS) were built and subjected to load testing in bending investigation using Abaqus software. Beams have been selected to ensure enhancement of yield point and local buckling in terms of steel elements’ varying material properties and thickness. The output concludes as follows,

- The local buckling effect was regulated in the compression area, which has the maximum width–thickness ratio.
- The local failure of both the steel and concrete occurred due to increasing force at the support.

- Local detaching between the steel and concrete due to buckling was investigated in the compression flange to present these values.
- Since the steel flange has a confinement effect, this arrangement implies that buckling does not represent the member's ultimate position where buckling activity has a specific impact on concrete crushing.
- The load–displacement curves summarised the impact of capacity as varied between the group of validated SCS beams compared to new strength material 1 and 2, indicating where proper design and optimum effect.
- A model of localised buckling was developed as the influence of concrete and steel strength emphasises on the local buckling effect.
- Since the specific concrete compressive strength ($f'c$) increases, the bending capacity will be increased in new strength materials 1 compared to the validation models.
- Compared to global codes for SCS calculation, the proposed method agrees well with the analytical outputs. It will be safely used in reality.

Acknowledgements The authors would like to express appreciation to the Indian Council for Cultural Relations, India, and the INPS's social security contribution under separate management (CHIETI, IT), Italy.

References

1. Liew JYR, Yan J-B, Huang Z-Y (2017) Steel-concrete-steel sandwich composite structures—recent innovations. *J Constr Steel Res* 130:202–221. <https://doi.org/10.1016/j.jcsr.2016.12.007>
2. Leng YB, Song XB, Chu M, Ge HH (2015) Experimental study and theoretical analysis of resistance of steel-concrete-steel sandwich beams. *J Struct Eng* 141(2). [https://doi.org/10.1061/\(ASCE\)ST.1943-541X.0001060](https://doi.org/10.1061/(ASCE)ST.1943-541X.0001060)
3. Wang Y, Lu J, Zhai X, Wang W (2022) Flexural behaviours of one-way steel-concrete-steel sandwich panels with novel hybrid connectors: tests and analysis. *J Constr Steel Res* 188:107013. <https://doi.org/10.1016/j.jcsr.2021.107013>
4. Roberts TM, Edwards DN, Narayanan R (1996) Testing and analysis of steel-concrete-steel sandwich beams. *J Constr Steel Res* 38(3):257–279. [https://doi.org/10.1016/0143-974X\(96\)00022-3](https://doi.org/10.1016/0143-974X(96)00022-3)
5. Chen J, Wang Y (2023) Finite element analysis of steel-concrete-steel sandwich beams with novel interlocked angle connectors subjected to impact loading. *J Constr Steel Res* 207:107977. <https://doi.org/10.1016/j.jcsr.2023.107977>
6. Kant R, Al Agha W, Thakur MS, Umamaheswari N (2022) Comparative study on seismic performance of steel-concrete composite structure without and with buckling—restrained braces. *Mater Today Proc* 56:2134–2144. <https://doi.org/10.1016/j.matpr.2021.11.461>
7. Guo YT, Nie X, Tao MX, Qiu SY, Tang L, Fan JS (2019) Bending capacity of steel-concrete-steel composite structures considering local buckling and casting imperfection. *J Struct Eng* 145(10). [https://doi.org/10.1061/\(ASCE\)ST.1943-541X.0002385](https://doi.org/10.1061/(ASCE)ST.1943-541X.0002385)
8. Bureau of Indian Standards (2000) New Delhi, Indian Standard Plain and Reinforced Concrete- IS 456
9. CEN (European Committee for Standardization) (1992). Design of concrete structures. Eurocode 2, CEN, Brussels, Belgium

10. JSCE (Japan Society of Civil Engineers) (1991) Standard specification for design and construction of concrete structures, JSCE, Tokyo
11. JSCE (Japan Society of Civil Engineers) (1992) Design code of steel- concrete sandwich structures. [In Japanese.] Concrete Library No. 73. JSCE, Tokyo

Experimental Investigation on Mechanical Properties of Steel Fibre in M50 Grade Concrete



S. Prakash Chandar and T. S. Lakshmi

1 Introduction

The manufacture of concrete consists of fine and coarse aggregate materials mixed with cement and water. In the construction area, there is an increasing for the requirement of concrete. Nowadays, many researchers are involved in this work to increase the strength of the concrete by adding some waste materials [1]. The use of waste RTSF strengthens concrete structures and promotes the development of sustainable construction by preserving natural resources [2]. Industrial steel fibres (ISF) have been compared to recycled steel fibres (RSF) derived from used tires [3]. The combination of steel fibres, aggregates, mortar matrix and the interfacial transition zone (ITZ) has been extensively employed to simulate the behaviour of steel fibre-reinforced concrete (SFRC) materials and structural elements. This approach aims to gain a deeper understanding of how steel fibres interact within the matrix, comprehend their action and behaviour, and ultimately recording the failure mechanisms of SFRC when subjected to varying loads [4]. The steel fibre is added in the concrete to make the concrete to achieve more strength. This research work explains about the addition of fibre in M50 grade mix concrete.

2 Materials

The required components for the manufacturing the concrete are cement, aggregate and water. The mineral admixture micro silica and superplasticizer are also added.

S. Prakash Chandar (✉)

SRM IST, Civil Engineering, Kattankulathur, Chennai, TN 603203, India

e-mail: prakashs2@srmist.edu.in

T. S. Lakshmi

Department of Infrastructure Engineering, Saveetha School of Engineering, Chennai, India

2.1 Cement

Cement is a substance in helping the material bond which each other. In this article, the ordinary portland cement OPC 53 is used as per the Indian standard 12,269: 2013 [5] specification.

2.2 Fine Aggregate

The aggregates are used in the production of concrete. The passing of 4.75 mm sieve size of materials is considered as fine aggregate as the code of provision Indian standard 383: 2016 [6].

2.3 Coarse Aggregate

The larger portion occupied in the concrete is coarse aggregate. The coarse aggregate is retaining the 4.75 mm sieve size which is considered as coarse aggregate, and the maximum of 20 mm aggregate is chosen as per the code provision of Indian standard of IS 383: 2016 [6] in the production of concrete.

2.4 Micro Silica

Micro silica is a very fine chemical material that improves the performance and quality of concrete. According to IS 15388: 2003 [7], the micro silica added is 12% in the production of concrete. Adding micro silica helps to achieve the higher mechanical properties.

2.5 Superplasticizer

The superplasticizer Conplast SP450 is used to enhance the concrete's working ability, shorten the time it takes for it to start setting and accelerate the strength development of the concrete.

3 Experimental Work

The mechanical characteristics of concrete were cast, and for fresh properties, slump cone value as 40 mm and the compaction factor value as 0.84 were found out, and the results are discussed below. Material characteristics are discussed in Table 1.

3.1 Compressive Strength Test

According to Indian Standard code IS 516:1959 [8] and the grade of concrete M50 (1: 1.47: 3.04: 0.35), the test on samples should be performed at after 3rd, 7th and 28th days. The mix ratio of the concrete is assumed to be M50 concrete grade. The test was carried on concrete sample sizes $150 \times 150 \times 150$ mm, and test outcomes are discussed in Table 2 and Fig. 1, respectively.

Table 1 Properties of materials

Description	Result	Requirement according to IS 12269:2013
<i>Physical properties</i>		
Fineness–specific surface	312 m ² /g	≧225 m ² /g
Initial setting time	34 min	≧30 min
Final setting time	468 min	≧600 min
Cement soundness	1.5 mm	≧10 mm
<i>Chemical composition</i>		
<i>Lime saturation factor</i>	0.96	≧0.8 and ≦1.02
Ratio of Al to Fe	1.19	≧0.66
Insoluble residue (%)	0.84	≧2
Sulphuric anhydride (SO ₃) (%)	2.10	≧3
Magnesia (MgO) (%)	1.31	≧6
Alkalies (%)	0.46	≧0.6
Chloride (%)	0.017	≧0.05
Loss on ignition (%)	1.8	≧4
SiO ₂ (%)	22	–
Al ₂ O ₃ (%)	4.3	–
Fe ₂ O ₃ (%)	3.4	–
CaO (%)	67	–

Table 2 Compressive strength test results

Steel fibre in %	Fresh density (kg/m ³)	Compressive strength (N/mm ²)		
		3rd day	7th day	28th day
Normal concrete	2424	18.77	32.92	54.3
0.5% steel fibre concrete	2428	18.75	32.36	55.9
1% steel fibre concrete	2436	20.36	33.09	57.82
1.5% steel fibre concrete	2442	19.85	32.68	55.41
2% steel fibre concrete	2434	19.07	30.82	54.36

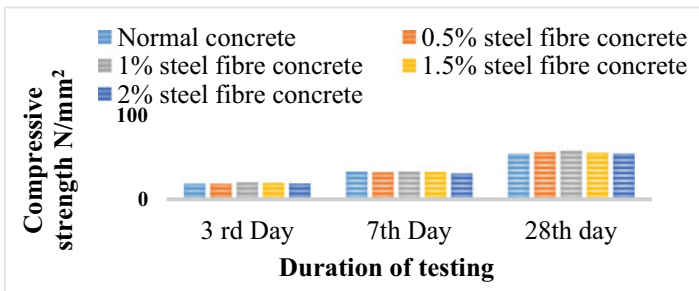


Fig. 1 Graphical representation on compressive strength with steel fibre

3.2 Split Tensile Strength

The splitting tensile strength properties of cylinder 150 × 300 mm are determined by a tensile strength test according to ASTM C496/C496M [9]. The split tensile strength of concrete is tested on day 3, day 7 and day 28 with steel fibres in the range of 0.5, 1, 1.5 and 2% which is shown in Fig. 2.

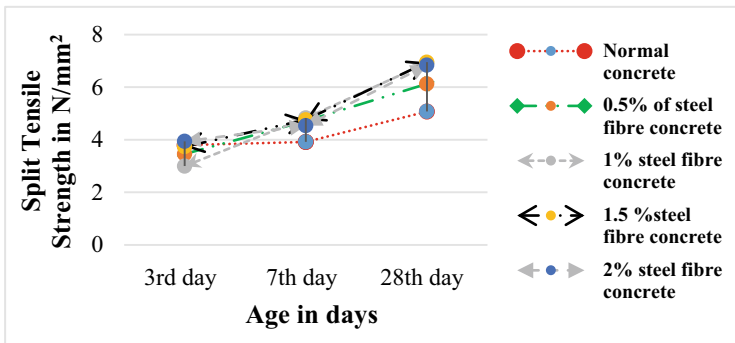


Fig. 2 Graphical representation on split tensile strength with steel fibre

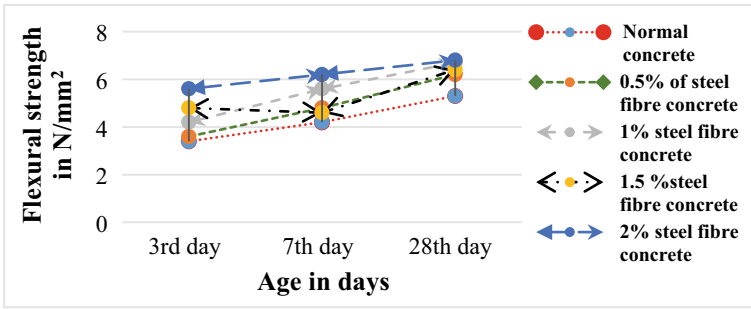


Fig. 3 Graphical representation on flexural strength with steel fibre

3.3 Flexural Strength Test

The flexural strength properties of the prism are determine according to ASTM C78-84 [10]. The maximum strains and stresses are determined due to the applied load. The flexural strength of the concrete with fibres are tested on the 3rd, 7th and 28th day, and the results are shown in Fig. 3.

4 Microstructural Analysis

Microstructural analysis of materials from various fields, including the study of failure mechanisms. Microstructure analysis is used to study the surface structure of materials.

4.1 SEM

Scanning electron microscope (SEM) research is used to examine the microstructure of the elements. The findings of microstructural analysis to study the clear surface structure of the concrete sample are shown in Figs. 4, 5, 6, 7, and 8. The C-S-H gel is evenly distributed in the hydrated cement concrete mix [10, 11]. The amount of ettringite in the concrete was evident in the SEM analyses, which is the proof for the increase of bonding. In the nondestructive test method of the concrete, the SEM analysis was involved to check the crack development in the ITZ, between the cement and aggregates. The steel fibre is added to reduce the cracks and temperature to enhance these properties. From the SEM analysis, this research works analysis the ITZ of the concrete made with steel fibre and is used to understand the nature of the ITZ region in the concrete with steel fibre.

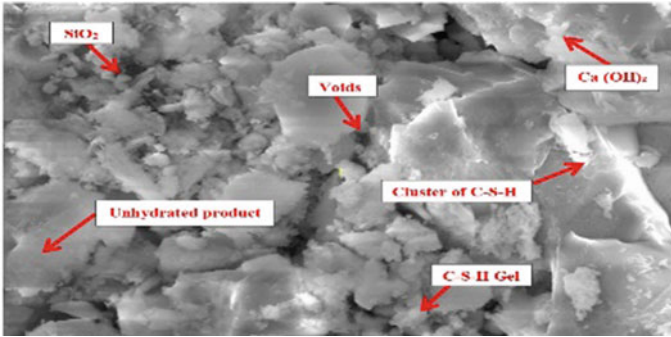


Fig. 4 SEM image of normal concrete

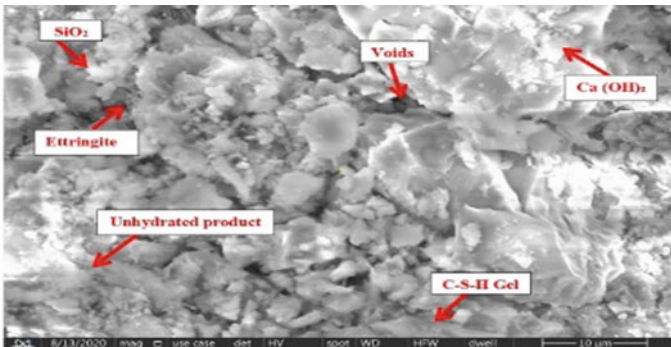


Fig. 5 SEM image of 0.5% steel fibre

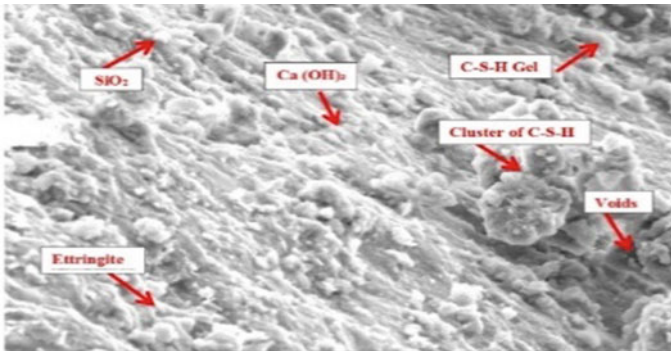


Fig. 6 SEM image of 1% steel fibre

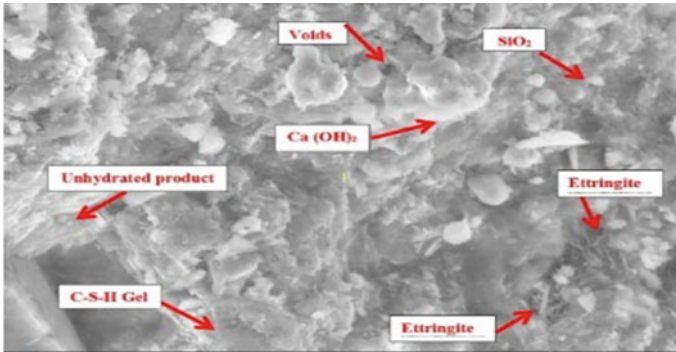


Fig. 7 SEM image of 1.5% steel fibre

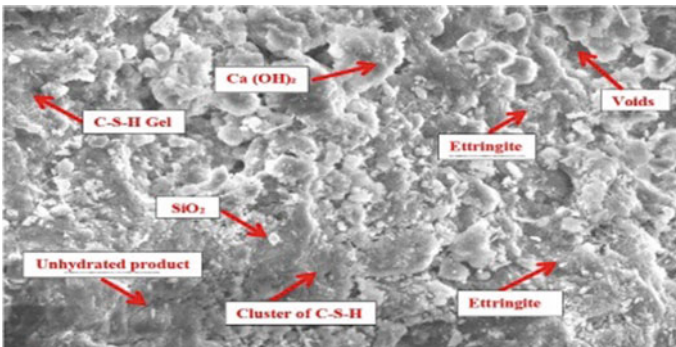


Fig. 8 SEM image of 2% steel fibre

4.2 XRD

XRD is the most important method to find the crystalline phase in concrete samples and also finding the correlating the diffraction peak present and intensities. Quartz, calcium silicate hydrates, calcium hydroxide, calcium silicates and calcite are all visible on the XRD [12]. The peak intensities were find to be C-S-H, CaCO₃ and Ca(OH)₂. The concrete with steel fibre samples are examined and shown in Figs. 9, 10, 11, 12, and 13.

4.3 FTIR

Every molecule or chemical structure will devolve a unique spectral fingerprint which also makes this analysis to become a great tool for chemical presence identification. This is clear with all the samples of FTIR patterns with normal wavelengths [2, 13].

Fig. 9 XRD analysis of normal concrete

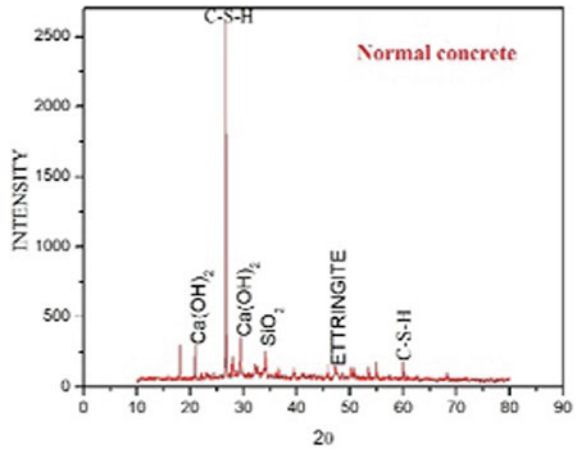


Fig. 10 XRD of 0.5% steel fibre concrete

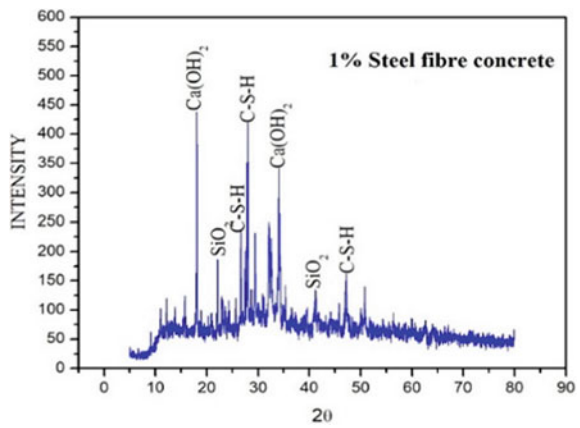


Fig. 11 XRD of 1% steel fibre concrete

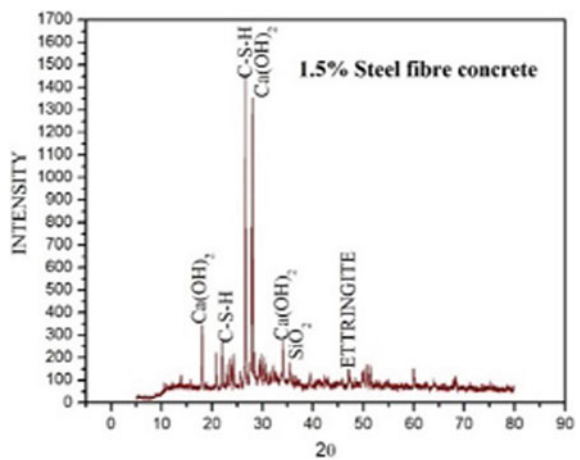


Fig. 12 XRD of 1.5% steel fibre concrete

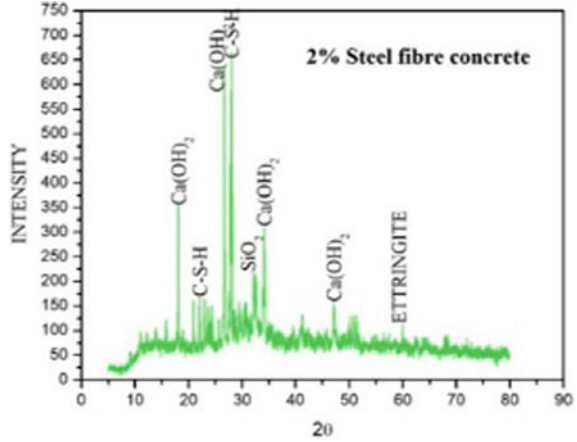
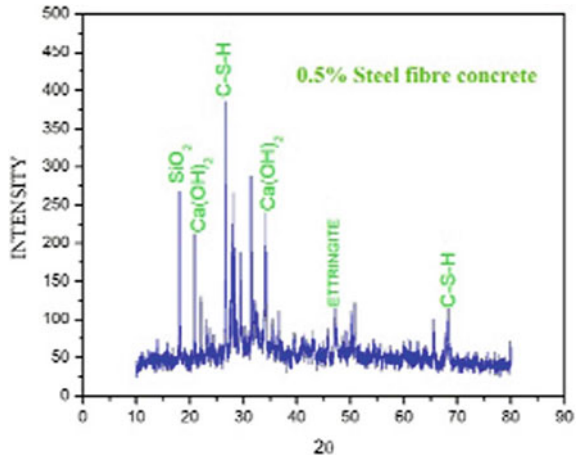


Fig. 13 XRD of 2% steel fibre concrete



The band at 1023 cm^{-1} is found to have normal peak wavelengths for 1% of steel fibre concrete. The bands at 534 cm^{-1} and 1022 cm^{-1} can be used to distinguish calcium carbonates (CaCO_3). The FTIR analysis of steel fibre concrete is shown in Figs. 14, 15, 16, 17, and 18.

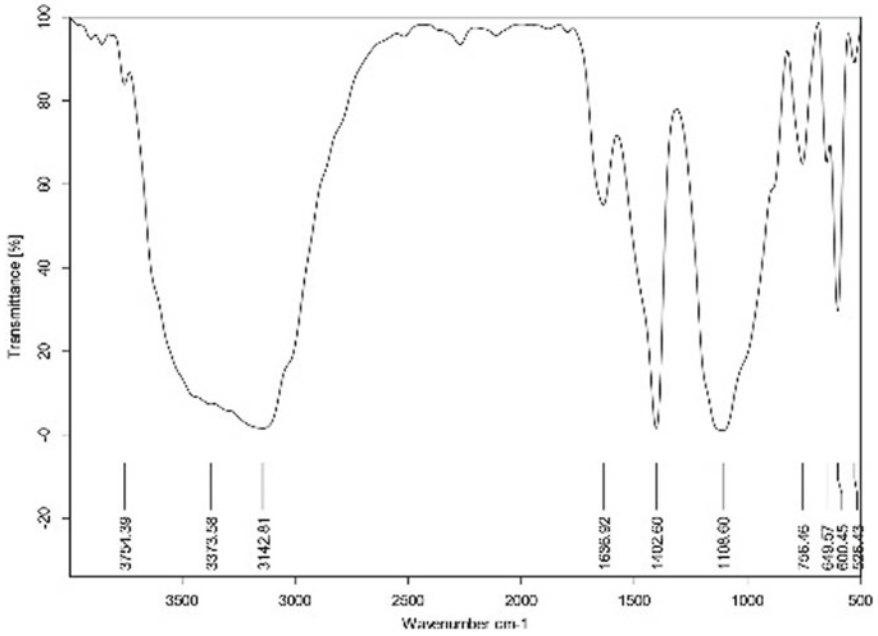


Fig. 14 FTIR of normal concrete

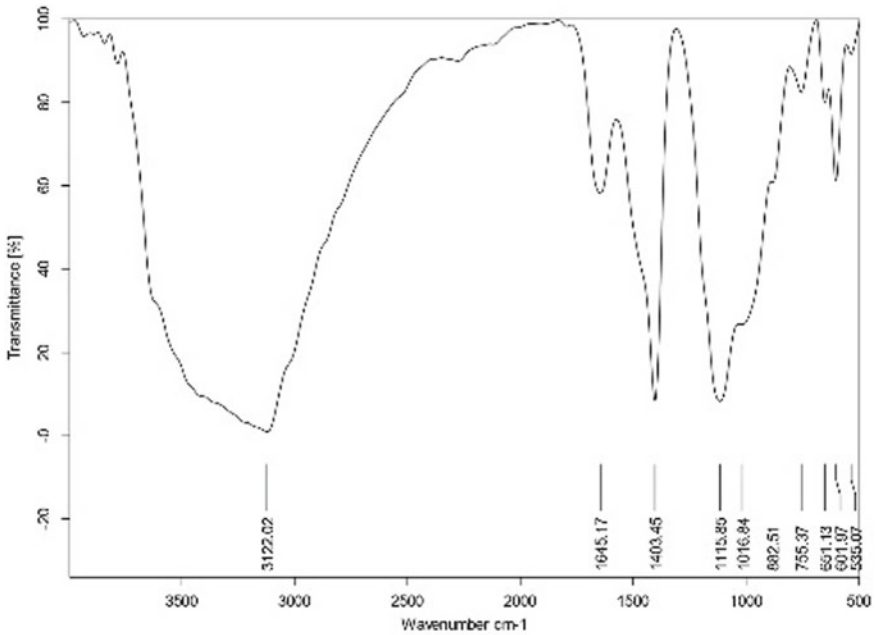


Fig. 15 FTIR of 0.5% steel fibre concrete

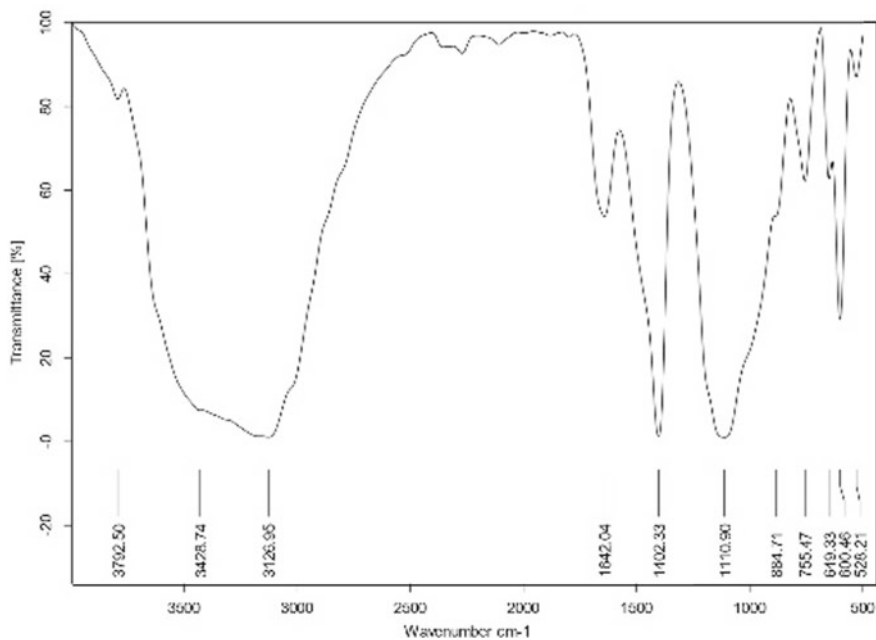


Fig. 16 FTIR of 1% steel fibre concrete

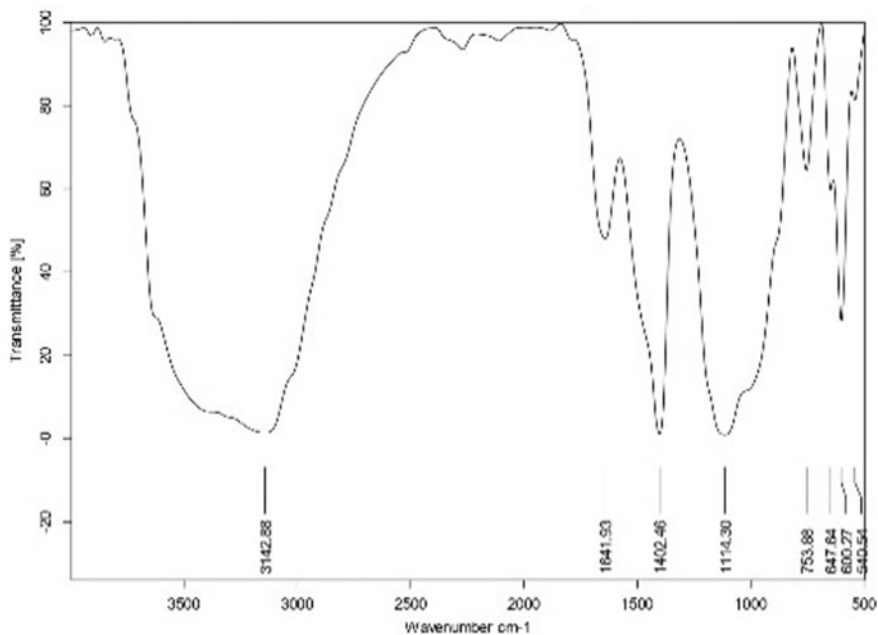


Fig. 17 FTIR of 1.5% steel fibre concrete

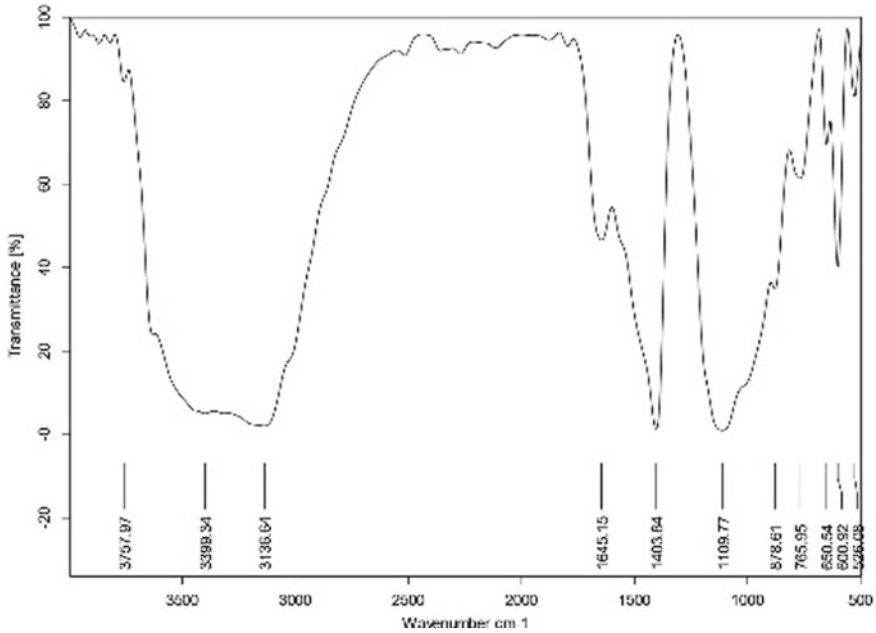


Fig. 18 FTIR of 2% steel fibre concrete

5 Failure Analysis of RCC Beams

RCC beam was used to analysis with the maximum load. This can be achieved by two point loading, and three deflectometers were used to find the deflection in the middle bottom of the specimen as depicted in Fig. 19. The concrete specimen size is 150 × 230 × 1500 mm. The reinforcement specifications are 10 mm dia main bars, and the stirrups sizes are 6 mm dia with 100 mm spacing [14–17]; the test result are discussed in Table 3 and Fig. 20.



Fig. 19 Load deflection test on RCC beam with steel fibre

Table 3 Load deflection values of steel fibre in RCC beam

Steel fibre in %	Breaking load (tonnes)	Maximum deflection at centre (mm)
Normal concrete	12.6	10.6
0.5% steel fibre concrete	12.8	11.4
1% steel fibre concrete	13.2	10.8
1.5% steel fibre concrete	13.4	10.6
2% steel fibre concrete	12.9	10.1

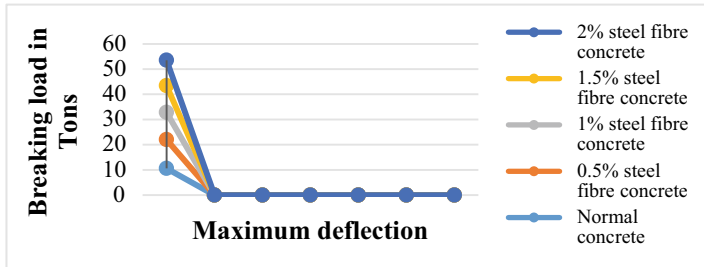


Fig. 20 Deflection of RCC beams with steel fibre

6 Conclusion

- According to the test results, concrete’s compressive, tensile and flexural strengths were discovered to be at their highest levels at 1% volume fraction of steel fibre.
- In comparison with conventional concrete, SFRC was found to have greater compressive, tensile and flexural strengths. When considering the volume fraction of fibre content in concrete, it becomes evident that once it surpasses 1%, there is a progressive decline observed in the compressive, tensile and flexural strength of the material.
- It has been noted that the addition of steel fibre to concrete transforms it from brittle to ductile.
- This outcome allows us to draw the conclusion that the steel fibre highlights the fundamental physical characteristics of concrete.
- The SEM analysis revealed the formation of hydration products of cement.
- The XRD pattern indicates the elemental position of compounds.
- The FTIR wave length exhibits the bonding of molecules.

The future studies are to evaluate thermal properties, structural elements and durability properties which are to be implemented.

References

1. Prakash Chandar S, Ravichandran PT, Gunasekaran K (2022) Mechanical and microstructure analysis of sustainable concrete using paper waste. <https://doi.org/10.21203/rs.3.rs-1721521/v1>
2. Michalik A, Chyliński F, Piekarczyk A, Pichór W (2022) Evaluation of recycled tyre steel fibres adhesion to cement matrix. *J Build Eng* 68(2)
3. Qin X, Kaewunruen S (2022) Environment-friendly recycled steel fibre reinforced concrete. *Constr Build Mater* 327(6)
4. Zhang J, Wu Z, Yu H, Ma H, Da B (2022) Mesoscopic modeling approach and application for steel fiber reinforced concrete under dynamic loading: a review. *Engineering* 16(4):220–238
5. IS-12269 (1987) Specifications for 53grade cement. *Bureau of Indian Standard*
6. IS 383 (1997) Coarse and fine aggregate from natural sources of concrete
7. IS 15388 (2003) Silica fume — Specification
8. IS 516 (2018) Method of tests for strength of concrete, Bur. Indian Standard
9. ASTM C496/C496M, Standard test method for splitting tensile strength of cylindrical concrete
10. ASTM C78–84 Standard test method for flexural strength of concrete (Using Simple Beam with Third-Point Loading)
11. Prakash Chandar S, Balaji SS (2022) A critical review on recycled aggregate concrete with m-sand as a fine aggregate. *AIP Conferen Proceed* 251(1)
12. Prakash Chandar S, Gunasekaran K, Kalpana Priya V, Ganapathyramasamy N (2019) An experimental investigation on partial replacement of sand by ceramic grains in coconut shell concrete. *Rasayan J Chem* 12(2):659–665
13. Nan S, Kung-Chung H, His-Wen C (2001) A simple mix design method for self-compacting concrete. *Cem Concr Res* 31:1799–1807
14. Arun B, Ravichandran PT, Divya Krishnan K (2020) Effect of pyrophyllite on behavioral strength of clayey soil. *IOP Conferen Series Mater Sci Eng* 912(6)
15. Prakash Chandar S, Gunasekaran K, Sai Sandeep N, Manikandaprabhu S (2017) An experimental investigation on strength properties of steel fibres along with recycled aggregate in cement concrete. *Rasayan J Chem* 10(2):528–533
16. Krishnaraj L, Ravichandran PT (2019) Investigation on grinding impact of fly ash particles and its characterization analysis in cement mortar composites. *Ain Shams Eng. J.* 10(2):267–274
17. Prakash Chandar S, Manivel S, Gunasekaran K, Jothiswaran A (2017) An experimental investigation of partial replacement of cement using micro silica and fly ash in production of coconut shell concrete. *Int J Civ Eng Technol* 8(4):1851–1859

Analytical Study on the Bending Behavior of the Composite Beam with T-shaped Shear Connector Under Partial Interaction



Rakesh Bhatia and R. Ramasubramani

1 Introduction

Practical design has high strength, dependability, and execution which is beneficial all around the globe as of now. This prompted advancement in new kind of the composite beam specifically bound concrete and steel composite. The impacts of steel–concrete composite beam bending are not yet tended to in global principles on composite steel–concrete development, e.g., the Euro code and the American Organization of Steel Development as well as in the Australian Norms [1–5].

Composite activity improves underlying productivity by joining the primary components to make a solitary composite part. Composite beam plans give a critical economy by decreased material, thinner floor profundities, and quicker development.

A basic point for underlying way of behaving and plan of composite beam is degree of connection, connection between concrete section, and steel segment. The term “full shear connection” connects with the situation wherein the connection between the mechanisms can completely oppose the powers applied to it.

To begin with, by firmly combining two sections, the subsequent system is firmly grounded compared to amount of its components. Secondly, composite action can all the more promptly utilize the properties of each and every constituent material. In composite beam, for instance, the substantial is expected to take the entire load while the steel takes the strain.

For a while now, steel bridges and multistory steel constructions have both been thought to have one of the most economical underlying frameworks: composite beams [6–9]. To give a surface to people and vehicles separately, buildings and bridges need a story chunk. Concrete was chosen as the material for the component because its density and firmness may be used to reduce floor system avoidances

R. Bhatia · R. Ramasubramani (✉)

Department of Civil Engineering, Faculty of Engineering and Technology, SRM Institute of Science and Technology, Kattankulathur, Tamil Nadu 603203, India
e-mail: ramasubr@srmist.edu.in

Table 1 Model description

Beam	Beam size (mm)	Number of shear connector	Spacing (mm)
A1	275 × 125 × 1500	3	250
B1	275 × 125 × 1500	3	200
C1	275 × 125 × 1500	5	250
D1	275 × 125 × 1500	7	200

and vibrations while still providing the desired level of fire safety. However, steel is frequently used for the supporting structure because it has a good strength-to-weight and firmness-to-weight ratio, is easy to maintain, and has a short development cycle.

2 Analytical Study

2.1 General

In this section, works done in the analytical study bending behavior of composite beam is done using Abaqus software, and the results are obtained. Abaqus software is widely used for FEM simulations due to its robust capabilities in handling nonlinear analysis, large deformations, and complex material behavior [7, 8]. The software offers a range of modeling capabilities, including geometric modeling, mesh generation, material modeling, and boundary condition application.

2.2 Modeling of Specimens

Analytical study is carried by modeling the composite beams in Abaqus software for finite element analysis. The modeling descriptions are mentioned in Table 1.

2.3 Geometry Creation

The first step in modeling is to create the geometric shape of the structure or system to be analyzed. In this, geometry of all the components of composite beams is created like concrete slab, T-shaped shaped shear connector, and steel-girder and is shown in Fig. 1.

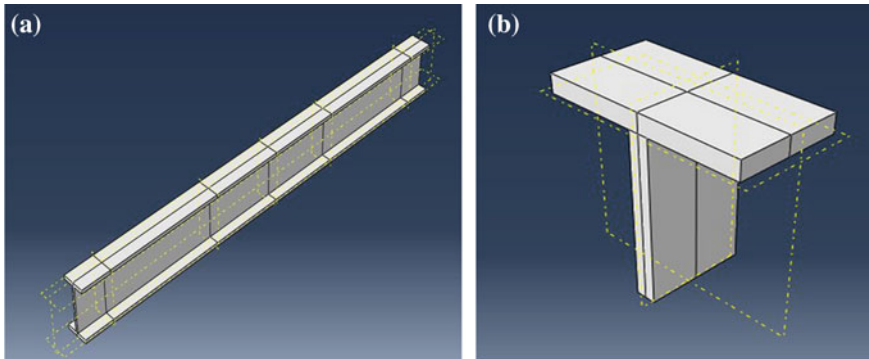


Fig. 1 a Steel section, b T-shaped shear connector

2.4 Assembly

Once individual parts are created, the next step is to create an assembly in Abaqus. The assembly module allows users to define the position and orientation of each part relative to the other parts in the system. In this section, the various parts of the composite beam are assembled. Initially, the shear connector is placed in the middle of the steel section, and shear connectors are placed at a distance of 250 and 200 mm center to center spacing based upon model description as mentioned in Table 6.1. Once the shear connectors are placed at the respective place over the steel beam, both the components are merged to act like a single component as shown in Fig. 2. After connecting the shear connectors with the steel beam, the concrete slab is assembled on the top as shown in Fig. 3.

2.5 Meshing

Meshing is a critical step in the finite element analysis (FEA) process, as it involves dividing the geometry of the model into smaller elements to perform numerical simulations. Abaqus software provides a range of meshing tools to create high-quality meshes for various types of models. Once the mesh is created, we can check the quality of the mesh using Abaqus's mesh quality checking tools. The quality check ensures that the mesh has the desired level of accuracy and is free from any errors. The meshing of each component and assembly of a composite beam is shown in Fig. 4.

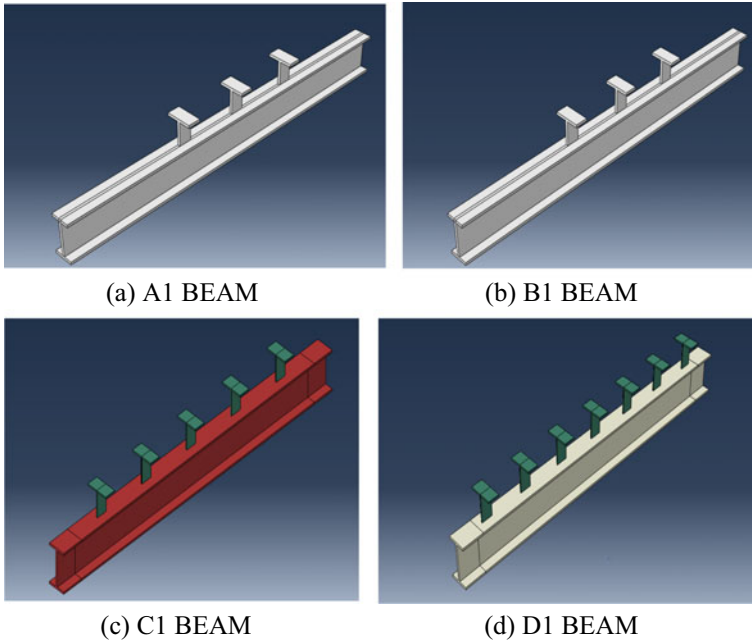


Fig. 2 Placement of shear connector

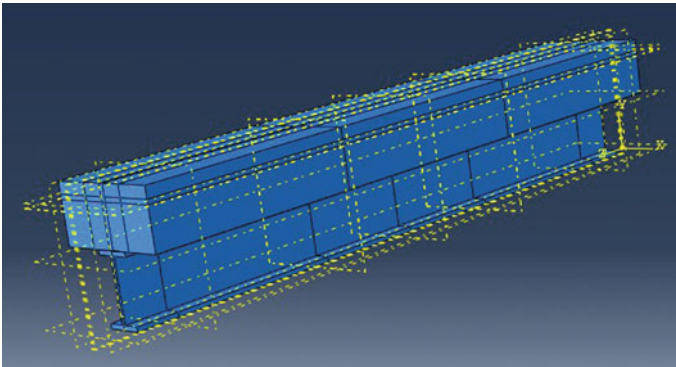


Fig. 3 Composite beam assembly

2.6 Loading Condition and Interaction

A node and two loading cell are prepared to distribute the load evenly. In this case, coupling interaction is given to the center node of the I-section to distribute the load or deflection to the loading cells. The deflection is applied to top node of I-section

Fig. 4 Meshed assembly of composite beam

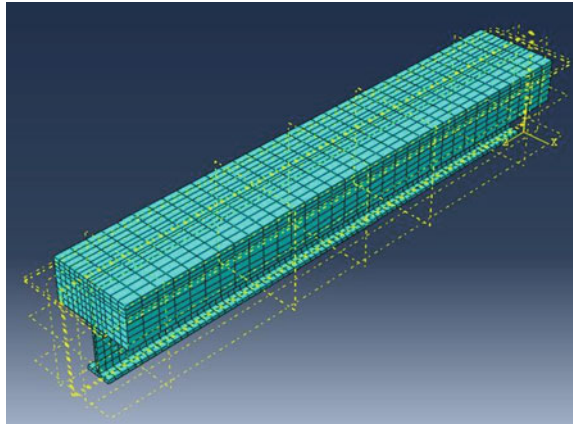
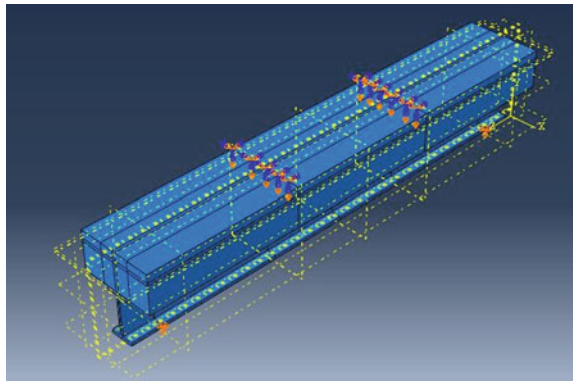


Fig. 5 Loading setup



as 10 mm in downward direction and for the supports boundary conditions as shown in Fig. 5.

In Abaqus software, interaction property refers to the definition of how different parts or components of a model interact with each other. It specifies the type of interaction, the contact behavior, and other relevant parameters that affect the behavior of the model. In other words, interaction properties are defined using specific elements, such as surface-to-surface, edge-to-edge, or point-to-surface interactions, depending on the geometry and nature of the problem [9–12]. They are essential for simulating complex mechanical systems, such as assemblies or structures composed of multiple parts that interact with each other, as given in Table 2.

Table 2 Interaction between the surfaces

S. No.	Element	Interaction
1	Concrete beam	–
2	Concrete steel	Surface-to-surface
3	Concrete and shear connector	Surface-to-surface
4	Connector and steel section	Surface-to-surface

Table 3 Material properties of steel

Material	Young's modulus (N/mm ²)	Density (kg/m ³)	Poisson ratio
Steel	200,000	7850	0.3

2.7 Material Properties

Material properties must be assigned to the model. Abaqus offers a range of material models and allows users to define material properties based on experimental data. Material properties of T-shaped shear connector and steel section are stated in Tables 3 and 4.

2.8 Analysis Setup

The next step is to set up the analysis in Abaqus. This involves defining the type of analysis to be performed, such as static or dynamic, and specifying the analysis parameters, such as time step or convergence criteria.

2.9 Analysis and Post-Processing

After setting up the analysis, the Abaqus model can be executed to produce results. Abaqus provides various post-processing tools to visualize and interpret the analysis results, including stress and strain plots, displacement contours, and animations. The deflected shape of composite beam is shown in Fig. 6.

3 Results and Discussion

In this section, the load versus deflection result obtained from analytical study by using Abaqus is compared. The results obtained shows that the C1 beam can carry maximum amount of load. The beam D1 with full interaction carry 14.1% lesser

Table 4 Material properties for concrete with CDP model in M40

Dilation angle	Eccentricity	fbo/fco	K	Viscosity parameter	Mass density	Young's modulus
35	0.1	1.16	0.667	0.007985	2.30E-09	21,082.51
Compressive behavior					Tensile behavior	
Yield stress	Inelastic strain		Damage parameter	Inelastic strain	Yield stress	Cracking strain
21.5	0		0	0	5.16	0
24.853717	6.00E-06		0	6.00E-06	2.862689	0.000354
28.098281	1.70E-05		0	1.70E-05	2.028134	0.000638
31.183016	3.50E-05		0	3.50E-05	1.588176	0.000904
34.047274	6.50E-05		0	6.50E-05	1.313788	0.001161
36.623184	0.000107		0	0.000107	1.125178	0.001415
38.840334	0.000167		0	0.000167	0.986998	0.001666
40.632164	0.000247		0	0.000247	0.881096	0.001916
41.94335	0.00035		0	0.00035	0.797156	0.002165
42.736969	0.000477		0	0.000477	0.728869	0.002413
43	0.000629		0	0.000629		
42.745873	0.000806		0.00591	0.000806	Damage parameter	Cracking strain
42.013436	0.001006		0.022943	0.001006	0	0
40.86256	0.001226		0.049708	0.001226	0.445215	0.000354
39.367388	0.001461		0.084479	0.001461	0.606951	0.000638
37.608688	0.00171		0.125379	0.00171	0.692214	0.000904
35.666697	0.001967		0.170542	0.001967	0.74539	0.001161
33.615471	0.002229		0.218245	0.002229	0.781942	0.001415
31.519179	0.002493		0.266996	0.002493	0.808721	0.001666
29.430323	0.002757		0.315574	0.002757	0.829245	0.001916
27.389502	0.003019		0.363035	0.003019	0.845512	0.002165
25.426272	0.003277		0.408691	0.003277	0.858746	0.002413
23.56061	0.003531		0.452079	0.003531		
21.804627	0.003779		0.492916	0.003779	Poisson's ratio	
20.164268	0.004022		0.531064	0.004022	0.18	
18.640845	0.004259		0.566492	0.004259		
17.232345	0.00449		0.599248	0.00449		
15.934482	0.004717		0.629431	0.004717		
14.74152	0.004938		0.657174	0.004938		
13.646888	0.005155		0.682631	0.005155		
12.9	0.005314		0.7	0.005314		

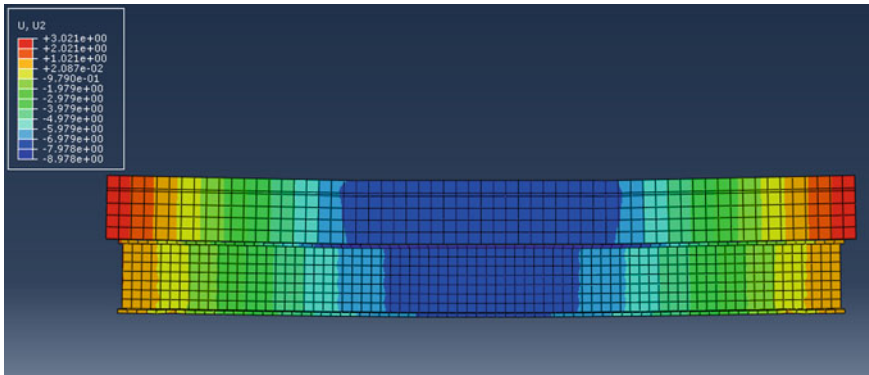


Fig. 6 Deflected shape of composite beam

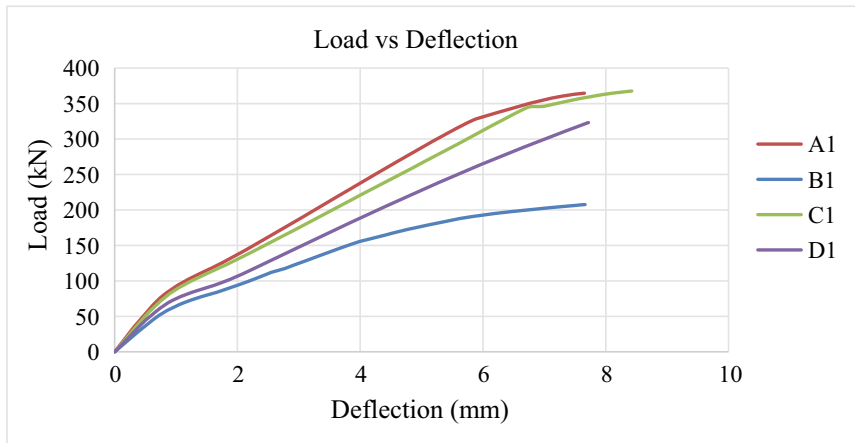


Fig. 7 Load versus deflection (analytical)

load as compared to C1 beam. The A1 beam and C1 beam almost shows similar behavior. Figure 7 shows the variation in the load versus deflection results obtained analytically.

3.1 Comparison of Experimental and Analytical Results

In this section, the experimental results are compared with analytical result. The results are compared with each other in order to validate the results values. The load versus deflection values for C1 beam is compared both analytical and experimental. The load value at a 10 mm deflection is compared, and it is observed that there is

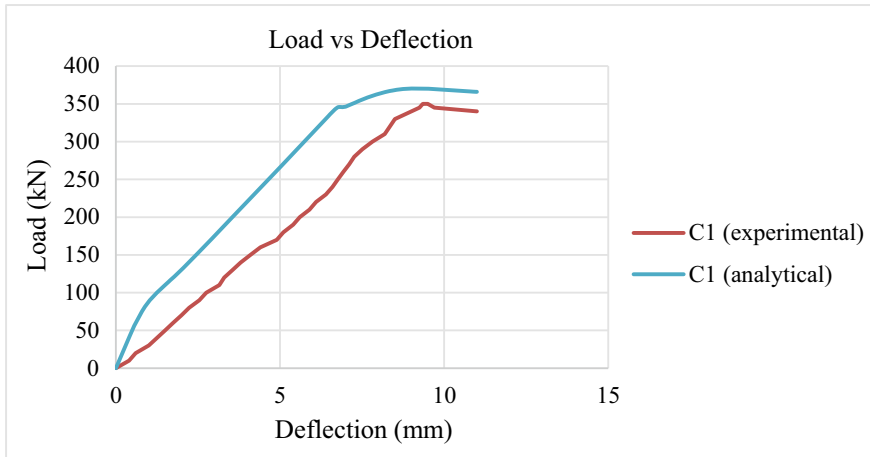


Fig. 8 Comparison of experimental and analytical results (C1 beam)

a difference of 4% between the load values. Figure 8 shows the difference between the experimental and analytical result.

The load versus deflection values for A1 beam is compared both analytical and experimental. The load value at a 10 mm deflection is compared, and it is observed that there is a difference of 10% between the ultimate load values [13–15]. Figure 8 shows the difference between the experimental and analytical result in beam A1.

The load versus deflection values for B1 beam is compared both analytical and experimental. It is observed that the experiment model can withstand more load before reaching to its ultimate load-carrying capacity [16, 17]. The comparison between the experimental and analytical result for B1 beam is shown in Figs. 9 and 10.

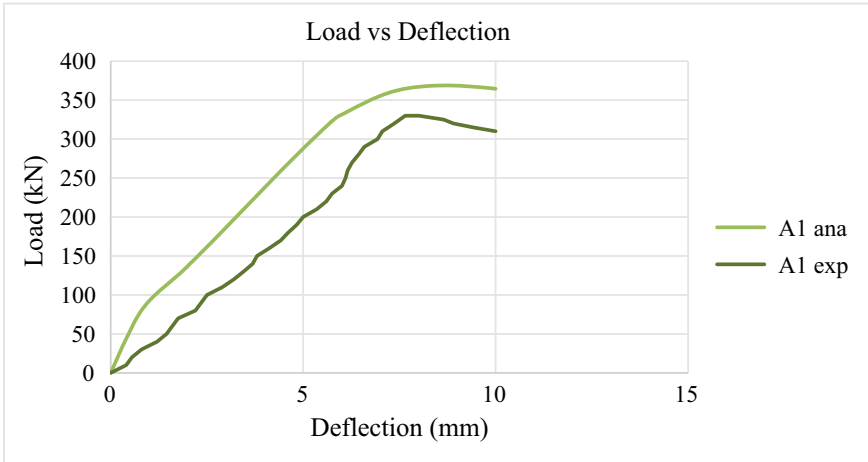


Fig. 9 Comparison of experimental and analytical results (A1 beam)

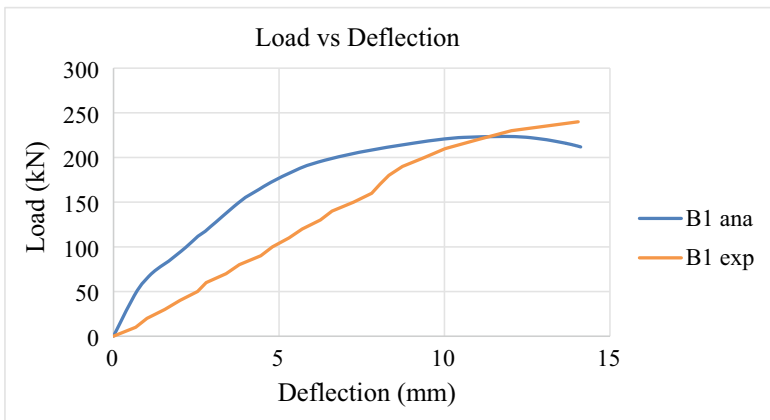


Fig. 10 Comparison of experimental and analytical results (B1 beam)

4 Conclusion

In this report, the bending behavior of composite beam with T-shaped shear connector under Partial interaction is investigated. Analytical study was carried in order to validate the result values obtained.

- The analytical results obtained shows that the C1 beam can carry maximum amount of load.
- The beams D1 with full interaction carry 9% lesser load as compared to C1 beam. The A1 beam and C1 beam almost show similar behavior.

- Based upon analytical results, the C1 beam, i.e., 5 connectors with 250 mm center to center spacing, carry the maximum number of load.
- The failure in the composite beam occurs due the buckling in steel section.
- As the grade of concrete increases, the strength of composite beam also increases.
- It is determined that as the number of shear connectors reduces the beam becomes more flexible.

References

1. Anju T, Smitha KK (2016) Finite element analysis of composite beam with shear connectors. *Procedia Technol* 24:179–187
2. Chen B, Liu A, Zhang J, Zhang F, Bradford MA (2022) Behavior of T-shaped embedded-nut bolted shear connectors in prefabricated steel-concrete composite beams. *Eng Struct* 272:114983
3. El-Sisi A, Alsharari F, Salim H, Elawadi A, Hassanin A (2023) Efficient beam element model for analysis of composite beam with partial shear connectivity. *Compos Struct* 303:116262
4. Fabbrocino G, Manfredi G, Cosenza E (1999) Non-linear analysis of composite beams under positive bending. *Comput Struct* 70(1):77–89
5. Girhammar UA, Gopu VK (1993) Composite beam-columns with interlayer slip—exact analysis. *J Struct Eng* 119(4):1265–1282
6. Newmark NM (1991) Test and analysis of composite beam with incomplete interaction. In: *Proceeding of society for experimental stress analysis* (1):75–92
7. Nie J, Cai CS (2003) Steel–concrete composite beams considering shear slip effects. *J Struct Eng* 129(4):495–506
8. Nie J, Fan J, Cai CS (2004) Stiffness and deflection of steel–concrete composite beams under negative bending. *J Struct Eng* 130(11):1842–1851
9. Oehlers DJ, Bradford MA (1995) *Composite steel and concrete structural members: fundamental behavior*. Kidlington
10. Peng K, Liu L, Wu F, Wang R, Lei S, Zhang X (2022) Experimental and numerical analyses of stud shear connectors in steel–SFRCC composite beams. *Materials* 15(13):4665
11. Ranzi G, Zona A (2007) A steel–concrete composite beam model with partial interaction including the shear deformability of the steel component. *Eng Struct* 29(11):3026–3041
12. SAP2000 14.2 [Computer software]. Berkeley CA Computers and Structures investigations on square CFST column to U-shaped steel-concrete composite beam joints with internal T-shaped diaphragms. *J Build Eng* 60:105172
13. Shariati A, RamliSulong NH, Shariati M (2012) Various types of shear connectors in composite structures: a review. *Int J Phy Sci* 7(22):2876–2890
14. Thivya J, Malathy R, Tensing D (2016) Behaviour of composite beams under combined bending and torsion. *Int J Adv Eng Technol* 7(2):563–566
15. Wang YC (1998) Deflection of steel-concrete composite beams with partial shear interaction. *J Struct Eng* 124(10):1159–1165
16. Xu X, Cheng R, Yang P, Yu Y (2022) Experimental and numerical investigations on square CFST column to U-shaped steel-concrete composite beam joints with internal T-shaped diaphragms *J Build Eng* 60:105172
17. Zona A, Ranzi G (2011) Finite element models for nonlinear analysis of steel–concrete composite beams with partial interaction in combined bending and shear. *Finite Elem Anal Des* 47(2):98–118

Planning and Analysis of G+2 Residential Building and Design of Slab and Beam with Sisal Fiber Polymer Reinforcement



Phumen Teron, Ningthoujam Khelendra, Shanmuga Raj,
and Balasubramanian Murugesan

1 Introduction

In the past two decades, the use of steel as a reinforcement material in concrete structures has been a vital part in the construction sector. But the production of steel for the construction purpose has its major disadvantages like discharge of greenhouse gases such as, CO₂, N₂O, and methane [1–5]. Therefore, the use of steel as reinforcement material with this process of production is not advisable as it is not sustainable, which would eventually affect the environment by global warming. Also, corrosion of the reinforcing steel is a prevalent mode of failure of steel-reinforced concrete structures in hostile settings. Corrosive elements, such as salt water or deicing chemicals, seep into the porous concrete and corrode the steel. Corrosion causes the steel to expand, causing harm to the surrounding concrete [6–8]. Moreover, rust reduces the stress capability of the steel. In recent times, some fiber reinforcements have been introduced to compensate these environmental issues and also to attain corrosion resistance without compromising the strength aspects.

Fiber-reinforced polymer (FRP) has emerged as a possible substitute of steel in the reinforcing of concrete structures. Number of fibers is available in the market such as glass-fiber-reinforced polymer (GFRP), basalt-fiber-reinforced polymer (BFRP), aramid-fiber-reinforced polymer (AFRP), and sisal-fiber-reinforced polymer (SiFRP). Natural fibers are easily available in the market and are economic. They are extracted from various plants and further processed with certain chemical and physical processes. The stirrups and bars used in the reinforcing of various structures can be replaced with the FRP composites to obtain more strength with cost effective construction. FRP composites are known for its easy production, availability, and economy friendly. It has proved to be a good replacement for steel in

P. Teron · N. Khelendra · S. Raj · B. Murugesan (✉)

Department of Civil Engineering, Faculty of Engineering and Technology, SRM Institute of Science and Technology, Kattankulathur, Tamil Nadu 603203, India
e-mail: balasubm1@srmist.edu.in

concrete structures, and it has shown considerable results when tested with various sections like beams, columns, and slabs. The perfect proportion of FRP is very important in obtaining its best performance. FRP composites are corrosion free which is a major problem in steel-embedded structures. In this invention, the plan and methodology for G + 2 along with the design and analysis of FRP incorporated beams and slabs are presented. FRP composites have proved to be the ultimate replacement of steel bars in the concrete structures. They eliminate the problem of corrosion in concrete structures when exposed to continuous water and sunlight. FRP reinforcement in concrete structures has shown impressive results when subjected to loads in various ways. The inclusion of FRP reinforcement is economically efficient, more durable, resilient, flexible, and free from corrosion in comparison with conventional steel reinforcement.

2 Methodology

Literature review: The topic was new to the group, and hence, journals were reviewed before the start of the project to get the better understanding of the title. After pursuing the related journals, the flow of the work was framed.

Characteristic study of FRP: FRP composites are progressively being explored as an upgrade to and/or change out for infrastructure components or systems made of traditional civil engineering materials such as concrete and steel [9–12].

Plan preparation for G + 2 residential building using AutoCAD: For the 2D drawing of the plan in this project, we utilized AutoCAD. The 2D drafting of a construction plan using AutoCAD is easier, faster, has less errors, and is easier to handle.

Analysis of G + 2 residential building using STAAD Pro: The STAAD Pro technology is used to evaluate loads, moments, and shear forces. Nowadays, most high-rise structures are built using STAAD Pro; therefore, the need for a civil engineer is to be familiar with this program. This program can handle RCC, steel, bridge, truss, and other materials according to various national norms.

Analysis of SiFRP and GFRP beams and slabs using Abaqus: Three-point load on beams and center point load are tested using Abaqus for results on deflections and stress developed [12–15].

Design of beams and slabs with SiFRP and GFRP reinforcement: Design of proper beams and slabs [16–18].

Results and discussion: The tests results are interpreted and discussed among the group for a conclusion.

3 Analysis

The structure is analyzed by using STAAD Pro software. The column dimensions are 350 mm × 350 mm for the columns at the ground floor and 300 mm × 300 mm for rest of the columns standing on the first and second floor. The beam dimension is 350 mm × 350 mm for the ground floor and 300 mm × 300 mm for the first and second floor. The STAAD Pro analysis is done in order of slab, beam, column, and footing. The load combination is composed in the software for manipulation of the design of the structure [19, 20]. The design of the structural components values was taken from the result of STAAD Pro. The sequence of the STAAD Pro is given below

- Seismic analysis by IS 1893-Part 1, zone 4
- Load in both X and Z direction (IS 875-Part 3)
- Dead load of self-weight by (IS 875-Part 1)
- Live load for residential building (IS 875-Part 2).

4 Abstract of Analysis

The above-mentioned values are the maximum and minimum of deflection (see Table 1), Shear force (see Table 2), and bending moment (see Table 3) when all the load cases are considered. The beams, column, and slabs are designed to withstand the different load combination possible to a structure. Hence, the structure is safe and is a secure residential building.

Table 1 Deflection value for different load combinations

Direction	Maximum positive (mm)	Maximum negative (mm)
Horizontal X	5.324	– 5.735
Vertical Y	0.373	– 2.115
Horizontal Z	3.566	– 4.445

Table 2 Shear force value for different load combinations

Direction	Maximum positive (mm)	Maximum negative (mm)
Fx	818.271	– 31.636
Fy	41.516	– 43.079
Fz	15.845	– 18.957

Table 3 Bending moment value for different load combinations

Direction	Maximum positive (kN)	Maximum negative (kN)
Mx	1.775	– 3.561
My	21.300	– 18.766
Mz	49.223	– 24.800

5 Results of Analysis

The FRP incorporated beams and slabs with the below mentioned specifications were analyzed using Abaqus; Table 4 represents the grade of concretes and dimensions of the reinforcement of the beam.

Figure 1a, b depict the FRP placement, deflection behavior in FRP (SiFRP and GFRP) incorporated beam and stress behavior distribution in FRP-incorporated beam. The critical sections in the beam are also highlighted with dark red color.

Figure 2 represents FRP incorporated slab, a shows the deflection behavior and b shows the stress behavior depict deflection behavior in FRP. The critical sections in the beam are also highlighted with dark red color. The plate section is subjected to center point load.

Table displays the stress and deflection values for different samples as mentioned in Tables 5 and 6 of beams and slabs incorporated with SiFRP and GFRP stirrups and bars, respectively.

Table 4 Beams with specification for three-point load testing

BEAMS (alternate replacement of SiFRP Stirrups)						
Sample no	Mix proportion	Cross section (mm)	Diameter size (mm)			
			Main bars	Spacing 150 mm c/c		
				Steel stirrups	SiFRP stirrups	GFRP stirrups
1	M20	300 × 300	16	8	8	–
2	M20			8	–	8
3	M20			10	10	–
4	M20			10	–	10
5	M25			8	8	–
6	M25			8	–	8
7	M25			10	10	–
8	M25			10	–	10

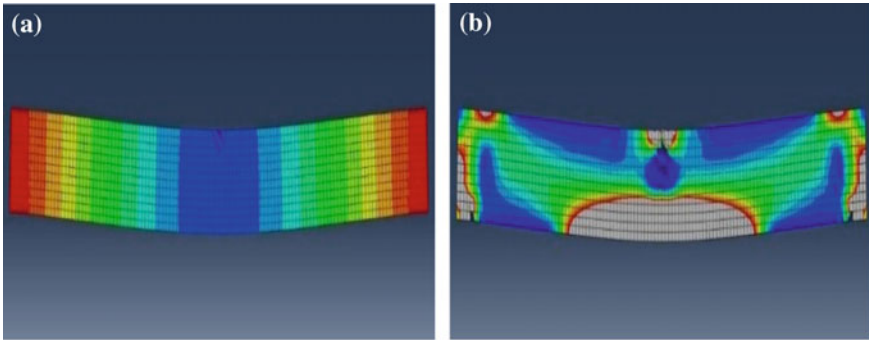


Fig. 1 a FRP (SiFRP and GFRP) stirrups placement (alternate) in a beam, b deflection in FRP incorporated beam

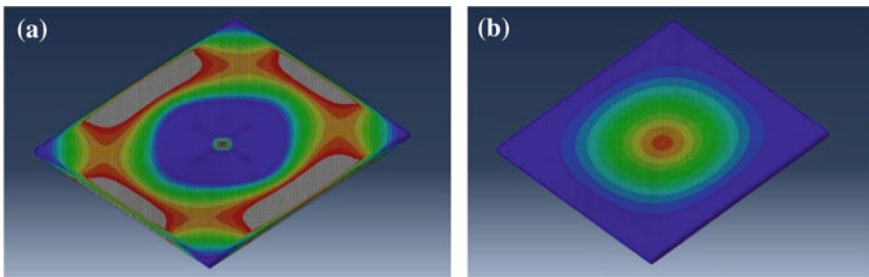


Fig. 2 a, b Deflection behavior in FRP, SiFRP and GFRP slab

Table 5 Slabs with specification for center point load testing

Slabs (with replacement of SiFRP bars as the distribution bars)

Sample no	Mix proportion	Dimension (m)	Thickness (mm)	Diameter size (mm)			
				Main bars	Distribution bars with spacing of 150 mm c/c		
					Steel bars	SiFRP bars	GFRP bars
9	M20	8 × 7	150	12	10	10	–
10	M20				–	–	10
11	M25				10	–	–
12	M25				–	–	10

Table 6 Deflection results for different samples of beams and slabs

Deflection results for different samples				
Sample	S. No.	Load (kN)	Stress (N/mm ²)	Deflection (mm)
Sample 1	1	20.00	1.39	- 3.02
	2	110.00	7.63	- 16.62
	3	200.01	13.87	- 30.21
Sample 2	4	20.00	1.39	- 3.02
	5	110.00	7.63	- 16.62
	6	200.01	13.86	- 30.22
Sample 3	7	20.00	1.39	- 3.02
	8	110.00	7.63	- 16.62
	9	200.01	13.87	- 30.21
Sample 4	10	20.00	1.39	- 3.02
	11	110.00	7.63	- 16.62
	12	200.01	13.87	- 30.21]
Sample 5	13	20.00	1.40	- 2.73
	14	110.00	7.69	- 14.99
	15	200.01	13.98	- 27.26
Sample 6	16	20.00	1.40	- 2.73
	17	110.00	7.69	- 14.99
	18	200.01	13.98	- 27.26
Sample 7	19	20.00	1.39	- 2.73
	20	110.00	7.69	- 14.99
	21	200.01	13.98	- 27.26
Sample 8	22	20.00	1.39	- 2.73
	23	110.00	7.69	- 14.99
	24	200.01	13.98	- 27.26
Sample 9	25	20.00	1.46	- 10.38
	26	110.00	8.02	- 57.07
	27	199.99	14.59	- 103.76
Sample 10	28	19.99	1.47	- 10.39
	29	110	8.07	- 57.14
	30	200.00	14.67	-103.88
Sample 11	31	20.00	1.46	-9.29
	32	110.00	8.05	-51.12
	33	200.00	14.63	-92.94
Sample 12	34	19.99	1.47	-9.30
	35	110.00	8.09	-51.17
	36	199.99	14.71	-93.04

6 Conclusion

In this invention, the plan and methodology for G + 2 along with the design and analysis of FRP incorporated beams and slabs are presented. The successful construction of any building is based on good comprehension of structure, application of software, theories of analysis, and methodology and explicit principle of design. The project involves the layout, planning analysis, and design of G + 2 residential building. FRP composites have proved to be the ultimate replacement of steel bars in the concrete structures. They eliminate the problem of corrosion in concrete structures when exposed to continuous water and sunlight. FRP reinforcement in concrete structures has shown impressive results when subjected to loads in various ways. The inclusion of FRP reinforcement is economically efficient, more durable, resilient, flexible, and free from corrosion in comparison with conventional steel reinforcement. The results obtained by the analytic tests conducted on beams and slabs have clearly proved that SiFRP incorporated beams and slabs show better deflection results compared to GFRP embedded concrete structures. SiFRP is prepared using a natural fiber which is obtained by a plant, and the extraction process does not affect the environment which boosts its advantages compared to the conventional steel. The use of SiFRP in concrete beams and column eliminates the issue of corrosion. As the presence of porous in sisal fiber work as traps and impeded the heat transfer to SiFRP, it slightly increases the performance than GFRP when replaced by steel in beams and slabs.

References

1. S Dinesh Kumar Raju, Balasubramanian Murugesan and Arul Jeya Kumar (2020), experimental studies on replacement of steel stirrups by sisal fiber reinforced polymers.
2. M. Konsta-gdoutos and Ch. Karayiannis (1998), flexural behavior of concrete beams reinforced with frp bars.
3. Gudonis e. Timinskas, e. Gribniak, v. Kaklauskas, g. Arnavutov, a. K. Tamulėnas, v (2013). Frp reinforcement for concrete structures: state-of-the art review of application and design, engineering structures and technologies.
4. N. F. Grace, g. A. Sayed, a. K. Soliman and k. R. Saleh (1999), strengthening reinforced concrete beams using fiber reinforced polymer (frp) laminates.
5. Jiho moon, Mahmoud M. Reda taha, and Jung j. Kim (2017), flexural strengthening of RC slabs using a hybrid frp-uhpc system including shear connector.
6. M. N Habeeb and A. F Ashour (2008), Flexural Behavior of Continuous GFRP Reinforced Concrete Beams.
7. Muhammad Masood Rafi, Ali Nadjai and Faris Ali (2007), Experimental Testing of Concrete Beams Reinforced with Carbon FRP Bars.
8. Adane Dagnaw Gudayu, Leif Steuernagel, Dieter Meiners and Rotich Gideon (2020), Effect of surface treatment on moisture absorption, thermal, and mechanical properties of sisal fiber.
9. Kiran Rohit and Savita Dixit (2015), A Review - Future Aspect of Natural Fiber Reinforced Composite.
10. M.Ramesha, K.Palanikumarb, K.Hemachandra Reddy (2013), Comparative Evaluation on Properties of Hybrid Glass Fiber- Sisal/Jute Reinforced Epoxy Composites.

11. Flávio de Andrade Silva, Romildo Dias Toledo Filho , João de Almeida Melo Filho, Eduardo de Moraes Rego Fairbairn (2009), Physical and mechanical properties of durable sisal fiber-cement composites.
12. Ramakrishna T. Sundararajan (2005), Impact strength of a few natural fibre reinforced cement mortar slabs: a comparative study.
13. Surendra P. Shah and James I. Daniel (1999), Measurement of Properties of Fiber Reinforced Concrete.
14. Gunasekaran Murali, Nandhu Prasad, Sergey Klyuev, Roman Fediuk, Sallal R. Abid, Mugahed Amran and Nikolai Vatin (2021), Impact Resistance of Functionally Layered Two-Stage Fibrous Concrete.
15. Jawad Ahmad1 , Mohamed Moafak Arbili2, Ali Majdi3, Fadi Althoey4, Ahmed Farouk Deifalla5 and Cut Rahmawati (2022), Performance of concrete reinforced with jute fibers (natural fibers): A review.
16. Hanfeng Xu, Sidney Mindess and Ivan Joseph Duca (2004), Performance of plain and fiber reinforced concrete panels subjected to low velocity impact loading.
17. Majid Ali (2012), Natural fibers as construction materials.
18. Marcin Małek, Waldemar Łasica, Marta Kadela, Janusz Kluczyński and Daniel Dudek (2021), Physical and Mechanical Properties of Polypropylene Fibre-Reinforced Cement-Glass Composite.
19. Hashim Mohd Khan, Sumitr Raj Shukla, Sarvi Shukla3, Akshay Kumar Gupta (2018), Enhancing mechanical properties of jute fibre/glass fiber and epoxy combined hybrid composite laminates.
20. Velu. S. Srinivasan. R (2013), Glass-Jute Fiber Reinforced Epoxy Composites.

Nonlinear Static Analysis Study on Progressive Collapse Behaviour of 2D RC Frame with Different Grades of Steel



P. Jagatheswari and R. Ramasubramani

1 Introduction

People were moving in our overpopulated world due to the excess population. To high-rise buildings, skyscrapers which require a limited area with easy livelihood provide safety, basic needs, and procurement of the people.

And when the buildings rise to a maximum height, many challenges are faced. In this, the important one that we should consider is structural design and material selection of the building and should satisfy the essential requirement such as fire safety, repair, maintenance, efficient plumbing system, basement provisions, geotechnical investigation, and seismic resistance; every category should be considered while constructing the tall building. If we fail to determine all this, failure may occur. One of the significant failures is progressive collapse. At the same time, progressive collapse is a failure of a single member or part of the structure that results in complete structural failure. In detail, progressive collapse is a structural failure, whereas the initial failure occurs in a structure that results in a continuous chain of structural damage, and at one stage, whole structure tends to collapse. And the cause of the progressive collapse is because of the load that acts on the building, and the load may be of impact load or pressure load on the building, such as gas explosions due to bomb blasts, winds, and waves occur, come under pressure load. And seismic actions like an earthquake, foundation settlement, and vehicle collision all come under the impact load [1–4].

The General Services Administration (GSA) and (DOD) Department of Defence have explained the detailed and stepwise procedure regarding the method to prevent the progressive collapse of the structure, and they put forward one crucial concept, i.e., vertical structural elements and their load path are studied. In that, column removal

P. Jagatheswari · R. Ramasubramani (✉)

Department of Civil Engineering, Faculty of Engineering and Technology, SRM Institute of Science and Technology, Kattankulathur, Tamil Nadu 603203, India

e-mail: ramasubr@srmist.edu.in

scenario is done to study the behaviour of the structure [5]. Several studies have been carried out in progressive collapse of column removal. Rakshith et al. (2013) analysed a 12-storey RC framed structure using ETABS. The demand capacity ratio is evaluated as per GSA guidelines. The linear static analysis is carried out by using software ETABS V9.7. The obtained demand capacity ratio values show that the columns are safe and beams are to be reinforced. Three column removal conditions are considered: corner, middle, and intermediate [6]. Patel [7] analysed a 15-storey 3D RC building using SAP 2000. Nonlinear static analysis is performed to see the formation of hinge pattern and rotation of the joint. Nonlinear dynamic analysis has been done to see the behaviour of the building under dynamic loading [7]. Chidambaram et al. (2016) analysed a moment-resisting frame. This is a G + 7 steel frame. This residential building is analysed using ETABS for progressive collapse caused due to fire loads. A temperature of 550 °C was given to the column at different levels with reducing material property and yield strength according to IS800. The load combination was considered according to GSA guidelines. Sanjay Kumar Sath et al. (2016) analysed a multi-storeyed RCC building under seismic effect. Building of different aspect ratios and plan configurations were considered. A total of 16 building models are analysed for different load combinations by linear elastic dynamic analysis (response structure analysis) using ETABS. They have focused on the vertical and horizontal aspects ratio of the building which decides the geometry strength and stiffness of the structure. Huang et al. [8] present two-bay by 2-storey reinforced concrete frames that took for the analysis with the loss of one corner column. However, it includes strengthening the high-performance ferro-cement laminate and the bonded steel plates, and strengthening effects are also determined. It also shows the crack development pattern, lateral deformation, load–displacement, load distribution, and strengthening effects. The frame's initial stiffness and bearing capacity are strengthened after the strengthening process [8].

This paper presents the study on two-dimensional RC behaviour of 5-, 10-, and 15-storey bare frame under the nonlinear static condition, which includes corner and middle column removal and to study the RC frame with different grades of steel.

2 Validation Study

A research paper for validation purpose has been chosen for the validation purpose research paper has been chosen. The selected paper was **a prototype and scaled computational model behaviour for RC frame with masonry infill walls** [9]. This paper investigated the push-over curves, stress–strain relation, and plastic point zone formation for 3D frame models. And a finite element model (FEM) was created to validate the study using the Abaqus software. A graph has been taken for the validation study in this load versus displacement. The parameters of the following model are the lengths of the beam and column which are 1 m and 0.75 m, the dimension of both beam and column is 100 × 60 mm, reinforcement beam 4 nos. of 6 mm dia., and the reinforcement details of column 4 nos. of 10 mm dia. However,

the material properties of the model are yield stress $f_y = 400$ MPa, ultimate stress = 520 MPa, yield strain = 0.001, ultimate strain = 0.09, and compressive strength of concrete = 24 MPa. The modelling and the analysis of the specimen are given in Figs. 1 and 2.

Comparison Graph for the Validated Model

In Fig. 3, the results show that the load versus displacement graph has a good agreement with the reference graph and the validated model graph.

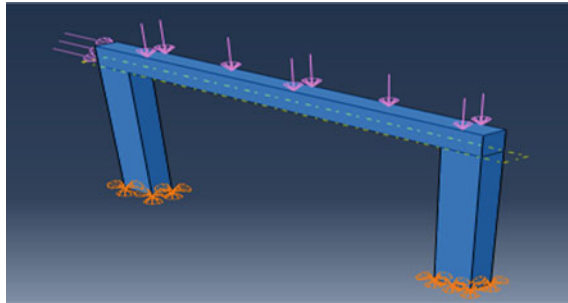


Fig. 1 Modelling of the frame

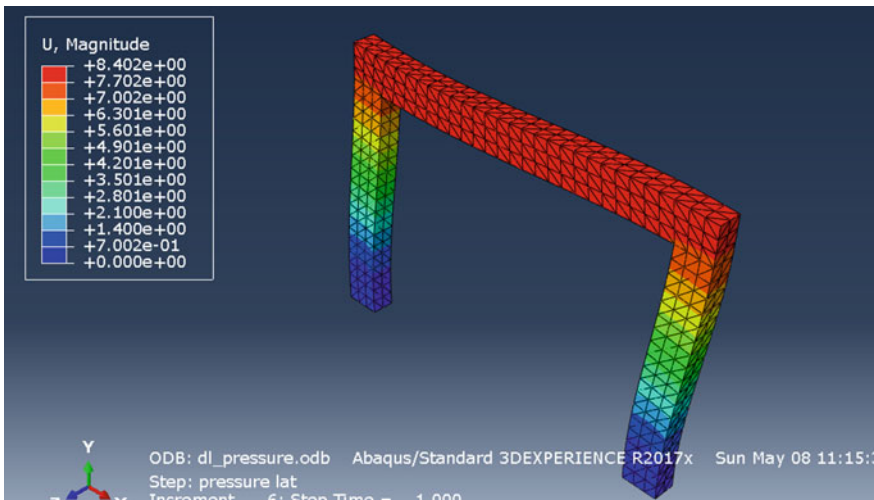


Fig. 2 Analysis of the frame

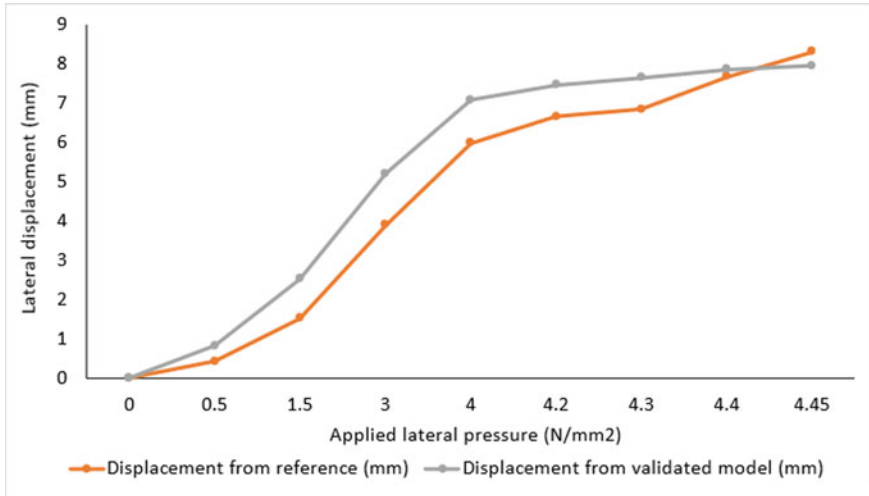


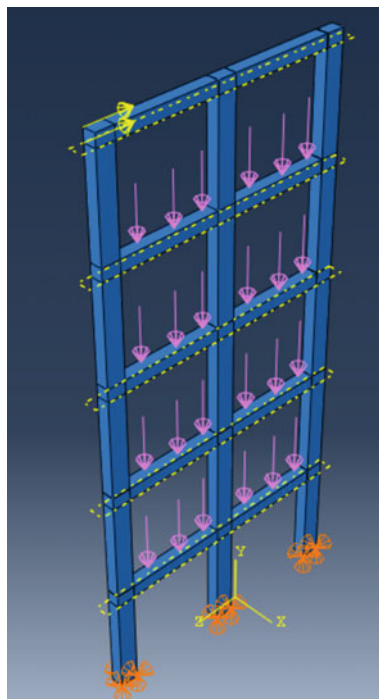
Fig. 3 Comparison graph for the validated model

3 Analytical Details

The structure was modelling and analysed using Abaqus (FEM software). This software accurately evaluates the results. Here, analytical studies on the progressive collapse behaviour of 2D RC frames with different steel grades were compared, and the column removal scenario is done at the corner and middle level. For the given structure, the results taken are compared with different grades of steel, and they determined the ductility behaviour of the RC frame when it is in the normal condition (without removing the column), robustness index of the 2D RC frame was identified for all the conditions, and base shear versus displacement of the RC frame was also determined. The boundary condition of the RC frame is a pinned end condition for the nonlinear static analysis to determine the extreme behaviours of the frames.

4 Geometry of the Structure

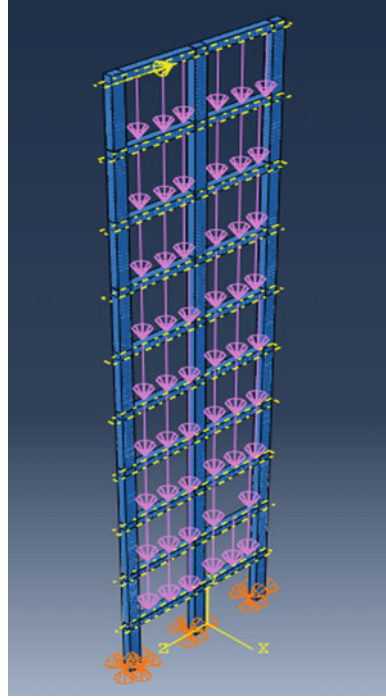
Preliminary data of the two-dimensional RC frame structure with the three different storeys 5, 10, and 15; each storey consists of height 15 m, 30 m, and 45 m, whereas no. of bay considered in these storeys are two bays, the height of each bay is 2.7 m, and the width of each bay is 2.5 m. Cross-section of the beam is 0.3 m × 0.3 m, and the cross-section of the column is 0.3 m × 0.45 m [10, 11]. Reinforcement details for the beam are the main bar 4 no. of 10 mm diameter with stirrups 8 mm diameter @ 100 mm spacing, and the clear cover is 25 mm overall the beam. Reinforcement details for the column are main bar 4 no. of 12 mm diameter along with ties 8 mm

Fig. 4 5-storey frame

diameter @ 150 mm spacing, and the clear cover is 40 mm [12]. The loads that act on the structure are dead load. DL is automatically calculated by the Abaqus software, and the self-weight of the structure is calculated manually. However, for the nonlinear static analysis of the 2D frame, only the self-weight of the beam and column is calculated as 0.447kN/m. The analysis process is carried out since the cyclic load point is given at the top of the frame until it reaches the maximum level point (Figs. 4, 5 and 6).

5 Material Properties

Material properties of the RC frame of different grades of steel and concrete were taken to compare the behaviour of steel at different storey levels and to give a better material for the frames. The properties are mentioned in Table 1.

Fig. 5 10-storey frame

6 Element Property of the Structure

Automated type mesh was chosen for modelling the frame. Thus, modification of geometry will result in the change of mesh automatically. (C3D8R) Solid element of deformable-type eight node was taken as the type of element. Automated square mesh and the meshing size of 250 mm were taken. The stress–strain behaviour of Fe415, Fe500, and Fe550 have been referred from the material characteristics, and design parameters for limit state method of design as per IS 456-2000 and IRC: 112–2011 (Fig. 7).

7 Nonlinear Static Analysis

Nonlinear static analysis is also known as push-over analysis. Nonlinear static analysis is an improvement over the linear static analysis, whereas it allows the inelastic behaviour of the structure, in which it is subjected to gravity load and monotonically increasing lateral load until the structure reaches the maximum or collapse pattern of the structure, and it provides information about the structure's strength, deformation, and ductility behaviour.

Fig. 6 15-storey frame

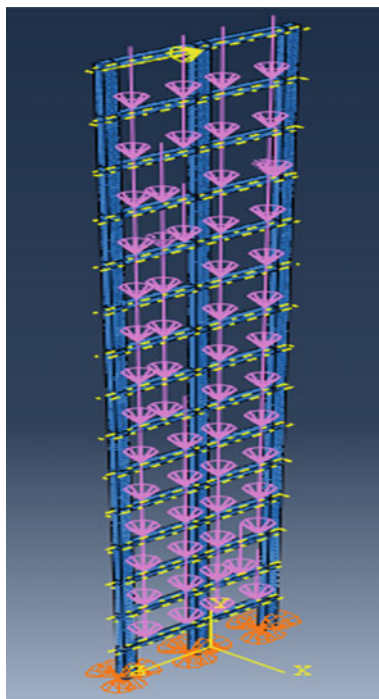


Table 1 Material properties of structure

Grade of steel	Grade of concrete	Poisson ratio of concrete	Poisson ratio of steel	Modulus of concrete	Modulus of steel
Fe415	M30	0.23	0.3	2×10^{10} N/m ²	2×10^{11} N/m ²
Fe500	M30	0.23	0.3	2×10^{10} N/m ²	2×10^{11} N/m ²
Fe550	M30	0.23	0.3	2×10^{10} N/m ²	2×10^{11} N/m ²

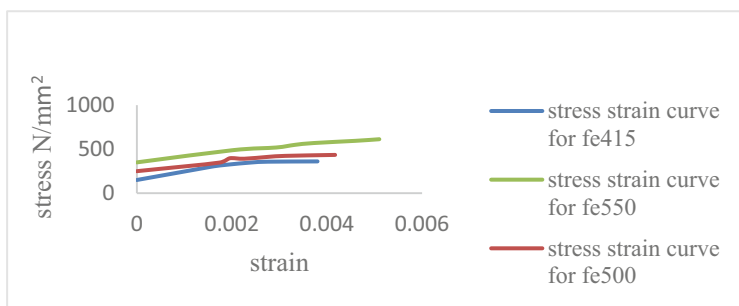


Fig. 7 Stress–strain curve for different grades of steel

In this project, nonlinear static analysis is carried out to determine the ductility behaviour of the 2D RC frame, base shear versus displacement of the frame under the bottom level is also determined, and the robustness index of the frame is also found. The analysis was done for a bare frame of 27 models with different grades of steel at the different storey levels, on the condition of column removal scenario at the corner and middle of an RC frame, and the loads are considered as per the GSA guidelines.

8 Procedure of Nonlinear Static Analysis

- A bare frame model is created in Abaqus for different storey levels like 5, 10, and 15. The material properties, load cases, and stress–strain behaviour for three steel grades were provided.
- The nonlinear static analysis is carried out for three cases at each storey. One is without removal of a column, the second case is corner column removal, and the third case is middle column removal.
- The analysis of three different cases is run, and the ductility behaviour of the concrete frame under the condition of without removal of a column is determined; base shear versus displacement and robustness index of the concrete frame is also found.
- As per the GSA guidelines, the obtained values are checked, whether the RC frame was safe according to the limits provided in the guidelines (Figs. 8, 9 and 10).

9 Results and Discussion for Nonlinear Static Analysis

The results analysed in the FEM are discussed below. Three storeys of buildings were analysed for the nonlinear static analysis, and different grades of steel were used. The results were compared with three-storey levels at three different grades of steel. Such ductility behaviour of the concrete frame, base shear versus displacement, and robustness index of the concrete frame were discussed below.

Ductility Behaviour of 2D RC Frame

The ductility behaviour of the 2D RC frame states that it is an ability of a material to undergo large deformation without any split or crack before failure [13].

Results for 5-Storey RC Frame Under Three Grades of Steel

In Fig. 11, the hysteresis loop was plotted for resisting force versus top most deformation of the 5-storey frame, where at the top most level point, the deformation is found to be the maximum point. According to the graph, the intensity of the space between the curves is very large when compared to the bottom-storey levels. And so, the

Fig. 8 Without removal of column

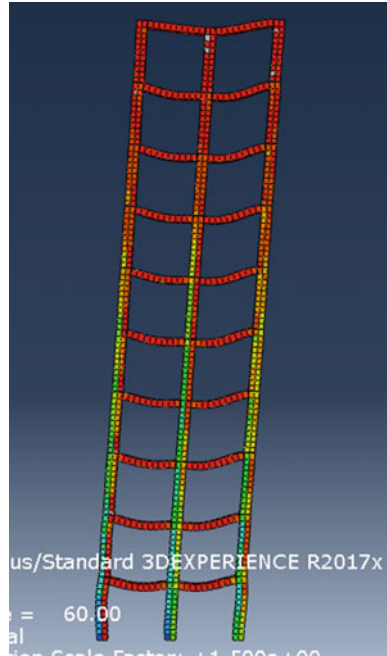
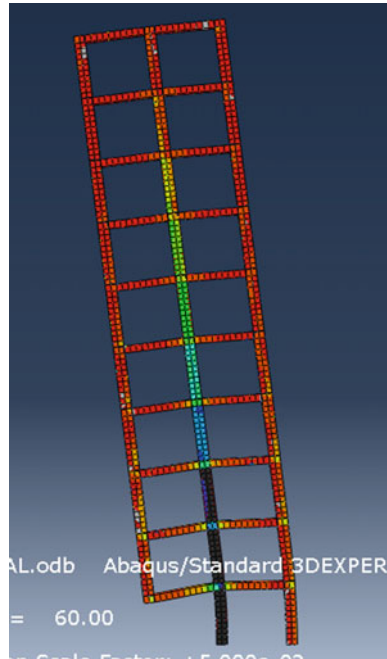


Fig. 9 Corner column removal



top-most deformation and resisting force values are taken for all three grades of steel as Fe415, Fe500, and Fe550. Comparatively, this Fe415 grade steel–concrete frame has more deformation elastic behaviour when compared to the other two constraints.

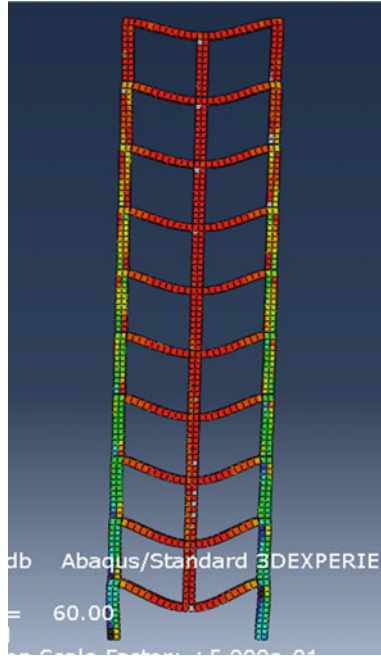


Fig. 10 Middle column removal

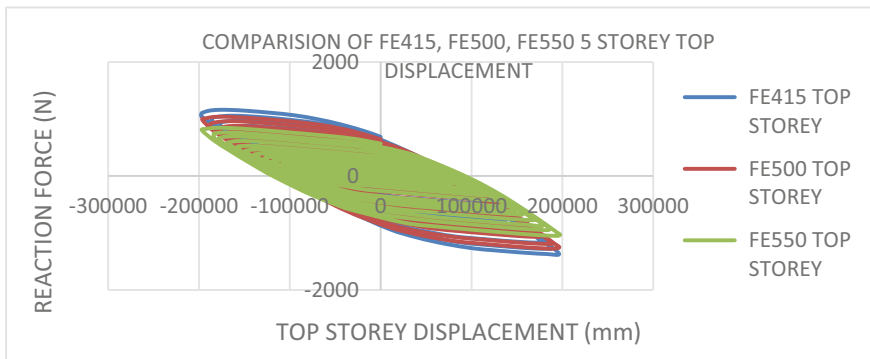


Fig. 11 Comparative graph for Fe415, Fe500, and Fe550 5-storey top displacement

Results for 10-Storey RC Frame Under Three Grades of Steel

In Fig. 12, the hysteresis loop was plotted for resisting force versus top most deformation of the 10-storey frame, where at the top most level point, the deformation is found to be the maximum point. According to the graph, the intensity of the space between the curves is very large when compared to the bottom-storey levels. And so, the top-most deformation and resisting force values are taken for all three grades of steel for Fe415, Fe500, and Fe550. Comparatively, this Fe415 grade steel–concrete frame has more deformation elastic behaviour when compared to the other two constraints.

Results for 15-Storey RC Frame Under Three Grades of Steel

In Fig. 13, the hysteresis loop was plotted for resisting force versus top most deformation of the 15-storey frame, where at the top-most level point, the deformation is found to be the maximum point. According to the graph, the intensity of the space between the curves is very large when compared to the bottom-storey levels. And so, the top-most deformation and resisting force values are taken for all three grades of steel Fe415, Fe500, and Fe550. Comparatively, this Fe415 grade steel–concrete frame has more deformation elastic behaviour when compared to the other two constraints.

Base Shear Versus Displacement of 2D RC Frame

Base shear states that the horizontal force occurs at the bottom of the structure or frame related to the lateral forces or load and displacement behaviour that act on the structure. And the following graphs describe the maximum and minimum load-bearing capacity of the frame according to its behaviour and the load pattern in the critical stage [14].

Base Shear Versus Top Storey Displacement for 5-Storey 2D RC Frame

Figure 14 shows base shear versus displacement for a 5-storey RC frame under different conditions. According to this Fe415 grade of steel, the RC frame has

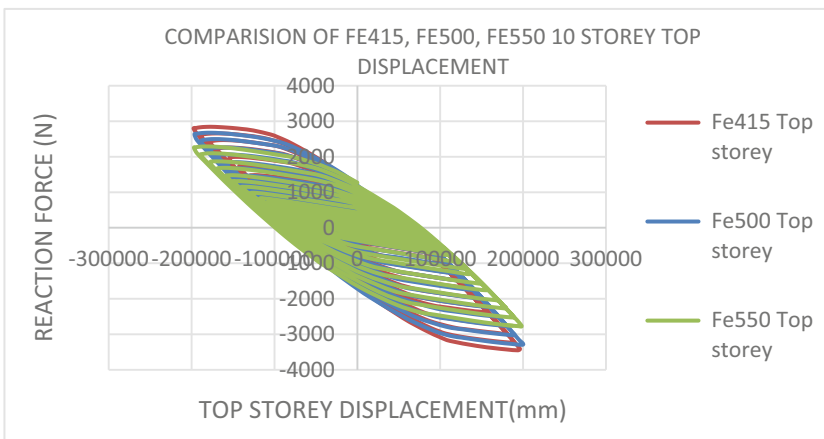


Fig. 12 Comparative graph for Fe415, Fe500, and Fe550 10-storey top displacement

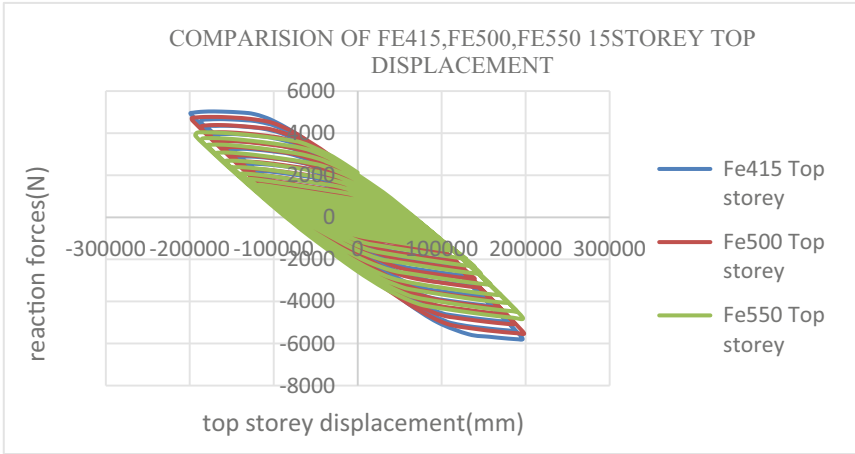


Fig. 13 Comparative graph for Fe415, Fe500, and Fe550 15-storey top displacement

very low load-resisting capacity compared to the other steel grades, and Fe550 has maximum base shear versus displacement value.

Base Shear Versus Top Storey Displacement for 10-Storey 2D RC Frame

Figure 15 shows base shear versus displacement for a 10-storey RC frame under different conditions. According to this Fe415 grade of steel, the RC frame has very low load-resisting capacity compared to the other steel grades, and Fe550 has maximum base shear versus displacement value.

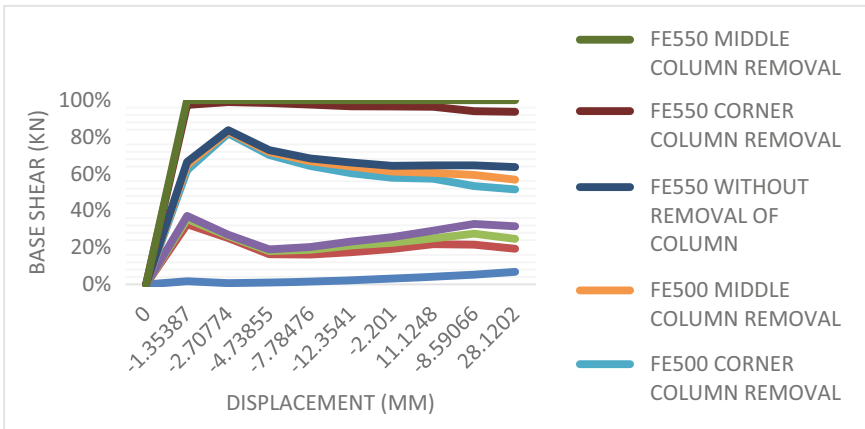


Fig. 14 Base shear versus displacement for 5-storey RC frame

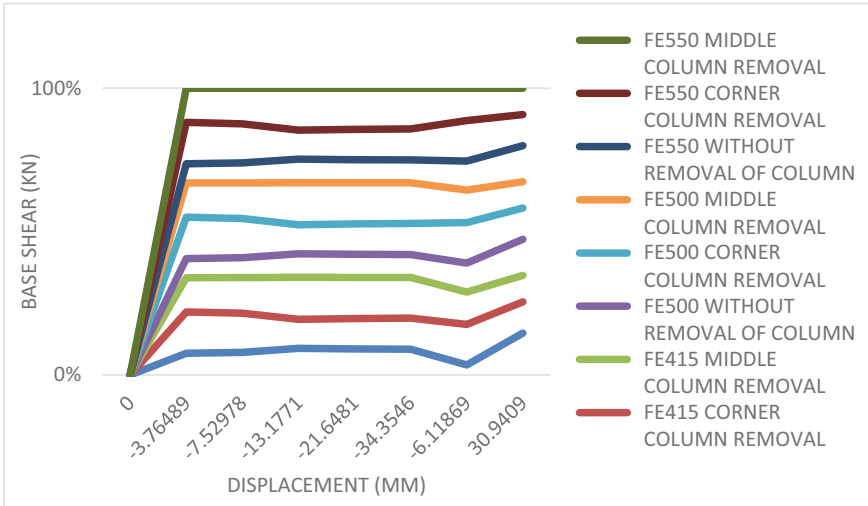


Fig. 15 Base shear versus displacement for 10-storey RC frame

Base Shear Versus Top Storey Displacement for 15-Storey 2D RC Frame

Figure 16 shows base shear versus displacement for a 15-storey RC frame under different conditions. According to this Fe415 grade of steel, the RC frame has very low load-resisting capacity compared to the other steel grades, and Fe550 has maximum base shear versus displacement value.

Robustness Index (R)

Robustness indicator (R) is defined as the capability of a building to hold on to the local failure to withstand the loading and not cause any disproportionate damage [15].

$$R = V_d / V_i$$

V_d is the base shear of a damaged building (removal of column).

V_i is the base shear of the intact building (without removal of column).

As per GSA guidelines, (R) must be equal to 1.

Robustness index of the value of 5-, 10-, and 15-storey RC frame is shown in Fig. 17.

Figure 17 shows that the Fe415 grade of steel–concrete RC frame has a maximum value of robustness index under both corner and middle column removal conditions. In that, corner column removal of Fe415 grade of the steel–concrete frame has at most critical value, or it is equal to the limit compared to the other two grade of steel, Fe500 and Fe550.

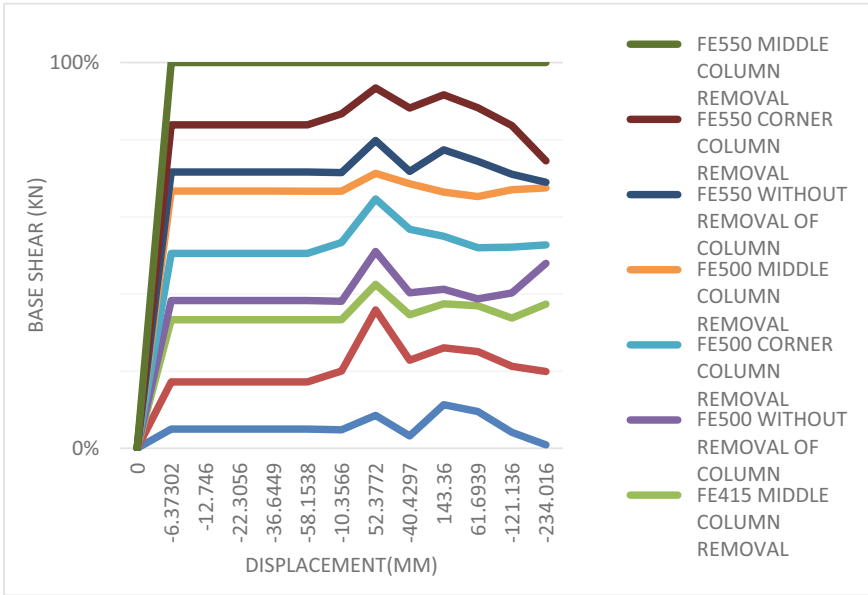


Fig. 16 Base shear versus displacement for 15-storey RC frame

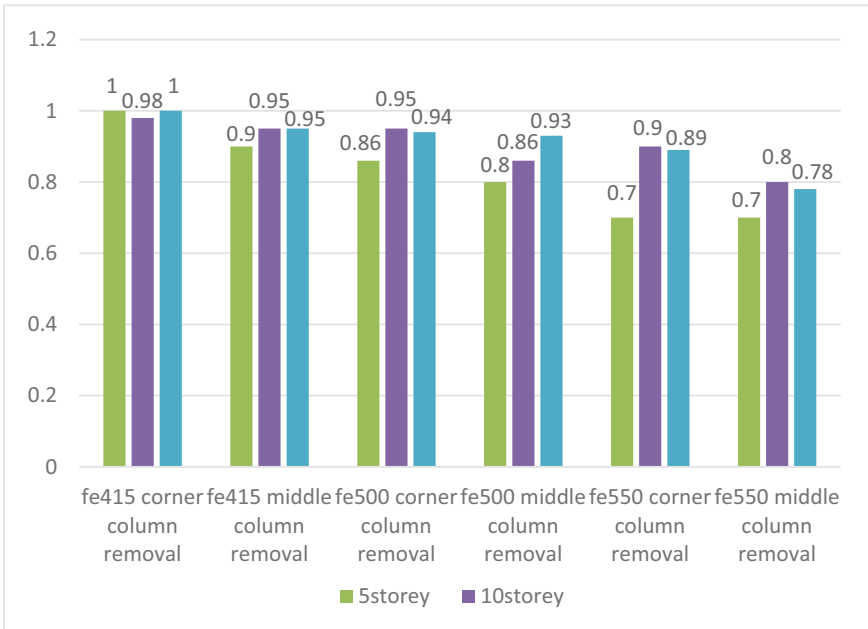


Fig. 17 Robustness index of 5-, 10-, and 15-storey RC frame

10 Conclusion

- In this study of 2D RC frame, nonlinear static analysis is carried over. And the behaviour of 5-, 10-, and 15-storey RC frames was determined by removing the corner, and middle column, i.e., progressive collapse behaviour of the frame is discussed under the consideration of three different types of steel like Fe415, Fe500, and Fe550.
- According to the above nonlinear static analysis, ductility behaviour of the RC frame, base shear versus displacement, and robustness of the frame were determined where the FE415 grade of steel frame have critical analysis value when compared to the other two grade of steel, especially the collapse pattern was critical in the corner column removal of the 2D RC frame compared to the middle column.

References

1. Starossek U (2009) Progressive collapse of structures, vol 153. Thomas Telford, London
2. Byfield M, Mudalige W, Morison C, Stoddart E (2014) A review of progressive collapse research and regulations. *Proc Inst Civ Eng-Struct Build* 167(8):447–456
3. Marjanishvili SM (2004) Progressive analysis procedure for progressive collapse. *J Perform Constr Facil* 18(2):79–85
4. Bao Y, Kunnath SK, El-Tawil S, Lew HS (2008) Macro model-based simulation of progressive collapse: RC frame structures. *J Struct Eng* 134(7):1079–1091
5. General service administration guidelines, 'alternate path analysis & design guidelines for progressive collapse resistance' October 2013
6. Birajdar YT, Shelke NL (2017) Progressive collapse analysis of multi-storied RCC building
7. Patel BR (2014) Progressive collapse analysis of RC buildings using nonlinear static and nonlinear dynamic method. *Int J Emerg Technol Adv Eng* 4(9):1640–1644
8. Huang H, Huang M, Zhang W, Guo M, Chen Z, Li M (2021) Progressive collapse resistance of multistorey RC frame strengthened with HPFL-BSP. *J Build Eng* 43:103123
9. Khoshnoud HR, Marsono AK, Prototype and scaled computational model behavior for RC frame with masonry infill walls
10. Lavendra S, Kumar P, Raghavendra T (2021) Progressive collapse behaviour assessment of steel frame structures—a review. *IOP Conf Ser: Earth Environ Sci* 822(1):012004
11. Sasi A, Joy T, Comparative study of static and dynamic seismic analysis of multi-storeyed RCC building by using E-tabs for different plan configurations
12. Gowtham S, Prakash M, Parthasarathi N, Satyanarayanan KS, Thamilarasu V (2018) 2D-Linear static and non-linear dynamic progressive collapse analysis of the reinforced concrete building. *Mater Today: Proc* 5(2):8775–8783
13. Liu M (2013) A new dynamic increase factor for nonlinear static alternate path analysis of building frames against progressive collapse. *Eng Struct* 48:666–673
14. Tavakoli HR, Alashti AR (2013) Evaluation of progressive collapse potential of multi-story moment resisting steel frame buildings under lateral loading. *Sci Iranica* 20(1):77–86
15. Jeyanthi R, Kumar SM (2016) Progressive collapse analysis of a multistorey RCC building using pushover analysis. *Int J Eng Res* 5(03)

Behaviour of Steel–Concrete Composite Beams Provided with Headed Stud Shear Connectors



Ammu C. Bose and N. Umamaheswari 

1 Introduction

A structural component made of two or more different materials that have been bonded jointly to function as a single entity called a “composite construction”. When compared to a mild steel construction, this one can withstand larger loads. This idea is built on utilizing both steel and concrete to their respective advantages. Shear connectors are primarily responsible for evenly distributing the load from the concrete slab to the steel beam without slipping, and they also need to keep the slab and steel component from vertically separating at the interface. Bending experiments were used to analyse the behaviour of the shear connection between the beam and composite slab.

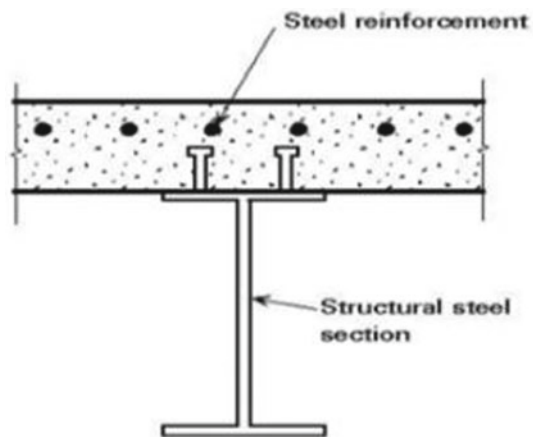
Laboratory testing is known to be more time consuming, expensive, and in some situations, not always viable. While this has been happening, the finite element approach has developed into a strong and practical instrument for the analysis of a variety of engineering issues. The model must accurately describe the constituent parts, incorporate relevant elements, and apply appropriate solution strategies in order to produce findings that can be trusted. Given that the behaviour of a composite beam is nonlinear, it is essential that the interactions between various components be accurately modelled. According to the models [1], a 3D model contains every structural component associated with nonlinearities. Under static and impact pressures, it was determined how steel stud connectors connecting a steel beam and concrete slab behaved in shear. The experiment consists of nine impact push out tests and four static testing. Along with examining the temporal evolution of impact load and slippage displacements, stud connections’ shear strength and failure modes were also examined. In comparison to static test results, it was discovered that the shear

A. C. Bose · N. Umamaheswari (✉)
Department of Civil Engineering, SRM Institute of Science and Technology,
Kattankulathur 603203, India
e-mail: umamahen@srmist.edu.in

capacities of the stud connections had increased by 33–63% in dynamic tests, and the static test results demonstrated that they reasonably satisfied the relevant standards [2]. Shear connectors were examined, and the best connector for a particular composite beam was predicted based on static load and the quantity of steel in the connector as a common factor. The following findings were reached based on the analytical results of the two models. When stud connections were utilized instead of bolted connections, the load carrying capability of the composite beam increased by 50% and slippage was found to be 50% less in the subassembly model with welded connections than with bolted connections [3]. Researchers investigated and studied the ultimate strength and behaviour of a novel form of composite beam known as a confined steel–concrete composite beam. An unreinforced concrete beam is confined to the concrete and used as a formwork during construction by having cold-formed steel sheet closed on three sides. Shear connections in the form of headed studs are provided to connect steel sheets to concrete. The behaviour of cold-formed steel sheet with shear connectors was investigated in this work. Both the numerical analysis and the experimental analysis used ANSYS, a finite element tool. These CSCC beams expedite construction by eliminating form work and reducing the amount of reinforced steel [4] (Fig. 1).

It was believed that each form of construction has a strong advantage that, when combined, produces an efficient system, therefore integrating steel and concrete systems made sense. The behaviour of composite construction with alternative shear connections was also studied [6]. It was determined from the results that the height of the shear connectors had no effect on the composite beam's deflection. This was determined by analysing 3D numerical models of steel–concrete composite beams structural behaviour. Additionally, it was shown that the cross-sectional geometry of the shear connector has an impact on how the composite beam behaves. Rectangular-shaped shear connectors are proven to be more successful than circular-shaped ones for preventing the deflection of composite beams [7].

Fig. 1 Composite structure with stud type shear connector [5]



Comparing the two types of connectors revealed that, under monotonic loading, channel shear connectors had a shear strength that was 7.5–36.4% larger than angle shear connectors, whereas angle shear connectors had a shear strength that was 23–49% greater under fully reversed cyclic stress [8]. The shear connectors are subjected to significant pull out forces around the web apertures, which have previously been ignored, according to a close inspection of the finite element models [9]. The capacity of headed shear studs in solid concrete slabs was increased as a result of the finite element model's improved grasp of the various mechanisms of failure seen during the experimental programme [10]. On simply supported composite beams, investigations on the three-dimensional combination of bending and shearing as well as the impact of the degree of shear connection on the vertical shear strength were made [11]. The impacts of shear slip and the deformation of steel–concrete composite beams were considered together with different forms of loads [12].

It has been noted from the literature review that the work done seeks to determine distinct shear connector qualities and its related behaviour by conducting various experiments by modifying its physical features including shape, size, length and spacing. The performance of steel–concrete composite beams with various span lengths, shear stud dimensions (diameters and height) and shear connector spacing is compared in the current study using numerical analysis.

2 Numerical Investigation

The finite element programme ANSYS was used to conduct the numerical investigation. In finite element analysis, a complicated system is divided into very small, so-called elements, using a numerical method. Equations governing the behaviour of all elements are implemented and solved by this software. These outcomes may be tabulated or graphically shown. A computational tool called the finite element method is used to obtain approximations of solutions to boundary value problems. A composite beam made of steel I section ISMB 300 and a 120 mm thick concrete slab is placed on top of the beam using different configurations of shear stud connectors. The boundary condition is simply sustained, and the concrete slab receives the load at its top and it is dispersed equally across its entire width. The accuracy of the results produced by the finite element model depends on the constitutive material model, boundary conditions and finite element mesh. Different components, such concrete slabs, stud connectors, and reinforcement bars, are handled on a part-by-part basis as opposed to employing global or sweep characteristics. Thus, a regular structured hexahedral mesh of 10 mm dimension was constructed for the I beam with a combination of hexahedral and tetrahedral elements provided for the slab, reinforcement and the studs. Figures 2, 3 and 4 shows model, meshing and loading and boundary condition of composite beam in numerical study. In the current finite element analysis, different types of headed stud shear connectors with 12, 19 and 25 mm diameters are used. Table 1 provides a description of the shear connector's dimensions.

Fig. 2 Full-scale model

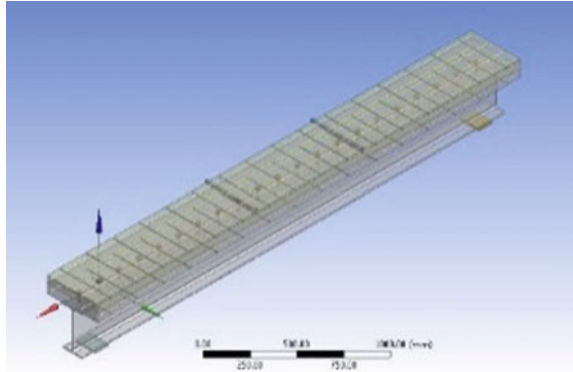


Fig. 3 Mesh generated

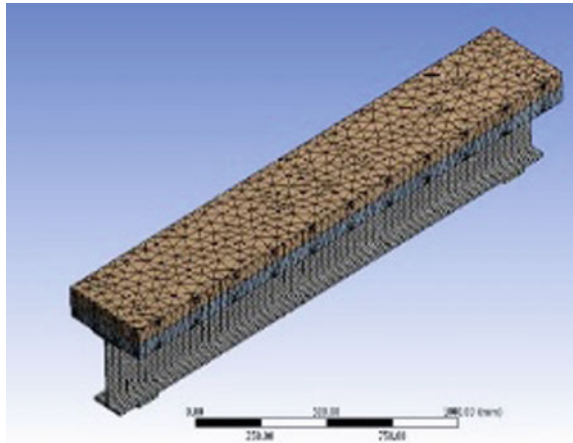


Fig. 4 Loading

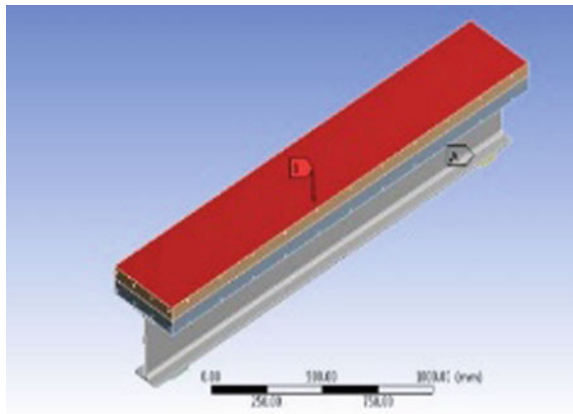


Table 1 Dimensions of shear connector

Head diameter (mm)	Shaft diameter (mm)	Overall height (mm)
18	12	62
30	19	100
38	25	100

Table 2 Details of geometry composite beam

Element	Description	Value
Concrete slab	Width, mm	380
	Thickness, mm	120
	Diameter of longitudinal bar, mm	10
	Diameter of transverse bar, mm	8
Steel	Cross sectional area, mm ²	5606
	Depth, mm	300
	Width of flange, mm	140
	Thickness of web, mm	7.4

In the current finite element analysis, different types of headed stud shear connectors with 12, 19 and 25 mm diameters are used. Table 1 provides a description of the shear connector’s dimensions.

Various spacing of shear connector being 150, 200 and 250 mm were used for the finite element model to choose the optimal spacing and to determine the optimal strength. To determine the deflection variables, the finite element model with a range of span lengths of 1, 2 and 3.2 m was examined with a range of stud spacing. Details of the composite beam’s geometry are given in Table 2 (Fig. 5).

Results of validation are given in Table 3.

Fig. 5 Validated load–deflection curve

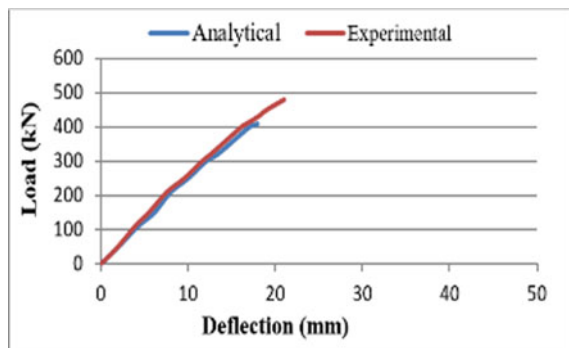
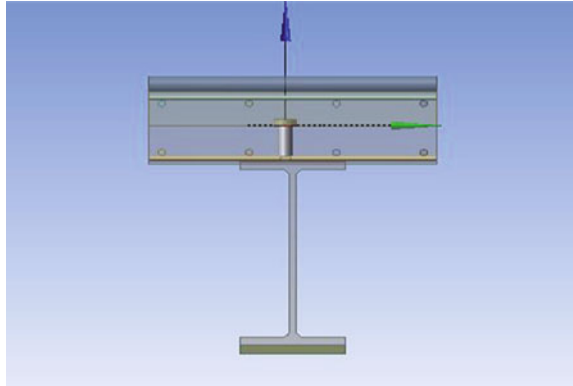


Table 3 Results of validation

Description	As per literature	Validated model	% Error
Maximum load (kN)	410.00	415.00	1.22
Maximum deflection (mm)	17.52	17.98	2.63

Fig. 6 Assemblage of the components

3 Numerical Programme

The parameters involved in the analysis consist of variation in the span length in which different diameter studs spaced at different spacing were embedded. Modelling was done using eight node linear hexahedral and tetrahedral components to represent concrete slabs, steel beams and the shear connector. Utilizing the three-dimensional, two-noded beam 188 element, steel reinforcing bars were simulated. The components are assembled in Fig. 6. Using interaction and constraint choices that accurately reflect the contact behaviour in test specimens, contact between various parts has been predicted. The contacts between a steel beam, a concrete slab and a shear connector were modelled using surface-to-surface interaction. With the previously specified material characteristics, the study of the beam is conducted, and load–deflection curves were derived for various spans with varied parameters. Figures 7 and 8 show deformation of section obtained from software and deformed section.

4 Results and Discussion

Figure 9a–c illustrates load–deflection curves for 1 m beam span for studs of various diameters and spacings, and the combined graph obtained for the spacing with the different size of the connector is illustrated in Fig. 9d–f.

Fig. 7 Deformation of beam

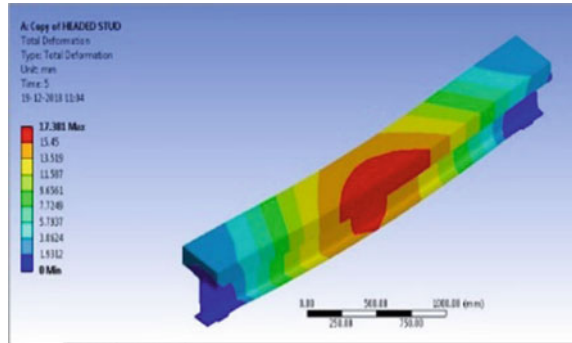


Fig. 8 Deformed section

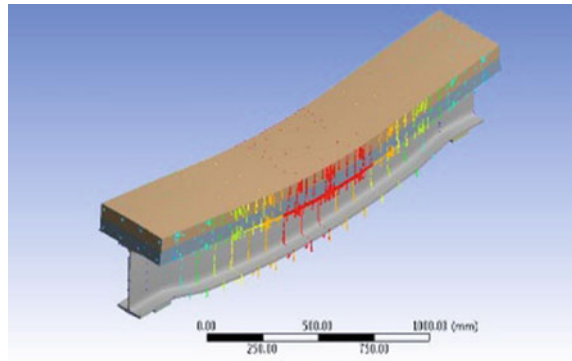


Figure 10a–c illustrates load–deflection curves for 2 m beam span for studs of varied diameters and spacing and the combined graph obtained for the spacing with the different size of the connector is illustrated in Fig. 10d–f.

Figure 11a–c illustrates load–deflection curves for 3.2 m beam span for studs of varied diameters and spacing, and the combined graph obtained for the spacing with the different size of the connector is illustrated in Fig. 11d–f.

From the load–deflection behaviour generated for beams of span 1, 2 and 3.2 m connected with headed stud shear connectors of diameters 18, 30 and 38 mm spaced at 150, 200 and 250 mm and various combinations of the parameters, it is found that headed stud shear connectors can be effectively utilized in steel–concrete composite beams in practice. The maximum load carrying capacity is found to be 410 kN. The deflection obtained is found to be more for beams of 3.2 m span compared to beams of 1 and 2 m. Diameter of stud is an important parameter influencing the performance of composite beams under static loading. Deflection was greatly reduced as stud diameter increased almost in all cases. Of three spacing of stud connectors considered, 150 mm is possessing the optimum strength compared to studs spaced at 200 and 250 mm.

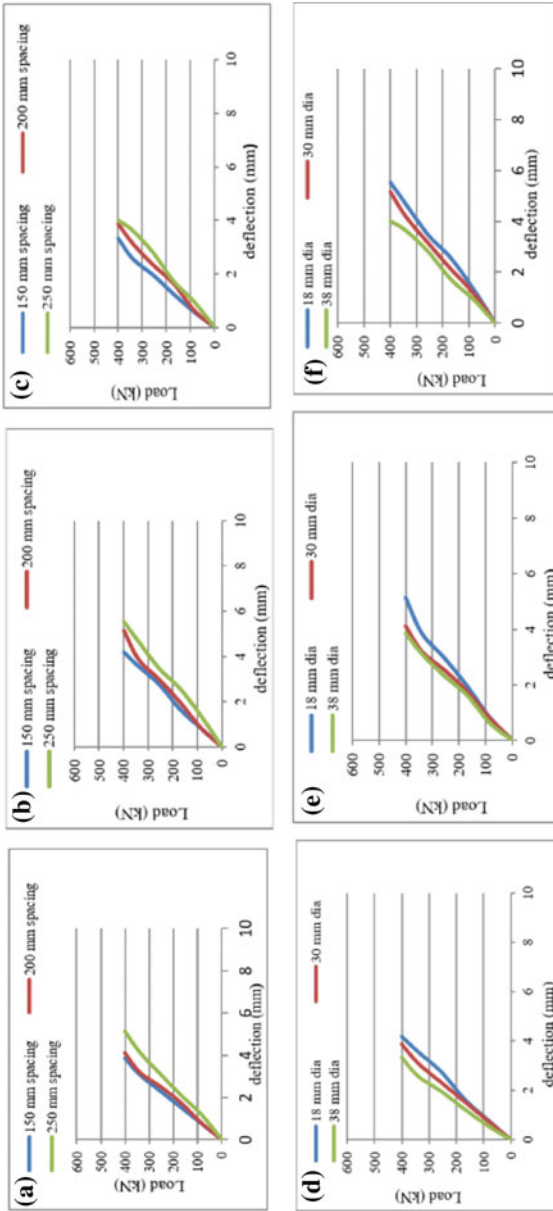


Fig. 9 Load-deflection curve for beam of span 1 m, **a** 18 mm diameter stud, **b** 30 mm diameter stud, **c** 38 mm diameter stud, **d** 150 mm spaced stud, **e** 200 mm spaced stud, **f** 250 mm spaced stud

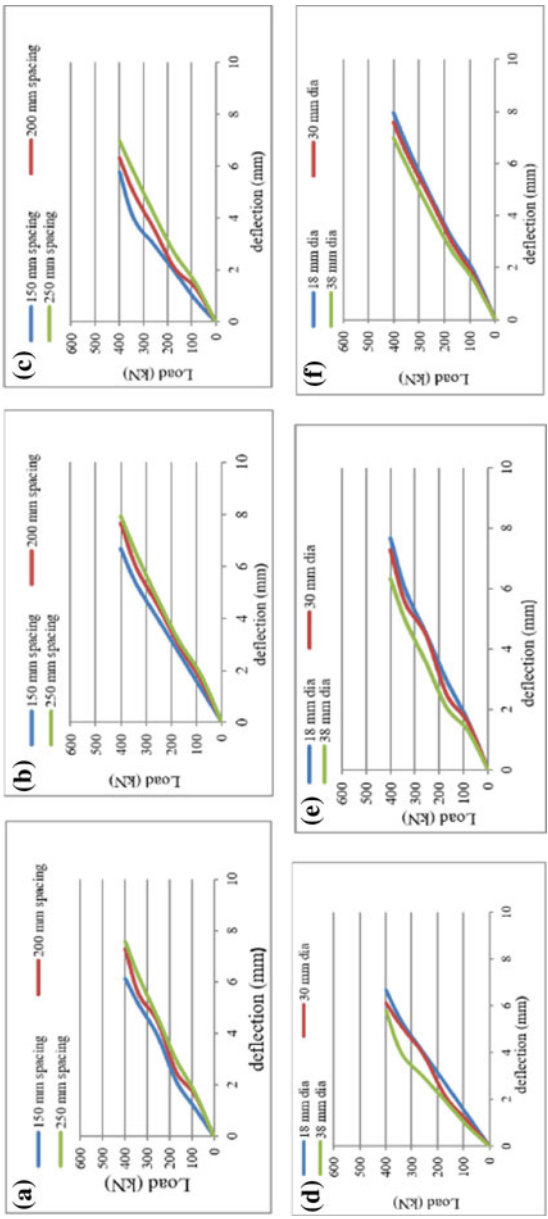


Fig. 10 Load-deflection curve for beam of span 2 m, **a** 18 mm diameter stud, **b** 30 mm diameter stud, **c** 38 mm diameter stud, **d** 150 mm spaced stud, **e** 200 mm spaced stud, **f** 250 mm spaced stud

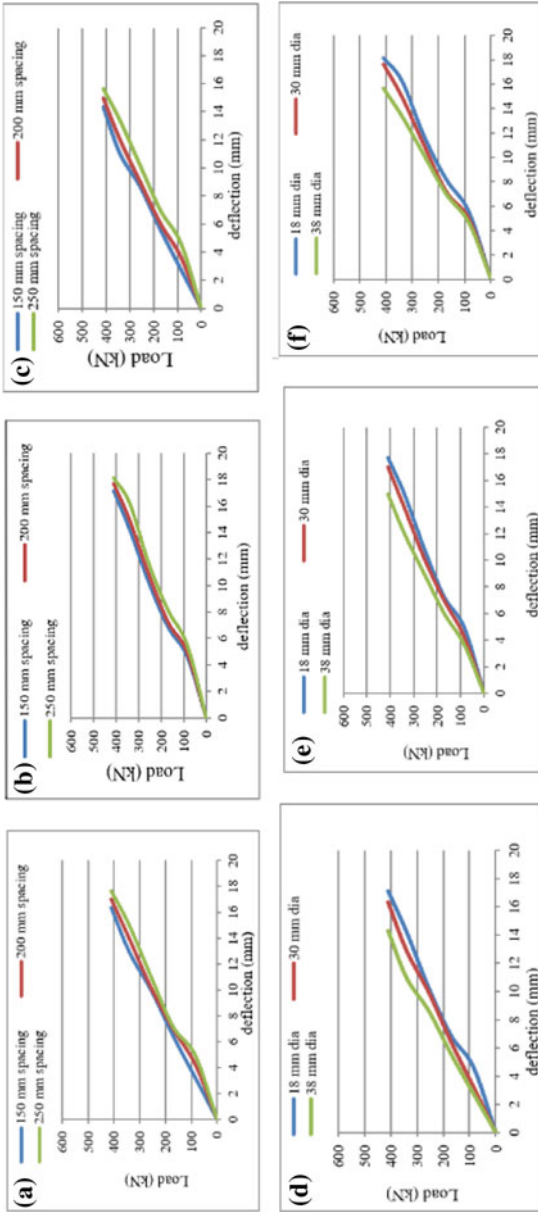


Fig. 11 Load-deflection curve for beam of span 3.2 m, **a** 18 mm diameter stud, **b** 30 mm diameter stud, **c** 38 mm diameter stud, **d** 150 mm spaced stud, **e** 200 mm spaced stud **f** 250 mm spaced stud

5 Conclusion

The flexural behaviour of a steel–concrete composite beam with a welded headed stud shear connector is examined using numerical analysis. The following conclusions are arrived.

The deflection obtained is more for beams of 3.2 m span compared to beams of 1 and 2 m, of three spacing of stud connectors considered, 150 mm is possessing the optimum strength compared to studs spaced at 200 and 250 mm and deflection was greatly reduced as the stud's diameter increased.

References

1. Raguvaran Balasubramanian B, Baskar R (2018) Performance study of steel-concrete Composite beam involving flexural shear connector. *Int J Struct Eng* 9
2. Huo J, Wang H, Zhu Z, Liu Y, Zhong Q (2018) Experimental study on Impact behaviour of stud shear connectors between concrete slab and steel beam. *J Struct Eng* 144:325–332
3. Subramani T and Zhong A A numerical, experimental and analytical study on confined steel concrete composite beam *International Journal of Science, Engineering & Technology Research* 5,1804–1809 (2016)
4. Preethi G, Elangovan R (2018) An experimental study on the shear strength of FRP perfbond shear connector. *IOP Conf Ser: Mater Sci Eng*
5. <http://fgg-web.fgg.uni-lj.si/~pmoze/esdep/master/wg10/10410.htm>
6. Gupta T, Ravi Sharma K (2015) Steel concrete composite structures: state of art. *Int J Latest Res Sci Technol* 4(15):149–153
7. Patil PS, Shaikh MG (2013) A study of effect of shear connector in composite beam in combined bending and shear by ANSYS. *Int J Innov Technol Explor Eng* 3
8. Shariati M, Sinaei H (2016) Comparison of behaviour between channel and angle shear connectors under monotonic and fully reversed cyclic loading. *Constr Build Mater* 38:512–523
9. Wang AJ, Chung KF (2008) Advanced finite element modelling of perforated composite beams with flexible shear connectors. *Eng Struct* 30
10. Lam D, ASCE M, El-Lobody E (2005) Behaviour of headed stud shear connector in composite beam. *ASCE J* 96
11. Liang Q, Uy B, Bradford A, Ronagh (2005) Strength analysis of steel-concrete composite beams in combined bending and shear. *J Struct Eng (AISC)* 131:1593–1600
12. Nie J, Cai CS (2003) Steel-concrete composite beam considering slip effects. *J Struct Eng (AISC)* 129:495–506

Bridge and Tunnel Engineering

Behavior of Double Layer Compound Cold-Formed Steel Columns



V. Hari Krishnan and C. Manoj Kumar

1 Introduction

Cold-formed steels are lightweight materials used for various small-scale/low-rise buildings for load applications [1–4]. Cold-formed steels are brake-pressed or bending flat sheets at room temperature Cold-formed steel is lighter than conventional RCC construction using and lesser in weight than structural steel. They are used in vehicles, agriculture, electrical equipment, etc. The yield strength of the CFS sheet comes to around 280 N/mm². CFS is used in prefabricated structures as truss elements. Cold-formed steels are being tested in various structural members for load-carrying capacity with less cost. The following cold-formed built columns shall be used in construction applications with providing appearance as well as load-carrying properties at less cost.

When designing a building or structure, the focus is on achieving strength at a lower cost, durability and a good return on investment. In such cases, steel is often the material of choice. Cold-formed steel, in particular, offers several advantages over hot-rolled steel. It can be easily bent and structured at room temperature [5], resulting in significant time and cost savings. In many developed countries, cold-formed steel is used even for constructing buildings with more than four stories, and some structures can go up to 10 stories. Further research on these materials reveals that they are widely used in other countries, and we are only beginning to adopt them as a developing technology.

The novelty of the research paper is using a compound form of cold-formed steel as columns with different shapes infused inside the outer layer of CFS.

V. Hari Krishnan (✉) · C. Manoj Kumar
Department of Civil Engineering, Sathyabama Institute of Science and Technology,
Chennai 600119, India
e-mail: Haricivilion@gmail.com

C. Manoj Kumar
e-mail: cmanoj1@gmail.com

2 Experimental and Numerical Results

The following 4 compound columns models were selected based on easy application in real-time projects. Based on the numerical results obtained from Abaqus, model CTTZ showed elevated load-carrying capacity when compared with models DCTT, CTTCA, and CTCB. Model CTTZ with a lesser area of cross-section performed well when compared to the higher cross-sectional area specimens, and this shows the cross-sectional area is not the key factor to achieve the strength. The Zed section used in model B with 5 screws on either side performed well as shown in Fig. 1b, where model CTCB performed poorly with a “C” channel and 2 “L” angles connected as a compound section inside the shell (2 face-to-face welded channels) of the model considered in our experiment [6].

2.1 Section Properties

The properties of the section chosen are based on the slenderness ratio value for intermediate column values ranging between 32 and 120. All four models created for testing are kept at a constant height of 1200 mm with the outer shell layer as 100 mm × 100 mm as shown in Figs. 1a, b, 2 and 3 respectively. The inner compound model alone changed in each sample studying the strength behavior when the same sheets are compounded into different shapes [6].

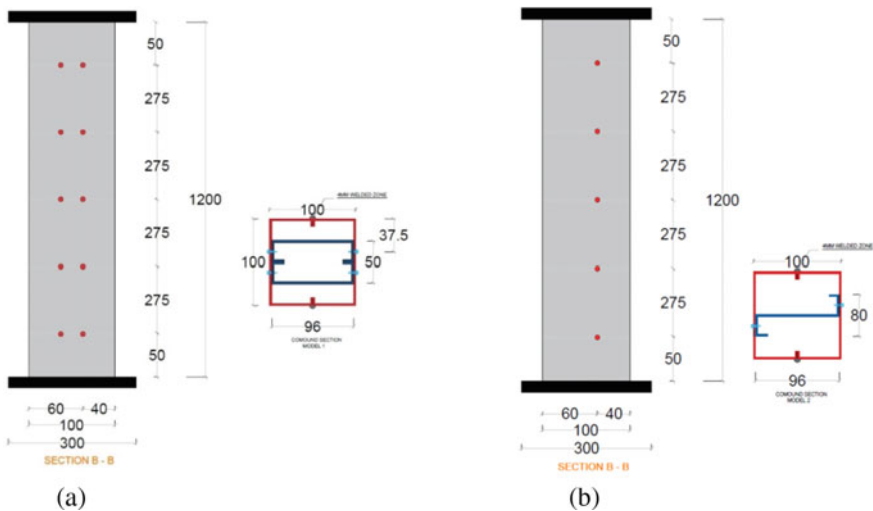


Fig. 1 a Model DCTT; b Model CTTZ

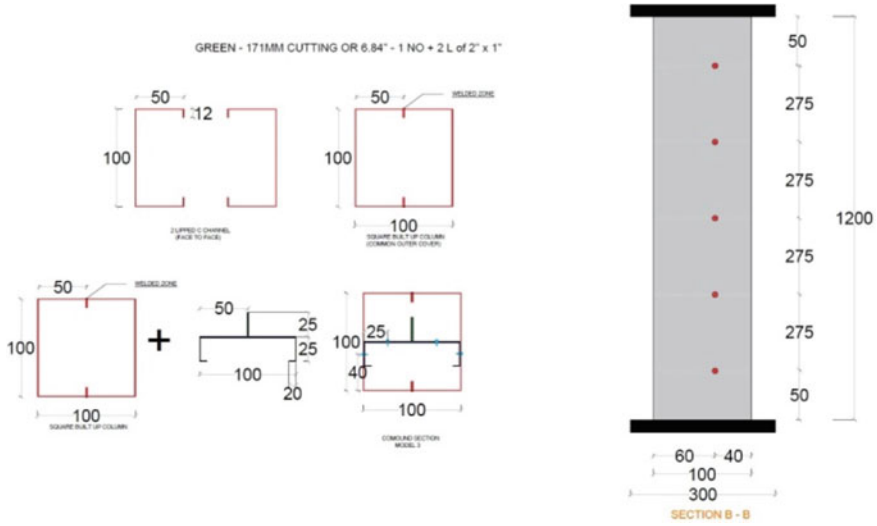


Fig. 2 Model CTTCA

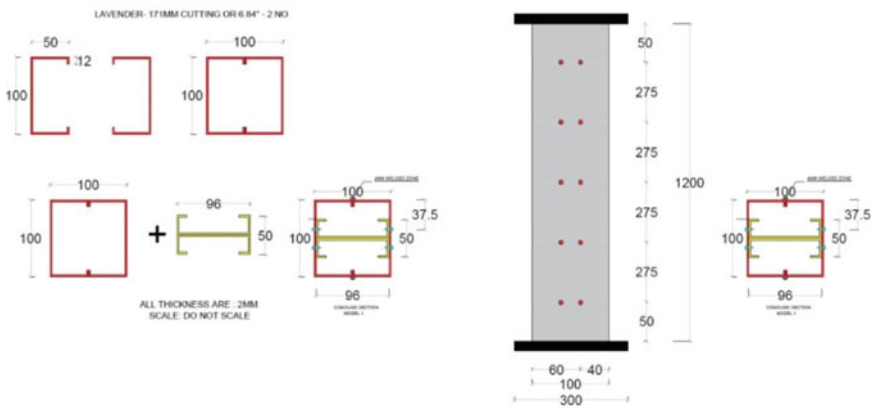


Fig. 3 Model CTCB

2.2 Coupon Test

A coupon test [7] was conducted as per American standard ASTM, on the sheet used for the fabrication of the built-up column as shown in Fig. 3a–d. The coupon test was conducted to understand the properties of the material such as Young’s modulus, yield stress, and breaking stress which can be used as input for an analytical procedure using Abaqus software. The coupon test cutting sample is shown in Fig. 4b and testing is conducted using the coupon testing machine [8] as shown in Fig. 4a.

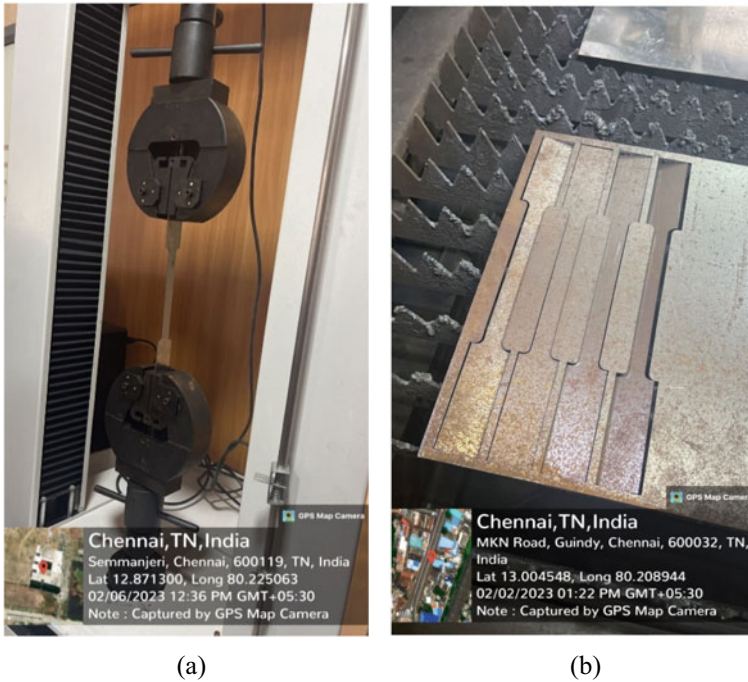


Fig. 4 a Coupon CNC cutting, b Coupon testing machine

2.3 *Abaqus Results*

The following 4 models show the buckling behavior as per the load-carrying capacity. Model DCTT and Model CTTZ have almost more load-carrying capacity compared to Model CTTCA and CTCB as shown in Fig. 3. The red zone indicates the maximum stress distribution area during the load application and also the deformed shapes show the buckling area similar to the experimental results [9]. The mesh size of 10 mm is used for detailed study on the stress distribution (Fig. 5).

2.4 *Fabricated Models*

The following 4 models are fabricated with the outer section welded using TIG inner sandwich layer which is screwed using a self-tapping screw as per the dimensions shown in Figs. 1a, b, 2a, 3a. The model is also coated with yellow primer and gray enamel paint to stop corrosion before testing it. The top and bottom of the column are TIG welded with a base plate for uniform load distribution to both the outer and inner section as shown in Fig. 6 [10, 11].

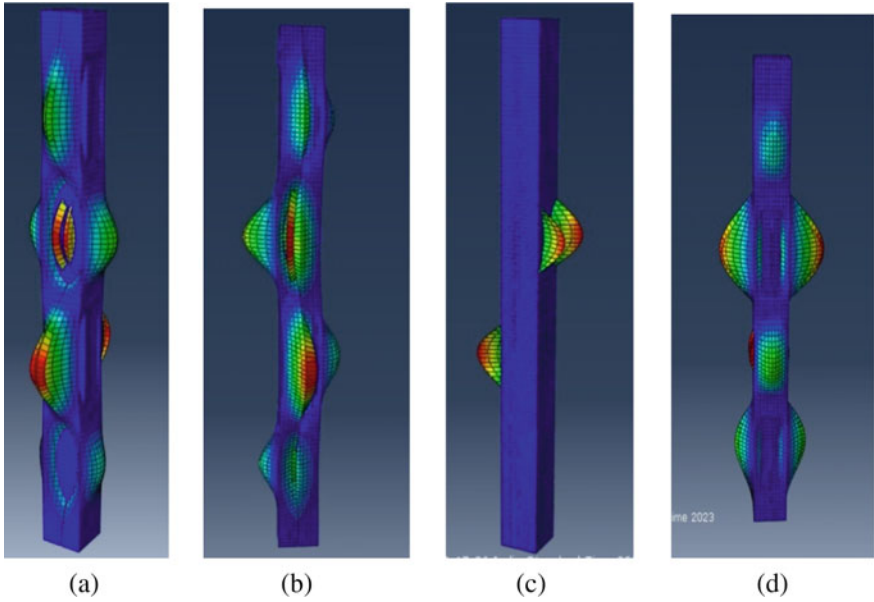


Fig. 5 Buckling behaviour from analytical study **a** Model DCTT; **b** Model CTTZ; **c** Model CTCA; **d** Model CTCB



Fig. 6 Fabrication process of columns **a** Bending; **b** fabrication; **c** fabricated models; **d** protective coating to models



Fig. 7 Buckling behaviour from experimental study **a** Model DCTT; **b** Model CTTZ; **c** Model CTTCA; **d** Model CTCB

2.5 Experimental Results

The 4 samples are tested using a loading frame by gradually applying load at Y -axis; at each increment, the values are noted down to formulate the load versus deflection graph to compare it with the analytical results. The buckling of the columns is visually noted down to compare it with the analytical buckling location and also the LVDT is attached over the suspected buckling zone to measure the deformation of the shape when the buckling is very minimal as shown in Fig. 7.

3 Results and Discussion

The load versus deflection graph shows the experimental deflection is higher when compared to the analytical results as in Fig. 8. The axial load-carrying capacity of the 4 models is 70–80% similar to the results obtained from the Abaqus software, hence the software can be used to determine the real-time load-carrying application of the models to be used in construction application. According to the slenderness ratio of an intermediate column which we used in the above experiment which showed

good performance in experimental and analytical can be used where the intermediate column is required in real-time application. Buckling in model CTTCA was at the center zone of the column exactly opposite to each other. Buckling in model CTTZ occurred on all 4 sides which shows the model has withstood heavier load [12]. Out of all the four specimen, the model-CTTZ outperformed with highest load carrying capacity from both analytical and experimental studies as mentioned in Fig. 9, with lesser area of section and unit weight. It is also the most economic section compared to other models. The curves in Fig. 9 shows the analytical value of the 4 different model performance in which green line that is model CTTZ with lesser cross-sectional area and weight it performed drastically which indicates the model with perfect balance in the inner layer of section will result in higher strength with reduction in cost. When compared with the experimental graph as shown in Fig. 10, similar results are seen with respect to Fig. 9 values with reduction in strength of 20–30% which may be due to man made errors and due to stitch welding and no of bolt holes and quality of the material.

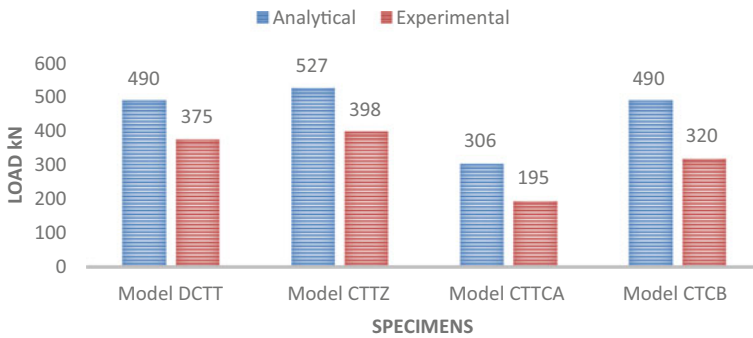


Fig. 8 Axial load-carrying capacity of experimental and analytical results

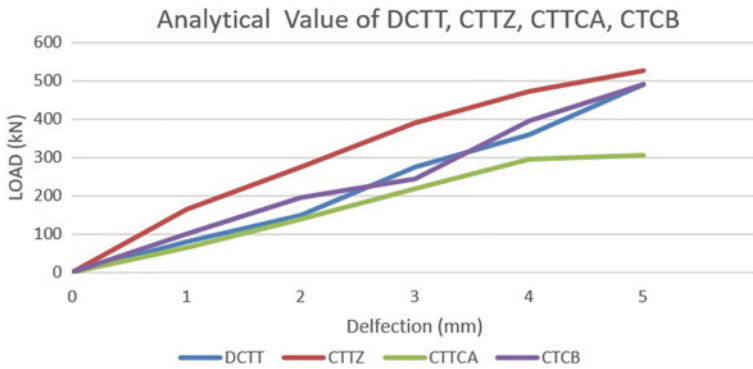


Fig. 9 Load versus deflection curve for Model DCTT, CTTZ, CTTCA, and CTCB-analytical values

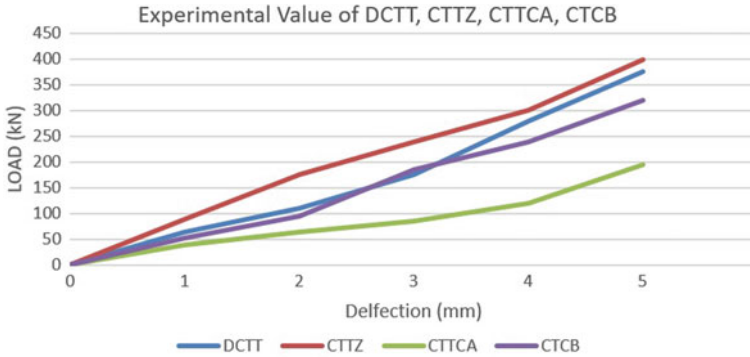


Fig. 10 Load versus deflection curve for Model DCTT, CTZ, CTCA, and CTCB—experimental values

4 Conclusion

Through an extensive review of the literature, the load-carrying capacity and buckling behavior of steel built-up columns were studied, leading to the following observations. Analysis of literature helped in defining the project objective and formulating a methodology flowchart. Selection of the column shape was based on its ease of folding and use in the field, beside its maximum load-carrying capacity.

The literature also provided insights into the behavior of cold-formed steel built-up columns under buckling and compression. The different shapes of built-up columns were studied through literature to understand their buckling behavior. The importance of incorporating lips in steel shapes was also realized through the literature review.

5 Limitation of Work

If this research is to be studied in detail, the following recommendations can be adopted. Increase the thickness of the sheet to enable a more detailed analysis of its performance in relation to varying thicknesses like 1, 2 and 3 mm. Increase the specimen size H of a well-performing specimen to study its performance when the same shape is required but at different heights as stub column, short column, and long column. To improve the reliability and durability of the samples, it is suggested to reduce the number of screw or bolt holes and fabricate the model with continuous or stitch welding. Furthermore, testing the performance with a continuous welding method without bolts may yield valuable insights.

Acknowledgements The authors would like to express appreciation to the Sathyabama Institute of Science and Technology and Hindustan Institute of Technology and Science, India, for the laboratory and equipment support.

References

1. Senthilkumar R, Divya M, Divya Roy S, Bahurudeen A, Avudaiappan S, Tsavdaridis KD (2022) Behaviour of cold-formed steel-concrete composite columns under axial compression: experimental and numerical study. *Structures* 44:487–502. <https://doi.org/10.1016/j.istruc.2022.07.086>
2. Babu SS, Selvan SS (2020) State of the art of cold formed steel members. *Mater Today: Proc*, pp 3069–3073
3. Kyprianou C, Kyvelou P, Gardner L, Nethercot DA (2020) Numerical study of sheathed cold-formed steel columns. In: *Proceedings of the 9th international conference on advances in steel structures, ICASS 2018*. Hong Kong Institution of Steel Construction
4. Liu J, Fang H, Chan TM (2022) Experimental investigation on material properties and residual stresses in cold-formed high strength steel irregular octagonal hollow sections. *J Constr Steel Res* 191. <https://doi.org/10.1016/j.jcsr.2022.107170>
5. Wu JR, Di Sarno L, Hesketh S, Phan N (2022) Buckling resistance of axially loaded cold-formed steel compound sections: numerical simulation and assessment of codified design approach. *Int J Steel Struct*. <https://doi.org/10.1007/s13296-022-00641-y>
6. Craveiro HD, Rahnavard R, Laím L, Simões RA, Santiago A (2022) Buckling behavior of closed built-up cold-formed steel columns under compression. *Thin-Walled Struct* 179. <https://doi.org/10.1016/j.tws.2022.109493>
7. Huang Y, Young B (2014) The art of coupon tests. *J Constr Steel Res* 96:159–175. <https://doi.org/10.1016/j.jcsr.2014.01.010>
8. Chen MT, Young B (2020) Tests of cold-formed normal and high strength steel tubes under tension. *Thin-Walled Struct* 153. <https://doi.org/10.1016/j.tws.2020.106844>
9. Evirgen B, Tuncan A, Taskin K (2014) Structural behavior of concrete filled steel tubular sections (CFT/CFSt) under axial compression. *Thin-Walled Struct* 80:46–56. <https://doi.org/10.1016/j.tws.2014.02.022>
10. Yan X, Gernay T (2022) Local buckling of cold-formed high-strength steel hollow section columns at elevated temperatures. *J Constr Steel Res* 196. <https://doi.org/10.1016/j.jcsr.2022.107403>
11. Singh TG, Singh KD (2021) Design of perforated cold-formed steel hollow stub columns using direct strength method. *Thin-Walled Struct* 168. <https://doi.org/10.1016/j.tws.2021.108265>
12. El Hady AM, El Aghoury MA, Ibrahim SM, Amoush EA (2022) Experimental investigation of steel built-up beam-columns composed of tracks and channels cold-formed sections. *J Build Eng* 51. <https://doi.org/10.1016/j.jobe.2022.104295>
13. IS 801-1975 (1975) Indian Standard code of practice for use of cold-formed light gauge steel structural members in general building construction

Flexural Behaviour of Cold-Formed Ferritic Stainless Steel Built-Up Joists



C. Manoj Kumar, Dinesh Kumar Marnadu, A. Harikaran,
M. Saran Kumar, and Venus David Rayan

1 Introduction

Cold-formed ferritic stainless steel (CFFSS) has gained recognition as a versatile structural material due to its high strength-to-weight ratio, elasticity, and long service life [1]. In a study on the flexural response of CFFSS closed-section built-up beams, mechanical properties were assessed through coupon tests, revealing a Young's modulus of 213 GPa and ultimate strength of 407.5 MPa [2]. These properties demonstrated good strength and ductility, meeting EN 1993-1-4 criteria for structural applications [2]. Another study using coupon tests confirmed CFFSS's Young's modulus and ultimate strength, suggesting its suitability for building structures [3]. Furthermore, a study evaluated the mechanical properties of CFFSS based on Australian and Indian standards, demonstrating its compliance with EN 1993-1-4 criteria for ductility and suitability for structural applications [4]. The flexural behaviour of CFFSS SHS/RHS beams, four-point bending tests, and parametric research was conducted, indicating that the bending and compression of these stainless steel elements adhered to design limitations [5]. In the pursuit of unified design equations for web crippling failure, a study focused on CFFSS unflipped channel sections with web holes [6]. By evaluating 18 sections per AISI S100 guidelines, the study provided insights into web crippling failure and the development of unified design equations [6]. Additionally, the design of CFFSS RHS perforated beams was explored, revealing that perforation had no significant effect on moment capacity

C. Manoj Kumar · M. Dinesh Kumar (✉) · A. Harikaran · M. Saran Kumar · V. D. Rayan
Department of Civil Engineering, Sathyabama Institute of Science and Technology (Deemed to be University), Chennai, Tamil Nadu 600119, India
e-mail: mrkcivil1923@gmail.com

C. Manoj Kumar
e-mail: cmanoj1@gmail.com

V. D. Rayan
e-mail: davidvenu06@gmail.com

and related curvature for hole diameters up to 20% of the web depth [7]. Composite shear transfer mechanisms between steel and concrete were proposed, enhancing the embedded flanges of C-sections and resulting in surface bonding [8]. The study verified the effectiveness of these enhancements highlighting the conservative nature of push-out test results compared to large-scale test results and their implications for steel–concrete structure design [8]. Nonlinear dynamic analysis using SAP2000 and ABAQUS software was conducted to evaluate the structural performance of buildings under dynamic loads [9]. The study focused on rotation moment capacity and provided insights into local buckling and the structural behaviour of buildings, aiding in the design of more resilient structures [9]. In a laboratory study, the flexural capacity of different floor joist layouts was investigated [10]. The study involved the construction of floor specimens using C-shaped joists with sheathing between two U-shaped spans. The findings indicated local buckling of the joist's flange and web after applying approximately 70% of the ultimate load, emphasizing the importance of careful experimentation and testing in structural engineering [10]. Through a comprehensive literature review, it was discovered that various forms of non-built-up sections made from ferritic stainless steel were examined. Limited investigations have been carried out specifically on joists fabricated with ferritic stainless steel.

2 Materials and Methods

2.1 Material Property

The nominal values for cold-rolled strip thickness less than 6 mm ferritic stainless steel grades have been given in EN 1993.1.4.2006. The yield and ultimate strength of the chosen steel grade are 260 N/mm² and 450 N/mm², respectively [11]. The mechanical properties of steel grade-EN-1.4016 were determined using tensile coupon test. The test involves tensioning four steel strips using a universal testing machine for determine the yield strength (F_y), ultimate tensile strength (F_u), elongation percentage, and breaking strength of the specimen. The dimensions provided according to ASTM E8/E8M-21a standards [12]. The steel coupon test was conducted to study the mechanical properties (see Fig. 1). Additionally, a stress–strain curve (see Fig. 2) has been generated based on the obtained data (see Table 1).

2.2 Section Property

Around four sections of joists are modelled. Among them, one is I-sectional profile, namely arrangement 1-I-sectional steel joist (A1-ISJ) and other three are trapezoidal sectional profile, namely arrangement 2-trapezoidal steel joist (A2-TSJ), arrangement 3-trapezoidal steel joist (A3-TSJ), and arrangement 4-trapezoidal steel joist

Fig. 1 Tensile coupon test set-up



Fig. 2 Four specimen tensile coupon test results

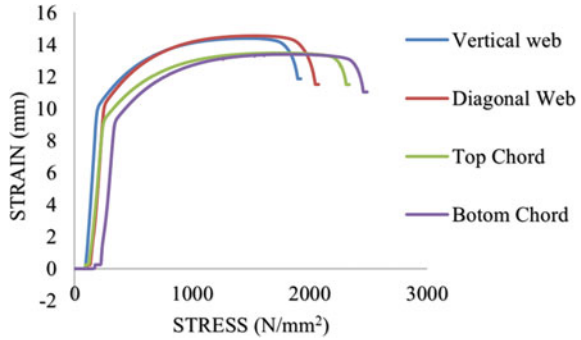


Table 1 Tensile coupon test results for steel grade-EN-1.4016

Specimen	Fy (N/mm ²)	Fu (N/mm ²)	Elongation %	Breaking strength (N/mm ²)
Top chord	332.333	480.017	23.73	383.38
Bottom chord	333.433	484.25	24.7	395.83
Vertical web member	310.933	448.95	28.57	367.6
Diagonal web member	302.05	445.85	28.8	383.3
Average	319.68	464.76	26.45	382.3

(A4-TSJ). The geometrical properties of all four sections are given in Table 2. The longitudinal and cross-sectional views of all four sections are shown in (Fig. 3).

2.3 Finite Element Model

A finite element analysis software ABAQUS is used to develop the numerical model based on static analysis [13]. There are two types of elemental bodies used—one is discrete rigid body, which has a 2D 4 node shell element, assigned for supports and loading points that shall not take any stress or strain, and the deformable body, which

Table 2 Section properties of joists used

Specimen	Top chord span (mm)	Bottom chord span (mm)	No. of struts	No. of diagonal member	Diagonal web length (mm)	Depth (mm)	Sectional profile	Mass (kg)
A1-ISJ	1300	960	10	12	220	180	I-Section	8.5
A2-TSJ	1300	960	0	12	240	180	Trapezoid	12.95
A3-TSJ	1300	960	6	12	230	180	Trapezoid	12.23
A4-TSJ	1300	960	10	12	220	180	Trapezoid	11.67

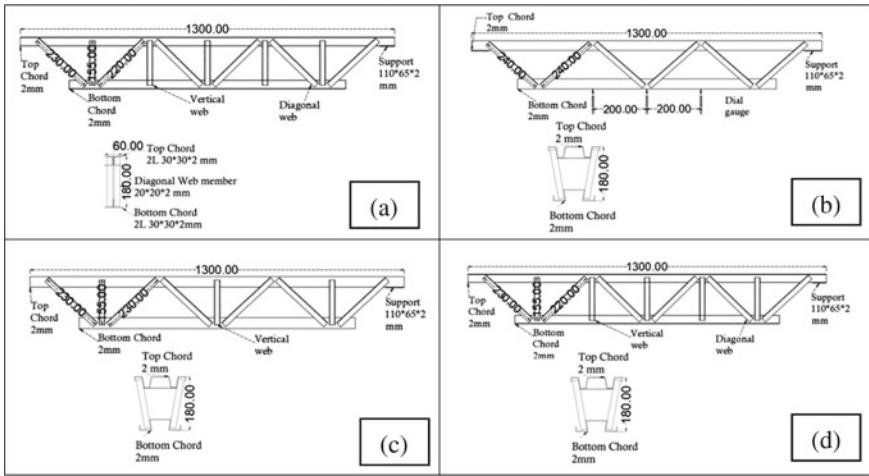


Fig. 3 Longitudinal and cross section views. **a** A1-ISJ, **b** A2-TSJ, **c** A3-TSJ, **d** A4-TSJ

has a 3D hexahedron 8 node element, assigned for joist members that shall take stress and strain.

2.4 Mechanical Property

The mass density of all the specimens is specified as 7800 kg/m^3 , which corresponds to the ferritic stainless steel EN-1.4016. The Young’s modulus is $200,000 \text{ N/mm}^2$ and the Poisson’s ratio is 0.28.

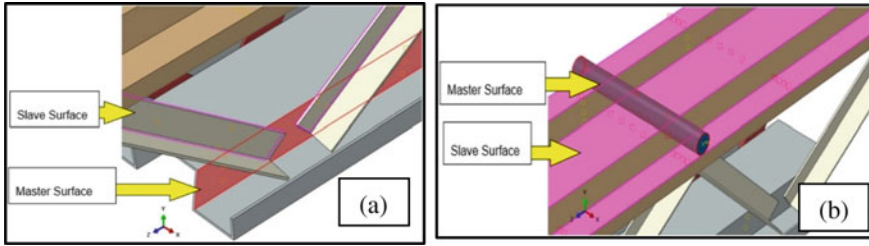


Fig. 4 Model interaction **a** Tie constrain, **b** surface-to-surface contact

2.5 Interaction

The tie constraint is assigned between two deformable bodies, such as chords and web connectors, to prevent the bodies from penetrating each other (see Fig. 4). Surface-to-surface contact is established between a discrete rigid body (acting as the master surface) and a deformable body (acting as the slave surface) with a friction coefficient of 0.1. This constraint models the contact properties, including normal behaviour and tangential behaviour [6].

2.6 Boundary Condition and Meshing Optimization

The boundary conditions in ABAQUS for all sections under static loading conditions are assigned with a roller support and a hinged support [14]. A prior study is carried out to select a suitable mesh size for the stainless steel joist based on computational efficiency, meshing accuracy to compare with the experimental study. The size is chosen between 5 and 20 mm according to the type of mesh and the different angles of the specimen. Structural mesh is used for right angle folding, and sweep mesh for less or greater than right angle is used (see Fig. 5).

3 Experimental Investigation

3.1 Fabrication

The sections are fabricated using 2 mm thick sheet metal of EN-1.4016 ferritic stainless steel using Tungsten Inert Gas (TIG) welding.

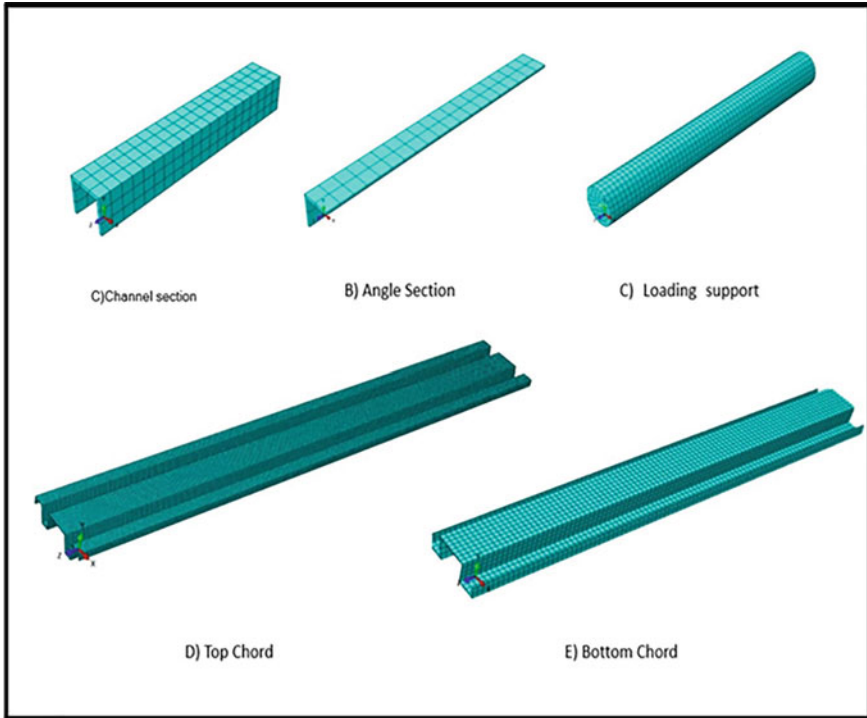
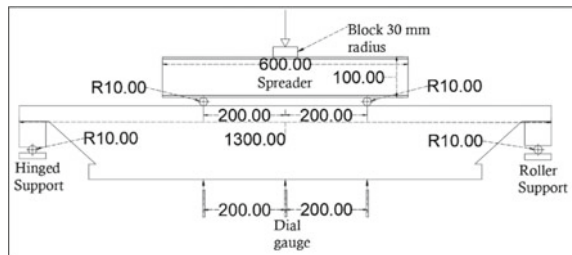


Fig. 5 Meshing of joist components in ABAQUS

3.2 Experimental Setup

All the joists are bent using two-point loads applied at 200 mm away from midspan on either side. Deflectometers are placed at midspan and load points. One end is provided with roller and other end is provided with pinned support (Fig. 6).

Fig. 6 Experimental set-up of joists (all dimensions are in mm)



4 Results and Discussion

4.1 Numerical and Experimental Results

This part presents the result obtained from the ABAQUS simulation software like the load Vs. deflection curve (see Fig. 7), and Deflection diagram in U2 (y axis) (see Fig. 8), for the Experimental setup made (see Fig. 9). The load carrying capacities of all specimens are being compared analytically and experimentally with respect to observed deflections in mm (Table 3).

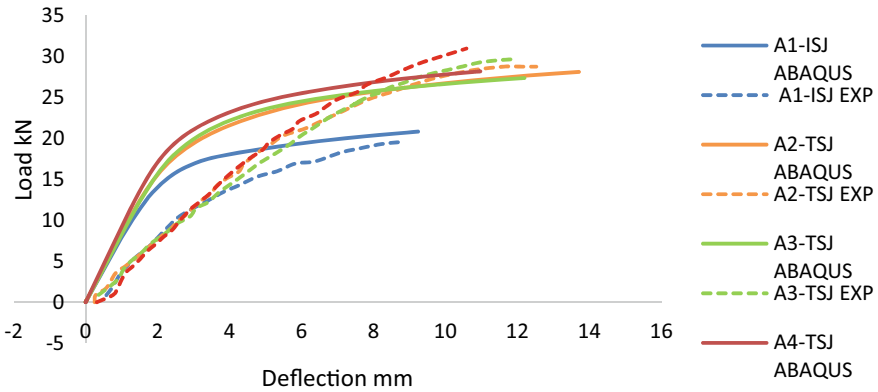


Fig. 7 Load vs. deflection curve for all the four finite element and experimental models

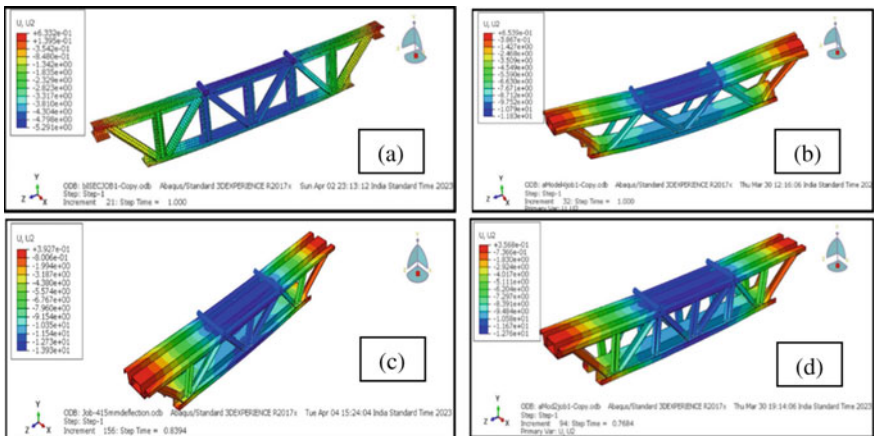


Fig. 8 Deflection diagram a A1-ISJ, b A2-TSJ, c A3-TSJ, and d A4-TSJ

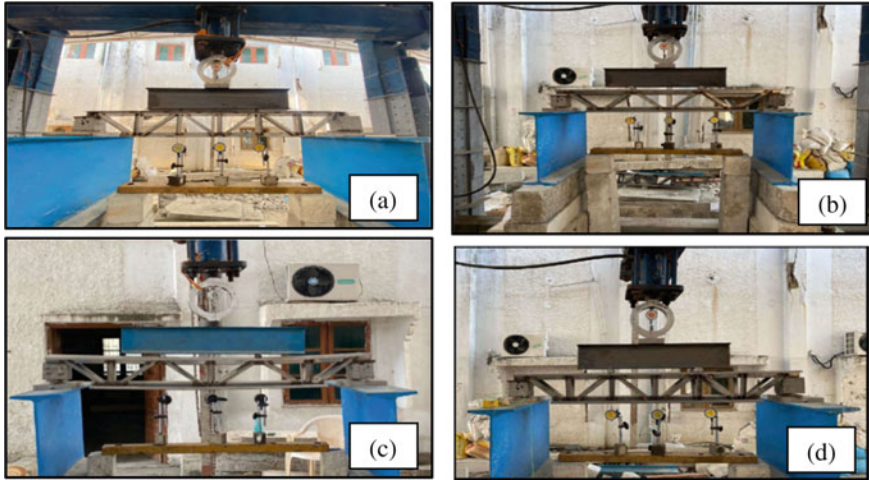


Fig. 9 Experimental test setup, (a A1-ISJ, b A2-TSJ, c A3-TSJ, and d A4-TSJ)

Table 3 Numerical and experimental results of load carrying capacity and deflection

Specimen	Numerical results		Experimental results	
	Load carrying capacity (kN)	Deflection (mm)	Load carrying capacity (kN)	Deflection (mm)
A1-ISJ	20.8	9.2	19.5	8.7
A2-TSJ	27.6	12.3	28.7	12.5
A3-TSJ	28.1	13.7	29.6	11.8
A4-TSJ	28.6	10.9	30.9	10.5

4.2 Failure Pattern

This analysis involved comparing the stress distribution diagram with the observed deformations from experiment. After carefully examining the non-slender section A2-TSJ diagram, (see Fig. 10b) it becomes apparent that the stress distribution along the entire span of the joist was not uniform. Notably, the stress experienced by the web connectors was significantly higher compared to the chords. This observation suggests that the web members must be designed stronger than the chords. In the experimental results, the brittle fracture was observed at the welding points of end web members as weld material is weaker than the member material.

In order to enhance the strength of the web member in sections A3-TSJ, additional vertical web members are provided. This modification resulted in increasing the ultimate load carrying capacity when compared to section A2-TSJ. During experimental testing, it was observed that a portion of the stress was transferred to the added vertical web member, which effectively prevented fractures in the diagonal end web member.

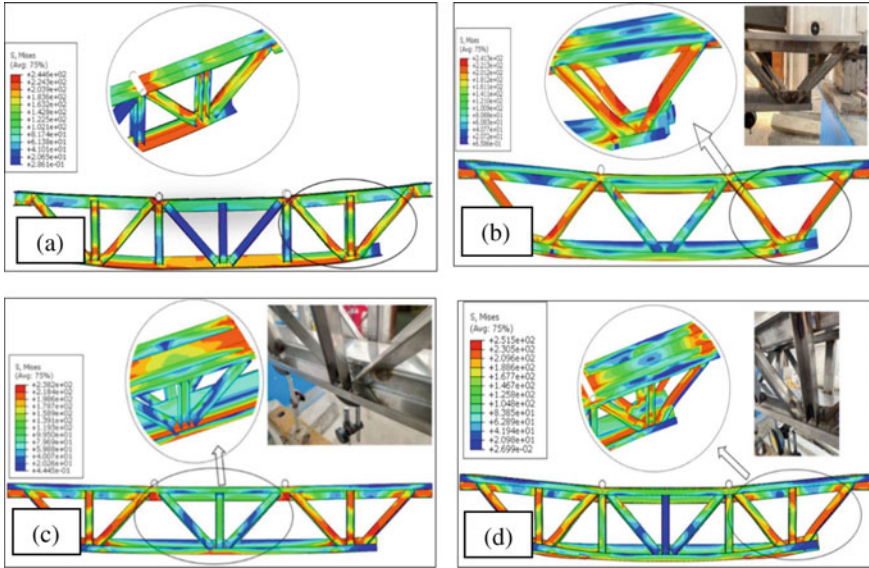


Fig. 10 Failure pattern comparison between numerical and experimental results using stress distribution diagram (Von Mises Stress N/mm^2) **a** A1-ISJ, **b** A2-TSJ, **c** A3-TSJ, and **d** A4-TSJ

However, it was also noted that the vertical web member became dislocated from the welded region (see Fig. 10c).

When a vertical web member is added between diagonal members in A4-TSJ, there is a slight increase in the load carrying capacity. However, in this model, there is no occurrence of brittle fracture or displacement of welded web member. The stress distribution diagram does not show any red spots, (see Fig. 10d) indicating that there is no concentration of stress in any part of the member.

In the comparative study, a typical I-joist A1-ISJ was utilized (see Fig. 10a). Due to the slender section design of the joist, it is susceptible to lateral torsional buckling, this failure pattern significantly reduces the ultimate load carrying capacity of the joist, when compared to other three non-slender trapezoidal joist sections. During the analytical testing of the specimen, buckling occurred in the lateral direction, approximately 6 mm outside the plane, further demonstrating the susceptibility of slender section designs to lateral torsional buckling failure.

4.3 Discussion

The detailed explanation of the results that are collected from the experimental and numerical key results was discussed by points below:

Trapezoidal joists typically outperform standard I-section floor joists. It is a result of the A1-ISJ I-section’s slenderness ratio, which caused it to buckle outside of the

neutral axis. Four different models' experimental findings were compared with one another. When compared to joist A1-ISJ, joist A4-TSJ's maximum load carrying capacity is 45.2% higher. Even though both have similar web arrangements and the mass difference is only 35.9% higher in A4-TSJ, with only an 18% difference in deflection. When compared to joist A1-ISJ, joist A3-TSJ's ultimate load carrying capacity is 41.1% higher, with 35.6% mass. Compared to joist A1-ISJ, joist A2-TSJ has a 38.1% higher ultimate load carrying capacity. Even though the mass difference is only 31% higher in A2-TSJ. By this comparison, it clearly shows that trapezoidal Joist are more economic than I-section steel joist. The next comparison is done using numerical model results. All three trapezoidal models were compared with I-section floor joists. Compared to joist A1-ISJ, joist A4-TSJ has a 31% higher ultimate load carrying capacity and 29.8% high when compared to joist A3-TSJ, and 28% high when compared to joist A2-TSJ (see Fig. 10). While the difference between the numerical and analytical results is more or less 10%, it is because of the type of connection used. It is clear from the graph that trapezoidal joists have performed well in experimental results. In contrast, I-section steel joist performed well in finite element model, which may be related to the fact that lateral torsional buckling occurred more quickly in experimental results, (see Fig. 11) when applying load to the joist. According to the graph (see Fig. 10), the relationship between A1-ISJ joist load and deflection is linear, and according to observations made throughout the experimental test processes, buckling only occurred on the top chord and no parts of the joist structure were fractured. There is lateral torsional buckling as the mode of failure. Models A2-TSJ and A3-TSJ were unsuccessful owing to brittle fracture, which is a failure mode where the welded region separates from the bottom chord and vertical web connector. Due to faulty welding technique, the material in the welded zone becomes harder as a result of a sudden shift in temperature during the welding process, which is common in welding ferritic stainless steel grades due to its chemical composition. On the other hand, in model A4-TSJ, brittle fracture didn't occur. Instead, the model experienced buckling at the diagonal web connectors that are provided on both ends. Based on observation, this is because the web connectors are inadequate to support the load that the top and bottom chords can support easily.

5 Conclusion

- Tensile coupon tests were carried out for accuracy purposes to define the material properties of cold-rolled ferritic stainless steel on ABAQUS for that a total of four specimens were cut down from each area of the specimen and the tensile test was carried out.
- The ASTM E8/E8M standard for cold-rolled stainless steel, which gives the dimensions for the tensile coupon test specimen.
- A loading frame with a 500 kN capacity was utilized to evaluate the flexural behaviour of the joists, and for the support condition, one end will have a roller support, while the other end will have a hinged support.

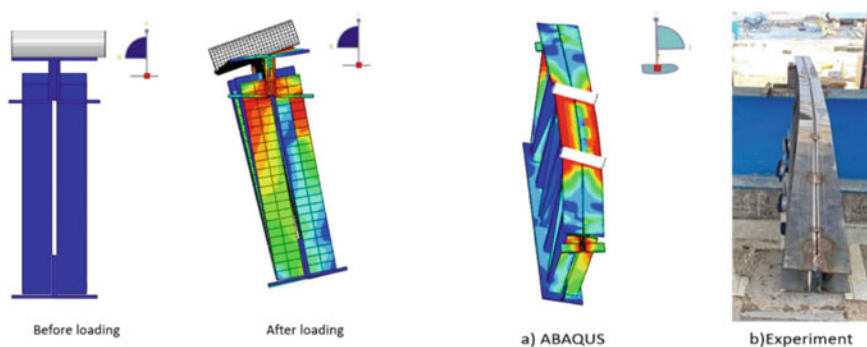


Fig. 11 Failure due to lateral torsional buckling of (AI-ISJ) Joist arrangement four I-section steel joist

- To investigate the flexural behaviour of joists during four-point static loading, a proving ring is used to gauge the load applied to the joists, and to calculate their values obtained simultaneously, the deflection values were collected from the bottom of the joist, and there were three deflectometer: one at the middle of the span, and other two were placed 200 mm away from the midspan on either side.
- The floor joist finite element model was accurately created, and all other modelling procedures were carried out as described in numerical investigation part after the model was assigned with the material properties obtained from the tensile coupon test.
- To conclude, the ferritic stainless steel grade that is used can be used for structural applications, but it is not recommended to go with the welding process; instead, bolted connections or Revit connections are recommended.
- To conclude the flexural behaviour of trapezoidal floor joists, their load carrying capacity is relatively high, and their strength by weight ratio is also 30% higher than that of the standard joist section. So, this type of joist section will have considerable cost effectiveness and completely restricted the lateral torsional buckling.
- To decrease the fracture in the web member, the steel strut thickness should be greater than the chord.

References

1. Bock M, Arrayago I, Real E (2015) Experiments on cold-formed ferritic stainless steel slender sections. *J Constr Steel Res* 109:13–23. <https://doi.org/10.1016/j.jcsr.2015.02.005>
2. Karthik C, Anbarasu M, Dar MA (2022) Cold-formed ferritic stainless steel closed-section built-up beams: tests and flexural response. *Thin-Walled Struct* 180. <https://doi.org/10.1016/j.tws.2022.109820>

3. Hou Z, Wan M, Wu X, Xu X (2018) Roll forming of aluminum alloy profile with hat-shaped section. *Procedia Manuf*, pp 759–766. <https://doi.org/10.1016/j.promfg.2018.07.315>
4. Karthik C, Anbarasu M (2021) Cold-formed ferritic stainless steel closed built-up beams: flexural behaviour and numerical parametric study. *Thin-Walled Struct* 164. <https://doi.org/10.1016/j.tws.2021.107816>
5. Li L, Li HT, Young B (2022) Cold-formed ferritic stainless steel SHS and RHS beams: testing, modeling and design. *J Constr Steel Res* 197. <https://doi.org/10.1016/j.jcsr.2022.107429>
6. Yousefi AM, Samali B, Hajirasouliha I, Yu Y, Clifton GC (2022) Unified design equations for web crippling failure of cold-formed ferritic stainless steel unlipped channel-sections with web holes. *J Build Eng* 45. <https://doi.org/10.1016/j.jobe.2021.103685>
7. Chen Z, Huang Y, Young B (2022) Design of cold-formed ferritic stainless steel RHS perforated beams. *Eng Struct* 250. <https://doi.org/10.1016/j.engstruct.2021.113372>
8. Lakkavalli BS, Liu Y (2006) Experimental study of composite cold-formed steel C-section floor joists. *J Constr Steel Res* 62(10):995–1006. <https://doi.org/10.1016/j.jcsr.2006.02.003>
9. Kim U, Leon RT, Galambos TV (2009) 3-D nonlinear dynamic behavior of steel joist girder structures. *Eng Struct* 31(1):268–274. <https://doi.org/10.1016/j.engstruct.2008.08.018>
10. Zhou X, Shi Y, Xu L, Yao X, Wang W (2019) A simplified method to evaluate the flexural capacity of lightweight cold-formed steel floor system with oriented strand board subfloor. *Thin-Walled Struct* 134:40–51. <https://doi.org/10.1016/j.tws.2018.09.006>
11. EN 1993-1-4: Eurocode 3: design of steel structures—part 1–4: general rules—supplementary rules for stainless steels (2006)
12. ASTM E8/E8M-13a Standard Test methods for tension testing of metallic materials 1. https://doi.org/10.1520/E0008_E0008M-13A
13. Pelletier B, Doudak G (2019) Investigation of the lateral-torsional buckling behaviour of engineered wood I-joists with varying end conditions. *Eng Struct* 187:329–340. <https://doi.org/10.1016/j.engstruct.2019.03.003>
14. Borkowski Ł, Grudziecki J, Kotełko M, Ungureanu V, Dubina D (2022) Ultimate and post-ultimate behaviour of thin-walled cold-formed steel open-section members under eccentric compression. Part II: experimental study. *Thin-Walled Struct* 171. <https://doi.org/10.1016/j.tws.2021.108802>

Flexural Behaviour of Corrugated Web Beams Using Cold-Formed Steel Sections



C. Manoj Kumar, S. T. Dhaarini, S. Rithish, and A. Thirunavukarasu

1 Introduction

Currently, the structural elements of light weight buildings such as columns, beams, joists, purlins, and built-up sections are being designed with cold-formed steel sections holding lots of advantages [1, 3, 4, 12, 19]. The type of cold-formed steel used in the study is stainless steel due to its good formability, ductility, corrosion resistance and has a high thermal conductivity [1, 2, 7, 8]. Nowadays, researchers are working on failure modes in beams, where failure occurs more in webs than in flanges hence to strengthen the web corrugated beams is an innovative design [5, 6, 11, 14]. Corrugated web beams support heavy loads over long spans. Corrugated beams are like lattice girders, in which the bending moment and normal force are transferred to the flanges and the transverse load is transferred to the vertical or diagonals of the lattice girder [9, 10]. To prevent the failures of steel beams like lateral torsional buckling, yielding, shear failure, local buckling, and vibration, the corrugated web beams are found to be helpful when reviewed from past literatures. The beams are designed with a unique web profile that resembles a series of corrugations or ridges, which helps to increase the beam's strength and stiffness [5, 10, 12, 13]. This design allows for a reduction in the amount of steel required, which makes corrugated web beams a more economical option than traditional solid web beams [2, 15, 16]. The corrugated web profile also provides better resistance to buckling and twisting, making these beams ideal for use in large-scale buildings such as warehouses, factories, and sports areas [8, 17, 18, 20]. This work is to study the span of the specimens of 1200 mm with webs corrugated. The failure mode, load–deflection curves, bending strength capacity, and shear capacity are compared with each specimen both experimentally and analytically.

C. Manoj Kumar (✉) · S. T. Dhaarini · S. Rithish · A. Thirunavukarasu
Department of Civil Engineering, Sathyabama Institute of Science and Technology,
Chennai 600 119, India
e-mail: cmanoj1@gmail.com

2 Material Property

2.1 Material

Cold-rolled steel sheet of Grade IS 513CR2 of 2 mm thickness is used to fabricate a built-up beam with desired conditions. The chemical composition of CR2 is given in Table 1, and the mechanical characteristics of cold-rolled sheet according to code IS 513:2008 are given in Table 2.

2.2 Coupon Test

A coupon test for CR2 steel sheet of 2 mm thickness involves taking a small sample or coupon of the steel sheet and subjecting it to various mechanical and chemical tests to evaluate its properties and performance. The tests typically include tensile testing to measure the steel’s strength and elongation, as well as hardness testing to assess its resistance to indentation and wear. Figure 1 is the samples of couple test and Figs. 2 and 3 are the stress strain curve of samples A and B, respectively.

Table 1 Chemical composition of CR2

Chemical constituents	%
Sulphur	0.035
Phosphorous	0.04
Carbon	0.7
Manganese	0.4
Silicon	0.05

Table 2 Mechanical properties of CR2

Properties	Max values	Units
Elongation %	38	%
Ultimate Stress	350	MPa
Yield stress	240	MPa

Fig. 1 Samples of coupon test



Fig. 2 Stress strain curve of Sample A

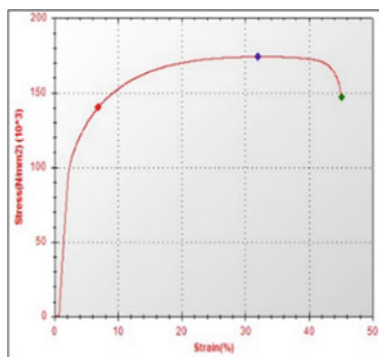
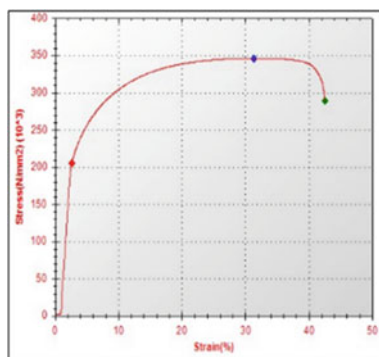


Fig. 3 Stress strain curve of Sample B



3 Test Specimen

3.1 Details of Specimen

A total of 3 I-section beams was fabricated using cold-formed steel sheet of 2 mm thickness with a span of 1200 mm, height of web 200 mm, and width of flange 160 mm lipped by 50 mm as shown in Fig. 4. As the study is based on corrugated web, three different web patterns are designed and studied. A beam consisting of flat web with stiffener size 50 mm width and 200 mm height is placed on both sides with a spacing of 170 mm as shown in Fig. 5, a beam with trapezoidal corrugated web of each corrugation of 300 mm as shown in Fig. 6, and a beam with rectangular corrugated web of each corrugation of 300 mm as shown in Fig. 7.

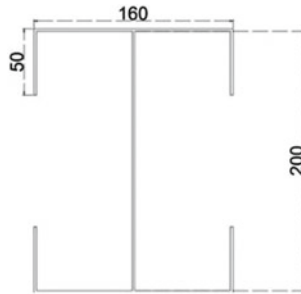


Fig. 4 Dimensions of I-Sections

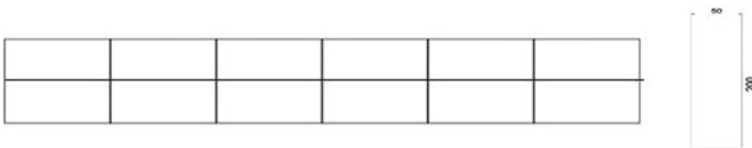


Fig. 5 Cross section of beam with flat web and stiffener and dimensions of stiffener

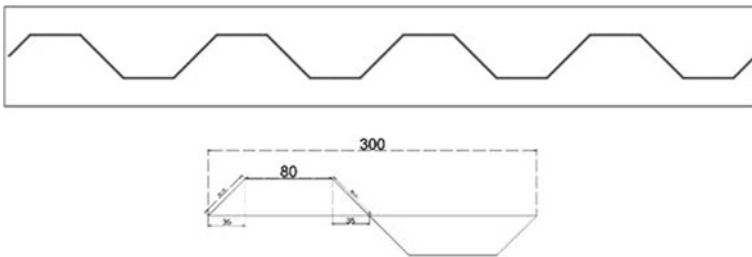


Fig. 6 Cross section of beam with trapezoidal corrugated web and dimensions of each corrugation

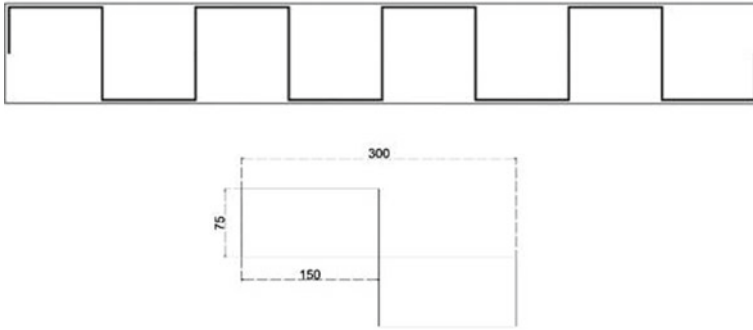


Fig. 7 Cross section of beam with rectangular corrugated web and dimensions of each corrugation

4 Analytical Investigation

The analytical investigation was carried out by finite element method using ABAQUS. All the three specimens were captured by a 3D scanner to ensure accurate dimensions and geometry was modelled in ABAQUS. Fine meshing was done to obtain an accurate result and a four-point loading condition was assigned. One end of the beam is provided with pinned support and other end is provided with roller support. The two point loads are passed through the rods of 50 mm diameter, placed at required loading points. The deflection and stress distribution of beam with flat web and stiffener is shown in Figs. 8 and 9, respectively. The deflection and stress distribution of beam with trapezoidal corrugated web is shown in Figs. 10 and 11, respectively. The deflection and stress distribution of beam with rectangular corrugated web is shown in Figs. 12 and 13, respectively.

Fig. 8 Deflection of beam with flat web with stiffener

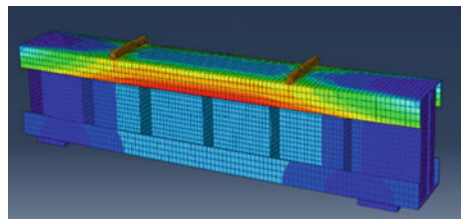


Fig. 9 Stress concentration of beam with flat web with stiffener

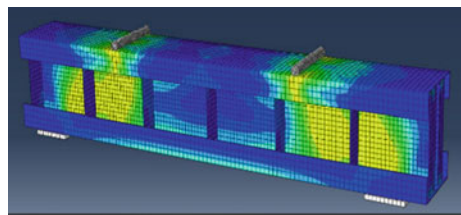


Fig. 10 Deflection of beam with trapezoidal corrugated web

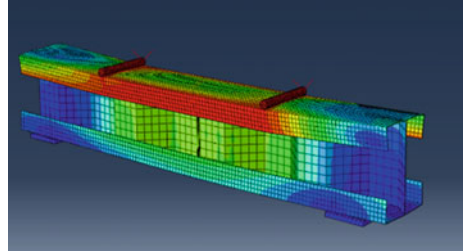


Fig. 11 Stress concentration of beam with trapezoidal corrugated web

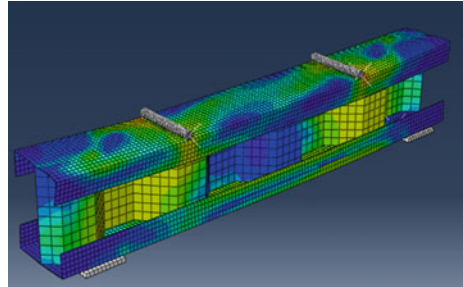


Fig. 12 Deflection of beam with rectangular corrugated web

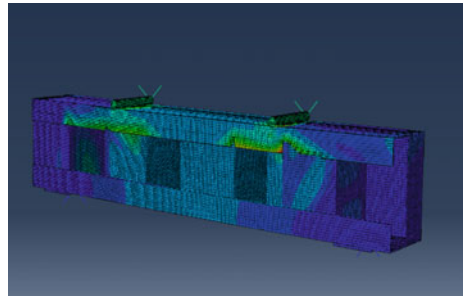
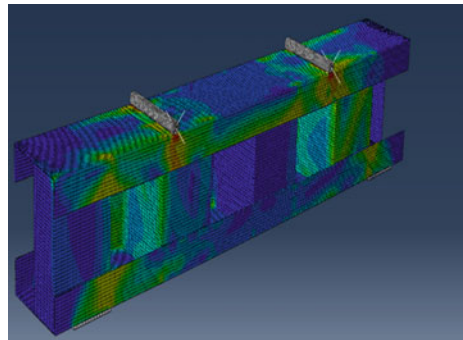


Fig. 13 Stress concentration of beam with rectangular corrugated web



5 Experimental Investigation

5.1 Fabrication

The CR steel sheet of 2 mm thickness is brought and for desired dimensions the sheet was cut into pieces and folded. According to the requirement, all the three specimens were welded using TIF welding. Figure 14 shows the fabricated beams.

5.2 Test Set-Up

To evaluate the bending strength and stiffness of beam, four-point loading test method is followed.

Each specimen is set up on the loading frame with 3 dial gauges to measure the deflection, hydraulic jack, and pivot ring. Figure 15 shows the experimental set up of specimen. The deflection of the beam is noted on gradual application of load till the yield point is reached. Figures 16, 17 and 18 show the beams with flat web and stiffeners, trapezoidal corrugated beams, and rectangular corrugated beams, respectively, at its yield point.

Fig. 14 Fabricated beams



Fig. 15 Experimental set up of fabrication beam



Fig. 16 Beam with flat web and stiffener at its yield point



Fig. 17 Beam with trapezoidal corrugated web at its yield point



Fig. 18 Beam with rectangular corrugated web at its yield point



6 Results and Discussion

6.1 Results

Analytical Investigation. The yield point is obtained at 23 kN, 29 kN, 8.5 kN for beams having flat web and stiffeners, trapezoidal corrugated beams, and rectangular corrugated beams respectively. The load–deflection graph for all three specimens is obtained from ABAQUS software. Trapezoidal corrugated beam carries the highest load. Figure 19 shows the load–deflection graph for all three specimens.

Experimental Investigation. The yield point is obtained at 25 kN, 30.4 kN, 12.5 kN for beams having flat web and stiffeners, trapezoidal corrugated beams, and rectangular corrugated beams, respectively. The load–deflection graph for all three specimens is obtained from a four-point loading method. Trapezoidal corrugated beam carries the highest load. Figure 20 shows the load–deflection graph for all three specimens.

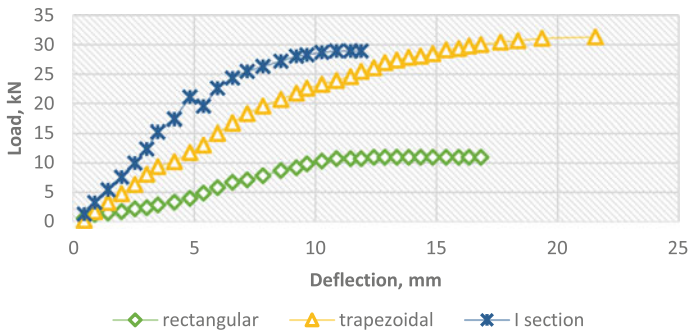


Fig. 19 Analytical results of load and deflection of all 3 beams

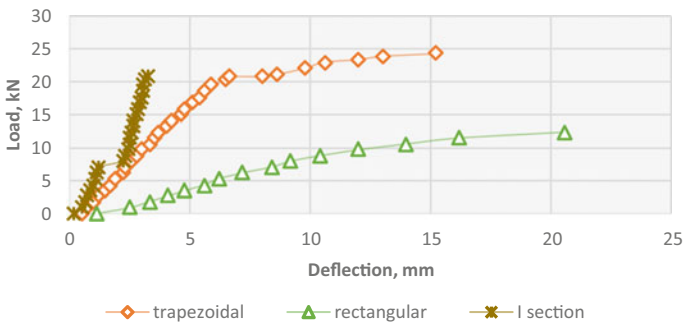


Fig. 20 Experimental results of load and deflection of all 3 beams

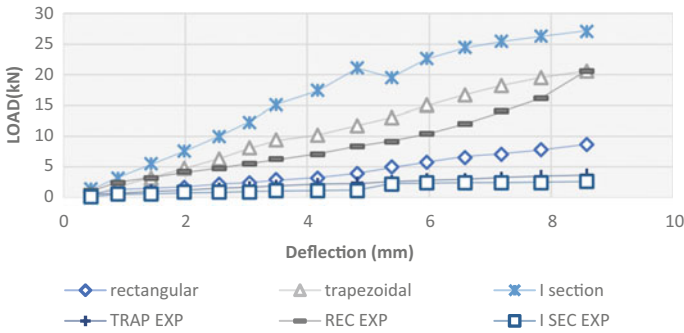


Fig. 21 Comparison of numerical and experimental results of load and deflection of all 3 beams

Comparison of Investigation. The yield point is obtained from analytical and experimental investigations for beams with flat web and stiffeners, trapezoidal corrugated beams, and rectangular corrugated beams which are plotted and shown in Fig. 21. The failure of beam was first noticed in analytical investigation than experimental in difference of 5%.

6.2 Discussions

The failure modes and properties of different types of beams under varying loading conditions were obtained and local buckling was noticed. The weight of the trapezoidal corrugated web beam was 13.84 kg, and it failed under a load of 30.4 kN, with a deflection of 5 mm. The local buckling took place at the web and at top flange at mid span for trapezoidal beam. The rectangular beam weighed 16.69 kg, and it failed under a load of 12.38 kN, with a deflection of 12 mm. The web of the rectangular beam was strong enough and did not buckle under the applied load. The local buckling took place in flange. The flat beam weighed 15.47 kg and failed under a load of 25 kN, with a deflection of 8 mm. The local buckling took place at the flange and did not shear for beam with flat web and stiffeners. The web of the rectangular beam was strong enough and did not buckle under the applied load. Understanding the failure behaviour of beams is essential for designing structures that can withstand the expected loads and prevent catastrophic failures, highlighting the importance of considering the beam’s properties and loading conditions. The total deflection of beam is higher in the middle of the beam for all specimens. Overall, trapezoidal corrugated beam has highest load of 30.4 kN, and rectangular corrugated beam carries the least load of 12.38 kN.

7 Conclusion

The performance of the corrugated web beams is studied, and it shows that exhaustion of the load capacity of corrugated beams occurs due to action of concentrated forces. This may be due to exceeding metal yield limit in the flanges or due to decrease in stability of corrugation. The load bearing capacity of corrugated beams is significantly influenced by eccentricity between the axes of flanges and webs. Addition to their superior strength and efficiency, corrugated web beams are also cost-effective and sustainable, as their unique shape allows them to be produced with less material than traditional beams. This can result in lower costs and reduced environmental impact compared to other structural solutions. Future works can be done with different distance of corrugation and design column with corrugated web and study their effectiveness. They can also be studied for composite construction with concrete slabs to create more efficient and sustainable structures.

References

1. Al-Kanon A-A, Suhail IA (2019) Flexural behavior of steel beam with corrugated web. *Int J Scient Technol Res* 8(10)
2. Elamary AS, Saddek AB, Alwetaishi M (2017) Effect of corrugated web on flexural capacity of steel beams. *Int J Appl Eng Res* 12(4) ISSN 0973-4562
3. Krishnan AB, Das S (2019) Finite element investigation on buckling behaviour of corrugated web beams. *Int Res J Eng Technol (IRJET)* 06(05)
4. Dubina D, Gilia L (2015) Experimental investigations of cold-formed steel beams of corrugated web and built-up section for flanges. *Thin-Walled Struct* 90
5. Fernandez-Lacabe I D, Lopez C, Serna MA (2022) Elastic lateral-torsional buckling of girders with corrugated web: equivalent section properties approach. 5(4)
6. Tahiliani D, Meena A, Narola D, Dave A (2019) Research on a steel built-up beam with varying corrugated webs. 148 Paper ICSECT 148 Rome, Italy, April 2019
7. Divahar R, Joanna P (2014) The effect of web corrugation in cold-formed steel beam with trapezoidally corrugated web. *Amer J Eng* 03(06):137-142
8. Sayed-Ahmed EY (2015) Behavior of steel and (or) composite girders with corrugated steel webs. In: Conference: international conference on advances in structural and geotechnical engineering (ICASGE'15), 6-9 April 2015, Hurgada, Egypt
9. Shu G, Zheng B, Shen X (2013) Experimental and theoretical study on the behavior of cold-formed stainless steel stub columns. *Int J Steel Struct* 13(1)
10. Ammash H, Albader M (2021) Shear behaviour of steel girder with web-corrugated core sandwich panels. *Thin Wall Struct* 45-32
11. Abbas HH, Sause R, Driver RG (2006) Behavior of corrugated web I-Girders under in-plane loads. *J Eng Mech* 132(8)
12. Huang ZY, Liew J (2016) Interactive shear buckling of plate girder with corrugated web design aspects of steel I-girders with corrugated steel web. *Thin-Walled Struct* 98:592-606
13. Iyappan G (2016) Experimental study on flexural behaviour of cold formed steel section. *IJSTE-Int J Sci Technol Eng* 2(10)
14. Khalid YA, Chan CL, Sahari BB, Hamouda AMS (2004) Bending behaviour of corrugated web beams. *J Mater Process Technol* 234-89
15. Krishnan L, Dineshraj CS, Prema S (2020) Experimental investigation of cold-formed steel section flexural member with triangular web. *IOSR J Mech Civil Eng (IOSR-JMCE)* 17:36-66

16. Limaye AA, Alandkar PM (2013) Strength of welded plate girder with corrugated web plate. *J Eng Res Appl* 3(5):1925–1930 ISSN: 2248–9622
17. Kumar M, Pradeep Reddy D, Senthil Pandia M (2018) A study on flexural capacity of steel beams with corrugated web. *Int J Civil Eng Technol (IJCIET)* 9:679–689
18. Nikoomanesh MR, Goudarzi MA (2020) Experimental and numerical evaluation of shear load capacity for sinusoidal corrugated web girders. *Thin-Walled Struct* 153
19. Leblouba M*, Karzad AS, Tabsh SW, Barakat S (2015) Plated versus corrugated web steel girders in shear: behavior, parametric analysis, and reliability-based design optimization. 12:987–453
20. Al-Kanon MA-A, Suhel IA (2019) Flexural behavior of steel beam with corrugated web. *Int J Scient Technol Res* 8:765–498

Analytical Behavior of Optimum Position of Multi-level Outriggers in RCC Frames



S. Naveen Kumar and K. S. Satyanarayanan

1 Introduction

To prevent a building from toppling over, engineers often install outriggers, which are horizontal support structures that connect the building's central core to additional columns at a considerable distance. The usage of outriggers in tall, narrow buildings extends back nearly half a century, though the design principle itself goes back millennia. The earliest known examples of “outriggers” are the horizontal beams that attach the outer stabilizing floats, or “amas,” to the main canoe-shaped hulls of Polynesian oceangoing boats (see Fig. 1). When pushed by sudden waves, a narrow boat hull can sink into the ocean or overturn, but a small amount of ama flotation (upward resistance) or weight (downward resistance) operating through outrigger leverage is enough to prevent overturning. Similarly, if outriggers are attached to perimeter columns that can withstand both upward and downward forces, the building will be far more resistant to toppling.

During the history of our evolution, humans have been fascinated by the idea of scaling great heights, and we've never stopped trying to literally touch the moon and stars. There is a long history of civilizations displaying their might and prosperity through the construction of extravagant monuments, from the ancient pyramids to the ultra-modern skyscrapers of today. The skyscraper has become the modern icon of economic dominance and leadership. Mankind's shown competitive nature has led to many efforts to construct the world's highest structure the Burj Khalifa and so on. However, lateral rigidity becomes more of a concern as buildings go taller; this is something that can be accomplished by adding an outrigger. An outrigger system uses the structure's perimeter columns to effectively mitigate the effects of overturning moments and the associated lateral displacements at higher levels in a building with

S. Naveen Kumar (✉) · K. S. Satyanarayanan

Department of Civil Engineering, Faculty of Engineering and Technology, SRM Institute of Science and Technology, Kattankulathur, Tamil Nadu 603203, India

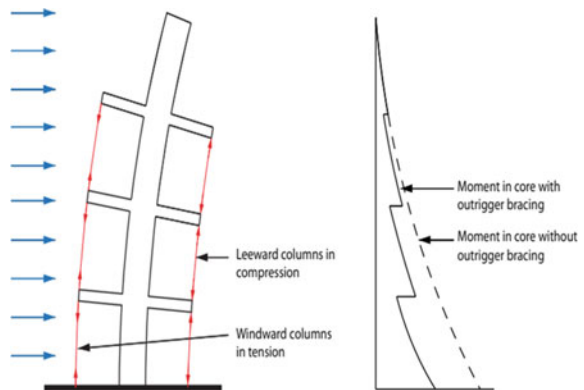
e-mail: naveenkumars3228@gmail.com

Fig. 1 Samoan outrigger canoe



a central core braced by the frame or shear walls as shown in Fig. 2. It also assists in uniformly distributing the resulting overturning loads to the base that causes the structure's effective depth to grow as a result. Although the outrigger arrangement does a great job of boosting the building's flexural rigidity. However, it only does a little to improve the structure's ability to resist shear, which is instead carried by the core. There will be tension in the windward columns and compression in the leeward ones. When compared to a free cantilever design, the core overturning moment of a tall building supported by an outrigger system can be reduced by as much as 40%. Due to the many advantages and practical benefits of outrigger systems, they can be built in any mix of steel, concrete, and composite construction.

Fig. 2 Interaction of core and outriggers



2 Literature Study

Many studies have been conducted on the topic of outrigger system behavior to highlight some of the recent papers. In this study, we provided a performance-based, optimized seismic design for a damped outrigger structure, one that accounts for outrigger and column flexibility. For the sake of the numerical example, a 50-story structure with three different column diameters was employed. As the perimeter columns grew more flexible, the optimal solution included more damped outriggers, which were located on lower floors than those in damped outrigger buildings with stiffer perimeter columns [1]. Analyzed the effectiveness of a three-level asymmetrical outrigger braced frame. There are a total of three potential offset ratios. Static analysis for wind loading and dynamic analysis for earthquake loading both make use of the same standard software package. Comparing the core frame's lateral drift natural frequency and base shear to those of the outrigger is one method of evaluating its effectiveness. By analyzing the structure's static and dynamic behaviors, the optimum position of the outrigger could be determined [2]. This study used an analytical approach to determine the best possible placement for up to four outriggers in a core-outrigger system. Two equations were devised to predict the top displacement and maximum height of a structure with an outrigger system. In addition, this work pioneers the use of curves as a straightforward alternative to the laborious and time-consuming FE analysis. These curves are useful for judging the viability of conceptual designs [3]. The research examines how a structure changes when supported by outriggers. The following findings were gleaned from the project analysis. As the size of the outrigger members grows, the displacement of the structural system of a tall structure grows smaller. A shear wall with an outrigger installed in the building's core can alleviate some of the pressure there. Different types of structures react differently to earthquake loads. Reduced construction time and increased overall rigidity are both benefits of using outriggers in both conventional and non-traditional building designs [5]. Different solutions will emerge depending on how flexible the perimeter columns are, highlighting the need for a well-formulated optimization problem when dealing with damped outriggers [7]. Examines the effects of outriggers for single-bay frames at single and two levels at 30 m, 45 m, and 60 m heights. Structural software performed finite element analysis. Static loads are considered for outrigger provisions, both symmetrical and unsymmetrical. For each outrigger level, the analysis calculates lateral displacements, internal forces, and base shear. Outrigger system efficiency is measured by core frame value lateral displacement. The outrigger position is optimized for efficiency [8, 10].

3 Methodology

Many resources were investigated to comprehend the workings and results of an outrigger. For frames of 10, 15, and 20 stories at 30, 45, and 60 m in height, both symmetrical and asymmetrical outrigger behavior are studied using static and dynamic analyses. The outrigger placements for both the single- and double-level configurations are optimized with the help of the analysis program ETABS.

4 Objectives and Details of the Present Study

The objective of this research is to find the optimum outrigger location for three distinct multi-story frames with symmetrical and unsymmetrical outrigger frames while under wind and earthquake load. IS 875 (Part 3) was used in the design process for calculating wind loads, while IS 1893 (Part 1): 2016 was used to determine earthquake loads.

Using the 2016 edition of IS1893 for the base shear calculation. For example, $VB = W \times Ah$ when $VB =$ Base shear. $W =$ Building's Seismic Weight. Yes, create a spectrum of the horizontal acceleration. $Z =$ Zone factor; $A_h = Z/2 \times I/R \times (S_a/g)$. The "I" stands for the "importance" component. R stands for "response reduction factor." $S_a/g =$ Spectral Velocity/Velocity [4]. In this case, IS: 456-2000 is used to examine the structure under a variety of loads. The maximum lateral deflection is calculated for the following load combination. (DL + LL \pm WL) The placement of the outrigger can be determined in order to lessen the effects of lateral movement, drift, and moments at the building's core. For this investigation, we opted to use the ETABS program. This research is limited to multi-story reinforced concrete (RCC) frames, both symmetrical and asymmetrical. Models of the same frame were analyzed with a 3-m outrigger length.

A 30 m, 45 m, and 60 m high-rise reinforced concrete frame model is used for this analysis. The frame bay width is 3 m, and each story is 3 m high. Darbhanga is assumed to be the location of the frame. Figure 3 provides an elevation view of a typical frame with an outrigger.

4.1 Details of Analytical Investigation

Analytical research of the dynamic behavior of a multi-story reinforced single-bay frame supported by single- and double-level outrigger systems. To Zone Factor (Z) 5, which is 0.36; hard soil type, a damping value of 5% is provided; the seismic characteristics examined are shown. Assume an I value of 1.5 and an R -value of 5 for the importance and response reduction factors, respectively [10].

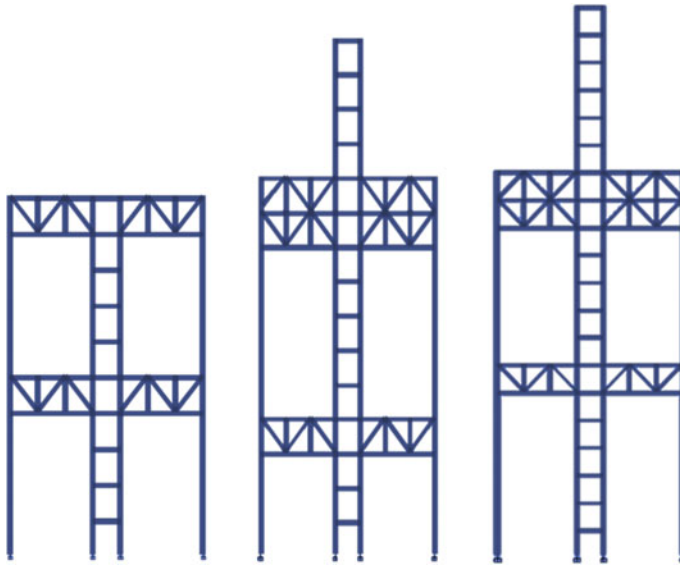


Fig. 3 Typical pattern for symmetrical outrigger added at the top story for 10, 15, and 20 story frame

The frame has a young's modulus of $22,360,679.78 \text{ kN/m}^2$ and a grade of concrete of M20 (as per IS 456-2000). Table 1 displays the various frame types and their corresponding geometrical specifications. Bay width of the frame: 3 m. Floor height of the frame: 3 m.

5 Analytical Results

The purpose of this analytical study is to examine the behavior and determine the optimum position of the outrigger for symmetrical and unsymmetrical outrigger frames for two levels under uniform horizontal loading and dynamic loading, with gravity loads, for frames with 10, 15, and 20 stories and floor heights of 3.0 m. Single- and double-level outriggers with core frames have been compared for their ability to mitigate movement. The core rotation occurs in the vertical plane when the outrigger structure is loaded from the side. Nevertheless, the tension in the windward columns and compression in the leeward columns created by the outriggers prevent this rotation from occurring. When subjected to lateral loads, the effective structural depth of the building is increased as a result of this.

Table 2 displays the maximum lateral displacement and base shear for 10-story frames with 1-level outriggers. Dynamic research reveals base shear changes in response to outrigger orientation changes at the top.

Table 1 Frame type and properties

S. No.	Type	Height (m)	Column size (mm)	Beam size (mm)	Bay width (m)
1	Core	30	500 × 500	300 × 450	3
2	Core	45	500 × 500	300 × 450	3
3	Core	60	500 × 500	300 × 450	3
4	Symmetrical outrigger	30	500 × 500	300 × 450	9
5	Symmetrical outrigger	45	500 × 500	300 × 450	9
6	Symmetrical outrigger	60	500 × 500	300 × 450	9
7	Unsymmetrical outrigger	30	500 × 500	300 × 450	6
8	Unsymmetrical outrigger	45	500 × 500	300 × 450	6
9	Unsymmetrical outrigger	60	500 × 500	300 × 450	6
10	Symmetrical outrigger	5.4	500 × 500	300 × 450	4.2

Table 2 Maximum lateral displacement and base shear of a 10-story frame with single-level outrigger

Position of outrigger from top	Maximum lateral deflection (mm)		Base shear (kN) dynamic analysis	
	Unsymmetrical outrigger	Symmetrical outrigger	Unsymmetrical outrigger	Symmetrical outrigger
0H	118.07	98.39	39.618	44.02
0.1H	113.32	94.43	39.816	44.24
0.2H	99.40	82.83	41.427	46.03
0.3H	100.82	84.02	43.083	47.87
0.4H	97.61	81.34	44.667	49.63
0.5H	96.40	80.33	45.702	50.78
0.6H	98.15	81.79	45.036	50.04
0.7H	104.40	87	41.742	46.38
0.8H	117.62	98.02	36.684	40.76

Figure 4 illustrates the maximum lateral displacement and Fig. 5 illustrates the maximum base shear for 15-story frames with single-level outriggers.



Fig. 4 Maximum lateral displacement of a 15-story frame with single-level outrigger

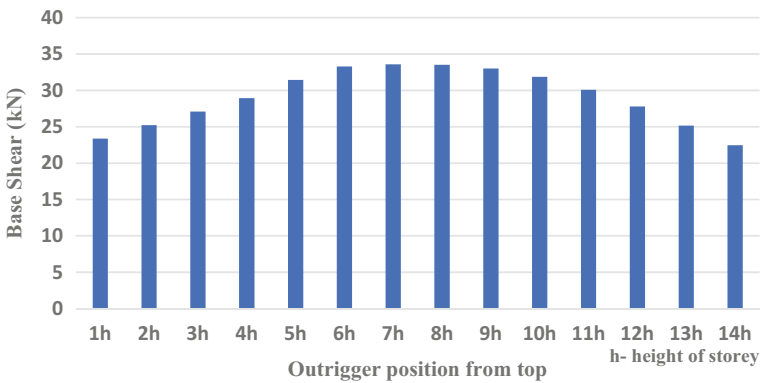


Fig. 5 Maximum base shear of a 15-story frame with single-level outrigger

5.1 Optimum Position and Efficiency of Core Frame with Single and Double Level Outrigger

The optimum position of the outrigger is established by contrasting the core’s maximum lateral deflection when it does not have an outrigger to the core’s maximum lateral deflection when it does have an outrigger. Figure 6 depicts the core frame in its optimal location with a single level of the outrigger.

The effectiveness of the outrigger is determined by comparing the lateral deflection of the core both before and after the installation of an outrigger and then taking the difference between the two measurements. The effectiveness of a core frame with a single-level outrigger with a double level of outriggers is compared and contrasted in Fig. 7.

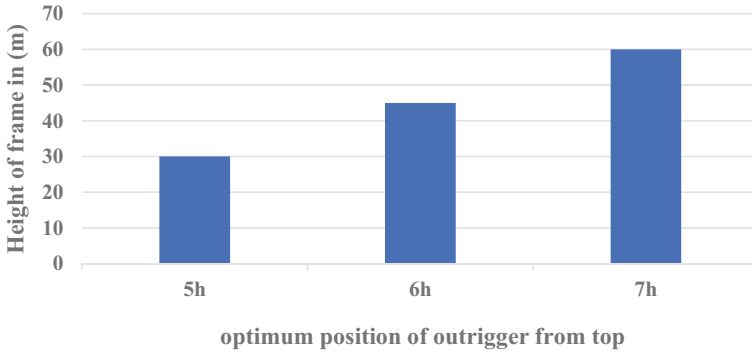


Fig. 6 Optimum position of single-level outriggers for a different types of frames

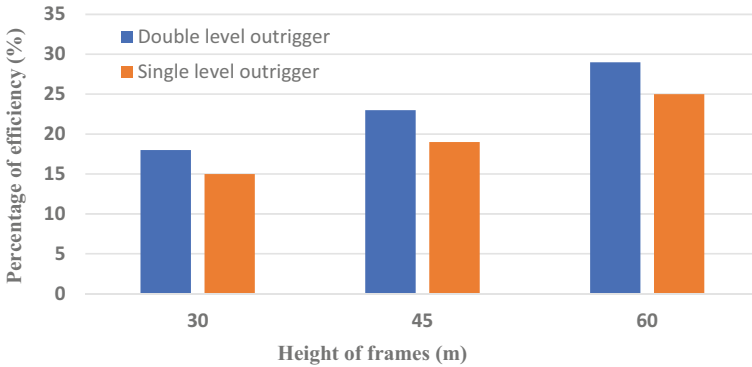


Fig. 7 Efficiency of core with single- and double-level outrigger

5.2 Optimum Position and Efficiency of Core Frame with Multi-level Outrigger

The best height for an outrigger is determined by trying out a few different positions and comparing the resulting lateral deflection in each story. For many level outriggers, one of the outriggers is fixed in position at the level that a single-level outrigger has decided to be optimum, while the other outrigger is given as a linked outrigger, which means that it consists of two outriggers combined and is modified from the top to the structure. The most effective positioning of the core frame while using a multi-level outrigger is shown in Fig. 8.

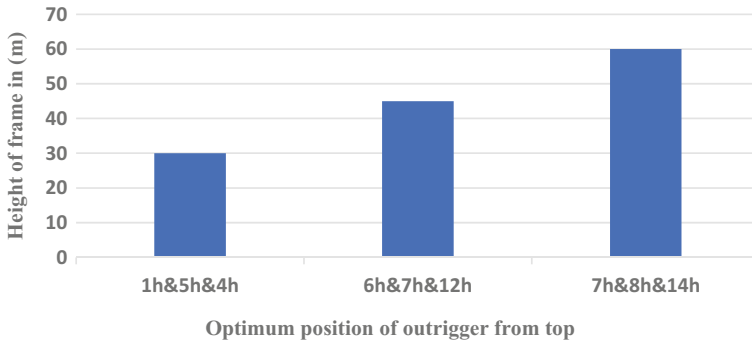


Fig. 8 Optimum position of multi-level outriggers for different type of frames

5.3 Optimum Position of 7-Story Frame with Outrigger

A prototype building with seven stories is scaled by a factor of four to reach a height of 5.4 m. In this investigation, the responses of symmetrical and unsymmetrical outrigger frame types under both static and dynamic loads are compared in order to locate their optimum position and efficiency. A comparison was made between the behavior of the core with and without outriggers in terms of lateral displacement and base shear. By comparing the lateral deflection of the core when it does not have an outrigger to the lateral deflection of the core when it does have an outrigger, the optimal position of an outrigger for a single bay, seven-story frame may be determined. Figure 9 illustrates the core frame positioned in the most ideal position, with just one level of the outrigger.

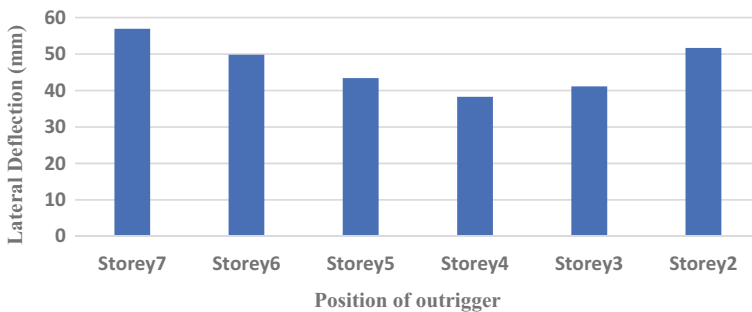


Fig. 9 Core frame positioned in the most ideal position

6 Summary of Work

The objective of this investigation was to analyze the effect of symmetrical and unsymmetrical outrigger bracings on the static and dynamic behavior of reinforced concrete core frames of three different heights, to find its optimum position for a single-level, double-level, and multi-level outrigger positions at various heights from the top for 30 m, 45 m, and 60 m. The research was also intended to determine the optimum position for a single-level, double-level, and multi-level outrigger. The results of the static analysis are used to calculate the maximum lateral displacement values, and the results of the static analysis and the dynamic analysis are used to calculate the base shear values. The ideal location of the symmetrical outrigger for buildings with 10, 15, and 20 stories and a height of 3 m. A single-level outrigger should be placed at $H/2$, $H/2.5$, and $H/2.85$ from the top at 30, 45, and 60 m, respectively. These are the best possible positions. When using an outrigger with two levels, the optimal position of the second outrigger is $H/1$, followed by $H/1.25$ and $H/1.4$. With a multi-level outrigger, the ideal position for one outrigger is fixed at its optimum position, which was derived from a single-level outrigger, and the optimum positions for the other two outriggers are added from different locations from the top, for 30, 45, and 60 m, respectively (H -height of the building). The symmetrical outrigger of the seven-story frame should be placed in the optimum location on the fourth floor at a height of 3.08 m. When performing dynamic analysis, the base shear value increases with each story as well as with the appropriate floor heights when outriggers are included.

References

1. Bayati Z, Mahdikhani M, Rahaei A (2008) Optimized use of multi-outriggers system to stiffen tall buildings. In: The 14th world conference on earthquake engineering, vol 64(2), pp 183–194
2. Devakumar (2002) Study on the performance of unsymmetrical outrigger braced frames. A thesis submitted in the partial fulfilment of the requirement for the award of Degree of Master of Engineering (Structural Engineering), University of Madras SRM Engineering College, Kattankulathur
3. Habrah A, Batikha M, Vasdravellis G (2022) An analytical optimization study on the core-outrigger system for efficient design of tall buildings under static lateral loads. *J Build Eng* 46:103762
4. IS: 1893:2015 (PART I), Criteria for earthquake resistant design of structures. Bureau of Indian Standards, New Delhi
5. Mulla AK, Srinivas BN (2015) A study on outrigger system in a tall RC structure with steel bracing. *Int J Eng Res* 4
6. Nanduri PRK, Suresh B, Hussain MI (2013) Optimum position of outrigger system for high-rise reinforced concrete buildings under wind and earthquake loadings. *Am J Eng Res* 2(8):76–89
7. Netzer I, Lavan O (2020) Optimized seismic design of passively damped outriggers considering perimeter column flexibility. *J Struct Eng* 146(12):04020254
8. Sathyanarayan KS, Vijay A, Balachandar S (2012) Feasibility studies on the use of outrigger system for RC core frames. Copyrights© 2012 Votrix Publication (team.ijaiti@gmail.com)

9. Smith BS, Coull A. Textbook—'tall building structures: analysis and design'
10. Thirumurugan V, Satyanarayanan KS, Ganesan TP. Feasibility studies on the use of pneumatic interface for mitigation of disasters in RCC frames with masonry infilling

Study on the Shear Behavior of Hybrid Fiber-Reinforced Concrete Beams



M. Bhuvaneshwari and Yaci Joshy

1 Introduction

Concrete has a high resistance to breakage under compression but a lower resistance to strain under tension. Fibers are mixed into concrete to increase its tensile strength. The tensile strength can be obtained by providing fibers. Many of the engineering features of the basic materials, such as fracture toughness, deflection under lateral stress, and durability can be improved through the addition of fibers to the concrete, mortar, and cement paste used for the construction process. By incorporating different fibers into traditional concrete to create hybrid fiber-reinforced concrete, the mechanical behavior of the material is improved. Concrete cracking can be prevented using FRC. The characteristics of FRC depend on the specific fiber types used. The behavior and characteristics of concrete are improved by the insertion of various types of fibers and their combinations. Several researchers have reported on their thorough testing of HFRC using both artificial and natural fibers, including steel, glass, organic polymers, nylon, coconut coir, jute, pine leaves, and bamboo. The results of previous studies have shown that the first-cracking character of fiber-reinforced concrete can be improved by the application of two or more fiber combinations, and this behavior is regulated by the fiber content and fiber mixture. They are also economical, lightweight, renewable, and eco-friendly. In this research, steel and jute fiber are used as hybrid fibers in the concrete. A sustainable way to improve the properties of concrete and promote environmental friendly buildings is focused in this paper. Jute fiber is inexpensive and widely accessible in several developing nations. Concrete physical properties may vary qualitatively when steel fiber is added in small amounts, greatly enhancing the material's resistance to cracking, impact, fatigue, and bending, as well as durability. There are several applications

M. Bhuvaneshwari · Y. Joshy (✉)

Department of Civil Engineering, Faculty of Engineering and Technology, SRM Institute of Science and Technology, Kattankulathur, Tamil Nadu 603203, India

e-mail: yj1346@srmist.edu.in

for steel fiber-reinforced concrete, including floors, maritime structures, concrete structure repair and retrofitting, etc. In this experiment, the concrete is mixed with hybrid fibers in beams at different ratios and the beam is tested under the four-point loading. The addition of hybrid fiber (HF) improves the tensile strength of concrete. The shear behavior of the HFRC beams was studied, and the shear properties will be analyzed and compared with the RC beams. The beam is analyzed in ABAQUS for load–deflection under certain loads for both HFRC beams and conventional beams and the results were compared.

1.1 Hybrid Fiber-Reinforced Concrete

Hybrid fiber-reinforced concrete (HFRC) is a type of concrete that involves the use of two or more fibers in its composition. The incorporation of fibers in concrete enhances its tensile strength and structural stability, leading to higher resistance to cracking and improved durability. The mechanical properties of HFRC depend on the type and ratio of fibers used in its composition. Fiber-reinforced concrete (FRC) has gained attention in the construction industry due to its unique properties. The fibers used in FRC can be synthetic or natural, such as steel, glass, organic polymers, nylon, coconut coir, jute, pine leaves, and bamboo. Each type of fiber contributes distinct mechanical properties to the concrete, such as toughness, ductility, and durability. In this study, a combination of natural and artificial fibers is used as a hybrid fiber in the concrete composition. Jute fiber, a natural and renewable fiber that is widely available in several developing countries, is combined with steel fiber, an artificial and highly durable fiber. The hybridization of fibers is expected to improve the mechanical properties of the concrete, such as its tensile strength and shear behavior. Overall, the use of hybrid fibers in concrete has the potential to enhance its properties and promote sustainable and eco-friendly building practices.

2 Literature Review

2.1 General

This survey gives us a comprehensive view of the progress that needs to be done. The process of performing a literature review includes examining up numerous studies that are similar to the one being done. Some of the papers are explained below.

Vinod Kumar et al. [1] have carried out the performance of HFRC beams in terms of bending and shear. HFRC beams made of SPF and GPF were put for test in a loading frame to see how well they bend and break (GPF). In this experiment, concrete was mixed with two distinct combinations of 1% steel fibers, 0.03% glass fibers, and 0.30% polypropylene fibers. Six beams of total were cast and tested each

of which contained three beams. An experiment was done to find out the behavior's maximum load as well as its crack patterns and width, load–deflection behavior, ductility, and stiffness relationships. The test results showed that HFRC beams could hold much more weight than control beams. An HFRC beam also reduces crack width and deflection.

Song et al. [2] have carried out studies on how the adding of JF affects the mechanical properties of cementations components. In this paper, the effects of using JF in CC for sustainable building are talked about. In addition, the jute fiber's microstructure is addressed, and the fiber and the matrix are described. It has been said what the best length and amount of JF are, and it has been shown how changing the length and amount of jute fibers affects the mechanical strength of CCs. It was found that jute fibers with small lengths and less volume contents make CC stronger, at the time, jute fibers with longer lengths and higher volume contents make CCs less strong.

Saravanakumar et al. [3] have carried out an experiment to see what happens when HFRC beams are obtained to torsion. Experiments were done to show the mechanical function and torsional characteristics of HFRC beams. Steel and glass fibers with varying fiber levels, including 0, 0.5, 1.0 and 1.5% by volume of concrete, were used to cast the specimens for this experiment. The mechanical property of the concrete was greatly enhanced by the inclusion of hybrid fibers up to 1% by volume. Depending on the amount of fiber component in the concrete, hybrid fiber-reinforced concrete has improved torsional strength in the first cracking and last cracking states. In HFRC beams, the number of failure increases but the width of the cracks decreased. 1% HFRC is created by adding 0.5% of each steel and glass fiber. Enhanced mechanical strength by about 20% over baseline. The HFRC beam's torsional strength continuously increased behavior for the additions of fiber. Maximum growth was discovered as much as 33% in 1.5% HFRC beams. In contrast to RC beams, HFRC beams failed gradually, and after the first crack, the specimen remained load-bearing for a longer time. The hybrid fiber-reinforced concrete displayed better post-cracking behavior than the RCC beam.

Vishaul et al. [4] have carried out to conducted research on the hybrid fiber-reinforced concrete's structural behavior. Experimental techniques were used to study the properties of M40 grade concrete of HF such as AR glass and coir fiber RC. The addition of various fibers increased the impact resistance and ductility of concrete proportionally. The compressive strength of concrete is increased when AR glass and coir fibers are added at a ratio of 2–1% as opposed to conventional concrete or concrete that contains both coir and AR glass fibers. In comparison to typical concrete, the compressive strength increased for the third day when coir and AR glass were added at a ratio of 1–2%. And split tensile strength of the similar mix types also produced better results.

Li et al. [5] have investigated how steel/polypropylene hybrid fiber affects concrete's ability to bend. This study, which involved 51 samples and four-point bending tests, examined the flexural behavior of SP HFRC. Three different kinds of SF straight, hooked end, corrugated, and monofilament polypropylene fiber are taken into consideration. Flexural behavior is examined and the synergistic effect of HF. The findings demonstrate that the combination of polypropylene fiber and all

three types of SF improve the flexural behavior of HFRC. The most effective flexural specimens are those that have fibers with hooked ends. The most obvious synergy, though, is between straight steel and polypropylene fibers. The volume content of steel and polypropylene fibers rises along with the properties of concrete [6].

3 Analytical Study

3.1 Modeling, Assigning Property, and Assembly

See Fig. 1.

The dimensions of the beam are first fixed and then parts created such as length, breadth and depth of the beam, reinforcement details. Once the model were created, the material property will be assigned to the model and assemble all the parts together [7]. The properties such as the tensile strength, density, Young's modulus, Poisson's ratio were given. The dimensions of the beam is shown in Fig. 1. Main bar of 12 mm provided at the bottom of the beam as per the design and as shown in Fig. 2. The length of the beam is 1.5 m; width of the beam is 0.15 m, and the depth of the beam is 0.18 m.

Fig. 1 Beam model (2 m × 0.15 × 0.25)

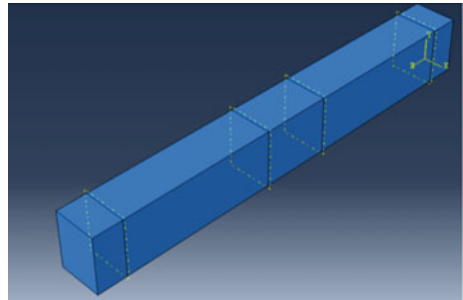
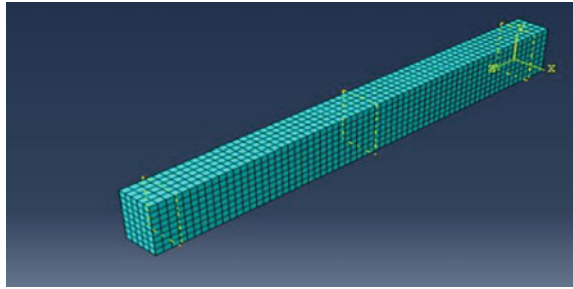


Fig. 2 Assembling of reinforcement and stirrups



Fig. 3 Meshing and loading of beam model



3.2 Meshing and Load Assigning

Meshing and load assigning are important steps in finite element analysis using the ABAQUS software for a beam model [8]. Meshing refers to dividing the beam geometry into a finite number of smaller elements. The load assigning involves defining the loads and boundary conditions that are applied to the beam during the analysis. Mesh provides accuracy to results for the analysis of beam and this helps to analyze the results such as stress and deflection at each of element in the beam [9]. The mesh size of wire is 15 mm and the beam is 25 mm, respectively (Fig. 3).

4 Results Obtained from the Analysis

The models were created and load–deflection was studied for the RCC beam using ABAQUS and finite element analysis (FEA) software. Beams were modeled and applied different loads, and the deflection is noted at a particular element in the beam. The deflection is noted and plot against load.

4.1 Deflection

Figure 4 shows the deflection of conventional concrete beam at 80 kN and Figure 5 shows the deflection of hybrid fiber-reinforced concrete beam at 80 kN.

4.2 Load–Deflection Relation

The beams are analyzed in the ABAQUS. The result obtained from the analysis is shown in Fig. 6. In the analysis, it is shown that the HFRCB performs better than CCB [10, 11]. The deflection at a particular node is plotted against the load. In the

Fig. 4 Deflection of the conventional beam

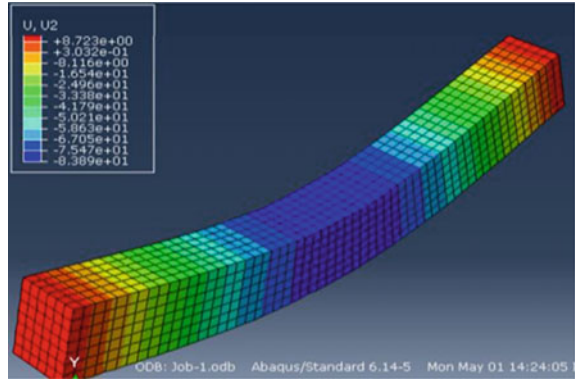
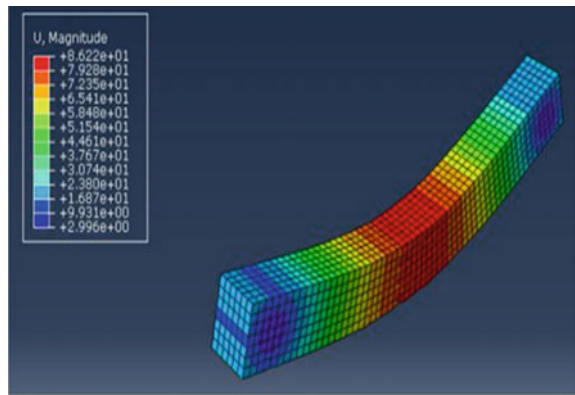


Fig. 5 Deflection of the hybrid fiber reinforced beam



analysis, it is observed that at 80kN load, the deflection of CCB and HFRCB is 8.72 and 8.62, respectively, as shown in the Figs. 5 and 6. The percentage of decrease in deflection is 1.14%, respectively.

5 Testing of Beams for Shear Behavior

A shear test on a concrete beam is a standard test used to determine the shear behavior of reinforced concrete. The test involves subjecting a beam to a gradually increasing load while measuring the resulting deflection and strain [12]. The beam is supported at two points and a load is applied at a point between the two supports. During the test, the concrete experiences both compressive and tensile stresses, as well as shear stresses. The shear strength of the concrete is determined by measuring the maximum load the beam can withstand before failure occurs. The shear test is an important measure of the quality and safety of concrete structures such as bridges, tunnels, and buildings. It is used to evaluate the ability of the concrete to resist

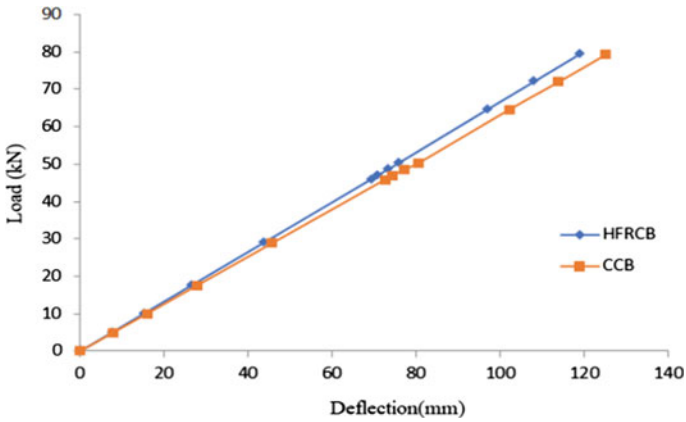


Fig. 6 Load–deflection relation of RC beam

lateral loads and to ensure that the structure can withstand the expected loads over its lifetime. The results of the shear test can be used to determine the need for additional reinforcement or other measures to increase the safety and durability of the structure. Beam of size 1500 mm length, 180 mm depth, and 150 mm width is casted for finding the shear behavior of CCB and HFRCB. In this proving ring, supports, hydraulic jack, deflectometer, strain gauge reading instrument are used for the experimental setup and as shown in Fig. 7.

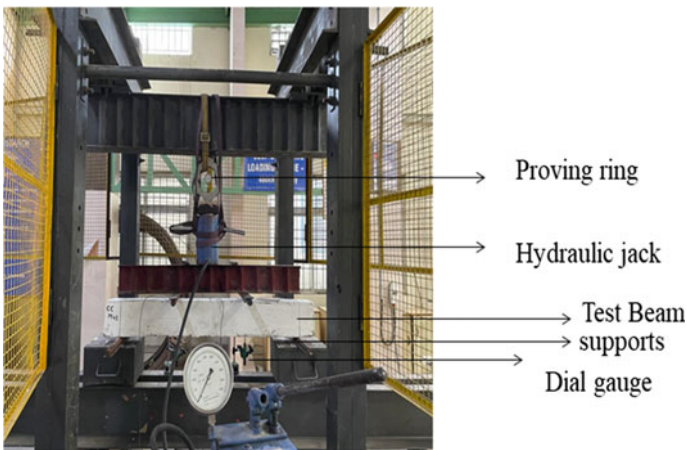


Fig. 7 Test setup for beam

5.1 Test on CCB and HFRCB

The Conventional Concrete Beam (CCB) testing is done which shown in Fig. 8. The initial crack happens at 30 kN at a deflection 3.04 mm and the beam failed at 80 kN at a deflection of 8.43 mm. The crack formation and the shear failure of the beam are marked in the beam. In the CCB, the cracks are extending from the bottom to the top while applying load. The hybrid fiber-reinforced concrete beam (HFRCB) testing is done which shown in Fig. 9. The initial crack happens at 35 kN at a deflection 3.26 mm and the beam failed at 100 kN at a deflection of 8.06 mm. The crack formation and the shear failure of the beam are marked in the beam. In the HFRCB, the cracks are arrested by the fiber and are not extending from the bottom to the top while applying load.

Fig. 8 Test setup for CCB

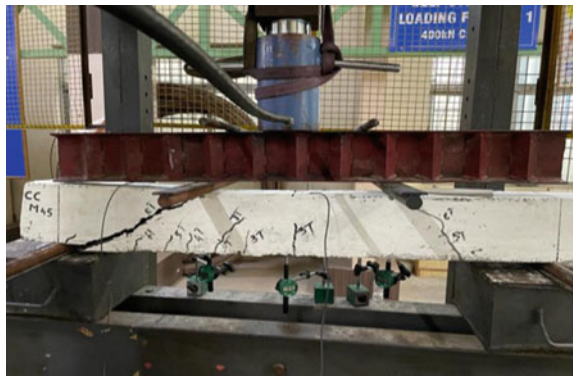


Fig. 9 Test setup for HFRCB



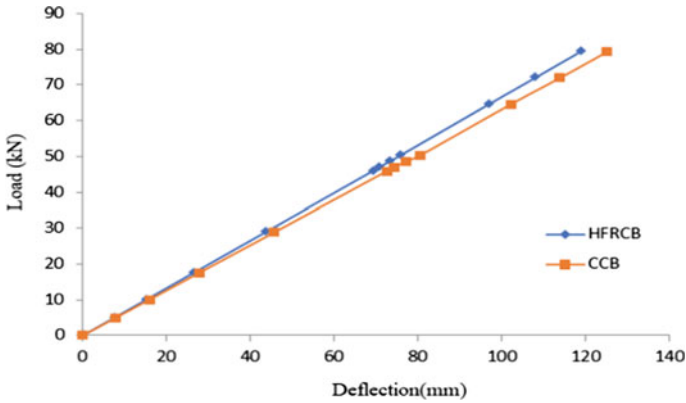


Fig. 10 Load deflection relation of the beams

5.2 Test Result of Beams

From the graph, Fig. 8 shows that the HFRCB performs better than the CCB. The HFRCB deflection is found to be less as compared to the CCB. The percentage of decrease in deflection is 4.3%. And from the Figs. 8 and 9, it is clear that the HFRCB has less cracks as compared to the CCB, and also the cracks are getting arrested by the fiber and the fiber does not allow the cracks to extend from bottom to the top while applying the load. The beams are analyzed in the ABAQUS. The result obtained from the analysis is shown in Fig. 9. In the analysis, it is shown that the HFRCB performs better than CCB. The deflection at a particular node is plotted against the load. In the analysis, it is observed that at 80kN load, the deflection of CCB and HFRCB is 8.72 and 8.62, respectively, as shown in Fig. 10. The percentage of decrease in deflection is 1.14%, respectively (Fig. 10).

6 Conclusion

- The compressive strength of JS0 specimen is 54.62 N/mm^2 and the fiber containing JS25 specimen is 56.52 N/mm^2 ; therefore, the percentage of increase in the strength is 3% more than the control specimen.
- The tensile strength of JS0 specimen is 3.5 N/mm^2 and the fiber containing JS25 specimen is 4.43 N/mm^2 ; therefore, the percentage of increase in the tensile strength is 26% more than the control specimen.
- The flexural strength of JS0 specimen is 7.53 N/mm^2 and the fiber containing JS25 specimen is 8.36 N/mm^2 ; therefore, the percentage of increase in the flexural strength is 11% more than the control specimen.
- The optimum percentage of fiber is 0.5% of steel and 0.2% of jute.

- Experimentally, the percentage of decrease in deflection is 4.3%. The HFRCB has less cracks as compared to the CCB, and also the cracks are getting arrested by the fiber and the fiber does not allow the cracks to extend from bottom to the top when subjected to load.
- In the analysis, it is observed that at 80 kN load, the deflection of CCB and HFRCB is 8.72 and 8.62, respectively. The percentage of decrease in deflection is 1.14%, respectively.

Acknowledgements I wish to express my sincere thanks to Department of Civil Engineering, SRM Institute of Science and Technology for giving this opportunity.

References

1. Kumar MV, Raj SJ, Kumar KR, Gurumoorthy N, Ganesh AC (2021) Flexural and shear performance of HFRC beams. *Mater Today: Proc* 42:816–820
2. Song H, Liu J, He K, Ahmad W (2021) A comprehensive overview of jute fiber reinforced cementitious composites. *Case Stud Construct Mater* 15:e00724
3. Saravanakumar P, Sivakamidevi M, Meena K, Yamini SP (2021) An experimental study on hybrid fiber reinforced concrete beams subjected to torsion. *Mater Today: Proc* 45:6818–6821
4. Vishaul K, Manikandaprabhu S, Radhakrishnan R (2021) Structural behavior of hybrid fiber reinforced concrete—an experimental study. *Mater Today: Proc* 39:818–822
5. Li B, Chi Y, Xu L, Shi Y, Li C (2018) Experimental investigation on the flexural behavior of steel-polypropylene hybrid fiber reinforced concrete. *Constr Build Mater* 191:80–94
6. Salih YA, Sabeeh NN, Yass MF, Ahmed AS, Khudhurr ES (2019) Concrete beams strengthened with Jute fibers. *Civil Eng J* 5(4):767–776
7. Rangasamy G, Mani S, Kolandavelu SKS, Alsoufi MS, Ibrahim AMM, Muthusamy S, Panchal H, Sadasivuni KK, Elsheikh AH (2021) An extensive analysis of mechanical, thermal and physical properties of jute fiber composites with different fiber orientations. *Case Stud Therm Eng* 28:101612
8. Gao D, Zhang L, Zhao J, You P (2020) Durability of steel fibre-reinforced recycled coarse aggregate concrete. *Constr Build Mater* 232:117119
9. Algassem O, Li Y, Aoude H (2019) Ability of steel fibers to enhance the shear and flexural behavior of high-strength concrete beams subjected to blast loads. *Eng Struct* 199:109611
10. Tran TT, Pham TM, Hao H (2019) Experimental and analytical investigation on flexural behaviour of ambient cured geopolymer concrete beams reinforced with steel fibers. *Eng Struct* 200:109707
11. Xu L, Huang L, Chi Y, Mei G (2016) Tensile behavior of steel-polypropylene hybrid fiber-reinforced concrete. *ACI Mater J* 113(2):219–229
12. Sajin JB, Paul RC, Binoj JS, Mansingh BB, Selvan MGA, Goh KL, Isaac RR, Saravanan MS (2022) Impact of fiber length on mechanical, morphological and thermal analysis of chemical treated jute fiber polymer composites for sustainable applications. *Current Res Green and Sustain Chem* 5:100241

Plastic Shrinkage and Microstructural Analysis of Butyl Rubber in Light-Weight Concrete



S. Prakash Chandar, Vishnu, and P. T. Ravichandran

1 Introduction

Because of the financial, environmental, and technological advantages of using alternative aggregate, it has become necessary for the construction industry [1–4]. They can be used as developing material or replacement material in the building industry in developing nations where medical wastes are dumped in large quantities. This will have two benefits: it will lower the construction material cost and provide a way to dispose of waste. The potential for developing new and alternative building materials using medical wastes is great, and this will partially lower the cost of building materials. Butyl rubber is a type of medical waste, is one such substitute [5]. The suitability of the aforementioned medical waste as a building material has been the subject of numerous studies. With its potential use as coarse aggregate in the creation of concrete, it is one of the most promising medical wastes. This has a good chance of being used in locations where crushed stone is expensive. When compared to conventional concrete, butyl rubber has better strength. The majority of compressive strength development occurs during the initial stages and increases with age.

S. Prakash Chandar (✉) · Vishnu · P. T. Ravichandran
Department of Civil Engineering, Faculty of Engineering and Technology, SRM Institute of Science and Technology, Kattankulathur, Tamil Nadu 603203, India
e-mail: prakashs2@srmist.edu.in

2 Materials

The following materials were selected in this experimental investigation.

2.1 Cement

Ordinary Portland cement of grade 53 (OPC 53) in accordance with standard confirming to IS 12269:1987 [6] is used for making of concrete mixes. Other building materials are bound together with cement so that they can harden and adhere.

2.2 Fine Aggregate

Fine aggregate that complies with zone III of IS: 383:1997 [7] and passes through a 4.75-mm IS sieve is used in concrete mixes. With fine aggregate specific gravity of 2.6.

2.3 Coarse Aggregate

The most crucial component of concrete is coarse aggregate. That was retained on an IS sieve with a 4.75-mm mesh. For the production of concrete, it must be angular with a size greater than 10 mm. Different properties of coarse aggregate according to Indian standard, which confirms IS: 383—1997 [7], were discovered in laboratories and the physical and chemical properties discussed in Table 1.

Table 1 Physical and chemical properties of materials

Description	Result	Requirement according to IS 12269:2013
<i>Physical properties</i>		
Fineness—specific surface	310 m ² /g	≧ 225 m ² /g
Setting time—initial	35 min	≧ 30 min
Setting time—final	480 min	≧ 600 min
Cement soundness	1.3 mm	≧ 10 mm
<i>Chemical composition</i>		
Lime saturation factor	0.95	≧ 0.8 and ≧ 1.02
Ratio of Al to Fe	1.17	≧ 0.66
Insoluble residue (%)	0.89	≧ 2

(continued)

Table 1 (continued)

Description	Result	Requirement according to IS 12269:2013
Sulphuric Anhydride (SO ₃) (%)	2.13	≠3
Magnesia (MgO) (%)	1.32	≠6
Alkalies (%)	0.48	≠0.6
Chloride (%)	0.0165	≠0.05
Loss on ignition (%)	1.3	≠4
SiO ₂ (%)	21.2	–
Al ₂ O ₃ (%)	4.05	–
Fe ₂ O ₃ (%)	3.18	–
CaO (%)	63.56	–

2.4 Butyl Rubber

Butyl rubber, also referred to as ‘butyl,’ is a synthetic rubber created from the copolymer of isoprene and butylene. IIR is the name for isoprene and isobutylene rubber. Polyisobutylene, also known as ‘PIB’ or polyisobutene, is the homopolymer of isobutylene, or 2-methyl-1-propene, on which butyl rubber is based as shown in Fig. 1.

**Fig. 1** Butyl rubber

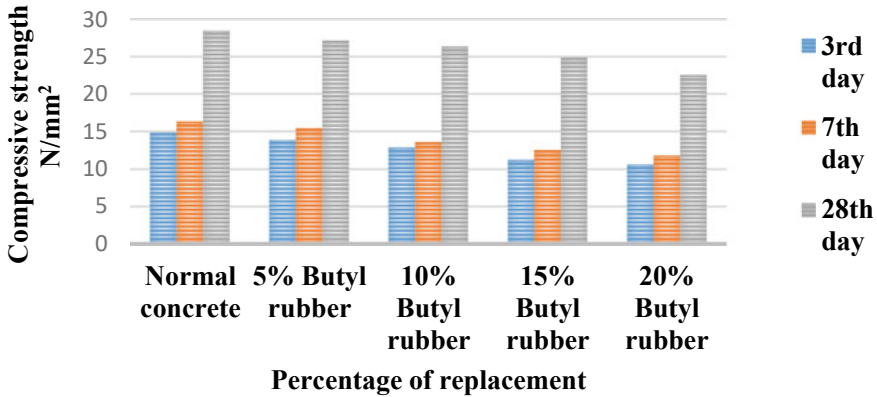


Fig. 2 Compressive strength test with LECA concrete

3 Experimental Program

The following experiments were conducted in this study including compressive strength, plastic shrinkage crack and microstructural characterization.

3.1 Compressive Strength

Compressive strength is the ability of concrete to withstand compression loading. A cube measuring $100 \times 100 \times 100$ mm is used to calculate the compressive strength of concrete [8, 9]. Compressive strength was measured in accordance with IS 516: 2016 at ages 3, 7 and 28 days. The M25 grade mix concrete (1:1:2:0.48) was chosen in this research and replaced with coarse aggregate by butyl rubber as follows. Utilizing various levels of coarse aggregate (5, 10, 15 and 20%) to replace butyl rubber, as shown in Fig. 2, and the replacement of 10% butyl rubber concrete results are shown.

3.2 Plastic Shrinkage

From the previous study, test procedure was used to evaluate the impact of butyl rubber on concrete cracking for plastic shrinkage. In accordance with the slabs of size $838 \times 533 \times 40$ mm, were prepared shown in Fig. 3 and subjected to the same procedure and environmental impacts. Atmospheric temperatures in this experiment was 27°C , and relative humidity readings between 40 and 90% were recorded during testing Table gives an outline of the quantity of framed cracks [11–14], least and greatest crack widths, and least and most extreme crack lengths on every

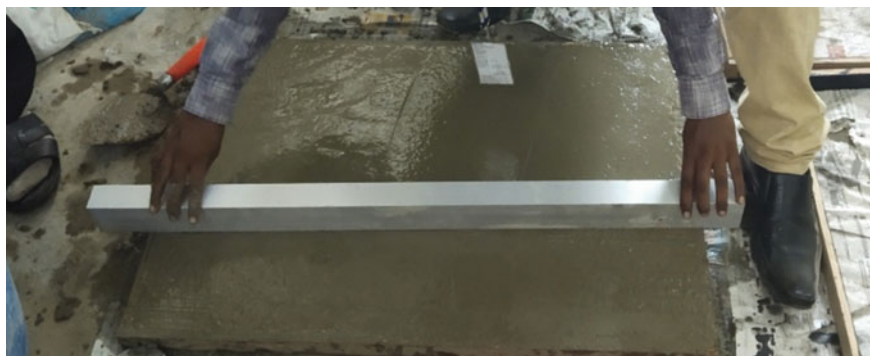


Fig. 3 Screeding

slab. According to the results of the plastic shrinkage tests, the area of the plastic shrinkage cracks decreases as the percentage of butyl rubber rises. In comparison to conventional mix, 10% replacement level of butyl rubber has fewer cracks and a smaller overall crack area. This demonstrates that butyl rubber has a big impact on lowering concrete plastic shrinkage cracks [9]. Thus, it can be said that the butyl rubber concrete, when compared to CC, lowering the overall crack area of plastic shrinkage. Floating was then done using an aluminium hand float as shown in Fig. 3 that was held flat against the slab surface and moved in a sweeping arc with a light sawing motion to fill holes, remove bumps, and smooth ridges. Leak water was then allowed to evaporate. After floating, a smooth and dense surface was created by troweling with a steel trowel as shown in Figs. 4 and 5. After 25 min after the mixer water addition, pedestal fans were allowed and allowed to run. A 150-mm diameter concrete cylinder filled with concrete was placed next to the slab panels and weighed throughout the test in order to determine the amount of water loosing from concrete during the experiment. To measure the rate at which free water evaporates, an open pan of water was filled and weighed. The emergence of the first plastic shrinkage cracks was observed visually. After five hours, the fans stopped. Crack widths were measured using a handheld microscope with an optical magnification of 40 and a sensitivity of 0.01 mm, and crack lengths were measured using thread and scale as shown in Fig. 6. Each crack's width was measured along its length three times, and the average of these measurements was taken into account. Crack length divided by the corresponding average. The crack area of the specific crack has been calculated using the crack's width. In a similar manner, the total crack area for each slab was calculated after measuring all the cracks as shown in Table 2.



Fig. 4 Wooden bull float application



Fig. 5 Slab specimen with butyl rubber



Fig. 6 Plastic shrinkage crack and measuring the length

Table 2 Plastic shrinkage cracks in butyl rubber replaced concrete

Mix with replacement	No. of cracks	Crack width (mm)		Crack length (mm)		Total crack (Area in mm ²)	% crack area in terms of CC
		Min	Max	Min	Max		
CC	9	0.2	0.9	20	70	63	100
5% Butyl concrete	8	0.2	0.8	18	66	52.7	90.4
10% Butyl concrete	8	0.2	0.9	18	68	61.2	96.7
15% Butyl concrete	9	0.2	1.0	20	74	74	117
20% Butyl concrete	11	0.2	1.2	26	78	93.6	148

3.3 SEM Analysis

The microstructure of the concrete itself controls how hardened it is. The amount of time the concrete is allowed to hydrate as well as the type of cement used all have a significant effect on the concrete structure. A material's topography and composition can both be analysed using SEM [15, 16]. The figure shows SEM morphology of light-weight concrete at a curing age of 28 days with various butyl rubber percentages. These micrographs show how CSH gel spreads clearly, creating voids and ettringite crystals in those spaces. As a result, the nano crystalline phase is where the strength of regular Portland cement, which is C-S-H gel comes from pictures of small fibre C-S-H and long, cylindrical ettringites that are transformed into calcium hydroxide fibre crystals. SEM images of butyl rubber concrete show similarities to images of traditional concrete as shown in Figs. 7, 8, 9, 10 and 11.

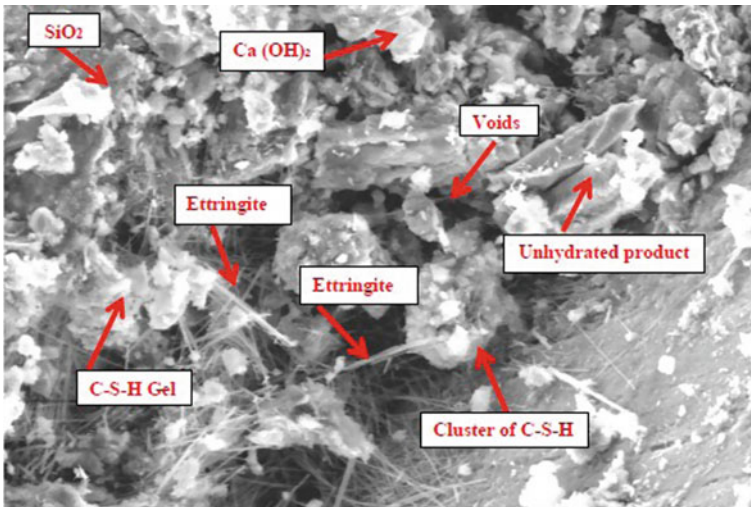


Fig. 7 Control concrete

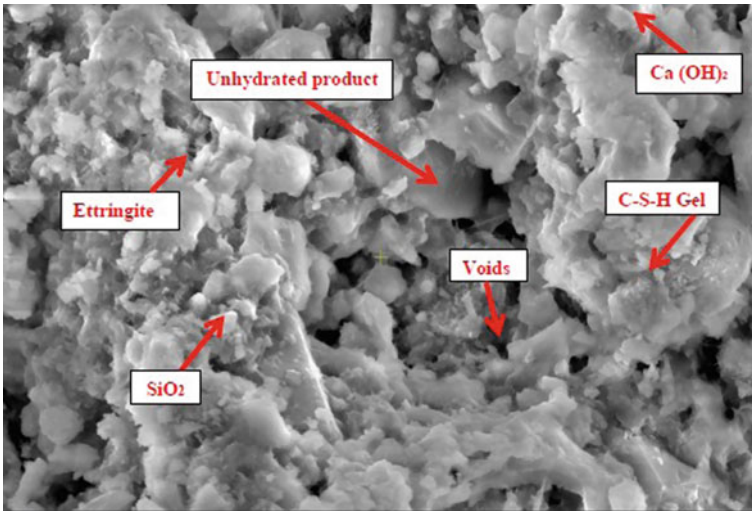


Fig. 8 5% butyl concrete

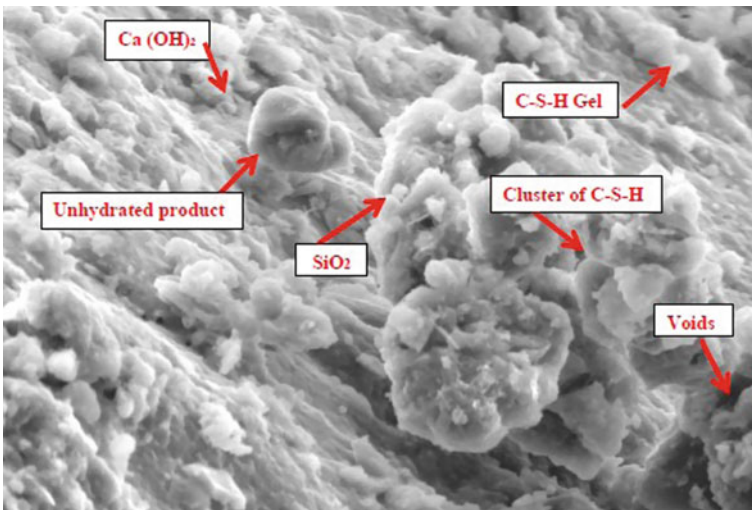


Fig. 9 10% butyl concrete

3.4 XRD Analysis

At the age of 28 days, concrete with varying percentages of butyl rubber as coarse aggregate was analysed using the X-ray diffraction method. XRD was used to determine the chemical phases using Panalytical X-Pert High Score Plus software. Diffraction angle 2 Theta measurements were made using XRD technology [13]. The

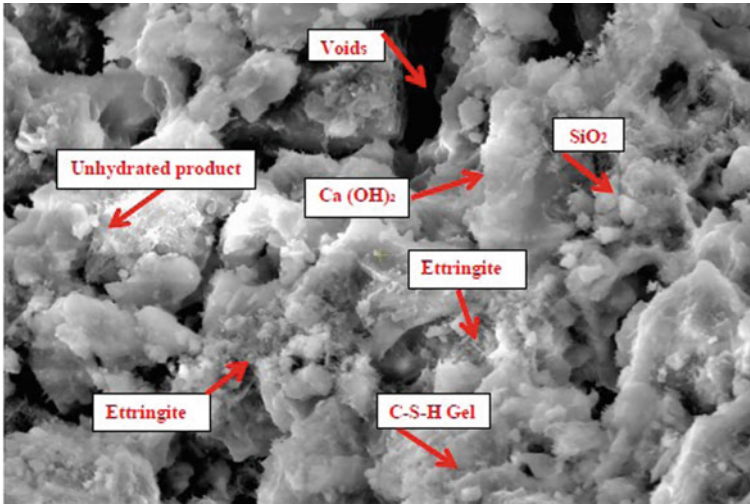


Fig. 10 15% butyl concrete

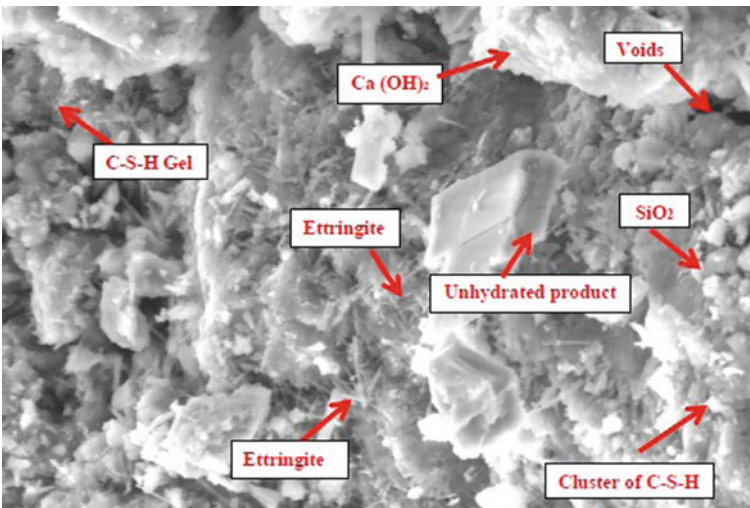


Fig. 11 20% butyl concrete

formation of CSH, SiO_2 , Ca(OH)_2 , CaCO_3 , and Ettringite is shown by the XRD pattern. C-S-H and Ca(OH)_2 are both significant constituents. Ettringite and calcite are insignificant components of crystalline materials. The butyl rubber concrete's XRD pattern resembles that of regular concrete as shown in Figs. 12, 13, 14, 15 and 16.

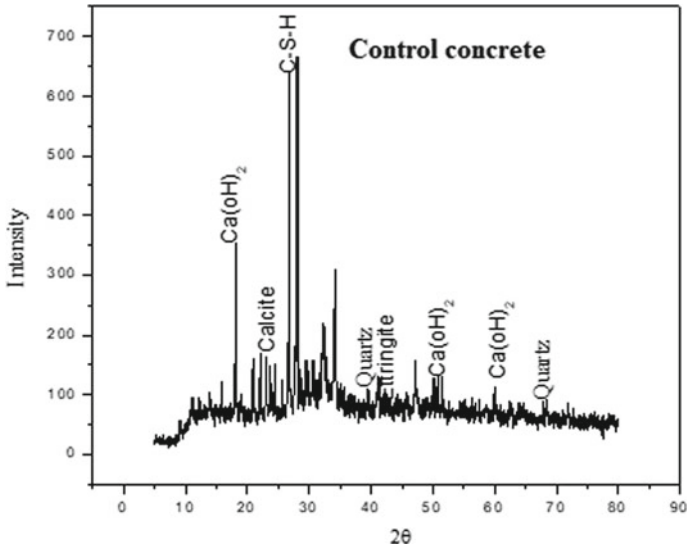


Fig. 12 Control concrete

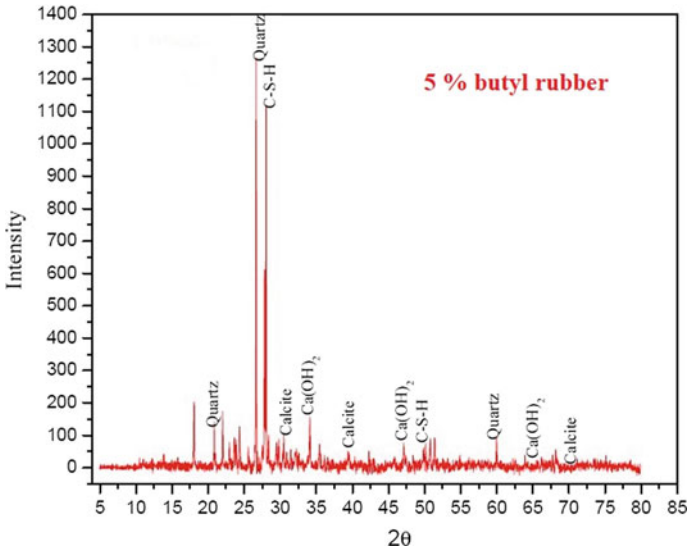


Fig. 13 5% butyl concrete

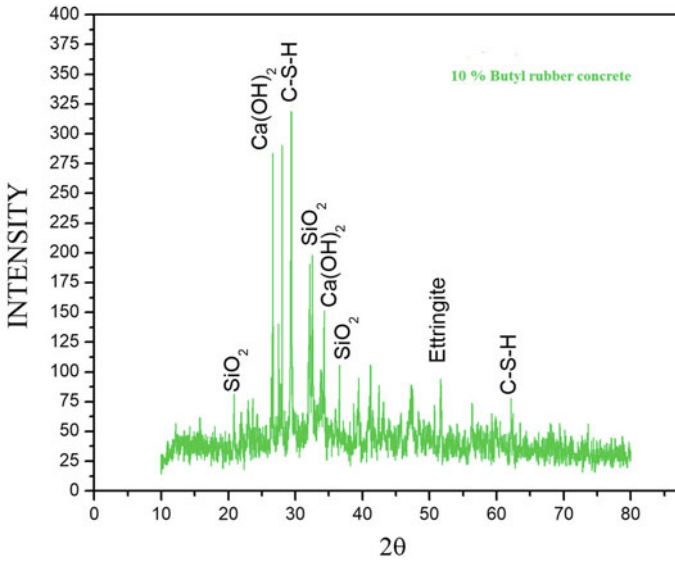


Fig. 14 10% butyl concrete

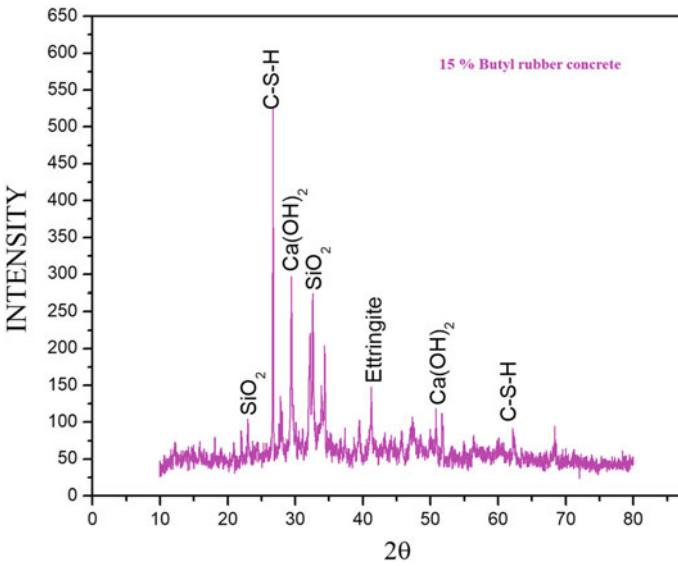


Fig. 15 15% butyl concrete

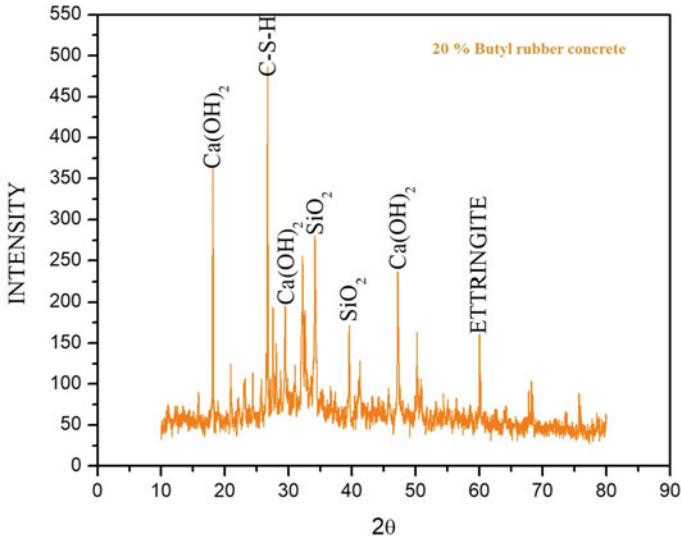


Fig. 16 20% butyl concrete

3.5 FTIR Analysis

As depicted in figure, FTIR analysis was done to look into the bond behaviour and bands of molecular groups found in different mixes [10]. The bands larger than 2000 cm^{-1} offered details regarding the hydration of cement paste. Conventional concrete and butyl rubber concrete have similar FTIR patterns as shown in Figs. 17, 18, 19, 20 and 21.

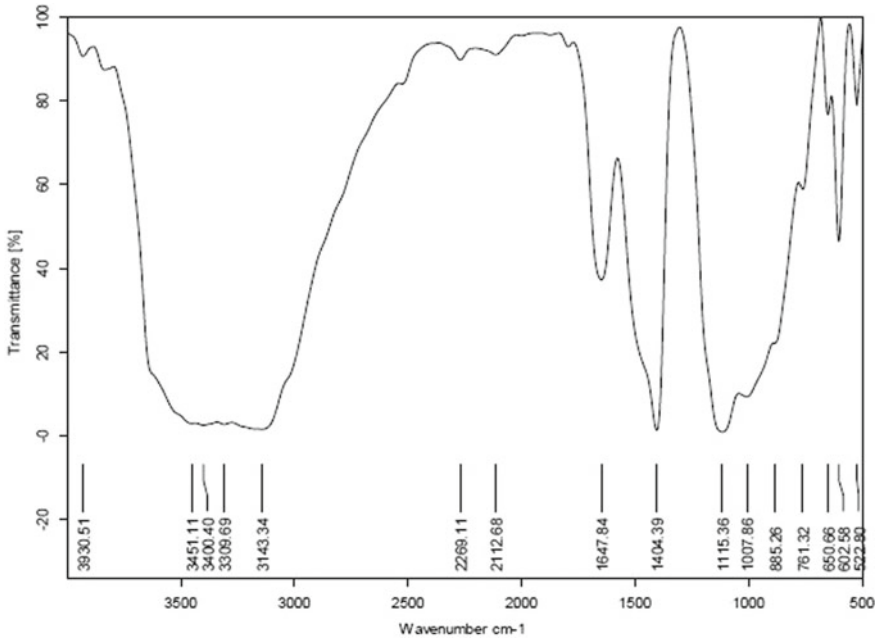


Fig. 17 FTIR in control concrete

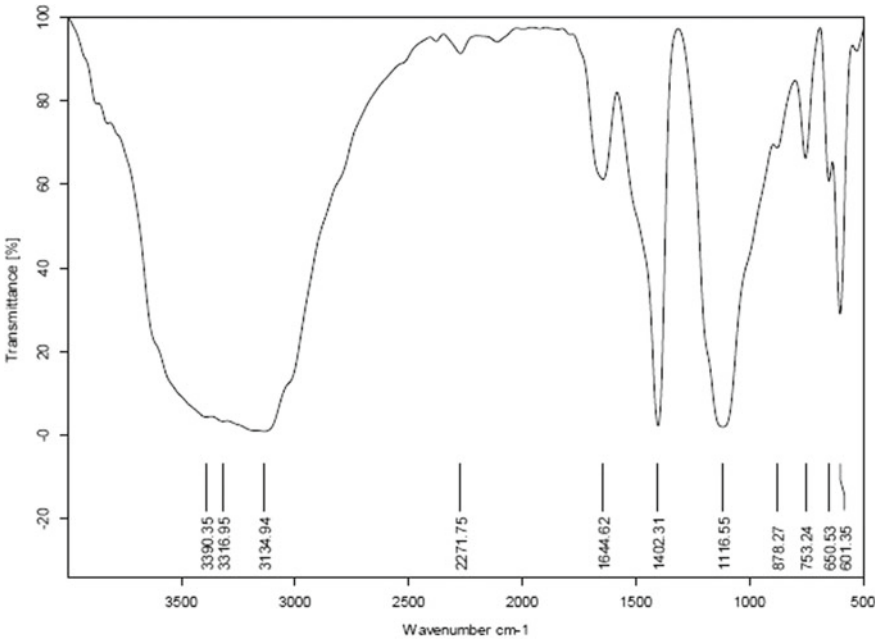


Fig. 18 FTIR 5% butyl concrete

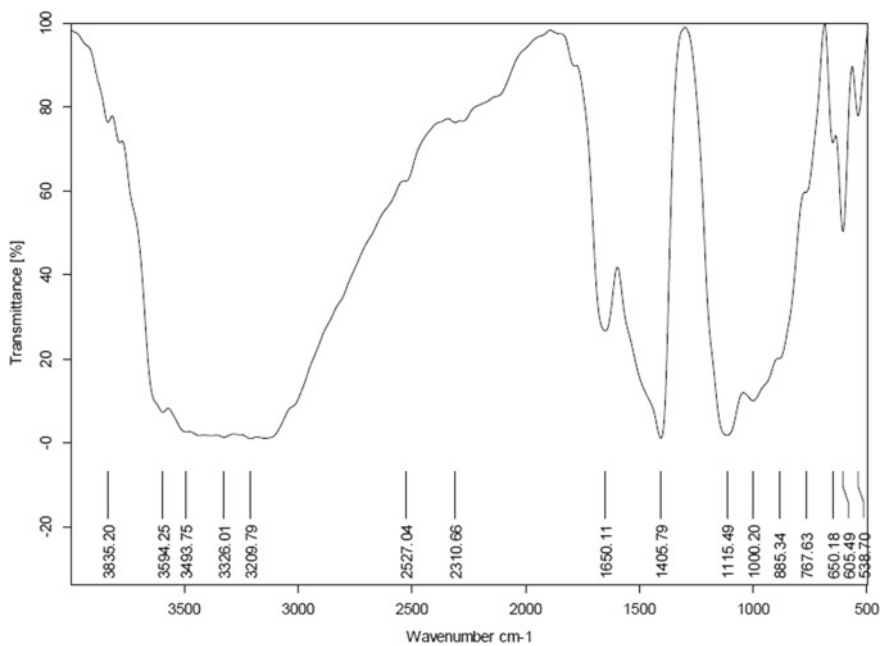


Fig. 19 FTIR 10% butyl concrete

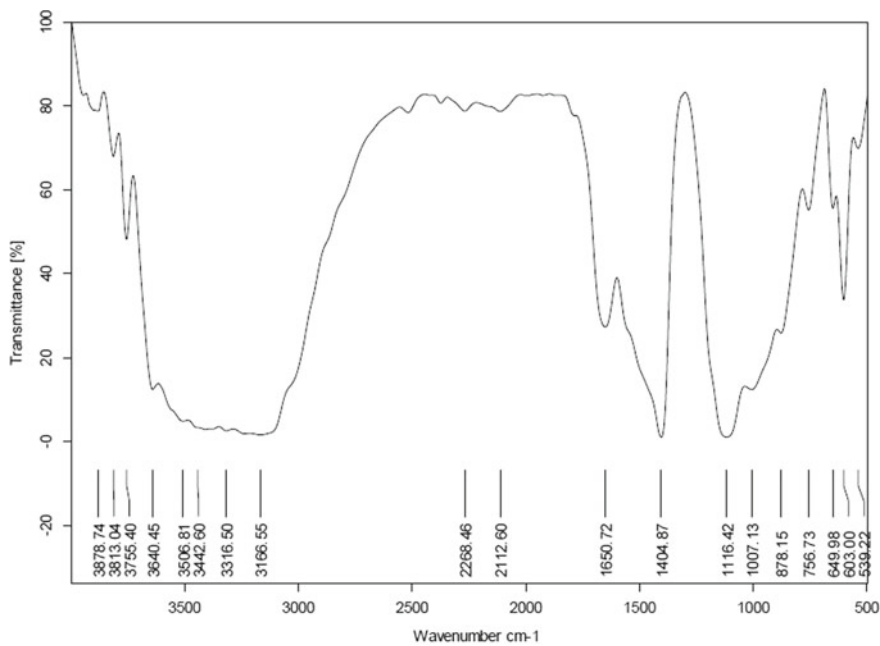


Fig. 20 FTIR 15% butyl concrete

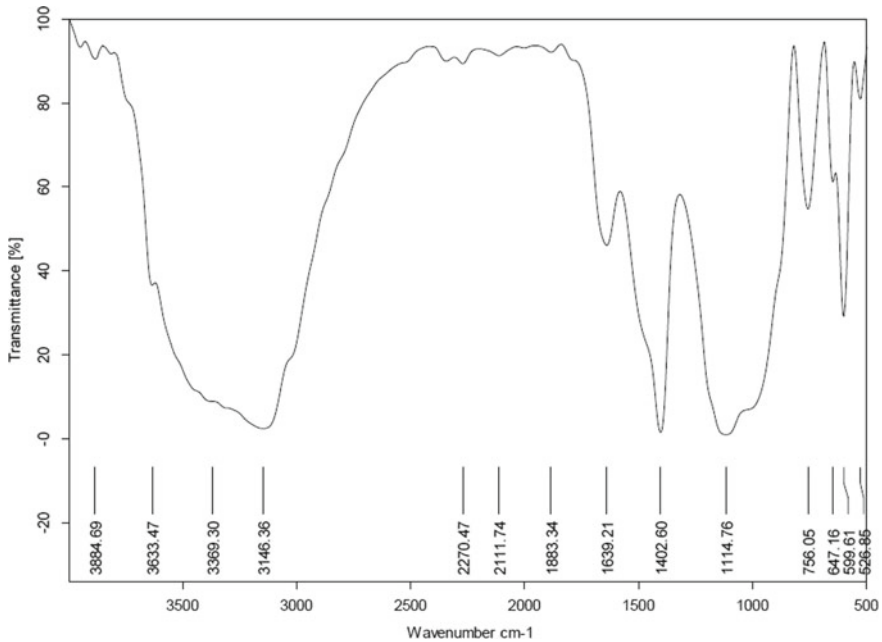


Fig. 21 FTIR 20% butyl concrete

4 Conclusion

- Butyl rubber concrete enhanced the compressive strength with the addition of 10% replacement level of butyl rubber.
- According to the test results, the area of cracks in plastic shrinkage decreases as the percentage of butyl rubber rises.
- This demonstrates the importance of butyl rubber in determining the degree of shrinkage of plastic and cracking concrete confidence.
- The butyl rubber concrete, as opposed to conventional concrete, lowering the plastic shrinkage area of crack.
- The SEM analysis of all mixes reveals the development of CSH gel and ettringite, which has a needle-like structure.
- The peak intensities of CSH, CaCO_3 , Ca(OH)_2 , and ettringite were visible in the XRD patterns of all mixtures.
- The butyl rubber used in concrete produced environmentally friendly concrete.
- The FTIR spectrum reveals the chemical bonding between the molecules with various wave lengths.

References

1. Ravichandran PT (2019) Investigation on grinding impact of fly ash particles and its characterization analysis in cement mortar composites. *Ain Shams Eng J* 10(2):267–274. <https://doi.org/10.1016/j.asej.2019.02.001>
2. Prakash Chandar S, Manivel S, Gunasekaran K, Jothiswaran A (2017) An experimental investigation of partial replacement of cement using micro silica and fly ash in production of coconut shell concrete. *Int J Civ Eng Technol* 8(4):1851–1859
3. IS 10262 (2009) Guidelines for concrete mix design proportioning. Bureau Indian Standard Delhi, pp 1–14
4. IS 516 (2018) Method of tests for strength of concrete. Bureau Indian Standard, pp 1–30
5. Prakash Chandar S, Gunasekaran K, Prasanth K (2018) An experimental investigation and durability property on recycled concrete with partial replacement to fine aggregate in coconut shell concrete. *Rasayan J Chem* 11(2):702
6. IS-12269 (1987) Specifications for 53 grade cement. Bureau of Indian Standard
7. IS 383 (1997) For coarse and fine aggregate from natural sources of concrete
8. Gunasekaran K, Kumar PS (2008) Lightweight concrete using coconut shells as aggregate. In: Proceedings of the ICACC-2008. International conference on advances in concrete and construction, Hyderabad, India; 7–9 February 2008. pp 450–9
9. Gunasekaran K, Kumar PS (2008) Lightweight concrete mix design using coconut shell aggregate. In: Proceedings of the IBMSDCP-2008. International conference on innovations in building materials, structural designs and construction practices, Sathyamangalam, India, 15–17 May 2008. pp 375–82
10. Gunasekaran K, Kumar PS (2008) An agricultural waste as aggregate in lightweight concrete. In: Proceedings of the SEC-2008, sixth structural engineering convention, Chennai, India, 18–20 December 2008. pp 1079–87
11. Gunasekaran K, Kumar PS, Lakshmipathy M (2011) Mechanical and bond properties of coconut shell concrete. *Constr Build Mater* 25(1):92–98
12. Gunasekaran K, Kumar PS, Lakshmipathy M (2011) Study on properties of coconut shell as an aggregate for concrete. *Ind J Ind Concr Ins* 12(2):27–33. [6] Gunasekaran K, Kumar PS, Lakshmipathy M (2010) Compatibility studies on the coconut shell cement composites. *Ind J Ind Concr Ins* 11(1):27–31
13. Gunasekaran K, Annadurai R, Kumar PS (2012) Long term study on compressive and bond strength of coconut shell aggregate concrete. *Constr Build Mater* 28:208–215
14. Gunasekaran K, Annadurai R, Kumar PS (2013) Study on reinforced lightweight coconut shell concrete beam behavior under flexure. *Mater Des* 46:157–167
15. Shetty MS (2006) Concrete technology theory and practice. Chand and Company Ltd., New Delhi
16. Soroushian P, Mirza F, Alhozaimey A (1995) Plastic shrinkage cracking of polypropylene fiber reinforced concrete. *ACI Mater J* 92(5):553–560
17. Samman TA, Mirza WH, Wafa FF (1996) Plastic shrinkage cracking of normal and high-strength concrete: a comparative study. *ACI Mater J* 93(1):36–40
18. Wang K, Shah SP, Phuaksuk P (2001) Plastic shrinkage cracking in concrete materials— influence of fly ash and fibres. *ACI Mater J* 98(6):458–464

Numerical Investigation of Encased Composite Beams with Reinforcements Passing Through the Web Openings



L. Vaishnavi and N. Umamaheswari 

1 Introduction

Over the past few years, steel–concrete composite structures have grown quickly and have been utilized widely in construction. Composite structural elements are often used in the construction of modern buildings and bridges. The advantages of composite construction include reduced dead weight, increased overload capacity compared to a non-composite beam under static ultimate loads, and for a given load, decreased construction depth with associated cost savings. The composite members have advantages over typical steel and concrete beams like high rigidity, excellent fire resistance, and outstanding durability, which improves structural stability. The complexity of the design limited its construction in numerous ways, despite the composite structure’s advantages. Steel-profile covered in reinforced concrete is an Encased steel–concrete composite beam. Encased steel–concrete composite beam contributes to higher load carrying capacity as buckling of web and flange plates were prevented [1]. Incorporation of concrete leads to economical design, as the required quantity of steel could be reduced. Encasing steel profile in concrete has many advantages such as: Fire resistance, increased strength, good corrosion resistance, resistance against lateral torsional buckling and also resists impact loads [2, 3].

Functionality of composite beam depends on the interaction between steel and concrete. Bonding of concrete to steel attained easily in case of fully encased composite beams which accounts for better composite action [2–4]. For reducing the overall structural depth of the beam, an encased beam can be employed effectively. An increase in bending stiffness and local buckling stiffness considerably in encased composite beams compared to conventional beams [5]. In a fully encased

L. Vaishnavi · N. Umamaheswari (✉)

Department of Civil Engineering, Faculty of Engineering and Technology, SRM Institute of Science and Technology, Kattankulathur, Tamil Nadu 603203, India

e-mail: umamahen@srmist.edu.in

section, maximum strain seen in steel than in concrete. The encased beam showed high ductility than any other beam due to high percentage of steel area [4, 6]. To accommodate ducts and pipes, composite beams with web openings are frequently utilized in construction [7]. Though the presence of web opening limited the load carrying capacity of the beam due to Vierendeel failure mechanism, on encasing the steel profile with a reinforced concrete enhance the flexural performance of the composite beam [6]. Abdul et al. experimentally investigated the perforated steel and partially-encased composite simply supported beams which were self-connected. Eight samples of those to determine how different forms of openings (square, rectangle, and circular) and also encasing the same in concrete affect the performance of the beams has been evaluated [8]. Ye et al. determined how to lower the self-weight of partially encased hollow-core composite beams without sacrificing their bearing capability. Tests carried conducted to compare the thickness, grouting strength, and shear stud design of hollow core partially encased composite beams (HPEC) with partially encased composite beams (PEC [9]). Du et al. examined the effects of reinforcement on the web openings and behaviour when the stiffeners' type and cross-sectional area were altered. The reinforced web openings in the composite beams exhibited good mechanical properties as well as the ductility performance [7].

Djebli et al. considered the Vierendeel mechanism and find solution for determining deformations of cellular composite beams. Various loading characteristics and geometry are considered for the analytical study [10]. Satyarno et al. presented the full height rectangular opening castellated steel beams which were compared with and without a partial encasement of reinforced mortar. The opening in the web for entire height limited the load carrying capacity due to Vierendeel truss mechanism. By strengthening the web by encasing it in reinforced mortar, it might be stopped. The diagonal strut mechanism was recommended [6]. Yang et al. experimentally studied the shear strength of partially castellated steel-reinforced concrete beams investigating the effects of steel shape openings and shear span-to-depth ratios on shear performance. Compared to reinforced concrete beams, encased steel beams demonstrated less brittleness [11]. Liu and Chung studied the behaviour of steel beams with web openings of various shapes and sizes and observed similar yield patterns after failure (shear/flexure/Vierendeel mechanisms). The shear and moment resistances of a perforated section were controlled by the opening depth, but the effect of local Vierendeel moments acting on the tee-sections was controlled by the critical opening length of the web opening [12]. The present work investigates the influence of steel profile with various dimensions of web openings, encased in a reinforced concrete beam. The effect of shape and size of web opening has been compared with a composite beam without web opening. A simulated beam demonstrated the flexural behaviour of encased steel-concrete composite beam. Numerical results were interpreted for assessing the performance of encased beams.

2 Beam Specifications

2.1 Material Properties

Material properties for the numerical analysis were chosen from available literature. Mid-range steel beam sections chosen was UB 457 × 152 × 60 kg/m [12] and UB 356 × 171 × 51 kg/m. The elastic modulus of the concrete (E_c) was 31,300 MPa. Elastic modulus of steel profile and reinforcing steel was taken as 273,500 and 360,000 MPa respectively. Elastic modulus of transverse bars was taken as 2×10^5 MPa. Poisson's ratio of concrete and steel was taken as 0.17 and 0.3, respectively.

2.2 Beam Models

Analysis was carried out for three group of beam models; each group consists of two models. Both the beam models have web openings, one was provided with steel reinforcements passing through the openings and the other was not provided with reinforcement. In addition, a control beam without web opening was analysed for comparative study. The total span of the models is 2000 mm (as shown in Fig. 1), of which 1000 mm is the pure bending zone and 900 mm is the shear span. The control beam and the other six beam models of same rectangular size 202 × 507 mm. Steel section UB 457 × 152 × 60 kg/m was selected, where thickness of flange and web were 13.3 and 8.1 mm respectively. Further, the analysis was carried out for reduced steel section where the control beam and the other six beams had the same size 220 × 405 mm. Steel section UB 356 × 171 × 51 kg/m was selected, where thickness of flange and web were 11.5 and 7.4 mm respectively.

2.3 Modelling of Composite Beams

To simulate the required encased steel–concrete composite beams with different web opening configurations for performing finite element analysis, as indicated in Fig. 2 and Table 1, Abaqus 6.14–5 was used. The web was cut in solid I-steel beam model with an extrusion cut option to create the apertures. Web openings were kept at 50 and 26.95 mm from the flange plates for UB 457 × 152 × 60 kg/m and UB 356 × 171 × 51 kg/m respectively. Linear patterning was used to keep the symmetry of the web openings throughout the beam. Both concrete encasement and steel section was composed of C3D8R elements. T3D2 element was used for the reinforcement part.

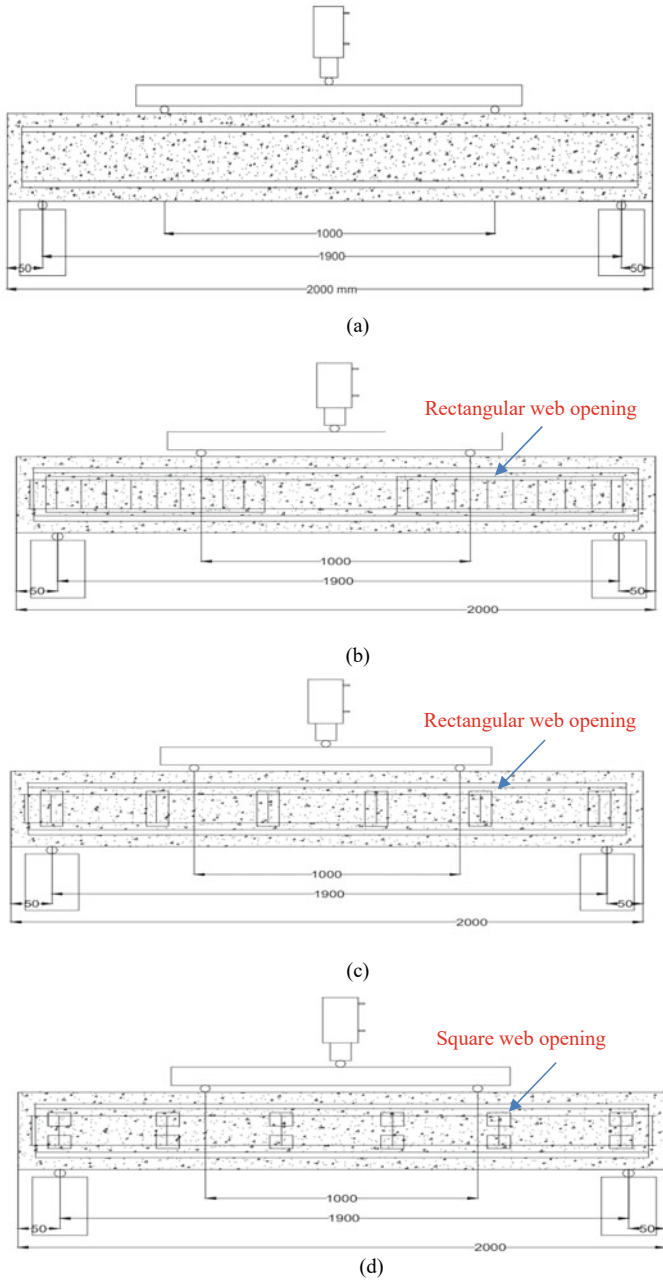


Fig. 1 Schematic representation of beam models a S1 b S2 c S3 d S4

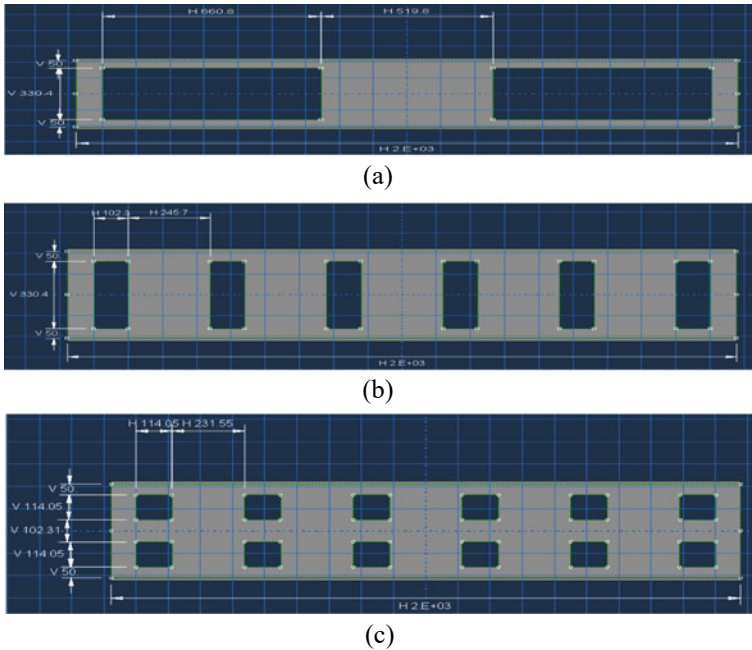


Fig. 2 Modelling of beams using Abaqus 6.14–5 a S2 b S3 c S4

Table 1 Dimensions of the web openings

Model	No. of openings	Dimensions of the web openings			
		UB 457 × 152 × 60 kg/m		UB 356 × 171 × 51 kg/m	
		Breadth (mm)	Depth (mm)	Breadth (mm)	Depth (mm)
S1	0	No openings		No openings	
S2	2	660.80	330.40	556.00	278.00
S3	6	102.30	330.40	86.90	278.00
S4	12 (two rows)	114.05	114.05	114.05	114.05

3 Finite Element Analysis

3.1 Analysis of Encased Composite Beam Without Web Openings

Abaqus 6.14–5 was used to analyse a steel–concrete composite beam without web openings. The concrete beam model of size 202 × 507 mm with the steel profiles, UB 457 × 152 × 60 kg/m or UB 356 × 171 × 51 kg/m, with the same sections preferred for both composite beams with and without web openings. The steel profile was

placed with a 25 mm cover. The embedded portion of the concrete and steel profile was constrained to allow for interaction. The beam model is of 2000 mm overall span with a 1000 mm pure bending zone and a 900 mm shear span.

3.2 Analysis of Encased Composite Beam with the Reinforcements Passing Through the Web Openings

Abaqus 6.14–5 was used to analyse steel–concrete composite beam with various dimensions of web openings. Dimensions of concrete beam models were 202×507 and 220×405 mm. The steel profiles chosen for composite beam are UB 457 \times 152 \times 60 kg/m and UB 356 \times 171 \times 51 kg/m. The steel profile was placed with a 25 mm cover. The longitudinal reinforcement and stirrups of 12 and 8 mm diameter was provided. During the assembly of the components, the web apertures were designed to allow the steel reinforcements to flow through. The concrete and steel reinforcements were given constraint of embedded region for interaction with each other and a coupling constraint was applied for having interaction of steel profile with concrete. The overall span of beam is similar to previous case. Shear span to depth ratio was 1.78 (lesser than 2.0) (Figs. 3, 4 and 5).

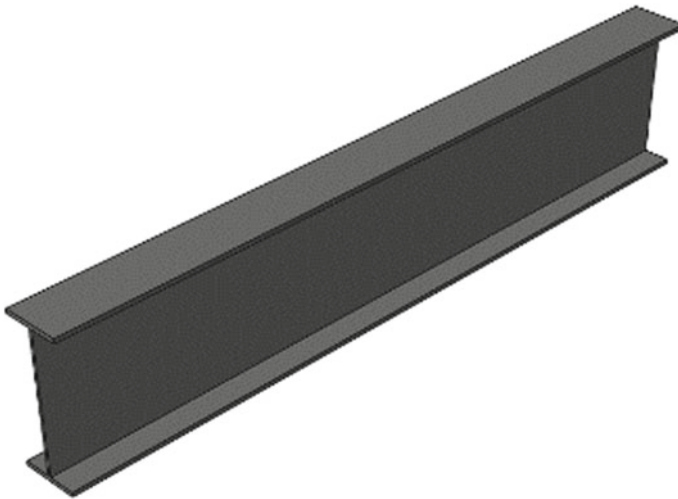


Fig. 3 Steel profile without web openings

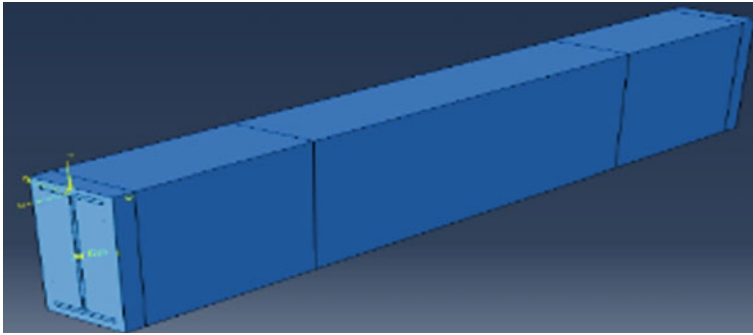


Fig. 4 Encased composite beam without web openings

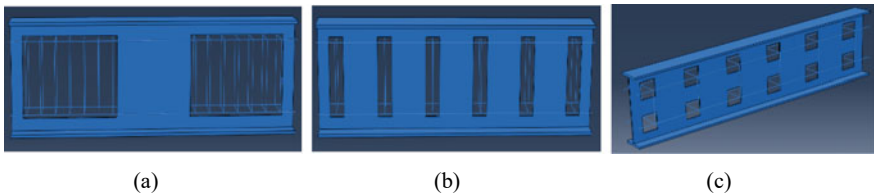


Fig. 5 Steel Reinforcements passing through the web openings **a** rectangular web openings ($B = 2D$) **b** rectangular web opening ($D = 3.2B$) **c** square web opening ($D = 3.2B$)

4 Results and Discussion

4.1 Convergence Study

The convergence was applied for various mesh sizes and graph is created by using the load versus displacement results for each size, as illustrated in Fig. 6. The findings of this mesh sensitivity analysis demonstrate that at element sizes of 20 and 15 mm, the load versus deflection curves converge and a global seed size of 20 mm was chosen.

4.2 S1- Encased Steel–Concrete Composite Beam (Without Web Opening)

The behaviour of an encased steel–concrete composite beam under two-point loading is shown in Fig. 7a–e, computed for a mesh size of 20 mm. For an allowable deflection of 25 mm, load capacity of 418.44 kN was observed.

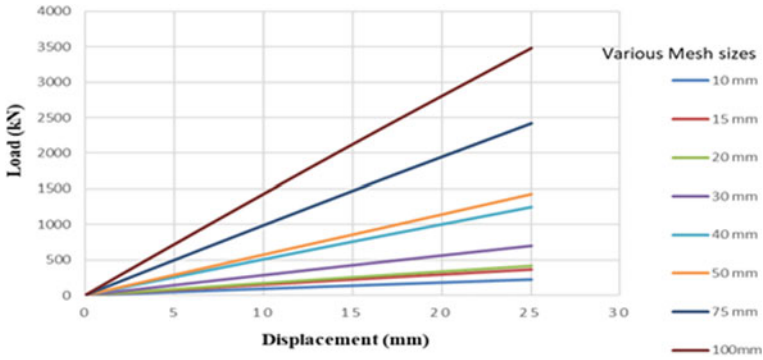


Fig. 6 Convergence study

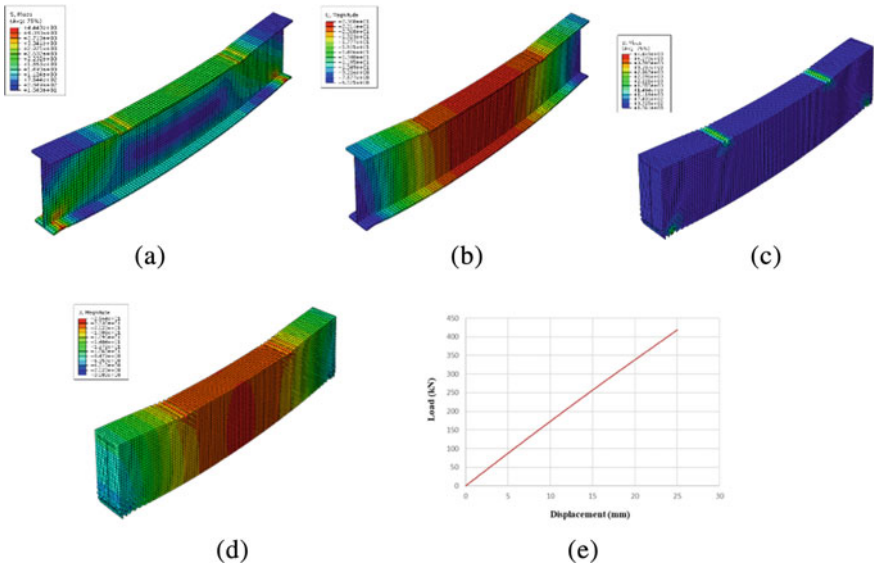


Fig. 7 Results for S1 a stress diagram-steel profile b displacement diagram-steel profile c stress diagram for S1 d displacement diagram for S1 e Load versus Displacement for S1

4.3 S2-Encased Steel-Concrete Composite Beam (Rectangular Opening, $B = 2D$)

Steel profile with rectangular web openings, whose breadth is twice the depth, reinforced with longitudinal bars and stirrups passing through the openings has been analysed. Stress diagram for S2, for steel profile with rectangular web openings and for steel reinforcements are shown in Fig. 8e, a and c, respectively. For S2, maximum stress concentrations were seen under the loading points. Displacement diagram for

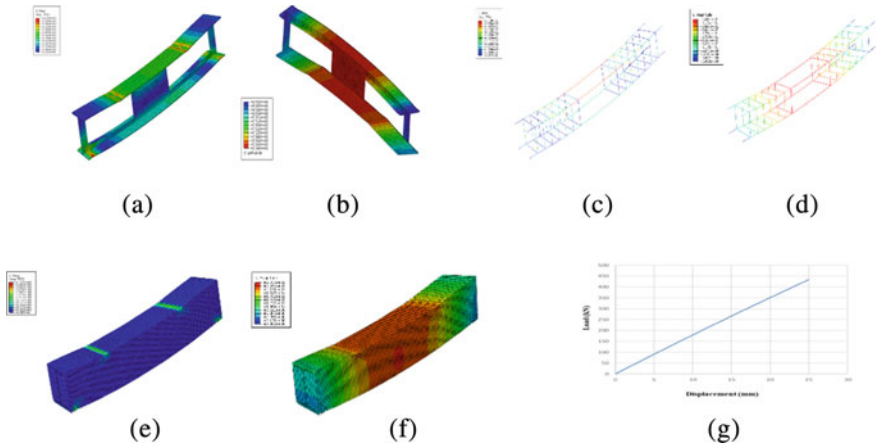


Fig. 8 Results for S2 **a** stress diagram-steel profile **b** displacement diagram-steel profile **c** stress diagram-steel reinforcements **d** displacement diagram-steel reinforcement **e** Stress diagram-S2 **f** displacement diagram for S2 **g** load versus displacement for S2

S2, for steel profile with rectangular web openings and for steel reinforcements are shown in Fig. 8f, b and d respectively. Reduced post buckling in the web of the steel section due to compressive stresses induced by shear transfer along the length of the beam is depicted in Fig. 8b. Maximum deflection was found in the pure bending region. The load versus displacement results is obtained as shown in the Fig. 8g. For 25 mm deflection, maximum load of 433.80 kN was obtained.

4.4 S3-Encased Steel–Concrete Composite Beam (Rectangular Opening, $B = 3.2D$)

Steel profile with rectangular web openings, whose breadth is 3.2 times the depth, reinforced with longitudinal bars and stirrups passing through the openings has been analysed. Stress diagram for S3, for steel profile with rectangular web openings and for steel reinforcements are shown in Fig. 9e, a and c respectively. Maximum stress concentrations were seen at ultimate load (443 kN). Displacement diagram for S3, for steel profile with rectangular web openings and for steel reinforcements are shown in Fig. 9f, b and d respectively. The load versus displacement results is obtained for linear hexahedral 20 mm mesh size as shown in the Fig. 9g.

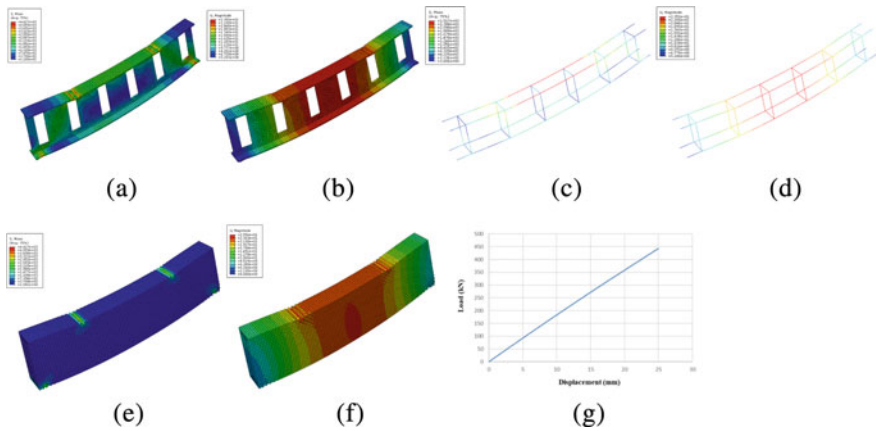


Fig. 9 Results for S3 **a** stress diagram-steel profile **b** displacement diagram-steel profile **c** stress diagram-steel reinforcements **d** displacement diagram-steel reinforcement **e** stress diagram-S3 **f** displacement diagram for S3 **g** load versus displacement for S3

4.5 *S4-Encased Steel-concrete Composite Beam (Square Opening, $B = D$)*

Steel profile with unique arrangement of square web openings and reinforced with longitudinal bars and stirrups passing through the openings has been analyzed. Stress diagram for S4, for steel profile with rectangular web openings and for steel reinforcements are shown in Fig. 10e, a and c respectively. S4 had a similar stress distribution to S3 along the length of the beam, where the maximum load (442 kN) increased from the normal steel profile with the Vierendeel failure mechanism and web post buckling. As a result, S4 contributes to slower yielding as compared to standard steel sections. Displacement diagram for S4, for steel profile with rectangular web openings and for steel reinforcements are shown in Fig. 10f, b and d respectively. The load versus displacement results is obtained for linear hexahedral 20 mm mesh size as shown in the Fig. 10g.

4.6 *Comparative Study*

The findings of linear finite element model for an encased composite beam with web openings of various forms has been listed in Table 2.

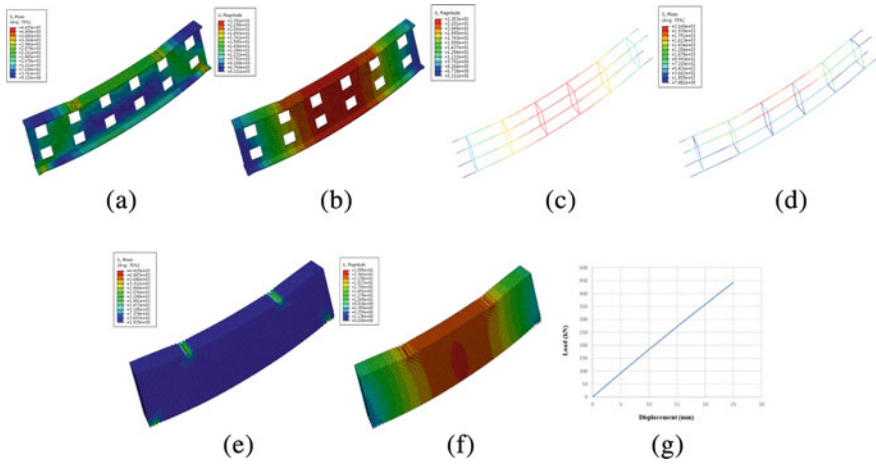


Fig. 10 Results for S4 **a** stress diagram-steel profile **b** displacement diagram-steel profile **c** stress diagram-steel reinforcements **d** displacement diagram-steel reinforcement **e** stress diagram-S4 **f** displacement diagram for S4 **g** load versus displacement for S4

Table 2 Ultimate load of Encased Composite Beams

Model	Web opening	Load resisted, kN		
		UB 457 × 152 × 60 kg/m		UB 356 × 171 × 51 kg/m
		For reinforcement through web openings	No reinforcement	For reinforcement through web openings
S1	0	418.44		372.25
S2	2	433.80	405.12	314.44
S3	6	443.11	411.35	400.67
S4	12	442.80	413.25	300.40

5 Conclusion

The importance of encasing a steel beam with web openings is studied through the finite element analysis. Steel beam with web openings showed Vierendeel failure mechanism contributing to the formation of plastic hinges at the corner of the web openings which eventually reduces the ultimate load. This study revealed that encased steel–concrete composite beams had immense effectiveness thereby showing increase in load carrying capacity. Wider study of web openings and its varied configurations in a steel beam has been included. Longitudinal bars and stirrups passing through the web openings also improved the results.

The control beam, for which there are no web openings, can support a maximum load whereas for a reduced section it decreases as 11% for the same allowable deflection. The encased composite beam with steel reinforcements passing through the

web openings showed an increase in load carrying capability. For a square opening, with reinforcements passing through it showed an increase in load carrying capacity compared to control beam by 6% and for reinforcements passing through the openings in reduced section, a decrease in load carrying capacity is observed. For the opening, whose breadth is equal to 3.2 times the depth ($D = 3.2B$) and reinforcements passing through it showed increased load carrying capacity in both the cases.

References

1. Nakamura SI, Narita N (2003) Bending and shear strengths of partially encased composite I-girders. *J Constr Steel Res* 59(12):1435–1453
2. Sadik SN (2012) Strength and ductility of concrete encased composite columns. *Behav Steel Struct Seism Areas* 30(15):681–688. <https://doi.org/10.1201/b11396-102>
3. Rana MM, Lee CK, Al-Deen S, Zhang YX (2018) Flexural behaviour of steel composite beams encased by engineered cementitious composites. *J Constr Steel Res* 143:279–290. <https://doi.org/10.1016/j.jcsr.2018.01.004>
4. Kabir MI, Lee CK, Rana MM, Zhang YX (2020) Flexural behaviour of ECC-LWC encased slender high strength steel composite beams. *J Constr Steel Res* 173:106253
5. Tsavdaridis KD, D’Mello C, Huo BY (2013) Experimental and computational study of the vertical shear behaviour of partially encased perforated steel beams. *Eng Struct* 56:805–822. <https://doi.org/10.1016/j.engstruct.2013.04.025>
6. Satyarno I, Sulisty D, Heldita D, De Oliveira ATCR (2017) Full height rectangular opening castellated steel beam partially encased in reinforced mortar. *Proc Eng* 171:176–184. <https://doi.org/10.1016/j.proeng.2017.01.324>
7. Du H, Hu X, Shi D, Fang B (2021) Effect of reinforcement on the strength of the web opening in steel-concrete composite beam. *Eng Struct* 235:112038
8. Abdul A, Maarooof A, Abdullah JA, Kasim SY (2022) Performance of steel perforated and partially-encased composite self-connected beams. 34(4):703–717
9. Ye Y, Yao Y, Liao H, Xin L, Liu Y (2022) Flexural performance of hollow-core partially-encased composite beams. *J Build Eng* 45:103432
10. Djebli B, Kerdal DE, Abidelah A (2019) Additional and total deflection of composite symmetric cellular beams. *J Constr Steel Res* 158:99–106
11. Yang Y, Zhou P, Yao X (2021) Study on the shear capacity of partially precast castellated steel reinforced concrete beams. *IOP Conf Ser Earth Environ Sci* 676(1):289–302
12. Liu TCH, Chung KF (2003) Steel beams with large web openings of various shapes and sizes: finite element investigation. *J Constr Steel Res* 59(9):1159–1176

Study on Behavior of Plastic Road—A Case Study



K. Surya Prakash, T. M. Jeyashree, and M. A. Venkiteswaran

1 Introduction

Plastic uses have primarily modified each critical space of the economy today, from agriculture to packaging, and automobiles. Plastic is present everywhere in today's society and all kinds of consumer items are packaged, protected, served, and even disposed of with plastic waste. The effective utilization and disposal of plastic waste are required for environmental protection. One attention-grabbing approach currently being investigated is using such waste plastic to vary the bituminous mixes used for road pavement. Studies in the past recommend the utilization of plastic waste for the construction of road pavement [1, 2]. Plastic and bitumen bond well since both are byproducts of the oil industry. This mixture enhances the performance of the road during its lifespan by increasing durability and reducing potholes [3]. The roads also show more considerable resistance to damages caused by severe rains. Modified polymers should be processed individually since they will be noninheritable from waste plastic, which is reduced by many million tonnes worldwide every year. These plastics can enhance a number of the qualities of the hydrocarbon combination and conjointly address environmental issues. Bitumen treated with polymer provides performance-related benefits by improving the physical qualities of the bitumen without affecting its chemical composition [4]. Pollution and disposal problems are reduced if plastic wastes are adequately utilized in route road development.

Many research works in the past have utilized waste plastic for the construction of road pavement since 1990. Plastic is utilized in pavement in various forms, such as plastic waste coated aggregate [5–7], Polymer modified bitumen [4, 8–10], and aggregate replacement with plastic waste. Collins et al. (1998) studied the rheological characteristics of bituminous binders with asphalt mixtures [1]. Significant

K. Surya Prakash · T. M. Jeyashree (✉) · M. A. Venkiteswaran
Department of Civil Engineering, Faculty of Engineering and Technology, SRM Institute of
Science and Technology, Kattankulathur, Tamil Nadu 603203, India
e-mail: jeyashrm@srmist.edu.in

improvement in properties of bituminous concrete mixes with Polymer is observed compared with conventional bituminous concrete mixes [3, 11].

The present study is focused on studying the performance of plastic roads with waste containing polyethylene terephthalate (PET or PETE), polypropylene (PP), and High- and Low-density Polyethylene (HDPE and LDPE) and the behavior of conventional bituminous road and plastic road is studied using damage analysis. This case study contains information on generated plastic waste from Potheri, Kancheepuram and SRMIST, followed by soil testing, traffic analysis, and design of road pavement. This study also includes assessing the deflection and stress patterns of plastic and conventional roads using KENPAVE Software and examining the results.

2 Data Collection of Plastic Waste

All plastics are made of chemical compounds that contain carbon and hydrogen. Many of these compounds also include halogen and nitrogen. Polymers are shaped by small molecules referred to as monomers differing in the kinds of polymers from which they are formed. All plastics are classified into seven categories depending upon their composition. The amount of waste generated from the selected location varies from 28 to 33 kgs on typical days, and on average, 35 kg/day of plastic waste is collected daily. The detailed classification of wastes generated at SRMIST is given in Table 1, as shown.

The collected plastic waste contains disposable carry bags, thermal cups, and PET bottles. Among the plastic waste of approximately 60 kg collected from Potheri, the plastic waste with polystyrene, polypropylene, and polyethylene can be used for the construction of pavement due to its good binding properties [5]. From the available data, the following observations are made.

1. Total plastic waste generated = 50 to 60 kg
2. Amount of usable plastic = 49 kg (Polystyrene, Polypropylene, Polyethylene)
3. Amount of non-usable plastic = 11 kg (Poly Vinyl Chloride).

Approximately 49 kg of generated plastic waste can be utilized effectively to construct road pavement in the selected location.

Table 1 Amount of plastic disposal generated per day

S. No.	Location	Papers (kg)	Plastics (kg)	Metals (kg)	Others (kg)
1	SRMIST Campus Weekdays	61	28	2	441
2	SRMIST Campus Weekends	93	40	1	508
3	Around SRMIST Campus (Potheri)	65	60	4	1026

3 Traffic Analysis

It is essential to grasp the magnitude of traffic information needed or collected, which can then verify the sort of road to be adopted. An automatic count approach was accustomed to perform a three-day survey during this study. The traffic flow was recorded employing a video camera, and the traffic movements were recorded for the SRMIST lake view road. Following the recording, the number of vehicles passing was counted and recorded for each fifteen-minute interval. An average number of vehicles passing during peak hours are counted. The data obtained during this period, which encompasses both the morning and evening, is shown in Tables 2 and Tables 3. The data obtained from traffic analysis are used for the design of the pavement.

Table 2 Average number of vehicles passing during peak hours in the morning

Time (AM)	Day 1	Day 2	Day 3	Average
7:30–7:45	101	100	92	97
7:45–8:00	160	163	146	156
8:00–8:15	316	398	249	321
8:15–8:30	340	484	333	386
8:30–8:45	414	512	402	443
8:45–9:00	258	206	252	239
9:00–9:15	224	191	185	200
9:15–9:30	154	116	130	133

Table 3 Average number of vehicles passing during peak hours in the evening

Time (PM)	Day 1	Day 2	Day 3	Average
3:00–3:15	60	55	64	50
3:15–3:30	102	95	97	98
3:30–3:45	161	149	148	153
3:45–4:00	238	241	257	245
4:00–4:15	262	295	294	284
4:15–4:30	357	352	354	354
4:30–4:45	270	267	264	267
4:45–5:00	176	172	174	174

Table 4 Tabulation for sieve analysis

IS sieve no/ Particle size	Weight of soil retained (kg)	Percent retained	Cumulative percent retained (N)	Cumulative percent finer (100-N)
4.75 mm	0.1465	14.65	14.65	85.35
2.36 mm	0.1485	14.85	29.5	70.5
1.18 mm	0.2235	22.35	51.85	48.15
600 μ m	0.0990	9.9	61.75	38.25
300 μ m	0.1785	17.85	79.6	20.5
150 μ m	0.1595	15.95	95.55	4.45
75 μ m	0.0345	3.45	99	1
Pan	0.01	1	100	–

4 Soil Testing

Soil testing was carried out on samples taken from the SRMIST lake road. Tests were conducted to find the soil properties. Soil properties were used for designing pavement. Following were the tests performed.

4.1 Sieve Analysis

According to IS 2720 (Part 4)-1985 [12] sieve analysis was done to classify the soil type based on its grain size. Table 4 shows the result of sieve analysis.

The results obtained from the sieve analysis test are as follows:

1. Effective size $D_{10} = 0.21$ mm
2. Uniformity coefficient $C_u = 4.09$
3. Curvature coefficient $C_c = 0.51$.

The results determined that the soil was sand since 50% of the soil particles passed through the 4.75 mm IS sieve. The sand was rated poorly because its uniformity coefficient was less than 6, and its curvature coefficient was less than 1.

4.2 Standard Proctor Compaction Test

According to IS 2720 (Part 7)-1980 [13] standard proctor test was done to determine the optimum moisture content at which a given soil type becomes most dense and achieves its maximum dry density. The maximum dry density of the sample was 1.95 g/cc, and the optimum moisture content was 11.9%.

4.3 California Bearing Ratio Test

According to IS: 2720 (Part 16)-1987 [14] California Bearing Ratio (CBR) test was conducted, and the test was performed with an optimum moisture content of the soil. As confirmed by IS Standards, the test results were consistent, with the CBR value of the collected soil sample at 2.5 mm penetration as 0.24% and 5-mm penetration as 0.28%.

5 Design of Pavement

The design was carried out using relevant data and equations from IRC: 37-2001 [15]. The design is carried out based on the computation of design traffic as given in Eq. 1.

$$N = \frac{365 \times [(1 + r)^n - 1]}{r} \times A \times D \times F \quad (1)$$

where, N —The cumulative number of standard axles to be catered for in design in terms of MSA.

A —Initial traffic in the year of completion of construction in terms of the number of commercial vehicles per day = 300 cv/day.

D —Lane distribution factor = 0.75 (Type of road: Two-lane single carriage way).

F —Vehicles damage factor = 3.5 [15]

n —Design life in years = 15 years.

r —Annual growth rate of commercial vehicles = 0.075.

The value of N is obtained as 7.5 MSA. For a CBR value less than 2%, the design should be based on a subgrade CBR value of 2%, and a capping of 150 mm thickness of the material is required [15]. The pavement design catalogue for Traffic range 1–10 MSA was used for the present study. The designed thickness of pavement and wearing course obtained are as follows:

Total pavement thickness = 822.5 mm (excluding 150 mm capping).

Wearing course = 33 mm BC.

Binder course = 85 mm DBM.

Granular base = 250 mm.

Granular sub base = 455 mm.

Hence, designed total thickness of the road is 972.5 mm including capping. Thickness of base course is 250 mm; sub base course is 455 mm and wearing course is 33 mm BC.

6 Analysis Using KENPAVE Software

The analysis of bitumen roads and plastic roads was done by using KENPAVE software. Input parameters like the Modulus of elasticity, Poisson's ratio, the thickness of layers, contact radius, contact pressure, load groups, and tolerance factor must be given for pavement analysis. Figure 1 shows the basic input parameters that need to be known for analyzing the pavement. The input parameters for plastic road and bitumen road were varied with respect to the modulus of elasticity and Poisson's ratio of pavement layers.

As an initial step, validation of model is done by comparing the graphical output with manual calculation for vertical and horizontal stresses and strains. The steps involved in the KENPAVE analysis are as follows:

- a. Assigning general information
- b. Assigning the z co-ordinates
- c. Assigning Layer thickness and Poisson's ratio
- d. Assigning load information
- e. Analysis of pavement
- f. Validation of model by comparing the graphical output with manual calculation.

Three-layer pavement structure with 300 mm thick bitumen layer and 150 mm crushed stone road-base was considered for the validation. CBR value of the subgrade

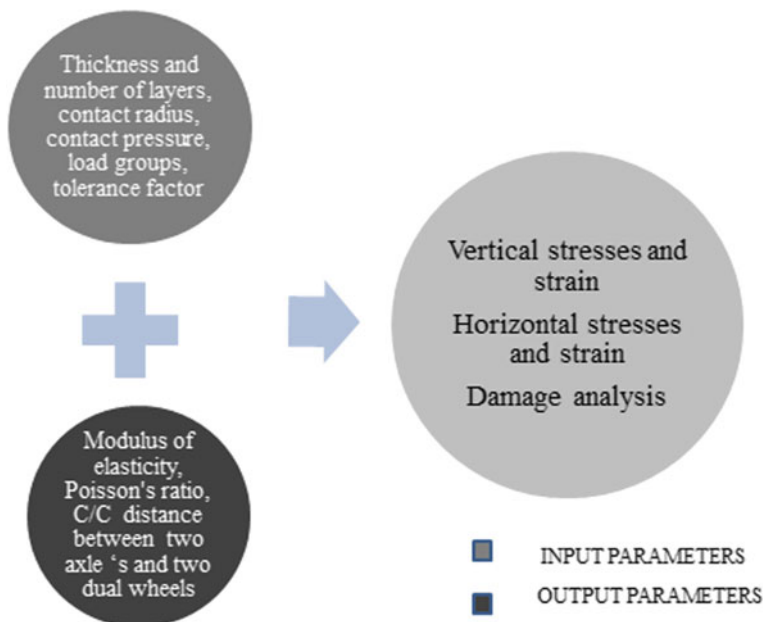


Fig. 1 Input and output parameters for pavement analysis

Table 5 Validation of KENPAVE model

Description	Calculated	Software	Error%
Vertical stresses (kN/m ²)	Layer 1: 17.06	Layer 1: 17.074	0.082
	Layer 2: 10.115	Layer 2: 10.120	0.049
Horizontal stresses (Top) (kN/m ²)	Layer 1: - 324.85	Layer 1: - 325.092	0.074
	Layer 2: - 5.35	Layer 2: - 5.342	- 0.14
Vertical strain	Layer 1: 0.000170	Layer 1: 0.0001711	0.64
	Layer 2: 0.000155	Layer 2: 0.0001546	- 0.25
Radial strain	Layer 1: - 0.0000855	Layer 1: - 0.0000855	- 0.046
	Layer 2: - 0.000077	Layer2: - 0.00007731	- 0.40

is 5 and a single wheel load with a tyre pressure of 0.5 MN/m² was applied over a circular contact area of 120 mm radius. The vertical stresses and strain, horizontal stresses, and the radial strain was calculated manually for the given input parameters. The obtained values are compared with the graphical output obtained from KENPAVE. Table 5 shows the % of error for the developed KENPAVE model.

7 Comparison on Performance of Plastic and Bitumen Road

As an initial step, general information was assigned for both plastic and bitumen road. The material type of the pavement layers was considered linear, the number of periods was assigned as 1 period per year, the number of load groups was taken as 1, the tolerance factor was 0.001, the maximum number of cycles was taken as 80, and interface of the layer was considered as 0 since all the layers are bonded.

Table 6 shows the input parameters defined for both conventional and plastic roads such as layer thickness, Poisson’s ratio, and layer modulus. Layer thickness remains the same for both conventional and plastic roads whereas Poisson’s ratio and layer modulus differ [16]. For the present study, polymer-modified bitumen layers utilizing plastic waste were considered for the wearing course and binder course. Load information was entered according to the traffic analysis of the considered road and the bus was considered a commercial vehicle. The load was assigned as 1 for a single axle with a dual tyre. Contact pressure and contact radius were assigned with the values of 0.2225 m and 620.52 kN/m² respectively. The value for center-to-center spacing between two dual wheels along the y axis was assigned as 0.005 m. The value for center-to-center spacing between two axles along the x-axis was given as 6 m.

Table 7 shows the comparison of the performance of bitumen roads and plastic roads at the vertical coordinates 0, 3.27, 11.7, 36.7, and 82.3 based on vertical stress and vertical deflection, and Fig. 2a, b shows the graphical representation of the

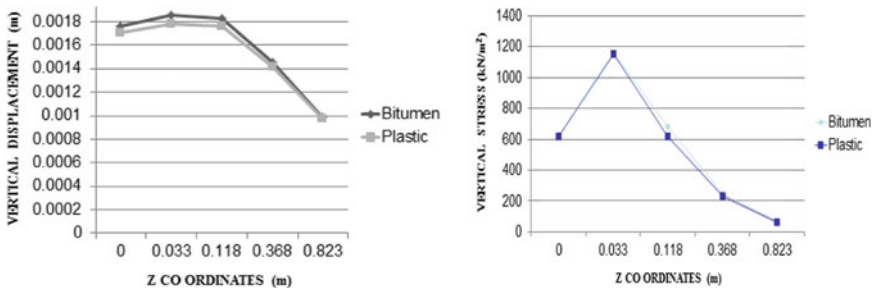
Table 6 Input parameters for analysis

Layer	Thickness (m)	Poisson's ratio		Layer modulus (N/mm ²)	
		Bitumen road	Plastic road	Bitumen road	Plastic road
Wearing Course	0.033	0.35	0.4	3000	3000
Binder Course	0.085	0.35	0.4	4000	6000
Granular Base	0.25	0.4	0.4	300	300
Granular Sub Base	0.455	0.4	0.4	150	150
Subgrade	∞	0.4	0.4	80	80

comparison of analysis results for vertical displacement and stress. The difference on basis of the vertical stress between the bitumen and plastic roads is about 63.448 kN/m² and vertical displacement is 0.0000634 m.

Table 7 Comparison of results

Points	Vertical coordinate	Type of road	Vertical stress (kN/m ²)	Vertical displacement (m)
1	0	Bitumen	620.520	0.0017585
		Plastic	620.520	0.0017038
1	3.27	Bitumen	1157.583	0.0018518
		Plastic	1150.244	0.0017810
1	11.7	Bitumen	684.091	0.0018271
		Plastic	620.648	0.0017637
1	36.7	Bitumen	244.4	0.0014511
		Plastic	230.411	0.0014184
1	82.3	Bitumen	68.112	0.0009901
		Plastic	66.352	0.0009768



a) Vertical displacement for bitumen and plastic road

b) Vertical stress distribution for bitumen and plastic road

Fig. 2 Comparison on vertical displacement and vertical stress distribution

Table 8 Comparison of design life

Output	Bitumen roads	Plastic roads
Design life (years)	7.19	8.06

7.1 Damage Analysis

Damage analysis is the type of analysis done on the pavements for calculating the approximate design life. Following were the steps carried out for the damage analysis.

- a. Assigning number of layers with bottom tension
- b. Assigning number of layers with top compression
- c. Assign values for fatigue coefficients and permanent deformation coefficients
- d. Assign total number of load repetitions for each load group during each period
- e. Damage analysis of pavement.

Fatigue coefficients for damage analysis F1, F2, F3, F4, and F5 were assigned as 0.0796, 3.291, 0.854, 1.365×10^{-9} and 4.477 respectively as per Asphalt Institute Model. Design life was obtained as output from the damage analysis. For damage analysis, each year was divided into 12 periods, and each period was given different load groups with the maximum value of 12. The damage from fatigue cracking, and irreversible deformation in each period across all load groups were added together to determine the design life. Damage analysis was performed for both plastic road and bitumen road. Table 8 shows the comparison on durability of both bitumen roads and plastic roads on the basis of design life. The comparison shows that the design life of plastic roads is almost 1 year more than the bitumen roads.

Based on the performance analysis using KENPAVE software, it is observed that durability of plastic road is higher, and it is expected to have design life one year more than the conventional road for the selected site location. The amount of bitumen required for the construction of the lake view road at Potheri, 0.5 km in length and 7 m in width is 52650 kg approximately. The percentage of plastic required for laying plastic road is 10% of the required quantity of bitumen and is 5265 kg approximately. As discussed in Sect. 2, approximately 49 kg/day of generated plastic waste can be utilized effectively to construct road pavement in the selected location.

8 Conclusion

The roads were designed manually in accordance with IRC specifications, considering the traffic data and soil testing results. The performance of the plastic and bitumen roads was compared with the KENPAVE software, and the following conclusions were arrived.

1. Plastic Roads has about 3.8% lesser vertical displacement and 9.2% lesser vertical stress than the bitumen road.

2. By performing damage analysis, the design life of plastic roads was found to be 1 year more than bitumen roads.

References

1. Collins JH, Bouldin MG, Gelles R, Berker A (1991) Improved performance of paving asphalts by polymer modification. *J Assoc Asphalt Paving Technol* 60:43–79
2. Verma SS (2008) Roads from plastics—point of view. *Indian Concr J*, pp 43–44
3. R. Vasudevan, R. Velkennedy, A. Ramalinga Chandra Sekar, B. Sundarakannan.: Utilization of waste polymers for flexible pavement and easy disposal of waste polymers. *International Journal of Pavement Research and Technology* 3(1) 34 – 42 (2010).
4. Ashok Pareek, Trilok Gupta, Ravi K. Sharma.: Performance of polymer modified bitumen for flexible pavements. *International Journal of Structural and Civil Engineering Research*, 1 (1) 77 – 86 (2012).
5. Amol S (2011) Bale: Potential reuse of plastic waste in road construction: A Review. *International Journal of Advanced Engineering Technology* 2(3):233–236
6. R. Vasudevan, A. Ramalinga Chandra Sekar, B. Sundarakannan, R. Velkennedy.: A technique to dispose waste plastics in an ecofriendly way – Application in construction of flexible pavements. *Construction and Building Materials* 28, 311 – 320 (2012).
7. Trimbakwala A (2017) Plastic Roads: Use of waste plastic in Road Construction. *International Research Journal of Scientific and Research Publications* 7(4):137–139
8. Huda Shafiq, Anzar Hamid.: Plastic Roads: A recent advancement in waste management, *International Journal of Engineering Research & Technology* 5(9) 684–688 (2016).
9. Akhilesh Yadav, Ruchi Chandrakar.: Construction of plastic roads: An effective way to utilize wastes. *International Journal of Engineering Research and Technology* 4 (11) 650–652 (2017).
10. Shabnum Masood, Ajay kumar Duggal, Shabina Masoodi, Gulam Mahi ud din Rather.: Evaluating structural integrity of plastic roads and their cost comparison with bituminous pavements. *International Journal of Multidisciplinary Educational Research* 10, 7(6). 77–81 (2021).
11. Sabina K, Tabrez A, Sangita, Sharma DK, Sharma BM (2009) Performance evaluation of waste plastic/polymer modified Bituminous concrete mixes. *J Sci Ind Res* 69:975–979
12. IS: 2720-Part 4. (1985). Methods of Test for Soils - Grain Size Analysis
13. IS: 2720-Part 7. (1980). Methods of Test for Soils – Determination of water content – Dry density relation using light compaction
14. IS: 2720-Part 16 (1987). Methods of Test for Soils – Laboratory determination of CBR
15. IRC: 37. (2001): Guidelines for the Design of Flexible Pavement.
16. Pereira, P.A., Pais, J.C., Azevedo, M.C.M.: Improvement of permanent deformation and fatigue life of bituminous mixtures by using modified bitumens (2000).

Holonic Construction Scheduling System for Construction Projects Using Python Programming Language



S. Gopinath and Rukhsar

1 Introduction

The complexity of a building project is commonly acknowledged. This is usually due to one or more of the following factors: physical restrictions, project scale, technical complexity, contractual agreements, client–consultant contractor interactions, and the project’s overall ‘one-off’ character [1]. Each project is distinct from the others, and the environment in which it takes place is always changing and evolving. The dynamic, turbulent, and complex nature of the construction industry leads to high uncertainty in construction projects and may adversely affect the performance of construction companies if uncertainty is not properly managed [2]. The primary goal of planning is to guarantee that things go as expected. This necessitates the establishment of goals, the identification of tasks, and the tracking of progress. The project schedule serves as the foundation for tracking progress and modifying the plan on a regular basis [3]. In practice, the timetable is disrupted throughout the implementation phase due to variable work and information flows [4].

The vast construction industry involves diverse kind of unique and unlike projects on which the stakeholders are working on. Each project is exclusive in terms of the activities involved, geographical factors, time, cost, materials availability, working power, and output. Not all projects has to schedule in the traditional way, so to provide differentiation among scheduling new methods of scheduling are introduced in construction industry. The commonly adopted project management approach is traditional plan-driven model, which sometimes is no appropriate approach to complex construction projects subject to successive changes, where more agile approaches might be more adequate [5]. The scheduling methods used widely in industry are CPM, PERT, LSM, LOB and CCM. All these methods have their characteristics,

S. Gopinath (✉) · Rukhsar

Department of Civil Engineering, Faculty of Engineering and Technology, SRM Institute of Science and Technology, Kattankulathur, Tamil Nadu 603203, India

e-mail: gopinats@srmist.edu.in

merit and demerits discussed in details. In order to provide freedom to the user to utilize any scheduling method irrespective of the type of project it's been applicable to give way to development of Holonic Construction Scheduling System (HCSS).

HCSS is a required scheduling system that gives project managers liberty to utilize the method which gives them the accurate result in the minimum duration. In HCSS, the concentration is to include all the constraints while scheduling a project unlike the traditional methods which had focus only in single constraint. HCSS include the characteristics of all the majorly used construction scheduling techniques that make it holon and user friendly.

2 Research Background

2.1 Time Management in Construction Industry

The project schedule is an estimate of how long it will take to complete the project. Time management is the act of tracking and regulating how much time employees spend on a project. Insufficient time management, procurement techniques, shareholder engagement, construction work planning, lack of software implementation, and poor site records are among the difficulties. As a consequence, these concerns may cause subtle delays, culminating in schedule and expense overruns, disagreements, litigation, and project termination [6].

Unlike traditional building scheduling in new structure scheduling, the construction sequence and accurate construction time of each component need to be specified in such component-level construction schedule, and the time unit of the schedule should be refined to hour or even minute [7]. In this situation, the critical path of the project is affected the most, hence any delay in critical activity may lead to project delay. However, a noncritical operation could still be harmed by a delay. Although the effect may not make the action important, it can still inflict financial damage.

2.2 Scheduling Methods

A construction business may use a number of schedules to reflect its construction plans in order to communicate its construction plans. As contemporary construction projects take place in a complex and dynamic environment, there is a need for project planning which concerns uncertainty from the early stages of a project life cycle [8]. The magnitude and complexity of the construction project, the preferences of the client who is developing the schedule, and the scheduling criteria specified in the contract all have an impact on the most appropriate scheduling strategy. In the construction industry, narrative schedules, Gantt charts or bar charts, linear schedules, and Critical Path Method (CPM) schedules are the most often utilised scheduling

tools. Apart from most commonly used scheduling methods PERT, LSM, LOB, and CCM are used under special conditions whenever required by the project manager. The use of scheduling tools assists the project manager in determining the available slack time between tasks and crucial routes for decision making over the course of the project. The scheduler manipulates and reschedules project activities based on this information in order to complete the project as efficiently as possible [9].

CPM and PERT are network-based scheduling methods used generally in determining the critical path, duration, and probability of project completion. LOB and LSM are used for repetitive scheduling projects, graphical scheduling is provided. Also, productivity rate and delivery rate is determined. In addition to critical path CCM uses explicit methods to eliminate resource conflicts. Consideration of uncertainties, Application of overlapping, Buffer size for particular situation, Multiple crew productivity rate, Time cost trade-off analysis are some of the common improvements discussed in the literatures. There is a significant distinction between an industrial scheduling challenge and a construction scheduling problem. This implies that not only resource information, but also 'site layout information,' such as the amount of space necessary for resources and the positioning of supplies, is required to arrange construction operations. Specifications, scheduling, resources, and other discipline-specific information should all be included in a comprehensive and integrated scheduling system [10].

2.3 Research Gap

The research gap which was determined from the study of all the scheduling methods in the construction project was that there is no single scheduling technique that can be used to schedule all the type of project. Each scheduling method has their own merits and demerits; effective strategies for arranging the best use of time and resources, running the project efficiently, and tracking progress [11]. The combination of all the method can strike out the limitations and result in the better scheduling system. The idea is to inculcate all the methods in a proper way to utilize its merits to maintain a time–cost trade off in it construction project. The research gap is explained in Fig. 1.

3 Methodology for Holonic Scheduling

To develop a Holonic scheduling system collaboration of all the existing scheduling techniques is done which will lead to the creation of a new system which can be developed using an interactive, interpreted, object-oriented, high-level programming language i.e. Python programming language. The methodology flowchart for HCSS development is shown in Fig. 2.

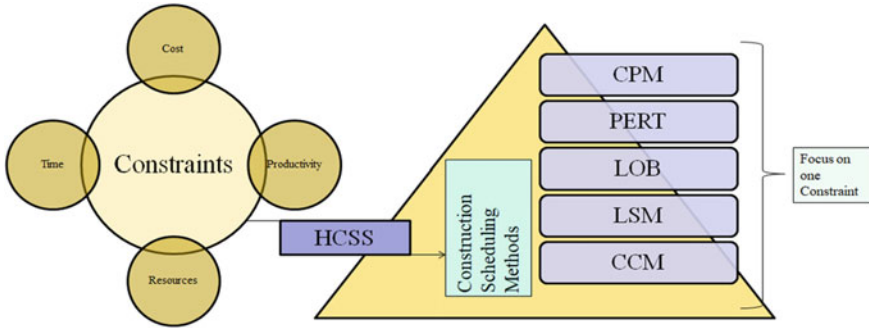


Fig. 1 Research gap and HCSS

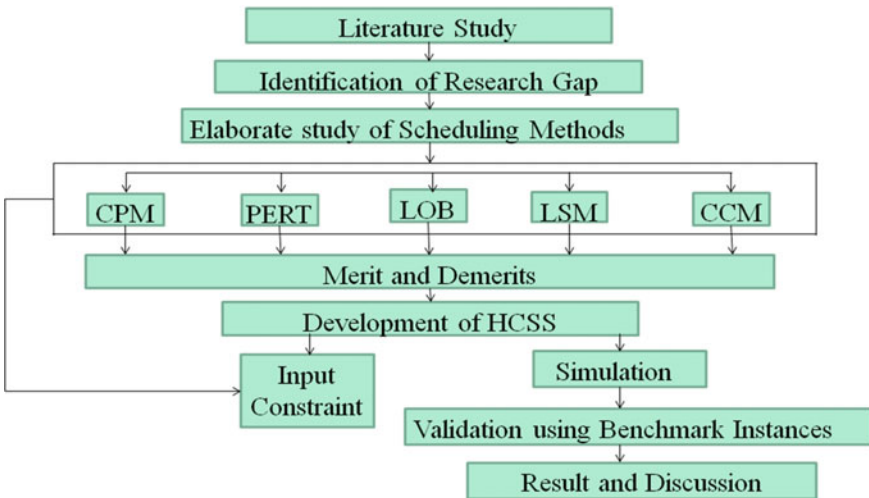


Fig. 2 Methodology flowcharts for HCSS

The methodology for HCSS is developed in various stages which include literature study at first. Taking HCSS development into consideration the constraints taken from them are as follows-

- Scheduling method concern with critical path.
- Scheduling method having probabilistic model.
- Scheduling method taking productivity rate into consideration.
- Scheduling method that provides proper resource allocation.
- Scheduling method that avoids procrastination.

Reading about the following factor has produced a requirement that has helped in identifying research gap in scheduling methods already existing. The concept which was developed by learning the research gap was that to produce a method that will

look into all the aspects of construction and work on all the constraints to produce and time–cost trade-off. So the idea is to develop a method suitable for all the different types of projects in construction industry and use it at a single interface all at a time. This will help to recovery the research gap which was created due to various scheduling methods and their demerits.

The elaborate study on scheduling methods, that is, CPM, PERT, LSM, LOB, and CCM is done on the basis of some factors in consideration these are as follows—How it works or Methodology, Merits, Demerits, Inference, Usability, Input, Output and Future Considerations.

Development of HCSS is after determining the data to be used from existing scheduling systems. This is to be done analytically, hence the open source Python programming language is proposed to make the interface which will help user to easily use the product for their usage. The product model is made by simulating various input data set for all the scheduling methods the coding part involved have various basic and advance codes that is executed to find the outputs the scheduling methods.

3.1 Analytical Study

Detailed study of all the scheduling method using a numerical example is done on the MS Excel to determine the working principle and calculative measures of the methods individually. The numerical involves different types of activities which are unique and repetitive in nature. The analytical study on MS Excel is first step for the development of HCSS, as turning the tradition calculations into soft computations. Once the input data, calculative data and output data are verified in MS Excel next Python Programming Language comes into process. The computations were done using basic formulas of MS Excel like SUM, AVERAGE, IF and some basic arithmetic operations like +, −, *, /, <, >, =. All these make the computation easier and within few steps determination of results. When MS Excel is used the calculation med to be performed by the user at each and every step but the concept is to make the process easier and computation can be done even by a layman by just entering the input data value, so the next step involves the soft computation using Python Programming Language.

While working on python programming language, it requires learning the syntax and expressions required for coding the computations. The basic required and used in computation while writing codes fro scheduling system are if, else, elif, for, while, sum, average, roundoff, def, del, return, import etc.

4 Result and Discussion

HCSS is a platform having CPM, PERT, LOB, LSM, and CCM codes compiled in it. According to the demand of the client the codes are used by the Project Manager. The codes are mostly designed in a user friendly way where the user need to put the input data required for the scheduling computations of that scheduling methods.

In CPM, the input data required are the number of activities, duration of each activity, predecessor, successor, logical relationship of activity, lag time and slag time, the coding is done in a systematic way as per the traditional calculation for CPM. The codes involve calculation of forward pass, backward pass, total duration of project, critical path of the project, early start time, early finish time, late start time and late finish time. The output remains same as in traditional calculation but the time required is minimized. The formulation can also be done in a way where the input data is directly taken from an excel sheet and the output data are provided to the Project Manager.

In similar way, the input data and calculation are formulated in Python code and output data are provided. To make the system more reliable and accurate, the real-time data are used as input value and simulation is performed.

The input data required, calculation and output for various scheduling methods in this study are shown in Table 1. From Table 1, users can identify the types of input data required for a particular type of scheduling method. The user has to insert the input values and within fraction of second it will give the output using the computation codes (Fig. 3).

The fundamental thought to use a programming language is to provide a common platform for all the scheduling systems unlike the outdated software like MSP and Primavera which can be used only for CPM and sometimes PERT. Also the simulation done with the real time data during this study use basic input data in all the scheduling methods and identify the best suitable scheduling method for the project.

The application of this type of scheduling can be done in a project having activities of mixed nature, that is, unique activities and repetitive activities, also it can be used as per the convenience of project manager and the scope of the project changes time to time due to resource, time or productivity constraints.

5 Conclusion

The literature study and the work conducted have a conclusive end stating that the scheduling is real important work done during planning. The project to be succeeded proper scheduling of resources and time is very crucial. Not only for the construction work these scheduling methods are used by they are used in other industries as well, to make sure that the method which is unique and has every aspect of solution within is much required. Also the scheduling platforms used are different for different type of project; development of HCSS has put an idea to give user a better picture

Table 1 Input data, calculation and output data for scheduling methods

Scheduling method	Input data	Calculation	Output data
CPM	Activities, duration of activities, predecessor, successor [12] Arrow diagram of network of activities[13]	Forward pass, backward pass	Critical path, critical activities, longest duration [14] EST, LST,EFT,LEFT
PERT	Most likely time, most optimistic time, most pessimistic time [12] Predecessor, successor activities	Duration of activity, variance and SD of activities, Z value	Critical path, critical activities, longest duration [14] variance of critical path, probability of project completion by Z-value
LSM	Productivity, buffer, total unit of work	Duration of each activity	Start date and end date of each activity, project duration
LOB	Productivity, buffer, total unit of work, worker-hours, crew sizes, and daily working hours	LUA, TPR, OTSUA, TTS, ATS[15]	Start date of first unit, finish date of first unit, start date of last unit, finish date of last unit, duration of project
CCM	Activities, duration of activities, predecessor, successor [12] Arrow diagram of network of activities [13], resources	Forward pass, backward pass, CCM calculations and network diagram	Critical path, critical activities, longest duration [14], project duration, feeder buffer, resource buffer, project buffer

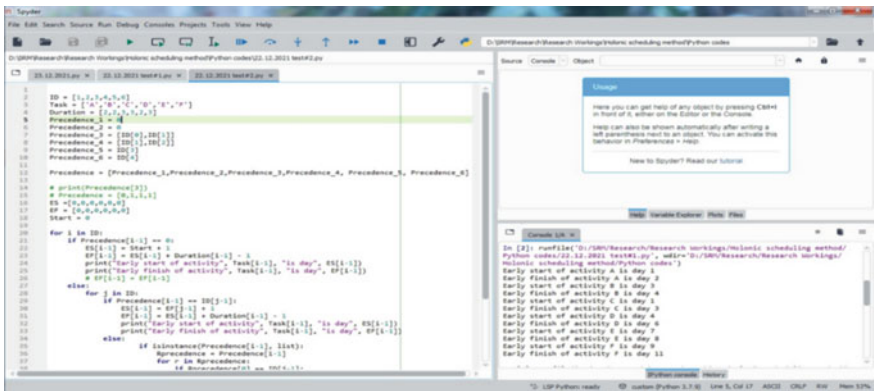


Fig. 3 Test code for CPM

of switching in between the scheduling methods at any stage of execution work. Python is kept in concentration to make it user friendly and accessible platform for scheduling and cost free. The merits of all the methods is tried to club together on the Python, the coding required lot of input data to be executed and analysed, simulated and validated. The current work is to put input and get the nearest possible output by maintaining the activity relationships like Finish-To-Finish, Start-To-Finish, Start-To-Start, and Finish-To-Start. Using HCSS user has multiple options to conduct the work using different scheduling methods. Its resolves the conflict of time, resources and money management at the time of planning and scheduling.

6 Future Scope and Improvement

The input data required are easily collected and can be inserted in the program to obtain desired result. Professionals having knowledge of python programming language as a beginner level will have advantage over the others, to make it simpler the system need to be more simplified using the programing structure which can retrieve the input data values for the database directly. The database used can be excel or SQL, this will ease the process of computation for a professional as well as other stakeholders of project to scheduling projects having n number of activities.

References

1. Barbara G, Skorupka D, Kuchta D, Duchaczek A (2015) Project risk time management—a proposed model and a case study in the construction industry. *Procedia - Procedia Comput Sci* 64:24–31. <https://doi.org/10.1016/j.procs.2015.08.459>
2. O. Okudan, C. Budayan, and I. Dikmen, “A knowledge-based risk management tool for construction projects using case-based reasoning,” *Expert Syst. Appl.*, vol. 173, no. January, p. 114776, 2021, doi: <https://doi.org/10.1016/j.eswa.2021.114776>.
3. F. Acebes, D. Poza, J. M. Gonz´alez-Varona, J. Pajares, and A. L´opez-Paredes, “On the project risk baseline : Integrating aleatory uncertainty into project scheduling,” *Comput. Ind. Eng.*, vol. 160, no. July, pp. 1–11, 2021, doi: <https://doi.org/10.1016/j.cie.2021.107537>.
4. Mani P, González VA, Raftery GM, Orozco F, Cabrera-Guerrero GG (2018) A multi-objective probabilistic-based method to determine optimum allocation of time buffer in construction schedules. *Autom Constr* 92:46–58
5. Lalmi A, Fernandes G, Souad SB (2021) A conceptual hybrid project management model for construction a conceptual hybrid project management model for construction projects. *Procedia Comput Sci* 181(2019):921–930. <https://doi.org/10.1016/j.procs.2021.01.248>
6. Siew L, Rahim A, Hamid A (2015) The practice of time management on construction project. *Procedia Eng* 125:32–39. <https://doi.org/10.1016/j.proeng.2015.11.006>
7. Z. Ma, S. Li, Y. Wang, and Z. Yang, “Component-level construction schedule optimization for hybrid concrete structures,” *Autom. Constr.*, vol. 125, no. August 2020, p. 103607, 2021, doi: <https://doi.org/10.1016/j.autcon.2021.103607>
8. Milat M, Knezic S, Sedlar J (2021) A new surrogate measure for resilient approach to construction a new surrogate measure scheduling for resilient approach to construction. *Procedia Comput Sci* 181(2019):468–476. <https://doi.org/10.1016/j.procs.2021.01.192>

9. G. Yogesh and C. Hanumanth Rao, "A study on linear scheduling methods in road construction projects," *Mater. Today Proc.*, vol. 47, no. xxxx, pp. 5475–5478, 2021, doi: <https://doi.org/10.1016/j.matpr.2021.07.393>
10. B. Yang, B. Liu, J. Xiao, B. Zhang, Z. Wang, and M. Dong, "A novel construction scheduling framework for a mixed construction process of precast components and cast-in-place parts in prefabricated buildings," *J. Build. Eng.*, vol. 43, no. June, p. 103181, 2021, doi: <https://doi.org/10.1016/j.jobbe.2021.103181>
11. D. Arditi, M. Asce, O. B. Tokdemir, and K. Suh, "Challenges in Line-of-Balance Scheduling," *J. Constr. Eng. Manag.*, no. December, pp. 545–556, 2002
12. Takakura Y, Yajima T, Kawajiri Y, Hashizume S (2019) Application of critical path method to stochastic processes with historical operation data. *Chem Eng Res Des* 149:195–208. <https://doi.org/10.1016/j.cherd.2019.06.027>
13. Bayraktar ME, Arif F, Hastak M, Gad NA (2012) Judiciary's Use of the Critical Path Method to Resolve Construction Claims. *J Leg Aff Disput Resolut Eng Constr* 4(1):10–16. [https://doi.org/10.1061/\(asce\)la.1943-4170.0000079](https://doi.org/10.1061/(asce)la.1943-4170.0000079)
14. S. Zareei, "Project scheduling for constructing biogas plant using critical path method," *Renew. Sustain. Energy Rev.*, vol. 81, no. May 2016, pp. 756–759, 2018, doi: <https://doi.org/10.1016/j.rser.2017.08.025>
15. Tokdemir OB, Erol H, Dikmen I (2019) Delay Risk Assessment of Repetitive Construction Projects Using Line-of-Balance Scheduling and Monte Carlo Simulation. *J Constr Eng Manag* 145(2):04018132. [https://doi.org/10.1061/\(asce\)co.1943-7862.0001595](https://doi.org/10.1061/(asce)co.1943-7862.0001595)

Study of Characteristics of Expansive Soil Stabilized with Tire Derived Aggregate and Fish Scale Powder



D. Gokulkumar, P. T. Ravichandran, and K. Divya Krishnan

1 Introduction

Naturally available materials in the Earth's crust are soil, and the geological origin of their constituents is sediment. Soil is classified into two types: that which results from physical and chemical weathering of parent rocks, and that which results from physical weathering and mechanical disintegration and retains the minerals found in the parent rock. Chemical weathering and breakdown of rock, on the other hand, is caused by hydration, oxidation, and carbonation. Various types of soils, such as alluvial soils, black cotton soils, laterites soils, and desert soils, are available in India as a result of this process. Soil, which is the uppermost part of the earth and readily available construction material, has been popular with civil engineers despite its poor properties. Its tensile and shear strengths are usually low, and its characteristics vary greatly depending on where it is found. Due to increasing urbanization and modernity, there is a scarcity of land for construction, this is usually done on tough soils like weak soil, problematic soils, and so on. Expansive soils are usually known to as problematic soils because their mechanical behaviour is subject to variations in their natural water. Several studies have discovered that, due to the negative qualities of expansive soil, its shear strength and bearing capacity are very low, while its compressibility is very high, necessitating some sort of soil stabilisation to improve subsurface parameters.

The infrastructure will suffer serious damage if it is not stabilised, resulting in poor performance. Over the years, numerous research has been conducted to assess the efficacy of soil stabilisation systems and building practices, as well as the process of altering soil properties in an attempt to optimise the soil's load bearing capacity

D. Gokulkumar · P. T. Ravichandran (✉) · K. Divya Krishnan
Department of Civil Engineering, Faculty of Engineering and Technology, SRM Institute of Science and Technology, Kattankulathur, Tamil Nadu 603203, India
e-mail: ravichap@srmist.edu.in

and stability, in which soil stabilisation improves expansive soil engineering properties such as bearing capacity and strength, compaction characteristics, and so on. Mechanical stabilisation, chemical stabilisation, thermal stabilisation, and electrical stabilisation are the four primary categories of soil stabilisation technologies based on soil improvement processing processes. Chemical additives are the most commonly utilised among them to stabilise soils by increasing their natural qualities through the incorporation of chemical additives into the soil. Chemical additives are used to stabilise soil, not only to prevent it from shrinking and swelling, but also to improve its strength, workability, and durability, so boosting its overall performance. Mechanical soil stabilisation can be achieved by combining and compacting two or more soils of various grades to produce a dense and well-graded material, or by altering the physical characteristics of soil using compaction or vibration techniques. Another technique to improve the soil properties is to fortify it. Natural and synthetic fabrics, plant roots, polymer fabrics, and shredded tyres are all included. The fundamental goal of soil mass reinforcement is to improve its stability and bearing capacity.

Several investigations on soil improvement in problematic soil, such as soil reinforcement and additive addition, have been conducted. Many studies have been conducted to address the problems that many stabilizing technologies, notably the usage of solid waste, have. Solid waste is divided into two groups based on the source of generation: agricultural and industrial trash. Bearing capacity has been considered as a means of stabilising weak soil. The UCS increased when 5% tyre waste was put to untreated soil, but it increased even more when 10% cement was applied, indicating a significant improvement in strength. Finally, the test findings reveal that a mixture of 5% tyre waste and 10% cement is the ideal quantity in terms of plasticity and strength [1]. Crushed rubber's potential for sub-grade ground enhancement in highway building. According to the test results, the amount of rubber particles used to improve soil quality ranged from 4 to 10%, indicating that both compaction properties decrease as tyre shreds are added, while CBR increases with increased shredded rubber content, with the maximum CBR value obtained when 8% shredded rubber is used, and the optimum value was also discovered from the CBR test [2]. On expansive soil stabilized by the addition of lime and Shredded Waste Tire (SWT) mixes, compaction characteristics, UCS, and CBR tests were performed. Tire debris passes through a 4.75 mm sieve and is caught by a 75 mm sieve in experiments. SWT was added to the mix in 5% doses, with a maximum of 20%, and the optimal quantity of SWT found to be 10%. The UCS and CBR values increase with a 5% lime addition to the soil-SWT combination as the SWT concentration grows, and the UCS and CBR values increase even more after adding 10% SWT to the soil. However, the ideal lime proportion for extending soil stability is found to be 5%, whereas the best percentage for SWT is discovered to be 10% [3]. The strength and compaction behaviour of pond ash, rice husk ash, cement, and fibre in soil sample were studied in a number of studies. For this experiment, 30–45% pond ash and 5–20% rice husk ash was used. For a various cure period, polypropylene fibres of 6, 12 mm length are used at 0.5, 1 and 1.5% by weight, while cement is used at 0, 2 and 4%. With unreinforced soil, there is a 7-day improvement in cement strength. The fibres change the stress situation and boost strength [4]. Natural coir fibre provides strength to this expansive

soil. Bottom ash is utilised in the soil as a cementing ingredient. Coir fibre of 0.25, 0.5 and 1% is mixed with bottom ash of 5, 10, 15 and 20%. The most effective ideal combination was found to be 20% bottom ash and 0.5% coir fibre, which yielded the highest value at UCS. The addition of bottom ash to the CF-soil matrix resulted in densification, according to a micro structural analysis [5]. According to the literature, incorporating waste objects such as rubber tyres into expanding soil improves the soil's strength properties. Calcium-based products added as additives to expansive soil boost the OMC, lower the MDD, and increase the soil's strength. The maximum compaction and strength qualities of various soils are given. Soil reinforcement with tyre debris improved the geotechnical qualities of the soil significantly.

The phrase 'solid waste' refers to any solids and semi-solids in which incorrect waste management has negative consequences for the environment, perhaps leading to disease outbreaks and epidemics. Solid wastes are divided into two categories: industrial waste and agricultural waste, for example, and these waste products are used as additives in the soil for a variety of purposes. Tire trash is chosen as a waste material to stabilise soil after recycling. India, a growing country, has experienced a significant annual spike in the number of automobiles, resulting in a continuous increase in the amount of trash vehicles decade after decade. The main source of this difficulty is that there are vast numbers of wasted tyres all over the world, according to the Indian situation, 112 million discarded tyres generated per year, and the main worry of the tire-based companies is to dispose of waste tyres safely and affordably. As a result, widespread use of discarded tyres in geotechnical projects will alleviate waste tyre industry concerns, while animal-based materials are also abundant biomass energy sources on the planet [6–22]. Animal-derived biomass is typically created from hazardous organic waste, and if not used properly, it can harm the environment significantly. The building sector may use a considerable quantity of this hazardous waste by using animal-derived biomass. The rising industrialisation of the world has resulted in a considerable increase in the volume of fish waste. Each year, approximately 18–30 million metric tons of fish residues are produced, with fish scales (FS) accounting for roughly 4% [6, 23]. FS is a type of waste protein that cannot be used as animal feed and is difficult for bacteria to breakdown. As a result, disposing of and treating such a massive volume of FS waste is problematic. It is critical to optimise this by-product disposal and to extend the application of FS waste in order to alleviate the environmental difficulties created by FS waste.

Biotechnology has been widely used to recycle bio-waste materials since its introduction to soil stabilization. Although several studies have been completed to employ other biomaterials to modify soil, no research has been done on the influence of FS on its qualities. In the extant literature, there is no mention of using FS in soil stabilization to recycle this sustainable resource. In comparison to conventional materials, FS is a cost-effective and sustainable biomaterial as a locally produced waste. This research aims to determine the best method for improving soil properties by stabilizing it with waste materials such as rubber tyres and fish scale, which will improve the soil property after stabilization, as well as the strength and compaction characteristics of soil when added to tyre waste, for soil with varying curing periods. There are several crucial considerations to consider when using waste materials like

Table 1 Geotechnical properties of expansive soil

Properties	Values
Specific gravity	2.69
Liquid limit	75%
Plastic limit	23%
Plasticity index	52%
Shrinkage limit	8.76%
MDD	1.69 (g/cm ³)
OMC	17.8%
UCC	148 kPa
CBR	4.17%

tyres and fish waste. They will look into making the most of solid waste products in order to improve soil and make it as environmentally friendly as feasible. Cost-effectiveness is achieved by reusing waste material in soil rather than the huge typical filler material.

2 Materials and Methodology

2.1 Soil Sample

The soil utilized in this experiment was widely available from Mahabalipuram—ECR road (Salavakkuppam) in Chennai was used to collect the sample. A height of 0.5–1.0 m below the actual soil surface is where sample specimens were obtained are showed in Table 1.

2.2 Tire Derived Aggregate

Tire Derived Aggregate was chosen as an addition to enhance the property of soil samples. Products based on TDA (e.g., crumbs, shadders and fibres). TDAs utilized in the study ranged in size from 1–2 mm. The TDA was identified by its specific gravity of 0.94, which was determined via a pycnometer test.

2.3 Fish Scale Powder

The fish scale powder (FSP) used in this study was produced using a consistent technique and came from a variety of fish. As a result, the energy dispersive X-ray

Table 2 Chemical elements of fish scale powder

Chemical constituents	Element content (%)
Calcium	46.09
Aluminium	4.84
Phosphorus	7.88
Silicon	1.32
Oxygen	32.53
Chlorine	5.62

characterization of FSP was depicted in Fig. 2. The figure also revealed the existence of components such as Ca, Al, O, P and Si. Ca (46.09%) was the most frequent component in this FSP (Table 2).

2.4 Methodology

Specific gravity, Atterberg limits (Liquid limit, Plastic limit, Shrinkage limit), and compaction characteristics (maximum dry density and optimal moisture content) were among the laboratory tests done on natural soil for the preparatory work programme, as prescribed by the IS code of practise [24–28]. The mineralogical parameters of FSP were evaluated using the scanning electron microscope, and the admixture properties were determined using the tests undertaken, such as specific gravity for TDA and FSP. The soil qualities were assessed using the IS code of practise as part of the experimental work programme. The standard proctor test was used to determine the maximum dry density and optimal moisture content of expansive soil when used alone or in combination with FSP and TDA. After determining the optimal for soil with TDA, soil and an optimal percentage of TDA mixed with a variable FSP percentage, the total number of samples required for the entire standard proctor test is 11, in which untreated soil and soil with additions of TDA content of about six samples will be prepared, and one sample for each varying percentage of TDA after determining the optimal for soil with TDA, soil and an optimal percentage of TDA mixed with a variable FSP percentage will be prepared. There will be about five samples made, one for each different % of FSP. IS-2720 Part-VII coding protocol is followed for conducting Standard Proctor Compaction Tests. Laboratory tests are conducted on treated and untreated soil to determine strength properties. IS 2720 part 10 was used to calculate the compressive strength unconfined. The total number of samples required for the casting is 93, with untreated soil and soil with TDA content additions of about 11 samples, one sample for each TDA content, soil and optimal percentage of TDA mix with variable FSP content of about 75 samples, and three samples for each varying percentage of FSP content.

3 Results and Discussion

3.1 Influence of TDA on Soil Compaction Characteristics

From the observation of the test results of standard proctor test, which conducted on the soil with varying percentage of TDA, shows that Maximum Dry Density and Optimum Moisture Content of untreated soil is about 1.69 g/cm³ and 17.8%. Then with the addition of TDA percentage with a increment of 3% to the untreated soil, they is reduction in Maximum Dry Density as well as in Optimum Moisture Content of treated soil as the inclusion of TDA percentage increases. TDA is specific gravity of 0.94 is lower than soil specific gravity of 2.69, resulting in a reduction in MDD. The decrease in OMC due to less attraction of TDA particle towards water molecules, the Optimum Moisture Content decreases, the Maximum Dry Density and Optimum Moisture Content of soil with TDA have been shown in Table 3, and the elastic reaction of TDA during compaction cause a reduction in compaction efficiency. According to the findings, it can be stated that the MDD and the OMC of the soil treated with TDA are both lower than those of the soil that was not treated, and that there is a relationship between the rise in the amount of TDA in the soil and a decrease in both Maximum Dry Density and Optimum Moisture Content. Figure 1 showing the compaction characteristics curve of soil with various TDA content.

Table 3 Compaction characteristics of TDA

Compaction characteristics	TDA of varying percentage				
	3	6	9	12	15
MDD (g/cm ³)	1.64	1.61	1.54	1.5	1.46
OMC (%)	17.2	16.8	1.61	15.7	15

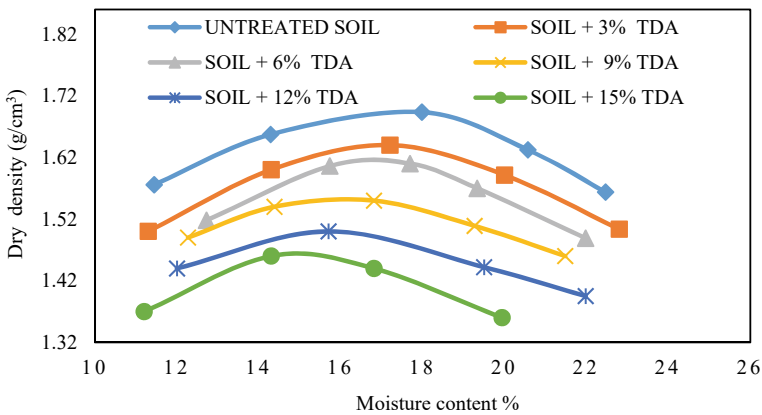


Fig. 1 Compaction characteristics curve of untreated soil with TDA content

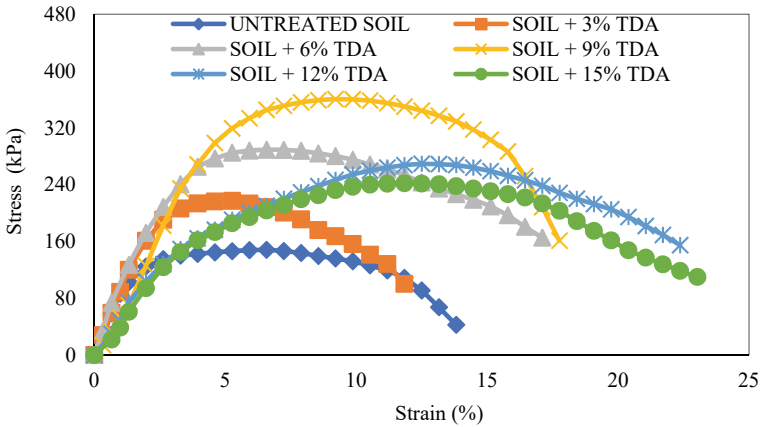


Fig. 2 Stress Strain characteristics curve of soil with TDA content

While coming to the 3% TDA is added to untreated soil, there Compaction characteristics as a reduction in both MDD and OMC content of the untreated soil as the addition of TDA percentage increases. Hence it is same for the TDA content of 6, 9, 12 and 15% is added to untreated soil. From the outcomes, it can be seen that MDD of TDA content is 1.64 g/cm³ it is less when compared to the untreated soil which as 1.69 g/cm³ and OMC of TDA content is 17.2% it is less when compared to the untreated soil which as 17.8%.

3.2 Influence of TDA on Unconfined Compression Strength

For the effect of addition of TDA on the Unconfined Compression Strength (UCS), at their Optimum moisture content and maximum dry density, the samples were created. condition respectively and the unconfined compression strength with addition of (3, 6, 9, 12 and 15) percentage of TDA with untreated soil. It has been seen that the UCS value rises as TDA content does, unconfined compression strength improves up to 9% and inclusion of TDA beyond that it drops gradually, from this it is clear that inclusion of 9% TDA to the untreated soil induces 212% increase in UCS as compared to untreated soil. From the results, the optimum amount of TDA for stabilization of untreated soil is found to be 9%. The unconfined compression strength of the soil sample with 15% TDA has a higher UCS value than the virgin expansive soil. From the results it is revealed that addition of optimal dosage of TDA with soil will enhance the strength characteristics as compared to the untreated soil.

Figure 2 shows the stress strain characteristics curve of soil with TDA content, when TDA content of 3% is added to untreated soil, they Strength characteristics as a increase in both stress and strain of the untreated soil as the addition of TDA percentage increases, the maximum stress of 220 kPa is achieved when the strain

is at 5% and thereafter it decrease gradually. While 3% TDA to the untreated soil induces 48.6% increase in UCS as compared to untreated soil. Then for the TDA content of 6% is added to untreated soil, there strength characteristics as a increase in both stress and strain of the untreated soil as the addition of TDA percentage increases, the maximum stress of 289 kPa is achieved when the strain is at 7% and thereafter it decrease gradually, which induces 95.2% increase in UCS as compared to untreated soil. For the TDA content of 9% is added to untreated soil, they Strength characteristics as a increase in both stress and strain of the untreated soil as the addition of TDA percentage increases, the maximum stress of 360 kPa is achieved when the strain is at 9.2% and thereafter it decrease gradually, which induces 143.2% increase in UCS. From the results, it is observed unconfined compression strength improves up to 9% and inclusion of TDA beyond that it drops gradually. The lesser stiffness of crumb rubber in comparison to clay and the challenges fitting light-weight TDA at significant rubber percentage may be the causes of the decreased maximum applied loads. Because of the elastic behaviour and ductility character of TDA, the increment of UCS value is quick as the TDA content increases. However, once the stress reaches the peak with respect to strain, it abruptly decreases because the yield strength of the treated soil sample will be lost after a certain axial load (strain).

3.3 Influence of Optimum% TDA with FSP on Soil Compaction Characteristics

From the observation of the test results of standard proctor test that performed on the soil and optimal percentage of TDA mix with variable FSP content (4, 8, 12, 16, 2%), which it shows that maximum dry density and optimum moisture content of untreated soil. Then, with the addition of FSP percentage with an increment of 4% to the soil mixed with optimal percentage of TDA as 9%. There is a reduction in maximum dry density and increase in optimum moisture content of soil as the inclusion of FSP percentage increases. The maximum dry density drops due to soil coagulant processes. The increase in optimum moisture content as FSP content increases is due to more water being required for the interaction of FSP with silica and alumina in untreated soil, resulting in an increase in optimum moisture content. Table 4 shows the variation of optimum moisture content and maximum dry density of soil and 9 percent TDA mix with varying percentages of FSP, as well as water requirements for hydration response and Fig. 3 showing the compaction characteristics curve of soil and 9% TDA mix with FSP content.

The findings indicate that FSP had a higher optimum moisture content than untreated soil. When 4% of FSP is added to soil with 9% TDA, the Compaction characteristics as a decrease in Maximum dry density and increase in Optimum moisture content of the treated soil as the inclusion of FSP percentage increases and it has an increment of 7.8% for the Optimum moisture content. When the 8% of FSP is added to soil with 9% TDA, and it has an increment of 12.35% for the

Table 4 Compaction characteristics of optimum% of TDA with FSP

Compaction characteristics	Optimum % TDA with FSP with varying percentage				
	4	8	12	16	20
MDD (g/cm ³)	1.47	1.44	1.38	1.24	1.22
OMC (%)	19.2	20	23.2	28.5	29

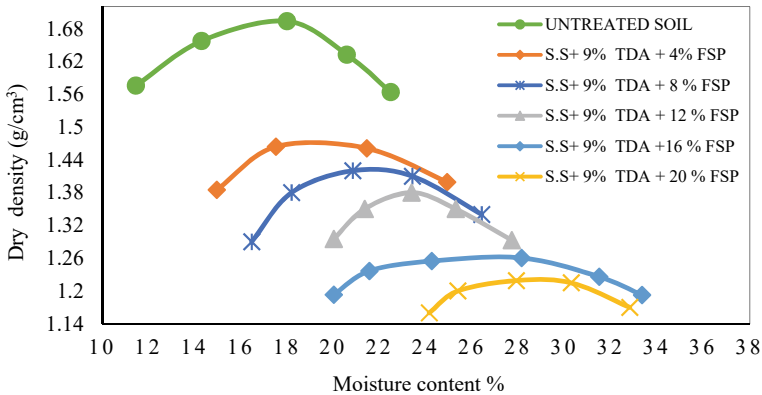


Fig. 3 Compaction characteristics curve of soil and 9% TDA mix with FSP content

Optimum moisture content and Maximum dry density will decrease, As FSP content increases, the Optimum moisture content and Maximum dry density will decrease. The rise in optimum moisture content as FSP content increases is owing to the fact that more water is required for FSP interaction with silica and alumina in untreated soil, resulting in an increase in optimum moisture content.

3.4 Influence of Optimum% TDA with FSP on Unconfined Compression Strength

For the effect of addition of 9% TDA with FSP on the Unconfined Compression Strength (UCS), the samples were prepared at their OMC and MDD condition respectively. Table 4.3 UCS of soil and 9% percentage of TDA mix with variable FSP content (4, 8, 12, 16, 20%) for (3, 7, 14, 28 and 60) days of curing periods. It is observed that the UCS value increase with increase in FSP content, for example addition of 4, 8, 12 and 16% of FSP and 9% TDA to the untreated soil generates a 243, 303, 157 and 139 kPa of UCS value for 14 days of curing, UCS increases up to 8% FSP with 9% TDA beyond that, it suddenly drops and also for the UCS of soil and 9% TDA mix with 8% FSP for (3, 7, 14 and 28) days of curing is 260, 288, 303 and 283 kPa. From this it is clear that inclusion of 8% FSP and 9% TDA to the

untreated soil induces 155% increase in UCS for 14 days of cure period. Similarly for inclusion of 4%, 12% FSP mix with stabilized treated soil induces a 95%, 18% increase in UCS for 14, 7 days of curing as compared to untreated soil. It was found that UCS of treated soil increase with increase in FSP content for 14 days, they is decrease in UCS value beyond 8% FSP and 14 days of curing, The drop in UCS with increasing curing days and FSP concentration is due to decomposition, as well as the infusion of more FSP, which interacted with less silica and alumina in expansive soil, creating a carbonation reaction and a loss in strength. The virgin expanding soil has a lower UCS value than the soil sample with 12% FSP. According to the findings, adding an appropriate dosage of FSP and a 9% TDA mix to soil for 14 days improves strength properties when compared to untreated soil, but the improvement is reduced. Figure 4 shows the stress strain characteristics curve of treated soil and 9% percentage of TDA mix with variable FSP content 8% for (3, 7, 14, 28 and 60) days of curing periods and Table 5 shows the values.

The addition of FSP content to the treated soil with 9% TDA is of 4% increment. For the strength characteristics of soil, the unconfined compression strength is 148 kPa. For the 8% of FSP for 3 days of curing, the strain is at 8% when the peak

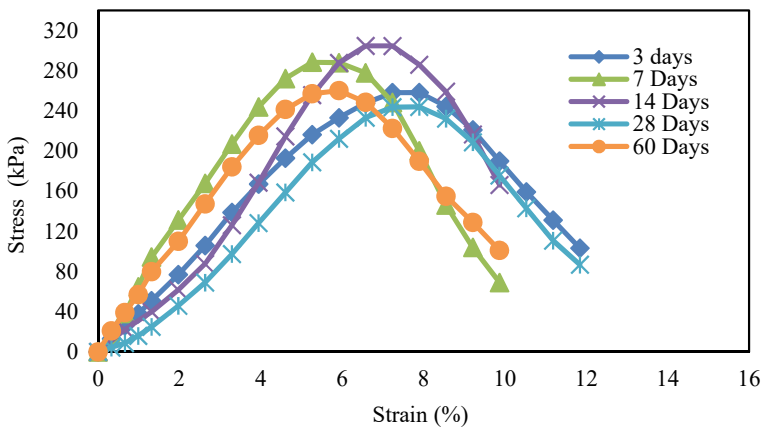


Fig. 4 Stress strain characteristics curve of treated soil with 8% FSP for various curing periods

Table 5 Strength characteristics of TDA and 9% TDA with FSP

9% TDA + FSP %	UCC for curing period (days) (kPa)				
	3	7	14	28	60
4	210	220	243	212	209
8	260	288	303	261	243
12	165	166	157	134	118
16	150	144	139	126	103
20	130	127	110	88	65

stress of 243 kPa is achieved after that gradually drops which induce the strength characteristics of 64.18% improvement in UCS for 3 days of curing as compared to untreated soil.

While coming to the FSP content of 8% is added to untreated soil for 3 days of curing periods, the strength characteristics as an increase in both stress and strain of the treated soil as the addition of FSP percentage increases, the maximum stress of 303 kPa is achieved when the strain is at 7.25% for 8% FSP for 14 days of curing and thereafter it decrease gradually. While 8% FSP to the treated soil induces 104.7% increase in UCS for 14 day of cure period. It was found that unconfined compression strength of treated soil increases with increase in FSP content for 14 days, they is decrease in UCS value beyond 8% FSP and 14 days of curing. Though the UCS of 8% FSP has a slightly increase from 3 to 14 days of curing period but after that sudden decrease from 14 to 60 days of cuing period. There is decrease in UCS value beyond 8% FSP and 14 days of curing and UCS value decrease after 14 days of curing, this is due the degradation behaviour of the FSP since its biodegradable in nature but for initial days of curing it enhances the soil strength characteristics then after certain days of curing periods its drops.

4 Conclusion

On soil samples and admixtures, experimental tests were performed, to evaluate the influence of TDA and FSP on expansive soil, the following conclusions can be drawn in the aspect of strength properties due to application of TDA and FSP. The final conclusion can be justified based on studies conducted as follows.

- Based on the results and discussions from the standard proctor test, it can be stated that with increase in percentage of TDA, there is a decrease in both MDD and OMC, on other hand increase in percentage of FSP with 9% TDA, There is reduction in MDD and increase in OMC of treated soil.
- For Unconfined compressive strength, by inclusion of 9% TDA to the untreated soil induces 212% increase in UCS as compared to untreated soil and while coming to FSP, there is a 155% increase in UCS for 14 days of curing as compared to untreated soil. From the results, the optimum amount of TDA and FSP for stabilization of untreated soil is found to be 9 and 8%.
- From the laboratory investigation conducted with TDA and FSP to stabilize the expansive soils, the results obtained shows that the soil stabilized with TDA has the higher strength characteristics when compared to the FSP blended with TDA to stabilize the soil.
- For addition of FSP, the strength characteristics is decreases with increase in curing days and FSP content because of it degradation behaviour, so when FSP treated with some additives like Fly-ash and lime which has the good cementitious property can improve the strength characteristics of expansive soil even more. Also it is easily available material which can be used in soil stabilization by replacing

the conventional material for additives such as fly ash, lime and cement etc. and it is very economic to use by which treating the soil by waste material will leads to less polluting of surrounding environment.

References

1. Md. Shah Azam (2020) Altering the geotechnical properties of clayey soil by using scrap rubber. *Int J Eng Res Technol* 9(7):199–203
2. Akshaya Kumar Sabat and Subasis Pati.: A Review of Literature on Stabilization of Expansive Soil Using Solid Wastes. *Electronic Journal of Geotechnical Engineering* 19(4), 6251–6267(2014).
3. Naseem, W. Mumtaz, Fazal-e-Jalal.: Stabilization of Expansive Soil using Tire rubber Powder and Cement Kiln Dust. *Soil Mechanics and Foundation Engineering* 56(1), 1–5 (2019).
4. Yoobanpot Naphol, Jamsawang Pitthaya, Horpibulsuk Suksun.: Strength behavior and microstructural characteristics of soft clay stabilized with cement kiln dust and fly ash residue. *Applied Clay Science* 141, 146–156 (2017).
5. Nitin Tiwari and Neelima Satyam.: Strength and durability assessment of expansive soil stabilized with recycled ash and natural fibers. *Transportation Geotechnics* 29, 2214–3912 (2021).
6. Hafez Jafari and Alberto Lista.: Fish collagen: Extraction, characterization, and applications for biomaterials engineering. *Polymers*12(4), 1–37 (2020).
7. Mukesh Kumar.: Clay soil stabilization by utilizing secondary lime and rubber tire powder. *Materials Today* 37, 3471–3474 (2020).
8. Basim Y. Alkhafaji, Roaa Jafar Elkheralla.: Effect of adding fish scales in agricultural soils and some characteristics of vignaradiata L. *Plant Archives* 19(1), 1041–1043 (2019).
9. Sheng-quan Zhou, Da-wei Zhou, Yong-fei Zhang.: Study on Physical-Mechanical Properties Microstructure of Expansive Soil Stabilized with Fly Ash and Lime. *Advances in Civil Engineering* 19(46) 37–57 (2019).
10. Melik Bekhiti, Habib Trouzine.: Influence of waste tire rubber fibers on swelling behavior, unconfined compressive strength and ductility of cement stabilized bentonite clay soil. *Construction and Building Material* 208, 304–313 (2019).
11. Arvind Kumar, Deepak Gupta.: Stabilized soil incorporating combinations of rice husk ash, pond ash and cement. *Geomechanics and Engineering* 12(1) 85–109 (2017).
12. Akshaya Kumar Sabat, Subasis Pati.: A review of literature on stabilization of expansive soil using solid. *Electronic Journal of Geotechnical Engineering* 19, 9–18 (2016).
13. Fauzi A, Djauhari Z, Fauzi UJ (2016) Soil engineering properties improvement by utilization of cut waste plastic and crushed waste glass as additive. *International Journal of Engineering and Technology* 8(1):15–18
14. T. Schanz, M.B.D. Elsawy.: Swelling characteristics and shear strength of highly expansive clay–lime mixtures: a comparative study. *Arabian Journal of Geosciences* 8, 7919–7927 (2015).
15. Vivek Singh, Rajesh Jain.: Effect of Cement Kiln Dust on Index Properties of Black Cotton Soil Recycling fish scale powder in improving the performance of asphalt. *International Journal of Engineering and Science Research* 5(4), 142–146 (2015).
16. Jan U, Kumar, Sonthwal and Kerni V.: Soil stabilization using shredded rubber tyre: A review. *International Journal of Civil and Structural Engineering Research* 3(1), 57–60 (2015).
17. H. Zhao, T.M. Petry, Y.Z. Sun.: Effects of chemical stabilizers on an expansive clay. *KSCE Journal of Civil Engineering* 18(4), 1009–1017 (2014).
18. M.Olgun.: Effects of polypropylene fibre inclusion on the strength and volume change characteristics of cement-fly ash stabilized clay soil, *Geosynthetics International* 20(4), 263–275 (2013).

19. Roy A (2014) Soil stabilization using rice husk ash and cement. *International Journal of Civil Engineering Research* 5(1):49–54
20. Effects of chemical stabilizers on an expansive clay (2014) Zhao H, Ge. L, Petry. T. M and Sun. Y. (2014). *J Civ Eng* 18:1009–1017
21. Hambirao GS, Rakaraddi PG (2014) Soil stabilization using waste shredded rubber tyre chips. *Journal of Mechanical and Civil Engineering* 11(1):20–27
22. Nareeman BJ (2010) A treatment of expansive soil using different additives. *Acta Montanistica Slovaca* 15(4):290–297
23. Suat Akbulut, Seracettin Arasan.: Modification of clayey soils using scrap tire rubber and synthetic fibers. *Applied Clay Science* 38, 23–32 (2007).
24. IS 2720 Part XL 2002 Methods of Tests for Soil Determination of Free Swell Index of Soils Bureau of Indian Standards New Delhi.
25. IS 2720 Part V 1985 Methods of tests for Soil Determination of Atterberg's limits Bureau of Indian Standards New Delhi.
26. IS 2720 Part III 1987 Methods of Tests for Soil Determination of Specific Gravity Bureau of Indian Standards New Delhi.
27. IS 2720 Part VII 1980 Methods of tests for Soil Determination of water content dry density relation using light compaction Bureau of Indian Standards New Delhi.
28. IS 2720 Part X 1973 Methods of Tests for Soil Determination of unconfined compressive strength Bureau of Indian Standards New Delhi.

Earthquake Engineering

Dynamic Response of Cable-Stayed Bridge Under Seismic Vulnerability Analysis: State of the Art



Inamdar Zakeer Ahamed Kadir Ahamed and Rajendra B. Magar

1 Introduction

Cable-stayed bridges have gained popularity for their esthetic appeal and strong load-bearing capacity. These modern architectural marvels utilize long cables to support the bridge deck. However, like all bridges, cable-stayed structures face dynamic loading challenges from wind, vehicles, and earthquakes. Researchers are particularly interested in understanding the seismic response of cable-stayed bridges, as earthquakes can impose complex and substantial loads that test the integrity of the structure. In countries like India and others, there is a growing need for constructing bridges at higher elevations to facilitate transportation in remote areas. However, this presents challenges such as higher lateral wind loads and the requirement for seismic-resistant design. Despite the significance, few studies have focused on the dynamic response of cable-stayed bridges at very high elevations. Numerical models have been used to assess the dynamic behavior, but few have specifically addressed bridges at these extreme heights. The literature review was carried out with a view to understand the concept of cable-stayed bridges and point out the need of research on cable-stayed bridges at higher elevations. A critical review of the papers has been presented here.

1.1 *Dynamic Response of Cable-Stayed Bridge:*

Gou et al. (2022) [12] studied the dynamic behavior of a cable-stayed bridge with hybrid girders made of steel and concrete. The authors created diverse train load

I. Z. A. K. Ahamed (✉) · R. B. Magar

Anjuman-I-Islam's Kalsekar Technical Campus, School of Engineering and Technology, New Panvel Affiliated to University of Mumbai, Navi Mumbai, Maharashtra 410206, India
e-mail: zakir.inamdar3@gmail.com

scenarios, including driving and braking, and equipped the bridge with sensors to monitor strains, deformations, and accelerations.

Li (2021) [21] analyzed the impacts of concrete carbonization on different elements of a bridge. The author carried out finite element time-dependent simulations of a cable-stayed bridge with one pylon and large deck. Ground motion data were chosen and matched first. The findings suggest that concrete carbonization can reduce steel and concrete strength by up to 23.30% and 12.66%, respectively.

Górski et al. (2021) [11] studied assessment of vibration serviceability of cable-stayed fiber line bridge composed of glass fiber reinforced polymer (GFRP). The investigation revealed that a one-person jump on the deck of the foot bridge was sufficient to detect seven bending and twisting types of modes of the structure.

Wei et al. (2020) [36] assessed the seismic performance of a multi-tower cable-stayed bridge having a height as super-high for the piers in mountainous locations using sixteen ground motion intensity metrics.

Zhang et al. (2020) [40] introduced the concept of an optimal proportion of structural variables, considering cost–benefit considerations. Finally, the best structural parameter ratio was estimated based on a cost–benefit analysis.

Tochaei et al. [35] studied the impacts of on field earthquake ground motion and soil–structure contact of cable-stayed bridges along with dynamic response with a particular focus on the impact of motions of earth and earthen material–structure interaction on bridges. The authors concluded that when the foundation of the bridge was on softer soils, the response was exacerbated.

Lu et al. (2020) [24] adopted a theoretical analysis of vibrations with various parameters for a stayed cable subjected to axial stimulation, and in this, the cable's sag was treated as a curve with the first phase of the cable as the only component. The findings by the authors indicate that when amplitude vibrations are lower than vibrations in the cable, then one must consider sag impact.

Ovett et al. [30] proposed vulnerability assessment paradigm for cable-stayed bridges. This research includes a precise approach for calculating wind loads that take into consideration varying wind speeds.

Bayraktar et al. [3] looked at static as well as dynamic field testing as well as observations from Turkey's Nissibi Euphrates cable-stayed bridge. The authors came to the conclusion that the experimental and theoretical cable frequencies obtained using the empiric formula are almost identical.

Kang et al. [17] evaluated cable-stayed bridge of two cables, using a new method of nonlinear dynamic, using Runge–Kutta direct integration method to investigate the stable equilibrium responses of the modulation formulas. The findings of the discrete equations' asymptotic and quantitative integrations have been compared.

Javanmardi et al. [15] confirmed that the base isolation system was a useful for decreasing seismic force transferring from substructure to the superstructure.

Park and Kim [31] took the impact of vibration in the core part of in-parallel twin cable-stayed bridges as the subject of their research. Six frequency ratios were tested to consider all possible possibilities of natural frequency variances between the two decks.

Sun et al. [34] presented an experiment where vibration data from a cable-stayed bridge of full scale were analyzed to determine its modal characteristics. The authors found that although the bridge's vibration level during the experiment was not very strong due to insufficient excitation, the approximation process could fail to identify all possible modes, especially the higher and lower modes.

Das et al. [6] used a nonlinear dynamic approach to simulate and analyzed a typical cable-stayed bridge. The findings indicated that as the failed cables approached the pylon, there was a decrease in the probability of progressive failure in the cable retention model.

Madrazo-Aguirre et al. [26] shown the dynamic behavior of under-deck cable-stayed bridges under lateral moving loading. The most effective approach to lower peak accelerations has been proven to be increasing the depth of the deck.

Larsen and Larose [19] examined the numerous forms of dynamic wind effects that suspension and cable-stayed bridges typically encounter, emphasizing the relevance of structural dynamics.

Atmaca et al. (2014) [2] figured out how earthquakes affect cable-stayed bridges that are isolated by concave-shaped pendulum bearings. The Manavgat cable-stayed bridge was chosen in this regard. The chosen bridge had a 202.0 m composite deck and a 42.0 m steel tower. SAP2000 was used to create 3D FEM models.

1.2 Long-Span Bridges and Super-High Cable-Stayed Bridges:

Lu and He (2022) [25] investigated the effect of cable's deterioration on elastic stability of long-span cable-stayed bridges. The authors concluded that bridges with densely distributed cables and shallower girders are more prone to switch failure modes when significant corrosion occurs.

Wei et al. (2020) [36] assessed the seismic performance of a multi-tower cable-stayed bridge having a height as super-high for the piers in mountainous locations using sixteen ground motion intensity metrics. The results revealed that peak velocity of the ground for this one is the optimum concentration measure for a bridge with super-high piers after their work.

Zhang et al. (2020) [40] proposed a method to address the challenge of ensuring the reliability of long-span cable-stayed bridges by introducing the concept of an optimal proportion of structural variables, considering cost-benefit considerations.

Lopez-Nuñez et al. (2020) [22] showed the variations of stability in terms of lessened wind speed and contrasted to other long-span bridges. The authors examined how the angle at which the windward side deck is positioned affects the stability of the long-span bridges.

Naderian et al. (2015) [29] developed an efficient finite band discretization approach for analyzing the behavior of long-span cable-stayed bridges. This approach

accurately simulated free vibration and static conditions, producing correct results quickly and demonstrating high convergence.

1.3 Damping System for the Bridges

Wen et al. (2021) [38] proposed an earthquake design procedure focused on optimizing the damping device design in cable-stayed bridges. By considering the structure's performance under earthquake forces, the researchers efficiently obtained optimal design parameters. Implementing damping devices with appropriate parameters led to a substantial reduction in overall repair cost.

Ferreira and Simões (2020) [9] utilized a refinement approach to address the structural-control challenge in a 350-m-long cable-stayed bridge. The results pointed out that viscous dampers were the most cost-effective solution for effectively resisting both static and dynamic forces.

Martínez-Rodrigo and Filiatrault (2015) [27] conducted a study on the performance under seismic conditions of an already-built steel cable-stayed bridge located in a highly seismic area exploring the possibility of retrofitting the existing bridge using different passive damping systems and seismic isolation technologies.

Heo et al. (2014) [14] investigated a semi-active control via magnetorheological damper with the goal of efficiently controlling the vibrations of asymmetrical cable-stayed bridges when an earthquake applied. A MR damper was also created by the authors in the appropriate size for model control.

1.4 Seismic Fragility Analysis

Fu et al. (2021) [10] introduced a technique for evaluating the susceptibility to damage over time of a cable-stayed bridge. The authors developed seismic fragility curves for both the component level and system level. The study found that stirrups deteriorated first, leading to significant declines in the tensile stress and strains of the restricted core concrete.

Li et al. (2017) [20] assessed seismic fragility of cable-stayed bridge along the length with five numbers of spans and with tall piers by method of fragility analysis. After the seismic response of members under time history analysis, the susceptible curves were also evaluated by the authors to check the seismic performance of the structure.

Martínez-Rodrigo and Filiatrault (2020) [28] studied the seismic behavior of an already-constructed steel cable-stayed bridge located in a highly seismic region. The authors proposed retrofitting the bridge using various passive dampening systems and seismic isolation technologies.

Wei et al. (2021) [37] solved the problem by creating an effective seismic fragility assessment skeleton based on the durability time approach (ETM). The fragility

curves computed by the ETM framework were compared to those calculated by the incremental dynamic analysis framework.

1.5 Recent Developments and Works and Few Case Studies of Cable-Stayed Bridges

Bera and Chandiramani (2022) [4] utilized the rational function approximation (RFA) to model self-excited aerodynamic drag in their study. The authors created a finite element (FE) model of the bridge and conducted a static analysis considering geometric nonlinearity.

Gou et al. (2022) [12] investigated the dynamic reactions of a large-length cable-stayed railway bridge with hybrid girders. The hybrid girder was made of steel and concrete. This research offered real test data as well as a tool for evaluating and designing cable-stayed railway bridges.

Martins et al. (2020) [28] conducted a literature review on optimization methods applied to cable-stayed bridges. The authors thoroughly reviewed 90 publications out of 155, summarizing test results, and important conclusions. The majority of the articles focused on refining cable force transfer, achieving optimal design with cost reduction. Researchers showed interest in optimizing foot over bridges, long-span bridges, and bridges with multiple spans using innovative cable arrangements, including crossing cables.

Jiang et al. (2020) [16] studied the North Channel Bridge of the Hangzhou Bay as an example to demonstrate a framework for cables of the bridge for both the load cases, i.e., traffic and wind velocity. The authors concluded that, with an increase in daily traffic volume, there is also a rise in the corresponding stress ranges and a reduction in the stress cycles.

Alkhawaldeh and Al-Rousan (2020) [1] discovered the best deck stiffness and girder contour with respect to vertical deformation and stresses in the cables. The study's viability was determined by analyzing and developing 18 models 2 times using ABAQUS software, 6 various deck stiffnesses, and 3 distinct profiles of girder of the bridge. The prior models were subjected to a nonlinear static finite element analysis. The highest stress was found at maximum deck stiffness.

Cid Montoya et al. (2018) [5] presented a new method for optimizing the deck design and cable size of a long-span cable-stayed bridge while taking into consideration both aero-elastic and structural constraints. It was discovered that in order to increase the deck's cross-section effectiveness, the structural and aero-elastic responses need opposite modifications in the deck breadth for the model under consideration in this work.

Kim et al. (2015) [18] examined the cable-stayed bridge during the construction, and the distribution of temperature in the steel box girder was observed. The authors studied the thermal behavior of bridge during the construction stage. The authors used a simple numerical approach in which the authors stated that the variation at

top flange was steep, and for bottom flange of the girder, it was uniform during the day time while estimating the temperature variations.

Zhang (2014) [39] proposed a calibration method for cable-stayed bridges using the universal design approach and a Kriging surrogate framework. To validate the effectiveness and accuracy of the proposed method using Kriging model, the authors conducted tests on a simple cable-stayed bridge.

Shao et al. (2014) [32] proposed a new type of bridge in the category of cable-stayed bridge which is arranged in such a way that there is partial anchorage in the ground and also the cross-stay cables to hold them. A comparison of this innovative bridge technology to a traditional self-anchored cable-stayed bridge with a main span of around 1400 m is made. The authors came to the conclusion that the new cable-stayed bridge system could be built utilizing the traditional cantilever method.

Lozano-Galant and Turmo (2014) [23] reviewed the existing literature, finding that a variety of software proposed the study of impacts of creep and shrinkage phenomena during the construction of cable-stayed bridges, but neither of the software were able to define a decided Objective Service Stage for a specified time.

2 Research Gap from Literature Review

Previous research has primarily focused on studying and analyzing super-span cable-stayed bridges in mild to moderate seismic conditions. However, there is a need to effectively analyze and design super-high cable-stayed bridges that can reach remote areas at higher elevations. The response of these bridges under dynamic loads needs to be thoroughly examined.

Constructing these structures in higher elevation areas presents challenges for conducting seismic analysis. Therefore, there is a requirement for seismic fragility analysis, which involves optimizing seismic forces and estimating the vulnerability of structures when subjected to ground motion vibrations.

In order to address the aforementioned challenges, the implementation of a damping system becomes necessary. A damping system helps to resist the forces generated by seismic activities, optimizing the bridge's response and reducing its vulnerability to potential damage.

By incorporating a damping system, it is possible to improve the performance and resilience of super-high suspension bridges in higher elevation areas. The damping system serves as an additional protective measure against seismic forces, ensuring the safety and stability of these structures.

Although the authors considered both traffic and wind load in their study, there is a gap in comprehensively analyzing the joint actions of various loads, including stochastic traffic and wind, on cable-stayed bridges. Further research is needed to understand the cumulative fatigue loss and stress ranges under different load combinations, particularly as daily traffic volume increases. Limited exploration of the combined effects of traffic and wind on cable-stayed bridges has been observed.

The previous research proposed structural modifications to mitigate specific issues in cable-stayed bridges. However, there seems a gap in comprehensively assessing the long-term effects and performance benefits of these modifications. Further investigation is needed to evaluate the durability, stability, and overall structural behavior of bridge systems after implementing such modifications.

3 Conclusion

Research Gaps in Bridge Design: Previous studies on super-high cable-stayed bridges in seismic zones and higher elevations have neglected their response to dynamic loads in remote regions. This research addresses these gaps and emphasizes the need for seismic fragility analysis and a damping system to enhance bridge safety and stability.

Comprehensive Load Analysis: Considering the combined effects of various loads, including stochastic traffic and wind, is crucial for cable-stayed bridges. This research identifies the need for analyzing fatigue loss and stress ranges under different load combinations, especially with increasing traffic volume.

Evaluating Structural Modifications: Assessing the long-term effects and performance benefits of structural modifications proposed in previous studies is essential. Further investigation is required to evaluate the durability, stability, and overall behavior of bridge systems after implementing these modifications.

Challenges in Bridge Construction: The construction of super-high bridges in remote, higher elevation areas faces challenges related to lateral wind loads and seismic design. This research aims to address these challenges through the design of a cable-stayed bridge with a damping system to mitigate oscillations during seismic and heavy wind loads.

Enhancing Seismic Response: The study focuses on analyzing the seismic response of super-high steel cable-stayed bridges in remote areas with higher elevations. It emphasizes the importance of seismic fragility analysis and highlights the effectiveness of a new damping system in enhancing the bridge's seismic response.

Conclusion and Impact: This research aims to contribute to the design and analysis of super-high cable-stayed bridges, making transportation to remote locations feasible and ensuring their safety under seismic and wind loads. By addressing research gaps and emphasizing the importance of seismic analysis and damping systems, the study enhances the overall performance and resilience of these bridges.

4 Implications of the Study

The findings and research presented in this study have several important implications for the analysis and design of super-high cable-stayed bridges in seismic zones and higher elevation areas. By addressing the identified research gaps, this study aims to enhance the overall performance, resilience, and stability of these bridges, making transportation to remote locations feasible and ensuring their safety under seismic and wind loads.

1. **Bridging Research Gaps:** This study addresses gaps in analyzing super-high cable-stayed bridges in seismic zones and higher elevation areas. It explores their response to dynamic loads and incorporates seismic fragility analysis, enhancing understanding in challenging environments.
2. **Optimizing Seismic Design:** The study emphasizes the importance of seismic fragility analysis for designing super-high cable-stayed bridges in higher elevation areas. It offers insights into optimizing seismic forces and enhancing their resistance to ground motion vibrations.
3. **Importance of Damping Systems:** The research highlights the effectiveness of damping systems in improving the seismic response of super-high cable-stayed bridges. It emphasizes their role in reducing vulnerability to potential damage and enhancing stability.
4. **Comprehensive Load Analysis:** The study emphasizes the need for comprehensive analysis considering combined effects of stochastic traffic and wind on cable-stayed bridges. It provides insights into fatigue loss, stress ranges, and the impact of increasing traffic volume.
5. **Evaluation of Structural Modifications:** The study evaluates the long-term effects and performance benefits of structural modifications proposed in previous research. It guides decision-making regarding their implementation, assessing their impact on the behavior of super-high cable-stayed bridges.

References

1. Alkhalwaldeh AA, Al-Rousan R (2020) The Optimum Reinforced Concrete Deck Stiffness of Cable-Stayed Bridge Decks. *Procedia Manufacturing* 44:342–349. <https://doi.org/10.1016/j.promfg.2020.02.240>
2. Atmaca B, Yurdakul M, Ateş Ş (2014) Nonlinear dynamic analysis of base isolated cable-stayed bridge under earthquake excitations. *Soil Dyn Earthq Eng* 66:314–318. <https://doi.org/10.1016/j.soildyn.2014.07.013>
3. Bayraktar A, Türker T, Tadla J, Kurşun A, Erdiş A (2017) Static and dynamic field load testing of the long span Nissibi cable-stayed bridge. *Soil Dyn Earthq Eng* 94:136–157. <https://doi.org/10.1016/j.soildyn.2017.01.019>
4. Bera KK, Chandiramani NK (2022) An element dependent multiple lag rational function approximation for aeroelastic analysis of cable bridge. *Appl Math Model* 105:95–113. <https://doi.org/10.1016/j.apm.2021.12.027>

5. Cid Montoya M, Hernández S, Nieto F (2018) Shape optimization of streamlined decks of cable-stayed bridges considering aeroelastic and structural constraints. *J Wind Eng Ind Aerodyn* 177:429–455. <https://doi.org/10.1016/j.jweia.2017.12.018>
6. Das, R., Pandey, A.D., Soumya, Mahesh, M.J., Saini, P., Anvesh, S., 2016. Progressive Collapse of a Cable Stayed Bridge. *Procedia Engineering* 144, 132–139. <https://doi.org/10.1016/j.proeng.2016.05.016>
7. Fabbrocino F, Modano M, Farina I, Carpentieri G, Fraternali F (2017) Optimal prestress design of composite cable-stayed bridges. *Compos Struct* 169:167–172. <https://doi.org/10.1016/j.compositestruct.2016.09.008>
8. Fathali MA, Dehghani E, Hoseini Vaez SR (2020) An approach for adjusting the tensile force coefficient in equivalent static cable-loss analysis of the cable-stayed bridges. *Structures* 25:720–729. <https://doi.org/10.1016/j.istruc.2020.03.054>
9. Ferreira F, Simões L (2020) Synthesis of three dimensional controlled cable-stayed bridges subject to seismic loading. *Comput Struct* 226:106137. <https://doi.org/10.1016/j.compstruc.2019.106137>
10. Fu P, Li X, Xu L, Xin L (2021) Life-cycle seismic damage identification and components damage sequences prediction for cable-stayed bridge based on fragility analyses. *Bull Earthquake Eng* 19:6669–6692. <https://doi.org/10.1007/s10518-021-01126-9>
11. Górski P, Tataru M, Stankiewicz B (2021) Vibration serviceability of all-GFRP cable-stayed footbridge under various service excitations. *Measurement* 183:109822. <https://doi.org/10.1016/j.measurement.2021.109822>
12. Gou H, Zhao T, Qin S, Zheng X, Pipinato A, Bao Y (2022) In-situ testing and model updating of a long-span cable-stayed railway bridge with hybrid girders subjected to a running train. *Eng Struct* 253:113823. <https://doi.org/10.1016/j.engstruct.2021.113823>
13. Guo X, Zhang C, Chen Z (2020) Dynamic performance and damage evaluation of a scoured double-pylon cable-stayed bridge under ship impact. *Eng Struct* 216:110772. <https://doi.org/10.1016/j.engstruct.2020.110772>
14. Heo G, Kim C, Lee C (2014) Experimental test of asymmetrical cable-stayed bridges using MR-damper for vibration control. *Soil Dyn Earthq Eng* 57:78–85. <https://doi.org/10.1016/j.soildyn.2013.10.007>
15. Javanmardi A, Ibrahim Z, Ghaedi K, Jameel M, Khatibi H, Suhatri M (2017) Seismic response characteristics of a base isolated cable-stayed bridge under moderate and strong ground motions. *Archives of Civil and Mechanical Engineering* 17:419–432. <https://doi.org/10.1016/j.acme.2016.12.002>
16. Jiang C, Wu C, Cai CS, Xiong W (2020) Fatigue analysis of stay cables on the long-span bridges under combined action of traffic and wind. *Eng Struct* 207:110212. <https://doi.org/10.1016/j.engstruct.2020.110212>
17. Kang HJ, Guo TD, Zhao YY, Fu WB, Wang LH (2017) Dynamic modeling and in-plane 1:1:1 internal resonance analysis of cable-stayed bridge. *Eur J Mech A Solids* 62:94–109. <https://doi.org/10.1016/j.euromechsol.2016.10.016>
18. Kim S-H, Park S-J, Wu J, Won J-H (2015) Temperature variation in steel box girders of cable-stayed bridges during construction. *J Constr Steel Res* 112:80–92. <https://doi.org/10.1016/j.jcsr.2015.04.016>
19. Larsen A, Larose GL (2015) Dynamic wind effects on suspension and cable-stayed bridges. *J Sound Vib* 334:2–28. <https://doi.org/10.1016/j.jsv.2014.06.009>
20. Li L, Hu S, Wang L (2017) Seismic fragility assessment of a multi-span cable-stayed bridge with tall piers. *Bull Earthquake Eng* 15:3727–3745. <https://doi.org/10.1007/s10518-017-0106-x>
21. Li, X., 2021. Assessing time-dependent damage to a cable-stayed bridge through multi-directional ground motions based on material strain measures. *Engineering Structures* 13.
22. Lopez-Núñez E, Ogueta-Gutiérrez M, Manzanares-Bercial R, Gómez-Ortega O, Franchini S, Roibás-Millán E, Sanz-Andres A (2020) Aerodynamic instability of a hinged-deck cross-section cable-stayed bridge. *J Wind Eng Ind Aerodyn* 198:104110. <https://doi.org/10.1016/j.jweia.2020.104110>

23. Lozano-Galant JA, Turmo J (2014) An algorithm for simulation of concrete cable-stayed bridges built on temporary supports and considering time dependent effects. *Eng Struct* 79:341–353. <https://doi.org/10.1016/j.engstruct.2014.08.018>
24. Lu Q, Sun Z, Zhang W (2020) Nonlinear parametric vibration with different orders of small parameters for stayed cables. *Eng Struct* 224:111198. <https://doi.org/10.1016/j.engstruct.2020.111198>
25. Lu W, He Z (2022) Effect of cable corrosion on nonlinear elastic stability of girder in Cable-Stayed bridges with floating systems. *Structures* 37:893–904. <https://doi.org/10.1016/j.istruc.2022.01.055>
26. Madrazo-Aguirre F, Ruiz-Teran AM, Ahmer Wadee M (2015) Dynamic behaviour of steel–concrete composite under-deck cable-stayed bridges under the action of moving loads. *Eng Struct* 103:260–274. <https://doi.org/10.1016/j.engstruct.2015.09.014>
27. Martínez-Rodrigo MD, Filiatrault A (2015) A case study on the application of passive control and seismic isolation techniques to cable-stayed bridges: A comparative investigation through non-linear dynamic analyses. *Eng Struct* 99:232–252. <https://doi.org/10.1016/j.engstruct.2015.04.048>
28. Martins AMB, Simões LMC, Negrão JHJO (2020) Optimization of cable-stayed bridges: A literature survey. *Adv Eng Softw* 149:102829. <https://doi.org/10.1016/j.advengsoft.2020.102829>
29. Naderian H, Cheung MMS, Shen Z, Dragomirescu E (2015) Integrated finite strip analysis for long-span cable-stayed bridges. *Comput Struct* 158:82–97. <https://doi.org/10.1016/j.compstruc.2015.05.031>
30. Ovelt M, Chorzepa MG, Durham S, Christian J, Davis B (2018) Vulnerability to failure of cable-stayed bridges for beyond-design basis wind events. *Eng Fail Anal* 91:182–200. <https://doi.org/10.1016/j.engfailanal.2018.04.038>
31. Park J, Kim H-K (2017) Effect of the relative differences in the natural frequencies of parallel cable-stayed bridges during interactive vortex-induced vibration. *J Wind Eng Ind Aerodyn* 171:330–341. <https://doi.org/10.1016/j.jweia.2017.10.010>
32. Shao X, Hu J, Deng L, Cao J (2014) Conceptual Design of Superspan Partial Ground-Anchored Cable-Stayed Bridge with Crossing Stay Cables. *J. Bridge Eng.* 19:06013001. [https://doi.org/10.1061/\(ASCE\)BE.1943-5592.0000534](https://doi.org/10.1061/(ASCE)BE.1943-5592.0000534)
33. Soyuluk K, Sicakic EA (2012) Soil–structure interaction analysis of cable-stayed bridges for spatially varying ground motion components. *Soil Dyn Earthq Eng* 35:80–90. <https://doi.org/10.1016/j.soildyn.2011.11.003>
34. Sun M, Makki Alamdari M, Kalhori H (2017) Automated Operational Modal Analysis of a Cable-Stayed Bridge. *J. Bridge Eng.* 22:05017012. [https://doi.org/10.1061/\(ASCE\)BE.1943-5592.0001141](https://doi.org/10.1061/(ASCE)BE.1943-5592.0001141)
35. Tochaei EN, Taylor T, Ansari F (2020) Effects of near-field ground motions and soil-structure interaction on dynamic response of a cable-stayed bridge. *Soil Dyn Earthq Eng* 133:106115. <https://doi.org/10.1016/j.soildyn.2020.106115>
36. Wei B, Hu Z, He X, Jiang L (2020) Evaluation of optimal ground motion intensity measures and seismic fragility analysis of a multi-pylon cable-stayed bridge with super-high piers in Mountainous Areas. *Soil Dyn Earthq Eng* 129:105945. <https://doi.org/10.1016/j.soildyn.2019.105945>
37. Wei K, He H, Zhang J, Yang C, Qin S (2021) An endurance time method-based fragility analysis framework for cable-stayed bridge systems under scour and earthquake. *Ocean Eng* 232:109128. <https://doi.org/10.1016/j.oceaneng.2021.109128>
38. Wen J, Han Q, Xie Y, Du X, Zhang J (2021) Performance-based seismic design and optimization of damper devices for cable-stayed bridge. *Eng Struct* 237:112043. <https://doi.org/10.1016/j.engstruct.2021.112043>
39. Zhang, J., 2014. Calibration of initial cable forces in cable-stayed bridge based on Kriging approach. *Finite Elements in Analysis and Design* 13.
40. Zhang Z, Li W, Ding Z, Wu X (2020) An approach to the selection of target reliability index of Cable-stayed bridge's main girder based on optimal structural parameter ratio from cost-benefit analysis. *Structures* 28:2221–2231. <https://doi.org/10.1016/j.istruc.2020.10.046>

Complex and Lightweight Tensegrity Structure Under Dynamic and Impact Loads; State of the Art



Shaikh Irfan Badiyoddin Shaikh and Rajendra B. Magar

1 Introduction

Recently, it is observed that, the interest in active structures has been increased drastically. Advances in active structure theory and practice have changed people's perceptions of structures. There are two design approaches for tensegrity structures: active design and passive design. The former can reduce use of material compared to the latter one, which will ultimately result in more lightweight tensegrity structures. However, complex tensegrity structures of varying geometries must be analyzed to explore the applications of tensegrity in practice.

The literature review extensively examined numerous scholarly articles from reputable journals to gain insights into tensegrity structures, including their advantages and limitations for practical implementation. It encompassed a comprehensive analysis of critical loadings such as dynamic and impact loading, finite element-based analysis, minimal mass design approaches, and shape optimization techniques for various geometries, particularly addressing complex geometries, which had been overlooked in the previous studies. A detailed review of the papers has been presented here.

1.1 Response and Behavior of Tensegrity Structure Under Dynamic Loading

Ma et al. [1] investigated tensegrity structures using finite element analysis. These structures consist of rigid bars and tensioned cables. The study examined both

S. I. B. Shaikh (✉) · R. B. Magar

Anjuman-I-Islam's Kalsekar Technical Campus, School of Engineering and Technology, New Panvel Affiliated to University of Mumbai, Maharashtra 410206, India

e-mail: irfofficial555@gmail.com

nonlinear and linearized versions, deriving mathematical equations to describe their dynamic behavior. Three instances were selected: a pair of pendulums connected in series, a beam supported at one end, and a tower consisting of two prisms arranged in a tensegrity configuration.

Boni and Royer-Carfagni [2] analyzed flexural tensegrity beams, for nonlinear effects for vibrations under harmonic excitations, considering the camber effect at initial stage of vibration.

Faroughi et al. [3] derived directly the inertia force vector and the tangent dynamic matrix by presenting the nonlinear dynamic analysis of truss structure in space frame. The effectiveness of the suggested approach was evaluated in relation to the traditional Lagrangian method, revealing potential savings of up to 55% in computational efforts.

Faroughi and Lee [4] used parametric studies to investigate the tensegrity footbridge's dynamic performance. The suggested tensegrity-based footbridge fits conventional static and dynamic design criteria, according to the results. Through the optimization of design and a dynamic investigation, the possibility of employing the tensegrity idea in a footbridge structural system is studied in this article.

Angellier et al. [5] did a vibratory study of the elements, a vibratory analysis of the entire structure, or a static loading analysis of the building. The experimental studies affirmed that when a structure is subjected to vertical loading, simulation results indicate that it undergoes a motion resembling a rotation; however, the exact cause of this rotation was not given.

Goyal and Skelton [6] made a significant breakthrough in balancing cable weights and bar stiffness in tensegrity structures. Unlike the previous methods, their approach accurately preserved the dynamics of rigid bars while allowing for rotational movements. The previous techniques either lacked rotational dynamics in finite element analysis or relied on massless wires. The researchers also demonstrated that incorporating flexible skin membranes improved structural stiffness.

Rimoli [7] discovered that when the impact velocity increases, the number of the worm-like oscillations increases, and the maximum load tends to saturate around the magnitude of the bar buckling load of a tensegrity-based structure.

Kan et al. [8] used two examples to demonstrate the effectiveness of the suggested element. The dynamic findings of their work also reveal that as the actuation speed tends to increase, the system's motion characteristics change from quasi-static solutions.

Sumi et al. [9] utilized finite element analysis to examine member characteristics and capture nonlinear behavior in tensegrity structures. The authors investigated the transition between different stable forms and discussed actuation principles for grippers. The authors demonstrated the importance of carefully adjusting member properties to achieve two stable equilibrium configurations.

Lu et al. [10] carried out dynamic analysis for arched shaped tensegrity structure. The authors that if the length to width ratio is reduced and pre-stress is increased, then it can significantly diminish dynamic load of wind response of arched tensegrity structures and when the height-span ratio is 0.25, the structure's overall stiffness improves.

1.2 Stability of Tensegrity Structure

Malik et al. [11] addressed the central issue and proposed a way to determine the topology of a super-stable tensegrity structure. For the complete stability of the tensegrity structures, the researchers suggested multiple topologies. The technique for identifying extremely stable (i.e., super-stable) tensegrity structures, according to the authors, began with determining the topology of fundamental extremely stable (i.e., super-stable) tensegrities taken from the graphs and then combining it to produce bigger tensegrity structures that are super-stable in nature.

Koohestani [12] proposed the form-finding and design of tensegrity structures with super-stability or without super-stability. The eigenvalues of a modified force density matrix were used to create the objective functions of two unrestrained minimization problems for tensegrities form-finding. Experiments reveal that the developed methods are both computationally and accuracy-wise very efficient.

Averseng and Dubé [13] explored the overall behavior of tensegrity structures, particularly their advantages for simply supported beam-like structures in static and dynamic scenarios. The authors focused on a 12 m footbridge as a case study, highlighting the essential steps for evaluating its performance under Ultimate Limit State and Serviceability Limit State stresses. The proposed system offered clear advantages for this application, as it could be easily transported and deployed efficiently in a folded state.

Muralidharan and Wenger [14] presented design methodologies for two types of activated tensegrity joints: revolute (R) joints and anti-parallelogram (X) joints. The article compared the characteristics of these joints and explored various case studies with different wrench-feasible workspace constraints and design requirements. The authors concluded that X-joints exhibited higher stiffness in the zero orientation range and displayed significant stiffness fluctuations within their wrench-feasible workspace.

Koohestani [15] introduced a new method for the identification of self-stabilizing equilibrium state of the tensegrity structure. The author stated the medium-scale tensegrities, the form-finding of irregular tensegrities can be performed and no need to pre-assign the unilateral response of components.

Dong et al. [16] looked at the subject of reverse form-finding for tensegrity structures in their paper. The study of their work introduced two novel algorithms. The authors did not focus on determination of practicability of this approach to scalable structures with more nodes.

Koohestani [17] provided a numerically efficient framework for tensegrity framework analytical form-finding. The proposed platform by the author Faddeev–LeVerrier method, which is a well-known method to construct needed connections among element force densities, resulting in explicit analytical parameters of self-stressed situations. The purpose of the paper was to develop a mathematical platform for tensegrity analytical form-finding. The method allowed researchers to use software tool with symbolic math abilities to identify the analytical form of tensegrities and

gave as simple as feasible mathematical connections for self-stressed equilibrium states.

Böhm et al. [18] used a strategy to find complying tensegrity structures with many stages of self-equilibrium. As illustrations, tensegrity structures in 4 planar coordinates with 2 or 3 stable equilibrium arrangements were examined and proven with experimental studies.

Xu et al. [19] presented a method for determining the topology of tensegrity systems. To validate the proposed method of quadratic computing, numerical examples were used by the authors.

1.3 Geometry, Shape, and Topology Optimization of Tensegrity Structure

Feng et al. [20] proposed a new topology of tensegrity system in such a way, which could get a new tensegrity dome structure curved in shape which will have less members than the traditional cable dome structure. At last, the authors analyzed the dynamic as well as static performance these structures and studied the defects which may likely to occur in the structure and found the possible weaknesses in the structures.

Roth and McCarthy [21] suggested that over-tensioning the tensegrities can have adverse effects, and it may reduce overall resistance against compressive load capacity. The researchers concluded that by optimizing the concept of pre-tensioning in the tensegrity, the structural integrity allows it to endure compressive loads that surpass previous literature-reported capacities by a factor of six.

Zhang et al. [22] presented a work based on solving a problem of optimization for the tensegrity structures. By solving numerical example, the authors suggested that the proposed method can be very much useful for complex tensegrity structures and its topology.

Schorr et al. [23] introduced a new way for developing reconfigurable systems based on the tensegrity principle. The issue is resolved by employing ropes that lack the ability to resist compressive forces. The Lagrange formula is used to develop structural dynamics, and numerical models are used to analyze structural behavior. The findings imply that using the tensegrity concept inside typical planar four-bar links could be beneficial.

Wang et al. [24] presented an approach for rigid tensegrity structures. As per authors, the existing design methods for the topology are invalid for the general tensegrities as they were focusing on tensegrity members which carries only axial forces. The authors treated topology as binary variable and the forces in the members as continuous variables.

Ma et al. [25] conducted shape optimization of a new tensegrity geometrical circular torus. The authors introduced the topology and configuration of the torus and parameterized it using four variables. Shape optimization was performed through

constrained nonlinear optimization, and numerical results demonstrated the effectiveness of the method. A physical model was also constructed to validate the structural system's feasibility.

Lee and Lee [26] proposed a novel way for topology design of tensegrity structures with the use of a force density approach paired with a genetic algorithm. This paper demonstrates efficiency through two well-known illustrative simulations. Finally, their findings reveal that the proposed technique performs exceptionally well. The paper also concludes that, the suggested approach does not require any element connectivity as initial input data; just nodal coordinates are required.

Gan et al. [27] developed a novel numerical technique to solve irregular tensegrity structure. Total 3 cases of test were presented in this research to demonstrate the efficiency of this method. The outcomes of this procedure serve as a reference for the design of an actual tensegrity object.

Faroughi and Lee [4] provided a design optimization study for a tensegrity-based footbridge in order to develop the tensegrity idea in current structural engineering. A new adaptive optimization approach is utilized to discover a cost-effective design solution.

Zargar and Alaghmandan [28] began by defining tensegrity hollow-rope structures, that have a broad range of applications in architectural design and building. The Force Density Method was then applied in a user-friendly context, and hollow-rope structure form-finding was performed utilizing this numerical technique in the second part. It is being developed as a new approach for tensegrity hollow-rope system design investigation, performance assessment, and structural optimization.

Zhu and Deng [29] examined the deployment and shape change of tensegrity structures. To address the inaccuracies stemming from the linear assumptions inherent in the formulation of the fundamental equation, a quantitative technique was proposed. The effectiveness of this method is substantiated by the results obtained from the analysis of a demonstrated cantilever tensegrity structure.

Branam et al. [30] offered the form-finding of tensegrity systems and along with that a nonlinear static study also. The presented method employed a Quasi-Newton method to overcome a shortcoming of the Newton–Raphson method, which is frequently utilized in commercial Finite Element software. Case studies were also shown and matched to experimental data described in the literature to illustrate the practicality of the suggested strategy, which is especially relevant for buildings with pre-tensioned components that are under-constrained.

Feron et al. [31] studied the strongest and lightest structures comparison, and a case study was created. The relevance and practicality of such tensegrity footbridges were examined.

Zhang et al. [32] produced large-scale tensegrities by combining truncated normal polyhedron tensegrities and prismatic tensegrities. This approach enabled them to create a variety of large-scale tensegrities that meet the size and topological requirements. The findings in the paper can be helpful in aiding in the production of large-scale tensegrities with delicate mechanical properties, as well as the construction of compound metamaterials.

Kan et al. [8] presented a sliding cable element for multibody system analysis. The originality of the methodology in contrast to the current previous research on sliding cables generated using the finite element method.

Spisak and Kmet [33] discussed the study for a suitable shape and adjustment of stress of a tensegrity mechanism based on predetermined criteria. The authors came to the conclusion that, if the active struts (i.e., actuators) are combined with technology, it can manage the flexibility behavior of tensegrity systems when they are subjected to the coming loads.

Sychterz and Smith [34] presented a framework with loosely connected movement spanning multiple degrees of freedom. Friction, both static and kinetic, was investigated both empirically and mathematically in this research work. To compensate for these impacts, simulations have been updated, and two approaches for quantifying friction effects were used. According to the findings in the paper, the section approach is the easiest to incorporate into dynamic-relaxation simulations.

Veuve et al. [35] observed and used the control approaches which lead to the creation of an effective learning approach and a mechanism for compensating damage for a deployable tensegrity structure.

Kmet and Mojdis [36] explored an adaptive cable dome which sensors in it. The dome consisted of 42 cables and 6 compressive struts with an addition of central strut. The authors carried out experimental as well as theoretical analysis and compared the results for the dome with cables and struts.

1.4 Minimal Mass Design Approach

Wang et al. [37] proposed an approach for designing active tensegrity structures for the minimal mass. As per this method, all 4 factors, i.e., pre-stress, actuator, cross-sectional areas, and the control strategies all designed simultaneously, treating these factors as continuous variables, and the layout is treated binary variable. The researchers further designed three tensegrity structures (active ones) through the proposed approach and they standardized the results with the passive method of minimal mass design.

Ma et al. [25] introduced the topology and configuration of a new tensegrity torus. The authors then proposed minimal mass design of the torus under loaded and unloaded conditions. Their aim was to minimize the total mass.

Chen and Skelton [38] presented an approach for minimal mass design of bar tensegrities or hollow tensegrities by applying any forces on them. Several nonlinear programming issues were generated as a result of the methodology. The paper gives a fundamental knowledge of materials and constructions.

Ma et al. [39] started with the prime objective of paper on the design of a novel cantilever structure and the refinement of its minimal mass under deformation and bending limitations. Initially, the least mass design of a double-element structure is investigated, either with or without a wall anchorage length constraint. The authors

came to the conclusion that as the compensation for joint weight grows, the optimal difficulty drops while total mass keeps increasing.

Goyal et al. [40] focused on developing compressive force-resistant tensegrity-based lattices with minimal mass. The authors calculated the weight of these structures considering pre-stress force and external force using analytical formulas. The author's innovative approach showcased how lightweight load-bearing architectural materials can be designed using minimal mass tensegrity T-bar lattices, demonstrating that maximizing the cross-sectional area of the strings yields lower mass solutions compared to enhancing pre-stress dispersion.

Fraddosio et al. [41] calculated the minimum mass of the modules by taking into consideration the buckling capacity of elements in self-equilibrium conditions, as per typical building codes.

2 Research Gap from Literature Review

Previously for the complex tensegrity structures, minimal mass design with only dynamic loading and active design consideration has been considered, but there is also need of consideration of minimal mass design along with parameters such as impact loading, energy absorption consideration and consideration of dynamic loading, temperature stresses, and blast loading.

Although previous studies have explored the two design approaches for tensegrity structure design—active design and passive design, there appears to be a gap in the literature regarding the comprehensive analysis of complex tensegrity structures with varying geometries. Furthermore, the consideration of special topological variables and shape optimization in such structures has been overlooked. Consequently, there is a need for further research to bridge this gap and enhance the understanding of creating more lightweight tensegrity structures while incorporating these crucial aspects.

3 Conclusion

With the current challenges of analyzing and optimizing the complex geometry of tensegrity structures, especially when considering dynamic and impact loads, there is significant potential for further research in this field. Previous studies have focused on minimal mass design and dynamic loading, as well as active design considerations. However, there is a need to also consider minimal mass design in relation to parameters such as impact loading, energy absorption, dynamic loading, temperature stresses, and blast loading.

While active designs have shown promise in reducing material consumption and creating lighter tensegrity structures compared to passive designs, there is still a requirement to analyze complex tensegrity structures with varying geometries. This

analysis should incorporate special topological variables and shape optimization techniques.

In essence, there is ample scope for studying complex tensegrity structures by adopting shape optimization and utilizing minimal mass design principles. These approaches can help create lighter weight structures capable of withstanding dynamic and impact loads. Additionally, it is important to consider parameters such as energy absorption, temperature stresses, and blast loading to enhance the overall performance and safety of the structures.

To summarize, the two main design approaches for tensegrity structures are active and passive design. While active design can reduce material consumption and result in lighter structures, further analysis is needed for complex structures with varying geometries. This analysis should take into account special topological variables and employ shape optimization techniques to achieve optimal performance.

References

1. Ma S, Chen M, Skelton RE (2022) Tensegrity system dynamics based on finite element method. *Compos Struct* 280:114838. <https://doi.org/10.1016/j.compstruct.2021.114838>
2. Boni C, Royer-Carfagni G (2021) Nonlinear effects in the vibrations of flexural tensegrity beams. *Int J Non-Linear Mech* 128:103616. <https://doi.org/10.1016/j.ijnonlinmec.2020.103616>
3. Faroughi S, Khodaparast HH, Friswell MI (2015) Non-linear dynamic analysis of tensegrity structures using a co-rotational method. *Int J Non-Linear Mech* 69:55–65. <https://doi.org/10.1016/j.ijnonlinmec.2014.11.021>
4. Faroughi S, Lee J (2015) Analysis of tensegrity structures subject to dynamic loading using a Newmark approach. *J Build Eng* 2:1–8. <https://doi.org/10.1016/j.jobe.2015.03.005>
5. Angellier N, Dubé JF, Quirant J, Crosnier B (2013) Behavior of a double-layer tensegrity grid under static loading: identification of self-stress level. *J Struct Eng* 139:1075–1081. [https://doi.org/10.1061/\(ASCE\)ST.1943-541X.0000710](https://doi.org/10.1061/(ASCE)ST.1943-541X.0000710)
6. Goyal R, Skelton RE (2018) Dynamics of class I tensegrity systems including cable mass, in: earth and space 2018. In: 16th biennial international conference on engineering, science, construction, and operations in challenging environments. American Society of Civil Engineers, Cleveland, Ohio, pp 868–876. <https://doi.org/10.1061/9780784481899.082>
7. Rimoli JJ (2018) A reduced-order model for the dynamic and post-buckling behavior of tensegrity structures. *Mech Mater* 116:146–157. <https://doi.org/10.1016/j.mechmat.2017.01.009>
8. Kan Z, Peng H, Chen B, Zhong W (2018) A sliding cable element of multibody dynamics with application to nonlinear dynamic deployment analysis of clustered tensegrity. *Int J Solids Struct* 130–131:61–79. <https://doi.org/10.1016/j.ijsolstr.2017.10.012>
9. Sumi S, Böhm V, Zimmermann K (2017) A multistable tensegrity structure with a gripper application. *Mech Mach Theory* 114:204–217. <https://doi.org/10.1016/j.mechmachtheory.2017.04.005>
10. Lu C, Lu S, Wang X (2014) Wind-induced dynamic analysis of the arched tensegrity structures in time domain, in: computing in civil and building engineering. In: 2014 international conference on computing in civil and building engineering. American Society of Civil Engineers, Orlando, Florida, United States, pp 1174–1181. <https://doi.org/10.1061/9780784413616.146>
11. Malik PK, Guha A, Seshu P (2022) Topology identification for super-stable tensegrity structure from a given number of nodes in two dimensional space. *Mech Res Commun* 119:103810. <https://doi.org/10.1016/j.mechrescom.2021.103810>

12. Koohestani K (2013) A computational framework for the form-finding and design of tensegrity structures. *Mech Res Commun* 54:41–49. <https://doi.org/10.1016/j.mechrescom.2013.09.010>
13. Averseng J, Dubé JF (2012) Design, analysis and self stress setting of a lightweight deployable tensegrity modular structure. *Procedia Eng* 40:14–19. <https://doi.org/10.1016/j.proeng.2012.07.048>
14. Muralidharan V, Wenger P (2021) Optimal design and comparative study of two antagonistically actuated tensegrity joints. *Mech Mach Theory* 159:104249. <https://doi.org/10.1016/j.mechmachtheory.2021.104249>
15. Koohestani K (2020) Innovative numerical form-finding of tensegrity structures. *Int J Solids Struct* 206:304–313. <https://doi.org/10.1016/j.ijsolstr.2020.09.034>
16. Dong W, Stafford PJ, Ruiz-Teran AM (2019) Inverse form-finding for tensegrity structures. *Comput Struct* 215:27–42. <https://doi.org/10.1016/j.compstruc.2019.01.009>
17. Koohestani K (2017) On the analytical form-finding of tensegrities. *Compos Struct* 166:114–119. <https://doi.org/10.1016/j.compstruct.2017.01.059>
18. Böhm V, Sumi S, Kaufhold T, Zimmermann K (2017) Compliant multistable tensegrity structures. *Mech Mach Theory* 115:130–148. <https://doi.org/10.1016/j.mechmachtheory.2017.04.013>
19. Xu X, Wang Y, Luo Y (2016) General approach for topology-finding of tensegrity structures. *J Struct Eng* 142:04016061. [https://doi.org/10.1061/\(ASCE\)ST.1943-541X.0001532](https://doi.org/10.1061/(ASCE)ST.1943-541X.0001532)
20. Feng Y, Yuan X, Samy A (2022) Analysis of new wave-curved tensegrity dome. *Eng Struct* 250:113408. <https://doi.org/10.1016/j.engstruct.2021.113408>
21. Roth JK, McCarthy TJ (2021) Optimizing compressive load capacity for differing tensegrity geometries. *Comput Struct* 249:106523. <https://doi.org/10.1016/j.compstruc.2021.106523>
22. Zhang P, Zhou J, Chen J (2021) Form-finding of complex tensegrity structures using constrained optimization method. *Compos Struct* 268:113971. <https://doi.org/10.1016/j.compstruct.2021.113971>
23. Schorr P, Chavez J, Zentner L, Böhm V (2021) Reconfiguration of planar quadrilateral linkages utilizing the tensegrity principle. *Mech Mach Theory* 156:104172. <https://doi.org/10.1016/j.mechmachtheory.2020.104172>
24. Wang Y, Xu X, Luo Y (2020) Topology design of general tensegrity with rigid bodies. *Int J Solids Struct* 202:278–298. <https://doi.org/10.1016/j.ijsolstr.2020.05.030>
25. Ma S, Yuan X-F, Samy A (2019) Shape optimization of a new tensegrity torus. *Mech Res Commun* 100:103396. <https://doi.org/10.1016/j.mechrescom.2019.103396>
26. Lee S, Lee J (2016) A novel method for topology design of tensegrity structures. *Compos Struct* 152:11–19. <https://doi.org/10.1016/j.compstruct.2016.05.009>
27. Gan BS, Zhang J, Nguyen D-K, Nouchi E (2015) Node-based genetic form-finding of irregular tensegrity structures. *Comput Struct* 159:61–73. <https://doi.org/10.1016/j.compstruc.2015.07.003>
28. Zargar SH, Alaghmandan M (2021) HALO: interactive equilibrium approach in designing tensegrity hollow-rope structures. *J Archit Eng* 27:04021026. [https://doi.org/10.1061/\(ASCE\)AE.1943-5568.0000487](https://doi.org/10.1061/(ASCE)AE.1943-5568.0000487)
29. Zhu D, Deng H (2020) Deployment of tensegrities subjected to load-carrying stiffness constraints. *Int J Solids Struct* 206:224–235. <https://doi.org/10.1016/j.ijsolstr.2020.08.022>
30. Branam NJ, Arcaro V, Adeli H (2019) A unified approach for analysis of cable and tensegrity structures using memoryless quasi-newton minimization of total strain energy. *Eng Struct* 179:332–340. <https://doi.org/10.1016/j.engstruct.2018.11.004>
31. Feron J, Boucher L, Denoël V, Lateur P (2019) Optimization of footbridges composed of prismatic tensegrity modules. *J. Bridge Eng* 24:04019112. [https://doi.org/10.1061/\(ASCE\)BE.1943-5592.0001438](https://doi.org/10.1061/(ASCE)BE.1943-5592.0001438)
32. Zhang L-Y, Li S-X, Zhu S-X, Zhang B-Y, Xu G-K (2018) Automatically assembled large-scale tensegrities by truncated regular polyhedral and prismatic elementary cells. *Compos Struct* 184:30–40. <https://doi.org/10.1016/j.compstruct.2017.09.074>
33. Spisak M, Kmet S (2017) Shape and stress modification of a chosen tensegrity system. *Procedia Eng* 190:637–644. <https://doi.org/10.1016/j.proeng.2017.05.391>

34. Sychterz AC, Smith IFC (2017) Joint friction during deployment of a near-full-scale tensegrity footbridge. *J Struct Eng* 143:04017081. [https://doi.org/10.1061/\(ASCE\)ST.1943-541X.0001817](https://doi.org/10.1061/(ASCE)ST.1943-541X.0001817)
35. Veuve N, Sychterz AC, Smith IFC (2017) Adaptive control of a deployable tensegrity structure. *Eng Struct* 152:14–23. <https://doi.org/10.1016/j.engstruct.2017.08.062>
36. Kmet S, Mojdis M (2015) Adaptive cable dome. *J Struct Eng* 141:04014225. [https://doi.org/10.1061/\(ASCE\)ST.1943-541X.0001189](https://doi.org/10.1061/(ASCE)ST.1943-541X.0001189)
37. Wang Y, Xu X, Luo Y (2021) Minimal mass design of active tensegrity structures. *Eng Struct* 234:111965. <https://doi.org/10.1016/j.engstruct.2021.111965>
38. Chen M, Skelton RE (2020) A general approach to minimal mass tensegrity. *Compos Struct* 248:112454. <https://doi.org/10.1016/j.compstruct.2020.112454>
39. Ma S, Chen M, Skelton RE (2020) Design of a new tensegrity cantilever structure. *Compos Struct* 243:112188. <https://doi.org/10.1016/j.compstruct.2020.112188>
40. Goyal R, Skelton RE, Peraza Hernandez EA (2020) Design of minimal mass load-bearing tensegrity lattices. *Mech Res Commun* 103:103477. <https://doi.org/10.1016/j.mechrescom.2020.103477>
41. Fraddosio A, Pavone G, Piccioni MD (2019) Minimal mass and self-stress analysis for innovative V-expander tensegrity cells. *Compos Struct* 209:754–774. <https://doi.org/10.1016/j.compstruct.2018.10.108>

Demountable Shear Connector in Steel–Concrete Composite Floors: A State-of-the-Art Review



G. Suba Sreenidhi and G. Senthil Kumar

1 Introduction

The rising use of non-renewable, finite resources on a worldwide scale, the ensuing shortages of essential raw materials, the ineffective management of garbage, and the limited space available for final garbage disposal are among the present global concerns. The issue of sustainability and material recycling has also become more obvious as the rate of carbon emissions into the atmosphere has increased. The building industry's demolition debris contributes significantly to this issue by creating pollution or energy consumption during the recycling process, both of which have an adverse impact on the environment. To correct this, steel components were recycled for additional use in steel–concrete composite construction. In the current construction method, composite action is performed by shear studs that are put into the concrete slab and attached to the steel beam flange by profiled sheeting. Due to the existence of welded shear connectors, deconstructing, modifying, and disassembling composite structures at the end of their design life is extremely challenging. As a result, steel beams undergo recycling rather than being utilized right away. Recycling uses a lot of energy and contributes to atmospheric carbon dioxide emissions. To get around this, demountable shear connectors are used in place of welded shear studs to form a monolithic connection between the deck sheet and the beam [1].

Steel–concrete composite structural systems are becoming more and more common because of their adaptability, adaptability, ability to be disassembled and reused, and impact on the economy and environment. This is especially true when combined with the controlled manufacturing processes used in the shop, just like in the mechanical and automotive engineering disciplines. Investigations into steel

G. Suba Sreenidhi (✉) · G. Senthil Kumar
Civil Engineering Department, Easwari Engineering College (Autonomous), Chennai, India
e-mail: subasreenidhi31@gmail.com

G. Senthil Kumar
e-mail: senthilkumar.g@eec.srmmp.edu.in

and concrete structures have focused on spanning longer spans, lowering floor self-weight, and minimizing floor depth [2]. The use of the demountable floor system (ReuseStru) in buildings results in the best level of ecological sustainability across many impact areas, according to additional research. When compared to conventional systems, the ReuseStru system considerably lowers greenhouse gas emissions by at least 80 kg CO₂-eq/m². Additionally, it significantly lowers primary energy use, with a drop of at least 800 MJ/m². ReuseStru is an environmentally friendly option because of these outstanding results, which help create a sustainable environment [3]. Despite being often used for shear connections, welded shear stud connectors are not ideal for preserving the original configuration during building demounting, deconstruction, or maintenance. Demountable shear connectors are used in place of shear studs. There are numerous authors and researchers who have studied the subject of demountable shear connectors in steel–concrete or reinforced concrete composite flooring. They have proposed suggestions, tested them experimentally and performing computational analysis of a lot of solutions. This article gives an overall review (state-of-the-art review) of demountable shear connections in steel–concrete composite floors to give readers a thorough grasp of the current concepts. The load-carrying mechanisms and other pertinent characteristics of the shear connections are categorized, allowing for a more thorough investigation of the subject. Each section's discussion of each category is succinct. Table 1 gives an overview and a chronological listing of the published studies on demountable shear connections for a consolidated reference or perspective [4, 5].

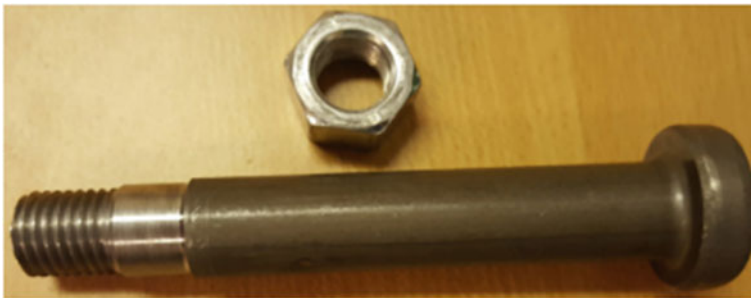
2 Studs with Threaded Heads

The experiments looked at variations in the studs' threaded and collar lengths as well as the strength of the concrete, the placement of reinforcement in the push-out test setup, the temperature during loading, and the height of the shear connector. Due to the stud-hole clearance, connections formed with threaded studs behaved considerably different from the connections made with welded studs in terms of initial stiffness. But the ultimate strength of shears for both connectors was almost identical. Threaded studs have two primary failure mechanisms, similar to welded shear connectors, i.e., connector failure and concrete crushing [6]. The complete transfer of shear force in demountable shear connectors occurs through the action of shearing between the bolt thread and the concrete bearing surrounding it. Although it is anticipated that the initial stiffness will be lessened by the presence of bolt slide within the hole. This loss of stiffness may have an impact on beam deflections and potentially introduce challenges related to serviceability [7] (Fig. 1).

Threaded bolts serving as shear connectors considerably improved the effectiveness of cold-formed steel–concrete combination slabs. The strength of these composite slabs is slightly influenced by where the bolts are placed across the cross section. The pre-yield stiffness properties are more influenced by the size of the bolts utilized, whereas the post-yield rigidity is influenced by the bolts' transverse

Table 1 Summarized reviewed studies on shear connectors

Reference No.	Year	Types of shear connectors used	Tests conducted	Experimental/ numerical
[6]	2016	Demountable headed stud shear connector	Push-off tests	Exp
[7]	2017	Threaded headed studs, welded headed studs	Push-off test	Exp
[8]	2020	Threaded bolts	Static load test	Exp
[9]	2022	Threaded headed bolts	Push-out test	Exp and Num
[10]	2022	Lockbolt demountable shear connector	Push-out test	Exp and Num
[11]	2010	Bolts with integrated nuts, adhesive anchors, and friction-grip bolts	Push-out test	Exp
[12]	1971	Friction-grip bolt	Push-out test	Exp
[13]	2015	High-strength friction-grip bolt	Push-out test	Exp and Num
[14]	2013	Bolt with embedded nuts	Push-out test	Exp and Num
[15]	2014	Bolts with embedded nuts	Beam test	Exp
[16]	2018	Bolts with couplers, welded headed studs	Static push-out test	Exp
[17]	2022	Steel block shear connector	Static load test	Exp
[18]	2019	Encased bolts, high-tension friction-grip bolts, Anchor bolts	Push-out test	Exp
[19]	2018	High-strength bolts	Push-off test	Exp and Num
[20]	2022	Hex head screws	Vibration test-heel drop test	Exp and Num
[21]	2020	Headed stud, rectangular steel pipe shear connector	Push-out test	Exp and Num
[22]	2021	Headed stud	Static load test	Exp and Num

**Fig. 1** Threaded headed stud [7]

distribution [8]. The bolt size and bolt grade are the key factors that affect the bolt shear connection's ultimate shear load capacity, according to a study based on finite element analysis. The degree of friction among the precast concrete slab with the steel beam is increased by increasing the preloading force supplied via the bolt in demountable shear connectors. In turn, this causes the amount of force needed to break the link to rise. Moreover, the clearance between the bolt and the slab, as well as the steel beam, decreases as the preloading force is augmented. Consequently, a higher force is needed to break the connection [9]. Threaded studs were used in place of welded studs to boost the deformation capabilities of composite shear connections made with ultra-high-performance concrete [10].

3 Friction-Grip Bolts

Recent years have seen a rise in interest in the study of friction-grip bolts. Testing has been conducted on three distinct types of shear connections, including friction-grip bolts, with the goal of post-installing bolts to produce a composite action in the structure. The study encompasses both finite element numerical simulations and single bolt shear tests conducted under static and fatigue loads [11]. In push-out tests, shear connectors made of high-strength friction-grip bolts of various sizes were assessed. In this test, the turn-of-nut method was used to post-tension the bolts into the slab once the concrete had attained the requisite strength. When exposed to service loads with a high rate of composite effectiveness, the high-strength bolted shear connectors gives the steel beam and slab an extremely rigid connection [12].

Friction-grip bolted shear connectors have been introduced as a development in the study. Experimental testing revealed that beams with embedded friction-grip bolts within monolithic slabs exhibited higher ductility but decreased ultimate capacity compared to beams in prefabricated slabs with friction-grip fasteners that have been inserted after the fact. The load-slip response of high-strength friction-grip bolt shear connectors was explained based on the findings. Slip occurred initially due to the space between bolts and prepared holes. Pretension in the shear connection eliminated friction at the steel–concrete interface. As the bolts made contact with the holes in the slab, a third behavior condition emerged. Slip resulted from clearance between prefabricated holes and bolts after preload-induced friction was removed. This slip was approximately equal to the sum of distances between bolts and holes in the steel flange and concrete slab. Overcoming this slip led to a nonlinear relationship between load and slip. These three stages of bolt behavior were added into the analytical framework for analyzing shear connections in composite beams utilizing pre-tensioned bolts [13] (Fig. 2).

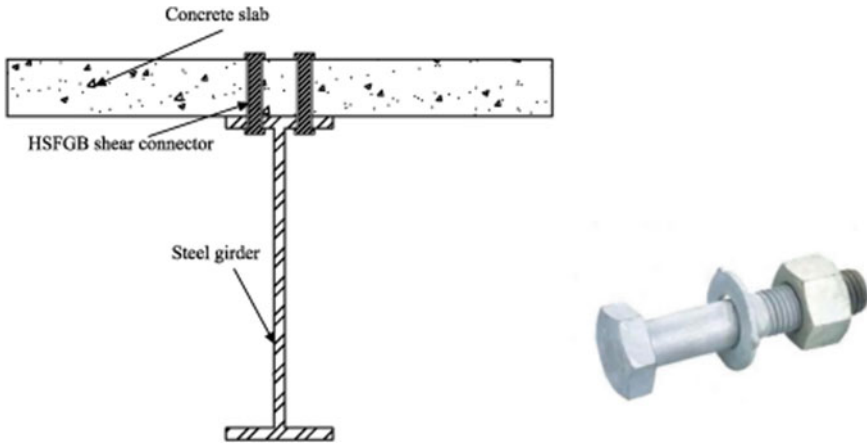


Fig. 2 Friction-grip bolt shear connector (high-strength) [13]

4 Bolt with Embedded Nuts

The structural behavior of bolts with embedded nuts has drawn the interest of researchers, along with high-strength friction-grip bolts and bolts without embedded nuts. Real push-out tests and finite element analysis were carried out to obtain a deeper comprehension of the failure mechanisms related to bolts with embedded nuts in order to provide design suggestions for bolted shear connections in contemporary buildings. It was discovered that the shear connection using bolts with a single integrated nut displayed less stiffness under serviceability loads than welded headed studs [14]. Using experimental testing on three beams of various spans, additional information regarding the characteristics of bolts with the embedded nut was provided. The researchers discovered that fastened beams showed equal resistivity when compared with headed studs, with lower moment capabilities [15] (Fig. 3).

5 Bolt with Coupler System

The use of bolts with coupler system in composite steel–concrete floors was an attempt to simplify the procedure of replacing bolts. The first evaluations of this kind of shear connectors involved changing the bolt properties and comparing the results of push-out experiments with welded headed studs to examine the performance [16]. The two coupler system types that were investigated were pre-tensioned bolts and bolts that had epoxy glue injected into the steel flange hole. A coupler of greater quality than the bolt was selected to be welded into the profile section because it provides the intended shear damage via the threaded part of an inferior bolt, which is conveniently replaceable (Fig. 4).

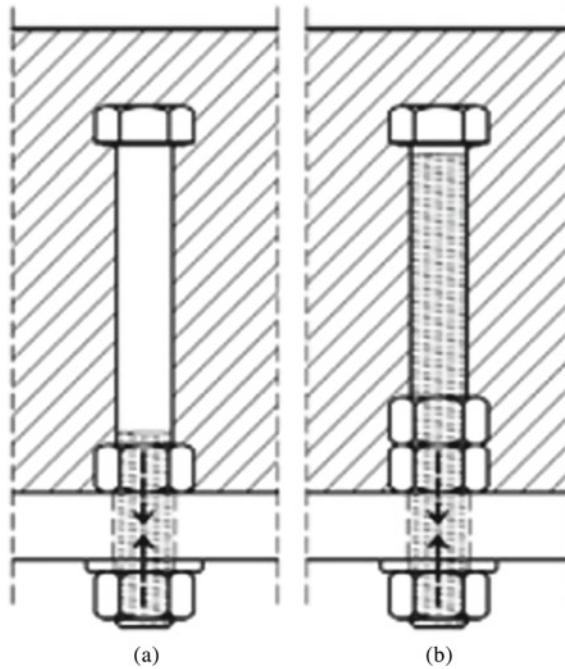


Fig. 3 a Bolt with single embedded nut and b bolt with double embedded nut [14]

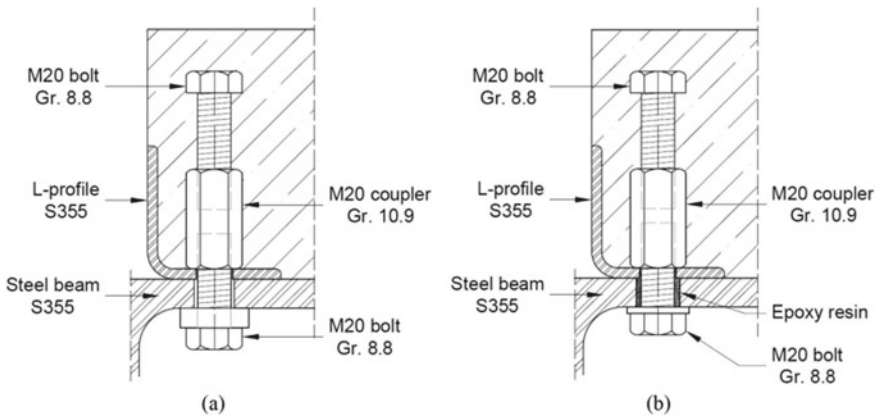


Fig. 4 Coupler system with a pre-tensioned bolts and b epoxy resin [16]

While epoxy resin coated bolts were used in the beam test on composite slabs with profiles metal decking, push-out tests on solid slabs tested both types of coupler connections. Although the initial stiffness of all the connectors is comparable, both

types of bolts experience a loss of stiffness when the friction resistance is overcome with applied pretension force. All of the bolted connectors that were exhibited experienced brittle shear failure of the bolts and no other damage were found [18].

6 Discussion

Shear connectors play a crucial role in composite systems, enabling efficient deconstruction in line with sustainable infrastructure goals. Unlike headed stud connectors that are welded to the steel flange, bolted shear connectors can be easily disassembled by unbolting them at the end of their service lives. Investigations have demonstrated that in composite systems, bolted shear connectors can achieve a high degree of stiffness against shear under static stresses, although they may not surpass the shear resistance provided by headed studs. However, bolted shear connectors exhibit significantly greater fatigue strength. While composite elements with headed studs initially exhibit higher stiffness than those with bolted shear connectors, they experience a sudden loss of interaction between the slab and steel beam once the connectors reach their strength capacity (Fig. 5).

The high-tension friction-grip bolt connector specimens exhibit exceptionally high stiffness at lower loading conditions because this method of connection uses friction as a shear-transfer mechanism during early loading. The average ultimate slip of the high-tension friction-grip bolt connector was significantly greater than that of the double-nut bolt connectors. Using the high-strength friction-grip bolt connector, a composite beam can complete its composite action without slipping at the steel–concrete contact before resistance is overcome.

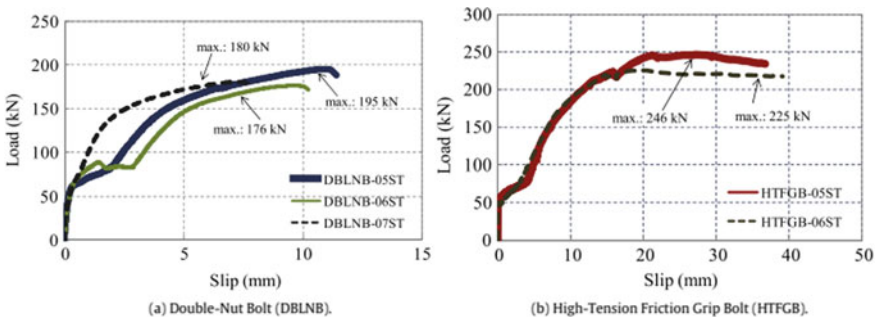


Fig. 5 Load-slip curves obtained from static test results [11]

7 Conclusion

A review of different shear connector types used in composite structures has been done. Numerous unique concepts and solutions may be expected in the future, as evidenced by the fact that several articles on friction-grip bolts, threaded studs, coupler systems, and bolt with embedded nuts have been published during the past few years. Undoubtedly, the bolt shear resistance indicated in the code cannot be implemented in the case of bolted shear connections due to the additional resistance provided by friction effects in bolts [14]. Furthermore, in order to permit structure reuse, it is required to restrict connector deformation during design and prevent beam plastic reaction. Using bolted shear connections with integrated nuts, certain recommendations for the analyzed connection with demountable steel–concrete beams have been supplied through study on the ideal span to depth ratio [15]. Other researchers highlight that certain demountable shear connectors are ineligible for experimental evaluation of connector ductility. Due to the fact that some bolted connectors exhibit substantial slip before reaching their maximum strength while welded studs exhibit significant deformations after reaching their maximum load, some bolted connectors behave differentially to load slip as welded headed studs.

References

1. Govindan SK (2020) A sustainable flooring system using cold formed-hot rolled steel built-up composite section. Ph.D thesis, IIT Hyderabad
2. Ahmed IM, Tsavdaridis KD (2019) The evolution of composite flooring systems: applications, testing, modelling and Eurocode design approaches. *J Constr Steel Res* 155:286–300. <https://doi.org/10.1016/j.jcsr.2019.01.007>
3. Brambillaa G, Lavagnaa M, Vasdravellisb G (2019) Carlo andrea castiglioni, environmental benefits arising from demountable steel-concrete composite floor systems in buildings. *Resour Conserv Recycl* 141:133–142. <https://doi.org/10.1016/j.resconrec.2018.10.014>
4. Govindan SK, Madhavan M (2019) Experimental and analytical study of lightweight floor system built-up with cold-formed profile steel sheet and hot-rolled steel plate (CFPSS-HRSP). In: *Structures*, vol 22. Elsevier, pp 291–309
5. Govindan SK, Madhavan M (2019) Study on cold-formed and hot-rolled steel composite panel system. In: *Structures*, vol 20. Elsevier, pp 886–902
6. Rehman N, Lam D, Dai X, Ashour AF (2016) Experimental study on demountable shear connectors in composite slabs with profiled decking. *J Constr Steel Res* 122:178–189. <https://doi.org/10.1016/j.jcsr.2016.03.021>
7. Rehman N, Lam D, Dai X, Ashour A (2018) Testing of composite beam with demountable shear connectors. *Proce Inst Civ Eng Struct Build* 171(1):3–16. <https://doi.org/10.1680/jstbu.16.00172>
8. Adil Dara M, Subramanianb N, Darc AR, Ghowsia AF, Sidiqic F, Fayazc S, Mirc MS (2020) Comparison of various shear connectors for improved structural performance in CFS concrete composite slabs. *Eng Struct* 220:111008. <https://doi.org/10.1016/j.engstruct.2020.111008>
9. Ataei A (2022) Modelling of demountable steel-concrete composite connections, Validation of finite element model and parametric study. *J Constr Steel Res* 198:107585. <https://doi.org/10.1016/j.jcsr.2022.107585>

10. Wang JY, Guo JY, Jia LJ, Chen SM, Dong Y (2017) Push-out tests of demountable headed stud shear connectors in steel-UHPC composite structures. *Compos Struct* 170(1):69–79. <https://doi.org/10.1016/j.compstruct.2017.03.004>
11. Kwon G, Engelhardt MD, Klingner RE (2010) Behavior of postinstalled shear connectors under static and fatigue loading. *J Constr Steel Res* 66(4):532–541. <https://doi.org/10.1016/J.JCSR.2009.09.012>
12. Marshall W, Nelson H, Banerjee H (1971) An experimental study of the use of high-strength friction grip bolts as shear connectors in composite beams. *Structural Engineer* 49(4):171–178
13. Liu X, Bradford MA, Lee MS (2015) Behavior of high-strength friction-grip bolted shear connectors in sustainable composite beams. *J Struct Eng* 141(6):04014149. [https://doi.org/10.1061/\(ASCE\)ST.1943-541X.0001090](https://doi.org/10.1061/(ASCE)ST.1943-541X.0001090)
14. Pavlović M, Marković Z, Veljković M, Buđevac D (2013) Bolted shear connectors versus headed studs behaviour in push-out tests. *J Constr Steel Res* 88:134–149. <https://doi.org/10.1016/j.jcsr.2013.05.003>
15. Moynihan MC, Allwood JM (2014) Viability and performance of demountable composite connectors. *J Constr Steel Res* 99:47–56. <https://doi.org/10.1016/j.jcsr.2014.03.008>
16. Yang F, Liu Y, Jiang Z, Xin H (2018) Shear performance of a novel demountable steel-concrete bolted connector under static push-out tests. *Eng Struct* 160:133–146. <https://doi.org/10.1016/j.engstruct.2018.01.005>
17. Xiong G, Li W, Wang X, Liu J, Bai Y, Frank Chen Y (2022) Flexural behavior of prefabricated high-strength steel-concrete composite beams with steel block connectors. *J Constr Steel Res* 197:107507. <https://doi.org/10.1016/j.jcsr.2022.107507>
18. Cicione A, Walls R (2022) The effect of shear connectors on the strength, serviceability and dynamic response of composite floors using cold-formed steel beams and concrete in decking. *Eng Struct* 269:114806. <https://doi.org/10.1016/j.engstruct.2022.114806>
19. Zhu X, Takimoto K, Tanaka H, Okubo N, Higashiyama H (2020) Properties of an innovative shear connector in a steel-concrete composite slab. *J Constr Steel Res* 172:106165. <https://doi.org/10.1016/j.jcsr.2020.106165>
20. Wang Z, Yan J, Lin Y, Fan F (2021) Influence of shear connectors on the ultimate capacity of steel-UHPC-steel slabs subjected to concentrated loads. *Eng Struct* 231:111763. <https://doi.org/10.1016/j.engstruct.2020.111763>
21. EN1993-1-1.: Eurocode 3: Design of steel structures. Part 1-1: General rules and rules for buildings. Brussels: CEN, 2005
22. EN1994-1-1.: Eurocode 4: Design of composite steel and concrete structures. Part 1-1: General rules and rules for buildings. Brussels: CEN, 2004

Effect of Steel Fibre and Plastering Sand on GGBS and Silica Fume Based Geo-Polymer Concrete



C. Gowthamaraj and G. Vimalanandan

1 Introduction

There has always been a need to find a technique to lessen the bitterness of materials used in civil engineering that are based on clay, lime, and cement. Today, steel fibre is primarily utilised to reinforce concrete and solve the bitterness issue [1, 2]. Professor Davidovits, introduced the geopolymer technology in 1978, and it has been emerged as one of the most significant advances in sustainable and affordable building materials. It can entirely replace the requirement for regular Portland cement. Geo-polymer cement is produced by polymerizing aluminium silicate minerals, such as GGBS, fly ash, rice husk ash, and others, with alkaline liquids, such as sodium hydroxide and sodium silicate or potassium hydroxide and potassium silicate [2–4]. If the superplasticizer dosage was increased in the mortar, both the workability and compressive strength increased [5]. Concrete's mechanical characteristics, durability, and serviceability are improved by the use of several types of fibres [6]. The production of geopolymer concrete reduces CO₂ emissions while also utilising an industrial by-product to produce a green and sustainable building material [7–12].

The 8 and 10 M of Molarity solutions are used to make the mixture. The cube compressive strength for 8 and 10 M of Molarity solutions was calculated for various combinations [8, 13]. Fresh concrete's workability significantly decreased as the sodium hydroxide content increased, but its matching compressive strength improved. Concrete specimens produced their greatest compressive strength when the sodium hydroxide level was 12 Molarity [13].

When subjected to sulphuric acid, five percent sodium sulphate, and sodium chloride, geopolymer concrete loses weight and strength at a pace that is substantially slower than that of cement concrete [14]. As a result, geopolymer concrete is viewed

C. Gowthamaraj (✉) · G. Vimalanandan

Department of Civil Engineering, Faculty of Engineering and Technology, SRM Institute of Science and Technology, Kattankulathur, Tamil Nadu 603203, India
e-mail: gc0290@srmist.edu.in

Table 1 Properties of GGBS

Specific gravity	2.84
IS code	IS12089 1987
CaO	39
SiO ₂	34
Al ₂ O ₃	14
Fe ₂ O ₃	0.2
MgOs	10

as a construction material free of environmental pollution [10]. Due to the widespread usage of concrete, mortar, and plastering products, natural sand is widely used globally [15]. This paper evaluates the steel fibre behaviour on silica fume and GGBS established geopolymer concrete with various trial mixes.

2 Materials and Methodology

2.1 Materials

This chapter covers the components needed to manufacture concrete, their characteristics, and the methodologies for mix designs. We use ground granulated blast furnace slag (GGBS) and silica fume as binders, M-sand as fine aggregates, broken stone as coarse aggregates, sodium silicate solution, and sodium hydroxide solution as alkaline activator solutions.

2.1.1 Ground Granulated Blast Furnace Slag (GGBS)

It is an outcome when slag and iron are melted together. When the furnace is filled with limestone, coke, and iron ore, the resultant molten slag will float above the molten iron at degrees of 1500–1600 °C. By tapping from the molten iron, siliceous, and aluminous residue-containing slag can be formed. The glassy granulate material can then be obtained by quenching the slag in water. To create GGBS, the material is acquired, dried, and ground to the required size (Table 1).

2.1.2 Silica Fume

Microsilica, another name for silica fume, is an outgrowth of making silicon metal/ferrosilicon alloys. Due to its chemistry and physical characteristics, it is also referred to as a highly reactive pozzolan. It is one of the admixtures used in the concrete most extensively. The placement, finishing, and curing of the concrete carrying silica fume

Table 2 Properties of silica fume

Specific gravity	2.21
IS code	IS15388 2003
Mean size	0.15 μm
Specific area	200,000 cm^2/g
SiO ₂	84%
Fe ₂ O ₃	1.87%
Al ₂ O ₃	1.89%
CaO	2.05%

Table 3 Properties of sodium silicate solution

Na ₂ O/SiO ₂	3.22
%SiO ₂	28.7
%Na ₂ O	8.9
Specific gravity	1.63
Ph	11.3
Viscosity (cp)	180

may require special consideration on the part of the contractor. When required to be mixed in concrete for the manufacturing of concrete, it does not require the assistance of trained labourers (Table 2).

A common nickname for sodium silicate is ‘water glass.’ Sand ($\text{Na}_2\text{SiO}_3 + \text{SiO}_2$) and soda ash are fused together at a high temperature to create it. It results in the formation of glassy materials that break down in the steam and produce sodium silicate solution. The ratio of SiO₂ to Na₂O in sodium silicate solution ranges from 1 to 3.23. They are mostly employed in applications involving water control. Sodium silicate solution is employed in the hand-dyeing process as a fixative. Additionally, it serves as an alum coagulant and an iron flocculant in waste water treatment facilities. Additionally, diluted soil applications work best because they have a lower viscosity and can penetrate farther into the desired zone (Table 3).

2.1.3 Sodium Hydroxide Solution

The alkaline activator solution that is usually used for geopolymer concrete is a combination of sodium silicate or potassium silicate and sodium hydroxide or potassium hydroxide. But because the potassium hydroxide solution has a high rate of alumina and silica ion leaching, sodium hydroxide is preferred over potassium hydroxide. As a result, the strength of concrete and the amount of silica and alumina leaching from GGBS particles are both influenced by the absorption of alkaline activator solutions. It is made by combining 480 gm of 99% pure sodium hydroxide

Table 4 Laboratory tests on M-sand

Sieve analysis	IS codes	Water absorption	Specific gravity	Bulk density (kg/l)
Zone II	IS2386 PART 3 1963	1.72%	2.63	1.68

Table 5 Laboratory tests on coarse aggregate

Sieve analysis	IS codes	Abrasion value	Specific gravity	Bulk density (kg/l)
Zone III	IS2386 PART 3 1963	0.72%	2.69	1.57

pellets with distilled water to create a solution with a 12 M molarity that fills a 1-L container. Its 1.29 specific gravity is determined.

2.1.4 Fine Aggregate

When making concrete, river sand can be used instead of manufactured sand (M-sand). Manufactured sand, used as fine aggregate in geopolymer concrete, is a great and cutting-edge substitute for river sand. Granite rocks with high density are crushed to create it. The particles, which are available after being cleaned and ground, are cubical in shape with sharp edges rather than round like river sand. Its dimension is less than 4.75 mm (Table 4).

2.1.5 Coarse Aggregate

The biggest and most static filler used in concrete is **coarse aggregate**. When sieving with IS sieves, aggregates that are maintained on 4.75 mm are referred to as coarse aggregates. Coarse aggregates are made from hard rocks that have been broken into smaller pieces. The geopolymer paste's ability to bond with the aggregates will be impacted by the durability, abrasion resistance, and cleanliness of the aggregates, which should be free of impurities like clay and silt particles. The 20 mm size of the coarse aggregates is utilized in this project (Table 5).

2.1.6 Superplasticizer

Superplasticizers (SP) are combined to concrete to make it more fluid and to lower the amount of water it needs. The water in the mixture tends to become entangled in the binder molecules, which makes concrete less workable. The 'zeta potential' created when SP is added to binder molecules causes repelling forces between them, enhancing the fluidity of concrete. As a superplasticizer, Primadon's Classic Superflo superplasticizer, which complies with BS 5075: Part 3 IS 9103, is employed. Naphthalene formaldehyde distillates are a dark liquid. With the use of superplasticizer, the

Table 6 Properties of superplasticizer

Physical state	Brown liquid
Specific gravity	1.20 @ 27 °C
Cl-content	0 according to IS 456
Air entrapment	Fewer than 1% air entrapped

amount of water needed can be reduced by roughly 30%, giving concrete a better strength and greater fluidity (Table 6).

2.1.7 Steel Fibre

The steel fibres (SF) are characterised as discrete, small lengths of steel with a length-to-diameter aspect ratio in the range of 20–100 and any of the various cross-sections, and are abundantly short to allow for easy and random dispersion in fresh concrete mix using conventional mixing procedures. Concrete's fundamental flaw is its inability to withstand pulling or tensile forces. Steel is utilized to solve this issue. A link between steel and concrete allows for the fulfilment of one's shortcomings by the other.

2.1.8 Plastering Sand

Plastering sand, often referred to as plasterer's sand, is fine-grained sand that has been thoroughly cleaned to get rid of any silt, salt, or clay. This procedure gives the sand a smooth surface and lessens shrinkage and cracking when dry. With this finish, they can be tiled, painted, or covered in wallpaper for a polished appearance. Plaster is only used for decoration and was not made to withstand moisture, thus it cannot be used externally.

2.1.9 Fly Ash

Alumino-silicate planted source substance is activated with an alkaline solution to create geopolymer concrete. It could be used as a source of geopolymer binder because it is primarily composed of silica and alumina. In order to improve the usage of this industrial debris by-product element, fly ash has been selected as the basis material for the geopolymer's synthesis.

2.2 Methodology

See Fig. 1.

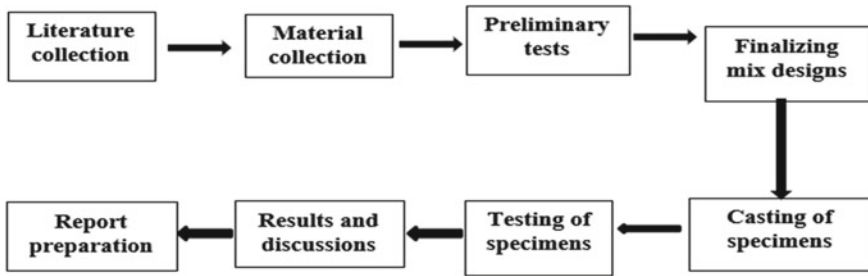


Fig. 1 Methodology flow chart

2.3 Casting Procedure

2.3.1 Mould Preparation

For mix design, the interior dimensions of cube (150 mm × 150 mm × 150 mm), cylinder (150 mm × 300 mm) and beam (150 mm × 150 mm × 700 mm) are gathered for compression testing of GPC. Given that geopolymer bonds to steel quite well, these moulds were lubricated on the inside to prevent stickiness.

2.3.2 Blending Concrete

The coarse aggregate (broken stone), binders like GGBS and silica fume, and fine aggregate (M-sand) are well mixed together before being added to the dry blend. The dry mixture is mixed with a sodium hydroxide solution that has been made and has a 12 M molarity. The water glass containing SP is next added to the mixture, which has now been blended with the superplasticizer and sodium silicate solution. The concrete is evenly mixed for five minutes using a mixer machine.

2.3.3 Casting of Specimens

Before being poured into the cube-shaped moulds, the concrete is thoroughly mixed. Each of the three layers is tamped at least 25 times using a tamping rod. After being left undisturbed for a day, the finished surface is demoulded.

2.3.4 Curing

The ideal curing method for geopolymer concrete is oven curing, however cast-in-situ concrete cannot use it since it is too expensive. As a result, the geopolymer concrete cures at ambient temperatures between 26 and 29 °C.

Table 7 Mix design—I

Materials used	Final quantity (kg/m ³)
<i>Mix I</i>	
GGBS	522.22
Silica fume	33.33
Sodium hydroxide (NaOH)	60
Sodium silicate (Na ₂ SiO ₃)	150
Superplasticizer	5.55
Fine aggregate	640
Coarse aggregate	1070

3 Experimental Study

The Trial mix for M60 has been prepared according to the code IS 10262-2019. The size of the cubes casted was 150 mm × 150 mm × 150 mm in dimensions.

3.1 Geopolymer Concrete of M60 Mix Design

See Table 7.

3.2 Geopolymer Concrete of M60 with Steel Fibre Mix Design

See Table 8.

Table 8 Mix design—II

Materials used	Final quantity (kg/m ³)
<i>Mix II</i>	
GGBS	522.22
Silica fume	33.33
Sodium hydroxide (NaOH)	60
Sodium silicate (Na ₂ SiO ₃)	150
Superplasticizer	5.55
Fine aggregate	640
Coarse aggregate	1070
Steel fibre	24.83

Table 9 Mix design—III

Materials used	Final quantity (kg/m ³)	
<i>Mix III</i>		
GGBS		522.22
Silica fume		33.33
Sodium hydroxi5cf0020de (NaOH)		60
Sodium silicate (Na ₂ SiO ₃)		150
Superplasticizer		5.55
Fine aggregate	M sand	428.3
	P sand	200.64
	Fly ash	10.56
Coarse aggregate		1070

3.3 Geopolymer Concrete of M60 with Plastering Sand Mix Design

See Table 9.

4 Testing of Specimens

4.1 Compressive Strength Test

The compressive strength test is highly important for figuring out the specimen's maximum load carrying capacity. The casting and curing of the cubical specimens followed the instructions in Sect. 2.3. At three days, seven days, and 28 days, the cubes were evaluated.

4.2 Split Tensile Strength Test

To ascertain the specimen's maximal tensile strength, the Split Tensile Strength Test is also crucial. The casting and curing of the cylindrical specimens followed the instructions in Sect. 2.3. The cylinders underwent testing after 3, 7, and 28 days.

Table 10 Compressive test results of M60

S. No.	Mix	Days	Average compressive strength (MPa)
1	Nominal mix	3	29.39
		7	56.23
		28	66.80
2	With steel fibre	3	52.56
		7	73.12
		28	81.41
3	With plastering sand	3	23.21
		7	53.76
		28	68.23

4.3 Flexural Beam Test

A material's ability to bend or flex is assessed using the flexural beam test. Flexural modulus is a measurement of a material's stiffness under flexure. The casting and curing of the beam specimens followed the instructions in Sect. 2.3. The beams were tested after 3, 7, and 28 days.

5 Results and Discussion

5.1 Compressive Strength Test

Table 10 illustrates the compressive strength test outcomes of geopolymer concrete including silica fume and GGBS with nominal mix, with steel fibre, and with plastering sand.

5.2 Split Tensile Strength Test

See Table 11.

5.3 Flexural Test

See Table 12.

Table 11 Split tensile test results of M60

S. No.	Mix	Days	Average compressive strength (MPa)
1	Nominal mix	3	2.2
		7	5.2
		28	6.8
2	With steel fibre	3	5.8
		7	10.1
		28	11.5
3	With plastering sand	3	1.8
		7	5.4
		28	6.2

Table 12 Flexural beam test results of M60

S. No.	Mix	Days	Average compressive strength (MPa)
1	Nominal mix	3	2.10
		7	3.46
		28	5.21
2	With steel fibre	3	3.33
		7	6.22
		28	8.33
3	With plastering sand	3	2.00
		7	2.68
		28	4.98

6 Conclusion

The materials utilised in this project underwent preliminary testing. While the geopolymer concrete takes 16 min to set initially and it takes 240 min to set completely. Sodium hydroxide (NaOH) with sodium silicate (Na_2SiO_3) are blended at a ratio of 1:2.50 to generate the geopolymer mix that works with alkaline activator solutions.

Steel fibre helped Geo polymer concrete's compressive, split tensile, and flexural beam strength to rise. Geopolymer concrete with plastering sand did not demonstrate any improvement in compressive, split tensile, or flexural beam strength.

References

1. Katzer J (2014) Steel fibers and steel fiber reinforced concrete in civil engineering harnessing of terrestrial laser scanning system for remote diagnostics of building and structures. View project Lunar soil simulants view project steel fibers and steel fiber reinforced concrete in civil engineering [Online]. Available: <http://www.wbiis.tu.koszalin.pl/ltb/>
2. Ryabchikov A, Tamme V, Laurson M (2015) Investigation of mechanical properties of steel fibre-reinforced concrete. In: IOP conference series: materials science and engineering. Institute of Physics Publishing. <https://doi.org/10.1088/1757-899X/96/1/012018>
3. Rangan BV, Cpeng F (Rtd), Faci, Fici H (2010) Fly ash-based geopolymer concrete. Allied Publishers Private Limited [Online]. Available: <https://www.researchgate.net/publication/230717147>
4. Nagral MR, Ostwal T, Chitawadagi MV (2014) Effect of curing temperature and curing hours on the properties of geo-polymer concrete [Online]. Available: www.ijceronline.com
5. Nuruddin MF, Demie S, Shafiq N (2011) Effect of mix composition on workability and compressive strength of self-compacting geopolymer concrete. *Can J Civ Eng* 38(11):1196–1203. <https://doi.org/10.1139/I11-077>
6. Shireesha N, Murugan SB, Kumar GN (2013) Experimental studies on steel fiber reinforced concrete [Online]. Available: www.ijsr.net
7. Shrestha P (2013) Development Of Geopolymer Concrete For Precast Structures
8. Mt. Student SBL, Professor A (2015) Effect of concentration of sodium hydroxide on strength of geopolymer concrete [Online]. Available: www.jetir.org
9. Pavithra P, Srinivasula Reddy M, Dinakar P, Hanumantha Rao B, Satpathy BK, Mohanty AN (2016) A mix design procedure for geopolymer concrete with fly ash. *J Clean Prod* 133:117–125. <https://doi.org/10.1016/j.jclepro.2016.05.041>
10. Sarath Chandra Kumar B, Ramesh K (2017) Durability studies of GGBS and Metakaolin based geopolymer concrete. *Int J Civ Eng Technol* 8(1):17–28 [Online]. Available: <https://www.iaeme.com/IJCIET/index.asp?IType=1>; <https://www.iaeme.com/IJCIET/issues.asp?JType=IJCIET&VType=8&IType=1>; <https://www.iaeme.com/IJCIET/issues.asp?JType=IJCIET&VType=8&IType=1>
11. Gopi V, Shyam Chamberlin K (2019) Experimental investigation on strength and durability of concrete incorporated with silica fume and fly ash 7(6C2)
12. Ahamed BS (2021) Issue 3 www.jetir.org (ISSN-2349-5162) [Online]. Available: www.jetir.org
13. Khan SU, Shafiq N (2013) Effect of sodium hydroxide concentration on fresh properties and compressive strength of self-compacting geopolymer concrete. [Online]. Available: <https://www.researchgate.net/publication/279527304>
14. Phoo-Ngernkham T, Phiangphimai C, Damrongwiriyanupap N, Hanjitsuwan S, Thumrongvut J, Chindaprasirt P (2018) A mix design procedure for alkali-activated high-calcium fly ash concrete cured at ambient temperature. *Adv Mater Sci Eng* 2018. <https://doi.org/10.1155/2018/2460403>
15. Patil MN, Khurd PVG (2022) Study of suitability of artificial sand in plastering & concrete [Online]. Available: www.irjet.net

Shear Resistance Behavior of Partially Sandwich Composite Structures Considering Elements Varying Dimension and Comparison Using Global Provisional Codes



Wesam Al Agha , Mohanad Ali Ishaq Najajra ,
Taha Ahmed Ghaleb Mohammed , and Nambiappan Umamaheswari 

1 Introduction

The Steel Concrete Steel (SCS) sandwich composite structure is formed from two sections of steel plates and a concrete core coated by a layer of epoxy resins [1]. Shear connectors, including headed studs, metal bars, and different mechanical variations, are used to connect steel and concrete. This material exhibits various advantageous characteristics, including superior strength, rigidity, ductility, blast and impact resistance, and effective construction efficacy and damage alertness. Due to the integration of steel and concrete, it is highly versatile. SCS might be utilized in various structures, which include but is not limited to protective offshore rigs, foundations,

W. Al Agha (✉)

Department of Civil Engineering, Delhi Technological University, Delhi 110042, India
e-mail: wesamalagha1@gmail.com; wa4977@srmist.edu.in;
wesamalagha_2k21phdce16@dtu.ac.in; wesam.alagha@unich.it

Department of Civil Engineering, Faculty of Engineering and Technology, SRM Institute Of Science and Technology, Kattankulathur, Tamil Nadu 603203, India

Department of Engineering and Geology, University G. d'Annunzio of Chieti-Pescara, Viale Pindaro 42, Pescara 65127, Italy

M. A. I. Najajra · T. A. G. Mohammed

Department of Civil Engineering, Cyprus International University, via Mersin 10, Haspolat, North Cyprus, Turkey

N. Umamaheswari

Department of Civil Engineering, SRM Institute Of Science and Technology, Kattankulathur, Tamil Nadu 603203, India
e-mail: umamahen@srmist.edu.in

bridge slabs, and submarine tunnels. During the early 1900s, steel shell structures established in the United States were primarily utilised as building frames and for preventing damage [2]. Nevertheless, shear connections were not made during this period. Despite the fact that the concrete core became reinforced and classified as the most important load-bearing structure, a slender steel shell was implemented subsequently to enhance the connection between steel and concrete [3]. During the 1970s, sandwich composite structures consisting of steel–concrete steel (SCS) were evaluated for their potential use as building and highway concrete slabs, as shown in Fig. 1b. The testing revealed that using bond epoxy was insufficient in providing effective transverse shear resistance. SCS evaluation was due to the fact that the concrete independently exhibited shear behaviour without the addition of reinforcements. The use of mechanical connections for linking the external steel plates of SCS composite structures was initially observed in the early 1980s. The shear resistance of SCS sandwich composite structures was investigated by academics who incorporated interacted-headed shear studs. The results indicated that the shear resistance of the frameworks with connectors was considerably more significant than that of SCS sections without connectors [1]. However, the impact resistance of the composite structures ended up low due to the separation resulting from concrete fractures [4]. The utilisation of the overlapping headed shear studs configuration was not implemented in practical applications owing to its elaborate manufacturing process of Bi-steel sandwich structures, as presented in Fig. 1a. Several projects have utilized structures incorporating exterior steel plates connected to concrete through friction-welded steel bars.

The Bi-Steel system was demonstrated through experiments. Nonetheless, using a sceptical methodology for estimating shear strength in this study, which relied on the Eurocode 2 Reinforced Concrete [5], proved insufficient to accurately identify different types of failure. In several underwater tunnel projects, Japanese engineers utilised a composite structure consisting of SCS, L-shaped steel shear connections, and bidirectional steel webs [2, 3]. A recently published design code for composite structures featuring SCS, L-shaped steel shear connections, and bidirectional steel webs has been developed based on deep study and practical expertise. This provisional code has a modification of the Japan Society of Civil Engineers (JSCE) guideline for concrete essentially [6]. In recent times, there has been a development and examination of SCS composite structures with novel mechanical connections

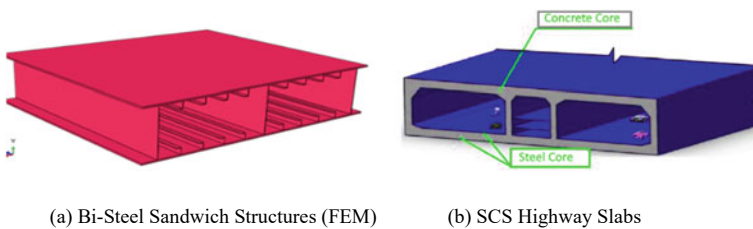


Fig. 1 Steel–concrete–steel sandwich element

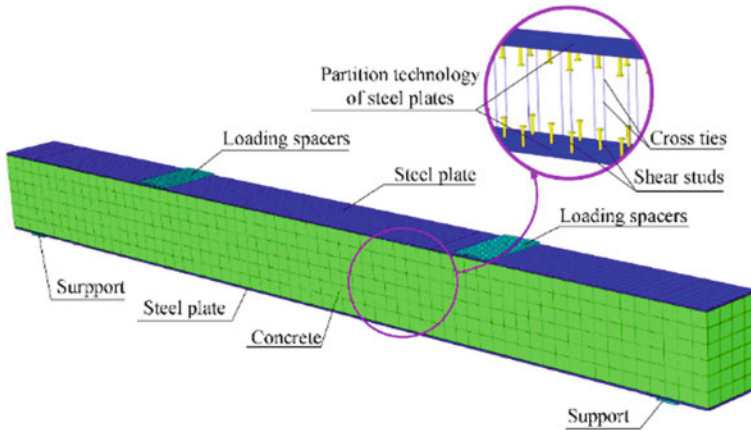


Fig. 2 FEM models of the SCS sandwich

that adjust to the requirements for design and performance requirements [2]. The yielding of steel in tension or compression and the crushing of concrete in compression is determined by selecting the suitable material and their respective mechanical characteristics [4]. Figure 2 depicts identified FEM models of the SCS component.

Lin et al. [7], An entire set of six composite beams was subjected to shear evaluation. The study’s findings reveal that SCS beams comprising separate procedures of Steel faceplate (SP) and Filled Concrete (FC) exhibit various options for failure, comprising shear without slip collapse, slip collapse, and flexural without slip collapse. The modified Strut-and-Tie simulation was utilised to identify the failure process. The researchers constructed Finite-Element (FE) models of SCS composite beams to derive the concrete diagonal strip width and the setup connection between SP and FC.

In summary, exploring the most significant effect of using the Steel–Concrete–Steel (SCS) composite in different concrete grades based on bending capacity and local buckling with varying thicknesses of SCS components is substantial.

2 Materials and Modelling Setup

The primary aim of this research is to assess the structural performances of Steel–Concrete–Steel (SCS) beams by examining shear resistance before and after modifying the materials FEM inputs of concrete and steel to correspond with Indian standards. Additionally, the study requires the creation of load–deflection plots pre and post-change of the Abaqus (6.14) input parameters. Table 1 presents the dimensions of the Steel–Concrete–Steel composite beam (SCS) in line with the literature review [8] to verify the connection to SCS components. In the reviewed study, the specimens comprised 16 beams established as groups of beam1 to beam14 and beam16

to beam17 [8]. Nevertheless, sample No. 15 was not modelled and tested due to experimental validation constraints that resulted from laboratory limits [8].

The model of all sixteen beams is classified and based on dimension in Table 1; The primary length is categorized into three steel core models per (mm), 1500, 3000, and 3600, as shown in Fig. 3a–c. Then assembling, all of them to create the main beam with concrete core and steel specimens, as shown in Fig. 3d. The (Concrete–Steel) specifications have been defined based on the relevant study for the validation models and as per Indian standards for the groups of materials’ strength.

The validation models simulated it as the relevant study material for beams (B1, B2, B3, B4, and B6) as the f_{cu} (48.5 MPa) concrete [8]. The literature review study presented specifications for beams (B7, B8, B9, B10, B11, B12, B13, B14, and B16) as the f_{cu} (25.4 MPa) concrete [8]. The new strength group material, as per Indian standard IS: 456-2000 [9], has been inserted into the Abaqus to be as M35 of beams where (B1, B2, B3, B4, and B6) as the f_{ck} (38.15 MPa) concrete and M20 for beams (B7, B8, B9, B10, B11, B12, B13, B14, and B16) as the f_{cu} (26.6 MPa). The same process has been done to define the steel properties of materials of thickness elements in the validation models as thickness 6 equals to f_u (536 MPa), thickness 10 equals to f_u (494 MPa), and thickness 25 equal to f_u (545 MPa), thickness 30 equals to f_u (538 MPa), thickness 40 equals to f_u (506 MPa) as f_u the minimum tensile strength [8]. The same insertion is for new strength material where models

Table 1 Dimension of SCS beam [8]

Beams	L (mm)	b_s (mm)	b_c (mm)	s_w (mm)	s_l (mm)	t_t (mm)	t_b (mm)	t_{wx} (mm)	t_{wy} (mm)
Beam 1	3000	600	600	1500	300	6	10	10	6
Beam 2	3000	400	400	1500	300	25	25	10	6
Beam 3	3000	400	400	1500	100	40	40	10	6
Beam 4	3000	400	200	1500	300	25	25	10	6
Beam 5	3000	400	100	1500	300	25	25	10	6
Beam 6	3000	400	200	1500	100	25	25	10	6
Beam 7	3000	400	200	1500	150	25	25	10	6
Beam 8	3000	400	200	1500	100	25	25	6	6
Beam 9	3000	400	200	1500	100	30	30	12	6
Beam10	3600	400	100	1800	300	25	25	10	6
Beam11	1500	400	200	750	100	25	25	10	6
Beam12	3000	400	200	750	300	25	25	10	6
Beam13	3000	400	200	500	300	25	25	10	6
Beam14	3000	400	400	1500	100	40	40	10	6
Beam16	3000	400	200	750	300	25	25	10	10
Beam17	3000	400	200	500	300	25	25	10	10

b_s = width of the steel plates, b_c = width of the concrete, s_w = spacing of transverse steel webs, s_l = spacing of L-shaped steel connectors, t_t = thickness of top steel plate, t_b = thickness of bottom steel plate, t_{wx} = thickness of axial steel web, t_{wy} = thickness of the transverse steel web

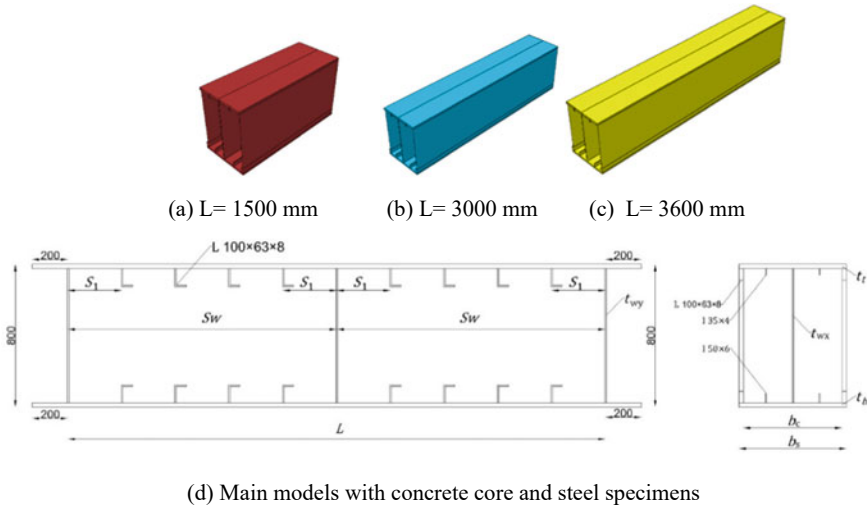


Fig. 3 Plan dimension (mm)

have included thicknesses 6, 10, 25, 30, and 40 (mm) as steel strength of Indian standard [9], Grade: f 345.

2.1 Numerical Methodology

The model of Abaqus is defined as the anticipated surface at a particular mode resulting from shear resistance using the plastic damage input as part of the analysis of the experimental literature review study [8]. A method for determining the composition of a system involves significant model specimens configuration of a structural SCS framework. Using the same approach from the previous steps as exact dimensions as the plan of the sandwich beam in Fig. 3, to be varied based on surface factors and the surface's boundary conditions. The nodes of interaction have taken points to points interaction, surface to points, and surface-to-surface. The steps of modeling for the beams are shown in Fig. 4.

In Fig. 4. The modelling steps started by defining the elements of steel materials as shown in Fig. 4a Axial web, Rib connector, and Top flange and bottom flange with Axial web based on dimensions and materials properties. Then, all the steel components were linked to formate the Fig. 4a flanges with shear connectors and assign the steel core with concrete as presented in Fig. 4b steel Beam with a concrete core. The next step is to release the meshing steps (thick-shell and four-node element) and define load cases as in the Fig. 4c by Assembly of steel model to the concrete core with proper mesh increments (100). The most significant step is the interaction between concrete and steel core, as illustrated in Fig. 4d Assigning the points as

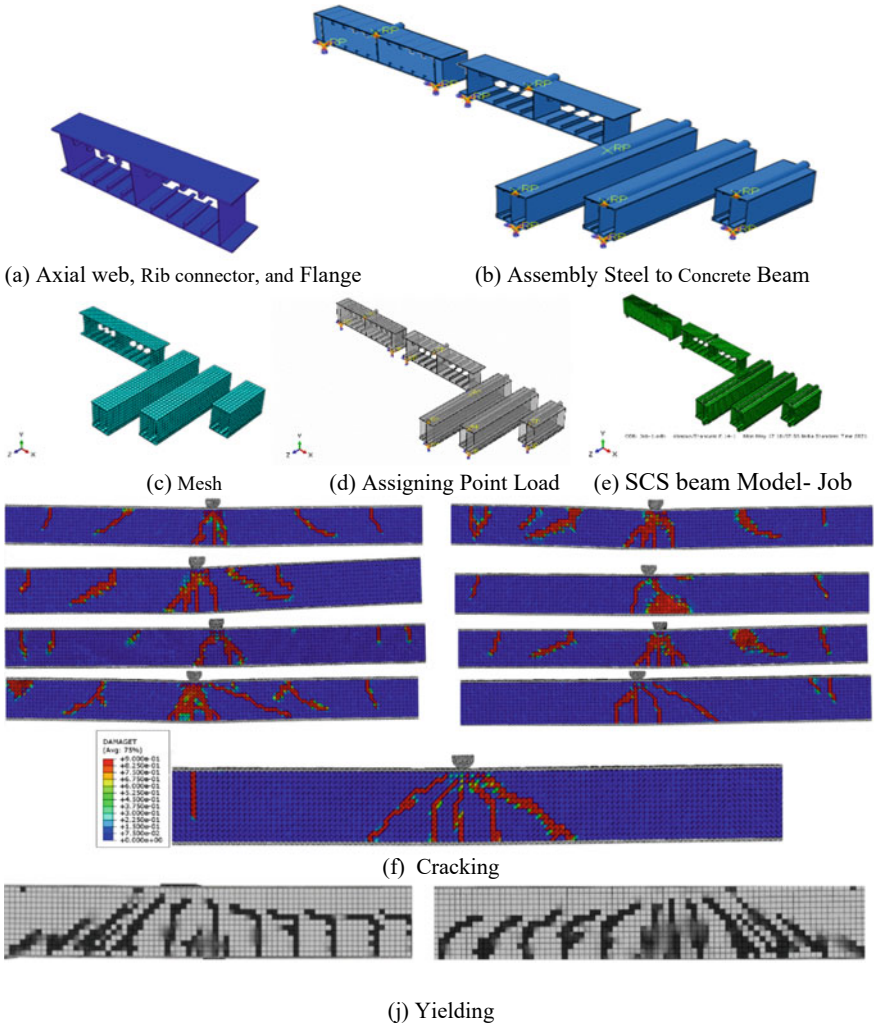


Fig. 4 Numerical modeling steps of SCS beams

interaction surface to surface. The following process of loads started as Fig. 4d defines the point load and duplicates as constraints under the SCS beam at edges. Finally, Fig. 4e Starts an analysis of Model—Job to present the visualization cracking progress in terms of SCS beam failure (Shear Mode) as in Fig. 4f Cracking behaviour and (j) Yielding behaviour. After analysis of the validation beams, the same process is followed for SCS beams, varying the new material strength.

3 Theoretical Method of Shear Beams as Per Global Codes

Theoretical approaches for predicting shear resistance have been recommended in design guidelines for shear connections with the development of SCS composite structures. This section examines the current design techniques and highlights that the primary principles governing shear in reinforced concrete (RC) are based on the connectors that integrate the two outer steel plates, which are considered shear reinforcements [5]. The credibility of this theory is predicated depending on the measure to which the code-based equations concerning the structural shear behaviour of the beam are integrated with the beam’s identified structural performance during assessment [5, 6]. In the European standard, numerous guidelines for design have been released to make the Bi-Steel design utilised as an instance in this case [5]. The SCS composite structure’s shear resistance comprises two distinct components, namely the concrete and steel bar portions. These components can be mathematically as follows.

$$V_u = V_c + V_s \tag{1}$$

$$V_c = 0.0525 f_c'^{2/3} \eta (1.2 + 0.4 \rho) B h_c \tag{2}$$

$$V_s = 0.9 k_T \frac{A_s w f_y B}{s_x} h_c \leq 0.3 f_c' B h_c \tag{3}$$

where the abbreviation V_u indicates the shear resistance of the structure to be divided into two sections: V_c , which represents the contribution of the concrete, and V_s , which illustrates the contribution of the steel bars. The abbreviation “ η ” represents the reduction factor of the height. The mathematical symbols ρ , B , h_c , and k_T represent the tension plate’s reinforcement ratio, the structure’s width, the concrete’s height, and the reduction factor, respectively. The variable “ $A_s w$ ” represents the area of the steel bar. The symbol f_{yB} represents the yield strength of the steel bar, while the symbol s_x denotes the spacing of the steel bar in the axial direction. The Japanese code maintains greater significance as it aimed to develop composite buildings of SCS with bidirectional steel webs (JSCE 1992) [6]. The present code classifies the structure into two distinct cases, axial steel webs and transverse steel webs [6]. The current code is primarily a modification of the JSCE guideline for reinforced concrete, wherein the axial web is treated as 60° reinforcements, and the angle of the shear cracks is taken as 30°. Nonetheless, the code asserts that limited research has been conducted on the shear capacity of bidirectional steel webs [6].

$$V_u = \min(V_{u1d}, V_{u2d}) \tag{4}$$

$$V_{u1d} = f_{vud} B h_c \tag{5}$$

$$V_{u2d} = \sin^2 \alpha_1 (\cot \theta + \cot \alpha_1) t_{wx} Z f_y \quad (6)$$

$$f_{vud} = 1.25 f_c^{1/2} \quad (7)$$

V_{u1d} represents the shear resistance when the concrete diagonal compression, and V_{u2d} , represents the shear resistance when the steel diagonal tension. The design methodology for SCS structures is not explicitly addressed by AISC 360. However, the design approach for filled or covered composite members exhibits certain resemblances, as per AISC 2016 [10]. It is determined entirely by the steel section, as per the guidelines outlined in AISC 360 [10]. The shear strength calculation excludes the concrete contribution for filled or wrapped composite elements [10].

$$V_u = 0.6 f_y t_{wx} h_c \quad (8)$$

As per the present research on RC and steel structures, it is established that an element involving a Reinforced Concrete (RC) part or a pure I-steel section might provide shear resistance.

4 Results

Thirty-two beams were tested using Abaqus, finite-element software, to present the shear resistance of the Steel–Concrete–Steel (SCS) sandwich effect compared to varying steel and concrete properties materials. The sixteen validated SCS beams with relevant studies have shown high accuracy of 96%; the new strength materials illustrate lower values than the initial validated SCS beams. Furthermore, a series of analyses have been performed to check the composite's performance to be presented the interaction that reveals the anti-shear mechanism accurately using concrete and steel infill of different grades. Abaqus investigated the SCS shear resistance of bottom and top steel plate thickness, steel connector's spacing, span-to-depth ratio, axial and transverse steel web thickness, and web shear studs. In conclusion, the shear resistance for numerical specimens is compared to be validated the ultimate loading of SCS beams with European code, Japanese standard (JSCE), American provisional design (AISC) and the proposed method from the relevant research. The shear resistance, yielding, and ultimate testing were observed in Tables 2 and 3. Where it has δ_t = testing displacement, F_t = testing load. The abbreviations *yt*: yielding and *ut*: ultimate are presented concerning the force and displacement. After reaching F_{yt} , which indicates the end of the elastic range in the load–displacement curve, the load caused the bottom steel flange of all 32 SCS beams to yield. Subsequently, the Crushing zone emerges due to the shear impact of F_{ct} , which arises from the effects of development until the ultimate load F_{ut} is reached. The comparison between 32 SCS-validated beams might have been observed in Table 2 by the ultimate to-yield ratio of displacement varied from 1.1 to 3.4. In contrast, Table 3 shows the SCS

values of the ultimate to-yield ratio of displacement of new strength materials to be exhibited a range of variability between 1.5 and 4.5.

The 32 SCS beams are presented with the comparison values of load—displacement in Fig. 5.

In Fig. 5a and c represents the SCS Beams (1–17) values from a group of validation models with relevant studies to compare with new strength material in Fig. 5b and d SCS beams. It has shown that the group of validation SCS beams for shear resistance exhibited higher values than the new material’s strength of the Indian standard. The same investigation is shown in Fig. 6 regarding the ultimate load of shear resistance comparison as validation SCS beams to be higher values than the new material’s strength, which is illustrated to SCS beams compared to Japanese code, European code, American code, and the proposed approach. Figure 7 shows the SCS composite effect by varying the concrete width b_c for the beam (3–4–5), steel web thickness t_{wx} for the beam (8–9), the L-shaped steel connectors spacing s_l for the beam (4–6), span of depth ratio λ for the beam (4–10–11), web shear studs for the beam (3–14), the influence of s_w and t_{wy} for beam (4–12–13–16–17) and shear resistance of new materials by the axial steel webs for beam SCS (4–6–8–14–16). In conclusion, Validation specimens verified manually approaching from codes show that the expected ultimate shear resistance of the current design methods and the proposed method are illustrated.

Table 2 SCS beams results, validation

Testing values validation					
Specimens	δ_{yt} (mm)	F_{yt} (kN)	δ_{ut} (mm)	F_{ut} (kN)	δ_{ut}/δ_{yt}
Beam1	20.9757	4798.229	70.504	5763	3.4
Beam2	15.9172	6003.9637	34.869	7056	2.2
Beam3	16.4244	6902.762	48.2691	8175	2.9
Beam4	12.6341	5149.1883	16.4244	5653	1.3
Beam5	10.3655	4009.4877	12.1268	4579	1.2
Beam6	13.395	5412.1021	22.7511	6070	1.7
Beam7	8.3891	4212.9233	12.1382	5010	1.4
Beam8	8.41691	3456.959	11.4242	4017	1.4
Beam9	11.0761	4966.3541	15.5823	5483	1.4
Beam10	12.807	3951.1675	14.5476	4173	1.1
Beam11	5.52563	5409.0826	8.9971	5705	1.6
Beam12	10.3799	4449.4944	12.9811	4689	1.3
Beam13	10.5539	4098.4004	18.1835	4560	1.7
Beam14	8.64898	5870.3438	19.5759	6775	2.3
Beam16	8.64898	4393.8959	11.7723	4948	1.4
Beam17	11.7723	4726.4571	19.75	5225	1.7

Table 3 SCS beams results, new strength materials

Testing values new strength					
Specimens	δ_{yt} (mm)	F_{yt} (kN)	δ_{ut} (mm)	F_{ut} (kN)	δ_{ut}/δ_{yt}
Beam1	14.6631	4096.31	66.4	5514	4.5
Beam2	21.9902	6178.83	38.4	6859	1.7
Beam3	18.7071	6792.71	49.3	7976	2.6
Beam4	16.1708	5083.15	23.2	5236	1.4
Beam5	15.6635	4294.41	20.7	4623	1.3
Beam6	17.1853	5456.12	25.3	5807	1.5
Beam7	8.12681	3969.7	11.4	4800	1.4
Beam8	7.95276	3101.75	10.7	3748	1.3
Beam9	10.0318	4430.96	15.1	4966	1.5
Beam10	12.4686	3360.18	14.4	3896	1.2
Beam11	6.74403	5187.72	12.6	5428	1.9
Beam12	10.728	4172.53	12.5	4487	1.2
Beam13	11.0761	3858.5	15.9	4375	1.4
Beam14	10.9021	5778.71	18.9	6498	1.7
Beam16	8.47493	3784.37	12.5	4615	1.5
Beam17	12.9811	4486.56	20.3	4985	1.6

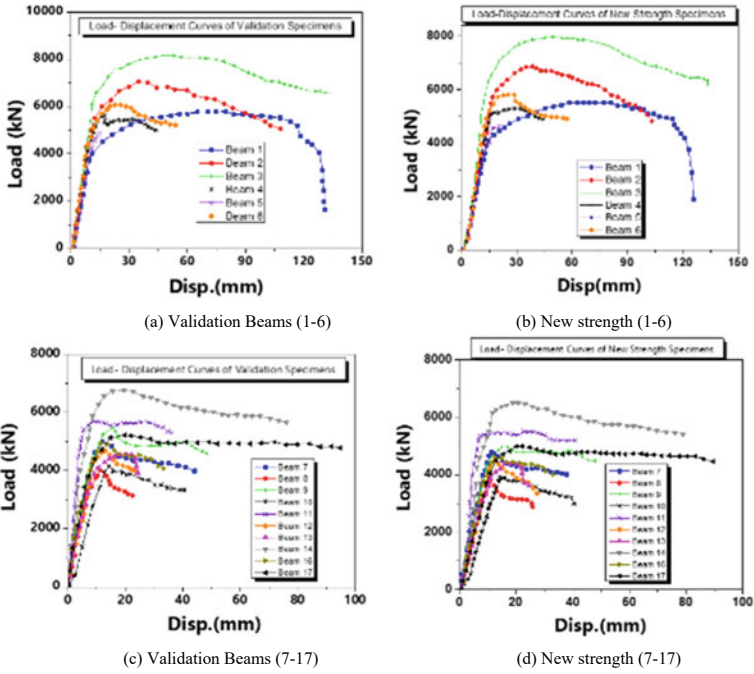


Fig. 5 Comparison of SCS beams, load–displacement

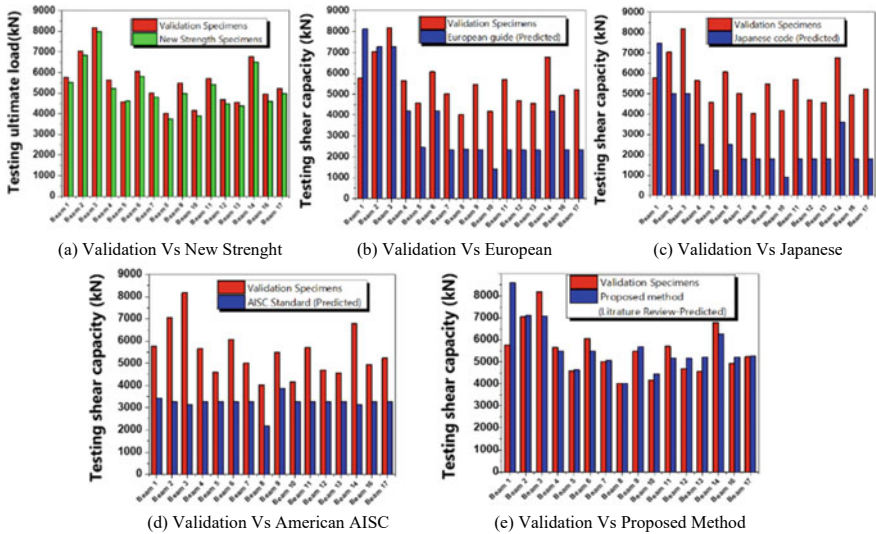


Fig. 6 Comparison SCS beams, ultimate load

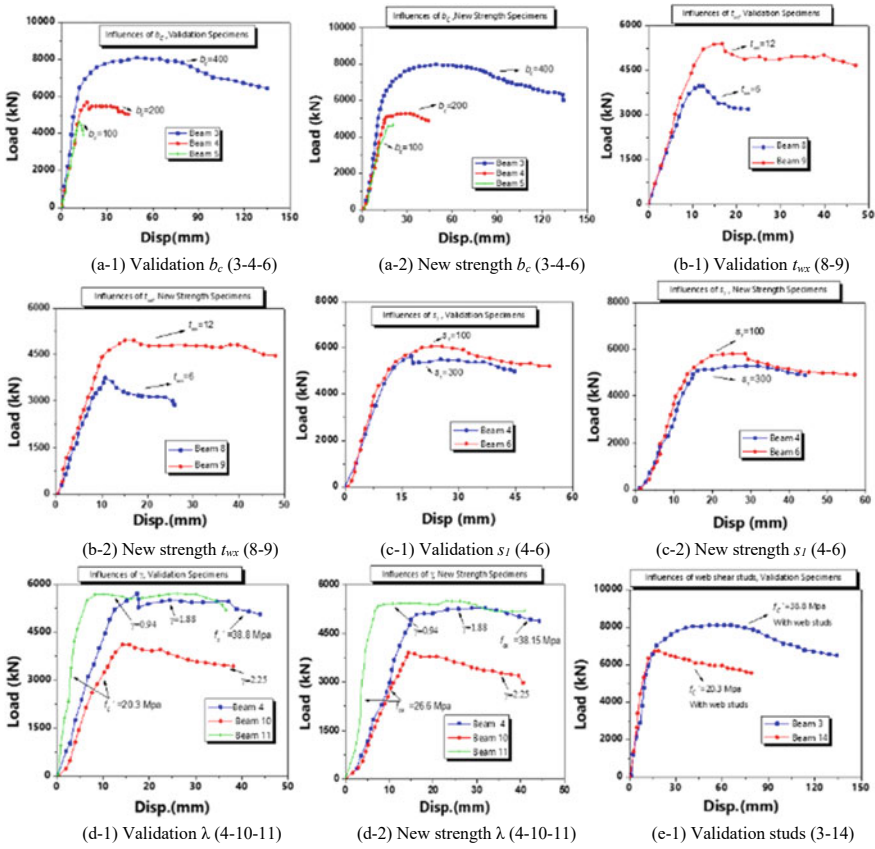


Fig. 7 Comparison of SCS beams parameters influences

5 Conclusion

In this study, thirty-two steel concrete steel (SCS) were modelled using Abaqus software to ensure yield point and shear resistance enhancement regarding steel elements’ varying materials properties and thickness. The output concludes as follows,

- The axial steel web exhibits shear stress that collapses within a range of approximately 30–60% of its shear capacity.
- The crack ratio was most significantly affected by the proportion of steel and concrete, and the width of the concrete primarily determined the failure direction.
- The integration of transverse steel webs positively impacted ductility, despite the relatively small magnitude of the observed effects.
- The incorporation of web shear studs and the ratio of span-to-depth are crucial factors that might significantly impact the shear capacity.

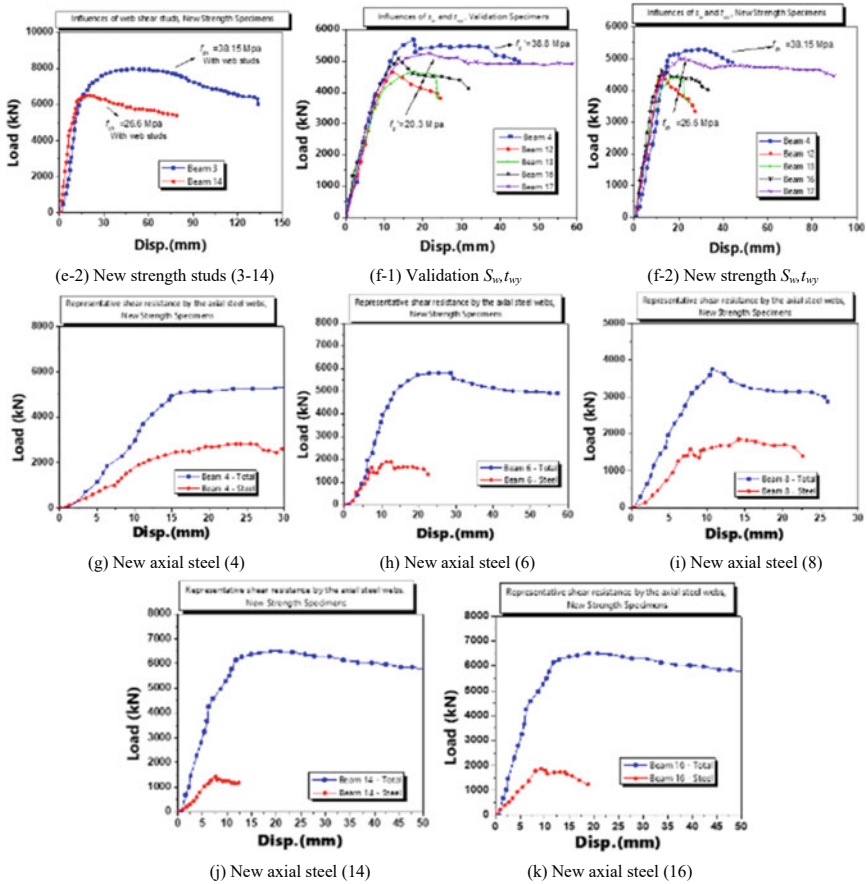


Fig. 7 (continued)

- Considering concrete strength is the most important to the shear capacity testing values that might be assumed to be greater than measuring values, owing to the development of local crushing and shear failure in SCS beams.
- The web buckling did not have any impact on the shear capacity.
- The verification of the existence of lateral concrete boundaries designed for preventing buckling and the potential ductile behaviour of the structure under shear might have been determined.
- Since the specific concrete compressive strength (f'_c) changed as new strength materials, the shear resistance might be affected dramatically compared to the validation models.
- Compared to global codes for SCS calculation, the proposed method agrees well with the analytical outputs.

Acknowledgements The authors express appreciation to ICCR, India, and the INPS's (CHIETI, IT), Italy.

References

1. Sayyad AS, Avhad PV (2022) A new higher order shear and normal deformation theory for the free vibration analysis of sandwich curved beams. *Compos Struct* 280:114948. <https://doi.org/10.1016/J.COMPSTRUCT.2021.114948>
2. Nguyen ND, Vo TP, Nguyen TK (2020) An improved shear deformable theory for bending and buckling response of thin-walled FG sandwich I-beams resting on the elastic foundation. *Compos Struct* 254:112823. <https://doi.org/10.1016/J.COMPSTRUCT.2020.112823>
3. Khatibi SH, Ghohani Arab H, Miri M (2023) The behavior of steel-concrete-steel sandwich composite beams with box-profile shear connectors: experimental and numerical. *Structures* 54:644–656. <https://doi.org/10.1016/J.ISTRUC.2023.05.054>
4. Lin Y, Yan J, Wang Y, Fan F, Zou C (2019) Shear failure mechanisms of SCS sandwich beams considering bond-slip between steel plates and concrete. *Eng Struct* 181:458–475. <https://doi.org/10.1016/J.ENGSTRUCT.2018.12.025>
5. CEN (European Committee for Standardization) (1992) Design of concrete structures. Eurocode 2. CEN, Brussels, Belgium
6. JSCE (Japan Society of Civil Engineers) (1992) Design code of steel-concrete sandwich structures. [In Japanese.] Concrete Library No. 73. JSCE, Tokyo
7. Lin Y, Yan J, Wang Z, Zou C (2023) Experimental study, finite element simulation and theoretical analysis on failure mechanism of steel–concrete–steel (SCS) composite deep beams with UHPC. *Eng Struct* 286:116124. <https://doi.org/10.1016/J.ENGSTRUCT.2023.116124>
8. Guo Y-T, Tao MX, Nie X, Qiu SY, Tang L, Fan J-S (2018) Experimental and theoretical studies on the shear resistance of steel–concrete–steel composite structures with bidirectional steel webs. *J Struct Eng* 144(10). [https://doi.org/10.1061/\(ASCE\)ST.1943-541X.0002182](https://doi.org/10.1061/(ASCE)ST.1943-541X.0002182)
9. Bureau of Indian Standards, New Delhi, Indian Standard Plain and Reinforced Concrete-IS 456, 2000
10. AISC (2016) Specification for structural steel buildings. AISC 360. AISC, Chicago

Effect of Bracing Structural System on the Seismic Response of High-Rise Reinforced Concrete Building for Strengthening with Soft Storey



Taha Ahmed Ghaleb Mohammed , Mohanad Ali Ishaq Najajra ,
and Wesam Al Agha 

1 Introduction

Earthquakes are catastrophic geological phenomena that result from an unexpected release of underground energy. It has been recognised as one of the most damaging natural disasters, causing frequent shaking of the earth's surface and affecting all living and non-living structures [1]. The release of energy from substances inside and outside a surface produces vibrations that might give rise to loss of life and damage to structures. Due to the varying intensities and magnitudes of earthquakes, it is imperative to thoroughly investigate the seismic behaviour of reinforced concrete structures with diverse parameters, particularly in terms of their response to shear at the base and displacement [2]. In order to mitigate the effects of lateral loads and attain sufficient rigidity, structural engineers utilised moment-resistant frames, diaphragms, and cross-braces. Irregularity might arise due to differences in the utilisation of a specific floor level compared to the adjacent floor level. Furthermore, numerous buildings are accidentally transformed into techniques during construction due to various factors, such as disconnects in construction methodologies and the utilisation of varying building materials. While investigating code limitations, it is prominent that most seismic codes offer comparable recommendations for design

T. A. G. Mohammed · M. A. I. Najajra

Department of Civil Engineering, Cyprus International University, via Mersin 10, Haspolat, North Cyprus, Turkey

W. Al Agha (✉)

Department of Civil Engineering, Delhi Technological University, Delhi 110042, India

e-mail: wesamalagha1@gmail.com; wesamalagha_2k21phdce16@dtu.ac.in;

wesam.alagha@unich.it

Present Address:

Department of Engineering and Geology, University G. d'Annunzio of Chieti-Pescara, Viale Pindaro 42, Pescara 65127, Italy

based on their magnitude while disregarding the irregularity's location of seismic dissipation technology. The significance of structure design lies in its type and distribution. Making the appropriate selection can contribute to improving both the functionality and visual appeal of tall buildings [3]. Despite urban buildings' functionality, historical earthquake records indicate that these structures have exhibited inadequate seismic performance. Structural performance is an inevitable occurrence in building design. Therefore, selecting and strategically positioning these dissipation technology is imperative [4].

1.1 Soft Storey

A soft storey, an open floor within a high-rise building, is typically necessary to accommodate various functions such as parking lots, retail stores and conference rooms. The fundamental issue that civil engineers encounter is the presence of soft story, as depicted in Fig. 1. According to the IS1893 (Part 1): 2016 standard, it has been established that the lateral stiffness of a soft floor is comparatively lower than that of the upper floor. The seismic lateral stiffness refers to the aggregate stiffness of all seismic forces that oppose the element and counteract the lateral seismic vibration impact in the specified direction. This study involves a parametric analysis of bare frame systems in response to alterations made to the bracing configuration structures featuring a soft storey [5]. Linear approaches have been applied to analyse frame systems of structures that exhibit linear damping, linear restoring, and linear inertia forces. A soft storey system of non-linear differential level is established when the structural frame system indicates non-linear relationships between the three reaction forces (inertia, damping, and stiffness) and corresponding response parameters, including displacements, velocity, and acceleration. It is essential to obtain accurate solutions [6, 7]. Stiffness and damping are the two most frequently discovered forms of linearity. With the exception of certain cases, it is generally observed that inertia forces exhibit linear behaviour. It is significant to explore the failure response in terms of soft storey buildings, as presented in Fig. 1.

1.2 Non-linear Pushover Analysis

Pushover analysis is a non-linear static procedure involving lateral load increments according to a determined pattern. The existing assumption implies that the behaviour of a structure is affected by its fundamental mode and that certain patterns occur in the form of both the fundamental period mode and storey shear. As the applied load magnitude increases, the non-linear response of different structural components becomes apparent, identifying the structure's failure modes and vulnerable connections. The pushover technique is also utilised for response spectrum analysis [8, 9]. Modifications have been made to the pushover analysis procedure in order



Fig. 1 Buildings failure due to soft storey

to account for the contribution of higher modes of structural vibration, as well as changes in the distribution of storey shear that correspond to the yielding of the structure's members. Pushover analysis has gained significant attention with an increase in widely used software applications such as ETABS. There exist two different types of Pushover analysis, namely force-controlled and displacement-controlled. The Force Controlled Method involves the application of force to a structure in small increments. This particular tool is applicable primarily in cases where the load is measurable, such as in the instance of a gravity load. The Displacement Controlled Method involves gradually increasing the displacement of a structure's top storey, allowing a horizontal force to laterally push the structure [10, 11]. The magnitude of the displacement resulting from applying an external force on a structure is directly proportional to the fundamental horizontal translational mode of the structure. The seismic performance of a structure can be evaluated based on various factors such as displacement ductility, plastic hinge formation, pushover curve, and performance point, as shown in Fig. 2. The performance level can be determined using the guidelines provided in FEMA 356. It's commonly analyzed in terms of the lateral displacement of the structure or the development of hinges. FEMA 356 specifies three different occupancy levels. Immediate Occupancy (IO), Life Safety (LS), and Collapse Prevention (CP).

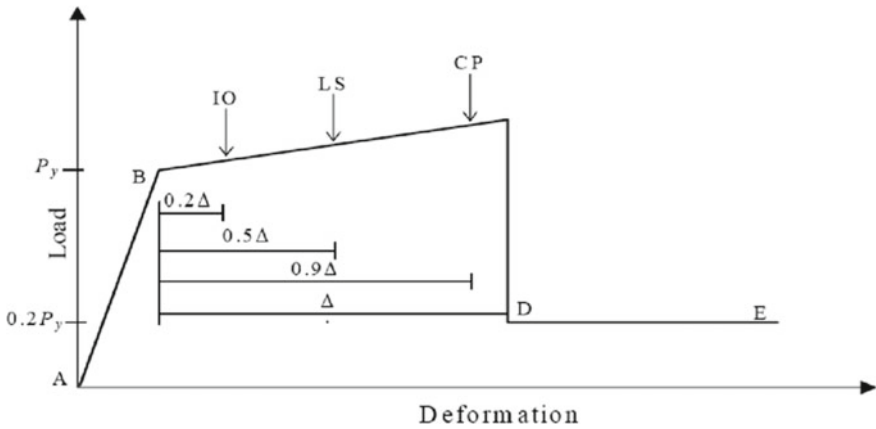


Fig. 2 Performance levels (ATC 40) [14]

ETABS has the capability to change the capacity curve into a capacity spectrum by utilising ATC 40, which enables the acquisition of the response spectrum [12, 13]. The point of intersection between the demand and capacity spectra determines the performance point within the analysed structure.

Immediate Occupancy (LO)

In the seismic magnitude effect, the building might be occupied. The structural integrity exhibits minor cracks, and no significant fractures are present. In the cracks, it is a minor effect. No structural deformation can result in the immediate occupation of a building subsequent to a sudden earthquake of this magnitude.

Life Safety Performance Level (LS)

The phenomenon is related to the reduction of the initial stiffness. The structural framework exhibits significant fractures. In contrast, the structure is capable of being repaired. In the event of restoration, a substantial amount of funds will be required.

Collapse Prevention Performance Level (CP)

The structure remains stable as it is not constructed to collapse. The damages occurred when a structure is exposed to excessive lateral loads and the structure's rigidity is inadequate to resist the lateral stresses. Certain structural elements have experienced failure and subsequent collapse. The structure cannot be repaired or maintained.

The performance metric evaluated through pushover analysis is compared to the target displacement determined through calculation. The determination of the performance point has been illustrated in ATC 40 by elucidating three distinct procedures. Procedure A involves the definition of a set of equations. The performance point is determined through a repetitive approach in Procedure B. Procedure C is a graphical method appropriate for manual and computer-based analysis. This methodology is

deemed appropriate for ascertaining the performance point within the ETABS software. The subsequent procedures outline the necessary steps to acquire performance points in Procedure C. A demand spectrum curve is generated for every point along the pushover curve. To create a constant period line, one must draw a radial line passing through a specific point (P) on the curve. Calculating the area under the curve up to a specific point (P) on the curve involves the consideration of damping. The demand spectrum can be derived by graphing it for a damping level equivalent to point (P) on the pushover curve. The Single Demand Spectrum, which features a Variable Damping Curve, can be characterised by the intersection point denoted as 'P' where the radial line intersects with the corresponding demand spectrum.

1.3 *Bracings*

Bracing is an effective device to resist the wind load for frame structures and is an economically vital approach. The brace arch is composed of standardised columns and beams that serve primarily to support vertical loads. Additionally, diagonal braces are incorporated into the structure to enable the assembly of the various components into a vertical truss that might withstand horizontal forces. Bracing is affixed to the joint located at the intersection of the column and beam. The classification of bracing materials is based on the materials used. (a) The cross-sectional shape of a Reinforced Concrete brace is either that of a beam or a column. The compressive strength of the braces is attributed to the high strength of the concrete material and the rigidity of the structure due to its limited usage. The high cost of these braces is due to their limited usability, as they are designed to be utilised only once in response to seismic activity. (b) Steel braces are constructed from steel and link various steel profile types, including angle, U, and tube sections [5, 15, 16]. Steel braces typically exhibit high tensile strength and are resistant to failure through buckling. Steel braces offer the benefit of being reusable multiple times following damage and are typically cost-effective. The categorization of the bracing is illustrated in Fig. 3, and its connections to frames are by the concentric elements which are joined together through beam and column connections. The following are instances of concentric braces that are based on configuration. The K-type, V-type, and X-type braces are structural dissipation supports commonly used in construction applications. The eccentric elements are linked to a different location within the designated segment [17]. The devices linked to members' support facilitate the transmission of energy from the seismic movements of plastic drift. Implementing these braces results in lateral stiffness and an elevation of energy dissipation. The frame's lateral stiffness is contingent upon the bending deformation when utilising eccentric braces..

In this study, X-bracing and V-bracing are provided in the corner and middle bays throughout the building with a soft storey to observe its effect on the behaviour of the building.

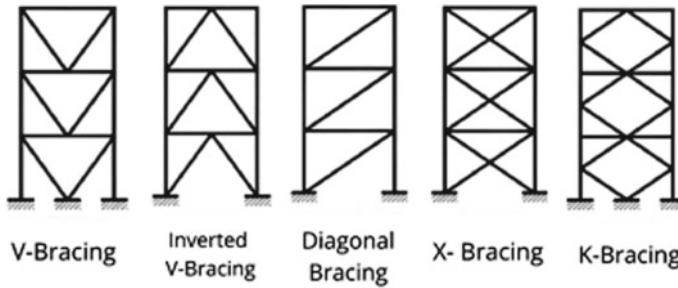


Fig. 3 Bracings types

2 Review of Literature

Akhila Lal [5] RCC Building of seven storeys is analyzed to be represented as a bare frame, a soft storey frame, and a frame equipped with steel bracings. The structural elements employed in this study comprise cross-bracing, concentric inverted V bracing, and eccentric inverted V bracing to mitigate the impact of a soft storey. The ETABS 2016 software is used to conduct linear and nonlinear dynamic analyses. The investigation involves determining the soft-storey building's response for each bracing type, specifically in terms of storey displacement and storey drift. The optimal bracing type is subsequently identified based on its efficiency.

In conclusion, there are insufficient design procedures for strengthening techniques by bracing. The code and relevant research have not covered theoretical aspects and case studies more deeply. Still, the design portion is mainly significant to evaluate the seismic performance of a building with a soft storey subjected to bracing as investigating the structure behaviour using Response Spectrum and pushover analysis.

3 Materials and Modelling Structures

The study analysed 10-storey reinforced concrete frame structure (SMRF) with a soft storey inserted to plan by 36×36 m. The design of the models is executed through a two-case approach, whereby the initial case involves the modelling of the building with a soft storey located at the ground floor level. During the second case, the structure of the building was designed to include bracing X and V types with a soft storey in the ground floor. ETABS is utilised to conduct various analyses, such as linear dynamic response spectra and nonlinear static pushover analysis. It is illustrated plan and 3D of two cases in Fig. 4.

The loading, that is, Dead, Live and Earthquake, were defined as per Indian Standard codes [18, 19]. Seismic analysis response spectra and pushover analyses were performed using IS 1893: 2016 [20–22].

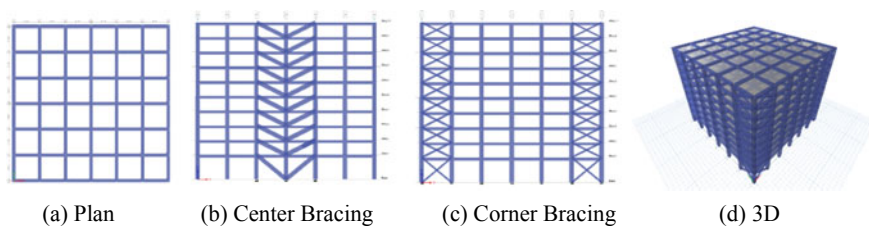


Fig. 4 ETABS bracing model

The properties of the materials (Steel and Concrete) in the building are presented in Table 1.

The non-linear material properties of steel and concrete are used as per compression-strain and tension-strain, presented in Table 2. Stress-strain graph of Steel and concrete is shown in Fig. 5.

ETABS presented the stress-strain plot of concrete M25 in Fig. 5a and illustrated the stress-strain plot Fe 500 in Fig. 5b.

Table 1 Properties of materials (Steel and Concrete)

Material	Steel	Concrete
Specific weight density	76.97 kN/m ³	25 kN/m ³
Specific mass density	7850 kg/m ³	2548 kg/m ³
Poisson's ratio (U)	0.3	0.2
Co-efficient of thermal	0.0000117 1/0c	0.0000055 1/0c
Expansion (α)	80,769.23 MPa	10,416.67 MPa
Shear modulus (G)	210,000 MPa	25,000 MPa
Modulus of elasticity (E)	76.97 kN/m ³	25 kN/m ³
	Isotropic	Isotropic

Table 2 Properties of non-linear materials

Material	Steel	Compression-strain	Concrete	Compression-strain
IO	0.01	- 0.005	0.01	- 0.003
LS	0.02	- 0.01	0.02	- 0.006
CP	0.05	- 0.02	0.05	- 0.015

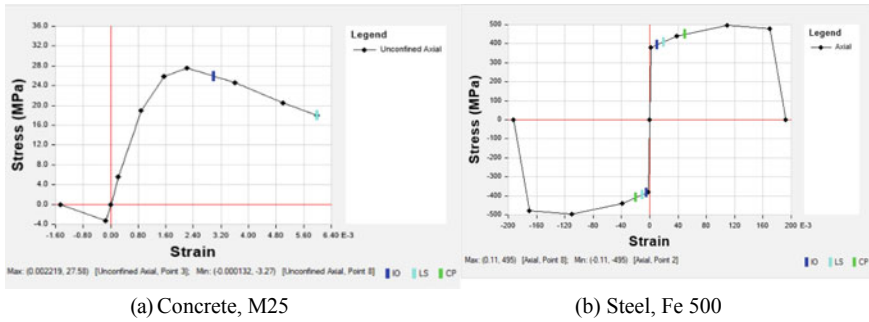


Fig. 5 Stress–strain plot of **a** concrete, **b** steel

4 Results

As a manual calculation of the stiffness in the case of the soft storey and validation using Indian standards, The stiffness is 21.6% compared with the second storey; therefore, the bottom storey has a lesser stiffness value. According to IS 1893 (Part 1): 2016: ‘Soft floors have less lateral stiffness than upper floors.’ Therefore, the selected model has stiffness irregularity in the bottom storey. The process of RCC frame modelling and their analysis in the first case of response spectrum analysis for Storey displacement, base shear, stiffness, and drift is presented in Fig. 6.

It is significant to explore in Fig. 5 that soft storey values are increased of storey displacement and storey drift; in the case without installing a bracing X and V types, it presented higher values compared with bracing X and V types usage in terms of storey shear and stiffness using Response spectrum methods. The displacements of all models conform to the maximum limits as prescribed in IS 1893:2016. The structure’s maximum storey displacement under pushover load in the X-direction is 24.65 mm. This displacement is most significant in the structure with a soft story model. However, in the structure model with cross bracings at the centre, the displacement is reduced to 8.187 mm. This reduction is the most significant among all model types. All models’ storey drifts confirm to the limits specified in IS 1893:2016. The results indicate that the maximum storey drift of 0.001181 is observed under pushover load. This value is found to be highest in structures with a soft story model. However, in structures with a model with cross bracing at the centre, the maximum storey drift is reduced to a minimum value of 0.000318 mm, the lowest among all models. Installing cross bracings at mid and corner bays results in a respective increase of 25.8 and 44% in the base shear. The placement of V-type bracings at mid and corner bays increases the base shear by 25% and 26%, respectively. Soft storey irregularity was reduced when the bracing was introduced in both corners and the core, giving a maximum stiffness value in the first storey. After analyzed RSM and Pushover analysis, the seismic performance parameters are varied to present in Fig. 7. In both RSM and Pushover analysis, the maximum storey shear is observed when bracings are positioned in the corner bays instead of mid-bays. In Pushover analysis, V-type

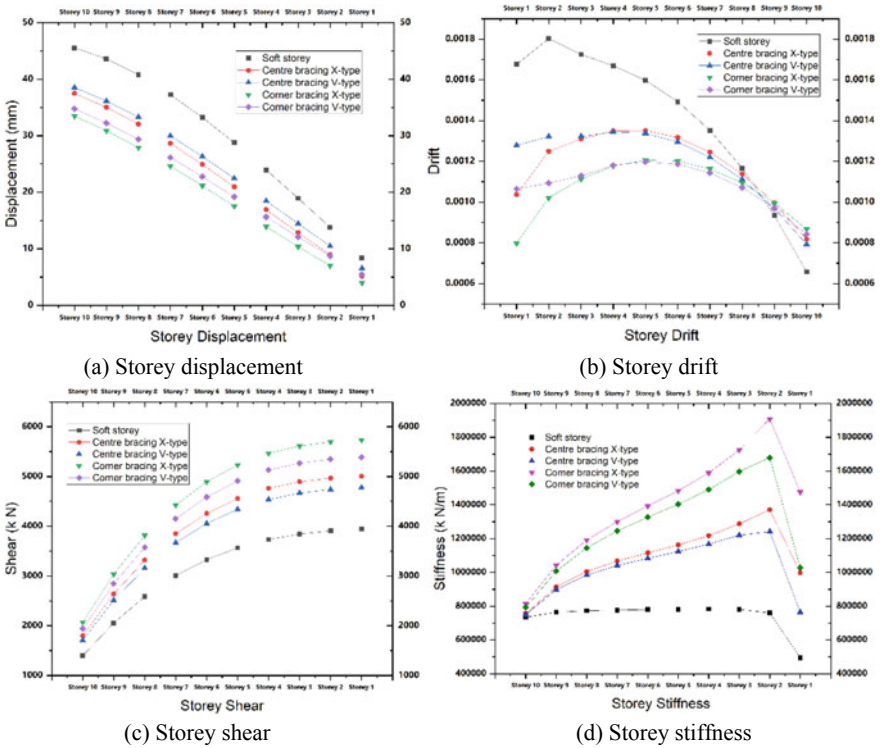


Fig. 6 Comparison results between soft storey and Bracing X and V types (centre and corner)

bracing at all corners in the RC frame model yields the computation of the minimum value of target displacement compared to other model types.

The comparison between the Response Spectrum and Pushover analysis in terms of maximum displacement, stiffness, base shear, and time period value is presented. Response spectrum analysis has a higher storey drift value than pushover analysis. The models with shear walls installed at all four corners had the lowest drift values, as seen from both response spectra and pushover studies. Non-linear time history analysis can be used to provide a more precise calculation of the structure’s capacity and simulate a more realistic demand instance. Shear barriers can be built and examined in many different places.

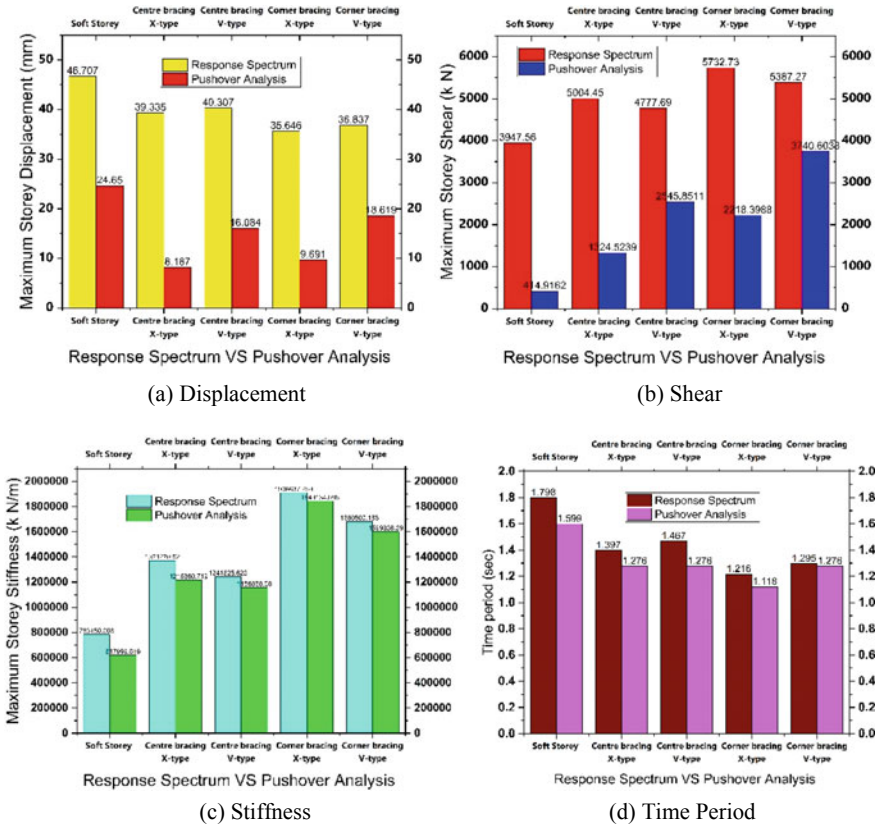


Fig. 7 Comparative results of response spectrum and pushover analysis

5 Conclusion

In this study, the regular shape plan of a 10-story reinforced concrete building in Zone V was analyzed in two phases, the first phase of which is a soft-storey building on the ground floor. In the second phase, the structure is analyzed with different types of X and V-type brace arrangements in the central and corner spans across the height of the building. The models are analysed using the ETABS 18.0.2 programme and the IS 1893 (Part 1): 2016 code. The seismic performance of soft-floor RC buildings is studied regarding maximum storey displacement, drift, story stiffness, base shear value, and time period by performing linear dynamic analysis, the Response spectrum method, non-linear static analysis, or the Pushover analysis method. It is concluded as the significant points of comparison as,

- The maximum storey shear occurs when the bracings are installed in the corner bays compared to mid-bays.
- V-type bracing exhibits a higher storey shear in comparison to X-type bracing.

- The utilisation of V-type bracing at all corners in modelling an RC frame results in the computation of the minimum value of target displacement when compared to other model types.
- The force–displacement plot, which represents an idealised model, was generated by transforming the pushover curve acquired during the structure’s loading until it reached the point of collapse.
- In a soft-storey scenario, most hinges are situated within the inter-storey drift limits, with only a few surpassing the collapse prevention level. Therefore, it is necessary to reinforce the column in the soft story.
- Using steel braces is considered a highly effective approach for enhancing the structural integrity of buildings that possess a soft storey.
- The X-bracing system demonstrates reduced displacement and time period, as well as increased stiffness and shear values compared to the V-bracing system.

Acknowledgements The authors would like to express appreciation to the Indian Council for Cultural Relations, India, and the INPS’s social security contribution under separate management (CHIETI, IT), Italy.

References

1. Al Agha W, Umamaheswari N (2021) Analytical study of irregular reinforced concrete building with shear wall and dual Framed-Shear wall system by using Equivalent Static and Response Spectrum Method. *Mater Today Proc* 43:2232–2241. <https://doi.org/10.1016/J.MATPR.2020.12.525>
2. Ravi K, Al Agha W, Thakur MS, Umamaheswari N (2021) Impact of the lead rubber base isolators on reinforced concrete building. *IOP Conf Ser Mater Sci Eng* 1026(1):012004. <https://doi.org/10.1088/1757-899X/1026/1/012004>
3. Kannan SS (2023) Seismic analysis of soft storey building in earthquake zones. In: *IOP conference series: earth and environmental science*. Institute of Physics. <https://doi.org/10.1088/1755-1315/1130/1/012023>
4. Kant R, Al Agha W, Alozzo Almorad W, Thakur MS, Umamaheswari N (2021) Study on seismic performance of reinforced concrete multi-storey building considering soil-structure interaction effect. *Mater Today Proc*. <https://doi.org/10.1016/J.MATPR.2021.11.475>
5. Lal A, Remanan M (2023) Analysis of soft storey building with different types of steel bracings under seismic load. pp 287–295. https://doi.org/10.1007/978-981-19-4040-8_24
6. Zaker Esteghamati M, Banazadeh M, Huang Q (2018) The effect of design drift limit on the seismic performance of RC dual high-rise buildings. *Struct Des Tall Special Build* 27(8). <https://doi.org/10.1002/tal.1464>
7. Kant R, Al Agha W, Thakur MS, Umamaheswari N (2022) Comparative study on seismic performance of steel-concrete composite structure without and with buckling—restrained braces. *Mater Today Proc* 56:2134–2144. <https://doi.org/10.1016/j.matpr.2021.11.461>
8. Torelli G, D’Ayala D, Betti M, Bartoli G (2020) Analytical and numerical seismic assessment of heritage masonry towers. *Bull Earthq Eng* 18(3). <https://doi.org/10.1007/s10518-019-00732-y>
9. Comparative study on seismic performance of reinforced concrete building with and without fluid viscous dampers. [Online]. Available www.ijerm.com

10. Kant R, Al Agha W, Thakur MS, Umamaheswari N (2021) Comparative study on seismic performance of steel-concrete composite structure without and with buckling—restrained braces. *Mater Today Proc.* <https://doi.org/10.1016/J.MATPR.2021.11.461>
11. Ahmed M, Tayyaba S, Ashraf MW (2016) Effect of buckling restrained braces locations on seismic responses of high-rise RC core wall buildings. *Shock Vibr.* <https://doi.org/10.1155/2016/6808137>
12. Pertile V, Stella A, De Stefani L, Scotta R (2021) Seismic and energy integrated retrofitting of existing buildings with an innovative icf-based system: design principles and case studies. *Sustainability (Switzerland)* 13(16). <https://doi.org/10.3390/su13169363>
13. Akhil Ahamad S, Pratap KV (2021) Dynamic analysis of G + 20 multi storied building by using shear walls in various locations for different seismic zones by using Etabs. *Mater Today Proc* 43:1043–1048. <https://doi.org/10.1016/j.matpr.2020.08.014>
14. ATC-40 , “ seismic evaluation and retrofit of concrete buildings”, vol 1, Report No. SSC 96-01, November 1996
15. Kanake S (2022) Seismic response of open ground multi-storey building retrootted with innll wall, shear wall and steel bracing. seismic response of open ground multi-storey building retrofitted with infill wall. *Shear Wall Steel Bracing.* <https://doi.org/10.21203/rs.3.rs-2183625/v1>
16. Della Corte G, D’Aniello M, Landolfo R, Mazzolani FM (2011) Review of steel buckling-restrained braces. *Steel Constr* 4(2). <https://doi.org/10.1002/stco.201110012>
17. Al Agha W, Alozzo Almorad W, Umamaheswari N, Alhelwani A (2021) Study the seismic response of reinforced concrete high-rise building with dual framed-shear wall system considering the effect of soil structure interaction. *Mater Today Proc* 43:2182–2188. <https://doi.org/10.1016/J.MATPR.2020.12.111>
18. IS: 456 (2000), ‘Code of practice for plan and reinforced concrete (fourth revision)’, Bu-reau of Indian Standard, New Delhi
19. IS 1893 (part1): 2016, “Criteria for earthquake resistance design of structures; Part 1 General provisions and buildings”, Bureau of Indian standards, New Delhi-110002
20. IS: 875 Part 1-5 (1987), ‘Code of practice for design load (other than earthquake) for build-ings and structures’, Bureau of Indian Standard, New Delhi
21. IS: 1893 Part I (2002), ‘Code of practice for criteria for earthquake resistance design of structure: generalprovisions and building’, Bureau of Indian Standard, New Delhi
22. IS: 4326 (1993), ‘Code of practice for earthquake resistantdesign and construction of buildings (second revision)’, Bureau of Indian Standard, New Delhi

Experimental Studies on the Flexural Strength Using Bagasse Ash and M-Sand in Concrete



S. Sundararaman and S. Azhagarsamy

1 Introduction

Manufacture of cement emits huge amount of carbon dioxide which is a major concern on greenhouse gas emissions, [1–5]. Hence there is an urgent requirement to have an environmentally and economically feasible alternate option to achieve a sustainable concrete production [5–7]. In India around 300 million tonnes of sugarcane are produced and generates 10 million tonnes of bagasse ash [4, 8]. The safe disposal of the ash is another concern nowadays. A study has been carried out to find out the cementitious property as well as the binding property of cement on its partial replacement [9]. Land filling is the only option of disposing the bagasse ash which requires a huge area of land in the outskirts and if it can be used in concrete will reduce the pollution [10]. The utilization of sugarcane bagasse ash replacement to cement in concrete is gaining importance among numerous research and studied the effect of replacing sugarcane bagasse ash in concrete [4]. The use of sugarcane bagasse ash when partially replaced in cement minimize the cement content as result 519.3 Kilotons of carbon dioxide is reduced. [11]. Various research on the partially replacement of cement with bagasse ash has been investigated on the physical, mechanical properties which revealed that up to 20% of replacement the required compressive strength has been attained. [12, 13]. The natural sand can effectively replaced with M-Sand which will reduced the cost of concrete and doesn't influence the properties of concrete [14]. Due to the non-availability of river sand and to have a sustainable environment, the utilization of manufactured sand has been expanded. Manufactured sand is a substitute of river bed sand for construction purposes [15]. Sugarcane

S. Sundararaman (✉) · S. Azhagarsamy
Department of Civil Engineering, Sri Manakula Vinayagar Engineering College, Madagadipet,
Puducherry, India
e-mail: sankaransundararaman@gmail.com

S. Azhagarsamy
e-mail: azhagarsamysekar@gmail.com

Table 1 Physical properties

Property	Value
Specific gravity	2.6
Fineness modulus	2.82
Water absorption	1.5%

bagasse ash a by-product from sugar manufacturing industry is replaced to cement in concrete [16]. Replacement of bagasse ash with different ratios of 5, 10, 15, and 20% by weight of cement possess a high strength in concrete [17]. It was observed that 10% replacement of bagasse ash sowed higher compressive strength, Flexural Strength than the concrete without sugarcane bagasse ash greater than 25 MPa [18–20].

2 Materials Used

In this study, OPC 53 grade as per IS: 10269-2009 was used [21]. River sand was used as fine aggregate in accordance with IS: 383-1970 standards [22]. For this investigation, coarse aggregate from nearby quarry units were used, conforming to IS: 383-1970 [22]. Potable water used for the study, conforms as per IS: 456-2000 [23].

2.1 *Manufactured Sand*

According to IS 2386-1963, manufactured sand was replaced to river sand and its physical properties are as shown in Table 1.

2.2 *Bagasse Ash*

Sugarcane bagasse ash was collected from a sugar industry near Erode, Tamil Nadu India. Bagasse ash Physical characterization was carried out to assess if cement partially replaced by it as a binder in mortar applications and physical properties are shown in Table 2.

Table 2 Physical properties of bagasse ash

Property	Value
Specific gravity	2.47
Mean grain size in (μm)	11.6
Density Kg/m^3)	2530
Particle shape	Spherical

3 Experimental Programme

Bagasse ash was used to replace 5, 10, and 15% of the cement for casting concrete cubes [4] and river sand is replaced with M-Sand of different ratio 10, 20, and 30% by weight. Mix ratio for M45 Grade of concrete and water cement ratio of 0.39 was used in this study as per IS: 10262-2009 [24]. The compressive strength and flexural strength of concrete at the end of 28 days was found out to study the mechanical properties of concrete. During the experimental programme, 90 cubes and 7 beams were casted. The compressive strength of Bagasse ash and M-sand for 10% and 20% replacement respectively has given a higher value of 55.4 N/mm^2 which is greater than the other varying percentages as shown in Table 3 and Fig. 1. Hence, this ratio is taken as the optimum percentage of replacement and hence Beam specimens of size $100 \times 150 \times 1100 \text{ mm}$ with an effective span of 1000 mm were casted to determine the midpoint and loading point deflection as shown in Fig. 2. For the experimental investigation, tension bars of two numbers 10 mm diameter, hanger bars of two numbers 8 mm diameter, and shear reinforcement of two legs of 6 mm diameter at 110 mm spacing were used. A loading frame of 300 kN capacity was used for testing the flexural strength where in a spreader beam with a constant-moment zone of 350 mm, a two-point loading was applied. A pair of steel hinge-roller supports with a span of 1000 mm serves as the specimens support. The mid-span deflections were recorded. Loading was gradually applied using the hydraulic jack. The beams were loaded to a maximum deflection of approximately 25 mm and a 5 mm wide crack formed or until concrete was crushed. When the beam attains final failure the tests were stopped. For every 5 kN during the loading procedure, crack developments were noted, and the patterns of the cracks were drawn on the beam. Additionally, load on the onset of the first crack seen was noted. The photographic view of the beam specimen to find out the flexural strength is shown in Fig. 3.

Table 3 Compressive strength of concrete

% Replacement of (BA and MS)	Compressive strength in N/mm ² 28 days
Conventional concrete (CC)	46.23
5% BA	46.58
10% BA	47.52
15% BA	44.07
10% BA + 10% MS	51.25
10% BA + 20% MS	55.4
10% BA + 30% MS	48.18

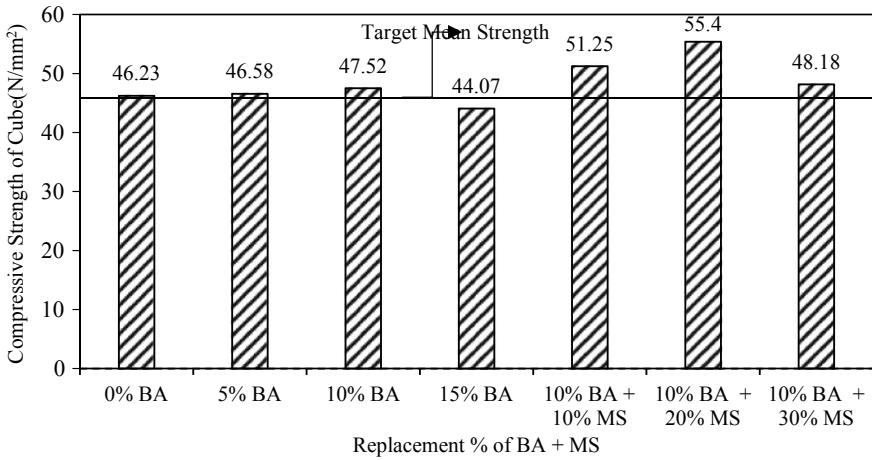


Fig. 1 Compressive strength of cubes on 28 days

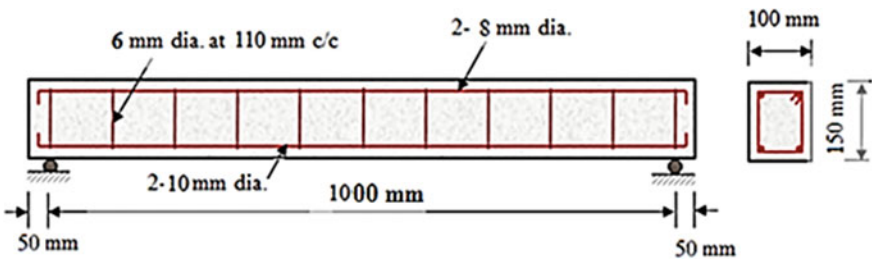


Fig. 2 Beam specimen



Fig. 3 Experimental setup

4 Result and Discussion

4.1 Flexural Strength and Deflection

From Table 4 shown it was observed that with various percentage of bagasse ash and replacement with cement (0, 5, and 10%) revealed that 10% of bagasse ash showed a maximum flexural strength 51.2 kN at the end of 28 days which is in comparable to the findings of [5] With increase in bagasse ash to 15% there was a sharp decline in the flexural strength to 42.9 kN. Hence 10% of bagasse ash is taken as the base to combine with various percentage of M-sand (10, 20 and 30%). It was found that when the M-sand is increase from 10 to 20% along with 10% of bagasse ash there is an increase in the flexural strength of 9 kN (that is from 49.62 to 58.6 kN). On increase of M-sand to 30% there was a drop in the strength to 53.8 kN as shown in Table 4. This shows that the increase of M-sand beyond 20% along with 10% of bagasse ash shows a decreasing trend in the flexural strength. A Similar trend of less deflection in the beam for 20% of M-sand was observed proving that 10% of bagasse ash and 20% of M-sand ass shown in Figs. 4 and 5 is optimum ratio showing maximum strength and minimum deflection.

4.2 Crack Pattern

1. Fig. 6 illustrates the crack patterns formed due to bending behaviour of the beams. The crack patters as carefully marked on the beam when it is subjected to the two point load.
2. The beam exhibits kinks due to the abrupt rise in deflection which was evidenced after the formation of the first crack and the steel yielding stage.

From the Fig. 7 it is observed that the starting yield of steel at 23.5 kN and the steel yield gradually increases from 36 to 42.8 kN when the bagasse ash is alone is increase from 0 to 10%. When the bagasse ash is combine with M-sand the yield strength is increased from 42.4 to 49.5 kN from 10 to 20% of M-Sand. The ultimate

Table 4 Flexural strength of concrete and the ultimate moment

S. No.	Beam specimen	Cube compressive strength, f_{ck}	Load at initial crack, (kN)	Load at ultimate stage, (kN)	Flexural Strength of concrete (N/mm ²)	Deflection at ultimate stage (mm)
1	0% BA	46.23	23.5	45.6	22.29	8.25
2	5% BA	46.58	23.5	46.8	22.88	8.98
3	10% BA	47.52	23.5	51.2	25.03	7.36
4	15% BA	44.07	23.5	42.9	20.97	10.1
5	10% BA + 10% MS	51.25	23.5	49.6	24.25	7.87
6	10% BA + 20% MS	55.4	23.5	58.6	28.65	6.20
7	10% BA + 30% MS	48.18	23.5	53.8	26.30	8.31

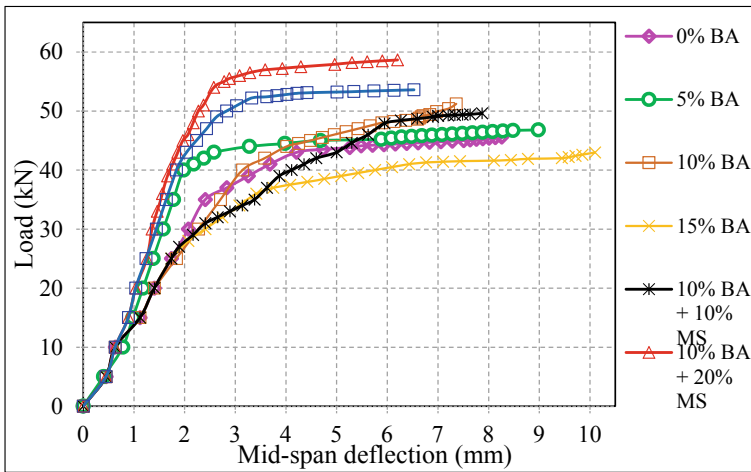


Fig. 4 Load versus Mid-span deflection

stage of flexural strength was increased 49.6 to 58.6 kN from 10 to 20% of M-Sand and 10% bagasse ash constant. After 20 to 30% replacement of M-sand it shows that decreasing in order from 58.6 to 53.8 kN.

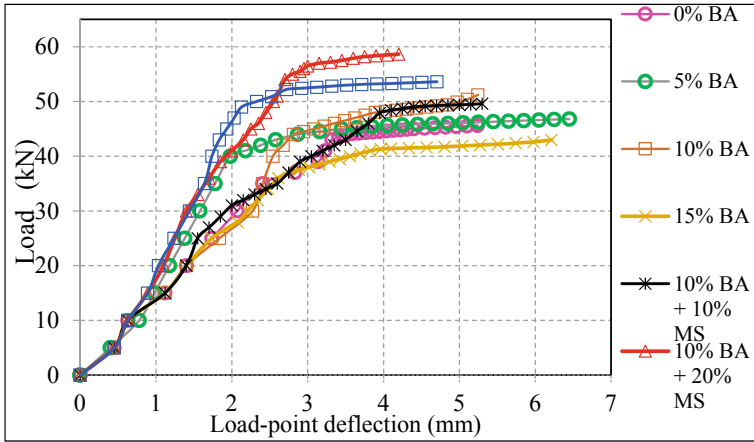


Fig. 5 Load versus Load-point deflection



Fig. 6 Typical crack pattern

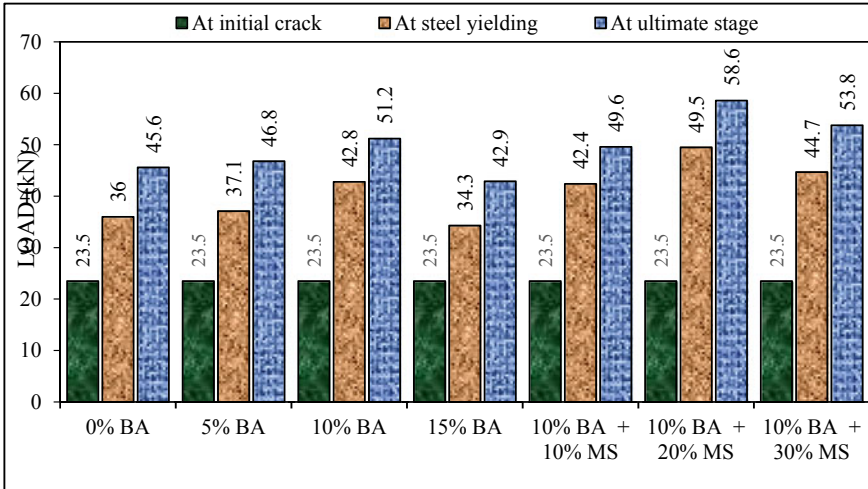


Fig. 7 Comparison of initial crack, steel yielding and ultimate moment

5 Conclusion

1. The bagasse ash which is replacement to cement showed a higher compressive strength value of 47.52 N/mm² for 10% bagasse ash.
2. 10% bagasse ash along with 20% of M-Sand replacement in concrete showed a compressive strength of 55.4 N/mm² at the end of 28 days.
3. When M-sand is increased to 30% keeping bagasse ash 10%, there is a decrease in compressive strength due to the higher percentage of bagasse ash. If it would have been 5% of bagasse ash 30% of m-sand might have a higher compressive strength.
4. The flexural strength of concrete beam for 10% of bagasse ash and 20% of M-sand showed 58.6 kN which is 9 kN higher value when compared to 10% of bagasse ash and 10% of M-sand.
5. The flexural strength showed a decline phase when the M-sand is increased to 30% in the above mix proportion. This shows that only 20% of M-sand could be an optimum percentage when combined with 10% of bagasse ash replaced to cement.
6. It is also observed that for 10% of bagasse ash and 20% of M-sand as a replacement to concrete there is a minimum deflection of 6.2 mm at the ultimate stage. This proves that the maximum flexure strength and minimum deflection is attained for 10% of bagasse ash and 20% of M-sand.
7. The compressive strength decreases beyond 20% of SCBA in the present study which is in the agreement with the finding of [4, 25].

References

1. Aghababai Beni A, Jabbari H (2022) Nanomaterials for environmental applications. Results Eng 15:100467. <https://doi.org/10.1016/j.rineng.2022.100467>
2. Gupta CK, Sachan AK, Kumar R (2022) Utilization of sugarcane bagasse ash in mortar and concrete: a review. Mater Today Proc. <https://doi.org/10.1016/j.matpr.2022.03.304>
3. Fort J, Šál J, Žák J, Cerný R (2020) Assessment of wood-based fly ash as alternative cement replacement. Sustainability 12. <https://doi.org/10.3390/su12229580>
4. Quedou PG et al (2021) Sustainable concrete: potency of sugarcane bagasse ash as a cementitious material in the construction industry. Case Stud Constr Mater 14:e00545. <https://doi.org/10.1016/j.cscm.2021.e00545>
5. Abdalla TA et al (2022) Mechanical and durability properties of concrete incorporating silica fume and a high volume of sugarcane bagasse ash. Results Eng 16. <https://doi.org/10.1016/j.rineng.2022.100666>
6. Bheel N, Sohu S, Jhatial AA, Memon NA, Kumar A (2022) Combined effect of coconut shell and sugarcane bagasse ashes on the workability, mechanical properties and embodied carbon of concrete. Environ Sci Pollut Control Ser 29(4):5207–5223. <https://doi.org/10.1007/s11356-021-16034-3>
7. Atoyebi OD, Gana AJ, Longe JE (2020) Strength assessment of concrete with waste glass and bankoro (Morinda Citrifolia) as partial replacement for fine and coarse aggregate. Results Eng 6:100124. <https://doi.org/10.1016/j.rineng.2020.100124>

8. Jagarapu DCK, Eluru A (2020) Strength and durability studies of lightweight fiber reinforced concrete with agriculture waste. *Mater Today Proc.* <https://doi.org/10.1016/j.matpr.2020.01.257>
9. Akash GS et al (2018) experimental study on partial replacement of sand with sugarcane bagasse ash in concrete. *Int Res J Eng Technol (IRJET)* 05(05)
10. Malagar L, Singh H (2023) Experimental research on ecofriendly high strength concrete with bagasse ash, jute fibre, and waste foundry sand. *IOP Conf Ser Earth Environ Sci.* <https://doi.org/10.1088/1755-1315/1110/1/012091>
11. Wani BJ (2021) Utilization of sugarcane bagasse ash in concrete as partial replacement in cement. *Int J Sci Res (IJSR)* 10(7)
12. Sundararaman S, Azhagarsamy S (2013) Experimental study on partial replacement of cement by bagasse ash and m-sand in concrete. *Int J Adv Technol Civ Eng* 2(2)
13. Lakshmi PS (2019) Influence of bagasse ash replacement on strength properties of cement mortar. *Int J Civ Eng Technol (IJCIET)* 10(05):954–962
14. Sai Kumar V (2018) Experimental Investigation on flexural behaviour of fly ash concrete by replacing sand with M-sand. *Int J Civ Eng Technol (IJCIET)* 9(6):348–354
15. Amin M (2022) Effects of sugarcane bagasse ash and nano eggshell powder on high-strength concrete properties. *Case Stud Constr Mater* 17. <https://doi.org/10.1016/j.cscm.2022.e01528>
16. Dayo AA et al (2020) Effect of sugarcane bagasse ash as fine aggregates on the flexural strength of concrete. *Int Conf Sustain Develop Civ Eng*
17. Abdalla TA (2022) Mechanical properties of eco-friendly concrete made with sugarcane bagasse ash. *Civ Eng J* 8(06)
18. Panda AK et al (2022) Study of properties of concrete by partial replacement of cement with sugarcane bagasse ash. *Int Res J Modernization Eng Technol Sci* 04(7)
19. Hathiram G et al (2023) Compressive strength of bagasse ash based M25 grade concrete. *Int J Eng Res Appl* 13(3)
20. Tarekegn M et al (2022) Experimental investigation of concrete characteristics strength with partial replacement of cement by hybrid coffee husk and sugarcane bagasse ash. *Adv Mater Sci Eng.* <https://doi.org/10.1155/2022/5363766>
21. IS 10262-2009 “IS method of mix design”, Bureau of Indian Standards, New Delhi
22. IS 383-1970 “Specification for coarse and fine aggregates from natural sources for concrete”, Bureau of Indian Standards, New Delhi
23. IS 456-2000 “Code of practice for plain and reinforced concrete”, Bureau of Indian Standards, New Delhi
24. Latha MS (2020) Strength characteristics of high performance concrete using bagasse ash and slag sand. *Int J Emerg Trends Eng Res* 8(6)
25. Dineshkumar R, Balamurugan P (2021) Behavior of high-strength concrete with sugarcane bagasse ash as replacement for cement. *Innov Infrastruct Solutions* 6(2). <https://doi.org/10.1007/s41062-020-00450-4>

Performance-Based Seismic Analysis of RC Multi-storey Framed Building Equipped with Dampers



R. Arvind, M. Helen Santhi, G. Malathi, and V. Vasugi

1 Introduction

India has the second highest population in the world, and 82% of its citizens live there despite about 60% of its landmass being vulnerable to moderate-to-severe earthquakes. Future seismic occurrences in earthquake-prone locations will rise as a result of rapid urbanization and population growth. An earthquake's effects on buildings and other structures cause deaths, injuries, and financial harm for a nation. Most of the buildings in the seismic prone regions are constructed by individual landholders and do not satisfy the design and construction guidelines specified in the Indian standard codes. Therefore, majority of the population live in these regions are under seismic threat. This forces the Government authorities to identify the vulnerabilities of building typologies all over the country against seismic forces and to formulate the recommendations to improve the safety of existing buildings. Lots of improvement have been carried out in Rapid Visual Screening (RVS) for common types of structures in the recent past [1–6].

Passive energy dissipation technologies perform wonderfully for all ranges of ground vibration. The passive control system is currently the most used damper system since it is widely available, affordable, easy to install and replace, and it runs without the usage of electricity.

Damage level of RC buildings under different ground motions was assessed by various methods by researchers in the past and out of which the performance-based methods are gaining importance due to their efficiency and accuracy in evaluation. Different developments were introduced in the performance-based safety assessment of RC buildings for the implementation in real structures [7–19].

R. Arvind · M. Helen Santhi (✉) · V. Vasugi
School of Civil Engineering, Vellore Institute of Technology, Chennai, India
e-mail: helensanthi.m@vit.ac.in

G. Malathi
School of Computer Science and Engineering, Vellore Institute of Technology, Chennai, India

The seismically deficient RC buildings are generally retrofitted with different techniques such as bracings, base isolation, seismic dampers, etc. to make them suitable to resist the future earthquakes [20–26]. There are lots of scope for the dampers for buildings and other structures as they show enhanced seismic behaviour during earthquakes of different intensities.

2 Modelling and Analysis

The modelling and analysis were performed in ETABS software version 2018. The building model consists of 5 bay by 5 bay G + 14 storeys with span 6.0 m and Fig. 1 shows the typical plan and elevation of the building. The storey height is taken as 3.2 m. The size of the column is taken as 750 × 750 mm for the lower 5 storeys, 600 × 600 mm in next 5 storeys above and 500 × 500 mm in the upper 5 storeys. The beam size is taken as 300 mm × 400 mm for the entire building. A 150 mm thick slab is used. The grade of concrete and steel are taken as M 25 and Fe 415, respectively. Live load on floors is considered as 3 kN/m².

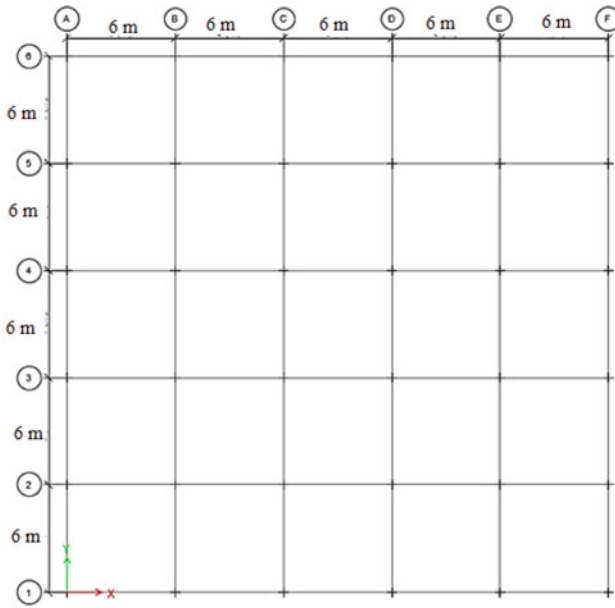
The friction and slit dampers are modelled as link elements with load-deformation characteristics as considered by Lee et al. [27]. The models with and without dampers were analysed using non-linear time history method.

2.1 Time History Analysis

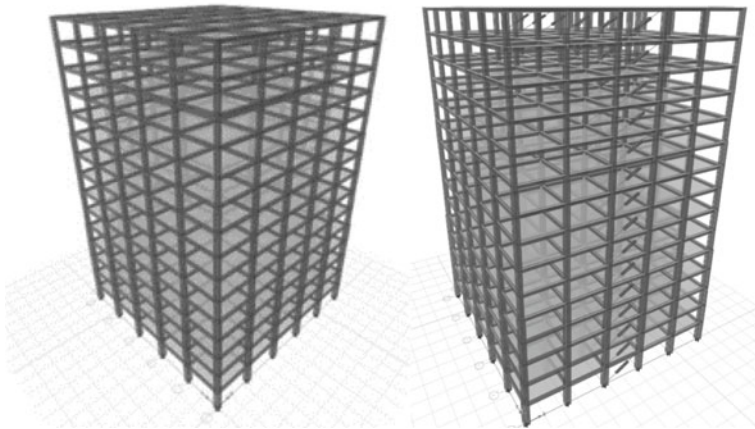
The input for the study, El-Centro earthquake values are scaled from 0.1 to 1.0 g PGA using Seismosoft software. El-Centro earthquake data of maximum PGA of 0.3172 g (Fig. 2) is scaled to have the ground motions. From the investigation, the top displacement, drift and, energy dissipation values of the models are observed under 0.1–1.0 g ground motions. From the obtained drift responses, the various damage levels of the structure under study are assessed.

3 Results and Discussion

From 0.1 to 1.0 g, PGA are applied to the structure and the top displacement, energy dissipation and maximum inter-storey drift ratio are obtained and compared. It is observed that the top displacement is reduced around 10% and 34% when the bare frame is retrofitted with friction damper and slit damper, respectively (Fig. 3). The energy dissipation of the models with and without dampers is given in Fig. 4. It can be seen that the energy dissipation is increased nearly 1.15 times and 1.74 times for the frames with friction damper and slit damper, respectively when compared to that



(a) Plan



(b) Elevation

Fig. 1 Building model with and without damper-typical

of the bare frame. The seismic responses of the frame with slit damper shows better behaviour than the frame with the friction damper.

The max inter-storey drift ratio of all the models for different ground motions is given in Table 1. In this study, 0.015 drift and 0.01 drift levels are considered as allowable drift and life safety limits, respectively to classify the damage level of the

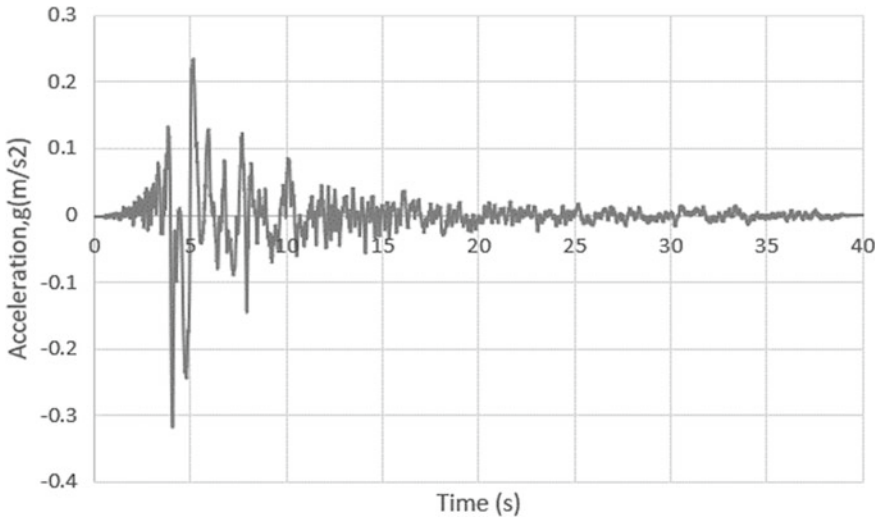


Fig. 2 El-centro earthquake data

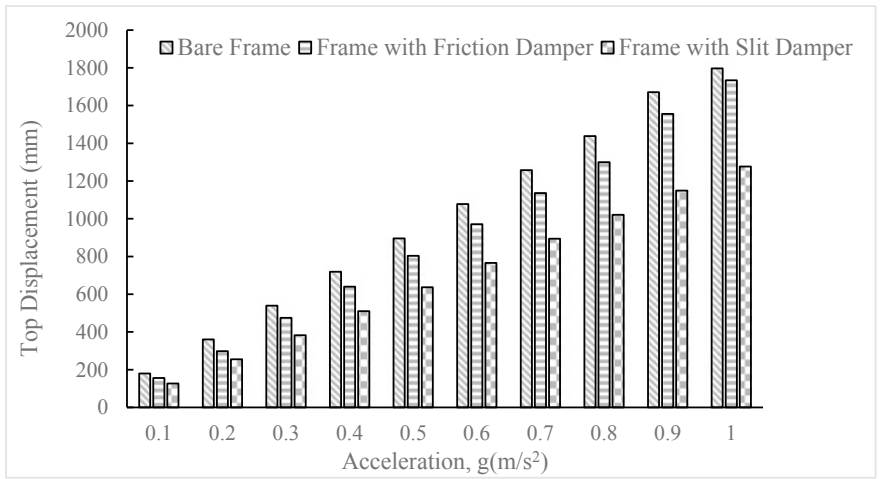


Fig. 3 Top displacement of all models

frames under study. From the observed values of drift ratio, it is understood that the frame with friction damper is able to control the allowable drift and life safety upto 0.2 g PGA. The drift control is appreciable in the frame with slit damper and the damage level shows that it is able to resist the drift nearly equal to 0.3 g PGA, beyond that there will be a significant structural and non-structural damages in the frame. For the enchancement of the lateral capacity of the structure for higher PGA, the following modifications may be preferred; (i) uniform column dimension of 750 mm

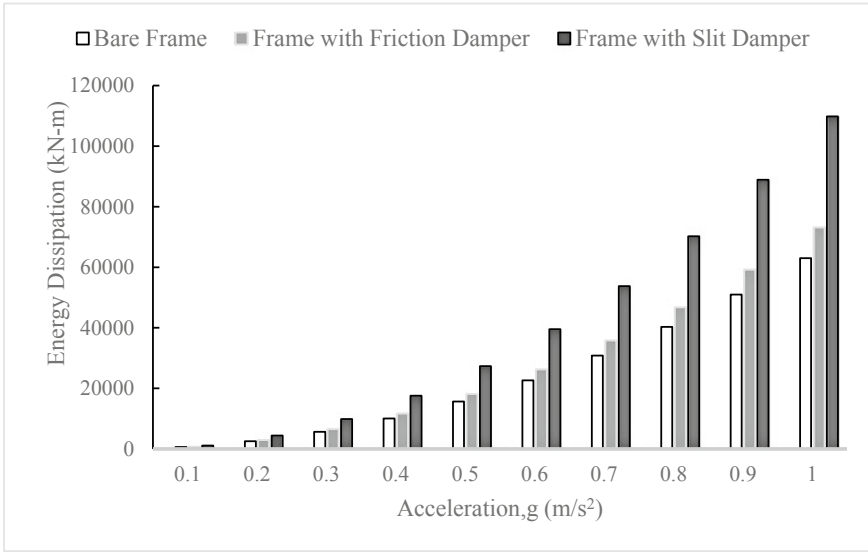


Fig. 4 Energy dissipation of all models

× 750 mm for the entire height of the building, (ii) more number of dampers, and (iii) hybrid damper.

Table 1 Maximum inter-storey drift ratio of all models

Acceleration, g(m/s ²)	Max inter-storey drift ratio		
	Bare frame	Frame with friction damper	Frame with slit damper
0.1	0.007	0.007	0.005
0.2	0.015	0.014	0.009
0.3	0.022	0.021	0.014
0.4	0.030	0.028	0.019
0.5	0.037	0.035	0.024
0.6	0.045	0.043	0.028
0.7	0.052	0.049	0.033
0.8	0.060	0.057	0.038
0.9	0.066	0.064	0.043
1.0	0.074	0.071	0.048

4 Conclusion

In this investigation, G + 14 storey RC framed building is analysed underground motions from 0.1 g to 1.0 g PGA and found not sufficient to meet the seismic requirements. In order to improve the seismic behaviour of the frame, friction damper and slit dampers are installed. The influence of friction damper on the frame is not much significant and its effect is meagre. The slit damper significantly enhances the seismic performance of the frame such as top displacement, drift and, energy dissipation. Also, the frame with slit damper is capable of resisting the PGA up to 0.3 g. Therefore, it is suggested to use slit damper in the frame under study to resist low to medium level ground motions.

References

1. Sinha R, Goyal A (2004) A National Policy for Seismic Vulnerability Assessment of Buildings and Procedure for Rapid Visual Screening of Buildings for Potential Seismic Vulnerability, Department of Civil Engineering, Indian Institute of Technology Bombay, India
2. Jain SK, Mitra K, Kumar M, Shah M (2010) A proposed rapid visual screening procedure for seismic evaluation of RC-frame buildings in India. *Earthquake Spectra* 26(3):709–729
3. Harirchian E, Kumari V, Jadhav K, Raj Das R, Rasulzade S, Lahmer T (2020) A machine learning framework for assessing seismic hazard safety of reinforced concrete buildings. *Appl Sci* 10(20):7153
4. A Primer on Rapid Visual Screening (RVS) Consolidating Earthquake Safety Assessment Efforts in India, National Disaster Management Authority, 2020.
5. Shendkar MR, Pradeep Kumar R, Mandal S, Maiti PR, Kontoni DPN (2021) Seismic risk assessment of reinforced concrete buildings in Koyana-Warna region through EDRI method. *Innovative Infrastructure Solutions* 6(3):1–25
6. Ghobarah A (2000) Seismic assessment of existing RC structures. *Prog Struct Mat Eng* 2(1):60–71
7. Goel R, Chandwell C. Evaluation of ASCE-41 nonlinear static procedure using recorded motions of reinforced-concrete buildings. In *Structures congress 2008: Crossing borders* :1–11.
8. Jaing HL, Chen LZ, Chen Q (2011) Seismic damage assessment and performance levels of reinforced concrete members. *Procedia engineering* 14:939–945
9. Habibi AR, M Izadpanah, Yazdani A. Inelastic damage analysis of RCMRFs using pushover method. *Iranian Journal of Science and Technology-Transactions of Civil Engineering*,2013; 37 (2): 345–352.
10. Heo Y, Kunnath SK (2013) Damage-based seismic performance evaluation of reinforced concrete frames. *Int. J. Concr. Struct. Mater.* 7(3):175–182
11. Hakim RA, Alama MS, Ashour SA (2014) Seismic Assessment of RC Building According to ATC 40, FEMA 356 and FEMA 440. *Arab J Sci Eng* 39:7691–7699
12. Anwar GA, Dong Y, Zhai C (2020) Performance-Based Probabilistic Framework for Seismic Risk, Resilience, and Sustainability Assessment of Reinforced Concrete Structures. *Adv Struct Eng* 23(7):1454–1472
13. Zameeruddin M, Sangle KK (2021) Performance-based seismic assessment of reinforced concrete frames. *J. King Saud Univ. Eng. Sci.* 33:153–165
14. Roy T, Agarwal P. Comparison of damage index and fragility curve of RC structure using different indian standard codes. In *Advances in structural engineering*. Springer, New Delhi, 2015; 2551–2563

15. Sriwastav RK . Seismic vulnerability assessment of high-rise buildings in Patna for future earthquakes. Master's thesis, Indian Institute of Technology Patna, 2016.
16. Paul S, Debnath S. Seismic Damage Evaluation of RC Buildings Using Nonlinear Static Method. Recent Advances in Structural Engineering, 2019; Lecture Notes in Civil Engineering, 12.
17. Das PK, Dutta SC, Sengupta P (2020) Damage Assessment of Recent Indian Earthquakes: Review of Existing Rapid Visual Screening Schemes. *Curr Sci* 119:2
18. Arvind R, Helen Santhi M (2022) A State of Art Review on Hybrid Passive Energy Dissipating Devices. *J. Vib. Eng. Technol.* 10:1931–1954
19. Kumar P, Samanta A. Seismic Fragility Assessment of Existing 9 Storey Reinforced Concrete (RC) Buildings in Patna, India. *Seismic Hazards and Risk. Lecture Notes in Civil Engineering*, 2021; 116.
20. Thermou G, Elnashai AS (2006) Seismic Retrofit Schemes for RC Structures and Local-Global Consequences. *Prog Struct Mat Eng* 8(1):1–15
21. Durucan C, Dicleli M (2010) Analytical study on seismic retrofitting of reinforced concrete buildings using steel braces with shear link. *Eng Struct* 32(10):2995–3010
22. Impollonia N, Palmeri A (2018) Seismic performance of buildings retrofitted with nonlinear viscous dampers and adjacent reaction towers. *Earthquake Eng Struct Dynam* 47(5):1329–1351
23. Moon KH, Han SW, Lee CS (2017) Seismic retrofit design method using friction damping systems for old low- and mid-rise regular reinforced concrete buildings. *Eng Struct* 146:105–117
24. Mazza F, Mazza M, Vulcano A (2018) Base-isolation systems for the seismic retrofitting of RC framed buildings with soft-storey subjected to near-fault earthquakes. *Soil Dyn Earthq Eng* 109:209–221
25. Anwar GA, Dong Y (2020) Seismic resilience of retrofitted RC buildings. *Earthq Eng Eng Vib* 19:561–571
26. Usmani S, Dabhekar K R, Khedikar I, Gautam N R (2021) Seismic retrofitting of Indian RC buildings using shear walls. In *Advances in civil engineering and infrastructural development*, pp 33–41
27. Lee J, Kang H, Kim J (2017) Seismic performance of steel plate slit-friction hybrid dampers. *J Constr Steel Res* 136:128–139

Numerical Studies on RC Beams Strengthened with an Externally Bonded Aramid FRP Sheets



Gurram Kalyani and N. Pannirselvam

1 Introduction

Reinforced concrete projects may need to be modified for a variety of causes. The concrete may have been systematically deficient due to the disintegration of substances, imperfect early design, the inadequacy of continuance, enhancement of organised loads, or mishap events. The performance of RC members can be improved throughout their service life by reinforcing, retrofitting and repairing them. Replacement of the structure may have certain disadvantages, such as higher material and labour costs, a greater natural effect, and discomfort due to the structure's inability to function. Steel plates or FRP laminates are commonly used to retrofit concrete structures with externally bonded reinforcement. FRP is also known as fibre-reinforced plastic. For a variety of reasons, FRP is more convenient than steel. They are less heavy than steel plates of the same size. They can be moulded into complex shapes on-site, and they can also be simply cut to length. Because FRP is lightweight, it makes installation easier and eliminates the need for temporary support until the adhesive reaches its full strength. The inclusion of FRP laminate to reinforced concrete beams has previously been shown to enlarge stiffness, utmost load, and crack widths, and the technology is frequently employed for concrete structural upgrades [1–4].

Numerous investigators have demonstrated the usefulness of FRP composites for concrete and masonry constructions over the last three decades. Few literature reviews are discussed below:

Zhang et al. [5] used Finite-Element Model (FEM) to demonstrate the effects of localised fractures on the response of Carbon Fibre-Reinforced Polymer (CFRP) sheets used to reinforce RC beams. They concluded that under simple conditions, FEM can be utilized to simulate crack propagation in structures. Spadea et al. [6]

G. Kalyani · N. Pannirselvam (✉)

Department of Civil Engineering, Faculty of Engineering and Technology, SRM Institute of Science and Technology, Kattankulathur, Tamil Nadu 603203, India

e-mail: pannirsn@srmist.edu.in

studied RC beam's strength and ductility repaired with CFRP laminates were investigated. The researchers looked at how retrofitting affected strength, deflection, curvature, and energy. The primary considerations were the ratio of lengthwise steel, the volume of inner connections, and the anchorage structure at the end. The authors discovered that appropriately planned and located outward anchorage allowed for additional ductile defeats of the CFRP reinforced beams.

Hamid and Allan [7] worked on the construction behaviour of concrete beams with adherently joined FRP sheets was investigated. The investigation utilised 2D nonlinear finite element modelling using the concrete damage replica for concrete. They discovered that prior ruptured beams were carried out ably; strengthened beams increased in strength and stiffness significantly; the magnitude of execution was impacted by tensile reinforcement as well as the type and quantity of outer reinforcement and non-linear finite element modelling can be used to predict the production of outer reinforcing concrete beams. Amer et al. [8] carried out a numerical examination of RC beams ANSYS finite part scheme, and the findings demonstrate the widespread ways of the finite element prototypes presented by the load–displacement loops at mid-spanned agree well with the experimental test data. In addition, they finished that the load-bearing capability of the flexure built-up beam anticipated by finite component investigation, is greater than that of the conventional beam. In their study of the probe, Wang and Li [9] provided methodical results for RC beams reinforced with CFRP laminates under prolonged loading. Six RC beams were utilised in the investigation. They examined how the ultimate strength of reinforced concrete beams is affected by previous loads and past loads. There was also a suggestion for an analytical model. The results of the experiments and the analysis agreed. After conducting a numerical analysis using the ABAQUS programme, Hsuan-Teh et al. [10] investigated the ultimate load-carrying capability of RC beams reinforced with FRP's placed on the tension side of the beams. The author explored the effect of reinforcement proportion, fibre inclination, and length of the beam on the maximum strength of beams. According to the investigators, the use of FRP's notably boosted the precision and final strength of RC beams. In addition, they found that the maximum strength of RC beams reinforced with FRP's at the bottom surface is greater than that of beams reinforced with FRP's at the side faces. Lua et al. [11] in the model, the behaviour of fractured concrete was approximated using the smeared crack technique, and concrete in condense was represented as an elastic–plastic substance. The authors discovered that the outcomes of the finite element replica were in acceptable unity with the test findings.

Experiments and finite element modelling with ABAQUS software were used in the majority of earlier efforts related to strengthening concrete beams with FRP to improve the flexure behaviour of RC beams. More theoretical and numerical investigations are needed to better understand the conduct of FRP-RC beams. The purpose of this research is to see how accurate the FEM is in representing RC beams reinforced with AFRP of various thicknesses under flexural loading. The numerical study goal is to use finite element analysis to characterise the behaviour of RC components in an experiment. Separate material models are used to idealise the macroscopic constituent of concrete and reinforcing steel. The material models are

integrated, specifying the interplay between reinforcing steel and concrete to mimic the integral behaviour of the composite RC material global reaction.

2 Analytical Modelling

2.1 General

Four-point bending under flexure, the reinforced concrete beams with overall dimensions of 3000 mm long, 250 mm depth and 150 mm width modelled using the simply supported boundary condition. The beam's effective span is calculated to be 2800 mm. To minimise shear defeat and make certain flexural measures of beams up to end, the longitudinal steel proportion employed for the beam sample was 0.603% (2 bars, 12 mm diameter) and 2-legged 8 mm diameter shear stirrups take place at 150 mm *c/c*.

2.2 Concrete

The modelling of concrete utilised a plastic damage model [12]. This model's primary two defeat ways are tensile splitting and compressive crushing. Until the defeat stress comes, the stress–strain reaction under uniaxial tension sticks to a linear elastic correspondence. The development of micro-rupturing in the concrete substance corresponds to the defeat stress. An easing stress–strain retaliation presents the production of micro-cracks beyond the breakdown stress. In Tables 1 and 2 give all material values.

2.3 Steel Reinforcement Bars

As depicted in Fig. 1, reinforcement bars were presumed to be an elastic–ideally plastic substance with similar tension and compression properties in tension and compression.

2.4 Procedure of Assembly, Interaction and Meshing

The usual assembly of the various pieces is depicted in Figs. 2 and 3. The loading plate and the upper surface of the beam form the tie constraint. As a rigid body, the loading plate is also limited. The reinforcement is distributed such that the tension

Table 1 CDP parameters for concrete

Compressive behaviour	Compression damage			
Yield stress	Inelastic strain	Damage parameter	Crushing strain	
15.3	0	0	0	
19.2	0.0001	0	0.0001	
22.5	0.0002	0	0.0002	
25.2	0.0003	0	0.0003	
27.3	0.0004	0	0.0004	
28.8	0.0005	0	0.0005	
29.7	0.0006	0	0.0006	
30	0.0008	0	0.0008	
29.7	0.0009	0.01	0.0009	
28.8	0.0011	0.04	0.0011	
27.3	0.0013	0.09	0.0013	
25.2	0.0014	0.16	0.0014	
22.5	0.0016	0.25	0.0016	
19.2	0.0017	0.36	0.0017	
15.3	0.0018	0.49	0.0018	
10.8	0.0019	0.64	0.0019	
5.7	0.0043	0.81	0.0043	
Tensile behaviour		Tension damage		
Damage parameter		Damage parameter	Cracking strain	
3	0	0	0	
0.03	0.0011673	0.99	0.0011673	
Dilation angle	Eccentricity	fb0/fc0	K	Viscosity parameters
31	0.1	1.16	0.67	0

Table 2 Mechanical properties

Properties	Concrete	Steel	AFRP
Density, kg/m ³	2400	7850	1440
Young's modulus, MPa	26,600	205,000	70,500
Poisson's ratio	0.2	0.3	0.25

Fig. 1 Reinforcement cage

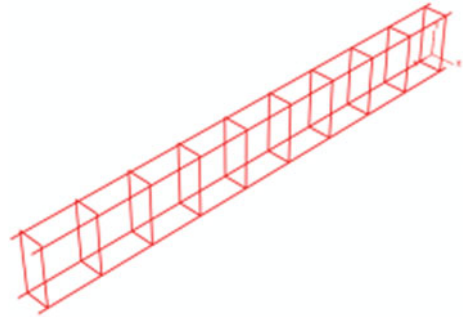
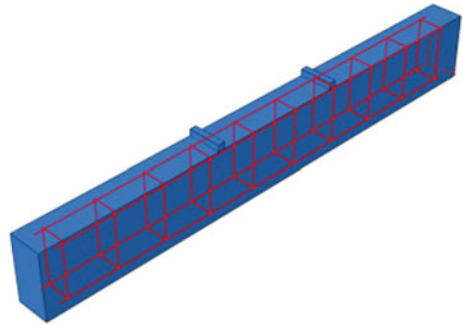


Fig. 2 Assembling of the RC beam

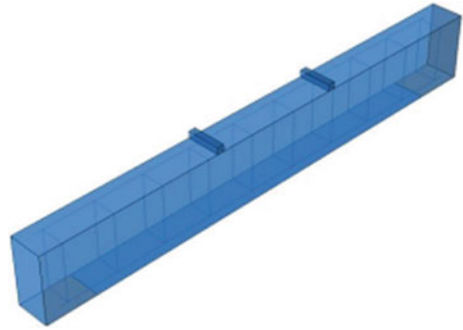


face of the beam has an effective cover of 25 mm and the compression face has an effective cover of 25 mm. This constraint specifies the interactivity between the concrete beam and reinforcing steel. Using the embedded element strategy, you can define that a set of components is submerged within a host element. ABAQUS looks for congruent correlations in the middle of the junction of submerged and host elements. When a junction of a submerged element is included inside a host element, the node loses its translational degrees of freedom and is referred to as an ‘embedded node.’ The rotational degrees of freedom of the submerged junction is managed by the interpose value of the in-tune degrees of freedom of the host element. Rotational degrees of freedom are allowed for embedded elements, but they are not bound by the embedding.

2.5 Load and Boundary Condition

For various beams, mechanical stacking is characterised by pressure load and descending deflection on a four-point flexing platform above a simulated steel loading plate. The simply supported partition state is idealised by specifying the node’s degree of freedom 150 mm from both ends across the breadth of the beam. The boundary

Fig. 3 Meshing of RC beam

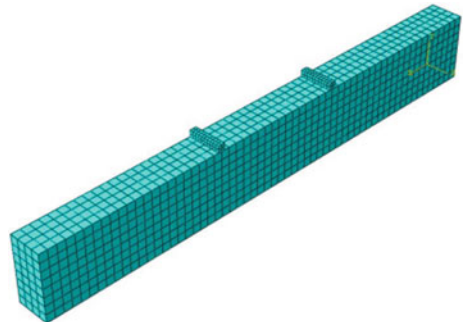


state is defined as a hinge with degrees of freedom $U1 = 0, U2 = 0$, and a roller with degrees of freedom $U2 = 0$ to generalise the simply supported boundary state.

2.6 Meshing

After that, the formed RC beams mesh with the required seed size. It is a well-known fact of FEM study that the precision of the analysis is all the time greater than that of refined mesh, despite the longer convergence time. The size of the element is governed by the kind and level of difficulty of the obstacle. To maintain mesh consistency, the seed size length for the concrete beam brick element and truss element of rebars is 10 mm. Figure 4 demonstrates the meshing of a modelled beam.

Fig. 4 Beam with AFRP at bottom



3 Results and Discussion

The load–deflection data for the conventional beam and retrofitting beams generated from finite element analysis will be illustrated in Table 3 and discussed in this section. Since the expected thorough association in the middle of concrete and reinforcement, the FEM investigation specifies that the beam will be modest rigid and well built. The high level of agreement implies that the concrete and reinforcement constitutive models may accurately predict failure behaviour.

Comparing all of the data, it is evident that the thickness of the AFRP laminates has a notable consequence on the conduct of the RC beam. The higher the highest load, the thicker the AFRP. From this study, it can be concluded that 4 mm thickness AFRP laminate is optimum for strengthening RC beams. The rigidity of the beam is increasingly overestimated by perfect bond models. This is required to the reality that the exact interaction does not account for the ‘shear strain’ connecting the concrete and the AFRP (Fig. 5).

Table 3 Load- deflection results

Specimen	Thickness, mm	Ultimate load, kN	Deflection, mm	Failure
SC	-	65	16.57	Flexure
A1	1	81	15.29	Flexure
A2	2	95	13.02	FRP rupture
A3	3	106	10.54	FRP rupture
A4	4	120	8.66	FRP delamination at the end
A5	5	107	8.00	FRP delamination at the end

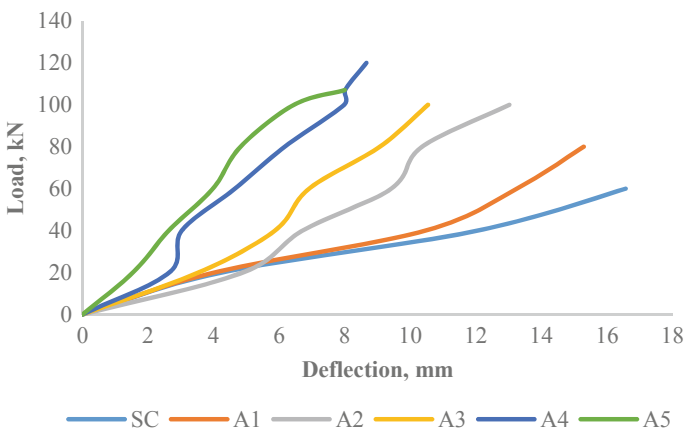


Fig. 5 Numerical FEM load–displacement results

4 Conclusion

The AFRP-refitted beams were examined using the finite-element method. Elastic isotropic exploits were utilised to approximate the AFRP actions. Using a cohesive model, the interfacial behaviour of AFRP and concrete was investigated. From this study, the resulting closures can be drawn:

The thickness of AFRP has an enormous effect on the performance of retrofitted beams. It is determined that the ultimate load is proportional to the AFRP thickness. Nevertheless, according to the finite element simulations, the concrete beam is marginally stiffer than the test results. Finally, environmental issues such as seasonal temperature variation, creep, and shrinkage that may affect the effectiveness of RC beams strengthened with AFRP were not taken into account. It is possible to investigate the impact of these characteristics over the course of a beam's lifetime.

References

1. Ai-hui Z, Wei-Liang J, Gui-bing L (2006) Behaviour of preloaded RC beams strengthened with CFRP laminates. *J Zhejiang Univ, Sci, A* 7(3):436–444. <https://doi.org/10.1631/jzus.2006.A0436>
2. Esfahani M, Kianoush M, Tajari A (2007) Flexural behaviour of reinforced concrete beams strengthened by CFRP sheets. *Eng Struct* 29:2428–2444. <https://doi.org/10.1016/j.engstruct.2006.12.008>
3. Saleem MU, Numada M, Amin MN, Meguro K (2016) Shake table tests on FRP retrofitted Masonry building models. *J Compos Constr* 20(5):1–19. [https://doi.org/10.1061/\(ASCE\)CC.1943-5614.0000684](https://doi.org/10.1061/(ASCE)CC.1943-5614.0000684)
4. Pham H, Al-Mahaidi R (2004) Experimental investigation into flexural retrofitting of reinforced concrete bridge beams using FRP composites. *Compos Struct* 66:617–625. <https://doi.org/10.1016/j.compstruct.2004.05.010>
5. Teng JG, Zhang JW, Smith ST (2002) Interfacial stresses in reinforced concrete beams bonded with a soffit plate: a finite element study. *Constr Build Mater* 16:1–14. [https://doi.org/10.1016/S0950-0618\(01\)00029-0](https://doi.org/10.1016/S0950-0618(01)00029-0)
6. Spadea G, Swamy RN, Bencardino F (2001) Strength and ductility of RC beams repaired with bonded CFRP laminates. *J Bridg Eng* 6:349–355. [https://doi.org/10.1061/\(ASCE\)1084-0702\(2001\)6:5\(349\)](https://doi.org/10.1061/(ASCE)1084-0702(2001)6:5(349))
7. Hamid Rahimi and Allan Hutchinson (2001) Concrete beams strengthened with externally bonded FRP plates. *J Compos Constr* 5(1):44–56. [https://doi.org/10.1061/\(ASCE\)1090-0268\(2001\)5:1\(44\)](https://doi.org/10.1061/(ASCE)1090-0268(2001)5:1(44))
8. Amer, M. Ibrahim, Wissam D and Salman, 2009. Finite element analysis of reinforced concrete beams strengthened with CFRP in flexural. *Diyala J Eng Sci* 02:88–104
9. Wang W, Li G (2006) Behaviour of preloaded RC beams strengthened with CFRP laminates. *J Zhejiang Univ-Sci A* 7(3):436–444. <https://doi.org/10.1631/jzus.2006.A0436>
10. Hu H-T, Lin F-M, Jan Y-Y (2004) Nonlinear finite element analysis of reinforced concrete beams strengthened by fiber-reinforced plastics. *Compos Struct* 63:271–281. [https://doi.org/10.1016/S0263-8223\(03\)00174-0](https://doi.org/10.1016/S0263-8223(03)00174-0)
11. Lua XZ, Yea LP, Tengb JG, Jianga JJ (2005) Meso-scale finite element model for FRP sheets/plates bonded to concrete. *Eng Struct* 27:564–575. <https://doi.org/10.1016/j.engstruct.2004.11.015>

12. Hafezolghorani M, Hejazi F, Vaghei R, Jaafar MSB, Karimzade K (2017) Simplified damage plasticity model for concrete. *Struct Eng Int* 27(1):68–78. <https://doi.org/10.2749/101686616X1081>

Analysis and Design of G+15 High-Rise Residential Structures with and Without Floating Column in Nepal



Nisha Jha, Pratiksha Simkhada, and R. Ramasubramani

1 Introduction

Recent urbanization in Nepal has demanded buildings with architectural complexities (soft story, heavy load, floating column, etc.). To cope with the growing population and limiting land area, high-rise buildings are required. Nowadays, floating column is embraced to enhance FSI and to create ample space for various purpose like parking, halls, lobbies, etc. The high-rise residential building (G+ 15) requires large uninterrupted parking area to facilitate all residents of building making use of floating column above ground floor unavoidable. Floating column is a vertical member which connects with slab or horizontal beam and to not take part in transferring load to the foundation directly, rather it acts as point load on slab or beam and then beam or slab transfer load to the nearest column and from column to foundation. When floating column is provided above ground floor, sub-column acts as point load on the ground floor beam and transfer load to nearest primary column. The primary column then transfers load to the foundation.

2 Literature Review

The examination of the literature reveals that the horizontal displacement, story drift, and story shear values derived from floating column buildings are maximum than those from regular buildings [1] when buildings with and without floating columns are analyzed and designed. Additionally, it was discovered that complicated models had larger displacements than models with merely floating columns. In every model, the

N. Jha · P. Simkhada · R. Ramasubramani (✉)

Department of Civil Engineering, Faculty of Engineering and Technology, SRM Institute of Science and Technology, Kattankulathur, Tamil Nadu 603203, India

e-mail: ramasubr@srmist.edu.in

displacement value grew as the seismic zone condition increased, while the maximum displacement and inter-story drift value decreased as the column size increased [2]. The maximum displacement is decreasing with increased ground floor columns, and base shear varies with column size as a building's height rises, decreasing the range in base shear from moderate to hard soil [3]. Some studies came to the conclusion that there may be a greater chance of failure when using a float column than when not using one [1]. As a result, nodal displacement, maximum shear force, maximum bending moment, and maximum axial forces were analyzed and compared for both scenarios in the planning, analysis, and design of G+ 15 residential buildings with and without floating columns.

3 Planning

A plan for the G+ 15 residential building is created in the AutoCAD with elevation and sectional view and 3D model is created in Revit 2022. The plan includes the location of flats, rooms, kitchens, bathrooms, and hallways, as well as other elements of the structure with suitable size. The plan for the proposed project has 8 apartments in each floor and parking in ground floor.

- Plot Size: 1000 m²
- Built-up Area: 630 m² (19 × 33 m)
- Building Height: 48 m (each floor 3 m)
- Number of staircases: 1
- Number of Lifts: 1
- Beam Dimension: 0.45 × 0.6 m
- Column Dimension
 1. 0.6 × 0.6 m
 2. 0.45 × 0.3 m
- Slab Thickness: 0.15 m
- Plan consists of 4—2BHK and 4—1BHK flats in each floor.
- An area of 118 m² is provided for 2BHK flats and 47 m² for 1BHK flats.
- Lift and staircase are provided to facilitate movement between floors.
- Parking area is allocated in ground floor with floating column for easily turning of vehicles and for enough parking (Figs. 1, 2, 3 and 4).

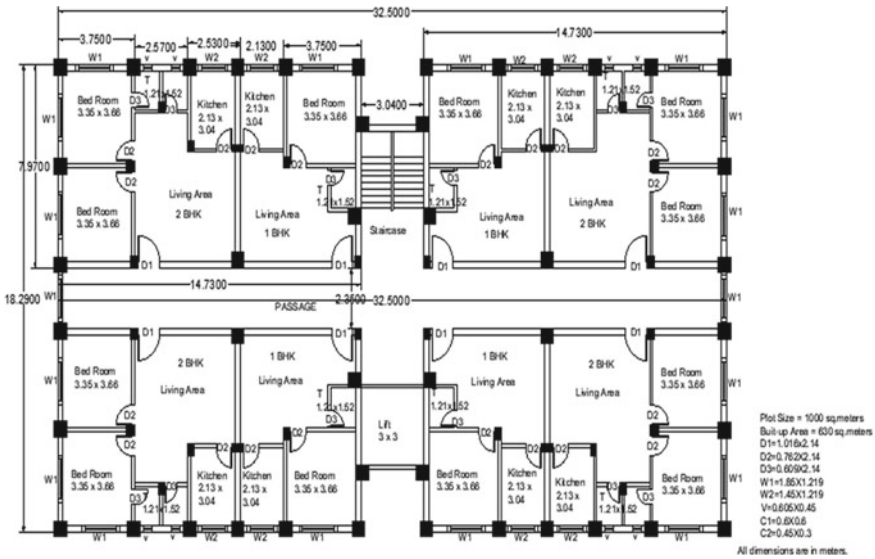


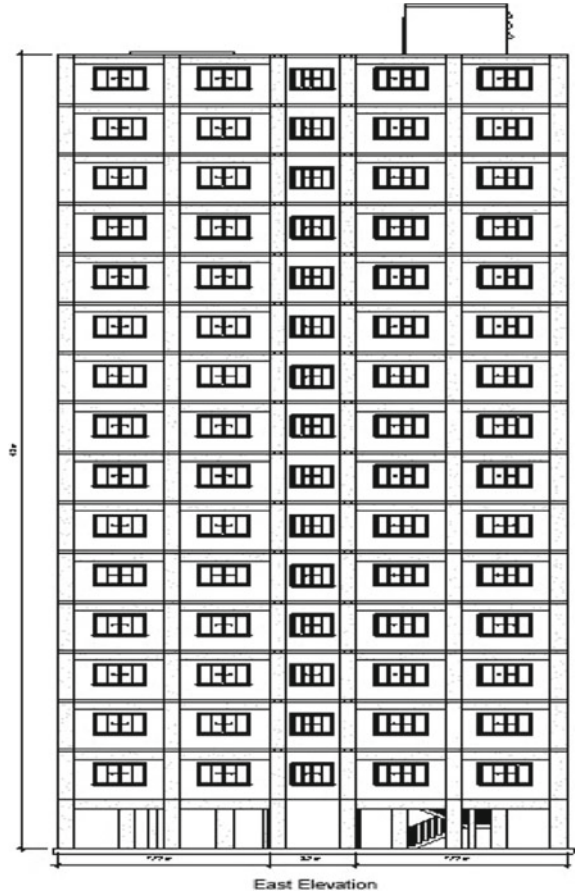
Fig. 1 Plan in AutoCAD

4 Analysis

Steps involved in analysis

- Analysis, designing of residential high-rise building has been done for G+ 15 both for floating column structure and for normal structure, and according to the plan of the building beams and column position are fixed.
- The analysis is done according to the plan of the building area. Hence, we must check whether the building is safe to bear loads.
- Then, a frame is drawn and as per the plan of the building the number of beam and column is designed and thus number of bays is also assigned.
- Beams (0.45 × 0.6) meters and two columns [Column1 (0.6 × 0.6 and Column2 (0.45 × 0.3)] meters are assigned as rectangular beam, and the property of material is assigned as concrete [4].
- The slabs are then classified as rectangular members of the appropriate value, with concrete as the material’s property.
- Then, the plates are created for slabs and the thickness is taken as 0.3. So, the floor thickness is assigned as 0.15 m.
- Type of support is fixed support.
- Suitable load combinations are assigned.
- Seismic load as per IS 1893 generated in STAAD.Pro itself for Zone III [5].
- Wind intensity at different heights is calculated and assigned in STAAD.Pro as input.
- Dead load for entire structure is auto-generated and assigned.

Fig. 2 Front elevation



- Floor load is calculated and assigned.
- Live load as per IS 875 part2 [6] is assigned (Figs. 5 and 6).

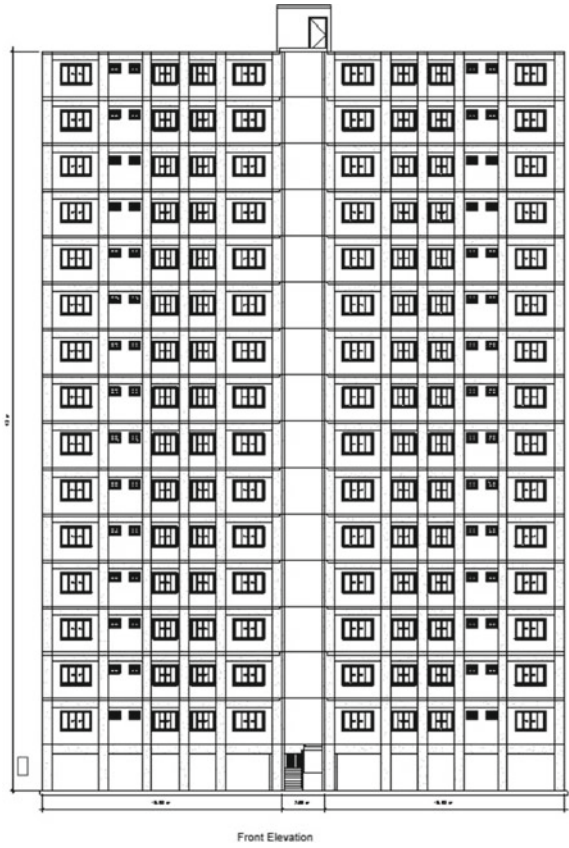
With Floating Column	Without Floating Column
Beam No.: 483	Beam No.: 5262
Maximum Bending Moment: 259.664 kNm	Maximum Bending Moment: 234.113 kNm

See Fig. 7.

With Floating Column	Without Floating Column
Beam No.: 584	Beam No.: 584
Maximum Shear Force: 423.381 kNm	Maximum Shear Force: 420.833 kNm

See Fig. 8.

Fig. 3 East elevation



With Floating Column

Beam No.: 5220

Maximum Displacement:
0.218 m

Without Floating Column

Beam No.: 5220.

Maximum Displacement: 0.211 m.

See Fig. 9.

With Floating Column

Beam No.: 503

Maximum Axial Force: 3474.771
kN

Without Floating Column

Beam No.: 503

Maximum Axial Force: 3274.756 kN

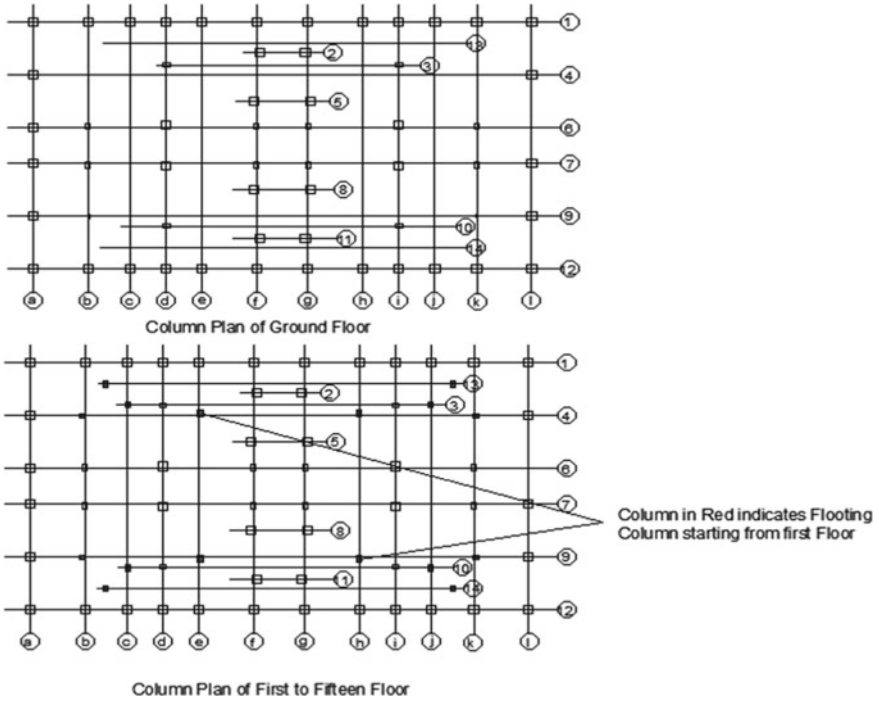


Fig. 4 Column plan of the building

5 Design

Design of Structural Elements

Structural components consist of slabs, beams, columns, staircase, and foundation [4]. These structural components are the most crucial part of the building and can be designed satisfying all elements according to IS codes and should be safe throughout the life. This project includes manual design of all structural components taking out the maximum values from STAAD.Pro software for both floating column and normal building. The manual design is discussed below (Fig. 10).

Design of Beam

See Fig. 11.

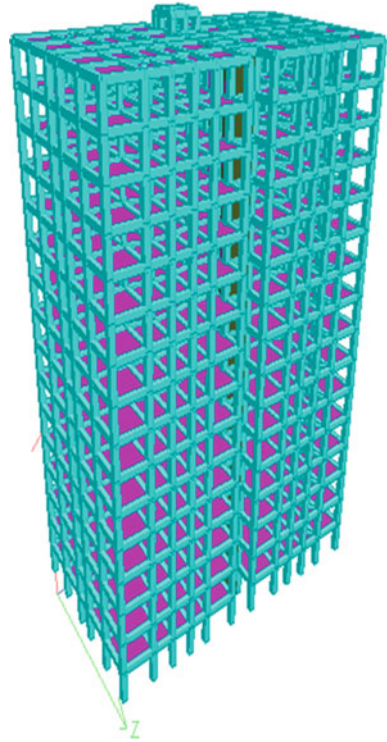
A. Beam Without Floating Column

See Fig. 12.

Design of Column 1

See Fig. 13.

Fig. 5 3D rendered view of structure



B. Without Floating Column Structure

See Figs. 14 and 15.

Design of Column 3—Floating Column

See Fig. 16.

C. Without Floating Column Structure

STAAD output (Fig. 17):

Design of Staircase

See Fig. 18.

Design of Footing

See Fig. 19.

Conclusion

- The population of Nepal is increasing tremendously and demand for commercial building is also high. The high-rise floating column building not only fulfill

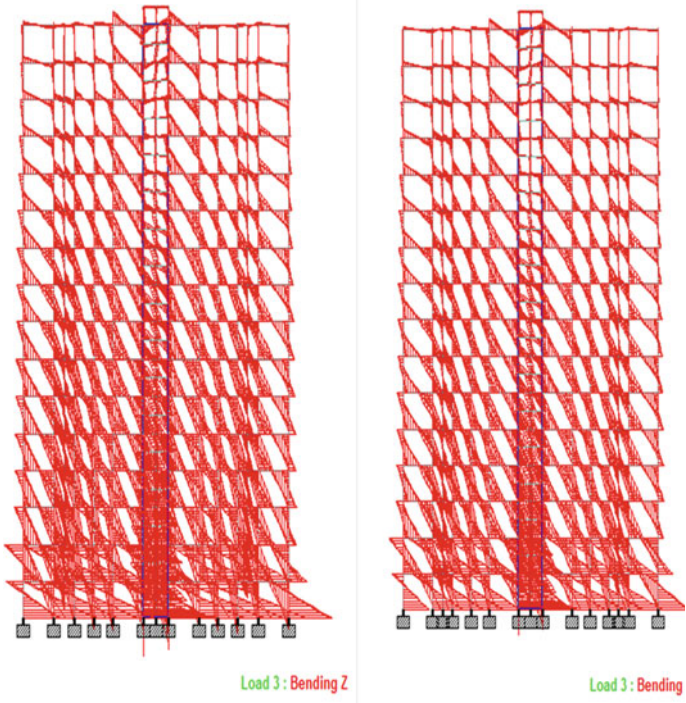


Fig. 6 Bending moment diagram

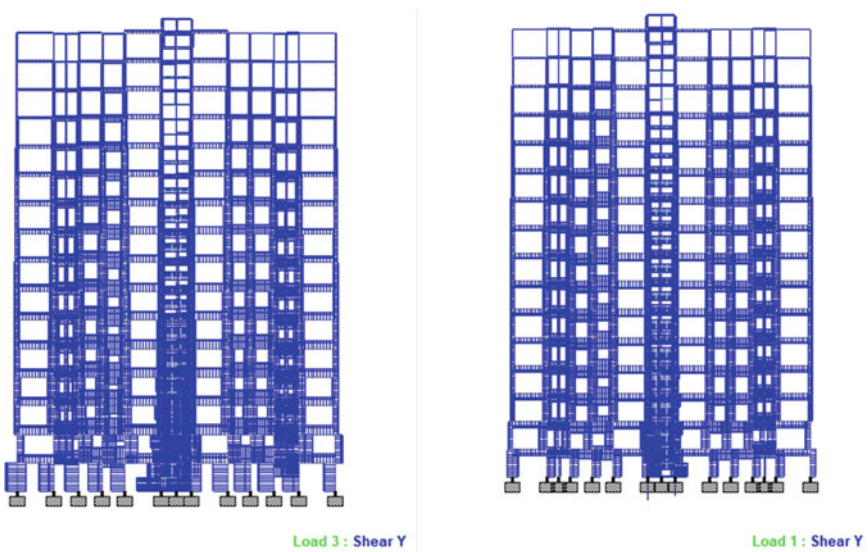


Fig. 7 Shear force diagram

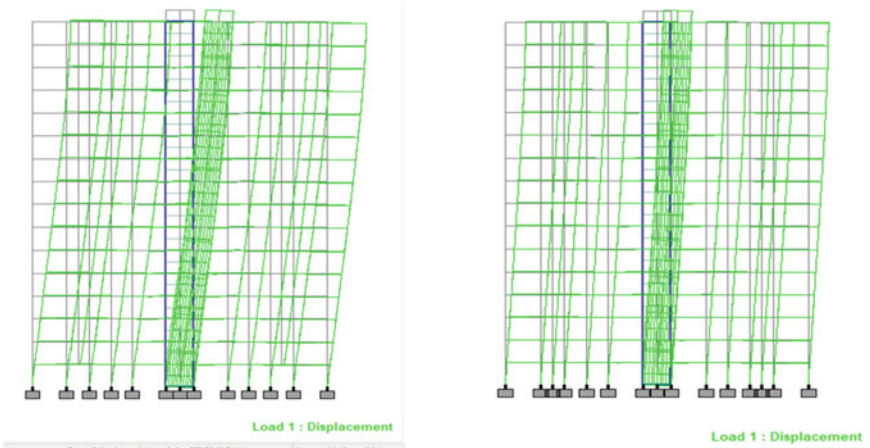


Fig. 8 Displacement diagram

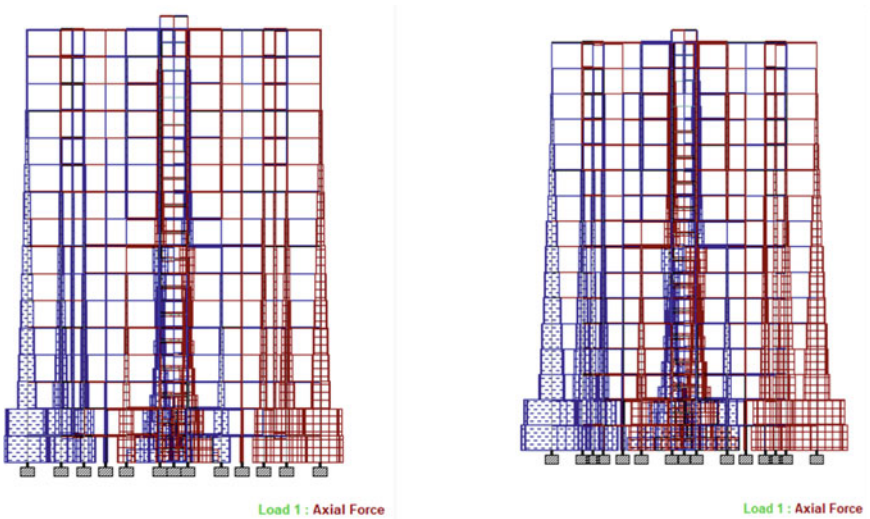


Fig. 9 Axial force diagram

the public demand but also give unique architectural benchmark for further construction.

- The building plan, structural analysis, and manual design of high-rise residential building with and without floating column is done according to proper orientation of the building and by taking load calculation from IS 875 1987 (part1 and part2).
- Design of the engineering components is done manually and by using STAAD.Pro., i.e., slab, beam, column, staircase, and foundation is designed by using IS456 2000.

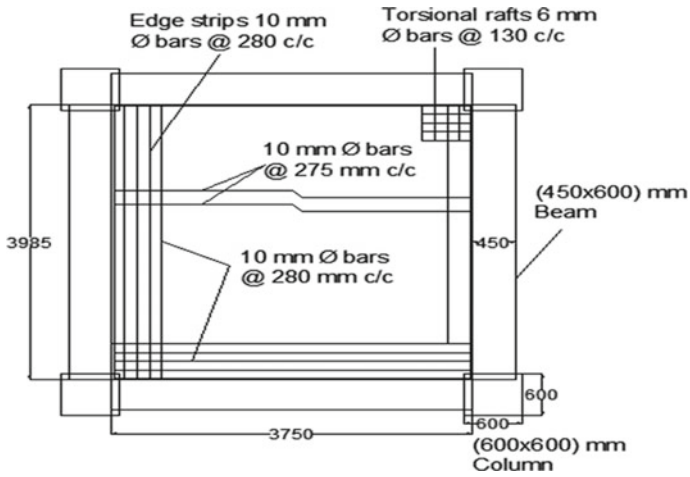


Fig. 10 Slab reinforcement details

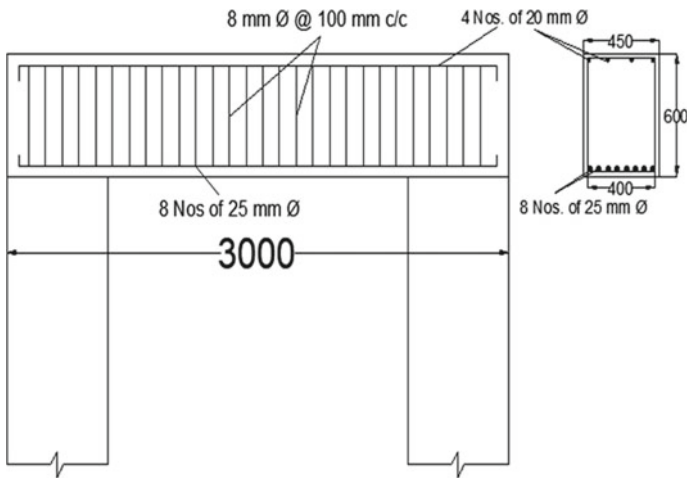


Fig. 11 Beam reinforcement details

- The behavior of G+ 15 residential building with and without floating column had been studied and structural parameters are designed for both floating column building and normal building and results obtained from STAAD.Pro concluded to have slight difference in the forces, moment and displacement and it reduces with the decrease in number of floating column.
- Here, the structure is created to be safe while having floating columns, and when compared to a typical building, it is noticeable and concluded that the building with floating column will lead to certain increase in reinforcement and constructed with following sustainable measures.

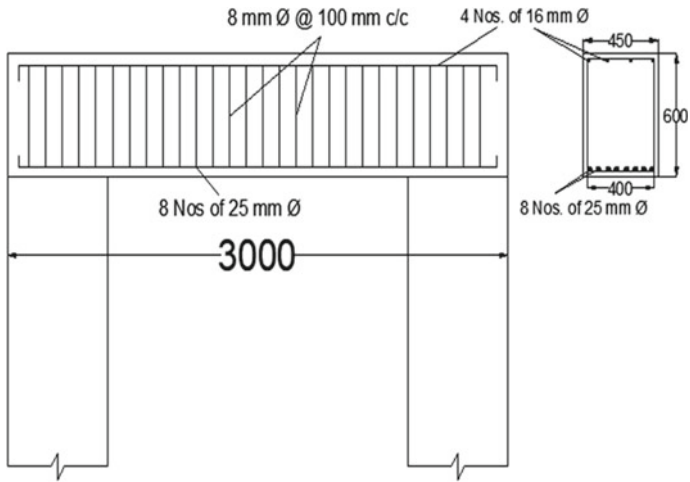


Fig. 12 Beam reinforcement details

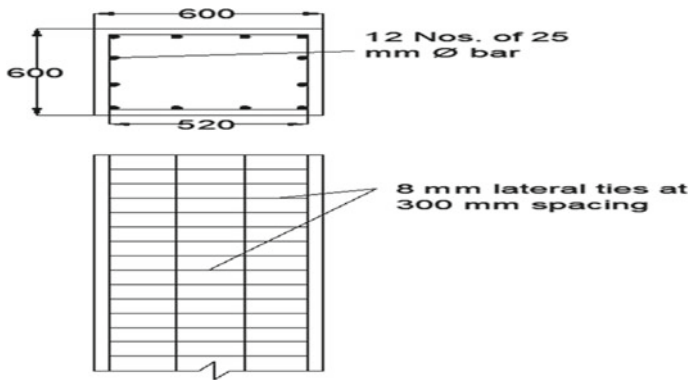


Fig. 13 Column reinforcement details with floating column structure

Fig. 14 Column reinforcement details without floating column structure

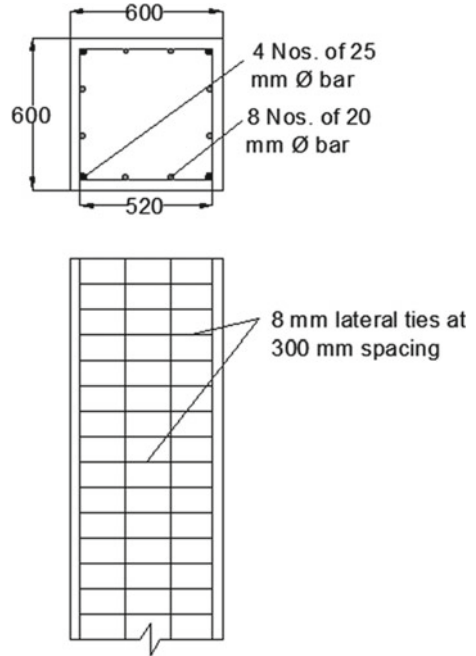


Fig. 15 Column reinforcement details without floating column structure

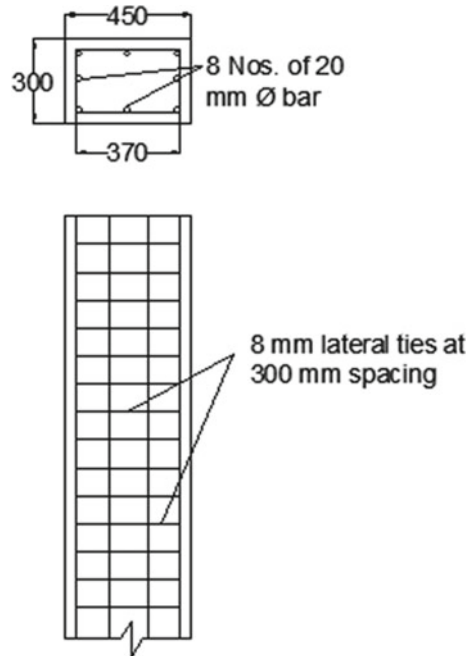


Fig. 16 Column reinforcement details with floating column structure

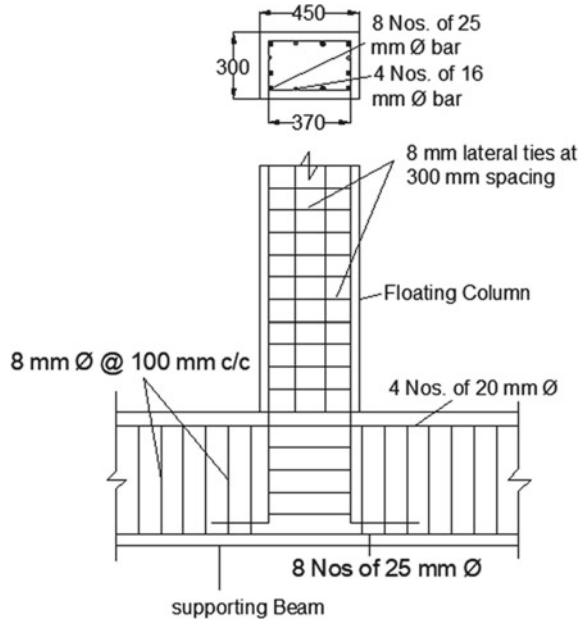


Fig. 17 Column reinforcement details without floating column structure

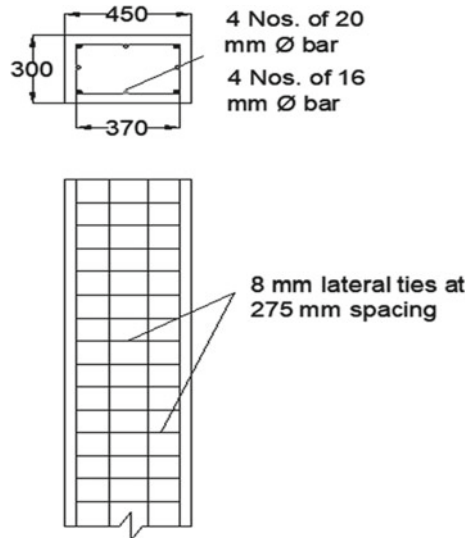


Fig. 18 Staircase reinforcement details

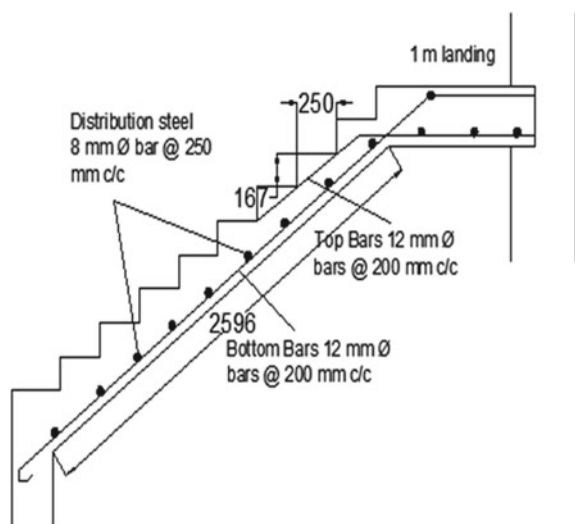
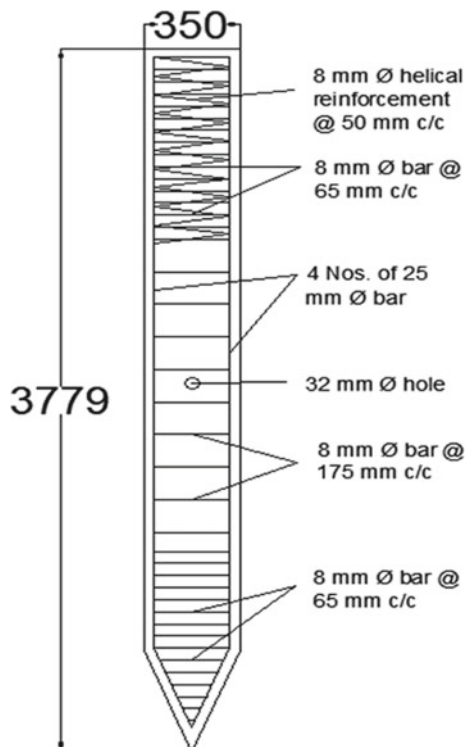


Fig. 19 Pile reinforcement details



References

1. Singh S, Priya S, Nadeem M, Alam M (2021) Analysis of G+ 5 storeys building with and without floating column. IOP Conf Ser Earth Environ Sci 889:012008. <https://doi.org/10.1088/1755-1315/889/1/012008>
2. Holebagilu YR (2014) Seismic response of complex buildings with floating column for zone II and zone. In: Srikanth V, Yogeendra MK, Holebagilu R (eds)
3. Nautiyal P, Akhtar S, Batham G (2014) Seismic response evaluation of RC frame building with floating column considering different soil conditions
4. IS 456 2000—plain and reinforced concrete
5. IS 1893 2002 (part 1 and part 2)—criteria for Earthquake resistance design of structure
6. IS 875 1987 (part 1, part 2 and part 3)—code for practice of design load

Disaster Management

Inferences on Strength and Ductility of High Performance Concrete Mixed with Steel and Macro-synthetic Fibres



S. Syed Ibrahim and S. Kandasamy

1 Introduction

Fibre-reinforced concrete (FRC) is often known as a type of high-performance concrete, in which short, discrete fibres effectively arrest/control the formation and propagation of structural cracks (right from pre-cracking to post-cracking stages) [1–3]. According to the current scenario, a single type of short-fibres has been predominantly used in the FRC for field applications. Studies reveal that a given single fibre type could be provided with a bridging effect only at any above one stage and have some degree of strain hardening/crack opening of FRC. To achieve an optimum (synergic) performance, multiple (i.e. more than one) types of fibres can combine suitably either based on fibre constitutive response or fibre dimensions or fibre function, which eventually produces a hybrid fibre-reinforced concrete (HFRC) matrix [4, 5].

The following salient observations draw an overview of distinctive studies on the HFRC. Nevertheless, studies wherein different shapes and sizes of steel fibres have been used, and referred to as ‘hybrid fibres’ by the various authors, have not been considered under. From 2000 onwards, there has been renewed interest in the study of HFRC. Most of the authors considered normal strength of concrete and few studies were conducted with high-strength concrete. Of all the combinations of hybrid system, combination of rigid with flexible fibres has been extensively used. In a hybrid fibre combination, steel fibres have been consistently mixed, which can be rigid by nature. Of the flexible type of fibres, polypropylene (PP) fibres have been

S. Syed Ibrahim (✉)

Department of Civil Engineering, Ilahia College of Engineering and Technology, Ernakulam, Kerala, India

e-mail: syed_ibms@yahoo.co.in

S. Kandasamy

Department of Civil Engineering, Vel Tech Rangarajan Dr Sagunthala R&D Institute of Science and Technology, Chennai, Tamil Nadu, India

extensively used in the study of HFRC, more so, in combination with steel fibres, until now. Almost all the studies were carried out with a fibre volume fraction ranges from 0.2 to 1.5%. Ratio between Young's modulus of (rigid/flexible) fibres was of ranges from 4.5 to 57.1. Various parameters like toughness, compressive strength, split-tensile strength, modulus of rupture, crack-width, deflection ductility, energy ductility, shear strength, fracture energy, and bond strength have been investigated to evaluate of performance of HFRC. And found significant enhancement in HFRC than using single fibre types. Apart from PP fibre, other types of flexible/non-metallic fibres used in the reported studies are polyvinyl alcohol fibre (PVA), recron, glass, polyolefin (PO), and nylon. However, such studies are a few. Among the above, PO fibre has been used rarely, especially with steel fibres in HFRC.

Consequently, the 'hybrid effect' in respect of fibre constitutive response by 3D hooked-end steel and polyolefin hybrid fibres with different total fibre volume contents-cum-proportions was experimentally evaluated in the present study. The primary purpose of the multiple types of fibre used in the HFRC matrix is that the steel fibres have strong and also stiff, which improves first-crack stress and ultimate strength, while the other one, polyolefin fibre, which is more flexible and ductile, leads to improve strain-capacity and toughness in the post-cracking zone. The study parameters include strengths (compressive and split-tensile), modulus of elasticity, modulus of rupture, and ductility indices.

2 Experiments

2.1 *Materials and Properties*

The required quantity of Portland Pozzolana Cement (PPC), conforming to IS 1489 Part I [6], was procured in a single batch stored in air-tight bags and used for the entire study. River sand and crushed granite (20 mm) as fine and coarse aggregates, respectively, were used. The salient properties of the aggregates are determined as per IS 2386 Part III [7] and IS 383 [8], as given in Table 1. Selecting the suitable type of fibre for preparing concrete is vital, especially in the context of assurance of strength, safety, and longevity of structures. Before adding a specific fibre type to concrete, it is necessary to understand the available fibres today and their potential for different applications. Polymeric fibres are divided into two classes: micro-fibre and macro-fibre. The size of micro-fibres is generally less than 0.3 mm dia. Features of the above fibre in concrete were to control the plastic shrinkage and to increase the impact resistance and inert protection from fire. However, concrete containing only these fibres has less structural benefit in a hardened state. Thereby, it can use for non-structural elements. Generally, the diameter of a macro-fibre is higher than 0.3 mm, which is more suitable for structural concrete. These macro-synthetic fibres increase the toughness at the post-crack stage, similar to steel fibres and improve the durability of the concrete [9].

Table 1 Properties of aggregates

Properties	Fine aggregate	Coarse aggregate	Unit
Specific gravity	2.63	2.70	–
Fineness modulus	2.70	7.98	–
Water absorption	0.60	0.50	%
Bulk density	1553	1530	kg/m ³
Zone	II	–	–

On the above aspects, two different types of short-fibres that is 3D hooked-ends steel (rigid) fibre and macro-synthetic polyolefin (flexible) fibre, were selected, both available commercially and were used in this study. As far as steel fibre is concerned, the hooked-ends act as an anchorage that resists cracking, which leads towards more durable concrete. In addition to steel fibre, commercially available straight polyolefin fibres bear a low aspect ratio mixed with concrete. There are several advantages of the above fibre, such as non-corrosive, non-magnetic, chemical inertness, and non-hazardous or nuisance conditions when fibres become loose or protrude from the concrete surface. This fibre can add a maximum of 20% (by volume) without causing any balling effect, segregation, or increase in air entertainment in concrete. However, the performance of these fibres in fresh and hardened concrete depends on the aspect ratio of the fibres. Figures 1 and 2 show hooked-end steel fibres and polyolefin fibre and their properties, given in Table 2. For casting potable water with the water-reducing admixture, ‘Classic Superflo SP’, which conforms to IS 9103 [10], was used.

Fig. 1 Hooked-end steel fibre



Fig. 2 Polyolefin fibre



Table 2 Properties of steel and polyolefin fibres

Properties	Steel fibre	Polyolefin fibre	Unit
Shape	Hooked ends	Straight	–
Length	30	48	mm
Diameter/size	0.5	1.22×0.732	mm
Aspect ratio	60	39.34	–
Tensile strength	532	550	MPa
Young's modulus	210	6	GPa
Specific gravity	–	0.90–0.92	–
Density	7850	920	kg/m ³

2.2 Preparation of Specimens

The concrete grade of M20, having a mix proportion of 1: 2.01: 3.36, was designed according to IS 10262 [11] with a water-cement ratio of 0.50. The design mix considered for casting control specimens that are in Table 3. Experimental investigations conducted in three different concrete matrices include (plain) concrete without fibre, concrete with steel fibre only (i.e. SFRC), and with steel-polyolefin hybrid fibre (i.e. HFRC) to study its various mechanical behavioural exclusively, compressive strength, splitting tensile strength, modulus of rupture, modulus of elasticity, and ductility index as per Indian standards. Cylindrical moulds having a diameter and height equal to 150 mm and 300 mm, respectively, were used to determine the compressive strength of the various types of concrete. Another size of a cylindrical mould having a diameter and height of 100 and 200 mm, respectively, was used to determine the splitting tensile strength of the concrete. Prisms having a cross section of 100×100 mm and a length equal to 500 mm were used to determine the flexural strength of the concrete. One plain concrete (HC0-S0P0) was left without fibres to act as a control specimen. Five HFRC containing various proportions of steel and polyolefin fibres (i.e. steel [S]: polyolefin [P] = 100:0, 80:20, 70:30, 60:40, 50:50) with a consistent V_f . The HFRC specimen details are as in Table 4.

Table 3 Details of concrete mix

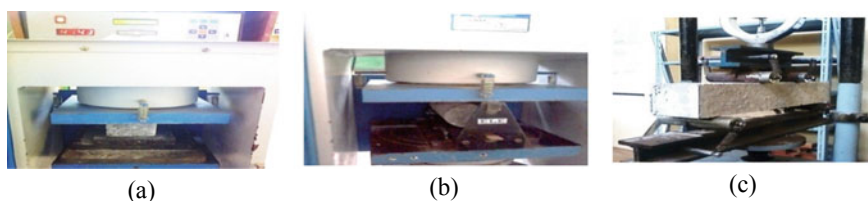
Material	Quantity	Unit
Cement	354	kg/m ³
Fine aggregate	710	kg/m ³
Coarse aggregate	1190	kg/m ³
Water	177	kg/m ³
Superplasticizer	1.77	kg/m ³
Slump	100	mm

Table 4 Details of HFRC specimens

S. No.	Specimen ID	Fibre volume fraction, V_f (%)	Fibre proportion	
			Steel (%)	Polyolefin (%)
1	HC0-S0P0	0	0	0
2	HC0.5-S100P0	0.5	100	0
3	HC0.5-S80P20		80	20
4	HC0.5-S70P30		70	30
5	HC0.5-S60P40		60	40
6	HC0.5-S50P50		50	50
7	HC1.0-S100P0		1.0	100
8	HC1.0-S80P20	80		20
9	HC1.0-S70P30	70		30
10	HC1.0-S60P40	60		40
11	HC1.0-S50P50	50		50
12	HC1.5-S100P0	1.5		100
13	HC1.5-S80P20		80	20
14	HC1.5-S70P30		70	30
15	HC1.5-S60P40		60	40
16	HC1.5-S50P50		50	50

2.3 Testing of Specimens

According to IS 516 [12], compression test on the cylindrical specimens was carried out with an extensometer to measure the deformation in concrete at equal intervals of loadings. The splitting tensile test was carried out on the cylinder specimens as per IS 5816 [13]. In accordance with IS 516, the prisms were supported with a span of 400 mm and tested. The readings were born at different load levels till the failure of the specimens. Figure 3a–c shows all three experimental test setups.

**Fig. 3** Experimental setup: **a** compression test; **b** split-tensile test; **c** flexural test

3 Results and Inferences

The experimental investigations were carried out on HFRC specimens, incorporated with ‘steel’ (rigid) and ‘polyolefin’ (flexible) hybrid fibres. A total of 144 samples using sixteen concrete mixtures with and without fibre, the specimens were cast and tested for obtaining the (average) compressive strength, splitting tensile strength, modulus of rupture, and ductility indices. The inferences have been highlighted below, based on the results of the tests.

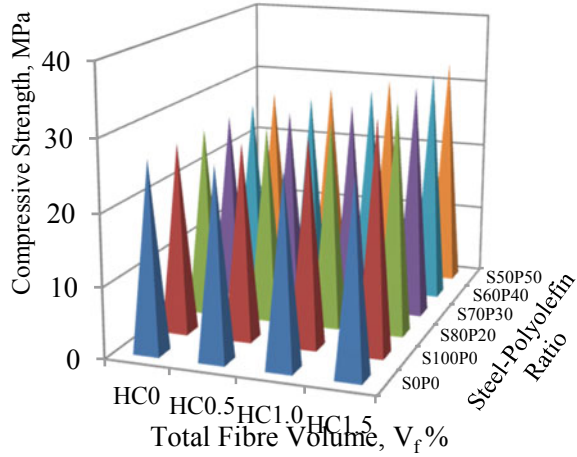
3.1 Strength Characteristics

Table 5 gives various HFRC specimens’ salient results in respect of the compressive strength (f_{ck}), split-tensile strength (T_{sp}), and modulus of rupture (MOR). The difference of compressive strength in respect of volume fractions (V_f) and the ratio of hybrid fibres [steel (S): polyolefin (P)] is shown schematically in Fig. 4. The discussion and also salient inferences are given below based on the above (V_f and S:P).

Table 5 Strength properties and ductility indices of HFRC

S. No.	Specimen ID	Compressive strength (MPa)	Split-tensile strength (MPa)	Modulus of rupture (MPa)	Deflection ductility ratio	Energy ductility ratio
1	HC0-S0P0	26.70	3.80	5.45	1.00	1.00
2	HC0.5-S100P0	27.50	4.10	6.25	1.17	1.24
3	HC0.5-S80P20	27.65	4.20	6.55	1.20	1.28
4	HC0.5-S70P30	27.90	4.35	6.80	1.22	1.33
5	HC0.5-S60P40	28.25	4.60	7.10	1.25	1.39
6	HC0.5-S50P50	28.10	4.40	7.00	1.23	1.35
7	HC1.0-S100P0	29.05	5.55	8.05	1.30	1.41
8	HC1.0-S80P20	29.20	5.80	8.25	1.34	1.45
9	HC1.0-S70P30	29.65	6.10	8.70	1.38	1.48
10	HC1.0-S60P40	30.10	6.40	9.05	1.41	1.52
11	HC1.0-S50P50	30.00	6.35	8.90	1.40	1.49
12	HC1.5-S100P0	32.25	7.65	10.35	1.46	1.54
13	HC1.5-S80P20	32.55	7.95	10.65	1.49	1.57
14	HC1.5-S70P30	32.85	8.20	10.90	1.54	1.62
15	HC1.5-S60P40	33.20	8.45	11.25	1.61	1.70
16	HC1.5-S50P50	33.05	8.25	11.10	1.58	1.66

Fig. 4 Compressive strength for specimens with and without fibres

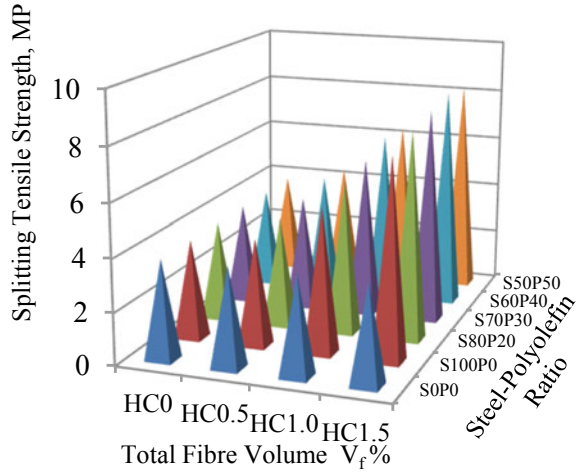


Compressive Strength: It observed that the characteristic compressive strength of HFRC specimens varies with respect to fibre volume content (V_f) and the proportion of hybrid fibres [namely: steel (S): polyolefin (P)]. Thus, not only the V_f but also the amalgamation of hybrid fibre plays a role in influencing the compressive strength. The above phenomenon seems to hold good for the range of V_f (i.e. 0.5–1.5%) and the various ratios of hybrid fibres (i.e. S:P = 100:0, 80:20, 70:30, 60:40, 50:50) considered in this study. As the V_f increases, the compressive strength of SFRC specimens also increases with respect to the control specimen for the range of V_f considered. However, the increase of the compressive strength is not significant up to $V_f = 1.0$, but it becomes considerable and substantially higher (20.8%) at $V_f = 1.5\%$. Thus, steel fibre incorporation contributes to a significant and higher compressive strength of SFRC specimens only if V_f is higher than 1.0% and at 1.5%. The above phenomenon highlights the role of steel fibres (alone) on the compressive strength (of specimens) [14, 15].

However, the increase in the above strength is maximum at the highest V_f (i.e. at 1.5%) and the lowest raise at the lowest V_f (i.e. at 0.5%). The increase in compressive strength of the HFRC specimen ranges from 3 to 5.8%, 8.8 to 12.7%, and 20.8 to 24.3%, over the control specimen, for the respective V_f equals 0.5, 1.0 and 1.5%. However, the rise of the compressive strength is significant for $V_f = 1.5\%$, and the compressive strength is maximum for the hybrid fibre combination 60:40 (S:P) for the range of V_f considered. The maximum increase of the compressive strength of HFRC specimens with respect to SFRC specimen is less than that of control specimen, for corresponding V_f considered. Further, the increase in the strength of the HFRC specimen over the SFRC specimen is found insignificant. It indicates the ‘hybrid fibres’ effect in influencing the compressive strength of HFRC specimens is inconsequential which are similar to the observation/(s) of some of the cited investigations [16, 17].

Splitting Tensile Strength: Variations of split-tensile strength with respect to fibre volume (%) and the ratio of hybrid fibres (S:P) as shown in Fig. 5. Based on the

Fig. 5 Splitting tensile strength for specimens with and without fibres

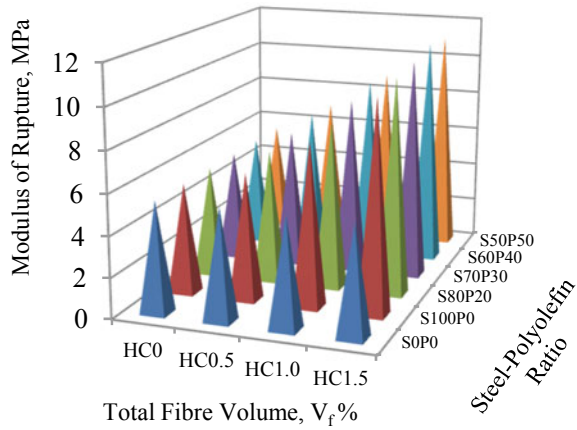


analysis of results in Table 5 and Fig. 5, the following are the salient inferences. The role of V_f and the combination of fibres in influencing the split-tensile strength are similar to that of the compressive strength. It observed that the split-tensile strength is maximum for the hybrid fibre combination 60:40 (S:P) for the range of V_f considered, which is the same as in the case of the compressive strength. However, the increase in the above strength is not significant up to $V_f = 0.5\%$. Afterwards, there is a sudden increase and much higher jump in the above strength for $V_f = 1.0$ onwards. The maximum increase in split-tensile strength is 3.6, 5.4, and 5.9 times that of compressive strength under identical conditions. In other words, the maximum split-tensile strength ranges from about 3–6 times the compressive strength under similar conditions. It highlights the significant role played by the ‘hybrid fibres’ in enhancing the split-tensile strength, unlike the case of compressive strength, where the role of the ‘hybrid fibres’ is found to be insignificant.

Modulus of Rupture: Comparison of modulus of rupture (MOR) with respect to fibre volume content (V_f) and the ratio of hybrid fibres (S:P) is shown in Fig. 6. Based on the analysis of results in Table 5 and Fig. 6, the following are the salient inferences. The role of V_f and the combination of fibres in influencing the MOR are similar to that of compressive strength. The trend with respect to the increase in MOR over the control specimen and SFRC specimens is similar to that of compressive strength. The maximum increase in the MOR of SFRC specimens with respect to the control specimen is 14.7, 47.7, and 89.9%, for $V_f = 0.5, 1.0,$ and 1.5% , respectively. It can be seen that the above increase becomes not only significant but also becomes very high for $V_f > 0.5\%$. The above behaviour is similar to that of the behaviour of split-tensile strength.

The maximum increase in the MOR of HFRC specimens over the control specimen is 30.3, 66.1, and 106.4% for $V_f = 0.5, 1.0,$ and 1.5% , respectively. This highlights the significant role of hybrid fibres in enhancing the MOR. It is seen that

Fig. 6 Modulus of rupture for specimens with and without fibres



the above maximum increase in MOR of HFRC specimen over SFRC specimen with respect to control specimen under identical conditions is considerably increased due to the ‘hybrid’ effect between the steel and polyolefin fibres used in this study. Such improvements can be made possible by the ability of fibres to modify the failure mechanisms of composite material [18]. Further, the above maximum increase in MOR of HFRC specimens with respect to SFRC specimens can be considered as closer to significant but not significant for all the V_f considered.

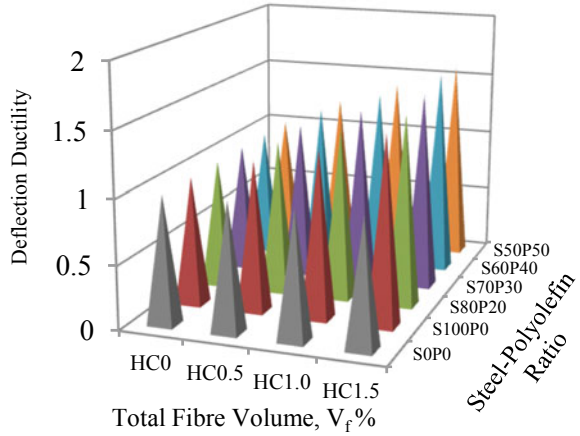
3.2 Ductility Indices

Ductility is measured via deflection and energy by a ratio called the ductility index or factor. Table 5 gives the indices of deflection and energy ductility of HFRC specimens.

Deflection Ductility: Fig. 7 shows variations of the ‘deflection ductility index’ in respect of fibre volume (%) and the ratio of hybrid fibres (S:P). The deflection ductility of HFRC specimens increases with an increase in V_f and with respect to the proportion of hybrid fibres (S:P) used in this study. The deflection ductility was highest for the hybrid combination 60:40 (S:P) for the V_f range considered. The maximum increase in the deflection ductility index of the SFRC specimen is 1.17, 1.30, and 1.46 with respect to the control specimen, for V_f : 0.5, 1.0, and 1.5%, respectively. Thus, the increase in the deflection ductility index was highest for $V_f = 1.5\%$. The deflection ductility of HFRC specimens seems to be higher than that of SFRC specimens, irrespective of V_f , due to the ‘hybrid’ effect of the types of fibres used. Further, the above increase in deflection ductility index is significant for the V_f considered attributed to the ‘role of hybrid fibres’ used.

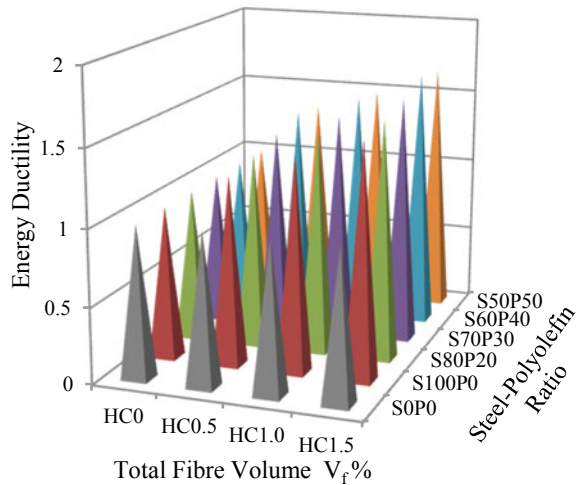
Energy Ductility: Comparison of the energy ductility index with respect to V_f and the ratio of hybrid fibres (S:P) is in Fig. 8. The energy ductility of HFRC specimens

Fig. 7 Deflection ductility for specimens with and without fibres



increases with an increase in V_f and with respect to the proportion of hybrid fibres (S:P) used in this study. The energy ductility index increases to the maximum for the SFRC specimens are 1.24, 1.41, and 1.54 with respect to the control specimen, for V_f : 0.5, 1.0, and 1.5%, respectively. It seems that the energy ductility of HFRC specimens is higher than that of SFRC specimens irrespective of V_f due to the ‘hybrid’ effect of the types of fibres used. The maximum increase in energy ductility index of HFRC specimens is 1.39, 1.52, and 1.70 times, over the control specimen, for V_f : 0.5, 1.0, and 1.5%, respectively. The above phenomenon is also similar to that of deflection ductility. However, energy ductility is consistently slightly higher than the deflection ductility for all V_f considered. Thus, the ‘role of hybrid fibres’ used is better in energy ductility than deflection ductility.

Fig. 8 Energy ductility for specimens with and without fibres



4 Conclusions

- The compressive strength, split-tensile strength, and modulus of rupture (MOR) of the HFRC specimens influences by the fibre volume content (V_f) and the combination of hybrid fibres [that is, steel (S): polyolefin (P)]. The above phenomenon holds good for the range of V_f (i.e. 0.5–1.5%) and various ratios of hybrid fibres ($\geq 20\%$ to $\leq 100\%$) considered in this study. All the above three strengths are maximum for the hybrid fibre combination 60:40 (S:P) for the range of V_f considered. Further, the highest strength is attained at $V_f = 1.5\%$ and for the above combination. However, the influence of ‘hybrid fibres’ on the above three strength parameters is dissimilar.
- In the case of compressive strength, the effect of ‘hybridization of fibres’ is not significant, whereas it is significant and very high in the case of the other two strength parameters for all the V_f considered. The above effect of fibres, in general, on the compressive strength is along expected lines and in line with the reported results in the literature. The maximum increase in the split-tensile strength of ‘HFRC specimens’, over the ‘control specimen’, ranges from 21 to 122.3% for the range V_f 0.5 to 1.5%, with the highest increase in strength occurring at the highest V_f ($= 1.5\%$).
- The maximum increase in the ‘MOR’ of HFRC specimens over the control specimen ranges from 30.3 to 106.4%, for the V_f ranging from 0.5 to 1.5%, with the highest increase in the above strength occurring at the highest V_f content ($= 1.5\%$). It highlights the role of hybrid fibres in enhancing the above strength and is similar to that of the split-tensile. The modulus of elasticity (MOE) of HFRC specimens ranges from 26.19 to 28.79 MPa. It seemed that the MOE of the HFRC specimen is maximum for the hybrid fibre combination 60:40 (S:P) for the range of V_f considered. The above behaviour is similar to the strength behaviour of HFRC specimens. The MOE of HFRC specimens is not significantly different from that of the ‘control concrete’.
- The maximum increase in ‘deflection ductility ratio’ of HFRC specimens ranges from 1.25 to 1.61 times the ‘control specimen’, for the V_f range 0.5–1.5%, with the highest increase occurring at $V_f = 1.5\%$ and S:P = 60:40. The above phenomenon may also be attributed, to the ‘positive and very high influence of the hybrid fibres’. Similarly, the maximum increase in the ‘energy ductility ratio’ of HFRC specimens ranges from 1.39% to 1.70 times the ‘control specimen’ for the V_f range from 0.5 to 1.5%, with the highest increase occurring at $V_f = 1.5\%$, and S:P = 60:40. However, the effect of hybrid fibre seems to be slightly higher in the ‘energy ductility ratio’ than in the other ratio for the range of V_f considered. Thus, the role of hybrid fibres is ‘consistently better’ in ‘energy ductility’ than in ‘deflection ductility’.

References

1. Ali A, Iqbal S, Holschemacher K, Bier TA (2017) Comparison of flexural performance of lightweight fibre reinforced concrete and normal weight fibre reinforced concrete. *Periodica Polytechnica Civil Eng* 61:498–504
2. Kytinou VK, Chalioris CE, Karayannis CG, Elenas A (2020) Effect of steel fibers on the hysteretic performance of concrete beams with steel reinforcement—tests and analysis. *Materials* 13:1–32
3. Ramadoss P, Li L, Fatima S, Sofi M (2023) Mechanical performance and numerical simulation of high-performance steel fiber reinforced concrete. *J Build Eng* 64(1):105424
4. Soner G, Demet Y, Fuat K, Ashraf A (2018) Strength prediction models for steel, synthetic, and hybrid fiber reinforced concretes. *Struct Concrete* 1–18
5. Júnior LAO, Borges VES, Danin AR, Machado DVR, Araújo DL, Debs MKE (2010) Stress-strain curves for steel fiber reinforced concrete in compression. *Revista Matéria* 15(2):260–266
6. IS 1489-1 (1991) Specification for Portland pozzolana cement, Part 1: Flyash based [CED 2: Cement and Concrete]. New Delhi
7. IS 2386-3 (1963) Methods of test for aggregates for concrete, Part 3: Specific gravity, density, voids, absorption and bulking [CED 2: Cement and Concrete]. New Delhi
8. IS 383 (2016) Coarse and fine aggregate for concrete—specification. New Delhi
9. Veronica G, Antonio C, Giovanni P, Shiho K (2018) Influence of steel and macro-synthetic fibers on concrete properties. *Fibers* 6:47
10. IS 9103 (1999) Specification for Concrete Admixtures—[CED 2: Cement and Concrete]. New Delhi
11. IS 10262 (2009) Concrete mix proportioning, New Delhi
12. IS 516 (1959) Methods of tests for strength of concrete. New Delhi
13. IS 5816 (1999) Method of test splitting tensile strength of concrete. New Delhi
14. Ferrari VJ, De Hanai JB (2012) Flexural strengthening of reinforced concrete beams with carbon fibres reinforced polymer (CFRP) sheet bonded to a transition layer of high performance cement-based composite. *IBRACON Struct Mater J* 5(5):596–626
15. Qureshi LA, Sheikh MI, Sultan T (2013) Effect of mixing fiber cocktail on flexural strength of concrete. In: *Proceedings of the second international proceedings on rehabilitation and maintenance in civil engineering*. *Procedia Engineering* vol 54, pp 711–719
16. Hockenberry J, Lopez MM (2012) Performance of fiber reinforced concrete beams with and without stirrups. *J Civil Environ Archit Eng* 4(1):1–7
17. Zhan Y, Meschke G (2014) Analytical model for the pullout behavior of straight and hooked-end steel fibers. *J Eng Mechan* 140(12):1–13
18. Chen Y, Qiao PE (2011) Crack growth resistance of hybrid fiber-reinforced cement matrix composites. *J Aerosp Eng ASCE* 24(2):154–161

Study the Interaction Behaviour of Integrated Infilled Frames with Interface Materials



S. Jaya Harish, S. Muthu Kumar, and K. S. Satyanarayanan

1 Introduction

High-rise or multi-storey buildings are more prevalent in urban regions because of industrialisation and population concentration. Using masonry or concrete brickwork as infills, infilled frames are made of steel or reinforced concrete columns and girders. Multi-storey concrete buildings always have infill masonry walls in framed constructions, notably for use in sealing functions. Under the influence of an in-plane lateral stress, the infilled frame functions as a composite system where the frame and infill wall converse. Partition walls typically come with frames for practical reasons. Because they absorb and disperse greater seismic forces. In earthquake-prone areas, infill walls have an impact on the ductility, stiffness, and strength of framed structures. In regions with greater seismic zones, infill frames perform better. Because of the coordinated movement of the filler and the frame, infill frames are more resistant. In this, Fig. 1 shows the detachment of infills in the frame which due to lateral loading on the frames.

1.1 Infilled Frame

When a frame is constructed first, then it is filled with one or more masonry panels, this is referred to as an “infilled frame.” When an infilled frame is subjected to in-plane loading, the frame’s components and the infills work together to produce a combined resistance to the load, with the frame’s parts deforming mostly under bending and axial pressures and the infills mostly under in-plane shear and diagonal

S. Jaya Harish · S. Muthu Kumar (✉) · K. S. Satyanarayanan
Department of Civil Engineering, College of Engineering and Technology, SRM Institute of Science and Technology, Tamil Nadu, Kattankulathur 603203, India
e-mail: muthukus1@srmist.edu.in

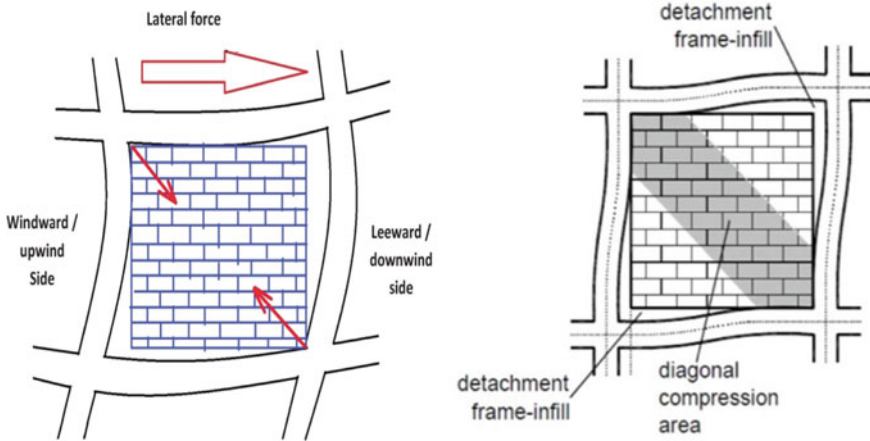


Fig. 1 Detachment of infilled frame

loads. When the frame is filled, a structure is produced that combines the containment provided by the frame with the stiffness of the infill. When the infill fractures, this structure keeps the infill from falling apart. Another benefit is a subsequent in-plane rigidity that is higher than the total of the frame and infill's separate stiffness.

1.2 Interface Materials

The medium between the frame and the infill walls is interface materials. It improves the frame's ductility.

1.2.1 Interface Materials (Cement Mortar)

In order to provide a dense, homogenous lining that will stick securely to the surface of the substance, cement mortar must be made up of cement, sand, and water, be well mixed, and have the right consistency.

1.2.2 Interface Materials (Foam Rubber)

Foaming agent (Polyurethane) has been used in the manufacturing of foam rubber to form an air-filled matrix structure.

1.2.3 Interface Materials (Cork)

The cork oak's phellem layer of bark tissue, which is predominantly obtained for commercial purposes from *Quercus suber*, is a buoyant impermeable substance.

1.2.4 Interface Materials (Bitumen)

Bitumen is a viscous material that transitions between liquid and semi-solid states. It is often made of asphaltene resin and other petroleum compounds, and it has a blackish-brown appearance.

1.2.5 Interface Materials (Recycled Plastic)

Reprocessing used plastic into fresh products is known as recycling plastic. Typically, recycled plastic requires relatively little maintenance. It is completely coloured, resistant to UV rays, does not splinter, shatter, or rot, and any damage's visual impact is minimised.

2 Literature Review

2.1 General

Literature review grants us a comprehensive view of the work that has to be done. A literature review entails looking at several studies that are comparable to the experiment being done. This chapter discusses several papers.

2.2 Study on Infilled and Interface Materials

Liauw et al. [1], Multi-storey infilled frames' static and cyclic behaviours under various interface conditions, *Sound and Vibration Journal*. It has been proven that the appropriate usage of infilled panels integrated into the plane of a frame, as seen in various types of infilled frames, is extremely practical and economical when it comes to resisting earthquake, wind, and blasting loads.

Asteris et al. [3], This paper's major goal is to propose a broad classification method infilled frames' failure mechanisms, including both those with and without openings. Based on a survey of the literature, the former classification is summarised, the latter identifies and categorises a variety of distinct failure modes (crack patterns) of masonry-filled frames. A greater understanding of how earthquake resistant infilled

frames behave and improved methodological approaches to their modelling, analysis, and design are both made possible by such a classification of failure modes.

Muthu Kumar et al. [5], The objective of this work is to investigate the linear behaviour of infilled frames with different interface materials. This study presents the analytical analysis of a two-phase, three-storey-reinforced concrete infilled frame that was subjected to static lateral loading. A frame that was empty as well as frames that had been filled with various interface materials were used in the analysis (cement mortar, cork, and foam). The study evaluates how different interface materials affect the frames' lateral stiffness under static lateral stress, paying particular attention to the discussion of the stiffness of the frames. The interaction between infilled with cement mortar interface is found to be more robust. The findings of this work can serve as the foundation for more research on how these interface materials behave when subjected to seismic loading.

Muthukumar et al. [6] The goal of this study is to use an experimental, theoretical, and numerical approach to examine the behaviour of (RCC) square frames made of two different infill materials, bricks, and aerated blocks, with different interface materials. Utilising numerical analysis and an existing theoretical model, the findings point to the potential of an alternative interface material.

3 Analytical Study

3.1 Modelling, Assigning Property, and Assemble of Frame

The model of bare frame is created first and infill (brick masonry) with different interfaces are like cement mortar, cork, bitumen, foam rubber, recycled plastic which are also created and assigned properties to them. The cross section area of frame is 600×600 mm, the thickness of frame is 60 mm, and the breadth of the frame is 85 mm in Fig. 2. In this frame, 6 mm dia bars are provided as main reinforcement and stirrups, providing 50 mm cover to the frame.

3.2 Properties of Infilled Frame

The materials used in the infilled frames are concrete, reinforcement, infill as brick masonry, and the interfaces are cement mortar, cork, bitumen, foam rubber, recycled plastic. And these materials have separate Poisson's ratio, density, and modulus of elasticity which are given in Table 1.

Fig. 2 Infilled frame model

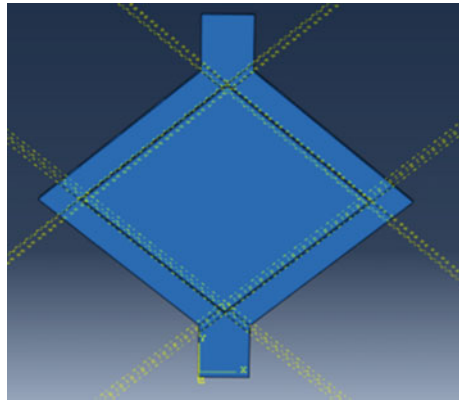
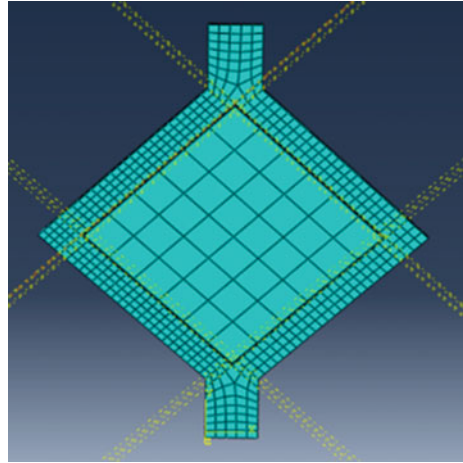


Table 1 Properties of infilled frame

Name of materials	Modulus of elasticity (KN/mm ²)	Poisson's ratio	Density (KN/m ³)
Concrete	24.451	0.16	5.19
Reinforcement	200.1	0.21	6.1
Infill (brick masonry)	1.021	0.16	9.56
Interface (cement mortar)	9.527	0.16	0.58
Interface (cork)	0.021	0.098	0.766
Interface (bitumen)	4000.1	0.36	1.06
Interface (foam rubber)	0.012	0.49	0.81
Interface (recycled plastic)	620.1	0.36	1.48

3.3 Analysis of Frame

In infilled frame, different interface materials are used likely cement mortar, cork, bitumen, foam rubber, and recycled plastic. In compare to bare frame, deformation is less in infilled frame Fig. 2. There are 45,718 numbers of nodes are present in this frame Fig. 3. In infilled frame, homogenous mesh is provided and the size of the meshes is 25 mm for frame 100 mm for infill and 5 mm for interface. In this frame, 20 kN loading is given and the time period is 19 with 10,000 increments.

Fig. 3 Nodes of frame

3.4 Loading on Frame

In this frame, model bottom surface is fixed and give boundary condition to the frame. Applying pressure force load on the top surface of the frame as cyclic loading is given to the frame and see the seismic response of the frame. Rate of increment for bare frame and infill frame is 0.5 per cycle.

3.5 Deformation of Frame

A deformation frame consists of beam and column with bent on the rigid corners. It shows the de-attachment of infill and interface material on the frame due to the ductility of the infilled frame.

3.5.1 Deformation Bare of Frame (BF)

In bare frame, there is no infill and interface. So the deformation is higher in lower amount of loading. In this frame, deformation is 49 mm (Fig. 4).

3.5.2 Deformation of Infilled Frame (Cement Mortar) (IFCM)

In this infilled frame, cement mortar is an interface medium. This interface is commonly used in all the frame structures. In this frame, deformation is 52 mm (Fig. 5).

Fig. 4 Deformation of BF

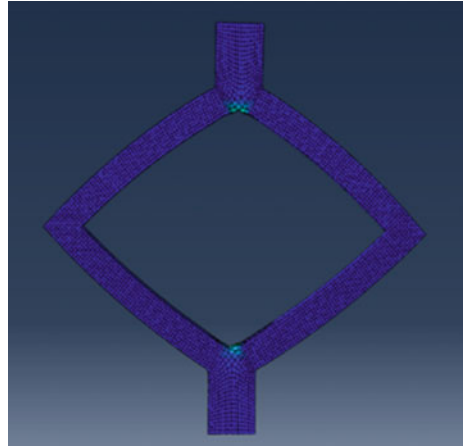
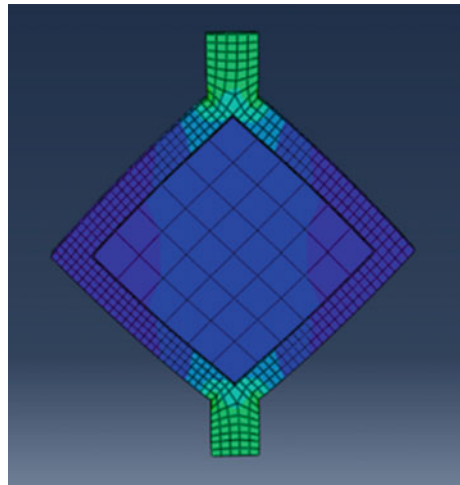


Fig. 5 Deformation of IFCM



3.5.3 Deformation Infilled Frame (Cork) (IFC)

In this infilled frame, cork is an interface medium. In this frame deformation is 61 mm deformation and failure takes place in the joint of the frame (Fig. 6).

3.5.4 Deformation of Infilled Frame (Bitumen) (IFB)

In this infilled frame, bitumen is an interface medium. In this frame, deformation is 67 mm deformation and failure takes place in the joint of the frame (Fig. 7).

Fig. 6 Deformation of IFC

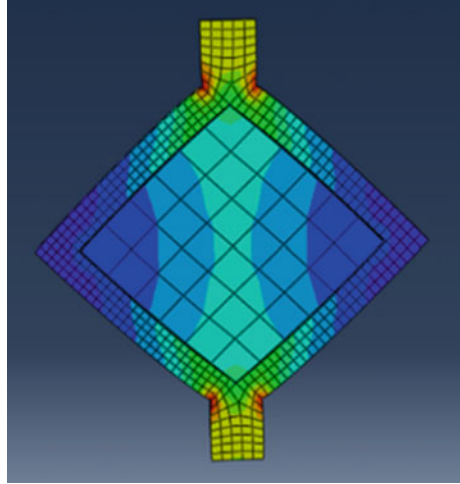
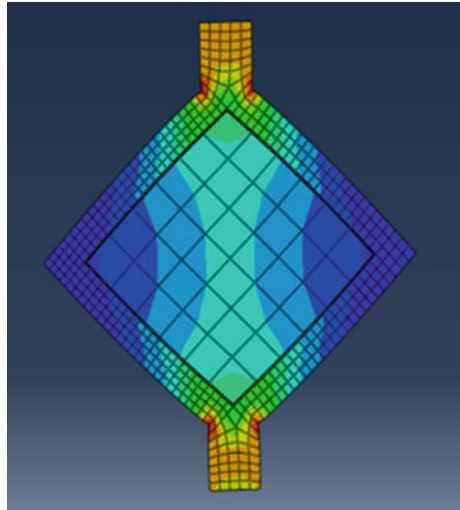


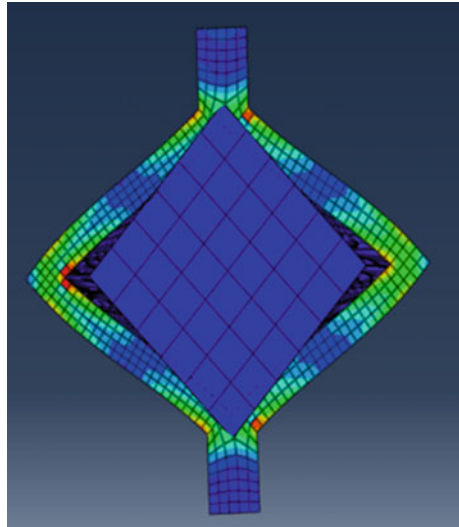
Fig. 7 Deformation of IFB



3.5.5 Deformation of Infilled Frame (Foam Rubber) (IFF)

In this infilled frame, foam rubber is an interface medium. In this frame, deformation is 73 mm deformation and failure takes place in the joint of the frame and also the detachment of interface medium also takes place. Due to the low density of the foam, rubber frame has least stiffness (Fig. 8).

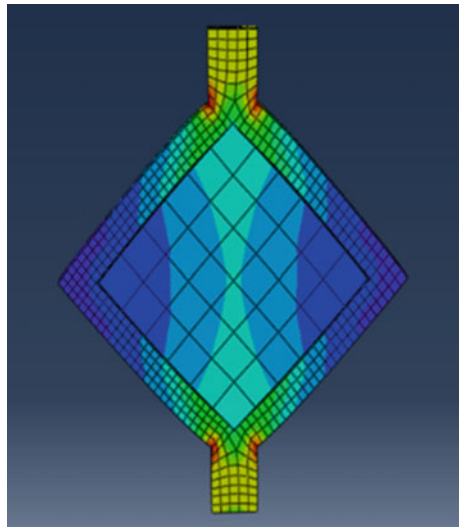
Fig. 8 Deformation of IFF



3.5.6 Deformation of Infilled Frame (Recycled Plastic) (IFP)

In this infilled frame, bitumen is an interface medium. In this frame, deformation is 54 mm deformation and failure takes place in the joint of the frame (Fig. 9).

Fig. 9 Deformation of IFP



4 Results and Discussion

In bare frame, there is no infill and interface, so the deformation is higher in lower amount of loading. In this frame, deformation is 49 mm. In bare frame, cyclic loading is given and the ultimate load is 5 kN. The average time period is 5 and the increment is 10,000. In infilled frame, different interface materials are used likely cement mortar, cork, bitumen, foam rubber, and recycled plastic; their stiffness profiles are compared which is shown in Fig. 10, and their values are given Table 2. In compare to bare frame, deformation is more than infilled frames even same set of loading. In cyclic loading of infilled frame is given and the ultimate load of 20 kN at an average time period is 18 and their increment is 10,000.

In this analysis, infilled frame with cement mortar is less in deformation than the other interface materials and the recycled plastic is also less in deformation. Both of the interfaces performed well under the cyclic loading.

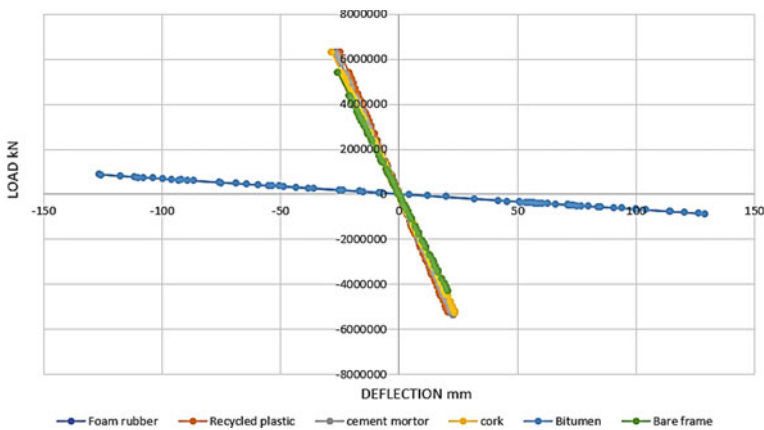


Fig. 10 Stiffness profile of infilled frames with interface materials

Table 2 Results of infilled frame

Type of frame	Max load (kN)	Deformation (mm)	Cyclic steps	Ultimate load (kN)
BF	20	49	5	2.5
IFCM	20	52	19	9.5
IFC	20	61	19	9.5
IFB	20	67	19	9.5
IFF	20	73	16	8
IFP	20	54	19	9.5

5 Conclusion

This analytical study examines how an infilled frame with various interface materials deforms at various stages. When modifying with various interface materials, the deflection also varies. While comparing the cement-mortar interface frame with other interfaces frame deflections are increased. Due to its low density, foam rubber and bitumen interface is more prone to deformation of frame. In this analytical investigation, the frame deformation for the cement-mortar interface is considerably more similar to the interface made of recycled plastic. In future investigation, the recycled plastic can be explore more as interface material.

Acknowledgements I wish to express my sincere thanks to Department of Civil Engineering, SRM Institute of Science and Technology for giving this opportunity.

References

1. Liauw TC, Kwan KH (1985) Static and cyclic behaviours of multistorey infilled frames with different interface conditions. *J Sound Vib* 99(2):275–283
2. Ravichandran SS, Klingner RE (2012) Seismic design factors for steel moment frames with masonry infills: part 1. *Earthq Spectra* 28(3):1189–1204
3. Asteris PG (2003) Lateral stiffness of brick masonry infilled plane frames. *J Struct Eng ASCE* 129(8):1071–1079
4. Kumar SM, Saranya G, Lakshmiopathy M, Satyanarayanan KS (2016) Modeling and study of behavior of infilled frames with different interface materials under static loading. *Indian J Sci Technol* 9(23):1–6
5. Muthukumar S, Satyanarayanan KS, Senthil K (2017) Studies on two bay and three storey infilled frame with different interface materials: experimental and finite element studies. *Struct Eng Mech* 64:543–555
6. Kumar SM, Satyanarayanan KS (2018) Study the effect of elastic materials as interface medium used in infilled frames. *Mater Today Proc* 5(2):8986–8995
7. Vinod Kumar M, Siddharamaiah YM, Aswin Sidhaarth KR (2019) Structural behaviour of lightweight RC frames contains fibres subjected to lateral loading. *Int J Eng Adv Technol (IJEAT)* 8(6):2640–2643
8. ABAQUS Standard User's Manual (2010) Dassault Systèmes, Version 6.10, USA. The Abaqus Software is a product of Dassault Systèmes Simulia Corp.: Providence, RI, USA
9. Maruthish K, Satyanarayanan K, Pradeep S, Muthukumar S (2021) Study on infilled frames with partial interface materials under inplane monotonic loading. *Mater Today Proc* 43:3256–3260

Experimental Investigation on Lightweight Expanded Clay Aggregate (LECA) as a Coarse Aggregate in Concrete



S. Prakashchandar and R. Senthamilselvi

1 Introduction

Cement, fine, and coarse aggregate, as well as other building materials, are all combined to make concrete. In recent years, a concrete type has been developed that uses lightweight expanded clay aggregate (LECA) as coarse aggregate instead of conventional coarse aggregate. Lightweight expanded clay aggregates (LECA), a manufactured product, are frequently utilized in the building constructions. LECA is made by heating natural clay to 1100 °C in a kiln. A honeycomb structure is created by sintering the outer surface of the plastic clay and burning the organic material inside. The finished product is very light, it floats on the water surface easily, chemically inert, and has a natural pH value; it does not contain any harmful or non-biodegradable materials, does not need to be crushed in water, and is chemically and frost-resistant. The LECA can be used in a variety of applications, including construction sectors [1]. Economically, LECA is preferable to coarse aggregate because they provide high strength, are lightweight and strong, and cause less environmental harm. To increase strength, coarse aggregate is used in the place of LECA. It is typically believed that improving the compressive strength of concrete will improve its mechanical properties [2]. The development of LWC was a significant step toward improving working conditions, efficiency at construction sites, and the quality and appearance of concrete structures. It is possible to improve the performance of concrete structures by incorporating LECA into LWC. LECA lightweight concrete combines the advantages of fresh with the improved performance of hardened concrete.

S. Prakashchandar (✉)

Department of Civil Engineering, Faculty of Engineering and Technology, SRM Institute of Science and Technology, Kattankulathur, Tamil Nadu 603203, India
e-mail: prakashs2@srmist.edu.in

R. Senthamilselvi

Bharath Institute of Higher Education and Research, Chennai 600073, India

Table 1 The properties of coarse aggregate

S. No.	Test	Results
1.	Specific gravity	2.5
2.	Unit weight kg/m ³	24
3.	Bulk density kg/m ³	15.80
4.	Impact strength	14%

2 Materials

In this research work, the materials are used in the production of concrete as given below.

2.1 Cement

Ordinary Portland cement of 53 grade (OPC 53) was applied in this research work for the production of concrete as per IS 12269: 1987 [3] reference and the specific gravity is 3.1.

2.2 Fine Aggregate

In this research, the aggregate that comes under the zone II as per the IS: 383:1997 [4] and passes through a 4.75 mm is used in the fabrication of concrete mixes. The fine aggregate specific gravity value is 2.6.

2.3 Coarse Aggregate

The stone aggregate was used in the fabrication of concrete and the size is greater than 4.75 mm and less than 20 mm. Different properties of coarse aggregate according to Indian standards, which confirms IS: 2386-1963 [5], were discovered in laboratories are shown in Table 1.

2.4 LECA

Natural clay is heated to 1100 °C in a kiln to create LECA and the size is not more than 20 mm. This produces a honey comb structure by sintering the plastic clay's

Table 2 The properties of LECA

S. No.	Test	Results
1	Specific gravity	1.68
2	Water absorption	19%
3	Impact strength	52.4%

outer surface and burning the organic material inside. The finished product does not need to be crushed in water, is chemically and frost-resistant, is extremely light, floats on the water surface easily, is chemically inert, and has a natural pH value, and the physical properties are shown in Table 2. It also does not contain any harmful or non-biodegradable materials.

3 Experimental Investigation

To achieve the aim of the research, the first step is to study the mechanical properties of the LECA concrete and the second step is to analyze the microstructural characterization of SEM, XRD, and FTIR.

3.1 Mechanical Properties

According to Indian standards, compressive, split tensile, and flexural strength were determined at ages 3, 7, and 28 days. The capacity of concrete to withstand compression loading is known as compressive strength. The concrete specimens $150 \times 150 \times 150$ mm size were used in accordance with IS 516 (2018) [6]. As per Indian standard 5816 (1959) [7] guidelines, $150 \text{ mm} \times 300 \text{ mm}$ long cylinders were used for splitting strength test. As per IS 516 (2018) [6] guidelines, $500 \text{ mm} \times 100 \text{ mm} \times 100 \text{ mm}$ prisms were used for flexural strength test.

3.2 Microstructural Analysis

Using X-ray diffraction (XRD), scanning electron microscopy (SEM), and Fourier transform infrared spectroscopy (FTIR) tests, the effect of LECA concrete on the cured specimen was investigated for microstructural study.

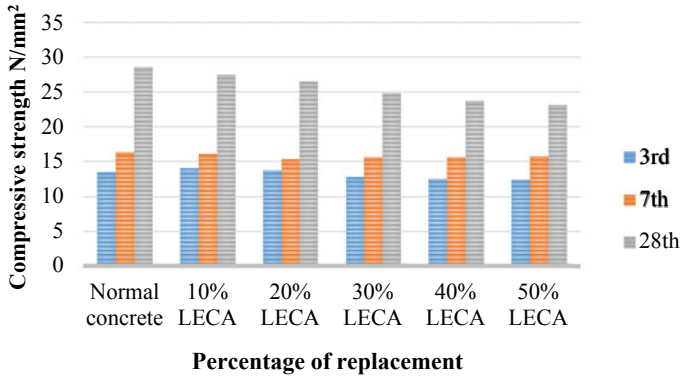


Fig. 1 Compressive strength results in LECA concrete

4 Result and Discussion

The following test results including mechanical properties and microstructural analysis like, SEM, XRD, and FTIR are discussed in this section.

4.1 Compressive Strength Test

The concrete specimens $150 \times 150 \times 150$ mm size were used. After 3, 7, and 28 days of curing, the compressive strength was assessed according to IS 516 (2018) [6]. The test results of concrete by using 10, 20, 30, 40, and 50% replacement level of LECA by coarse aggregate is shown in Fig. 1. According to findings, the 20% substitution level of LECA as coarse aggregate increased strength. The better strength is due to the properties of LECA.

4.2 Split Tensile Strength Test

According to Indian standard 5816 (1959) [7] guidelines, $150 \text{ mm} \times 300 \text{ mm}$ long cylinders were used for splitting strength test. After 3, 7, and 28 days of curing, the split tensile strength was evaluated and the results are shown in Fig. 2. The test results revealed that the tensile strength was enhanced for LECA concrete related with conventional concrete [8]. The 20% substitution of LECA shows the better split tensile strength compared with other replacements. The better strength is due to the properties of LECA.

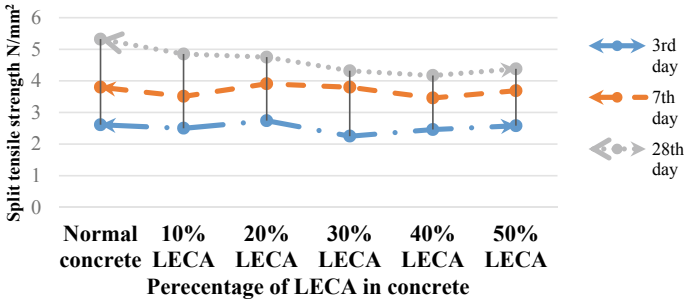


Fig. 2 Split tensile strength of LECA concrete

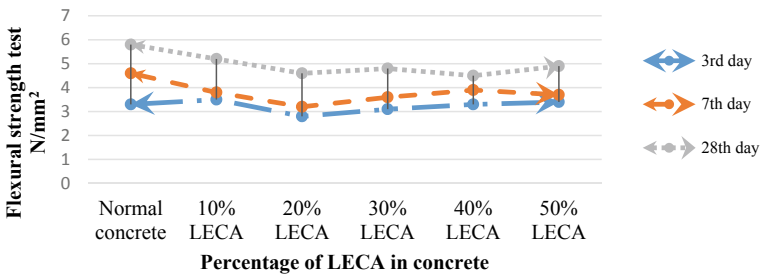


Fig. 3 Flexural strength of LECA concrete

4.3 Flexural Strength Test

As per IS 516 (2018) [6] guidelines, 500 mm × 100 mm × 100 mm prisms were used for flexural strength test. The test results of flexural strength are shown in Fig. 3. This result proves the LECA replaced concrete have good flexural strength. The better strength is due to the properties of LECA.

4.4 SEM Analysis

Concrete inherent microstructure determines how hardened it becomes. The curing period and cement type used in the concrete production are the major impact on the concrete structure. Scanning electron micrograph (SEM) can present both topographic and compositional analysis of material. At 28 days of curing, SEM images of lightweight concrete with different ratio of LECA percentages are displayed in the Figs. 4, 5, 6, 7, 8 and 9. These micrographs demonstrate the distinct spreading of CSH gel, voids and ettringite formation in void spaces [1, 2]. The SEM images of LECA concrete is similar to conventional mix.

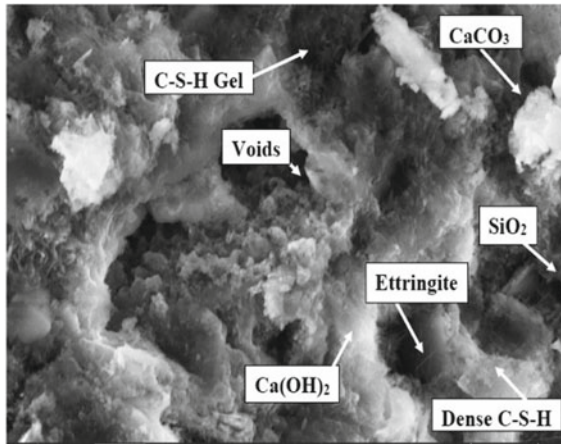


Fig. 4 SEM analysis of normal concrete



Fig. 5 SEM of 10% LECA

4.5 XRD Analysis

The X-ray diffraction analysis was used to analyze the concrete with varying percentage of LECA as coarse aggregate at of 28 days of curing. The chemical phases were identified through XRD using Panalytical X-Pert High Score Plus software. XRD measurements were made for diffraction angle 2 Theta. The XRD pattern demonstrates the formation of CSH, SiO₂, Ca (OH)₂, CaCO₃, and ettringite [9, 10] as shown in Figs. 10, 11, 12, 13, 14 and 15. The XRD pattern of LECA concrete is similar to conventional concrete.

Fig. 6 SEM of 20% LECA

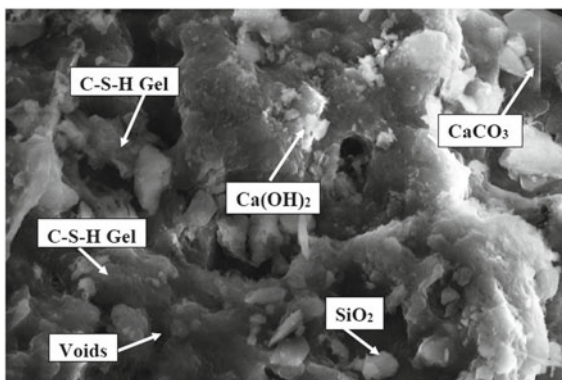


Fig. 7 SEM of 30% LECA

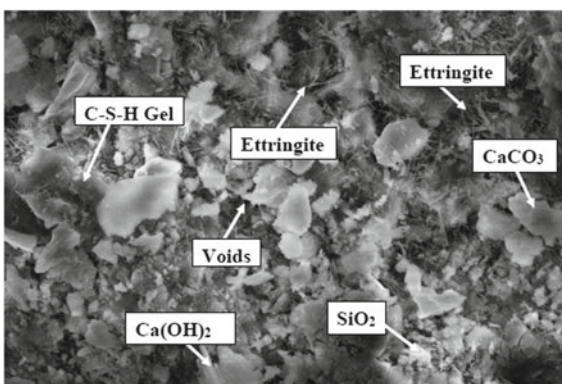


Fig. 8 SEM of 40% LECA

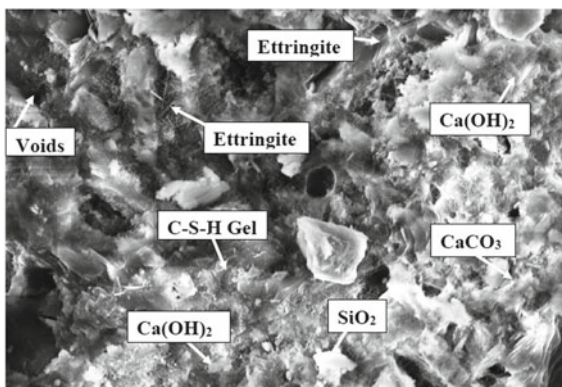


Fig. 9 SEM of 50% LECA

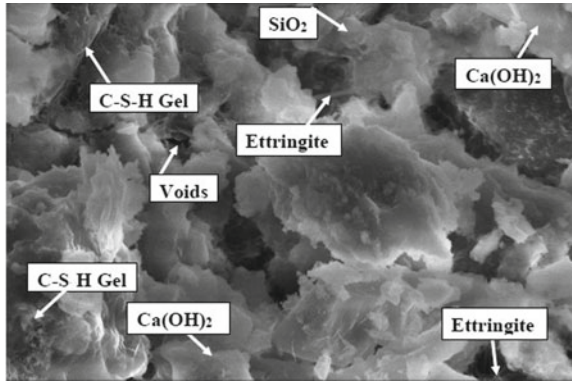


Fig. 10 XRD analysis of normal concrete

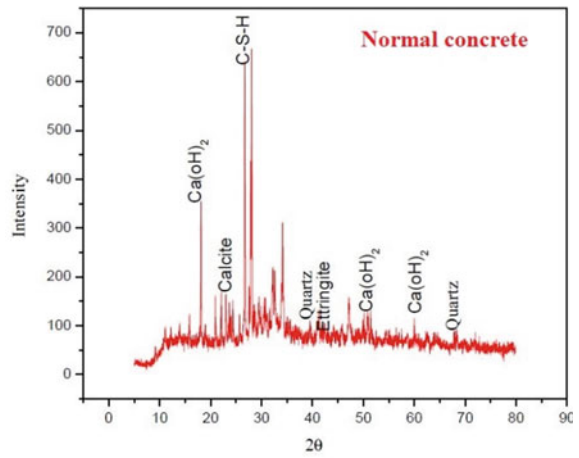
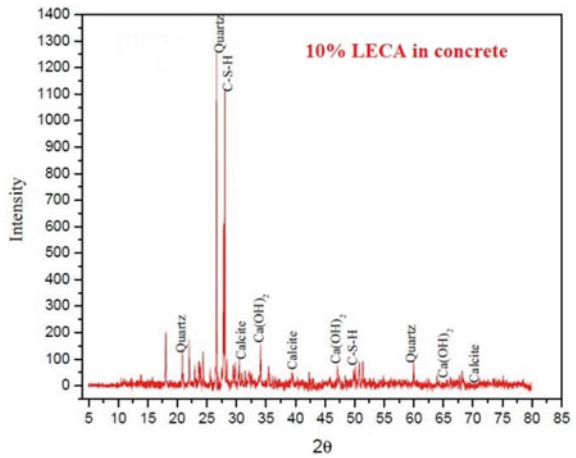


Fig. 11 XRD of 10% LECA



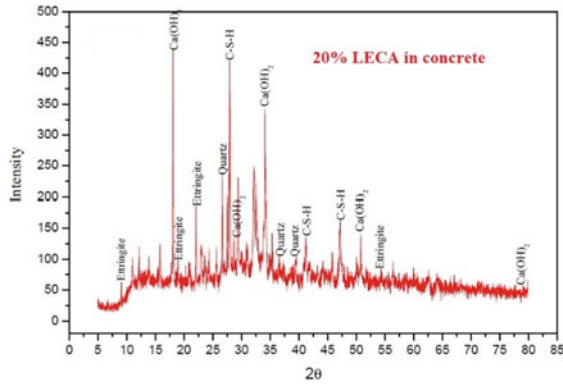


Fig. 12 XRD of 20% LECA

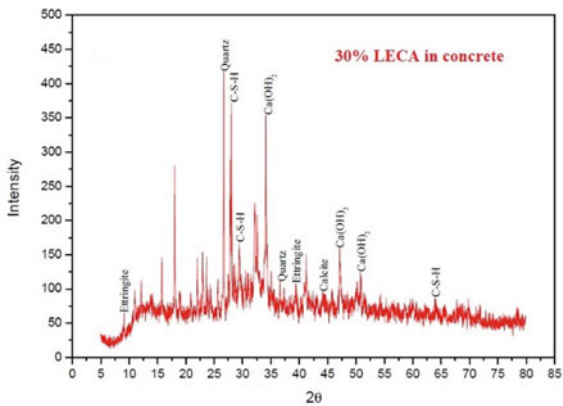


Fig. 13 XRD SEM of 30% LECA

4.6 FTIR Analysis

FTIR analysis was conducted to investigate the bond behavior and bands of molecular groups present in various mixes, as shown in Figs. 16, 17, 18, 19, 20 and 21. Information about the hydration of cement paste was provided by bands larger than 2000 cm^{-1} . The FTIR pattern of LECA concrete is similar to conventional concrete [9–13].

Fig. 14 XRD of 40% LECA

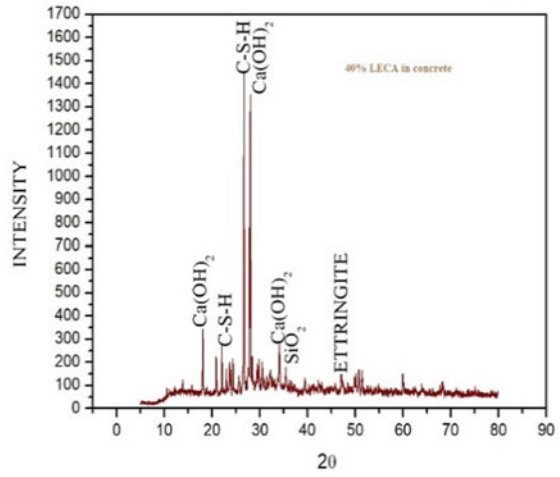
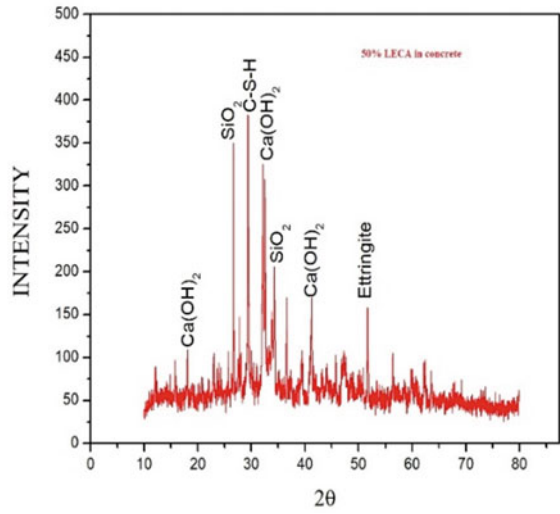


Fig. 15 XRD of 50% LECA



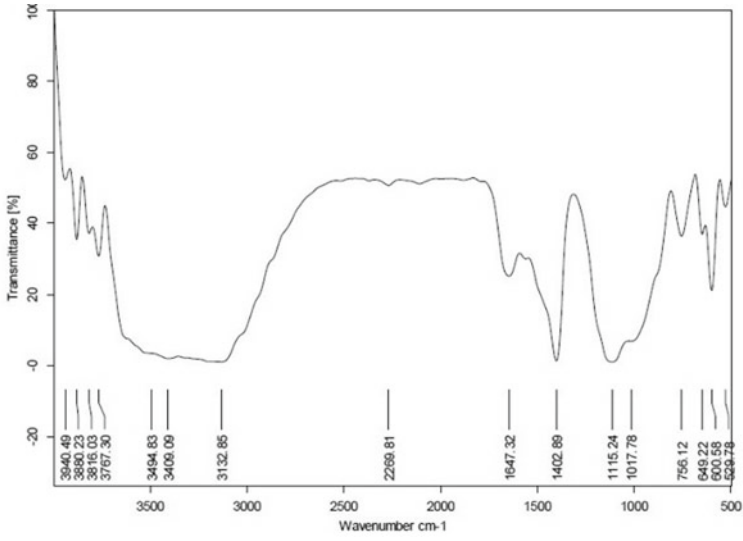


Fig. 16 FTIR analysis of normal concrete

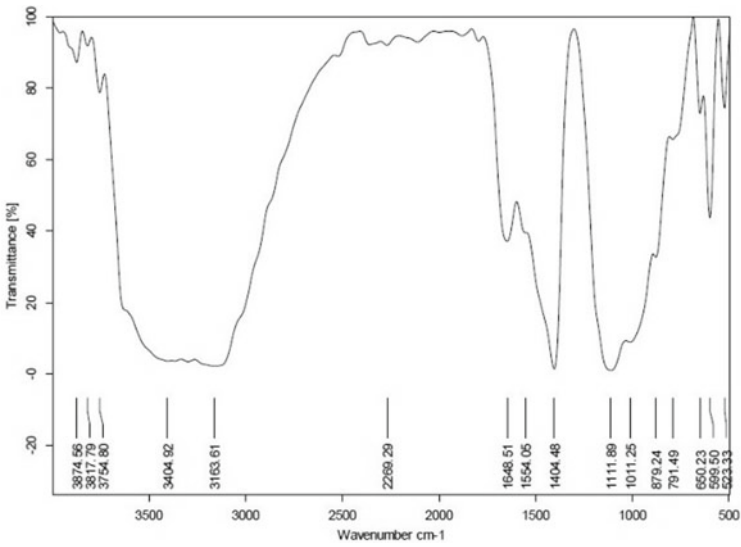


Fig. 17 FTIR of 10% LECA

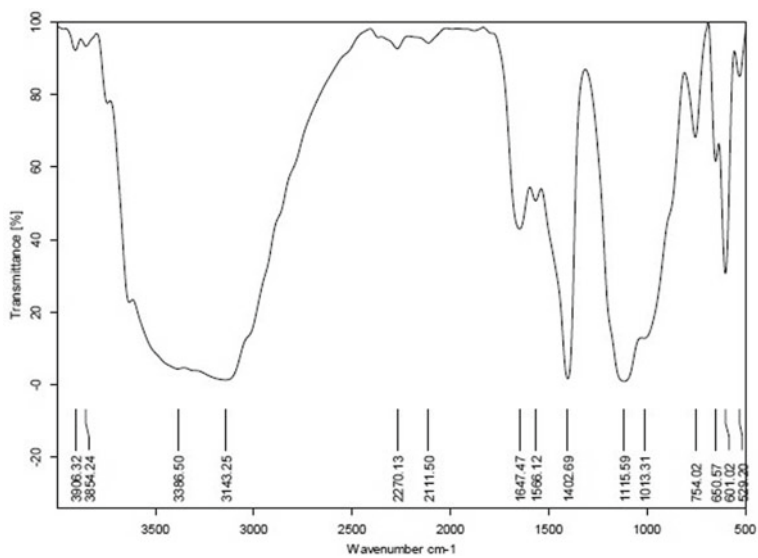


Fig. 18 FTIR of 20% LECA

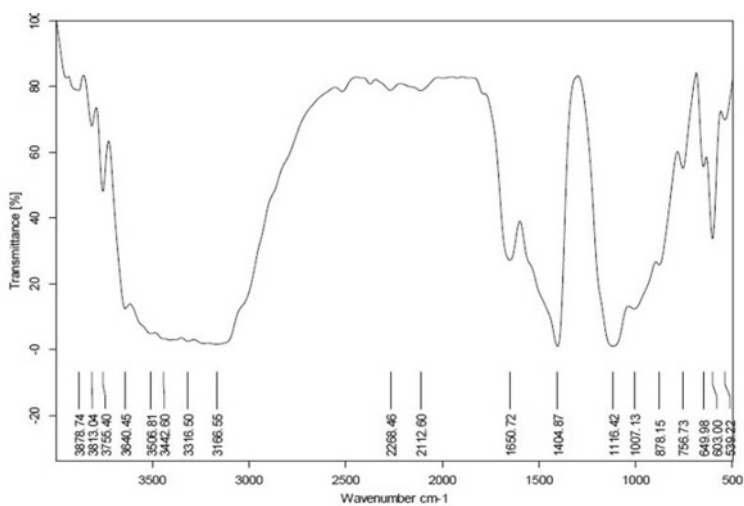


Fig. 19 FTIR SEM of 30% LECA

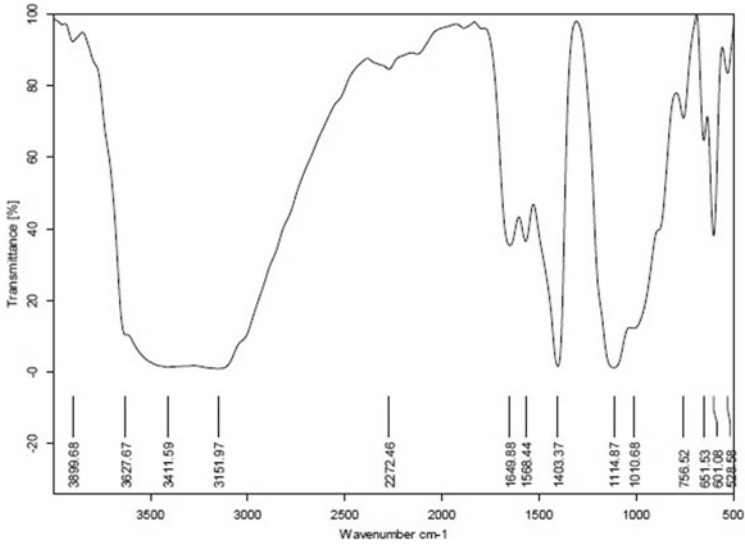


Fig. 20 FTIR of 40% LECA

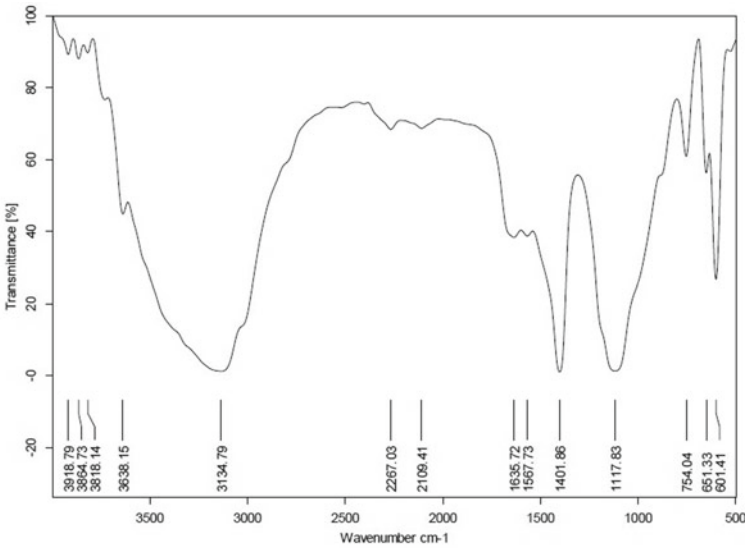


Fig. 21 FTIR of 30% LECA

5 Conclusion

In this research work, the effects of LECA as a partial substitution in the fabrication of lightweight concrete were investigated, and based on the research results, the conclusions are drawn as follows:

- The LECA concrete was possible to produce structural lightweight concrete with less density when compared with conventional concrete.
- The properties of LWC, including compressive, split tensile, and flexural strength, improved with the addition of 20% LECA.
- The concrete made with 20% replacement of LECA as coarse aggregate improved the split tensile strength compared with normal concrete.
- According to the test results, concrete flexural strengths were found to be at their highest levels at 20% substitution of LECA
- The SEM analysis of all mixes identifies the formation of CSH gel and needle-like structure ettringite.
- The XRD pattern of all mixes observed the peak intensity of CSH, CaCO_3 , $\text{Ca}(\text{OH})_2$, and ettringite.
- The FTIR spectrum reveals the chemical bonding in between the molecules with different wavelength.
- The LECA used in concrete produced eco-friendly concrete.

References

1. Ravichandran PT, Divya Krishnan K (2020) Effect of pyrophyllite on behavioural strength of clayey soil. *IOP Conf Ser Mater Sci Eng* 912(6):062063. <https://doi.org/10.1088/1757-899X/912/6/062063>
2. Ravichandran PT (2019) Investigation on grinding impact of fly ash particles and its characterization analysis in cement mortar composites. *Ain Shams Eng J* 10(2):267–274. <https://doi.org/10.1016/j.asej.2019.02.001>
3. IS-12269 (1987) Specifications for 53grade cement. Bureau of Indian Standard
4. IS 383 (1997) For coarse and fine aggregate from natural sources of concrete
5. IS: 2386 (Part III) (1963) Methods of test for aggregates for Cqconcrete
6. IS 516 (2018) Method of tests for strength of concrete. Bureau of Indian Standards, pp 1–30
7. IS: 5816 (1959) Splitting tensile strength of concrete “method of test”. Bureau of Indian Standard
8. Prakash Chandar S, Ravichandran PT, Gunasekaran K, Mechanical and microstructure analysis of sustainable concrete using paper waste. <https://doi.org/10.21203/rs.3.rs-1721521/v1>
9. Kumar VRP, Gunasekaran K, Shyamala T (2019) Characterization study on coconut shell concrete with partial replacement of cement by GGBS. *J Build Eng* 26. <https://doi.org/10.1016/j.jobe.2019.100830>
10. Prakash Chandar S, Santhosh R (2022) Partial replacement of cement with alternative cementitious material in the production of concrete: a review. *Mater Today Proc* 68(1). <https://doi.org/10.1016/j.matpr.2022.09.140>
11. Prakash Chandar S, Manivel S, Gunasekaran K, Jothiswaran A (2017) An experimental investigation of partial replacement of cement using micro silica and fly ash in production of coconut shell concrete. *Int J Civ Eng Technol* 8(4):1851–1859

12. Prakash Chandar S, Gunasekaran K, Kalpana Priya V, Ganapathyramasamy N (2019) An experimental investigation on partial replacement of sand by ceramic grains in coconut shell concrete. *Rasayan J Chem* 12(2):659–665. <https://doi.org/10.31788/RJC.2019.1225227>
13. Prakash Chandar S, Balaji SS, A critical review on recycled aggregate concrete with m-sand as a fine aggregate. *AIP Conf Proc* 2515(1):020004. <https://doi.org/10.1063/5.0103019>

Experimental Study on Strengthening of Damaged Steel Flexural Members Using CFRP Composite Wraps



G. Arun Kumar, S. A. Vengadesh Subramanian, and N. Umamaheswari 

1 Introduction

FRP is considered as one of the efficient materials used in the rehabilitation of structures. The feasibility of using carbon fiber-reinforced polymer as external reinforcement for strengthening steel structures is studied since 1980s. As per the available literature, the first ever application of CFRP to strengthen a bridge structure occurred in 1990s. Though the cost of material of CFRP is more than that of steel plates which are more commonly used for strengthening, the efficiency proves to be more in the case of CFRP. The traditional method of strengthening such as attachment of plates may not be helpful since there will be considerable increase in weight and extended construction period. CFRP plates/sheets have also been capable of increasing flexural, fatigue, and shear strength as well as serviceability criteria of beams [1–7]. In this paper, an attempt has been made to rehabilitate the failed steel beam specimens using FRP sheets and strips by using wrapping technique. Carbon has high bonding strength and stiffness compared to other fibers, and hence, CFRP is used in this experimental study. The development of modern retrofitting techniques has been focusing on concrete structures rather than steel structures. Nowadays, the researchers have been doing experimental, numerical, and analytical studies related to retrofitting of concrete structures using advanced composite materials, and the results are encouraging for the improvement in the strength of existing concrete structures, while the research on retrofitting of steel structures is under developed. FRP wrapping is one of the modern techniques used in retrofitting of concrete structures showing high strength to weight ratio. Carbon, Kevlar, Glass are the commonly used fibers in FRP wrapping technique. This technique can also be implemented in retrofitting steel structures if adequate research is carried out. Repairing or retrofitting

G. Arun Kumar · S. A. Vengadesh Subramanian · N. Umamaheswari (✉)
Department of Civil Engineering, Faculty of Engineering and Technology, SRM Institute of
Science and Technology, Kattankulathur, Tamil Nadu 603203, India
e-mail: umamahen@srmist.edu.in

of steel structures with FRP composites takes only less time for construction. The idea of implementing CFRP wrapping technique to steel structures increases the corrosion resistance and reduces the time for construction and hence the cost involved. However, many critical issues need to be resolved before adopting this advanced material for retrofitting of structures. The available research papers describe about using FRP for the retrofitting techniques for the buildings that are not capable of withstanding seismic forces. The FRP materials are used for retrofitting RC structures as well as steel structures. From the research, it has been known that the FRP retrofit can increase 10–37% of the elastic stiffness of damaged steel structure [8–10]. It is suggested that the repairing techniques for steel framed structure and the damaged steel structure is analyzed by loading tests. The damaged portion of the steel structure is rehabilitated using steel cover technique and the specimen is tested again. The results show that the strength and ductility of the repaired specimen is increased when compared to the original specimen.

Retrofit of steel structures using FRP materials has not gained importance similar to RC structures. The effect of using FRP to repair or strengthen steel structures requires additional research. It has been tried on steel girders to repair/strengthen the damaged parts due to corrosion or fatigue. Elastic stiffness of damaged parts can be improved by up to 37% which is reported in the literature. The capacity of steel section which is lost can be restored in addition to higher load resistance when FRP sheets/strips are used as repair materials by reducing the crack propagation. This technique is found to increase service load also [11–13].

2 Details of Materials Used

Finite element analysis has been carried out using ABAQUS V.14. The analysis deals with the behavior of non-prismatic beams subjected to monotonic loading conditions. From the analysis using plastic strain, plastic hinge length and location was calculated.

2.1 Selection of Polymer Type

Carbon fiber is the preferred type in FRP composites, though other fibers such as glass, basalt, or aramid are also available. The main reason for choosing glass or basalt fiber is reduced cost. Carbon fibers will be expensive but the increased cost can be compensated by the high level of enhancements in strength characteristics obtained from using them for rehabilitation techniques. The digital image of woven carbon fiber is shown in Fig. 1. Carbon fiber possesses high tensile strength and exhibits lightweight. When bonded to the exterior part of a steel column or beam, it can add significant strength without increasing much weight which in turn increases the load on other structural members. CFRP wraps are easy to apply and can be used

Fig. 1 Woven carbon fibers**Table 1** Physical and chemical properties of carbon fabric

Materials	Properties
Woven pattern	Unidirectional
Tensile strength (MPa)	≥ 2750
Thickness (mm)	0.115
Width (mm)	500
Area weight (g/m^2)	245
Material code	403-112

on any size or shape of structural member. Traditional techniques for strengthening, such as welding of steel plates to beams and columns, can be replaced by wrapping technique [14–16].

The important reason to apply the idea of CFRP addition is to improve strength of old structure. But for rectifying some smaller errors in construction, it will be used in new structures also. Because of easier application, this technique of strengthening proves to be less costly up to 50% compared to conventional methods.

2.2 Carbon Fiber Fabric

Carbon fibers have high strength to weight ratio. These fibers are corrosion-resistant, chemically stable and fatigue-resistant. The orientation of the fibers and the different fiber layer orientation have a great influence on their performance. Carbon fiber is classified as noncombustible. The physical and chemical properties of carbon fiber fabric are shown in Table 1.

2.3 Epoxy Resin and Hardener

Epoxy resin is used to bind the strengthening fibers, to lock them in position and it helps to protect the fibers from damage from external agents and provides impact resistance. Epoxy has proved to be a relatively safe material. The image of epoxy

Fig. 2 Epoxy resin and hardener



Table 2 Physical and chemical properties of epoxy resin and hardener

Property	Epoxy resin 520	Hardener
Appearance	Colorless liquid	Clear liquid
Specific gravity (g/cc)	1.15–1.18	0.98
Type	Solvent modified resin	Polyamine
Storage stability	12 months	6 months

resin and hardener is shown in Fig. 2. The physical and chemical properties of epoxy resin and hardener is shown in Table 2.

2.4 Properties of Steel Beam Specimens

The property of failed steel beam specimens for which retrofitting has to be done is given in Table 3.

Table 3 Properties of steel beam specimens

Designation of beam section		Types of section	Dimensions (mm)
Original	Retrofitted		
C4	RC4	C section	100 × 60 × 20
C5	RC5	C section	120 × 50 × 20
R2	RR2	Rectangular section	80 × 50 × 20
R3	RR3	Rectangular section	90 × 40 × 20
R4	RR4	Rectangular section	100 × 60 × 20

Fig. 3 Identification of local buckling



3 Wrapping Process

The wrapping process involves preparation of specimen, coating of epoxy resins along the surface of the specimen, wrapping of CFRP sheets around the steel beam for the required number of layers.

3.1 Preparation of Specimen

The specimen for which the retrofitting is to be done using CFRP sheets is physically inspected, to prepare the specimen for wrapping since any amount of dust or rust appearing on the surface of steel specimens may cause serious problem in affecting the bonding strength between CFRP, epoxy, and steel member. Hence, it is cleaned using sand paper.

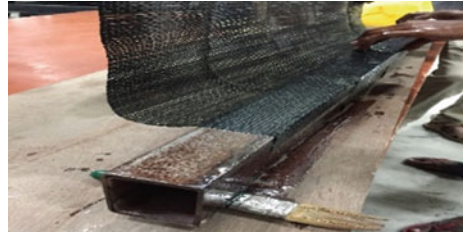
3.2 Physical Analysis of Defect

After removing rust from the surface of steel specimen, the steel beam specimen is observed for the defects. Local buckling has been occurred only on the places where the supports have been placed during the testing process. These buckling points are marked as shown in Fig. 3.

3.3 CFRP Wrapping Process

The epoxy resin coating is done all around the surface of the steel beam specimen, to enhance the bonding strength between the CFRP wrapping layers and also to prevent member to undergo further corrosion. The epoxy coating is left dry for 6 h. When the epoxy coating is dried, the CFRP wrapping process is done (as shown in Fig. 4) by laying epoxy resins for each layer.

Fig. 4 CFRP wrapping method



4 Experimental Investigation

The experimental investigation includes applying retrofitting technique on failed steel beam specimens and testing of specimens in computerized universal testing machine of 40 T capacity, as shown in Fig. 5. Different methods of retrofitting techniques are tried for C and rectangular sections.

4.1 Retrofitting Techniques

Different methods of wrapping techniques are adopted for C and rectangular beam sections and it is explained in detail in this section.

Retrofitting of beam specimens of C sections. Initially it was decided to adopt CFRP wrapping only in the buckled area to check the response of the steel beam specimen (RC4), and if the strength regained is insufficient, wrapping can be done over the entire surface of the specimen. The specimen is prepared by removing the rust, and epoxy coating is done all over the surface of specimen to resist corrosion. When the epoxy is made to dry for 6 h, wrapping is done on the buckled area for



Fig. 5 Flexural testing of retrofitted beam specimen using UTM

3 rotations by applying epoxy resins in all layers. It is allowed to cure for 24 h before testing. The wrapped specimen tested under flexure showed higher strength compared to original specimens. Hence, the same process is repeated for another beam specimen of C section (RC5).

Retrofitting of beam specimens of rectangular sections. Similar to beams of C section, initially wrapping is done on buckled area of rectangular section (RR4) also to check the response of the specimen. The specimen is tested and found to possess lesser strength compared to original specimen. The alternate method of retrofitting is tried with initial wrapping on the two locally buckled areas for three complete rotations followed by complete wrapping of CFRP sheet over the surface of the specimen (RR2). The retrofitted specimens RR4 and RR2 are shown in Figs. 6 and 7, respectively. While retrofitting of concrete structural elements using CFRP, carbon strips (shown in Fig. 8) are used when the strength of carbon fabric is insufficient. The carbon strips can also be used in steel specimens. The carbon strips have higher strength and stiffness compared to carbon fabrics and hence increases the strength of the retrofitted steel specimen. This method is adopted for beam specimen of rectangular section (RR3), as shown in Fig. 9. The results obtained showed increase in flexural strength compared to original beam specimen.

Fig. 6 Retrofitting of specimen (RR4)



Fig. 7 Retrofitting of specimen (RR2)

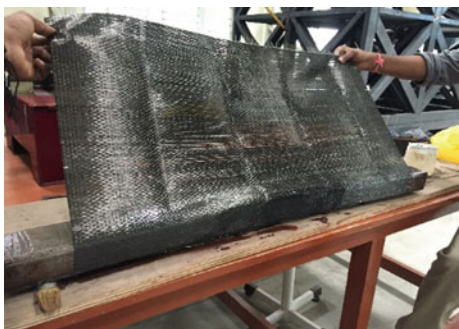


Fig. 8 Carbon Strip used**Fig. 9** Retrofitted specimen (RR3)

5 Results and Discussions

The results obtained from experimental investigation carried on retrofitted C and rectangular sections are tabulated (Table 4). The percentage increase in strength obtained shows the effectiveness of wrapping technique adopted in strengthening process of steel beam specimens. Further percentage decrease in deflection at maximum load shown in Table 4 indicates the efficiency of repair method adopted. All type of retrofitting methods show improvement in strength and stiffness (except for specimens RR2 & RR4) of steel beam specimens. There is a decrease in deflection at maximum load is obtained for all beam specimens. It apparently shows that the method is efficient. The percentage increase in strength varies from 4 to 72%, whereas the percentage decrease in deflection at maximum load ranges from 5 to 82%. The percentage increase in stiffness goes up to 166%. Reduction in deflection at maximum load is marginal only for rectangular sections. Overall, the performance of retrofitted C section beam specimens is better compared to retrofitted rectangular sections in terms of strength and reduction in deflection. It is evident from the results that wrapping of steel beam specimens can be conveniently adopted to strengthen the flexural members made of C sections either existing or repaired.

Table 4 Results obtained from experimental investigation

Section	Dimension (mm)	Ultimate load (kN)		Displacement (mm)	
		Original specimen	Retrofitted specimen	Original specimen	Retrofitted specimen
C4	100 × 60 × 20	14.00	24.18	8.20	1.40
C5	120 × 50 × 20	22.70	23.64	6.98	2.00
R2	80 × 50 × 20	63.41	60.85	4.00	3.80
R3	90 × 40 × 20	57.67	64.07	4.18	3.27
R4	100 × 60 × 20	80.96	76.14	3.63	3.20

C4, C5, R2, R3 and R4-Original specimens and RC4, RC5, RR2, RR3 and RR4-Retrofitted specimens

Section	Dimension (mm)	Ultimate load (kN)		Displacement (mm)	
		Original specimen	Retrofitted specimen	Original specimen	Retrofitted specimen
C4	100 × 60 × 20	14.00	24.18	8.20	1.40
C5	120 × 50 × 20	22.70	23.64	6.98	2.00
R2	80 × 50 × 20	63.41	60.85	4.00	3.80
R3	90 × 40 × 20	57.67	64.07	4.18	3.27
R4	100 × 60 × 20	80.96	76.14	3.63	3.20

The load versus deformation curves were plotted for both C and rectangular sections before and after retrofitting. The variations are shown in Fig. 10.

6 Conclusions

The rehabilitation of steel structural elements using advanced composite materials offers many advantages such as cost-effectiveness and feasibility to adopt so that strengthening and stiffening is made possible. The success of the method lies in the selection process of adhesives that should provide adequate durability under a variety of field conditions. The experimental study described in this paper focused on applying advanced composites to steel beams for retrofitting. Already tested steel beam specimens were rehabilitated using CFRP sheets/strips. Load tests were performed after the rehabilitation indicates a reduction in total deflection (up to 82%) of beams. The test results showed that significant increase in strength (up to 72%) and stiffness (up to 166%) were obtained with the composite repair. However, durability of bond between CFRP sheets/strips and steel beam needs to be assessed. The test results revealed that this rehabilitation approach is a feasible and potentially cost-effective repair method which offers a better solution for damaged steel structural elements.

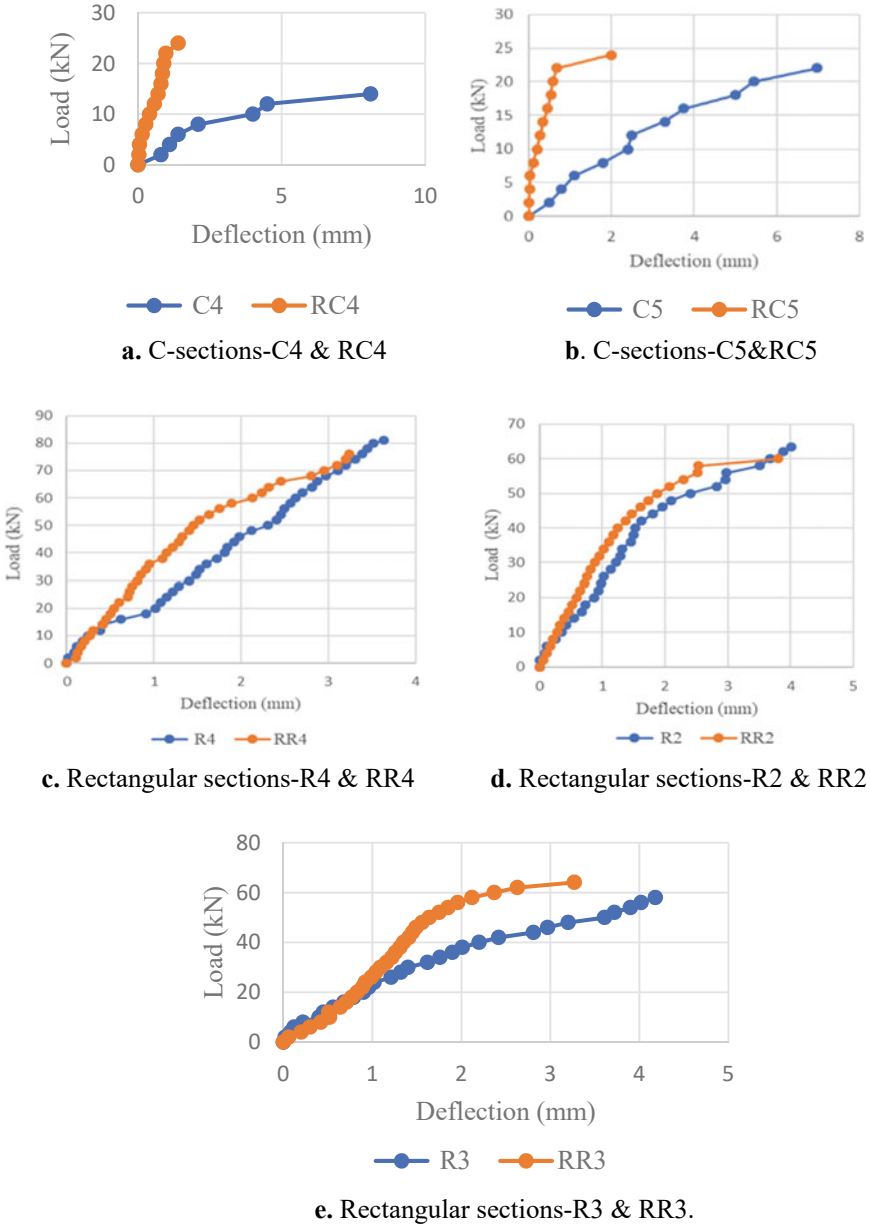


Fig. 10 Load versus deflection of steel beam specimens

References

1. Baky HA, Ebead UA, Neale KW (2007) Flexural and interfacial behaviour of FRP-strengthened reinforced concrete beams. *ASCE* 1(6):629–639
2. Bonacci JF, Maalej M (2000) Externally bonded fibre-reinforced polymer for rehabilitation of corrosion damaged concrete beams. *ACI Struct J* 97(5):703–711
3. Bousias SN, Triantafillou TC, Fardis MN, Spathis L, O'Regan BA (2004) Fiber-reinforced polymer retrofitting of rectangular reinforced concrete columns with or without corrosion. *ACI Struct J* 101(4):512–520
4. Brena SF, Bramblett RM, Wood SL, Kreger ME (2003) Increasing flexural capacity of reinforced concrete beams using carbon fibre-reinforced polymer composites. *ACI Struct J* 100(1):36–46
5. Bruneau M, Reinhorn A (2006) Overview of the resilience concept. In: Proceedings of 8th U.S. national conference on earthquake engineering
6. El-Hacha R, Green MF, Weight RG (2003) Innovative system for prestressing FRP sheets. *ACI Struct J* 100(3):239–252
7. Fujisaki T, Hosotani M, Ohno S, Mutsuyoshi H (1997) JCI state of the art on retrofitting by CFRM—research. In: Proceedings of 3rd conference on non-metallic (FRP) reinforcement for concrete structures. *JCI*, vol 1, pp 613–620
8. Gillespie JW, Mertz DR, Kasai K, Edberg WM, Demitz JR, Hodgson I (1996) Rehabilitation of steel bridge girders: large scale testing. In: Proceedings of the American society for composites 11th technical conference on composite materials, pp 231–240
9. Kobatake Y, Kimura K, Katsumata H (1993) Fiber-reinforced-plastic (FRP) reinforcement for concrete structures: properties and applications. In: Nanni A (ed) Elsevier Science Publishers, pp 435–450
10. Kotynia R, Baky HA, Neale KW, Ebead UA (2008) Flexural strengthening of RC beams with externally bonded CFRP systems: test results and 3D nonlinear FE analysis. *J Comp Constn* 12(2):190–201
11. Millar D, Scott P, Clenin R (2004) Bridge strengthening with prestressed CFRP plate system. In: Proceedings of 2nd international conference on FRP composites in civil engineering. Taylor and Francis, Adelaide, pp 463–469
12. Mori K, Ito T, Sato H, Munemura H, Matsumoto T (2015) Repairability performance and restoring force characteristics of damaged H-shaped steel members after repair. *Int J High-Rise Build* 4:57–61
13. Motavalli M, Czaderski C (2007) FRP composites for retrofitting of existing civil structures in Europe: state-of-the-art review, composites and polycon. American Composites Manufacturers Association, Tampa, pp 17–19
14. Tanaka A, Izumi M, Narihara H (1990) Experimental study on the statistical characteristics of repaired or reinforced steel structures. *J Struct Eng* 36B:377–384
15. Triantafillou TC, Deskovic N, Deuring M (1992) Strengthening of concrete structures with prestressed fiber reinforced plastic sheets. *ACI Struct J* 89(3):235–243
16. Triantafillou TC, Fardis MN (1997) Strengthening of historic masonry structures with composite materials. *Math Struct* 2:96–104

Strengthening of Structures Using FRP Composites Fibres



D. Murugan and N. Pannirselvam

1 Introduction

Cement, fine and coarse aggregate, and water were used to create reinforced concrete (RC). Fibre-reinforced polymer (FRP), which is externally strengthened, enhances the structural behaviour of the structural components. Since FRP is lightweight, installation is simple and no temporary support is needed. The choice of adhesives is crucial because it prevents the separation of FRP from concrete. Studies on the ultimate load carrying capacity and failure mode of beams take into account the number and orientation of GFRP layers [1]. The strength behaviour of the structure where GFRP is used is influenced by the orientation of the GFRP layers. Using externally attached polymer and fibre reinforcement, a reinforced concrete beam's strength was simulated [2]. Evaluations are made of analytical models and design strategies for the bonding of FRP composites and concrete [3]. The attached beam cannot delaminate since composite laminates are produced flawlessly [4]. Ductile strengthening using near-surface mounted composite materials that are externally bonded [5]. Utilizing BFRP textiles, RC beams are reinforced in shear and flexure [6]. To support any deficient structural member, the use of FRP composites in the form of laminates, rods, sheets, or dry fibres that are fastened to the surface of the damaged region with adhesives and fasteners improved stiffness and load bearing capacity of the material. FRP systems are more advantageous than conventional reinforcing methods since they are noncorrosive, lightweight, and relatively simple to install. Strengthening structural members is a need to increase their strength [7]. By using ACI report the design performed to evaluate the strength of the member [8–10].

D. Murugan · N. Pannirselvam (✉)

Department of Civil Engineering, Faculty of Engineering and Technology, SRM Institute of Science and Technology, Kattankulathur, Tamil Nadu 603203, India

e-mail: pannirsn@srmist.edu.in

The use of FRPs in the construction sector has a lot of promise for both new construction and the renovation of existing buildings. FRPs can enhance a material's strength capacity as well as its resistance to crack propagation [11–15].

- To assess the effectiveness of manual wet lay-up application using cold-cured adhesive bonding.
- The external FRP reinforcement is adhered to the meticulously cleaned concrete surface with the fibres running parallel to the main tensile stress direction.
- To carry out extensive investigation on utilization of FRP for structural strengthening.

2 Materials Used

FRP is synthetic in nature extracted from glass and made into ductile to reach as like the thread and different orientations followed to achieve in the form of cloth. The thickness can be achieved by adding resin between the layers.

3 Methodology

The beam is cast and cured. After curing, the soffit of the beam has to be fixed to FRP using resin by a mechanical grinding machine. By using a wire brush, the dust particles are removed and the layer of prepared resin. The beam with FRP at the soffit after curing is tested to evaluate the strength characteristics.

4 Flexural Strengthening of Beams

The most common method of flexural strengthening using FRP composites is to connect a FRP plate to the beam soffit. Numerous studies and practical applications of RC beams with unanchored and unstressed FRP plates have been conducted [11–17].

5 Experimental Investigations

Experimental investigations were carried out on fifteen beam specimens. Five beams were cast for three steel ratios of 0.419, 0.603, and 0.905%. CSM and WR GFRP laminates having 3 and 5 mm thicknesses were plated to the soffit of the beams. The beams were tested under monotonically increasing loading as shown in Fig. 1. The specimen details and material are presented in Tables 1, 2 and 3.

Table 3 FRP properties

FRP type	Thickness	Tensile strength	Elongation (%)	Elasticity modulus
FRP (CSM)	3	125.20	1.68	7456.61
	5	155.00	1.37	11,386.86
FRP (WR)	3	146.40	2.15	6855.81
	5	177.09	1.98	8994.44

**Fig. 2** Testing in progress

6 Preparation of Surface

The soffit of the beam surface is organized by mechanically grinding the surface to make it smooth. The surface was then thoroughly cleaned, and resin was then applied. After that, the CSM was attached to the resin, which was then followed by the roving and, ultimately, the surface mat with resin sandwiched in between each layer. Experimental testing results are shown in Fig. 2.

7 Results and Discussion

The failure modes of beam are represented in Fig. 3 (Tables 4, 5 and 6).

8 Conclusions

1. The increase in ultimate load for beams with CSM and WR GFRP laminates of 3 and 5 mm thickness ranged from 3.84 to 111.78%.
2. The deflections in concrete beams with WR GFRP laminates were reduced to a level up to 22.14% at the ultimate load level of the control beam.



Fig. 3 Failure modes of beam

Table 4 Test result at first crack load

S. No.	Specimen designation	First crack load (kN)	Deflection at first crack load (mm)	Radius of curvature (radian/m)	Crack width (mm)
1	S1	17.17	4.52	4.61E-06	0.002
2	S2	17.17	3.29	3.36E-06	0.002
3	S3	24.53	3.75	3.83E-06	0.002
4	S1 CSM3	17.17	3.38	3.45E-06	0.002
5	S2 CSM3	26.98	5.09	5.19E-06	0.002
6	S3 CSM3	22.07	4.52	4.61E-06	0.002
7	S1 CSM5	24.53	6.55	6.68E-06	0.002
8	S2 CSM5	24.53	3.89	3.97E-06	0.002
9	S3 CSM5	46.60	7.51	7.66E-06	0.002
10	S1 WR3	29.43	7.77	7.93E-06	0.002
11	S2 WR3	36.79	6.32	6.45E-06	0.002
12	S3 WR3	41.69	7.47	7.62E-06	0.002
13	S1 WR5	34.34	7.39	7.54E-06	0.002
14	S2 WR5	49.05	11.72	1.20E-05	0.002
15	S3 WR5	53.96	9.2	9.39E-06	0.002

3. The test beams with GFRP laminates failed mostly due to the yielding of tensile steel. The size and density of crack in such class of beam were less than those in the control beam.
4. The concrete beams provided with WRGFRP laminates of 5 mm thickness exhibit enhanced ductility ranging from 95.60 to 141.58%.

Table 5 Test result at yield load

S. No.	Specimen designation	Yield load (kN)	Yield deflection (mm)	Radius of curvature (radian/m)	Crack width (mm)
1	S1	17.17	11.17	1.14E-05	0.12
2	S2	34.34	10.91	1.11E-05	0.36
3	S3	36.79	10.40	1.06E-05	0.12
4	S1 CSM3	22.07	8.04	8.20E-06	0.14
5	S2 CSM3	41.69	9.64	9.84E-06	0.16
6	S3 CSM3	51.50	9.57	9.77E-06	0.20
7	S1 CSM5	39.24	8.44	8.61E-06	0.18
8	S2 CSM5	44.15	8.43	8.60E-06	0.28
9	S3 CSM5	58.86	9.11	9.30E-06	0.10
10	S1 WR3	44.15	11.58	1.18E-05	0.36
11	S2 WR3	49.05	9.85	1.01E-05	0.12
12	S3 WR3	74.80	9.86	1.01E-05	0.30
13	S1 WR5	51.50	7.98	8.14E-06	0.24
14	S2 WR5	56.41	10.63	1.08E-05	0.06
15	S3 WR5	58.86	9.20	9.39E-06	0.08

Table 6 Test result at ultimate load

S. No.	Specimen designation	Ultimate load (kN)	Ultimate deflection (mm)	Radius of curvature (radian/m)	Crack width (mm)
1	S1	34.34	30.20	3.08E-05	1.20
2	S2	41.69	33.70	3.44E-05	1.04
3	S3	63.77	33.89	3.46E-05	0.90
4	S1 CSM3	36.79	32.73	3.34E-05	1.00
5	S2 CSM3	53.96	33.82	3.45E-05	0.64
6	S3 CSM3	66.22	35.05	3.58E-05	0.40
7	S1 CSM5	49.05	35.60	3.63E-05	0.60
8	S2 CSM5	61.31	37.15	3.79E-05	0.52
9	S3 CSM5	80.93	38.68	3.95E-05	0.54
10	S1 WR3	58.86	32.83	3.35E-05	0.82
11	S2 WR3	73.58	35.05	3.58E-05	0.66
12	S3 WR3	78.48	37.52	3.83E-05	0.54
13	S1 WR5	63.77	35.49	3.62E-05	0.62
14	S2 WR5	88.29	44.38	4.53E-05	0.58
15	S3 WR5	105.46	45.64	4.66E-05	0.52

References

1. Josy J, Johny MA (2019) Effect of GFRP wrapping on flexural behaviour of reinforced concrete beams, pp 4348–4353
2. Pannirselvam N, Raghunath PN, Suguna K (2008) Strength modeling of reinforced concrete beam with externally bonded fibre reinforcement polymer reinforcement. *Am J Eng Appl Sci* 1(3):192–199. <https://doi.org/10.3844/ajeassp.2008.192.199>
3. D'Antino T, Pellegrino C (2014) Bond between FRP composites and concrete: assessment of design procedures and analytical models. *Compos B Eng* 60:440–456. <https://doi.org/10.1016/j.compositesb.2013.12.075>
4. Biswas S, Anurag J (2019) Fabrication of composite laminates. In: Reinforced polymer composites: processing, characterization and post life cycle assessment, pp 39–53. <https://doi.org/10.1002/9783527820979.ch3>
5. Rasheed HA, Harrison RR, Peterman RJ, Alkhrdaji T (2010) Ductile strengthening using externally bonded and near surface mounted composite systems. *Compos Struct* 92(10):2379–2390. <https://doi.org/10.1016/j.compstruct.2010.03.009>
6. Madotto R, Van Engelen NC, Das S, Russo G, Pauletta M (2021) Shear and flexural strengthening of RC beams using BFRP fabrics. *Eng Struct* 229:111606. <https://doi.org/10.1016/j.engstruct.2020.111606>
7. Saribiyik A, Abodan B, Balci MT (2021) Experimental study on shear strengthening of RC beams with basalt FRP strips using different wrapping methods. *Eng Sci Technol Int J* 24(1):192–204. <https://doi.org/10.1016/j.jestch.2020.06.003>
8. ACI Committee 338, Building code requirements for structural concrete and commentary. American Concrete Institute, Farmington Hills, Michigan
9. ACI Committee 440 (1996) State-of-the-art report on fibre reinforced plastic (FRP) reinforcement for concrete structures. American Concrete Institute, Farmington Hills, Michigan
10. ACI Committee 440.1R-01 (2001) Design and construction of concrete reinforced with FRP bars. American Concrete Institute, Farmington Hills, Michigan
11. Baky HA, Ebead UA, Neale KW (2007) Flexural behaviour of FRP-strengthened reinforced concrete beams. *J Compos Constr ASCE* 11(6):629–639
12. Bonacci JF, Maalej M (2000) Externally bonded fiber-reinforced polymer for rehabilitation of corrosion damaged concrete beams. *ACI Struct J* 97(5):703–711
13. Brena SF, Bramblett RM, Wood SL, Kreger ME (2003) Increasing flexural capacity of reinforced concrete beams using carbon fiber-reinforced polymers composites. *ACI Struct J* 100(1):36–46
14. Choi HT, West JS, Soudki AK (2008) Analysis of the flexural behavior of partially bonded FRP strengthened concrete beams. *J Compos Constr ACSE* 12(4):375–386
15. Kobatake Y, Kimura K, Katsumata H (1993) A retrofitting method for reinforced concrete structures using carbon fiber. In: Nanni A(ed) Fiber-reinforced-plastic (FRP) reinforcement for concrete structures: properties and applications. Elsevier Science Publishers, pp 435–450
16. Nitereka C, Neal KW (1999) Analysis of reinforced concrete beams strengthened in flexure with composite laminates. *Can J Civ Eng* 26:646–654
17. Saadatmanesh H, Ehsani MR (1990) RC beams strengthened with GFRP plates I. *J Struct Eng ASCE* 117:3417–3433

The Behavior of RC Beam with an Opening Filled with the Hollow Square Section Under Static Loading



P. Gokul and L. Sabarigirivasan

1 Introduction

As the urban cities grow and land becomes scarce, ever more rising structures and tall structures spring up. People's expectations of building function are continually evolving, and skyscrapers are allowing the structural function to reach new heights. Pipelines in high-rise buildings are now laid crosswise beneath the beams, occupying 1/6th to 1/5th of the floor height. The opening through the role of the beam arrangement reduces self-weight and allows for a more compact and cost-effective construction. The holes in the beams reduce the building's overall height and self-weight. The presence of a fracture in a beam reduces its strength and increases deflection and cracking behavior. Hollow structural square sections are cold-formed, hot-rolled tubes used in the welded as well as bolted building structures, bridges, and other structures, as well as a range of concepts with multiple. The hollow element at the openings increases load-carrying capacity while reducing the number of plastic hinges at the openings.

Cracks pose significant challenges to the structural integrity of concrete buildings, as they can result from various failure modes such as flexural and shear forces. In order to analyze crack formation and its effects, a plastic damage behavior was employed in utilizing the ABAQUS software to model concrete and embedded reinforcing steel in RC beams [1]. This study focuses on the flexural behavior of steel I-beams with rectangular web openings. To address this issue, advanced nonlinear three-dimensional finite element models (FEM) were developed using ABAQUS. The current research examines the impact response of steel beams with rectangular perforations, considering factors such as the size, depth, number, and reinforcement of the web apertures. Various impact velocities ranging from 2.214 to 7 m/s were investigated to gain

P. Gokul · L. Sabarigirivasan (✉)

Department of Civil Engineering, Faculty of Engineering and Technology, SRM Institute of Science and Technology, Kattankulathur, Tamil Nadu 603203, India
e-mail: sabarigl@srmist.edu.in

comprehensive insights into the flexural effects [2]. To demonstrate maximum resistance, stress–strain, stiffness, strength damage, ductility, energy absorption capacity, but also the behavior of the specimens' fatigue strength under cyclic load, seven rectangular RC beams were poured and improved with outside bonding of CFRP sheets around beam web entrance with different positions. The inclusion of FRP sheets enhanced the highest capacity and maximal displacement for RC beams by roughly 66.67% as well as 77.14%, correspondingly, including the data. The validated finite element model may be used as a numerical basis for parameterized research such as investigating the impacts of hole diameter and bond length [3]. Similarly, the (CFRP) is double the load necessary to produce the first diagonally crack in approaches with $(a/h) = 0.9$, whereas the load required in modeling techniques with $(a/h) = 1.1$ is only completely different [4]. It uses ABAQUS, a generalized finite element program, to computationally evaluate the behavior of a restricted structurally sub-assembly of steel beams featuring web holes to concrete-filled tubular columns under fire load variations. The behavior of this study examines the characteristics of structural sub-assemblies of steel beams including holes in fire scenarios using a complete finite element (FE) analysis. To understand the significance of their effects, four sizes of ruptured steel sections with seven various opening compositions are modeled and analyzed [5]. Steel beam: In numerical and computational investigations, the web size of the steel beam, the average diameter, the strength, and elongation between the concrete floor and the unit organization for WO connectors are all relevant characteristics. The spaces between the apertures were filled with infill concrete for optimal shear strength, and the gives the optimum between group WCO shear interconnections which were found to be 250 mm, while the effective distance between WSO and WRO shear connects was discovered to be 300 mm. Finally, utilizing COVs of 0.032 but also 0.021, the highest tensile resistant of the WCO but also WSO/WRO shear connectors was anticipated and validated [6]. Utilizing the finite element method, the stress-deformation of a deep beam with openings can be calculated. Additionally, a total of seventeen deep beams were simulated under static stress conditions to investigate the effects of opening position, size, and shape, as well as the depth, span, and shear span over depth ratio on the overall influences of opening position, size, and shape. The computational findings were found to be in excellent agreement with the experimental studies in terms of predicting the pattern of stress and displacement. The average shear strength was reduced by 35% when the aperture size was increased from 200 to 250 mm. Deep beams with circular holes deflect less than square perforations and are hence recommended. When the depth was extended from 500 to 550 mm, the deflection was decreased by 78% [7].

In this study, the finite element method was used to investigate the behavior of reinforced concrete beams also with web holes, and the finite element approach was used to determine the evaluation of RC members with and without web holes. Experiments were conducted using the damaged elastic–plastic model. The model assessment has demonstrated a strong level of agreement with experimental data. According to the simulation findings, web apertures that intersect the projected compression components should be disregarded, and the depths of the gaps should not exceed 20% of the overall depth of the beam. In the case of simply supported concrete beams, the

concentration of reinforcement should fall within the range of 0.1–0.2 times the depth of the beam [8]. A computational analysis employing FEA software and a modeling approach for reinforced concrete structures with circular apertures examines the stress behavior of structural members with various types of reinforcement across gaps [9]. This serves as the central theme connecting all aspects of the study. The damaged plasticity model, utilized in the 2010 version of the International Code for the Design of Concrete Structures and in this research, can be employed. Finite element analysis using ABAQUS was conducted to determine the capacity of the concrete beams. The ABAQUS methodology was employed to model the behavior of reinforced concrete (RC) beams in this study. Our stress–strain approach was incorporated into the finite element model, which can be used to validate theoretical results and contribute to laboratory investigations of behavior. The results indicate a close correspondence between the finite element model (FEM) and the actual data in terms of displacement, main reinforcement, flexural strength, concrete compression strain, and fatigue crack patterns [10].

2 Finite Element Modeling

All reinforced concrete equal spacing and closer spacing near the holes the beams filled with hollow square sections would be simulated using Abaqus software, which is a broader terms analytic tool that can handle a wide range of nonlinear partial differential equations. For concrete and reinforcing elements such as various products and pins, a four-node bi-linear solid element (CPS4R), a 2-node normal 2D truss element (T2D2) with inner reinforcement, and an enhanced linear beam element for outside bars were used, respectively.

2.1 Details of Test Specimens

Every one of the beam groups is 2500 mm in length, 200 mm wide, and 250 mm deep. The concrete cover is 25 mm thick. They reinforced both the compression and tension zones. 2 nos. 12 mm diameter bar and 8 mm diameter bar in shear reinforcement at 150 mm center to center spacing. The mild steel hollow square section has a 200 mm opening length and a thickness of 5 mm. The hollow square sections utilized in this project were $150 \times 150 \times 5$ and $125 \times 125 \times 5$. For each group of beams, the openings are located at the lengths of $L/6$, $L/5$, $L/4$, $L/3$, and $L/2$ m. 125×125 mm and 150×150 mm are the sizes of the openings. The hollow square section was 5 mm thick. Table 1 shows the material properties of young modulus, Poisson's ratio, density, yield, and tensile strength. Equally spaced stirrups and closer spacing stirrups at the opening were the two types of concepts studied.

Nine groups of 41 nos reinforced concrete with and without opening beams were studied. The nine group beam details were presented in Tables 2 and 3. There is one

Table 1 Properties of material

Material	Elastic modulus N/mm ²	Unit weight N/mm ²	The Poisson coefficient	Yield strength N/mm ²	Tensile strength N/mm ²
Concrete	16,000	2.3×10^{-8}	0.18	31	3.5
Steel bar	2.1×10^5	7.85×10^{-9}	0.3	250	480
Hollow square section	2.1×10^5	7.85×10^{-9}	0.3	210	310

conventional beam in Group A. In groups B, C, D, and E, there were five pairs of equally spaced stirrup beams demonstrated in Table 2. The opening size of groups B and C was 125×125 mm, and they had 5 nos of beams with a hollow square section at the opening and 5 nos of beams without a hollow square section at the opening. The opening size of groups D and E was 150×150 mm with 10 nos of hollow square section at the opening and without hollow square section at the opening of beams. Closer spaced stirrups the opening with a hollow square section at the opening and without a hollow square section at the opening is located in the F, G, H, and I group. Table 3 gives the four sets of closer-spaced stirrups (F, G, H, and I) at the opening beam details. The distance between closer stirrups was 50 mm. The mesh sensitivity is depicted in (Fig. 1).

2.2 Interaction, Meshing, and Boundary Condition

This study used three interaction approaches. Surface-to-surface contact, embedded region, and tie. To analyze the concrete-reinforcement bar contact, a full connection was assumed. Figure 2 shows an extensive numerical reinforcement model. Tie interaction connected shear and major reinforcement. Joining the hollow square portion to the concrete beam using surface-to-surface contact. Surface-to-surface friction is 0.25. Embedded regions joined reinforcement and concrete. ABAQUS lets you pick automated or fixed analysis and step increment for model execution. ABAQUS analysis methods have multiple steps. The analysis depends on loading conditions and reactions. Static analysis, automatic-step increment, and given model are implemented. The increment size is 0.01.

The mesh sensitivity study, as depicted in Fig. 1, revealed that there was no notable sensitivity to mesh size when the components were larger than the specified size. Additionally, the test results were deemed satisfactory. Consequently, a mesh size of 35 mm, with a detailed percentage of 1, was selected for the investigations to optimize computational speed. Figure 3 illustrates the mesh model operation. Concrete, reinforcing, and hollow square section mesh were 35 mm. $U_x = U_y = U_z = 0$ fixed the 100 mm left and right beam ends. Two-point load at $L/3$ support. 10 mm y-axis displacement imposed the load.

Table 2 Results for equal spaced stirrup beams

Size	Group	Beam name	Location of the opening	No of the opening	Load (kN)	Displacement (mm)	
125 × 125 mm	A	Control beam	–	–	155.768	12.817	
	B	BS1	L/2	1	141.667	12.232	
		BS2	L/3	2	134.634	11.925	
		BS3	L/4	3	132.851	11.735	
		BS4	L/5	4	141.212	12	
		BS5	L/6	5	138.152	11.892	
	C	CS1	L/2	1	140.5	12.707	
		CS2	L/3	2	134.634	11.925	
		CS3	L/4	3	119.767	10.9	
		CS4	L/5	4	125.512	10.981	
		CS5	L/6	5	128.306	11.407	
	150 × 150 mm	D	DS1	L/2	1	129.507	12.709
			DS2	L/3	2	136.306	11.844
			DS3	L/4	3	130.209	11.104
			DS4	L/5	4	141.4	11.718
DS5			L/6	5	116.162	11.417	
E		ES1	L/2	1	129.014	12.427	
		ES2	L/3	2	104.891	11.575	
		ES3	L/4	3	75.351	10.198	
		ES4	L/5	4	77.6	9.414	
		ES5	L/6	5	74.877	10.623	

3 Results and Discussion

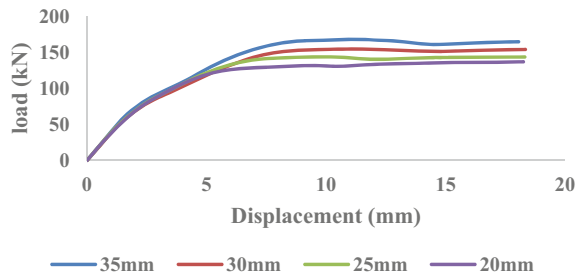
All beams in the investigation had their applied loads securely set at 100 mm from the support end. Beams with square apertures of 125 × 125 mm and 150 × 150 mm were investigated to determine their maximum displacement and ultimate load. These measurements were collected at various distances from the support end, specifically at L/2, L/3, L/4, L/5, and L/6, where L is the beam span length. In addition, alternative square entrance layouts were examined. Static analysis is used for all 41 beams in FEM analysis. The displacement diagram and compressive stress distribution diagram of one of the examined beams are shown in Figs. 4 and 5.

The conventional beam had the maximum ultimate load of all the beams with and without openings, with a value of 155.76 kN. The maximum ultimate load of equal spacing stirrups beams of 125 × 125 and 150 × 150 mm square openings with and without the hollow square section of the opening was recorded from the BS1 beam, which has a value of 141.66 kN. The largest ultimate load of closer spacing

Table 3 Results for closed spaced stirrup beams

Size	Group	Beam name	Location of the opening	No of the opening	Load (kN)	Displacement (mm)
125 × 125 mm	F	FS1	L/2	1	141.435	12.421
		FS2	L/3	2	137.306	11.974
		FS3	L/4	3	137.905	12.332
		FS4	L/5	4	141.842	12.03
		FS5	L/6	5	138.532	12.012
	G	GS1	L/2	1	140.545	12.585
		GS2	L/3	2	134.856	11.934
		GS3	L/4	3	132.296	11.952
		GS4	L/5	4	132.686	11.297
		GS5	L/6	5	129.543	11.496
150 × 150 mm	H	HS1	L/2	1	129.407	12.702
		HS2	L/3	2	136.303	11.848
		HS3	L/4	3	130.443	11.167
		HS4	L/5	4	142.671	11.784
		HS5	L/6	5	117.691	11.439
	I	IS1	L/2	1	129.201	12.468
		IS2	L/3	2	105.186	11.567
		IS3	L/4	3	76.741	10.204
		IS4	L/5	4	87.016	10.272
		IS5	L/6	5	78.232	10.66

Fig. 1 Variations of mesh sensitivity



stirrups near the opening beams of 125 × 125 and 150 × 150 mm square openings with and without the hollow square section of the opening was obtained from the HS4 beam, with a value of 142.671 kN. Figure 6 presents a load vs displacement graph of equal spacing stirrups of L/2 location of 125 × 125 and 150 × 150 mm opening beams with and without hollow square sections, as well as conventional beam comparative results. In equal spacing stirrups of groups B, C, D, and E, the highest ultimate load was determined to be 141.66 kN of BS1 beam. As a result, the

Fig. 2 Interaction diagram

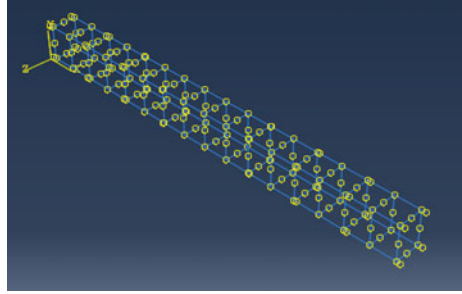


Fig. 3 Meshing

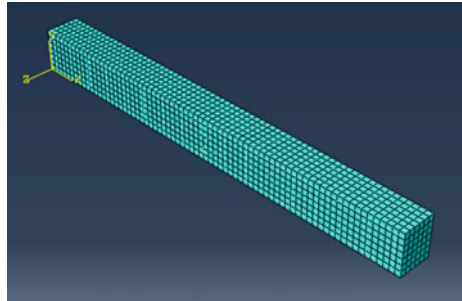


Fig. 4 Displacement diagram

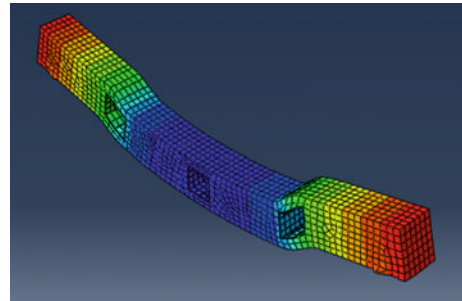


Fig. 5 Stress distribution diagram

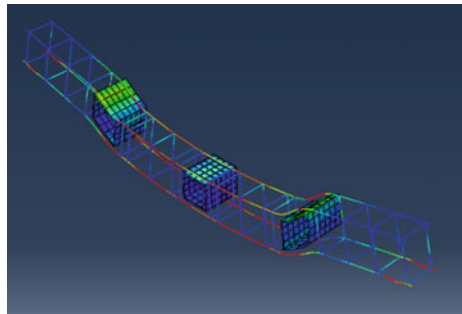


Fig. 6 Equal spacing stirrups of L/2 opening

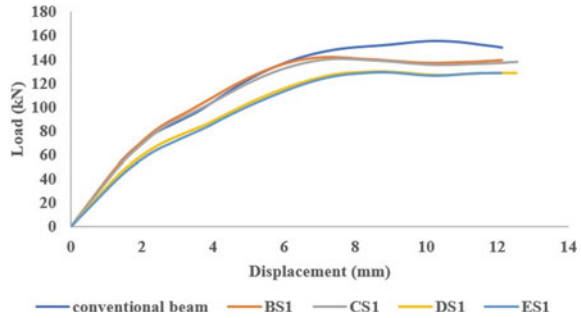
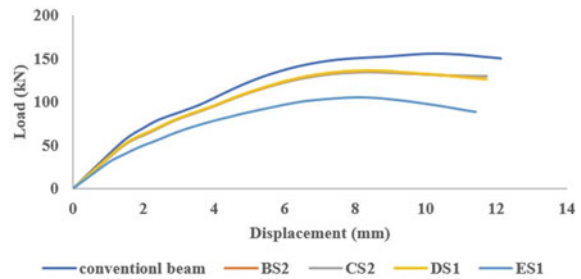


Fig. 7 Equal spacing stirrups of L/3 opening



load was raised by 0.83% for the 125 × 125 mm L/2 opening and 0.39% for the 150 × 150 mm L/2 opening by providing the hollow square section at the opening. Aload vs displacement graph of equal spacing stirrups of L/3 location of 125 × 125 and 150 × 150 mm opening beams with hollow square section and without hollow square section and conventional beam comparison results was shown in Fig. 7.

The maximum ultimate load was found in equal spacing stirrups of groups B, C, D, and E which is 141.66 kN of BS2 beam. Figure 8 shows a load versus displacement graph of equal spacing stirrups of L/4 location of 125 × 125 and 150 × 150 mm opening beams with and without hollow square sections, as well as conventional beam comparison findings. The highest ultimate load of the BS3 beam was determined to be 132.851 kN in equal spacing stirrups of groups B, C, D, and E. As a result, the load was raised by 9.84% for the 125 × 125 mm L/4 opening and 42.13% for the 150 × 150 mm L/4 opening by providing the hollow square section at the opening. Figure 9 demonstrates a load versus displacement graph of equal spacing stirrups of L/5 position of 125 × 125 and 150 × 150 mm opening beams with and without hollow square sections, as well as conventional beam comparison data. In equal spacing stirrups of groups B, C, D, and E, the maximum ultimate load was determined to be 141.4 kN of DS4 beam.

As a result, the load was raised by 11.17% for the 125 × 125 mm L/5 opening and 45.12% for the 150 × 150 mm L/5 opening by introducing the hollow square section at the opening [11, 12]. Figure 10 shows a load versus displacement graph of equal spacing stirrups of L/6 position of 125 × 125 and 150 × 150 mm opening beams

Fig. 8 Equal spacing stirrups of L/4 opening

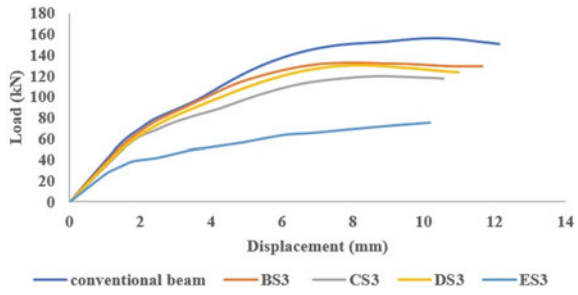
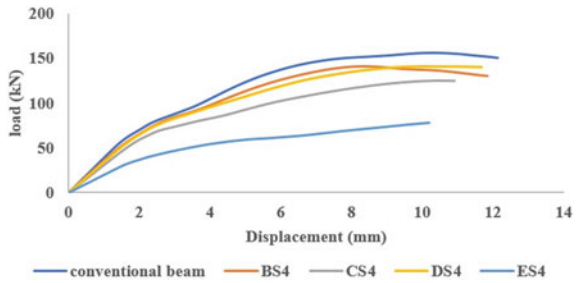


Fig. 9 Equal spacing stirrups of L/5 opening



with and without hollow square sections, as well as conventional beam comparative findings [13]. In equal spacing stirrups of groups B, C, D, and E, the highest ultimate load was determined to be 138.15 kN of BS4 beam. As a result, the load was raised by 7.12% for the 125×125 mm L/6 opening and 35.54% for the 150×150 mm L/6 opening by installing the hollow square section at the opening. Figure 11 presents a load vs displacement graph of closer spacing stirrups near the openings of L/2 location of 125×125 and 150×150 mm opening beams with and without hollow square sections, as well as conventional beam comparative results. In equal spacing stirrups of groups F, G, H, and I, the highest ultimate load was determined to be 141.435 kN of FS1 beam. As a result, the load was raised by 0.62% for the 125×125 mm L/2 opening and 0.2% for the 150×150 mm L/2 opening by providing the hollow square section at the opening. A load vs displacement graph of closer spacing stirrups near the opening of L/3 location of 125×125 and 150×150 mm opening beams with hollow square section and without hollow square section and conventional beam comparison results was shown in Fig. 12. The maximum ultimate load found in closer spacing stirrups of groups F, G, H, and I is 137.306 kN of FS2 beam. Figure 13 shows a load versus displacement graph of closer spacing stirrups near the opening of L/4 location of 125×125 and 150×150 mm opening beams with and without hollow square sections, as well as conventional beam comparison findings [14]. The highest ultimate load of the FS3 beam was determined to be 137.905 kN in equal spacing stirrups of groups F, G, H, and I. As a result, the load was raised by 3.64% for the 125×125 mm L/4 opening and 41.16% for the 150×150 mm L/4 opening by providing the hollow square section at the opening. Figure 14

demonstrates a load versus displacement graph of closer spacing stirrups near the opening of L/5 position of 125 × 125 and 150 × 150 mm opening beams with and without hollow square sections, as well as conventional beam comparison data.

In closer spacing stirrups of groups F, G, H, and I, the maximum ultimate load was determined to be 142.671 kN of HS4 beam. As a result, the load was raised by 6.38% for the 125 × 125 mm L/5 opening and 39% for the 150 × 150 mm L/5 opening by introducing the hollow square section at the opening. Figure 15 shows a load versus displacement graph of closer spacing stirrups near the opening of L/6 position of 125 × 125 and 150 × 150 mm opening beams with and without hollow square sections, as well as conventional beam comparative findings. In closer spacing stirrups of groups F, G, H, and I, the highest ultimate load was determined to be 138.532 kN

Fig. 10 Equal spacing stirrups of L/6 opening

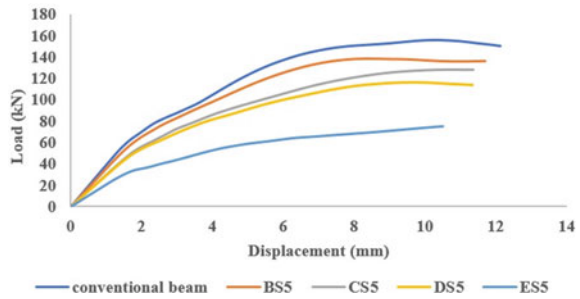


Fig. 11 Closer spacing stirrups of L/2 opening

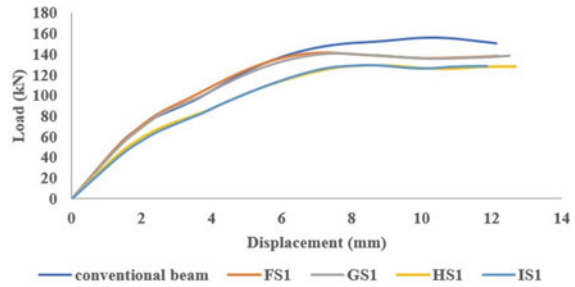


Fig. 12 Closer spacing stirrups of L/3 opening

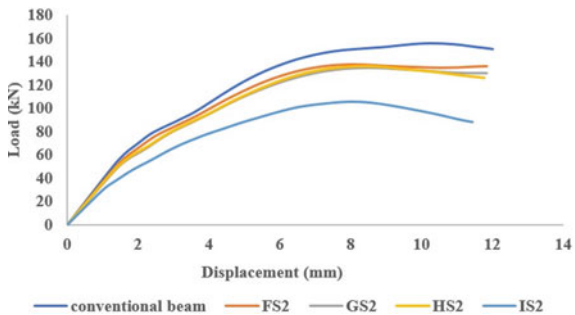


Fig. 13 Closer spacing stirrups of L/4 opening

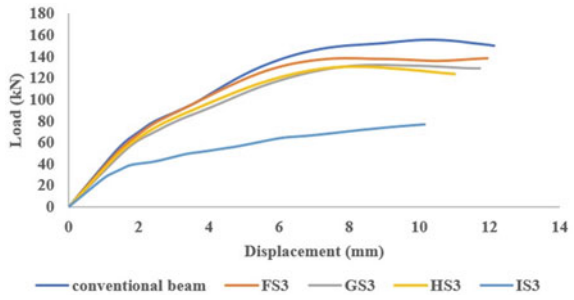


Fig. 14 Closer spacing stirrups of L/5 opening

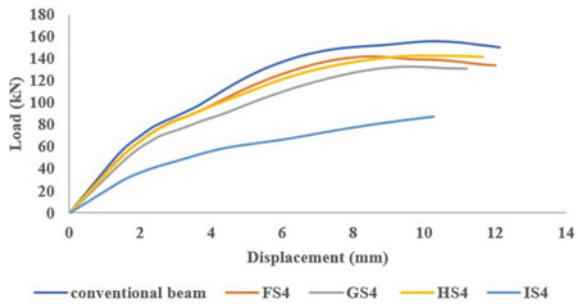
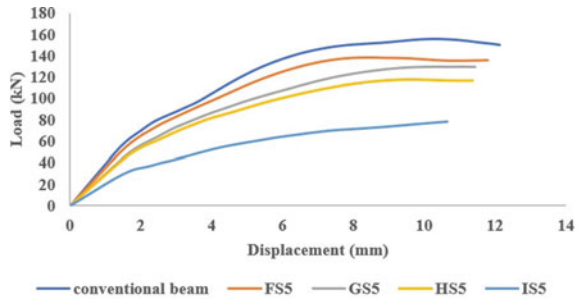


Fig. 15 Closer spacing stirrups of L/6 opening



of FS5 beam. As a result, the load was raised by 6.52% for the 125 × 125 mm L/6 opening and 33.34% for the 150 × 150 mm L/6 opening by installing the hollow square section at the opening.

4 Conclusion

The study includes a numerical nonlinear FE analysis of 41 RC beams with and without openings fitted with a hollow square section that has been tested. For that purpose, the evaluation of the specimen is confirmed until it achieves a satisfactory

degree of accuracy via the use of a required FE modeling technique and suitably exact material modes.

- This study compared finite element analysis of beams with and without holes. Different beam diameters and locations were analyzed. The typical beam analytical approach yielded maximum displacement and ultimate load of 12.817 mm and 155.768 kN, respectively.
- Finite element analysis of equal spacing stirrups and closer spacing stirrups B, C, D, E, F, G, H, I group of 40 reinforced beams with the square section as well as without square section opening results showed that the HS4 beam has the highest ultimate load-bearing capacity. The ultimate load on the HS4 beam is 142.671 kN.
- By providing the opening with a square hollow section on the beams, plastic hinges and shear cracks may be minimized, and the ultimate load can be enhanced.
- The resilience of hollow square section beams was nearly identical to that of normal concrete beams.
- The load-carrying capacity of the beam may be improved by increasing the thickness of the hollow square section and placing closer stirrups at the opening and shear region of the beam.

References

1. Al Hasani S, Nasrellah HA, Abdulraeg AA (2021) Numerical study of reinforced concrete beam by using ABAQUS software. 4(3):733–741, ISSN: 2613-7305. <https://doi.org/10.15157/IJTIS.2021.4.3.733-741>
2. Al-Rifaie A, Al-Husainy AS, Al-Mansoori T, Shubbar A (2021) Flexural impact resistance of steel beams with rectangular web openings. Case Stud Constr Mater 14:e00509. <https://doi.org/10.1016/j.cscm.2021.e00509>
3. Salih R, Zhou F, Abbas N, Mastoi AK (2020) Experimental investigation of reinforced concrete beam with openings strengthened using FRP sheets under cyclic load. Materials 13:3127. <https://doi.org/10.3390/ma13143127>
4. Jasim WA, Abu Tahnat YB, Halahla AM (2020) Behavior of reinforced concrete deep beam with web openings strengthened with (CFRP) sheet. Structures 26:785–800. <https://doi.org/10.1016/j.istruc.2020.05.003>
5. Elswaf SA, Hassan MM (2018) Behaviour of structural sub-assemblies of steel beams with openings in fire conditions. J Constr Steel Res 148:627–638. <https://doi.org/10.1016/j.jcsr.2018.06.023>
6. Hosseinpour E, Baharoma S, Badaruzzaman WHW, Al Zand AW (2018) Push-out test on the web opening shear connector for a slim-floor steel beam: Experimental and analytical study. Eng Struct 163:137–152. <https://doi.org/10.1016/j.engstruct.2018.02.047>
7. Senthil K, Gupta A, Singh SP (2018) Computation of stress-deformation of deep beam with openings using finite element method. Adv Concr Constr 6(3):245–268. <https://doi.org/10.12989/acc.2018.6.3.245>
8. Sabarigirivasan L, Umamaheswari N (2023) Temperature gradient impacts on concrete-encased steel I-girder: an ANN optimization approach. Asian J Civ Eng. <https://doi.org/10.1007/s42107-023-00699-x>
9. Mohamed AR, Shoukry MS, Saeed JM (2014) Prediction of the behavior of reinforced concrete deep beams with web openings using the finite element method. Alexandria Eng J 53:329–339. <https://doi.org/10.1016/j.aej.2014.03.001>

10. Han X, Liu Z (2014) Numerical simulation on the form of reinforcement of reinforced concrete beam with openings. *Appl Mech Mater* 444–445:884–888. <https://doi.org/10.4028/www.scientific.net/AMM.444-445.884>
11. Sinae H, Shariati M, Hosein Abna A, Aghaei M, Shariati A (2012) Evaluation of reinforced concrete beam behaviour using finite element analysis by ABAQUS. *Sci Res Essays* 7(21):2002–2009. <https://doi.org/10.5897/SRE11.1393>
12. Gokul P, Sabarigirivasan L (2022) Finite element analysis of RC beams with and without openings. *Mater Today Proc* 68:2541–2550
13. Bonopera M, Chang KC, Chen CC, Sung YC, Tullini N (2019) Experimental study on the fundamental frequency of prestressed concrete bridge beams with parabolic unbonded tendons. *J Sound Vib* 455:150–160
14. Lakshmi Narayanan S, Nambiappan U (2023) Long-term impacts of temperature gradients on a concrete-encased steel I-girder experiment—field-monitored data. *Buildings* 13(3):780. <https://doi.org/10.3390/buildings13030780>

Application of Data Mining Techniques and Hedonic Pricing Methods to Determine the Real Estate Land Prices in the Chengalpattu District



K. Mahima Christin, M. B. Sridhar, B. Divya, and R. Sathyanathan

1 Introduction

Real estate is an essential instrument for both short- and long-term investments. It influences the economic space, project design, finance regulation, and taxes. Experts with proper knowledge carry out real estate evaluation processes. Housing, as a component of public–private affluence, explains a country’s unprecedented increase in wealth relative to gross domestic product. In industrialized nations, the real estate industry contributes considerably toward economic output and the state’s tax revenue. Thus, property prices are essential not just to real estate owners but also to legislators, directors, bank executives, architects, and estate agents; in brief, the general citizens [1, 2]. Economic shifts significantly impact the housing sector [3]. Land and property transactions are critical to the government’s revenue generation and financial institution banking policies, especially in emerging nations with rising urbanization and dependence on land-based financing. Before making prudent buy or rental choices, investors and property brokers should do a market study considering the various attributes affecting the price [4]. Due to the variations in the property’s sales price, the uniqueness and heterogeneity of the relevant parties that engage in the housing market might have varying contributions [5].

Land is a unique commodity since it cannot be transported from one location to another. Having sufficient knowledge of the real estate evaluation field is critical. A precise estimate of a property’s price is essential for buyers, sellers, and those interested in investing in real estate. Forecasting the future value of real estate is challenging due to the multifaceted influence of climatic, geographical, and physical characteristics. An objective perspective and future prediction abilities are also

K. Mahima Christin · M. B. Sridhar (✉) · B. Divya · R. Sathyanathan
Department of Civil Engineering, Faculty of Engineering and Technology, SRM Institute of Science and Technology, Kattankulathur, Tamil Nadu 603203, India
e-mail: sridharb@srmist.edu.in

crucial [6]. The method for selecting and using relevant factors for projecting real estate sales prices remains uncertain [7].

Consequently, a precise property price prediction model is essential [8]. Notably, the model must comprehend and adapt the relation between house prices and their potential individual factors [9]. The most significant issues in valuation are the unknown characteristics that impact the value and the inadequacy of classical valuation methods [10]. A specific real estate valuation method must address all technical, economic, and legal considerations, as the accuracy of property value assessment is critical to all parties involved. As a result, there has been a move toward a sophisticated valuation approach compared to older methods, which tend to be more accurate and dependable [11]. The hedonic price method (HPM) is a sophisticated estimation system extensively employed theoretically and practically for many years [2]. It adequately reflects the linear connection between property values and characteristics [12]. Historically, the fundamental objective of most hedonic analyses has been to interpret the computed coefficients as implicit marginal trait prices [13]. While other analytical tools were utilized in the property price evaluation, real estate researchers often adopt HPM [14]. HPM is used to analyze house price transaction behavior data to determine the land values of various estates.

As a quasi-approach to information extraction, data mining methods identify the connection between various records through existing data [15]. It is the method of extracting usable information patterns from unstructured abstracts. The data mining methods also help in information discovery and observation [16]. The capacity of data mining approaches in real estate appraisal to address mixed issues is the method's most significant advantage over other methods [6]. In this study, a hybrid of two data mining approaches, classification and regression trees (C&RT) and Chi-square automatic interaction detection (CHAID) [17], is used to identify the factors affecting the price of the land. The variables impacting the land price for residential use in the context of the Chengalpattu division of land pricing considerations are considered in this study. The decision tree represents the relationship between the specified components and land price. The SPSS program was utilized to determine data mining techniques and HPM.

In India, real estate prices are determined according to the buyer's preferences. Buying a property in India is skewed since there is no standard way to determine the property's selling price. A typical income property market appraisal is based on a collection of existing economic circumstances and movements in the market that are often considered reasonably steady in the years ahead [1, 18]. This study aims to determine land prices for consumers in the Chengalpattu district. Recent years have seen an enormous surge in land prices in this area. Since then, the real estate industry in the Chengalpattu district has developed in lockstep with economic growth. This article offers substantial research on the link between real estate qualities and prices.

The HPM approach has been widely utilized for property evaluation in various property investment sectors across the globe to quantify the extent of the impact of the variables on the property's worth. The property price variables have been studied using data mining techniques. It uses the decision tree technique, which incorporates the CHAID, C&RT, and other elements that influence the price of land.

The quantitative approach employed well-known statistical tools of correlation and regression. ANOVA was utilized to establish the significance and correctness of the model developed after the regression study.

2 Data Source and Methodology

2.1 Study Area

This study was conducted in Chengalpattu district, located on the north-east coast of Tamil Nadu, adjacent to the Bay of Bengal. The Chengalpattu district was chosen as the research region for three key reasons. Before this research, there was no rigorous valuation analysis of property values in this region. Additionally, there has been a land price boom in some areas of the district due to increased infrastructure facilities. Finally, residential property procurement funding has become simpler throughout the nation. In residential finance, market-based instruments such as mortgage loans and savings products are often supported with various state subsidies to increase the district's rental market and affordability. Therefore, the housing sector in Chengalpattu has gained dynamism.

2.2 Methodology

The collection of land prices was done in the Chengalpattu district with the use of online websites and onsite visits. Twenty variables were collected during the literature survey, affecting the district's land prices. For twenty factors, nine hundred eighty two data for land parcels were gathered and analyzed using the hedonic pricing approach (HPM). The essential factors affecting land prices were determined using data mining techniques, CHAID (Chi-square automatic interaction detector) and C&RT (Correlation and regression technique). CHAID is used to estimate variables using the best-class method. CHAID is a method for analyzing the crucial variables that significantly affect land prices. The C&RT approach creates the classification model when the relying variable is changed, and the predictor is continuous. It is important to note that the recommended classification tree method can be used for inspections or enhancement to forecast accuracy in various predictive scenarios, provided a sufficient training sample is available [19]. Regression has been done for the essential factors from the CHAID and C&RT techniques.

The crucial factors identified by CHAID and C&RT were combined. The combined essential factors were further utilized for correlation and regression analysis. Correlation coefficients are used to demonstrate an approximate linear connection between independent variables. Correlation and regression are two methods for

examining the link between variables. This method may be used to undertake a quantitative or qualitative association study. It measures the linear relationship between two random factors. Data and sample means may be used to calculate a linear correlation coefficient [20]. Finally, the hedonic price model (HPM) was created. According to the hedonic theory, pricing requires an exact valuation of the offering's characteristics [13]. The influence of each characteristic on pricing is referred to as its hedonic price. The hedonic pricing model aims to describe the accuracy of diverse market prices in terms of model quantity changes. The accuracy of the HPM prediction was determined by comparing the predicted land values with the actual values.

3 Results and Discussion

3.1 Factors Identified

SPSS was used to analyze the 20 parameters chosen based on a literature review and expert interviews. Price is the sole dependent variable, with the other 20 values being independent. The effect of several variables on the land market's activity and pricing was determined. The following criteria were investigated to ascertain their impact on land market activity and price: Distances from the land to the paved road, the nearest town, railway, highway, bus stop, hospital, commercial capabilities, industries, agriculture, forest, MRTS, places of worship, central business district, universities, park, view of mountains, availability of garden, whether the land was previously part of a gated community or not, approval status, and orientation of the land.

The twenty factors and the dependent variable of land price are given in Table 1.

3.2 Data Mining

The property price elements have been studied using data mining techniques. The primary benefit of data mining techniques in land price appraisal is their capacity to tackle various challenges. An in-depth examination of efficient data mining methods has the potential to expedite data reduction and interpretation procedures and close existing knowledge gaps. Herein, the predictive data mining techniques CHAID and C&RT were used.

The CHAID method is extensively utilized for ongoing and discrete inputs. CHAID can tolerate nonmonotonic connections between the dependent and predictor variables. CHAID was used to identify the significant elements affecting the land unit price, represented in Fig. 1. According to CHAID, the following characteristics were effective: price (F1) being dependent, and the independent variables are distance to the central business district (F15), distance to universities (F16), distance to the bus

Table 1 Factors affecting the land price

Factors	ID	Description
Price/m ²	F ₁	Price of the land parcel per square-meter
Paved road	F ₂	Distance to the paved roads
Nearest town	F ₃	Distance to the nearest town
Railway	F ₄	Distance to railway station
Highway	F ₅	Distance to national highway
Bus stop	F ₆	Distance to the bus stop
Hospital	F ₇	Distance to hospital or clinic
Commercial amenities	F ₈	Distance to commercial abilities like shopping malls, markets, and banks
Industries	F ₉	Distance to industries or factories
Agriculture	F ₁₀	Proximity to agriculture
Forest	F ₁₁	Proximity to forest
MRTS	F ₁₂	Distance to nearest metro station
Place of worship	F ₁₃	Distance to temples, churches, mosques, and monasteries
Orientation of land	F ₁₄	Orientation of land (8 categories: North = 1, North-East = 2, North-West = 8)
Central business district	F ₁₅	Distance to central business district
Universities	F ₁₆	Distance to universities or institutions
Park	F ₁₇	Proximity to parks
Mountains	F ₁₈	Proximity to mountains
Garden	F ₁₉	Availability of garden (2 categories: Yes = 1, No = 2)
Gated community	F ₂₀	Availability of gated community (2 categories: Yes = 1, No = 2)
Approval	F ₂₁	Land approval (3 categories: 1 = Chennai Metropolitan Development Authority (CMDA), 2 = Directorate of Town and Country Planning (DTCP), 3 = Not Approved)

stop (F₆), distance to the highway (F₇), distance to the hospital (F₁₈), distance to the mountain (F₁₈), distance to industries (F₉), and distance to commercial facilities (F₈).

The C&RT approach has various benefits, including handling missing data using any mix of discrete/continuous characteristics and making the variable selection. C&RT determined that the factors distance to the CBD (F₁₅), distance to commercial facilities (F₈), distance to MRTS (F₁₂), and distance to universities (F₁₆) were impacting the price of the land (F₁). The C&RT results are depicted in Fig. 2.

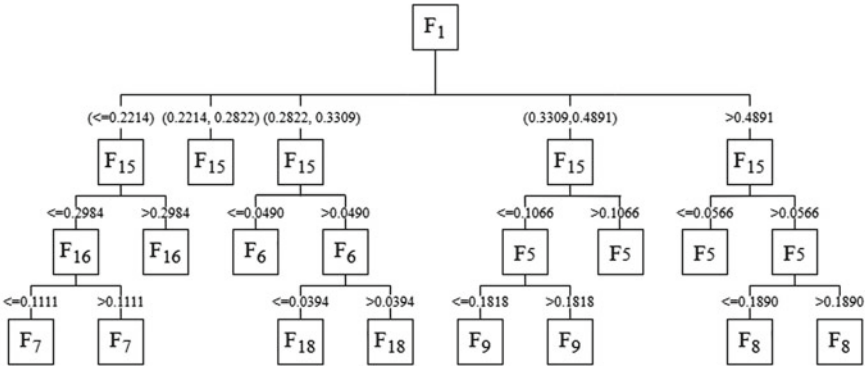


Fig. 1 CHAID

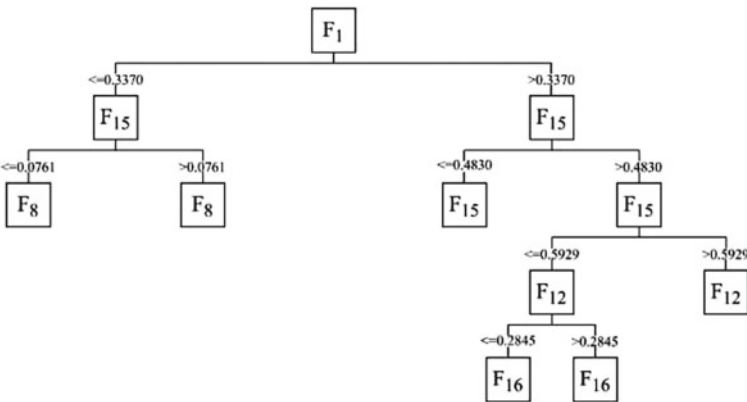


Fig. 2 C&RT

3.3 Correlation

The Pearson correlation coefficient determines the statistically significant linear relationship between the variables. When a change in one variable’s value influences another variable’s value, the variables are correlated. Cohen’s frequently used criteria consider a correlation of $r = 0.1$ to be minor, $r = 0.3$ to be fair, and $r = 0.5$ to be high. A correlation value between 0 and 1 (i.e., positive value) indicates a perfect positive correlation and that both variables tend to rise in tandem. 0 denotes no correlation, implying that the variables have no relationship. A correlation value between 0 and -1 (i.e., a negative number) indicates a complete negative correlation in which one variable increases while the other falls [21]. Table 2 gives the correlation values for the independent variables. The negative value, in this case, refers to a decrease in the parameter price. For example, the distance to a central business district’s Pearson’s

Table 2 Correlation applied to variables

Variable	Pearson’s correlation	Significance
Price/m ²	1	–
Paved road	– 0.008	0.797
Nearest town	– 0.182	0.000
Railway	– 0.003	0.927
Highway	– 0.039	0.220
Bus stop	– 0.182	0.000
Hospital	– 0.296	0.000
Commercial abilities	– 0.310	0.000
Industries	– 0.230	0.000
Agriculture	0.315	0.000
Forest	0.225	0.000
MRTS	– 0.542	0.000
Place of worship	0.113	0.000
Orientation of land	– 0.010	0.755
Central business district	– 0.601	0.000
Universities	– 0.221	0.000
Park	– 0.088	0.006
Mountains	0.034	0.289
Garden	– 0.049	0.126
Gated community	– 0.014	0.647
Approval	– 0.265	0.000

correlation is – 0.601, which means there is a respective decrease in the price for the increase in the distance.

Many present modeling techniques are built on the foundation of linear regression. When the information is faint, the regression model is often an excellent estimate of the actual coefficient of determination [22]. The R value of the regression was 0.69 which means the price is affected by 69% of the variables. The R square reveals how much of the total variance in the dependent variable (costs) can be explained by the independent variables. It demonstrates that the independent factors account for 43% of the total variation. The standard error of the estimates is 1242.81.

3.4 Hedonic Price Model

After deciding on the variables to include in the regression model, the regression analysis was considered to create the HPM. Hedonic pricing is a strategy for estimating the advantages of environmental amenities that affect land prices on the open market. The hedonic pricing model disintegrates the studied item into several

component qualities and uses a regression model to derive the coefficients of the individual variables [23]. By regressing the sale price on specific attributes, the effect of each variable on price is distinguished [24]. Thus, the price will reflect the worth of a collection of characteristics that consumers consider relevant when purchasing. Running a linear regression model on the standardized version of the variables yields standardized coefficients. If all other predictor variables are consistently associated, unstandardized coefficients indicate the degree to which a response variable varies with a predictor variable. For every one-unit increase in the distance of the land from the highway, there will be a consequent decrease in 0.032 units of price. These tests indicate if the slope coefficient found in a particular sample represents a genuine link between two variables [25]. Unstandardized coefficients are derived by running a regression model on observed variables in their primary sample, i.e., in the same units as the dataset used to train the model. In this case, the unstandardized coefficient B assists in relating the individual values when determining the expected value of the land. The standardized coefficients are normalized to compare the coefficients' magnitude and which has the more significant influence. Table 3 presents the regression and significance of each variable.

The significance test can be carried out by analysis of variance (ANOVA). It is used to examine the changes in the overall average values of the dependent variable caused by the impact of the regulated independent variables after accounting for the effects of the unregulated independent variables. The F ratio test has a value of 83 with a significance of 0.000. Higher the F value, the higher the variation between samples. In the Hedonic function, the property price (P_p) can be estimated using the independent variables and the coefficients of the variables from the regression. Their variances are derived based on forecasting models for the derivatives of the market value and the supply function.

Table 3 Regression analysis

Attributes	Unstandardized coefficients		Standardized coefficients	Sig.
	B	Std. error	Beta	
(Constant)	5389.752	232.590		0.000
Bus stand	246.683	44.872	0.158	0.000
Distance to hospital	- 210.297	20.431	- 0.293	0.000
Distance to commercial amenities	- 76.393	34.144	- 0.065	0.025
Distance to industry	- 5.820	25.956	- 0.008	0.823
Proximity to MRTS	- 32.403	6.891	- 0.283	0.000
Distance from the central business district	- 38.092	6.115	- 0.330	0.000
Distance to universities	- 39.542	14.923	- 0.075	0.008
View of mountains	- 29.050	13.557	- 0.063	0.032

Table 4 Regression applied to variables

Plot no.	Actual	Predicted	Accuracy
Land 1	2400	2149	89.54
Land 2	3100	2541	81.97
Land 3	2600	3472	66.46
Land 4	2900	3154	91.24
Land 5	2850	2483	87.12
Land 6	2100	2454	83.14
Land 7	4250	3524	82.92
Land 8	3600	2784	77.33
Land 9	2900	2458	84.76
Land 10	2700	3218	80.81

The price prediction is carried out for a land parcel not included in the model development. The price and land data for the required characteristics are collected. The predicted land prices are represented in Table 4. The model was able to predict with an accuracy of 83%.

4 Conclusion

Using data mining techniques, the research attempted to explore the influence of housing characteristics on property value. The study was conducted in the Chengalpattu area, and the factors were selected from expert interviews. The data were collected for the land price and the factors. This research was conducted to evaluate the association between land prices and factors. Additionally, the area’s topographical and structural factors were considered. One thousand data were collected for various parameters with the help of online websites and offline site visits. Data were collected for 21 parameters. CHAID and C&RT algorithms have been utilized in data mining. When the model’s effectiveness was reviewed, it was determined that both methods’ estimated outputs could be employed. The most important parameters were collected. Using regression analysis is to determine the independent variables and their impact on existing market price. Finally, ANOVA was done to test the significance of the study. At last, hedonic pricing model was created, and the land price was predicted using the model. The model produced an accuracy of around 80%. The larger sample of land value in different ranges would affect the model’s accuracy.

References

1. Schulz R, Werwatz A (2004) A state space model for berlin house prices: estimation and economic interpretation. *J Real Estate Finance Econ* 28:37–57
2. Selim H (2009) Determinants of house prices in Turkey: Hedonic regression versus artificial neural network. *Exp Syst Appl* 36(2 PART 2):2843–52
3. Yavuz Ozalp A, Akinci H (2017) The use of hedonic pricing method to determine the parameters affecting residential real estate prices. *Arab J Geosci* 1:10(24)
4. Sirmans GS, Macpherson DA, Zietz EN (2005) The composition of hedonic pricing models. *J Real Estate Lit* 13:3–43
5. Abidoye RB, Chan APC (2017) Critical review of hedonic pricing model application in property price appraisal: a case of Nigeria. *Int J Sustain Built Environ* 6:250–9
6. Ersoz F, Ersoz T, Soydan M (2018) Research on factors affecting real estate values by data mining. *Baltic J Real Estate Econ Constr Manage* 6(1):220–239
7. Bin O (2004) A prediction comparison of housing sales prices by parametric versus semi-parametric regressions. *J Hous Econ* 13(1):68–84
8. Hu S, Cheng Q, Wang L, Xie S (2012) Multifractal characterization of urban residential land price in space and time. *Appl Geogr* 34:161–170
9. Zhang P, Hu S, Li W, Zhang C, Yang S, Qu S (2021) Modeling fine-scale residential land price distribution: an experimental study using open data and machine learning. *Appl Geogr* 1:129
10. Yalpir S, Sisman S, Akar AU, Unel FB (2018) Feature selection applications and model validation for mass real estate valuation systems. *Land Use Policy* 1:108
11. Gilbertson PricewaterhouseCoopers, Preston J, LaSalle JL. Practice briefing: a vision for valuation [Internet]. Available from: www.emeraldinsight.com/researchregister
12. Abidoye RB, Chan APC (2018) Improving property valuation accuracy: a comparison of hedonic pricing model and artificial neural network. *Pac Rim Prop Res J* 24(1):71–83
13. Bao HXH, Wan ATK (2004) On the use of spline smoothing in estimating hedonic housing price models: empirical evidence using Hong Kong data. *Real Estate Econ J* 32(3):487–507
14. Babawale GK, Ajayi CA (2011) Variance in residential property valuation in Lagos, Nigeria. *Prop Manage* 29(3):222–237
15. Larose DT, Larose CD. *Discovering knowledge in data an introduction to data mining*, 2nd edn. Wiley Series on Methods and Applications in Data Mining
16. Ramageri BM. *Data mining techniques and applications*. Indian J Comput Sci Eng (1)
17. Medina-Borja A. *Uncovering complex relationships in system dynamics modeling: exploring the use of CHAID and CART*
18. Born W, Pyhrr S (1994) Real estate valuation: the effect of market and property cycles. *J Real Estate Res* 9(4):455–485
19. Antipov EA, Pokryshevskaya EB (2012) Mass appraisal of residential apartments: an application of Random forest for valuation and a CART-based approach for model diagnostics. *Exp Syst Appl* 39(2):1772–1778
20. Zou KH, Tuncali K, Silverman SG (2003) Correlation and simple linear regression. *Radiology* 227:617–22
21. Pandey R, Dhoundiyal M, Kumar A (2015) Correlation analysis of big data to support machine learning. In: *Proceedings—2015 5th international conference on communication systems and network technologies, CSNT 2015*. Institute of Electrical and Electronics Engineers Inc., pp 996–999
22. Su X, Yan X, Tsai CL (2012) Linear regression. *Wiley Interdiscip Rev Comput Stat*. 4(3):275–294
23. Nishi H, Asami Y, Shimizu C (2018) The illusion of a hedonic price function: nonparametric interpretable segmentation for hedonic inference. *J Hous Econ* 52:101764
24. Liang J, Yuan C (2021) Data price determinants based on a hedonic pricing model. *Big Data Res* 25:100249
25. Lindner AM, Larson RP (2018) Regression and regression analysis. In: *The Blackwell encyclopaedia of sociology*. Wiley, New York, pp 1–2

Optimization of Inventory Control Management to Impact on the Profitability of Construction Projects



S. Sarath Babu and A. Arokia Prakash

1 Introduction

Stock control on a global scale has often involved either an excessive quantity of inventory with poor management or a poor amount of stock with poor management. Amount of inventory with excessive management. There is no shadow of a doubt that effective inventory management improves the operations of many different enterprises. According to Kasim et al. [1], poor material management and handling on the job site are the major problems preventing the project from being completed successfully. In order to raise the overall efficiency of the production process, specialized material management systems for accelerated construction projects are needed. As was said before, one of the challenges that come with managing materials is a lack of accessible storage, material shortages, supply delays, pricing fluctuation, damage, and waste which are all factors to consider. Kasim [2] conducted research into the first stages of a revolutionary information and communications technology (ICT)-based material management system for construction projects. The results of the survey indicate that a significant majority of the businesses operating in the infrastructure sector is classified as either small or medium in size. Large organizations have the ability and the expertise to control the prices of labour and materials on projects by making use of modern information and management technologies.

Donyavi and Flanagan [3] say that every step that helps cut down on waste and boosts productivity results in significant cost and time savings. It is because material costs might make up a significant amount of the whole. They came to the conclusion that by implementing these three processes, small and medium-sized enterprises (SMEs) had the potential to enhance their performance in the areas of materials management, cost reduction, and project execution. Sánchez-Rodríguez et al. [4]

S. Sarath Babu · A. Arokia Prakash (✉)

Department of Civil Engineering, Faculty of Engineering and Technology, SRM Institute of Science and Technology, Kattankulathur, Tamil Nadu 603203, India
e-mail: arokipa@srmist.edu.in

present an example that compares the ABC model with the analysis model. The research shows an extended method for several inventory management ABC analysis criteria. Patel and Vyas [5] came to the conclusion that the organization and the site ought to work together by means of a centralized material management team, that the system ought to be adequately regulated, recorded, and monitored, and that the company ought to encourage a sense of awareness and responsibility among its employees. Meghani et al. [6] provide a summary of the results of a research that was carried out in Anand (Gujarat), India. In spite of the fact that each project was permitted a certain amount of waste, the limit was exceeded, which caused a decrease in the profit or return on investment generated by the project (ROI). Georgekutty [7] noted that projects are always susceptible to schedule overruns for a variety of reasons. This was one of the reasons why they arrived at this result. As a direct result of this, inventory management and control are critical issues that need to be addressed and considered. Madhavi et al. [8] have focused their attention on the problems that are prevalent in the construction sector. The processing of the materials in an inaccurate manner will result in a variation in the price of the materials. As a direct consequence of this factor, a case study was carried out by Kafle [9] on a selection of locations within the state of IMO in Nigeria. Vipin and Rahima Shabeen [10] stated that a void is created by the absence of proper materials management on construction sites. Research has shown that construction materials account for 60–70% of the total cost in construction projects. Material mismanagement decreases the contractor's profit leading to huge losses, and leaving the project in big troubles, and therefore, the proper management of this single largest component can improve the productivity and cost efficiency of a project and help ensure its timely completion. Here, introduce the paper, and put a nomenclature if necessary, in a box with the same font size as the rest of the paper.

2 Methodology

The study was carried out through questionnaire survey for the projects that are currently under consideration to investigate the suggestions of industry professionals for inventory management systems in the construction industry. Using SPSS 25.0 ranking analysis and multiple regression analysis, the questionnaire survey is analysed in order to determine the primary challenging management practices that need to be implemented in order to improve the overall performance of the project and implement efficient inventory management in order to maximize the profit that the construction project generates. Primary sources are those that are defined by the context [11]. In addition to this, it explores other ideas related to both theory and practice. A complete analysis of the published literature was carried out with the purpose of determining current approaches to material management. Interviews with the primary personnel engaged in the project are a part of the questionnaire survey.

Secondary data is information that has been derived from primary data that has previously been collected for a specific purpose: MRN, ledger register, daily material report, and running amount bill.

The research was conducted using a survey format, and the researchers acquired quantitative data from construction experts working for a variety of different firms [12]. The material, construction, quality, store managers, and site managers who worked in the private or public sector as building material suppliers or contractors. These individuals were responsible for supplying building materials or providing construction services. The method for collecting the data was a questionnaire that was very nicely organized. The questionnaire was separated into six parts as per the factors considered in framing these questions, consisting of a total of 60 questions. The challenges that must be overcome before the Indian construction industry can make effective use of emerging technology are discussed in the second part [13]. First being cost factors included within are cash flow for the project, price variations and currency differentiation, material procurement and storage, machinery and equipment, and manpower. Second being time factors included within are stock out and material shortage, planning of resources, payment delay, performance of the project, and natural factors. Third being quality factors included within are unavailability of experienced personnel, quality decision making, improper inspection, transportation and delivery, and poor material management. Fourth being productivity factors included within are work schedule sequencing, management–labour relationship, resource allocation, contractor and owner coordination, effective planning, and waste management. Fifth being people factors included within are owner–employee coordination, consultants and contractors understanding, employee motivation, design changes coordination, and project manager and work allocation. Sixth being client satisfaction factors included within are leadership skills of project manager, reworks upgradation–client changes, dispute management, owner–client relationship, and cash flow management. Seventh being regular and community satisfaction factors included within neighbourhood dispute management, site conditions, proper documents, quality materials and handling, easement, and pollution management [14].

3 Results and Discussion

The replies to the questionnaire came from 188 individuals working for 30 different construction businesses. These individuals had varying levels of experience and designations within the construction sector. This information is processed by the ranking analysis programme known as SPSS. This analysis is done by ranking (rankings are used to rate the hurdles in the execution of material management), and contractors employ suitable solutions to handle these limits in order to meet their obligations. The data are recoded into their rank ordering using ranking, which may go in either direction, from smallest to biggest or largest to smallest. This will

be shown by using SPSS statistics to rank some data once it has been entered into the programme [15].

3.1 Ranking Analysis/RII(Relative Importance Index)

The relative importance index is computed for each of the indicators, and then, those indices are sorted in the appropriate order. The RII was developed utilizing the Likert scale in order to describe the significance of each indication.

$$RII = \Sigma W / (A * N)$$

W Weighting as assigned or total sum,
 A Highest weight in Likert scale (here it is 5),
 N is the total number of respondents.

The greater the value of RII, the more significant the question, which therefore has an effect on the profit of the project. Table 1 represents the frequency and the percentage of the total respondents for the top ten most important ranked questions which affect the profitability of the project. Factors such as consultants and contractors affect the project and effective planning at every stage of work, and natural seasonal factors preparation is necessary. Inventory control tools and AMP models improve material ordering time which have most responses in the range of strongly agree and agree. All other factors have maximum responses in the range of agree and slightly disagree. The factor consultants and contractors affect the project has the least strongly disagree of 9%, hence being most important criteria.

- “Consultants and contractors understanding affects the project” as being the study question was noted to be 30.9% for agree for its impact on the factor of design changes coordination and work allocation with proper coordination which is important for effective working strategy.
- “Effective planning at every stage of work” as being the study question is noted to be having a higher percentage of disagree 27.1% as there can be variation in resource allocation and other natural factors affecting the site conditions. Hence, variations can be seen in the planning which has to be well coordinated. Then, positive impact can be observed.
- “Performance of the project is important” as being the study question is noted to be having more inclination towards disagree 28.2% as in case of time factor the delay in payment is most important which will rule the performance; hence, priority is mainly the cost consideration and not the up-to-date performance of the project.
- “Selection of vendors” and “Natural seasonal factors preparation is necessary” are noted to have majority votes in the neutral conditions as 27.7% and 25.5%, respectively. These factors have such conditions as it is variable in nature based on the scale and time.

Table 1 Percentage and frequency of responses from SPSS 25.0

Questions/scale	Factor	Strongly agree	Agree	Neutral	Dis.agr	Strong. Dis.agr	Total
Consultants and contractors understanding affects the project	Frequency	46	58	40	27	17	188
	Percentage	24.5	30.9	21.3	14.4	9	100
Effective planning at every stage of work	Frequency	36	25	44	51	32	188
	Percentage	19.1	13.3	23.4	27.1	17	100
Performance of the project is important	Frequency	26	41	42	53	26	188
	Percentage	13.8	21.8	22.3	28.2	13.8	100
Selection of vendor	Frequency	28	38	52	37	33	188
	Percentage	14.9	20.2	27.7	19.7	17.6	100
Natural seasonal factors preparation is necessary	Frequency	35	34	48	33	38	188
	Percentage	18.6	18.1	25.5	17.6	20.2	100
Quality and handling of materials affect the project	Frequency	25	45	43	51	24	188
	Percentage	13.3	23.9	22.9	27.1	12.8	100
Owner and client relationship affects the project	Frequency	26	49	41	41	31	188
	Percentage	13.8	26.1	21.8	21.8	16.5	100
Procurement and holding or storage cost spent on inventory	Frequency	29	44	45	40	30	188
	Percentage	15.4	23.4	23.9	21.3	16	100
Neighbourhood coordination is important	Frequency	29	37	50	51	21	188
	Percentage	15.4	19.7	26.6	27.1	11.2	100
Inventory control tools and applications improve material ordering time	Frequency	33	38	44	47	26	188
	Percentage	17.6	20.2	23.4	25	13.8	100
Un-experienced personnel affects the project	Frequency	27	38	56	48	19	188
	Percentage	14.4	20.2	29.8	25.5	10.1	100

- “Owner and client relationship affects the project” as being the study question is a very important area of discussion. It is mainly voted to be agreed as 26.1% of the population of study considered this important. Proper coordination between the two entities would ensure good management of planning as well as finance.
- “Procurement and holding or storage costs spent on inventory” has an almost equal vote share for agree and neutral of 23.4 and 23.9%. This denotes that the materials procurement schedule has a very important role in the proper execution of the site as even storage for a longer duration is not acceptable. Hence, timely delivery is to be planned.
- “Neighbourhood coordination is important” has about 27.1% of disagree as it is not constant for all projects as the place is variable. Also due to scale, its issues would vary. Overall, a properly approved project would not have any major disturbances in the neighbourhood.
- “Inventory control tools and applications improve material ordering time” has 23.4% neutral and 25% as disagree due to major setbacks in the skillset unavailability in the current Indian construction industry conditions.

Table 2 represents the identified factors for all the 60 questions which are analysed through SPSS software; the average, mean, median, mode, standard deviation, variance, and the sum value are used further in the analyses to find the relative importance index for the questions using the ranking formulae.

- Standard deviation of range 1–1.4 is lesser than the mean value. This shows that variability measure is more appropriate. The data points are clustered around the mean equally representing standard normal distribution.
- The standard error of the mean is spread equally almost ranging from 0.08 to 0.09 representing the accuracy of the mean sample data. So the standard deviation values are also more precise compared to standard error, as we can vary the differences accurately by comparing the mean values.
- The mean, median, and mode values from the analysis depict that the responses are varying almost equally and the attributes of variables are occurring most frequently.
- The maximum and minimum values are ranged from 1 to 5 based on the Likert scale.
- The variance values from the analysis fall between 1 and 1.9 which gives more distribution and deviation, whereas the standard deviation values are considered here as it gives clear values of the deviation of data around the mean values.

Considering all the data, sum value of every question is generated. The value varies between 400 and 600 for the 60 questions from 188 responses. From this data, the relative importance index is calculated from the ranking analysis. This denotes the major factor influencing the project. After the ranking analysis has been completed, we have identified the top ten ranked questions that have an impact on the total profit of the project. The regression analysis is then carried out specifically for these top ten ranked questions, taking into account all of their respective data. Table 3 represents that the RII values are derived from the ranking formulae considering majorly the

Table 2 Statistical data obtained from analysis of responses

	Valid	Mean	Std. error of Mean	Median	Mode	Std. deviation	Variance	Range	Maximum	Minimum	Sum
Consultants and contractor understanding affects the project	188	3.11	0.091	3	4	1.249	1.561	4	1	5	584
Effective planning at every stage of work	188	3.1	0.099	3	4	1.361	1.852	4	1	5	582
Performance of the project is important	188	3.06	0.093	3	4	1.269	1.611	4	1	5	576
Selection of vendor	188	3.05	0.095	3	3	1.305	1.704	4	1	5	573
Natural seasonal factors preparation is necessary	188	3.03	0.101	3	3	1.385	1.919	4	1	5	569
Quality and handling of materials affect the project	188	3.02	0.091	3	4	1.249	1.561	4	1	5	568
Owner and client relationship affects the project	188	3.01	0.095	3	2	1.304	1.7	4	1	5	566
Procurement and holding or storage cost spent on inventory	188	2.99	0.095	3	3	1.308	1.711	4	1	5	562
Neighbourhood coordination is important	188	2.99	0.091	3	4	1.241	1.54	4	1	5	562
Inventory control tools and applications improve material ordering time	188	2.97	0.096	3	4	1.31	1.716	4	1	5	559
Un-experienced personnel affects the project	188	2.97	0.088	3	3	1.201	1.443	4	1	5	558

sum that we arrived at for every question considering all the data. The RII values vary between 0.42 and 0.62. Based on the RII, the top ten ranked questions which is shown in Fig. 1 majorly affect the overall project.

In this study, multiple regression analysis was performed, and analysis results were obtained as given in Tables 4 and 5 to determine the amount of influence that the application of the constraints of material management, the impact of delays in the delivery of materials, and the contracting company solution to addressing the issue of the application of materials management all had. Dependent variable—Years of experience. Independent variable—top ten ranked questions as given in Table 3. Because of this, we are able to determine the ANOVA df-critical factor and the F-static value, and as a result, we are able to draw the conclusion from our study on whether or not the strength of the ranking questions influences the project's profit.

F—Static value or major factor,

Df—Indicator of criticality.

These rated questions will have an impact on the profitability of the project if $F < df$ occurs.

Table 3 Relative importance index and ranking

S. No.	Top ranked questions	RII	Rank	Factor
1	Consultants and contractors understanding affects the project	0.62128	1	People
2	Effective planning at every stage of work	0.61915	2	Productivity
3	Performance of the project is important	0.61277	3	Time
4	Selection of vendor is important	0.60957	4	Quality
5	Natural seasonal factors preparation is necessary	0.60532	5	Community satisfaction
6	Quality and handling of materials affects the project	0.60426	6	Community satisfaction
7	Owner and client relationship affects the project	0.60213	7	Client satisfaction
8	Procurement and holding or storage cost spent on inventory	0.59787	8	Cost
9	Neighbourhood coordination is important	0.59787	8	Community satisfaction
10	Inventory control tools and applications improve material ordering time	0.59468	9	Time
11	Un-experienced personnel affects the project	0.59362	10	Quality

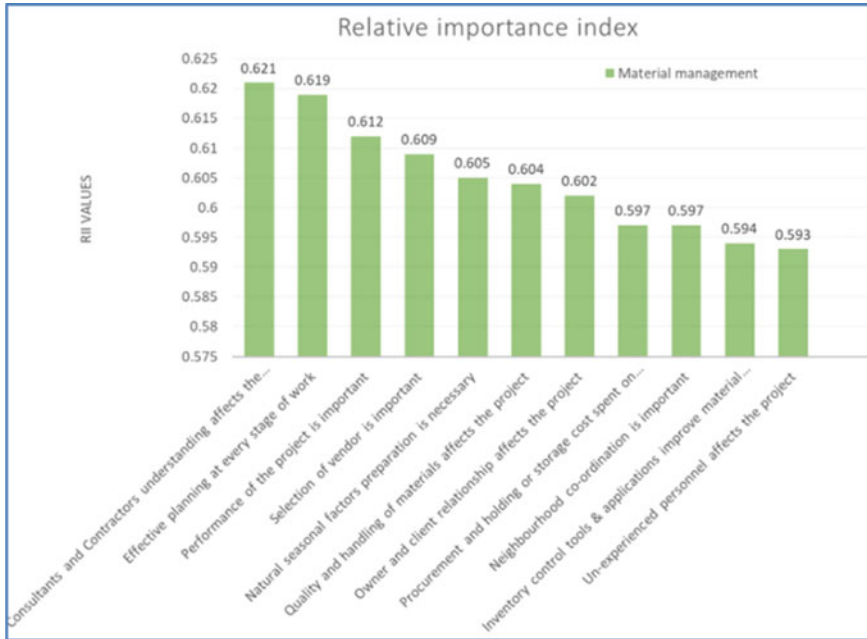


Fig. 1 RII and ranking of top ten questions

Table 4 Simple correlation and standard error from regression analysis

Model	R	R. sq	d R	Std. err. of estimate
1	0.247a	0.061	0.002	1.759

Table 5 Critical factor and significance from regression analysis

Model	Sum of sq	df	Mean sq	F	Sig
Regression	35.384	11	3.217	1.04	0.414 b
Residual	544.595	176	3.094		
Total	579.979	187			

- If F is higher than df, then the profit generated by the project will not be impacted by these ranking questions. The study reveals that $F < df$, and as a result, the ranking questions will be the primary factor in the profit that the project generates. Table 4 represents the standard error of the estimate value of 1.759 derived considering the simple correlation R and the R square value 0.247 and 0.06, the error falls in range with the regression line. The standard value for the significance in regression analysis should not be lesser than 0.05.
- The significance value ought to be larger than 0.05, and the F value should be more than the significance value and should fall between 1% significance levels

in accordance with the conventional analysis theory; if it falls within this range, the analysis is successful, and it demonstrates that the ranked questions satisfy the analysis. If it falls outside of this range, the analysis is unsuccessful. The F value of 1.040 was found to be more than the significance value (0.414) representing the positive result of the analysis of regression. Here, the null hypothesis is rejected leaving an effect on the hypothesis.

- This demonstrates that the top ranked queries do, in fact, have an effect on the overall profit of the project. Therefore, the inventory management techniques for any construction project should take into consideration the following criteria in order to maximize the profit of the project while simultaneously reducing the amount of time wasted on it and the amount of delay it experiences.

4 Conclusion

The profitability of the project varies based on the saving mainly from tangible costs. Inventory management accounts for about 30–80% of the construction cost, saving contributed from the same will enhance the project profitability. Materials and Labour are two major factors that if not properly managed through inventory control could lead to wastage. This research was aimed at assessing the ground reality of the construction industry and its professionals' ideology for the impact of inventory control management on the profitability of projects on a medium to large scale. The study was conducted in the Indian context covering majorly large-to medium-scale industries and their working mechanism. The variables in the study as discussed earlier are based on the critical factors and the set of questions derived from these factors based on real-time conditions in the construction industry. The top ten ranked questions were analysed using regression analysis to prove their impact on the project. Based on this, the F value was found to be 1.040 which falls within the range and lesser than the critical factor df. Hence, through the analysis, the project proves that the top ten questions analysed have a considerable impact on the project. Construction projects could take into consideration of the discussed factors in order to maximize the profit of the project while simultaneously reducing the amount of time wasted on it and the amount of delay it experiences. Inventory management helps to optimize the project.

References

1. Kasim NB, Anumba CJ, Dainty ARJ (2005) Improving materials management practices on fast-track construction projects. In: 21st annual ARCOM conference
2. Kasim N (2003) Improving material management practices in construction. In: International symposium in developing economics communalities among diversities

3. Donyavi S, Flanagan R (2009) The impact of effective material management on construction site performance for small and medium sized construction enterprises. In: ARCOM 2009—proceedings of the 25th annual conference
4. Sánchez-Rodríguez C, Hemswoth D, Martínez-Lorente ÁR, Clavel JG (2006) An empirical study on the impact of standardization of materials and purchasing procedures on purchasing and business performance. *Supply Chain Manage An Int J*. <https://doi.org/10.1108/13598540610642475>
5. Patel KV, Vyas CM (2011) Construction materials management on project sites
6. Meghani MD, Vyas CM, Bhavsar JJ, Hingu RJ (2011) A study on basic material waste in building Industry: main causes and prevention. In: National conference on recent trends in engineering and technology
7. Georgekutty CK (2012) Hall marks in construction material management: a literature review. *IOSR J Mech Civ Eng*
8. Madhavi T (2013) Material management in construction—a case study. *Int J Res Eng Tech* <https://doi.org/10.15623/ijret.2013.0213075>
9. Kafle SC (2019) Corelation and regression analysis using SPSS. *OCEM J Manage Tech Soc Sci*
10. Vipin VP, Rahima Shabeen S (2019) Factors affecting material management in construction industry. *Int J Recent Tech Eng* <https://doi.org/10.35940/ijrte.C6337.098319>
11. Lenin P, Krishnaraj L, Prasad DN, Kumar VP (2014) Analysis of improper material management affecting cost in construction projects. *Int J Res Appl Sci Eng Tech*
12. Subramani T, Nair VB, David A, Ghouse BM, Kumar NS (2017) A study of inventory management system in construction industry. *Int J Appl Innovat Eng Manage*
13. Sindhu S, Nirmalkumar K, Krishnamoorthy V (2014) Performance analysis of inventory management system in construction industries in India. *Int J Innovat Res Sci, Eng Tech*
14. Nayak R, Pandey M (2016) Management of construction materials on project site. *Int Res J Eng Tech* e-ISSN: 2395-0056
15. Vignesh S, Shanmugapriya S (2016) Improvement of decision making process in construction supply chain management using analytical hierarchy process. *Int J Emerg Tech Adv Eng*

Developing Management Information System for Construction Equipment Maintenance



B. Indhu and J. Ajay

1 Introduction

In terms of both quality and productivity, construction machinery may effectively replace human labour in the construction industry. It does, however, result in significant suffering when equipment is unavailable at critical moments, resulting in delays in the building project's completion [1]. Delays in a construction project are one of the major factors affecting the economy of the country [2]. Delays in project raise disputes among the stakeholders, leading to lawsuits and results in loss of firm's reputation [3]. There is a history of inadequate equipment management in developing countries, which leads in cost overruns as a consequence of delays [4]. A penalty provision is usually included in the contract if the contracting business fails to finish their operations or the project on time [5, 6]. Delay of the project with respect to equipment is often caused due to sudden failure of equipment and low productivity [7]. Irregular daily maintenance by the operators is one of the causes of sudden failure of equipment [8]. Poor equipment maintenance leads to low productivity [9]. Lack of scheduled lubrication and cleaning results in sudden breakdown of equipment. An inadequate maintenance management team is the primary cause for all the factors affecting sudden failure of equipment [1]. Irregular failure analysis causes the increased risk of equipment downtime [10].

Maintenance, as a system, plays a key role in reducing cost, minimizing equipment downtime, improving quality, increasing productivity, providing reliable equipment, and as a result achieving organizational goals and objectives [11]. There has been a considerate amount of research concerning construction equipment management which has concluded that improper equipment maintenance is one of the major causes for construction project delay [12]. Improper construction equipment maintenance

B. Indhu (✉) · J. Ajay

Department of Civil Engineering, Faculty of Engineering and Technology, SRM Institute of Science and Technology, Kattankulathur-603203, Tamil Nadu, India

e-mail: indhub@srmist.edu.in

leads to sudden failure of equipment stopping the entire work in site [13, 14]. Also, poor maintenance of equipment leads to low productivity [15]. Several researches have been done on the causes and effects of improper equipment management, yet these researches do not meet the practical requirement of the issue [16]. Since there is a thriving need for the use of equipment in site, it is mandatory to plan the maintenance of equipment effectively [17].

Past studies on construction equipment management issues have suggested control measures in general to avoid delay. But there is no solution proposed mitigate sudden failure of equipment due to improper construction equipment maintenance. Hence, the novelty of this paper lies in giving a solution to overcome one of the major issues, i.e. improper construction equipment maintenance by proposing software architecture to track the regular maintenance of construction equipment at site to avoid sudden failure.

2 Past Studies on Software Architecture

Software architecture is associated with the identification of apt elements required to form a framework of the desired design. Implementation of the software architecture is dependent on the algorithms and the database provided with respect to field study [18]. The researchers implemented automation in construction industry for advanced performance software prototype, based on quality function deployment (QFD) technique is designed and developed for material handling equipment [19]. The researchers in USA have developed data storage in construction management information systems which is growing rapidly due to the extensive adoption and widespread usage of information technology in construction. Automated techniques to organize and improve access to information included in these papers are now important to construction data [20]. A study in India researched that the software architecture implementation for lean management focuses on combining traditional management systems with lean construction, resulting in the development of a streamlined lean implementation framework and recording format for measuring daily performance in construction projects [21]. Processing elements, data elements, and connecting elements are the three different types of architectural elements. The raw data collected is processed to be entered in database. These processed elements are then used and transformed to data elements as per requirement to fit into the framework. Connecting elements acts as a bond to get the preferred design of software architecture [22].

3 Research Design

The equipment causes of delay in residential and road construction project were identified through pilot study and background study. To frame a software architecture model construction equipment spare parts maintenance schedule was collected. The data was collected by various dealers and showrooms. The data was interpreted as software architecture using graphical user interface. This software architecture will help to track the maintenance schedule for effective maintenance management. Figure 1 shows flow chart of research design.

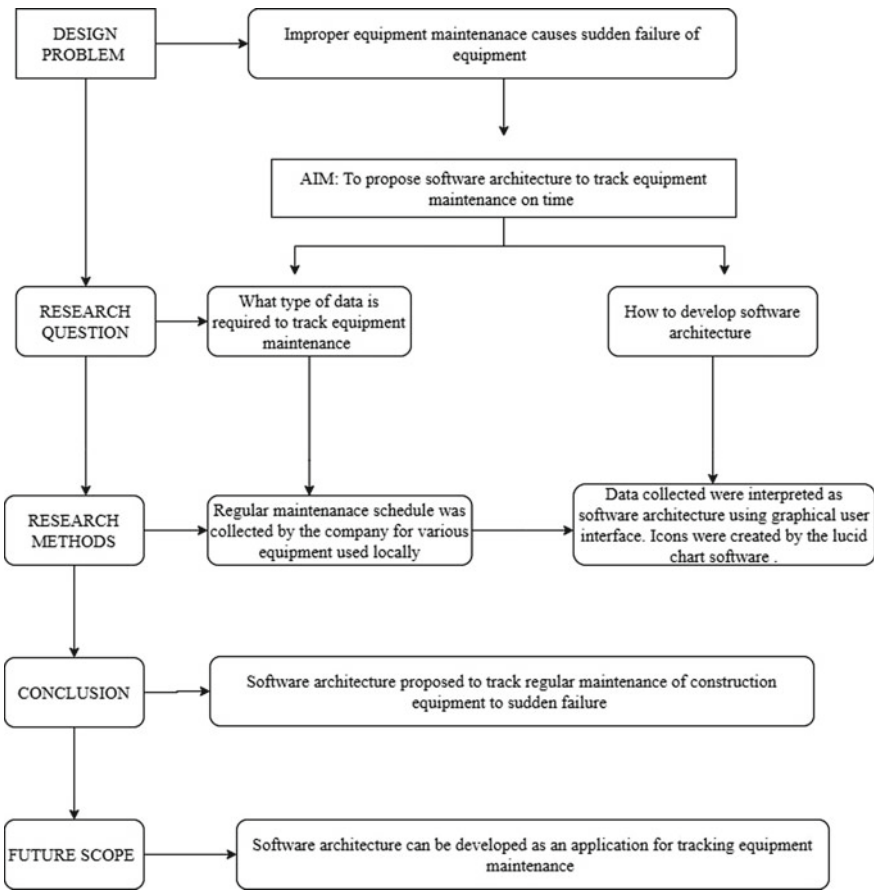


Fig. 1 Flow chart of research design

4 Data Collection

Personal observation of a few construction sites revealed the most often seen pieces of equipment in the area. Backhoe loader, vibratory compact roller, tandem roller, excavator, dump truck, grader, and hydra crane were some of the equipment that were recognized as being used. Spare components were classed according to the kind of equipment they were used with. The maintenance schedule of each spare part of respective equipment was collected from the local dealers and showrooms. The data collected is given in Table 1.

5 Software Architecture

In the proposed work on effective construction equipment management, there are four modules. First is data collection, second module is data management then user interface module and finally algorithms. Figure 2 shows software architecture improper equipment maintenance.

Module I: Data Collection:

Various sources, including manufacturers, showrooms, and dealers, are used to compile the most basic information regarding construction equipment. These data include the equipment description, configurations, guidelines, and maintenance. The database is updated with this information when it is processed.

Module II: Data Management:

The information of construction equipment will be maintained in a subsystem catalogue on the database server, and the administrator will have the ability to add, retrieve, and modify the database. It also has a connection to the user interface, which allows the machinery operators to update the working hours of the machines. This will be automatically updated in the database.

Module III: User Interface:

The user interface will have a registration page for new members and a login page for existing members. The interface is a site-based interface so only machinery operators and project managers will have the access. Admin and supervisor have the ability to add vehicle details and tag them with the corresponding type. Once an operator uses a machine, he/she will update the usage details of that machine which will be available in the subsystem catalogue for example: If excavator works 5 h, the data should be updated; the detail will show subsystem catalogue. Also, there will be a dashboard for each machine which will tell the depreciation details, and it will be dynamic.

Module IV: Algorithms:

Table 1 Data collection

		Description	Interval hours	Change
1	Backhoe loader	Radiator hose connection	500 h	Yes
		External bolts and nuts	500 h	If required
		Fuel connections	500 h	Yes
		Fuel tank to remove sediments	250 h	Yes
		Lubricant oil check	500 h	Yes
		Engine oil	500 h	Yes
		Secondary fuel filter canister	1000 h	Yes
		Level in battery	250 h	If required
		All connection	250 h	Yes
		Brake oil	2000 h	Yes
		Hydraulic oil	2000 h	Yes
		Hydraulic filter	500 h	Yes
		Bucket teeth	90 Days	If required
		Change of tyre	365 days	Yes
Oil hose	3 years	Yes		
2	Vibratory compact roller	Air clean filter	50 h	Yes
		Hydraulic cylinders	50 h	If required
		Drum oil level	250 h	Yes
		Lubricant grease for hinges	250 h	Yes
		Fuel filter	500 h	Yes
		Bleeder filter on hydraulic tank	500 h	Yes
		Engine oil and oil filter	500 h	Yes
		Hydraulic filter	1000 h	Yes
		Drum gear oil	1000 h	Yes
		Oil in axle planetary	1000 h	Yes
		Drum oil	2000 h	Yes
		Forward reverse lever and lubricant	2000 h	Yes
		Tyre	2 years	Yes
		Oil hose	3yrs	Yes
3	Tandem Rollers	Engine oil and filter (every 250 h)	100 h	Yes
		Secondary filter	100 h	Yes
		Radiator oil	500 h	Yes
		Battery water level	500 h	If required
		Air cleaner outer element	500 h	Yes
		Fuel tank	1000 h	Yes

(continued)

Table 1 (continued)

		Description	Interval hours	Change
		Hydraulic filter	1000 h	Yes
		Hydraulic oil	2000 h	Yes
		Coolant	2000 h	If required
4	Excavator	Engine oil and oil filter	500 h	Yes
		Fuel filter	500 h	Yes
		Infused bushes and pivot pins and lubricant	1000 h	If required
		Battery check	250 h	If required
		Brake oil	2000 h	Yes
		Bucket teeth	90 days	If required
		Hydraulic oil	5000 h	Yes
		Oil hose	3 years	Yes
5	Hydra cranes	Radiator hose connection	500 h	Yes
		External bolts and nuts	500 h	If required
		Fuel connections	500 h	Yes
		Fuel tank to remove sediments	250 h	Yes
		Lubricant oil check	500 h	Yes
		Engine oil	500 h	Yes
		Secondary fuel filter canister	1000 h	Yes
		Level in battery	250 h	If required
		All connection	250 h	Yes
		Brake oil	2000 h	Yes
		Hydraulic oil	2000 h	Yes
		Hydraulic filter	500 h	If required
		Bucket teeth	90 Days	If required
		Change of tyre	365 days	Yes
		Oil hose	3 years	Yes
6	Grader	Engine oil and filter	150 h	Yes
		Air filter elements	150 h	If required
		Exhaust system	150 h	Yes
		Wire connection	150 h	Yes
		Lubricant oil check	250 h	Yes
		Battery check	250 h	If required
		Front ends	150 h	Yes
		Axle oil	150 h	Yes
		Fuel filter	300 h	Yes
		Transmission filter	300 h	Yes

(continued)

Table 1 (continued)

		Description	Interval hours	Change
		Radiator oil	300 h	Yes
		Hydraulic filter	500 h	If required
		Engine check	1000 h	Yes
		Wheel bearings	1000 h	Yes
		Pivots pins and bushings	1000 h	Yes
		Hydraulic tanks	1000 h	Yes
7	Dump truck	Engine oil and oil filter	100 h	Yes
		Fuel filter	350 h	Yes
		Lubricant check	350 h	Yes
		Battery check	350 h	Yes
		Brake oil	500 h	Yes
		Hydraulic filter and oil	650 h	If required
		Change of tyres	365 days	Yes
		All faults and wire check	365 days	Yes

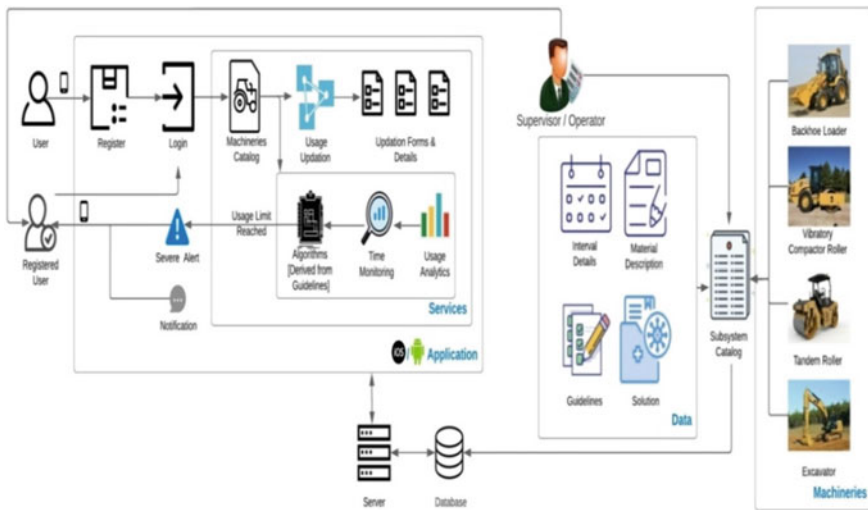


Fig. 2 Software architecture for improper equipment maintenance

The algorithms are constructed using recommendations offered by the manufacturers; for each type of machinery spare parts and for each of its components, there will be certain rules. If the depreciation rate goes over the guideline, depending on the algorithm, it will trigger use restriction and send an alert message to the user and project manager. By understanding the warning, they can constantly prevent the

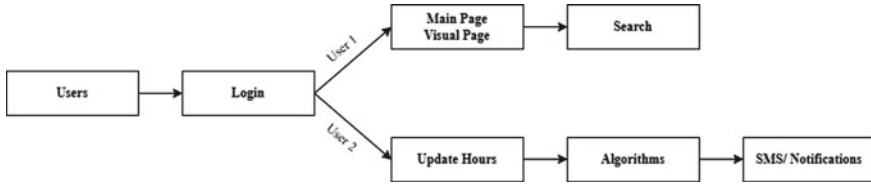


Fig. 3 Parallel process shared structure architecture

machinery from unintentional damages and save maintenance expense.

$$H_i = T_i - U_i$$

where

- i* Component
- H* Balance hours
- T* Total hours
- U* Used hours

5.1 Parallel Process, Shared Structure Architecture

In this paper, the parallel process shared structure architecture data is applied because this process where multiple users can use at same time and also the process which acts parallel. As self-contained processes fed by a shared source internal representation, that is, the shared representation acts as the connecting element, and each processing is independent of the others. Element does a fast assessment. Figure 3 shows the how the structure acts.

5.2 Process/Data/Connector Interdependence

A significant lesson from building architecture is the concept of many perspectives. Processing, data, and connectivity are three critical perspectives in software architecture. The processing element means buttons which change the value in database and algorithm which checks usage limit and triggers alerts notification is processing element. Moreover, data elements store data in backend for example: Machinery details and user details which help to give alert for personnel. The connecting element is meaning its connecting user authentication and database and data validation. Figure 4 explains how the elements acts.

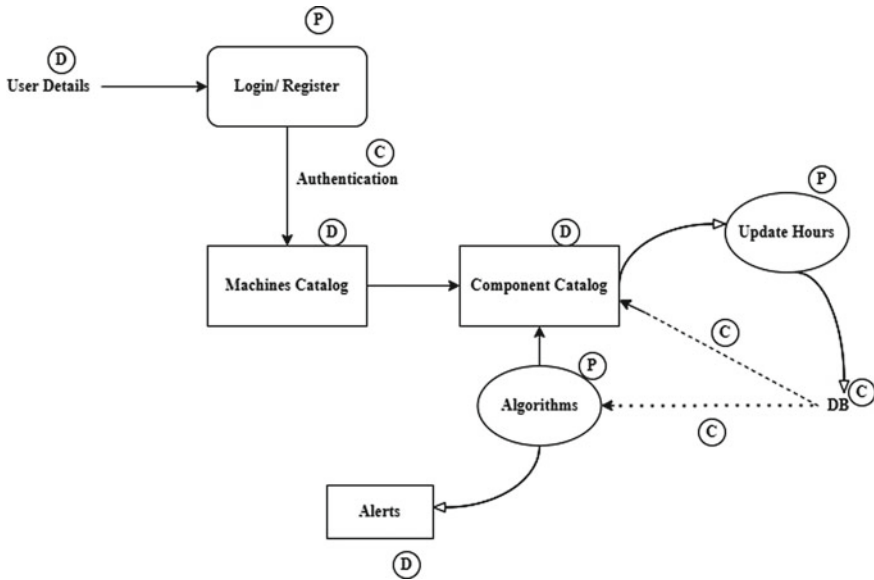


Fig. 4 Elements in software architecture

6 Conclusion

According to the findings of previous research, improper construction equipment maintenance results in equipment failures that occur suddenly, causing a delay in the completion of the project. When construction projects are delayed, they may result in negative consequences such as lawsuits, fines, and cost overruns, which can result in the business’ image being ruined. Hence, software architecture is proposed to track the maintenance schedule of each equipment, and its spare parts used locally. Developing software architecture provides tool for collecting of maintenance schedule of each spare part of equipment, data management by interpreting the acquired data using graphical user interface and ultimately developing algorithms based on guidelines established by the manufacturers. Parallel process, shared structure architecture is the type of architecture used here to support multiple users.

Future Scope:

This proposed software architecture can be developed as an application and updated for the tracking of equipment maintenance.

Limitations:

1. Only the most common equipment used locally is been considered for research.
2. The construction equipment is limited to road and residential project only.

Funding There is no conflict of interest for the any of the authors in this paper.

References

1. Indhu B, Yogeswari K (2020) Review on delay factors due to improper construction equipment management. *Int J Emerg Tech* 11(1):209–214
2. Aziz RF (2013) Ranking of delay factors in construction projects after Egyptian revolution. *Alex Eng J* 52(3):387–406. <https://doi.org/10.1016/j.aej.2013.03.002>
3. Cristóba JRS (2014) Cost allocation between activities that have caused delays in a project using game theory. *Proced Tech* 16:1017–1026. <https://doi.org/10.1016/j.protcy.2014.10.056>
4. Mansfield N, Ugwu O, Doran T (1994) Causes of delay and cost overruns in Nigerian construction projects. *Int J Project Manage* 12(4):254–260. [https://doi.org/10.1016/0263-7863\(94\)90050-7](https://doi.org/10.1016/0263-7863(94)90050-7)
5. Bergantiños G, Lorenzo L (2019) How to apply penalties to avoid delays in projects. *Eur J Oper Res* 275(2):608–620. <https://doi.org/10.1016/j.ejor.2018.11.056>
6. D'Alpaos C, Moretto M, Valbonesi P, Vergalli S (2013) Time overruns as opportunistic behavior in public procurement. *J Econ* 110(1):25–43. <https://doi.org/10.1007/s00712-013-0352-6>
7. Al-Khalil MI, Al-Ghafly MA (1999) Important causes of delay in public utility projects in Saudi Arabia. *Constr Manag Econ* 17(5):647–655. <https://doi.org/10.1080/014461999371259>
8. Tracking of construction progress concerning activity wise equipment delay (2019) Regular Issue 8(3):1883–1892. <https://doi.org/10.35940/ijrte.c4459.098319>
9. Abd El-Razek ME, Bassioni HA, Mobarak AM (2008) Causes of delay in building construction projects in Egypt. *J Const Eng Manage* 134(11):831–841. [https://doi.org/10.1061/\(asce\)0733-9364\(2008\)134:11\(831\)](https://doi.org/10.1061/(asce)0733-9364(2008)134:11(831))
10. Bashiri M, Badri H, Hejazi TH (2011) Selecting optimum maintenance strategy by fuzzy interactive linear assignment method. *Appl Math Model* 35(1):152–164. <https://doi.org/10.1016/j.apm.2010.05.014>
11. Naskoudakis I, Petroutsatou K (2016) A thematic review of main researches on construction equipment over the recent years. *Proc Eng* 164:206–213. <https://doi.org/10.1016/j.proeng.2016.11.611>
12. Indhu B, Yogeswari K (2021) Structural equation modelling (SEM) approach on inappropriate construction equipment delay factors. *Civ Eng J* 7(7):1156–1168. <https://doi.org/10.28991/cej-2021-03091717>
13. Indhu B, Yogeswari K, Dhivya D (2019) Ranking of delay factors in road construction project due to improper construction equipment management. *Int J Recent Tech Eng* 8(3):1962–1971. <https://doi.org/10.35940/ijrte.C4485.098319>
14. Le-Hoai L, Lee YD, Lee JY (2008) Delay and cost overruns in Vietnam large construction projects: a comparison with other selected countries. *KSCE J Civ Eng* 12(6):367–377. <https://doi.org/10.1007/s12205-008-0367-7>
15. Akhavian R, Behzadan AH (2015) Construction equipment activity recognition for simulation input modeling using mobile sensors and machine learning classifiers. *Adv Eng Inform* 29(4):867–877. <https://doi.org/10.1016/j.aei.2015.03.001>
16. Yang J-B, Kao C-K (2012) Critical path effect based delay analysis method for construction projects. *Int J Project Manage* 30(3):385–397. <https://doi.org/10.1016/j.ijproman.2011.06.003>
17. Lopes RS, Cavalcante CAV, Alencar MH (2015) Delay-time inspection model with dimensioning maintenance teams: a study of a company leasing construction equipment. *Comput Ind Eng* 88:341–349. <https://doi.org/10.1016/j.cie.2015.07.009>
18. Perry DE, Wolf AL (1992) Foundations for the study of software architecture. *ACM SIGSOFT Softw Eng Notes* 17(4):40–52. <https://doi.org/10.1145/141874.141884>
19. Prasad K, Zavadskas EK, Chakraborty S (2015) A software prototype for material handling equipment selection for construction sites. *Autom Constr* 57:120–131. <https://doi.org/10.1016/j.autcon.2015.06.001>
20. Caldas CH, Soibelman L (2003) Automating hierarchical document classification for construction management information systems. *Autom Constr* 12(4):395–406. [https://doi.org/10.1016/s0926-5805\(03\)00004-9](https://doi.org/10.1016/s0926-5805(03)00004-9)

21. Kasiramkumar T, Indhu B (2016) An implementation framework for integrated lean construction system for Indian scenario. *ARPN J Eng Appl Sci* 11(15):9388–9394
22. Campbell RH, Habermann AN (nd) The specification of process synchronization by path expressions. *Operat Syst* 89–102. <https://doi.org/10.1007/bfb0029355>

Research Advancements in the Study of Microbiology of Aerosols



Rajitha J. Rajan and Sathyanathan Rangarajan

1 Introduction

According to World Health Organization (WHO), “air pollution is contamination of the indoor or outdoor environment by any chemical, physical, or biological agent that modifies the natural characteristics of the atmosphere”. Air pollution arises from various common origins. They are rapid development of industrialization and urbanization, increase in vehicle fleet, forest fires and household combustion devices [1]. Particulate matter, CO_x, ozone, NO_x, and SO_x are the major pollutants of health concern [2]. This pollutants are inhaled by human beings and other living organisms and are responsible to many harmful effects in them.

Airborne microorganisms are omnipresent and are found attached to the particulate matter in the atmosphere. Atmosphere is not a hospitable climate for microbes because of stress due to dehydration and limited active time frame. Microbes that are suspended in air are also called bioaerosols. Pathogenic or nonpathogenic, live or dead bacteria and fungi, viruses, fungal spores, pollen, organic and inorganic particulates, toxins, plant fibers, etc., are some of the examples of bioaerosols present in the atmosphere [3].

Depending upon several aerodynamic properties, the biological particles can reside in the atmosphere from less than a day to few weeks. The biological characterization of aerosols involves different sampling techniques using equipment of several kinds in aseptic conditions and storing it in ambient conditions until further analysis [4].

The samples are then cultured to explore the microbial flora present in it. Wind is considered as responsible for the microbial dispersion and transportation for a

R. J. Rajan · S. Rangarajan (✉)

Department of Civil Engineering, College of Engineering and Technology, SRM Institute of Science and Technology, Kattankulathur, Tamil Nadu 603203, India

e-mail: sathyanr5@srmist.edu.in

long distance [5]. The change in meteorological parameters, time, source of formation, human and animal activities can cause variations in the nature and diversity of airborne microorganisms [6]. The morphological analysis can give a vague idea about the identity of microbe present in the sample. If we want to get a clear idea about the identity, then sophisticated techniques like PCR analysis and other molecular biological techniques need to be employed.

The physical and chemical characteristics of the pollutants in the atmosphere are widely studied in many urban countries while the biological studies are limited. The temporal and spatial variability of the microbes are yet to be studied, and several experiments are done across the globe regarding that. The objective of this review is to highlight the different techniques that are employed in the research area for the biological characterization of microorganisms present in the atmosphere. Different sampling techniques used for the collection of samples and further experiments done in order to identify several parameters related to the microbial flora are explored here.

1.1 General

Earth's primary atmosphere was inhospitable for microorganisms and other living forms. The present day atmosphere evolved as a result of series of changes in the atmosphere gradually encouraging the metabolic and reproductive activities of microorganisms in it. This gradually promoted the movement of vast number of microbes through the troposphere and worldwide dispersal of microorganisms in the earth's atmosphere [7]. Moreover, microorganisms can enter the atmosphere through various pathways such as soil, dust, plants, and animals. These surfaces are exposed to air currents, allowing microorganisms to become airborne and contribute to the atmospheric microbial load [8, 9].

Bacteria make up approximately 80% of the microorganisms detected in the atmosphere, with concentrations ranging from 10 to 10^7 cells per cubic meter. These bacteria are identified using various techniques, including culture methods and molecular biological techniques. [10, 11]. For example, it ranged from 8.49×10^4 to 2.11×10^6 cells/m³ in Qingdao coastal region, China, and 4800–24,000 cells/m³ in Beijing, a mega city of China [12, 13]. This observation indicates that the concentration of microorganisms in the air can differ based on geographic locations, climatic factors, and environmental conditions. These variations can influence the types and abundance of microorganisms present in the atmosphere at different places and times. The particulate matter in the atmosphere provide habitat for these airborne microorganism by a phenomenon called adhesion. It also provides the microorganisms shield from the harmful radiations of the atmosphere and air with nutrients supported by cloud, rainwater and particles provide essential nutrients for the survival of microbes [14]. The microorganisms attached to PM particles have chances of survival more than that of those that exist individually in the atmosphere. Thus, concentration of such attached microbes becomes abundant, and the interaction of

these microbes among themselves and the external environment provide amazing knowledge regarding the properties of microorganisms in the atmosphere which can form the basics of consequent studies.

1.2 Recent Studies in the Area

Sampling can be done using M air T sampler and Mas sampler. After sampling, the plates containing Dichloran Rose Bengal Chloramphenicol (DRBC) medium should be incubated at a temperature of 300 ± 2 °C for a maximum of seven days. This incubation period allows for the isolation and phenotypic identification of microorganisms present in the samples. Specifically, during this timeframe, various fungi such as *Aspergillus*, *Curvularia*, *Penicillium*, *Neurospora*, *Rhizopus*, and *Trichoderma* were identified. These are the specific types of fungi that were detected and characterized during the incubation period [15–17].

According to the findings of Chen Cao, microorganisms present in PM_{2.5} (particulate matter with a diameter of 2.5 μm or less) and PM₁₀ (particulate matter with a diameter of 10 μm or less) particles play a significant role in causing allergies and respiratory diseases. These microorganisms, when inhaled, can trigger immune responses and respiratory inflammation, leading to various respiratory health issues. Prebaked tissuquartz filters were used in high-volume samplers for aerosol collection, and DNA extraction was done by doing centrifugation of the PM samples. The resuspension is filtered using a disc filter which was used for DNA extraction DNA isolation kit. The Illumina MiSeq and HiSeq 2000 sequencing systems were used for sequencing [18].

The microbial characteristics and concentrations of bioaerosols vary according to the environmental conditions. This is experimentally illustrated in the experiment conducted during the autumn haze days in Xi'an, China by Yanpeng Li. Bacterial and fungal aerosols of various size ranges were collected using an Andersen six-stage sampler, which consists of six glass Petri dishes. The sampler allows for the separation and collection of aerosols based on their particle sizes, enabling the analysis and characterization of bacterial and fungal populations present in each stage of the sampler. Standard disinfection procedures were adopted, and sterile conditions were maintained throughout the experiment. Nutrient agar and Sabouraud dextrose agar were used for culturing bacteria and fungi. After incubation at 37 °C for 48 h, positive-hole correction method for counting the colonies is employed [19].

Studies conducted in Beijing, China, included the collection of PM_{2.5} particles from roof top of building was collected using a high-volume air particulate matter sampler using prebaked quartz filters. Their approach for the DNA extraction was a little different from the usual practice in which a particular area of the PM_{2.5} filter paper was clipped grinded into a powder using which is loaded into a PowerSoil DNA isolation kit to extract DNA. After the DNA extraction, the bacterial 16S ribosomal RNA (rRNA) gene was amplified by polymerase chain reaction (PCR), using primers

338F and 806R, and primers 1737F and 2043R were used for the amplification of the fungal rRNA [20].

Low-volume air samplers were used for the collection of microbial communities of Urumqi. PM₁ was collected for 72 h using quartz fiber filters and high-volume samplers for PM₁₀ for 24 h using glass fiber filters. The primers 319F and 806R. Bacterial community is mainly composed of Actinobacteria, Proteobacteria, and Firmicutes, and fungal microbial community constituted Ascomycota and Basidiomycota. *Acinetobacter*, *Delftia*, *Serratia*, and *Chryseobacterium* were the pathogens identified [21].

High-volume samplers were used to collect samples from Hangzhou, China, in rectangular glass fiber membrane. DNA extraction from the airborne particulate matter (PM) samples was performed using a PowerSoil DNA extraction kit, and water samples were extracted using a Power Water DNA extraction kit. 515-F and 907-R were the primer pairs used for the sequence analysis. Sequence processing was done using QIIME package, and statistical analyses were done using Origin. A “Human Pathogen Database” was created, and the available pathogenic gene sequences were compared using the prepared “Human Pathogen Database” [22].

With an aim to study the nature of microbes in airborne particles of urban and rural areas, PM_{2.5} and PM₁₀ samples were collected from different areas of Hangzhou. Sample collection sites were the top of a residential building (urban) and forest scenic spot (rural). Air samplers and glass fiber were employed for sampling. DNeasy PowerSoil Kit was used for the extraction of bacterial and fungal DNA. Phenol–chloroform–isoamyl alcohol was used to extract sufficient quantities of DNA from the filter papers. The primer pairs 515-F and 806-R were used for bacterial sequence, and for fungal analysis, 2045-F and 2390-R were used. The concentrations of bacteria and fungi were calculated using quantitative PCR technique (qPCR) [23, 24]. The bacterial and fungal genes need sequencing which can be accomplished on an Ion Torrent platform. Ion plus Fragment Library Kit and QIIME package can be used for the sequence analysis and further processing.

The air quality is indeed influenced by the health and condition of both land and marine ecosystems. In Shandong Province of China, 23 h triplicate samples were collected using PM_{2.5} samplers and stored in -80°C. NanoDrop spectrophotometer was used for the quantification of extracted DNA followed by qPCR technique. qPCR technique was validated by the addition of ultra-pure water to check PCR contamination [25].

In the Xi'an city, in sterilized polycarbonate membranes using an Omni air sampler. This is followed by shaking in Erlenmeyer flasks at the rate of 120 r/min for 20 min containing phosphate buffer and Tween-80 solution. The blue fluorescence emitted by DAPI (4',6-diamidino-2-phenylindole) was quantified by counting using a fluorescent microscope. This technique allows for the visualization and enumeration of cells or particles that emit blue fluorescence when bound with DAPI. The data is used to find out the concentration and number of microorganisms which is later used to find the mean and standard deviation of the microbial population of the air mass [26]. Similar type of analysis is done Lijie Dong using a six-stage microorganism FA-1 cascade impactor [12].

A 13 staged Micro-Orifice Uniform Deposit Impactor was used for the collection of particulate matter samples during Sep. 11–14, 2017. The aluminum membranes were weighed prior and after the sampling procedure. Membrane of each stage with sample is placed in 0.05% tween 20 water, shaken at 200 r/min for 4 h. The samples are then stored in -20°C until analysis. The supernatant in the tubes are subjected to Limulus ameocyte lysate (LAL) assay after centrifugation. The standard curve was prepared using endotoxin free water. The bacterial concentration is then determined from the experimental results obtained [27].

Sampling was conducted using a high-volume total suspended particle (TSP) sampler in the urban hospitals of China using glass fiber filters. Total genomic DNA was extracted using a FastDNA Spin Kit, Qubit 3.0 was used to check the quality, and extracted DNA was diluted and for further use. Quant Studio 6 Flex system was used for RT-qPCR technique. The amplified products were purified using a purification kit and then fed Illumina MiSeq system for sequencing. Further taxonomical details were found out using FLASH, UPARSE algorithm, and BLAST [28].

Kai Wei et al. collected air samples during haze and sunny days using the button aerosol sampler in mixed cellulose ester (MCE) filter. Filters were placed in centrifuge tubes, and centrifugation was done in the presence of 2 mL sterile water and an addition of one drop of Tween 20 for two hours. Polymerase chain reaction was used to amplify the V1–V3 region of the bacteria using primers 27F and 533R [29].

Rui Lu and coworkers found out that there is no significant effect of haze pollution in bacterial community structures through his work conducted in Xi'an, China. Samples collected in sterilized polycarbonate membranes were subjected to fluorescent microscopic analysis after standard laboratory procedures of isolation and storage. DNA sequencing was done using OMEGA Soil DNA Kit, and the extracted DNA was then subjected for PCR amplification using 338F and 806R primers to amplify the V3–V4 hypervariable regions of the bacterial 16S rRNA gene [30].

In a study conducted in an urban city in India, a novel technique called the Becton Dickinson (BD) BBL Crystal Mind Auto reader was utilized for the enumeration and characterization of airborne microbial communities. The BD BBL Crystal Mind Auto reader is an automated system designed to analyze and identify microorganisms based on their biochemical properties. This advanced technology allows for efficient and high-throughput analysis of airborne samples, providing valuable insights into the composition and diversity of the microbial communities present in the urban environment. PM_{10} and $\text{PM}_{2.5}$ aerosol samples were collected using respirable dust sampler in GFA (glass fiber filter) and Polltech finedust Sampler in Teflon filter paper, respectively. 48 samples, one sample every week in each month was taken from March 2013 to February 2014. Sabouraud dextrose agar (SDA) and nutrient agar medium media was used for the isolation of fungi and bacteria using pour plate technique. Optimization of bacterial isolates was done after optimizing the culture media using nutrient broth (NB) and Trypticase soya broth (TSB) while in the case of fungal isolates the media was sabouraud dextrose agar (SDA), potato dextrose agar (PDA), and Czapek Dox Agar (CDA) media. This was followed by identification of selected fungal isolates using an optical microscope [31, 32].

Passive air sampling was conducted in a tertiary care institute hospital. Bacteria and fungi were collected on nutrient agar, blood agar and sabouraud dextrose agar (SDA) by exposing the petridishes for 60 min in the morning and afternoon [33].

Air sampling was done in slaughter hall, processing room, chilling room and further processing room for a slaughter house and milk reception area, pasteurization unit, and packaging rooms for a dairy plant. HI Media. No LA002air sampler system, whose working principle is centrifugal impaction, was used for air sampling. Sterile plastic air sampler strips were also used for the collection of microbes [34].

1.3 Conclusion

Most of the studies of airborne microorganisms are concentrated on collection of air samples, extraction of microorganisms from filter paper followed by DNA extraction and sequencing. Several equipment were used for the sampling of air particulates which includes respirable dust sampler, button aerosol sampler, high-volume total suspended particle (TSP) sampler, etc. Several DNA extraction kits are available in the market, and some of them are mentioned in this review. PowerSoil DNA extraction kit, OMEGA Soil DNA Kit, E.Z.N.A. Soil DNA Kit, and DNeasy PowerSoil Kit are some of them. Each study has employed different primers for the characterization of samples according to the requirement of the microbe to be identified. Thus, this paper represents a brief idea about the different unique methodologies adopted by different researchers in the area of airborne microorganisms.

References

1. Weltgesundheitsorganisation (2021) World Health Organization, European centre for environment. WHO global air quality guidelines: particulate matter (PM_{2.5} and PM₁₀), ozone, nitrogen dioxide, sulfur dioxide and carbon monoxide. World Health Organization
2. Goodsite ME, Hertel O, Johnson MS, Jørgensen NR (2021) Urban air quality: Sources and concentrations. *Air Pollution Sources, Statistics and Health Effects*, 193–214
3. Gupta A, Gupta R, Singh RL (2017). Microbes and environment. In: *Principles and applications of environmental biotechnology for a sustainable future*, Springer, Singapore, pp 43–84
4. Parshintsev J, Hartonen K, Riekkola ML (2017) Environmental analysis: atmospheric samples. *Liquid Chromatogr* 2017:769–798
5. Pepper IL, Gerba CP (2015) Aeromicrobiology. *Environmental Microbiology Academic Press*, pp 89–110
6. Cavicchioli R, Ripple WJ, Timmis KN, Azam F, Bakken LR, Baylis M, Behrenfeld MJ, Boetius A, Boyd PW, Classen AT, Crowther TW (2019) Scientists' warning to humanity: microorganisms and climate change. *Nat Rev Microbiol* 17(9):569–586
7. Henderson TJ, Salem H (2016) The atmosphere: its developmental history and contributions to microbial evolution and habitat 1–41
8. Zhang Y, Huang W, Cai T, Fang D, Wang Y, Song J, Hu M, Zhang Y (2016) Concentrations and chemical compositions of fine particles (PM_{2.5}) during haze and non-haze days in Beijing. *Atmospheric Res* 174:62–69

9. Zhang F, He J, Lin L, Jin H (2015) Dominance of picophytoplankton in the newly open surface water of the central Arctic Ocean. *Polar Biol* 38(7):1081–1089
10. Albrecht A, Witzemberger R, Bernzen U, Jackel U (2007) Detection of airborne microbes in a composting facility by cultivation based and cultivation-independent methods. *Ann Agric Environ Med* 14(1)
11. Liu Z, Li H, Cao G (2017) Quick estimation model for the concentration of indoor airborne culturable bacteria: an application of machine learning. *Int J Environ Res Public Health* 14(8):857
12. Dong L, Qi J, Shao C, Zhong X, Gao D, Cao W, Gao J, Bai R, Long G, Chu C (2016) Concentration and size distribution of total airborne microbes in hazy and foggy weather. *Sci Total Environ* 541:1011–1018
13. Fang Z, Ouyang Z, Zheng H, Wang X (2008) Concentration and size distribution of culturable airborne microorganisms in outdoor environments in Beijing, China. *Aerosol Sci Tech* 42(5):325–34
14. Maier RM, Gentry TJ (2015) Microorganisms and organic pollutants. Environmental microbiology. Academic Press, pp 377–413
15. Santos D, Pukinskas SR, Oshida JT, Oliveira L, Carvallho AF, Melhem MS (2015) A new culture medium for recovering the agents of Cryptococcosis from environmental sources. *Braz J Microbiol* 46:355–358
16. e Silva DD, Marcusso RM, Barbosa CG, Gonçalves FL, Cardoso MR (2020) Air pollution and its impact on the concentration of airborne fungi in the megacity of São Paulo, Brazil. *Heliyon* 6(10):e05065
17. Moura ML, Caldas CC, Santos DC, Andrade MD, Gonçalves FL (2015) Castro e Silva DM. The impact capacity of Millipore M air T® and Merck MAS-100® in an external environment. *Access J. Environ Res* 1:1–6
18. Cao C, Jiang W, Wang B, Fang J, Lang J, Tian G, Jiang J, Zhu TF (2014) Inhalable microorganisms in Beijing's PM_{2.5} and PM₁₀ pollutants during a severe smog event. *Environ Sci Tech* 48(3):1499–507
19. Li Y, Fu H, Wang W, Liu J, Meng Q, Wang W (2015) Characteristics of bacterial and fungal aerosols during the autumn haze days in Xi'an. *China Atmos Environ* 122:439–447
20. Du P, Du R, Ren W, Lu Z, Zhang Y, Fu P (2018) Variations of bacteria and fungi in PM_{2.5} in Beijing, China. *Atmospheric Environ* 172:55–64
21. Gou H, Lu J, Li S, Tong Y, Xie C, Zheng X (2016) Assessment of microbial communities in PM₁ and PM₁₀ of Urumqi during winter. *Environ Pollut* 214:202–210
22. Liu H, Hu Z, Zhou M, Hu J, Yao X, Zhang H, Li Z, Lou L, Xi C, Qian H, Li C (2019) The distribution variance of airborne microorganisms in urban and rural environments. *Environ Pollut* 247:898–906
23. Liu H, Zhang X, Zhang H, Yao X, Zhou M, Wang J, He Z, Zhang H, Lou L, Mao W, Zheng P (2018) Effect of air pollution on the total bacteria and pathogenic bacteria in different sizes of particulate matter. *Environ Pollut* 233:483–493
24. Speth DR, Guerrero-Cruz S, Dutilh BE, Jetten MS (2016) Genome-based microbial ecology of anammox granules in a full-scale wastewater treatment system. *Nat Commun* 7(1):1
25. Wei M, Liu H, Chen J, Xu C, Li J, Xu P, Sun Z (2020) Effects of aerosol pollution on PM_{2.5}-associated bacteria in typical inland and coastal cities of northern China during the winter heating season. *Environ Pollut* 262:114188
26. Xie Z, Li Y, Lu R, Li W, Fan C, Liu P, Wang J, Wang W (2018) Characteristics of total airborne microbes at various air quality levels. *J Aerosol Sci* 116:57–65
27. Zhang T, Li X, Wang M, Chen H, Yao M (2019) Microbial aerosol chemistry characteristics in highly polluted air. *Sci China Chem* 62(8):1051–1063
28. Gao XL, Shao MF, Wang Q, Wang LT, Fang WY, Ouyang F, Li J (2018) Airborne microbial communities in the atmospheric environment of urban hospitals in China. *J Hazard Mater* 349:10–17
29. Wei K, Zou Z, Zheng Y, Li J, Shen F, Wu CY, Wu Y, Hu M, Yao M (2016) Ambient bioaerosol particle dynamics observed during haze and sunny days in Beijing. *Sci Total Environ* 550:751–759

30. Lu R, Li Y, Li W, Xie Z, Fan C, Liu P, Deng S (2018) Bacterial community structure in atmospheric particulate matters of different sizes during the haze days in Xi'an, China. *Sci Total Environ* 637:244–252
31. Raghav N, Shrivastava JN, Satsangi GP, Kumar R (2020) Enumeration and characterization of airborne microbial communities in an outdoor environment of the city of Taj India. *Urban Climate* 32:100596
32. Tyagi P, Mukhopadhyay K. Assessment of bio aerosols in rooms of tertiary care hospital in New Delhi, India. *Iasta Bulletin* 461 (2012)
33. Kotgire S, Akhtar R, Damle A, Siddiqui S, Padekar H, Afreen U (2020) Bioaerosol assessment of indoor air in hospital wards from a tertiary care hospital. *Indian J Microbiol Res* 7:28–34
34. Vinayananda C, Deepak S, Elango A (2018) Analysis of microbial quality of the air in meat and dairy plants by impactation technique. *Bull Environm Pharmacol Life Sci* 7:7–13

Coastal and Harbour Engineering

Behaviour of Quartz Powder-Based Fibre-Reinforced Concrete



P. Kaviya and A. Sattainathan Sharma

1 Introduction

Reinforced concrete has reached its heights in construction industry. The materials used in concrete can be hardly replaced by other materials. This is because of its versatility, being strong, and stable. Though the materials cannot be completely replaced, it can be partially replaced with suitable materials. The utilization of novel materials as partial replacements for cement in concrete, while ensuring the preservation of mechanical properties, has garnered significant attention in recent times. Certain raw materials, when incorporated into the concrete, have the potential to enhance its strength. These materials work in conjunction with the replacement of existing components, contributing to the overall improvement in concrete strength. Among many additive materials, we have opted quartz powder as a partial replacement of cement because it is naturally fine, chemically inert at normal ambient temperature more importantly the chemical composition. The chemical composition which mainly constitutes of silica which when mixed with cement accelerates the pozzolanic reaction. Along with the chemical reaction there will be physical advantages such as packing and filling effect on concrete matrix. The effectiveness of quartz powder as a replacement for cement in concrete is influenced by its size, chemical composition, and the mixing method employed. The interaction of these parameters plays a crucial role in facilitating pozzolanic activity and improving the mechanical strength of the concrete. The size of QP is responsible for filling the matrix, whereas the method of introducing QP into the dry mix of concrete starts the pozzolanic effect early. The QP is introduced in concrete by pre soaking it for 6 h in the water required to mix the concrete. This is done in order to dissolve the SiO_2 , CaO and Na_2O ion. The Na^+ ion being more mobile than Ca^+ ion, more Na^+

P. Kaviya (✉) · A. S. Sharma
Department of Civil Engineering, SRM Valliammai Engineering College, Kattankulathur,
Chennai, Tamil Nadu 603203, India
e-mail: kaavi2405@gmail.com

ion is formed in the solution. Higher surface area of QP results in increased ion exchange. As a soaking effect the concentration of Na^+ ion decreases. The chemical bond breaks as a result of hydrolysis which leads to the formation of silinol group. Therefore it reacts to form secondary calcium silicate hydrate (C–H–S) known as pozzolanic reaction. The density of concrete is increased which in turn reduced the water absorption and porosity of concrete. Polyolefin, a synthetic fibre, offers valuable properties in concrete applications. Its remarkable features include high abrasion resistance and minimal water absorption, ensuring that it does not interfere with the water–cement ratio. Additionally, polyolefin exhibits corrosion resistance, high strain capacity, chemical resistance, excellent bonding with the cement matrix, and long-term crack control. These attributes provide added advantages, enhancing the strength, durability, and post-cracking behaviour of hardened concrete. Consequently, polyolefin fibres are widely utilized in concrete construction due to their beneficial properties. The aim of this work is to effectively utilize the chemical and physical properties of quartz powder with polyolefin fibre in concrete. The results are correlated with the conventional concrete.

1.1 Literature Review

Bignozzi et al. [1] conducted a study on different types of glass powder as a substitute for cement. They investigated the composition of glass powder in cement mortar by replacing 25% of its weight. Prism specimens dimension 40 mm in length, 40 mm in width, and 160 mm in height were cast and cured for various duration. The results manifested that the use of glass powder as a supplementary cementitious material contributed to the pozzolanic reaction. In another study by Lin et al. [2], the influence of water–cement ratio and quartz content on cement paste was examined. Two water–cement ratios (0.5 and 0.2) and three percentages of quartz powder (0, 10, and 20%) were investigated. The findings revealed that a water–cement ratio of 0.5% significantly decreased the compressive strength, while a ratio of 0.2% showed no significant difference compared to the controlled paste. Elaqla et al. [3] explored the utilization of local glass powder as a replacement to cement. Four different replacement percentages (0%, 10%, 20%, and 30%) were employed. The results indicated that a 10% replacement of glass powder exhibited higher compressive strength, approximately 130% higher than conventional concrete. Smirnova et al. [4] investigated the influence of polyolefin fibres on the mechanical properties of concrete, including the method of fibre introduction. The study revealed that the fibre introduction method improved the uniform distribution of fibres in fresh concrete. In a study by Elaqla et al. [5], the effect of differing water–cement ratios along with soaking time of glass powder on the activation of pozzolanic reaction and mechanical properties of concrete was determined. These previous research studies collectively demonstrate that incorporating quartz powder as a partial replacement to cement in concrete enhances the pozzolanic reaction during the early stages of concrete life. Furthermore, the inclusion of polyolefin fibres in concrete improves its resistance

against cracking. The current study aims to investigate the mechanical properties of quartz powder when soaked at different percentages, in combination with polyolefin fibres. The findings will accord to a clearer vision of the benefits associated with the utilization of these materials in concrete, ultimately leading to the construction of more durable structures.

1.2 Objective of Study

- To optimize the percentage of quartz powder as a partial replacement of cement.
- To determine the effectiveness of polyolefin fibre in concrete.
- To compare the characteristic compressive strength of quartz powder replaced concrete with conventional concrete.

1.3 Materials

The experimental investigation utilized Portland pozzolana cement (CEM), which is fly ash-based, along with quartz powder (QP). The chemical and physical characteristics of CEM and QP, as per the specifications outlined in IS 1489:1991 Part 1 [6], are presented in Tables 1 and 2, respectively. These tables provide comprehensive information regarding the chemical composition and physical properties of CEM and QP, facilitating a deeper understanding of their suitability for the experimental study. Coarse aggregate with nominal maximum size of 20 mm down grade was used to satisfy the requirement of IS 383-2016 [7]. Fine aggregate with 2.67 fineness modulus was used satisfying the requirement of zone II, similar to medium river sand. Table 3 displays sieve analysis and physical properties of the coarse aggregate (CA) and fine aggregate (FA) used in the experiment. Portable water was used in accordance with the conditions of IS 456-2000 [8]. The locally available superplasticizer (conplast SP-430) having specific gravity and density of 1.2 and 1260 kg/m³, respectively, was used.

2 Experimental Program

2.1 Mix Combination

The concrete mix was designed as per requirements of IS 456-2000 [8] and IS 10262-2009 [9]. Considering the requirements, concrete mix of grade M40 for reference (RC), concrete with varying percentage of QP (<90 μm in diameter), and concrete

Table 1 Material properties of cement and quartz powder

Properties	Experimental value of CEM	Experimental value of QP	Values as per IS 1489: 1991
Specific gravity	3.13	2.94	3.15
Finesses (Blaine) m ² /kg	356	790	300 (minimum)
Normal consistency (%)	30	–	–
Initial setting time (min)	56	–	30 (minimum)
Final setting time (min)	245	–	600 (maximum)
Soundness (le-chatelier expansion) (mm)	3	2.4	10 (maximum)
Compressive strength (MPa) 3 days	16	–	16 (minimum)
7 days	25		22 (minimum)
28 days	34		33 (minimum)

Table 2 Chemical properties of cement and quartz powder

Chemical composition	Experimental value of CEM	Experimental value of QP	Values as per IS 1489: 1991
Insoluble residue (%)	2.3	1.89	3 (maximum)
Lime (CaO)	61.3	9.2	–
Silicon dioxide (SiO ₂)	20.4	71.1	–
Aluminium oxide (Al ₂ O ₃)	4.56	0.95	–
Magnesia (%)	1.65	4.4	6 (maximum)
Sulphuric anhydride (SO ₃) (%)	2.6	–	3.5 (maximum)
Loss of ignition (%)	3.06	2.5	5 (maximum)
Chloride content (%)	0.06	–	0.1 (maximum)
Sodium oxide (Na ₂ O + 0.658 K ₂ O) (%)	0.1	–	0.6 (maximum)

with 0.15% of polyolefin fibre as given in Table 4 were experimented. A water-cement ratio of 0.36 and 1% dosage of superplasticizer was kept constant throughout the investigation.

Table 3 Properties of CA and FA

Properties	CA	FA
Specific gravity	2.83	2.68
Water absorption (%)	0.5	2.60
Fineness modulus	–	2.67
Aggregate impact value	23	–
Aggregate crushing value	25	–

Table 4 Composition of the tested concrete

Specimen designation	% CEM	% QP	% Fibre
RC	100	0	–
10QP	90	10	–
15QP	85	15	–
20QP	80	20	–
0.15PF	100	0	0.15

2.2 Mixing Methods, Casting, and Curing

In the case of reference concrete (RC[']) and 0.15PF (0.15% polyolefin fibre), the mixing process followed the guidelines specified in IS 456-2000 [8]. Initially, cement, aggregate, and polyolefin fibre were dry mixed for two minutes to achieve a uniform blend. Subsequently, the liquid components, including water and superplasticizer, were added to the dry mix, and the mixing continued for an additional four minutes. On the other hand, for the concrete containing quartz powder (QP), the QP was first soaked in water for a duration of six hours, utilizing a predetermined amount of water. After soaking, the QP was gradually introduced into the dry concrete ingredients. The entire mixture was thoroughly mixed until a homogeneous consistency was attained. The homogeneous mixtures obtained from both cases were then cast into cubes with uniform dimensions of 150 mm on each side. Additionally, cylinder specimens of dimension 150 mm diameter and 300 mm height were prepared for each type of mix. These specimens were carefully cured for duration of 7, 14, and 28 days under normal ambient temperature. By following this methodical approach, the specimens were prepared and cured, allowing for subsequent testing at different curing periods.

3 Results and Discussion

Workability: The slump value increased gradually with the increase of QP content as shown in Fig. 1. This is because the water absorbing capacity of QP is nearly zero. The 0.15PF mix showed almost same slump value as that of RF. The compaction factor value of concrete with QP content showed an increasing trend from RC to 20

QP as shown in Fig. 2; this is due the smaller particle size of (<90 μm in diameter) of QP as shown in the particle size distribution curve. Therefore, it is clear that the particle size being less than that of cement, which effectively contributed to the packing and filling of concrete matrix.

Density: The density (ρ) of concrete was obtained by dividing the measured mass to the volume of the same as per IS: 1199-2018 [10]. Density of concrete improved with the addition of QP. The maximum density was observed in 20QP. The increase in density is due the smaller particle size of (<90 μm in diameter) QP, thereby creating a denser matrix. It is clear that the particle size being less than that of cement, which effectively contributed to the packing and filling of concrete matrix.

Compression Testing: The test was as per IS: 516-1959 [11] on cubes-shaped specimens cured in batches for 7, 14, 28 days as illustrated in Fig. 3a. The test results were compared with the results of conventional cube of similar size and curing period, respectively. Based on the experimental results obtained in this study, the

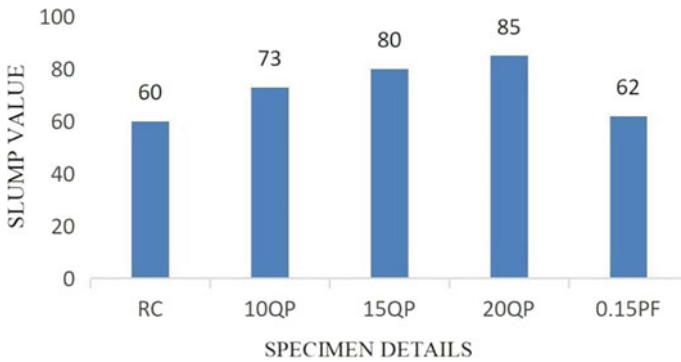


Fig. 1 Slump value results

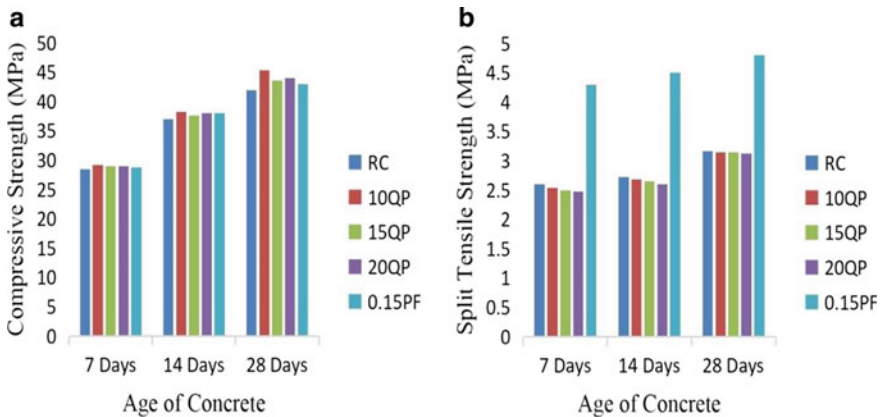


Fig. 2 a Compression test results; b Split tensile strength results

characteristic compressive strength of concrete reached maximum value for 10QP when compared to other concrete mix whilst 0.15PF performed equally with the RF satisfying the requirements. From Fig. 2a, the strength seems to be sensitive to the combination in different proportion of QP, and increase in QP content more than 10 percent to the weight of cement showed a negative results on compression strength. Therefore, the research findings suggest that the optimal dosage for replacing cement with quartz powder in concrete is 10%. This dosage has demonstrated a significant increase in concrete strength. The study also established a formula to calculate the percentage increase in strength, enabling accurate comparisons between different QP percentages. These findings provide valuable insights for engineers and practitioners, guiding them in selecting the appropriate QP dosage for stronger and more resilient concrete structures.

$$\text{CS increase} = 100 \times \frac{\text{CS with QP} - \text{CS of reference mix}}{\text{CS of reference mix}}$$

Table 5 provides insights into the percentage increase in strength for various concrete mixes compared to the reference mix.

Split tensile strength: The test was conducted on cylinders of 150 mm diameter and 300 mm height as per IS 5816-1999 [12] as illustrated in Fig. 3b. The results of different composition of quartz powder are presented in Fig. 2a Split tensile strength

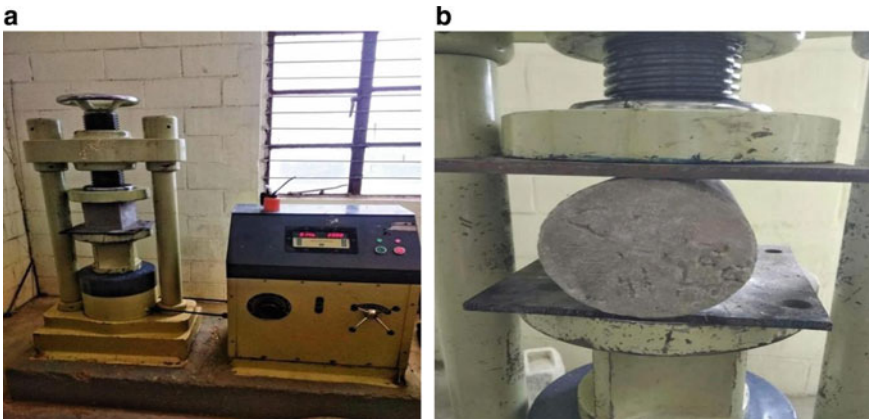


Fig. 3 a Cube compression test setup; b Split tensile strength test setup

Table 5 Percentage increase in strength

Specimen designation	7 days (%)	14 days (%)	28 days (%)
10QP	2.46	3.24	7.86
15QP	1.75	1.62	3.81
20QP	1.75	2.70	4.76
0.15PF	1.05	2.70	2.38

Table 6 Activity index calculation

Specimen designation	7 days	14 days	28 days
10QP	0.902	0.903	0.907
15QP	0.853	0.853	0.856
20QP	0.804	0.805	0.809

and Fig. 3b of each specimen with different percentage of quartz powder was better than that of the reference concrete (RC). The specimen with 0.15% polyolefin fibre had the highest splitting tensile strength; by this it is evident that tensile strength of concrete improves effectively by the active influence of adding fibre.

Activity index calculation: X. Pu [13] in his study have put forward the subsequent mathematical calculate to interpret the activity of any addition or cement replacement material:

Relative index or activity index

$$1 - \frac{\text{Compressive strength of RC} * \text{QP} \%}{\text{Compressive strength of QP mix} * 100}$$

The activity index associated with the incorporation of quartz powder (QP) in concrete can exhibit three possible scenarios. Firstly, a negative value indicates that QP exhibits no activity and leads to a decrease in compressive strength. Secondly, a zero value signifies that the addition of QP does not bring about any significant change, and the compressive strength remains the same. Finally, a positive value suggests that QP demonstrates reactivity, resulting in a constructive effect on the compressive strength of the concrete. These observations regarding the activity index provide valuable insights into the influence of QP replacement on the overall performance of concrete structures. With respect to the above calculation as shown in Table 6, positive results are obtained to all percentage of QP mix, among all 10QP showed the highest activity index.

4 Conclusion

The main conclusion of this study are presented below:

Increasing the replacement of cement with quartz powder (QP) gradually enhances the workability of fresh concrete. QP effectively contributes to the packing and filling effect of the concrete, improving its workability during construction. Typically, the characteristic compressive strength of the concrete mixture with 10% quartz powder (10QP) showed improvement compared to other mixes. At 28 days, the percentage increase in compressive strength was measured to be 7.86%. The experiment also revealed that the addition of polyolefin fibre in concrete enhanced the splitting tensile strength. In addition to the experimental result, mathematical calculation of relative

activity index also showed a positive value, highest of 0.907 for 10QP at the age of 28 days indicating an increase in compressive strength due to QP replacement.

References

1. Bignozzi MC, Saccani A, Barbieri L, Lancellotti I (2015) Glass waste as supplementary cementing materials: the effects of glass chemical composition. *Cement Concr Compos* 55:45–52
2. Lin R-S, Wang X-Y, Zhang G-Y (2018) Effects of quartz powder on the microstructure and key properties of cement paste
3. Elaqla HA, Haloub MAA, Rustom RN (2019) Effect of new mixing method of glass powder as cement replacement on mechanical behavior of concrete. *Constr Build Mater* 203:75–82
4. Smirnova O, Kharitonov A, Belentsov Y (2019) Influence of polyolefin fibers on the strength and deform ability properties of road pavement concrete
5. Elaqlabrahim HA, Elmasry H, Tabasi Mohamme AM, AlwanHisham D, Shamia Mostapha Eln N (2021) Effect of water - to-cement ratio and soaking time of waste glass powder on the behaviour of green concrete
6. IS 1489 (Part 1) : 1991 Portland-Pozzolanacemetspecipication Part 1 Fly Ash Based.
7. IS 383: 2016 Coarse and fine aggregate for concrete—Specification
8. IS. 456: 2000 Plain and reinforced concrete—code of practice (Fourth Revision).
9. IS 10262: 2009 Concrete mix proportioning—Guidelines (First Revision).
10. IS 1199 (Part 1) : 2018 Fresh concrete -methods of sampling, testing and analysis part 2 determination of consistency of fresh concrete (First Revision)
11. IS 516 - 1959 Methods of tests for. Strength of concrete
12. IS 5816: 1999 splitting tensile strength of concrete—Method of test (First Revision)
13. Pu X (2004) Ultra-high strength high performance concrete. Chongqing University Press, Book

Investigations on Ambient Cured Alkali-Activated One-Part Geopolymer Concrete



F. Stellamary and T. Ch. Madhavi

1 Introduction

Inorganic polymers are called as geopolymers. They are also called as alkali-activated materials (AAMs). They can be produced by using raw materials such as industrial waste materials in alkali activation reaction. They have advantages of achieving properties such as fire resistance, resistance against chemical corrosion, adequate mechanical strength, and exceptional durability. After 1980s, ordinary Portland cement (OPC) is replaced by GPC mainly because of their less CO₂ emissions and high performance comparing with OPC [1–5].

The processing technique of GP is a composite chemical reaction by developing dissolution of raw materials, conveyance, and polycondensation of the reaction products. If sodium silicate usage is avoided, two-part or traditional GP will be more energy efficient with a lower CO₂ emission. In addition to that current geopolymeric mixes could be affected from efflorescence because of the less utilization of alkaline silicates which are mixed at the time of processing in polymerisation mechanism [6–8]. The main drawback of GPC is the alkaline solution which is already corrosive in nature for activating aluminosilicate precursor in the two-part method and at the same time impedes their overall productivity.

So, the one-part GPC emerged in which solid alkaline activator and solid Al-Si precursor were prepared to improve their huge production and marketable potentiality. So, we need to get upgraded geopolymer mixes. It was first introduced by French scientist Joesph Davidovits and his team in 2007. The major factor exhorted to the advancement of one-part GP using solid activators in terms of safety concerns are solid activators replaces activating solutions.

F. Stellamary (✉) · T. Ch. Madhavi
Department of Civil Engineering, SRM Institute of Science and Technology, Ramapuram,
Chennai, Tamil Nadu 600089, India
e-mail: sf9003@srmist.edu.in

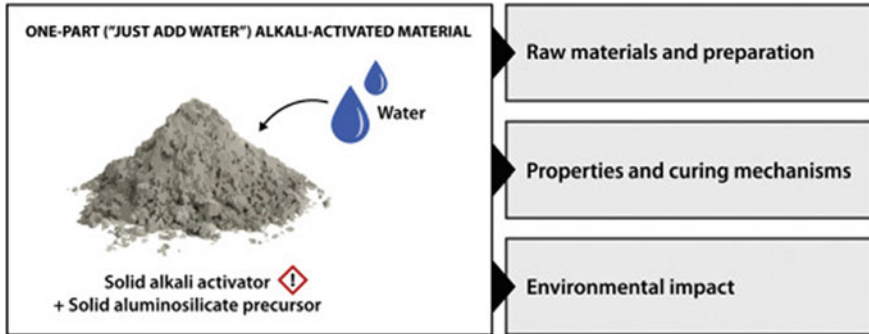


Fig. 1 One-part geopolymer concrete

1.1 What is One-part Geopolymer?

One-part (water added) GPC constitutes a blend of solid alkaline activator and Al-Si precursor, and it can be used same as conventional concrete. One-part GP is the mixture of dry powder and sufficient water Fig. 1.

1.2 Differentiation and Advantages Between Conventional Geopolymer and One-Part Geopolymer

See Table 1; Figs. 2 and 3 and 4.

Table 1 Differentiate between conventional and one-part geopolymer

S. No.	Two-part geopolymer	One-part geopolymer
1	Produced by reaction in between strenuous alkaline solution of first part: NaOH, Na ₂ CO ₃ , Na ₂ SiO ₃ , NaAlO ₂ , Na ₂ SO ₄ , and KOH and second part: solid rich in alumina and silica	Completely solid (powder form) + water added same as conventional OPC
2	Less potential for cast in situ	Greater potential for cast in situ
3	Difficult in handling, storage, and transportation	Easy to handle, storage, and transport
4	Less convenient mixing procedure	Convenient mixing procedure

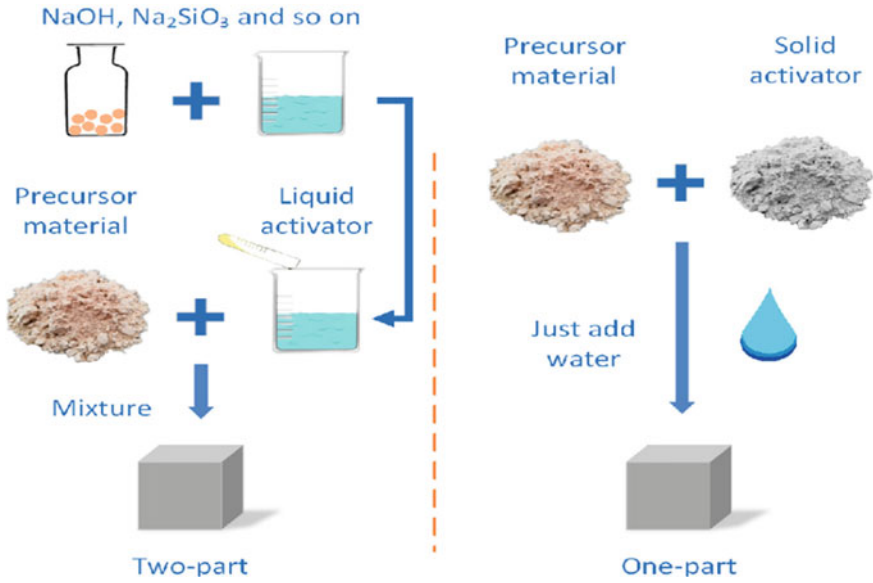


Fig. 2 Differentiation between one-part and two-part geopolymer

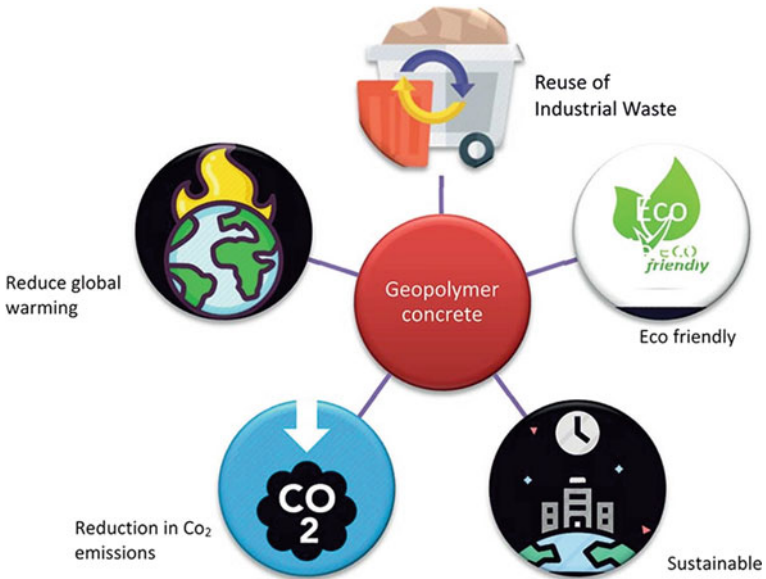


Fig. 3 Benefits of one-part geopolymer

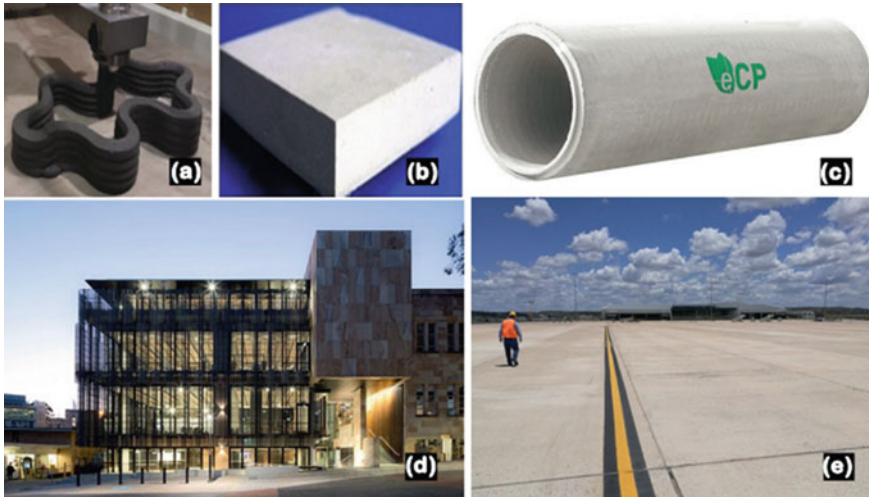


Fig. 4 a 3D printed geopolymer product b geopolymer foam c UG sewer pipes d Building: The University of Queensland's Global Change Institute e precast construction

1.3 Applications of One-Part Geopolymer

Geopolymer concrete can be utilized for construction of pavements/blocks, retaining walls, water tanks, precast bridge decks, and sewer pipe in infra works.

2 Materials or Precursor Used for One-Part Geopolymer Mix

2.1 Aluminosilicate Precursors

- Fly ash from coal combustion with class F (containing less calcium) as defined by ASTM standard C618. Fly ash with classification class C (containing high calcium) is rarely used as its quick setting and less availability [9].
- Blast furnace slag-GGBFS: high calcium content. It hardens at room temperature.
- Al-Si-rich materials such as silica fume, rice husk ash, Kaolin, Metakaolin, geothermal silica, red mud, natural zeolite, and many more [10].

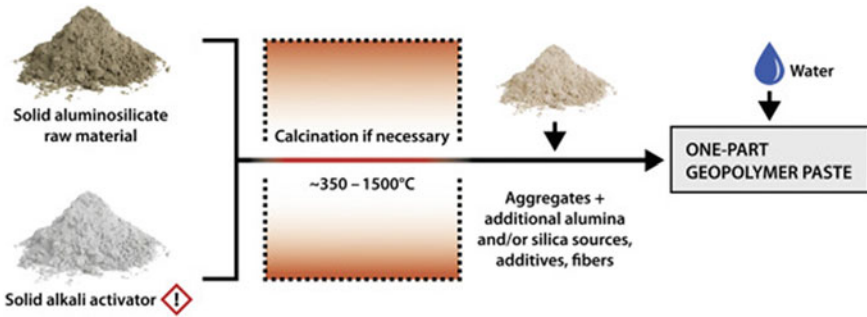


Fig. 5 Preparation method of one-part geopolymer.

2.2 Solid Activators

Activators can be consumed in the formation of GP mix such as solid NaOH, Na_2CO_3 , Na_2SiO_3 , NaAlO_2 , Na_2SO_4 , and KOH.

2.3 Curing Condition

The nature and the property of aluminosilicate precursor plays a major role in curing activity whether in ambient or in elevated temperatures for one-part GP [11].

The heat discharged from dissolving dry activator in solid precursor enhanced the early-ages compressive strength. GP samples are more advantageous as microcracks have been avoided while sealing and is helpful for mechanical aspects [12].

3 Preparation of One-Part Geopolymer

While preparing the GP mix, the water is added to the ingredients at the site itself whenever it is required. This is the method same as Portland cement as explained in Fig. 5. This means omitting alkaline solutions can contribute to the marketable promotion of GP.

4 Properties of One-Part Geopolymer Concrete

Factors deciding the properties are strength of the activator, precursor, and curing circumstances [13–15].

- Fresh one-part GP paste slump test value = 3.52–3.69.

- The setting time has been limited as 23–150 as initial and final 69–230 min, respectively. It has been found out that the setting time increases when fly ash content is included more.
- Also, it has been observed that when NaOH remains constant and quantity of blast furnace slag was added more, then setting time also increased. These are the statements from Nematollahi et al.
- Water absorption for blast furnace slag was 7–16%. (As curing time increased, water absorption reduced.)
- The PH value for the one-part GP pastes made up of residue from silica fume (activated by sodium aluminate) is 13.4–14.7.

5 Geopolymerization Process and Their Phases [16]

Following steps can be occurred after adding water into GP mixtures:

1. ion exchange
2. hydrolysis
3. network breakdown
4. release of Si and Al.

After completion of the above steps, the formation of one-part GP will be similar to two-part GP process as mentioned below:

- (i) speciation (ii) consolidation (iii) restructuring (iv) polymerization.

6 Mechanical Properties of One-Part Geopolymer Concrete

See Table 2.

Table 2 Mechanical properties

Parameters	One -part geopolymer
Compressive strength	<ul style="list-style-type: none"> • Achieved 45 MPa by adding Al-Si along with Na₂SiO₃ at air curing • Resulted as 39 Mpa and 36 MPa by using Al-Si along with Na₂SiO₃ at air and heat curing, respectively • Reported as 66 MPa by including BFS along with sodium metasilicate at ambient curing
Split tensile strength	Recorded the results as 3.5, 3.1, and 4.75 MPa at water, air, and solar curing, respectively
Flexural strength	6, 5, 8.3, and 4.2 MPa at ambient, water, plastic, and air curing, respectively
Fire resistance	It has a good fire resistance

7 Durability Properties of One-Part Geopolymer [17]

The below factors affect the durability properties, namely

- Effect of chemical attack such as sulphate and chloride attack,
- Freeze/thaw cycles,
- Climatic conditions,
- Carbonation and efflorescence,
- Environmental changes and weathering actions.

8 Conclusion

The following is the summary of points discussed:

1. One-part GP is more eco-friendly than two-part GP. It is having a great influence on the products/project as it is added with water at the time of the usage such as cement with ample curing in ambient temperatures, and further, it has better attainable properties.
2. The major sources of Al-Si-based industrial by-products are preferred widely as they are easy available and meet the required properties while major activators such as sodium silicate, sodium metasilicate, sodium hydroxide, and sodium carbonate used to produce the GP mixtures.
3. As compared with OPC, the price of alkali activators is very high. But at the same time the price of industrial waste by-products is lesser as added advantage and affordable as a whole.
4. The compressive strength of one-part AAMs are up to 80 MPa values on 28th day. Also, it has been identified that value of compressive strength and elasticity has been increased, if $\text{SiO}_2/\text{Al}_2\text{O}_3$ molar ratio is increased. It also has been observed that porosity increases when $\text{SiO}_2/\text{Al}_2\text{O}_3$ ratios are low [14]
5. The environmental impact studies/analysis like life-cycle assessment analysis (LCA), global warming potential (GWP) of one-part GP showing the results are comparatively lower than that of two-part GP and OPC concrete. The mix design criteria are also a deciding factor in this. The quantity of activator added is also the major factor affecting environmental impact specifically. Thus, one-part geopolymers are sustainable and more eco-friendly [14].

References

1. Abdollahnejad Z, Pacheco-Torgal F, Aguiar JB, Jesus C (2015) Durability performance of fly ash based one-part geopolymer mortars. *Key Eng Mater* 634:113–120
2. Hajimohammadi A, Jannie S, van Deventer J (2017) Characterisation of one-part geopolymer binders made from fly Ash. *Waste and Biomass Valorization* 8:225–233

3. Nematollahi B, Sanjayan J, Ahmed Shaikh FU (2015) Synthesis of heat and ambient cured one-part geopolymer mixes with different grades of sodium silicate. *Ceram Int* 41(4):5696–5704
4. Nematollahi B, Sanjayan J, Qiu J, Yang E-H (2017) High ductile behavior of a polyethylene fiber-reinforced one-part geopolymer composite: a micromechanics-based investigation. *Arch Civ Mech Eng* 17(3):555–563
5. Nematollahi B, Sanjayan J, Qiu J, Yang E-H (2017) Micromechanics-based investigation of a sustainable ambient temperature cured one-part strain hardening geopolymer composite. *Const Build Mater* 131:552–563
6. Zhang H-Y, Liu J-C, Wu B (2021) Mechanical properties and reaction mechanism of one-part geopolymer mortars. *Const Build Mater* 273:121973
7. Abdel-Gawwad HA, Abo-El-Enein SA (2016) A novel method to produce dry geopolymer cement powder. *HBRC J* 12(1)
8. Neupane K (2022) Evaluation of environmental sustainability of one-part geopolymer binder concrete. *Cleaner Mater* 6:100138
9. Ming LY, Wan En O, Cheng Yong H, Mohd Mustafa Al Bakri Abdullah & Ong Shee Ween: Characteristic of one-part geopolymer as building materials. *Lect Notes Civil Eng* 129:97–118
10. Askarian M, Tao Z, Samali B, Adam G (2019) Shuaibu: mix composition and characterisation of one-part geopolymers with different activators. *Const Build Mater* 225:526–537
11. Ghazy MF, Abd Elaty MA, Mostafa SM Properties of one-part versus two-part geopolymers composites—a review. *Am J Eng Res (AJER)* 11(06):01–14. e-ISSN: 2320-0847 p-ISSN : 2320-0936
12. Cong P, Cheng Y (2021) Advances in geopolymer materials: a comprehensive review. *J Traffic Transp Eng (English Edition)* 8(3):283–314
13. Sturm P, Gluth GJG, Brouwers HJH, Kühne H-C (2016) Synthesizing one-part geopolymers from rice husk ash. *Const Build Mater* 124:961–966
14. Luukkonen T, Abdollahnejad Z, Yliniemi J, Kinnunen P, Illikainen M (2018) One-part alkaliactivated materials: a review. *Cement Concrete Res* 103:21–34
15. Dong M, Elchalakani M, Karrech A (2020) *Construction and building materials* 236 (2020) 117611 Development of high strength one-part geopolymer mortar using sodium metasilicate
16. Askarian M, Tao Z, Adam G, Samali B (2018) Mechanical properties of ambient cured one-part hybrid OPC-geopolymer concrete. *Constr Build Mater* 186(20):330–337
17. ASTM standard C618 ASTM C618-23 standard specification for coal ash and raw or calcined natural pozzolan for use in concrete

Experimental Investigation on the Incorporation of Reed Plant Ash in Concrete



P. Eshanthini, K. Sarayu, and K. Srishanth

1 Introduction

Concrete is an extensively utilized material in the construction industry, composed of a mixture of cement, sand, and aggregate. Utilization of river sand in concrete has significantly decreased in recent times [1, 2]. The major reason for less availability of sand is environmental sustainability. Researches have been made to find the alternate source for river sand in concrete. The fine aggregate present in concrete was partially replaced by various recyclable and eco-friendly material without compromising the strength of the concrete [3]. Several factors contribute to the strength of concrete, such as the quantity of water employed in the mixture and the selected concrete grade [4]. Reed plant is most prolific perennial plant species, with well-established arrangement and no clearly defined confines. Many harsh weather conditions, such as extreme cool or extreme hot, as well as dryness or dankness, have been adapted by the grass despite a few environmental drawbacks, such as invasiveness scientist are have demonstrated its potential to restore the consistency of environmental matrices. Apart from commercial uses, it is also environmental species [5, 6]. The property of a common reed plant is to construct a traditional low carbon building. It offers a cheap and low technology building that can be constructed as both temporary and permanent shelter.

P. Eshanthini (✉) · K. Sarayu · K. Srishanth
Department of Civil Engineering, Sathyabama Institute of Science and Technology, Chennai,
Tamilnadu, India
e-mail: eshaindia14@gmail.com

2 Materials and Methods

2.1 Cement

Cement is a binding material, combined with sand, gravel, and water to form concrete or mixed with water to form mortar [7, 8]. In this experiment, ordinary Portland cement (OPC) 53 grade manufactured by calcareous or other silica, aluminum, or iron oxide, confirming to IS 269: 2015 [9] was used. Table 1 shows the characteristics of cement after testing (Fig. 1).

Table 1 Characteristics of cement

Physical properties	OPC 53 grade	Requirements as per code book IS 269:2015
Fineness (m ² /kg)	290	> 225
Consistency (%)	29	30
Specific gravity	3.15	3.15
Setting time (min)	Initial	> 30
	Final	< 600



Fig. 1 Specific gravity and setting time test of cement



Fig. 2 Specific gravity test of fine and coarse aggregates

Table 2 Characteristics of fine aggregate

Physical properties	Values	
Specific gravity	2.62	
Water absorption (%)	2.65	
Bulk density (kg/m ³)	Loose	1637
	Rodded	1920
Fineness modulus (%)	2.66	

2.2 Fine Aggregate

Crushed aggregate derived from hard granite stone, known as M-sand, was employed as a fine aggregate. It has balanced properties and can withstand any climatic condition [10, 11]. The properties of fine aggregate were tested Fig. 2 as per IS 2386 (part 1 to part 8):1963 [12]. It has excellent fineness which helps the concrete to fill voids, honeycomb effect, etc. The properties of the M-sand were presented in Table 2.

Table 3 Characteristics of coarse aggregate

Physical properties		Values
Specific gravity		2.76
Water absorption (%)		0.33
Bulk density (kg/m ³)	Loose	1429.3
	Rodded	1652
Fineness modulus (%)		6.003

2.3 Coarse Aggregate

In this experimental study (Fig. 2), the coarse aggregate of size less than 20 mm has been used as a coarse aggregate (Table 3).

2.4 Reed Plant Ash

Reed plant is the globally available waste agricultural species. It has longest woody stalks. The reed plant ash was produced from the reed plant. The utilization of reed plant ash in concrete has reduced the environmental hazard [13, 14]. Reed plant ash was prepared by collecting the fresh plant and allowing it to air-dry for 2–3 days, followed by grinding the stalks into pieces and then burn the air-dried reed plant in a furnace at 750°C in order to obtain reed plant ash. The characteristics of reed plant ash was listed in Tables 4 and 5.

Table 4 Properties of reed plant ash

Physical properties	Values
Specific gravity	1.98
Water absorption (%)	4.85
Fineness (%)	2.66
Maximum gradation (mm)	2.36
Density (kg/m ³)	1275

Table 5 Chemical properties of reed plant ash

Chemical components	Results
SiO ₂	37.1
Al ₂ O ₃	0.6
Fe ₂ O ₃	0.7
CaO	6.8
MgO	3.3
Na ₂ O	3.6

Table 6 Mix proportion

Mix design	Cement (kg)	Fine aggregate (kg)		Coarse aggregate (kg)	Water (L)
		Sand (kg)	Reed plant Ash (kg)		
CC	12.30	26.51	0	32.43	6.12
MIX1	12.30	23.60	2.05	32.43	6.12
MIX2	12.30	21.09	4.11	32.43	6.12
MIX3	12.30	18.23	6.167	32.43	6.12

2.5 Mix Design

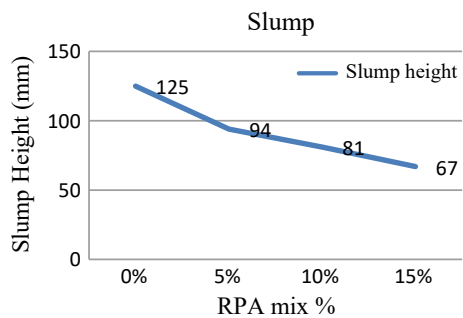
For the current study, the mix ratio of M25 grade concrete was determined based on IS 10262:2019 [15, 16], considering a water–cement ratio of 0.5. Table 6 shows the mix proportion for 0, 5, 10, and 15% replacement of fine aggregate with reed plant ash in concrete.

3 Results and Discussions Test on Fresh Concrete

3.1 Slump Test

The slump cone test procedure is employed to assess the workability or consistency of the concrete mix being prepared. The slump cone itself is a cone-shaped apparatus with dimensions of 10 cm at the top diameter, 20 cm at the bottom diameter, and a height of 30 cm. From the slump test, the slump value of conventional mix is 125 mm. The reed ash concrete mix has less workability compared to the standard mix M25 grade. The increase in RPA decreases the water content in the concrete mixture causes lower slump value (Fig. 3). It is due to poor geometry of RPA and the reduction in fineness modulus.

Fig. 3 Slump values plotted in graph



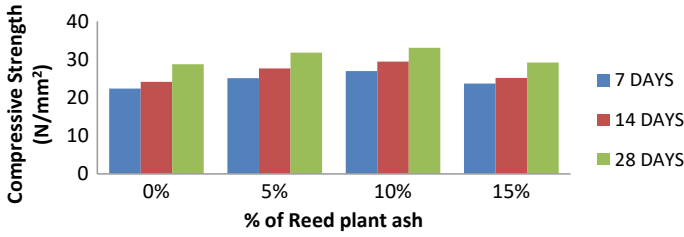


Fig. 4 Bar chart showing compression strength value

3.2 Test on Hardened Concrete

3.2.1 Compressive Strength

The outcome of the compressive strength tests (Fig. 5) for the reed plant ash concrete mixes (Fig. 4) is given in Table 7. As per the test results, the optimum 28-day compressive strength value of 33.38 N/mm² was acquired for the concrete mix made of 10% reed plant ash, which represents an rise in the compressive strength of up to 13.89% compared to the conventional mixture. As the content of RPA (5% and 10%) increases, the compressive strength also increases, but it decreases when the RPA content reaches 15%. By increasing the percentage RPA up to 10%, the value shows a tendency for compressive strength values of RPA-concrete mixes to increase below the simple mixes at each curing. This trend may be attributed to the pozzolanic effect of reed plant ash and the enhancement of cohesive strength between the surface of RPA and the cement adhesive. Additionally, in the initial stages, reed plant ash exhibits a slow reaction with free calcium hydroxide during cement hydration.. By addition of the RPA from 10% up to 15%, the result reveals a propensity for compressive strength values of RPA-concrete mixes to improve. However, by adding the proportion of RPA up to 15% only, the compressive strength values fall. This phenomenon might be attributed to the possibility that increasing the amount of RPA in the concrete could hinder the penetration of water necessary for cement hydration during the curing phase of the cement specimens.



Fig. 5 Compression test on cube

Table 7 Compression strength test results

Mix % of reed plant ash (%)	Average compression strength value (N/Mm ²)		
	7 days	14 days	28 days
0	22.34	24.11	28.74
5	25.09	27.63	31.78
10	26.93	29.43	33.03
15	23.66	25.14	29.18

3.2.2 Split Tensile Strength

The outcome of the split tensile strength tests (Fig. 6) for the RPA-concrete mixes 0, 5, 10, and 15% (Fig. 7) was given in Table 8. As per the test results, the optimum 28-day split tensile strength test value of 4.10 N/mm² was obtained for the concrete mixture made with RPA, which replaced M-sand by 10%, which represents an increase in the split tensile strength of up to 11.8% compared to the conventional mix.



Fig. 6 Split tensile strength test on cylinder

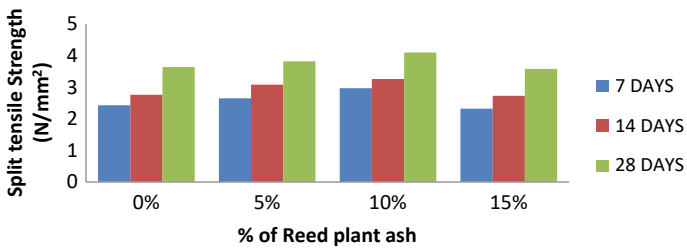


Fig. 7 Bar chart showing split tensile strength value

Table 8 Split tensile strength test result

Mix % of reed plant ash (%)	Average split tensile strength value (N/Mm ²)		
	7 days	14 days	28 days
0	2.43	2.76	3.64
5	2.65	3.08	3.82
10	2.97	3.26	4.10
15	2.32	2.73	3.58

4 Conclusion

In this experimental study, the main work is to find an efficient and promising method for use of the unwanted reed plants in concrete. The reed plant ash (RPA) as a partial replacement for fine aggregate had no discernible impact on the color of the concrete. The decrease in the slump value for the 15 percentage increase of RPA is the consequence of water content from the RPA. The addition of 10% reed plant ash (RPA) was found to be the optimal ratio that produces the highest values of compressive and split tensile strengths above which the effect falls with increases in reed plant ash. This is because adding the content of RPA in the concrete may hamper the impede the water required for hydration process.

References

1. Aziz A, Rama Krishnan A (2019) Analysis on mix design of M25 grade of concrete- case study on modification of terminal building 7:2321–9653
2. Ibrahim A, AL-Jumaily S, Najj N, Kareem Q (2015) An overview of influence of pozzolonic materials on properties of concrete 4:81–92
3. Saraswathy V, Seung Lee H, Yang H-M, Kwon S-J, Karthick S (2017) Comparative study of strength and correction resistance properties of plain and blended cement concrete 2017:306–791
4. Nahata Y, Tank TG, Kholia N (2014) Effect of curing methods on efficiency of curing of cement mortar 9:222–229.
5. Ismail ZZ, Jacel AJ (2014) Environmental friend concrete using giant reed as undesirable wild species 6:68–73
6. Tvukavkina VV, Gerasimova LG, Semushin Mehta VV et al (2019) Properties of composition based on cement with Al_2O_3 —Inorganic materials. *Appl Res.* 255(119358):35–42
7. Xiw N, Akin M, Shi X et al (2018) Permeable concrete pavements using TiO_2 : a review of environmental benefits and durability. *J Cleaner Prod.* 248(119281):3327–3339
8. Gopalakrishnan R, Vignesh B, Jeyalakshmi R et al (2018) Mechanical, electrical and micro structural studies on nano- SiO_2 admixture cement mortar cured with industrial wastewater. *Eng Res Express* 248(119278):3356–3368
9. IS 269:2015. Specifications for 53-grade ordinary Portland cement bureau of Indian Standards, 1–14
10. Li Z, Ding S, Yu X, Han B, Ou J et al (2018) Multifunctional cementitious composites modified with nano Titanium Dioxide- Composites Part-A *Appl Sci Manuf.* SAGE, 128:215–225
11. Yu QL (2018) Application of nanomaterials in Alkali- activated materials et al (2018)—Nanotechnology in Eco-efficient construction (Second Edition) 175:483–495
12. IS 2386 (Part 1 to Part 8):1963 Methods of test for aggregates of concrete
13. Gao L, Ren K, Ren Z, Yu X-J et al (2017) Study on the shear property of nano-MgO modified soil- Marine Georesources and Geotechnology 43(06)
14. Yang LY, Jia ZJ, Zhang YM, Dai JG et al (2016) Effects of nano- TiO_2 on strength, shrinkage and microstructure of alkali activated slag pastes, *Cement Concrete Compos* 35:874–883
15. IS 456–2000, Plain and Reinforced Concrete Bureau of Indian Standards
16. IS 10262–2019, Concrete mix proportioning guidelines

Study on the Bonding Behavior of Hybrid Fiber-Reinforced Concrete Using Ramie and Glass Fibers



S. Torhffi David, R. Ramasubramani, and P. T. Ravichandran

1 Introduction

Concrete is a well-liked composite structural member because of its great compression strength, basic formability, and resistance to harsh climatic conditions. Its extremely low tensile strength is its biggest flaw. Due to the concrete's brittleness, structural concrete members are prone to tensile stresses and crack. By incorporating different fibers into the concrete mixture, it is possible to reduce the brittleness of the concrete and produce a composite material known as fibers reinforced concrete (FRC). Fibers can generally be divided into two categories: natural fibers and synthetic fibers. Steel, carbon, polypropylene, glass, and aramid fibers are artificial fibers, whereas banana, coir, sesal, cotton, and ramie fibers are natural fibers. These fibers increase the concrete's strength to impact loads, reduce shrinkage cracking, and increase concrete's longevity [1].

A form of natural fiber called ramie fiber is obtained from the stem of ramie plants (scientific name: *Boehmeria nivea*), one of nature's toughest fibers, and it finds extensive usage in the textile industry. Ramie fibers outperform the majority of natural fibers worldwide in terms of mechanical qualities. Ramie fiber does have some advantages over synthetic fibers in terms of the environment, that is why it is referred to as an eco-friendly fiber source. Ramie fibers feature unusually long fiber cells that range in length from 110 to 140 mm. Ramie has a length that is almost six times that of cotton and almost eight times that of silk. Glass fiber is a material composed of a number of incredibly fine glass fibers [2–5]. These two fibers are used in our study to improve the compressive, tensile, flexural strength, and bonding of the concrete and to reduce plastic and drying shrinkage cracks. The early hydration stage, plastic shrinkage, environmental cracking caused by thermal changes, drying shrinkage as

S. Torhffi David · R. Ramasubramani (✉) · P. T. Ravichandran
Department of Civil Engineering, Faculty of Engineering and Technology, SRM Institute of Science and Technology, Kattankulathur, Tamil Nadu 603203, India
e-mail: ramasubr@srmist.edu.in

concrete hardens, and the alkali-silica reaction process are among the frequent causes of fractures in concrete. A slab will be casted to find the plastic shrinkage cracks of the optimized concrete and compared with conventional concrete [6, 7].

To examine the bonding behavior of HFRC, pull-out test is carried out. It identifies the amount of force necessary to remove a steel rod or disc with a specific shape from the hardened concrete into which it was casted. Concrete with steel, glass, jute, sisal, and coir fibers had their mechanical properties, shrinkage, and bonding behavior explained by a number of experimental programs, but only a small amount of research had been done using ramie and glass fibers. This study analyzes the mechanical characteristics, shrinkage, and bonding manners of HFRC using ramie and glass fibers [8].

2 Experimental Study

2.1 General

In this section, works done in this project on mix proportion practiced for the preparation of fiber-reinforced concrete for the study. Experimental procedures for assessing concrete properties: Workability, compressive, split tensile, flexural, deflection, and bonding behavior are discussed for various proportions. Size and shape of specimen proposed for the study are mentioned.

2.2 Mix Proportion of Concrete

The mix design of concrete for casting of cubes is M40 grade. The mix proportion is calculated in accordance with IS10262-2019 [9]. The concrete's mix proportioning is shown in Table 1.

The trial mix of grade M40 has been prepared. Six different fiber percentages were used to make six distinct mixes (0.25% glass fiber alone, 0.5% ramie fiber +

Table 1 Mix proportion of concrete

Materials	M40 grade mix
Cement	420 kg/m ³
Fine aggregate	768 kg/m ³
Coarse aggregate	1111 kg/m ³
Water	151 L/m ³
Super plasticizer	4.20 kg/m ³
w/c	0.40
Ratio	1: 1.83: 2.68



Fig. 1 Casting of cube, cylinder, and prism specimens

0.25% glass fiber, 0.4% ramie fiber + 0.25% glass fiber, 0.3% ramie fiber + 0.25% glass fiber, 0.2% ramie fiber + 0.25% glass fiber, and 0.1% ramie fiber + 0.25% glass fiber), respectively, according to volume fraction [12, 13].

2.3 Casting of Specimens

The specimens which we have casted throughout the project are explained below. The specimens include cube, cylinder, prism, slab, and specimen for bond test.

2.3.1 Casting of Cube, Cylinder, and Prism

The cubes, cylinders, and prism are casted in a steel cubical molds size of 100 mm × 100 mm × 100 mm, cylindrical molds size of 100 mm × 200 mm and cuboidal molds size of 100 mm × 100 mm × 500 mm, respectively, on the inside. Nine cubes have been cast out using the mix design specification that was obtained above. To verify that the mix design is right, it is essential to get the compressive strength results of the cubes. After verifying the control concrete mix result, concrete cubes with fibers of different proportions have been casted of 9 numbers to get the results of 7, 14, and 28 days. After finding out the compressive results of concrete cubes with different fibers proportion, optimum percentage of fibers in concrete is found, and with that further specimens are casted. Figure 1 shows the casting of cube, cylinder, and prism specimens in their respective molds.

2.3.2 Slump Test

The workability of fiber-reinforced concrete is primarily determined by the water-cement ratio and fiber weight proportions. The strength parameters are reduced when the water-cement ratio increases. Super plasticizers were utilized at a rate of 0.5% by weight of cement. Workability will improve with the addition of super plasticizers [11]. The slump values for different mixes are shown in Table 2.

Table 2 Slump cone test results

S. No.	Mix	Slump value (mm)
1	M40 – Conventional	85
2	0.25% glass fiber alone	83
3	0.25% glass + 0.1% ramie	70
4	0.25% glass + 0.2% ramie	64
5	0.25% glass + 0.3% ramie	45
6	0.25% glass + 0.4% ramie	27
7	0.25% glass + 0.5% ramie	0

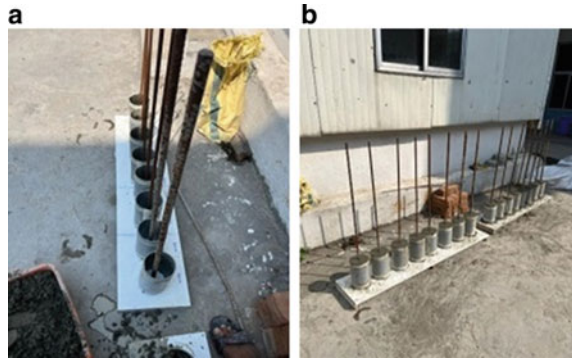
**Fig. 2** Slump cone test

Mix 1 (CC) has a slump value of 85 mm, which is a good sign of workability while mix 2 has a slump value of 83 mm, from these values, we come to know that glass fibers did not absorb water. Whereas, mix 3 has a slump value of 70 mm which is also a good slump, but ramie fiber absorbs some water. In mix 4, 5 6 and 7 further addition of fibers is incorporated, and due to this workability is greatly decreased. While mixing mix 7, balls were forming due to over addition of ramie fibers, and hence, true slump is formed. Sample images are represented in Fig. 2.

2.3.3 Casting of Specimen for Bonding Behavior

Plastic cylindrical pipes of size 100 mm × 200 mm placed in a custom made plywood bench with different set of deformed bars of size (10 mm, 12 mm, and 16 mm) are casted with conventional concrete as well as with optimum concrete to find out the bonding behavior of both mix by pull-out test with a curing intervals of 7, 14, and 28 days. In each specimen, steel rod was placed at the center of the cylinder leaving 25 mm un-bonded length at top and bottom positions of the cylinder, so that 150 mm bonded length was maintained for the entire specimen. ASTM C 234 were followed for the casting of specimens. Following Fig. 3 represents the sample of specimens for bonding behavior.

Fig. 3 **a** Empty bond specimen molds, **b** Molds after casting



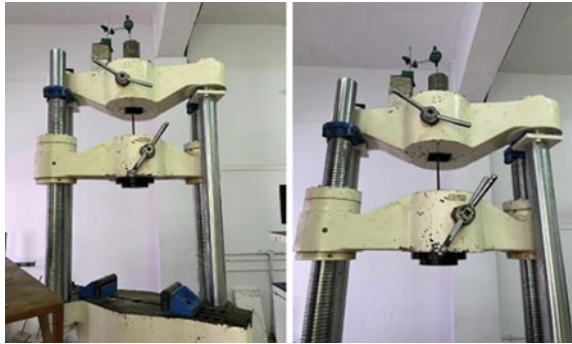
2.4 Experimental Setup for Pull-Out Test

As per ASTM C 234, pull-out test was executed on bond specimens prepared for all the mixes used. Cylinder specimen having 100 mm diameter and 200 mm height was used for this study. For pull-out test, twisted rods of 10, 12, and 16 mm diameters were used. All the bars used conformed to IS 1786: 2008 [10] with specified yield strength of 415 N/mm². In each specimen, steel rod was placed at the center of the cylinder leaving 25 mm un-bonded length at top and bottom positions of the cylinder, so that 150 mm bonded length was maintained for the entire specimen. Universal testing machine (UTM) of capacity 400 kN was used for this pull-out test. During testing, the machine gripped the bottom of the embedded rods shown in Fig. 4 and made a steady vertical pull from the specimen until failure; the load and slip were then recorded. The below equation is the expression for calculating bond stress in N/mm². Pull-out test bond specimen in UTM is shown in Fig. 4.

$$\tau = \frac{F}{\pi dl}$$

where

- τ Bond strength (N/mm²)
- F Failure load (N)
- d Diameter of steel rod (mm)
- l Bonded portion of steel rod (mm)

Fig. 4 Pull-out testing setup

2.5 Bonding Behavior by Pull-Out Test Study

Setup has been done as previously mentioned in experimental study of bonding behavior by pull-out test. The ASTM C 234 standard evaluated the bond's characteristics. Deformed Fe415 bars were employed in cylinders with a diameter of 100 mm and a height of 200 mm. 10, 12, and 16 mm deformed bars were taken into consideration. The top and bottom 25 mm of each specimen's 200 mm total embedment length were left un-bonded. This left a 150 mm effective bond length to determine the bond stress using the formula, $\tau = \frac{F}{\pi dl}$, where F , d , and l are the applied load in N , diameter and length are in mm, respectively. Bond stress was calculated as per the guidelines BS 8110 and IS 456: 2000 and is tabulated in Table 3, and it is used for comparison. Figure 5 shows the bond-tested specimen.

The bond stress results with different size of bars in CC and OC at 7 days are shown in Table 4 and Fig. 6. After curing is done, the specimens were subjected to bond stress in UTM to check the ultimate stress taken. The bond stress of specimen increases in OC when compared to CC in all dia of bars. As a result, in terms of the design bond stress of the concrete mixes investigated in this study, the use of fibers is structurally sound. The concrete with 10 mm bars took the most bond stress while the 16 mm took the least bond stress. Based on the results obtained, OC with 10 mm dia bars provides better bonding strength.

Table 5 and Fig. 7 show the bond stress findings with different bar sizes in CC and OC after 14 days. Following curing, the specimens were subjected to bond stress in UTM to determine the ultimate stress taken. In all dia of bars, the bond stress of

Table 3 Bond stress as per the guidelines

Mix	Theoretical bond stress, N/mm ²	
	IS 456: 2000 (Deformed rod)	BS 8110 (Deformed rod)
CC	2.24	2.88
Glass fibers only		2.59
OC		2.73

Fig. 5 Bond tested specimen



Table 4 Bond stress @ 7 days

Diameters of bar (mm)	Bond stress (N/mm ²)	
	CC	OC
10	5.24	6.42
12	3.32	5.22
16	2.67	3.78

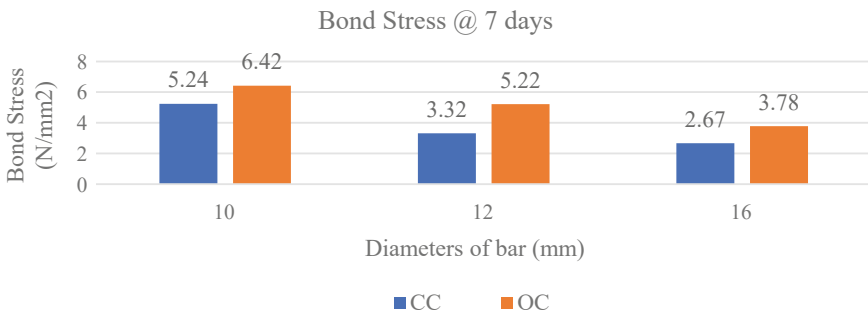


Fig. 6 Graph showing bond stress with different set of bars for CC and OC @ 7 days

the specimen increases in OC when compared to CC. As a result, in terms of the design bond stress of the concrete mixes investigated in this study, the use of fibers is structurally sound. The concrete with 10 mm bars absorbed the maximum bond tension, while the concrete with 16 mm absorbed the least bond stress. According to the data, OC with 10 mm dia bars gives superior bonding strength.

Table 6 and Fig. 8 show the bond stress findings in CC and OC after 28 days with varied bar widths. The specimens were subjected to bond stress in UTM after curing to ascertain the ultimate stress taken. The bond stress of the specimen increases in OC when compared to CC in all dia of bars. As a result, in terms of the design bond stress of the concrete mixes investigated in this study, the use of fibers is structurally sound. The concrete with 10 mm bars absorbed the most bond stress, while the concrete

Table 5 Bond stress @ 14 days

Diameters of bar (mm)	Bond stress (N/mm ²)	
	CC	OC
10	6.89	8.73
12	4.77	6.62
16	3.92	5.83

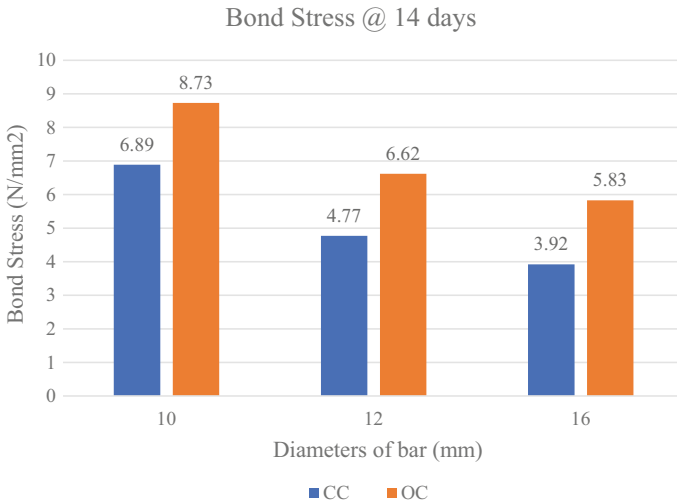


Fig. 7 Graph showing bond stress with different set of bars for CC and OC @ 14 days

with 16 mm bars absorbed the least. Similar to the previous results, that OC with 10 mm dia bars provides greater bonding strength.

In deformed bars (Fe415), there was formation of longitudinal cracks, and failure was sudden. This is because of projections present on the deformed bar and good grasp between the bar and concrete throughout the length of the specimen. Therefore, bond strength is improved by the exterior outcrop of the deformed bars.

The 28 days strength in bond of CC mix was in the range of 5.24–7.92 N/mm² for deformed bars. Likewise, the strength in bond of OC mix was in the range of 6.42–11.24 N/mm² for deformed bars.

Table 6 Bond stress @ 28 days

Diameters of bar (mm)	Bond stress (N/mm ²)	
	CC	OC
10	7.92	11.24
12	5.69	9.76
16	5.18	9.14

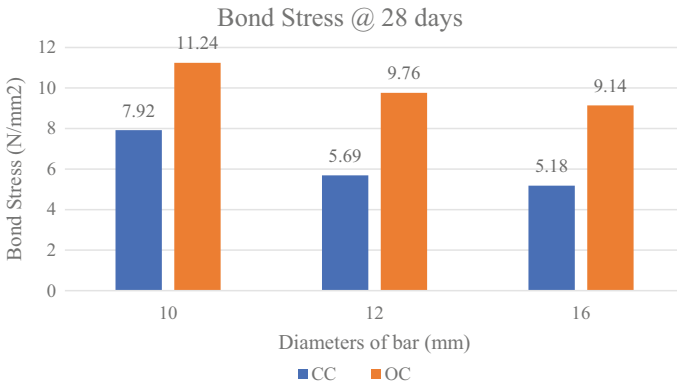


Fig. 8 Graph showing bond stress with different set of bars for CC and OC @ 28 days

In general, OC mix's bond strength was enhanced by the addition of hybrid fibers. All these results are higher than the values given by the guidelines mentioned in Table 3. As per some literature [15, 16], here also, whether it is a plain or deformed bar, bond strength decreased with increased bar diameter because of concrete volume and confining pressure on the bars.

3 Conclusion

Following are the results arrived from this study, and they are as follows:

- The use of hybrid fibers intensifies the mechanical properties of concrete furthermore in place of using single fiber.
- Over dosage of fibers significantly reduces its mechanical qualities of concrete.
- The concrete with 10 mm dia bars absorbed the most bond stress, while the concrete with 16 mm dia bars absorbed the least in case of both CC and OC. Overall OC with 10 mm dia bars provides better bonding strength.
- In terms of the design bond stress of the concrete mixes tested in this study, the usage of hybrid fibers is structurally sound.

References

1. Afroughsabet V, Teng S (2020) Experiments on drying shrinkage and creep of high performance hybrid-fiber-reinforced concrete. *Cement Concr Compos* 106:103481
2. Ali MAEM, Soliman AM, Nehdi ML (2017). Hybrid-fiber reinforced engineered cementitious composite under tensile and impact loading. *Mater Des* 117: 139–149. Sriram M, Sidharath

- KRA (2022) Various properties of natural and artificial fibers with cementitious composites in hybrid form
3. BS 8110, Structural use of concrete Part 1, Code of practice for design and construction. British Standard Institution, London
 4. Chandar SP, Gunasekaran K (2019) Study on the effect of quarry dust on plastic shrinkage in concrete slab made with the waste coconut shell as aggregate. *J Green Eng* 9(2):282–290
 5. Chandar SP, Gunasekaran K (2019) Study on the effect of quarry dust on deflection characteristics of coconut shell concrete slab. *Rasayan J Chem* 12(3):1038–1042
 6. de Melo FMC, de Jesus Cruz ACA, de Souza Netto LD, de Souza Símplicio MA (2021) Experimental study of bond between steel bars and hybrid fibers reinforced concrete. *Constr Build Mater* 275:122176
 7. Grzymiski F, Musiał M, Trapko T (2019) Mechanical properties of fibre reinforced concrete with recycled fibres. *Constr Build Mater* 198:323–331
 8. Hong L, Chen YD, Li TD, Gao P, Sun LZ (2020) Microstructure and bonding behavior of fiber-mortar interface in fiber-reinforced concrete. *Constr Build Mater* 232:117235
 9. IS 10262: 2019 Concrete mix proportioning—guidelines. Bureau of Indian Standards, New Delhi, India
 10. IS 12269: 2013, Specification for 53 grade ordinary Portland cement. Bureau of Indian Standards, New Delhi, India
 11. IS 456: 2000, Indian standard plain and reinforced concrete—code of practice. Bureau of Indian Standards, New Delhi, India
 12. IS: 2386 (Part IV): 1963, Indian standard methods of test for aggregate for concrete, Part IV mechanical properties. Bureau of Indian Standards, New Delhi, India
 13. IS: 2386 Part III): 1963, Indian standard methods of test for aggregate for concrete, part III specific gravity, density, voids, absorption and bulking. Bureau of Indian Standards, New Delhi, India
 14. Passuello A, Moriconi G, Shah SP (2009) Cracking behavior of concrete with shrinkage reducing admixtures and PVA fibers. *Cement Concr Compos* 31(10):699–704
 15. Ramasubramani R, Gunasekaran K (2022) Sustainable replacement materials for concrete production from renewable resources and waste on interfacial bond properties. *Innovative Infrastruct Solutions* 7(4):266
 16. Yuan C, Chen W, Pham TM, Hao H (2019) Bond behaviour between hybrid fiber reinforced polymer sheets and concrete. *Constr Build Mater* 210:93–110

Study on Effectiveness of Reinforced Concrete Beam Strengthening with Carbon Fibre-Reinforced Polymer



Taha Ahmed Ghaleb Mohammed , Mohanad Ali Ishaq Najajra ,
and Wesam Al Agha 

1 Introduction

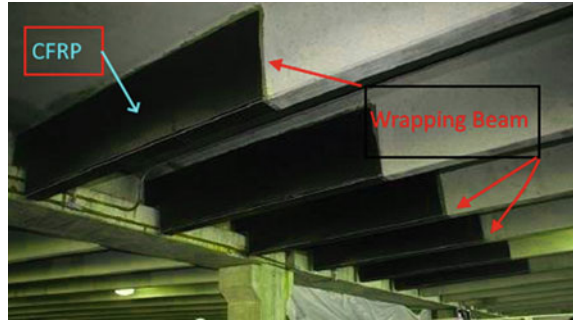
Integrating concrete and steel in a composite material might resist compression and tension. This process is commonly referred to as reinforced concrete. RCC structures frequently experience distress, the damage before estimated service life due to various factors such as not sufficient design, modification in usage and low-quality materials, high loading, seismic disaster, explosions, deterioration, and corrosion [1]. The significance of structural maintenance develops when observed through particular environments [2, 3]. The challenge lies in determining the optimal strengthening approach of substantially contributing to the concrete structure's strength and service life, considering critical factors such as durability, construction activities, and expenses [4, 5]. In instances where a structural element might not have the capacity to sustain the targeted load, this might have been caused by inadequacies in the design and incorrect implementation of the design, which might result from the design drawings' mistakes [6, 7]. The bonding of fibre-reinforced polymers (FRP) to the concrete member represents a recent development in the field of RC retrofitting [8, 9]. Fibre-reinforced polymer (FRP) composites consist of continuous and directional non-metallic fibres which possess advanced properties and are embedded within a polymer material matrix [5, 6]. The process of strengthening is

T. A. G. Mohammed · M. A. I. Najajra
Department of Civil Engineering, Cyprus International University, via Mersin 10 Haspolat, North
Cyprus, Turkey

W. Al Agha (✉)
Department of Civil Engineering, Delhi Technological University, Delhi 110042, India
e-mail: wesamalagha1@gmail.com; wesamalagha_2k21phdce16@dtu.ac.in;
wesam.alagha@unich.it

Present Address:

Department of Engineering and Geology, University G. d'Annunzio of Chieti-Pescara, Viale
Pindaro 42, 65127 Pescara, Italy

Fig. 1 CFRP specimens

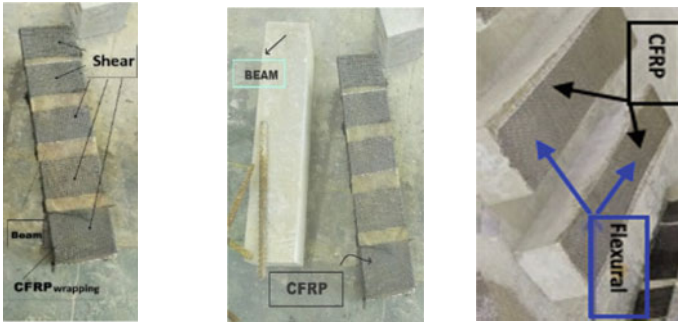
a professional aspect of rehabilitation that applies to the structure that has undergone a reduction in both its physical characteristics and performance, whether in part or in full. The proposed rehabilitation method entails establishing the structural framework as similarly as possible to its initial configurations [5, 9]. It is mandatory to relocate the damaged structures and protect the resilience to re-establish their functionality without compromising their safety and efficacy [10, 11]. The objective is to reduce visible cracks and rectify any problems that may affect the protection of humans and destroy the rigidity of a building [12]. The application of CFRP to envelop the structural members, as illustrated in Fig. 1, has the potential to enhance the ductility of the structural section.

2 Materials and Experimental Setup

The main objective of this study is to evaluate the structural efficacy of concrete beams regarding their flexural and shear characteristics. Moreover, the research necessitates finding and using load–deflection diagrams before and after strengthening. The present investigation assesses the effectiveness of CFRP materials in increasing the load-carrying capability in flexural and shear modes [5, 9] and evaluating the crack propagation by reducing crack width. A total of 12 reinforced concrete beams were fabricated for the purpose of examining the effectiveness of CFRP as a strengthening material. The constituents employed in the investigation of reinforced concrete comprise cement, aggregate, and water. Therefore, achieving the appropriate mix of design properties at a specific strength age is critical. The present study examines the practicability of entirely mixed concrete and its ability to withstand damage, utilising ordinary portland cement with a density of 3.15 and a grade of 43 [13, 14]. The properties of cement fines, including compressive strength and setting time, were tested. As a result, the principal aim of this investigation is to develop an achievable methodology for enhancing structural integrity. This study built 12 beams with $700 \times 150 \times 160$ mm dimensions using M20 grade concrete. After the curing process, the specimens were thoroughly cleaned and subsequently embedded with epoxy. A single layer of CFRP laminate was then manually applied at a close distance to the surface of

the member. Uniform pressure was used throughout the entire width of the prepared surface to eliminate any air bubbles, leading to a smooth and uniform final surface, as depicted in Fig. 2a. A period of 72 h is required for the air curing of CFRP composite materials. The specimens were appropriately arranged and staggered during the air drying to prevent adhesion to one another, the floor, or any other surface [15]. The present investigation applies Sika CarboDur as a reinforcement agent. The carbon fibre-reinforced polymer (CFRP) is bound to the beams in an external reinforcement capacity, utilising the Sikadur[®]-30 IN adhesive, as given in Table 1, an epoxy resin-based material suitable for standard operating temperatures. The shear-strengthening beams underwent an enhancement process using square wire mesh positioned at a 65-degree orientation. Subsequently, the beams were subjected to a curing period of seven days [13, 14]. Subsequently, the strengthened beams underwent flexural and shear testing with one and two-point loading, respectively. This was carried out similarly to the control beams and those reinforced with CFRP, aiming to identify the maximum load and corresponding deflections. Beams were subjected to load testing in flexural and shear failure modes where the function of damage accrued. The four control beams were castes to compare the strength of specimens before the strengthened approach using carbon fibre-reinforced polymers, as shown in Fig. 2. The loading capacity in flexural and shear cases illustrates the outputs. In the case of four flexural CFRP beams, the carbon fibre-reinforced polymer laminate bonded continuously on the surface of flexural effect to avoid crack growth, as shown in Fig. 2c. The flexural failure mode was evaluated using a one-point loading test, while the shear failure mode was assessed using a two-point loading test. Then, it was compared to the four carbon fibre-reinforced polymer beams in the flexural case with the outputs of control specimens. The final group of experimental setup demonstrated four carbon fibre-reinforced polymers under shear loads to study the structural performance of reinforced concrete beams reinforced with carbon fibre-reinforced polymer laminate, as shown in Fig. 2b. The CFRP laminate covered all surfaces of the beams to have higher resistance using shear loads, as shown in Fig. 2a. The experiment was vital utilising a 1000 kN universal testing machine (UTM) to apply a load at a regular rate until failure progressively, as shown in Fig. 2d. The initial findings suggested that there is an enhancement in load-carrying capacity. The beam specimens' flexural failure testing was at the beams' centre [16]. The shear failure has been assessed through a two-point loading test, with a distance of 400 mm between the loading points and 600 mm between the supports.

The Sikadur[®]-30 IN products manual has taken the properties of CFRP as in Table 1.



(a) CFRP Shear Beam (b) CFRP Wrapping (c) CFRP Flexural Beam



(d) Universal Testing Machine (UTM)

Fig. 2 Carbon fibre-reinforced polymer materials and experiments

Table 1 Properties of Sika CFRP laminate

Type of CFRP	Sika® CarboDur® S 1241 of 1.4 mm thick (black)
Width	50 mm
Area	70 mm ²
Density	1.60 g/cm ³
Mean tensile strength	3100 N/mm ²
5% fractile value	2900 N/mm ²
Mean modulus of elasticity	170,000 N/mm ²
5% fractile value	165,000 N/mm ²
Strain at break	> 1.8%
Fibre volume	> 68%

3 Numerical Prediction of Control and CFRP Beam as Per ACI Standard

The measurement of moment resistance in the section will be carried out using the formulas of design criteria presented in ACI-318 M-11 [17, 18]. The implementation of numerical forecasting will guarantee the seamless integration of mathematical calculations, per ACI-318-14, with the experimental results regarding the ultimate strength [19]. Consequently, these equations might be solved in order to determine the numerical values of “ a ” and “ M_n ” parameters. The M_n abbreviation indicates the theoretical resistance of the section. The evaluation of the concrete strength of an identified structural element, denoted as φM_n , involves multiplying its theoretical strength by a numerical value referred to as the strength reduction factor. The flexural strength of a member characterised as φM_n must equal the minimum requirement of being equal to the calculated factored moment, M_u , which arises from applying a factored load, as illustrated in Fig. 3 of the equation listings [17, 18].

$$\varphi M_n \geq M_u \tag{1}$$

The uniform distribution of concrete stress at 0.85 times the compressive strength of concrete needs to be considered over a compression zone equivalent to the cross-section limits. This zone is defined by a straight line parallel to the neutral axis and centred around a distance of 1 times the effective depth of the section from the fibre of maximum compressive strain. Section (10.2.7.3) of the American code displays the β_1 coefficients, which indicates that the appropriate index for f_c' values between 17 and 28 MPa is 0.85 [17]. The methodology outlined in Section (10.2.7.3) yields the β_1 coefficients, which define the value of 0.85 required for f_c' values to become within the range of 17–28 MPa. To achieve an f_c' value above 28 MPa, reducing β_1 in a linear case is essential, with a rate of 0.05 for each 7 MPa increment in strength. Nevertheless, the resulting value of β_1 must remain below 0.65. For concretes with a compressive strength (f_c) exceeding 30 MPa, the value of 1 might be calculated

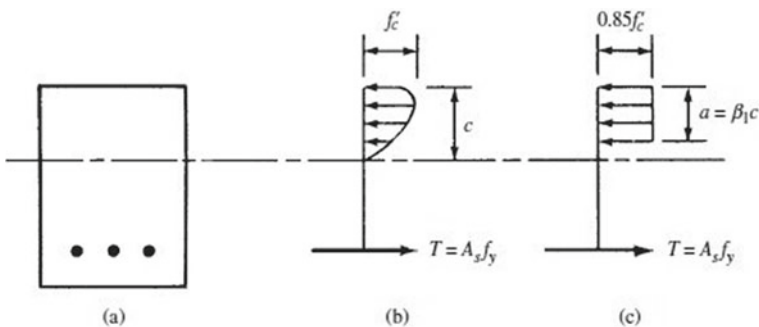


Fig. 3 Stress distribution at ultimate condition

using the following mathematical equation [18, 19]. Values obtained for “ a ” into this formula, replace A_s with ρ, bd , and equate ϕM_n to M_u , to be presented in the following equation.

$$\phi M_n = M_u = \phi b d^2 f_y \rho (1 - \rho f_y / 1.7 f_c) \quad (2)$$

- ρ Ratio of steel to section area
- F_y Yielding strength of steel
- M_n Nominal resistance of the section
- M_u Moment applied on the section.

The shear resistance of RC control beam section, as per ACI-318 M-11, is presented in terms of shear forces rather than shear stresses. Total shear forces are calculated by multiplying the average shear stresses mentioned in the equations below by the effective beam area.

$$V_n = V_c + V_s \quad (3)$$

- V_n Member’s theoretical shear strength
- V_c Shear strength of concrete

$$\xi v = V_u / b d \quad (4)$$

$$V_u = \phi V_c + \phi V_s \quad (5)$$

$$V_c = (\lambda \sqrt{f_c} / 6) b w d \quad (6)$$

In the validation of control beams calculation with CFRP sections as per the strength design methodology, the flexural strength of any particular member’s design must exceed the required factored moment [19], as demonstrated by the equation of moment M_u that is factored is derived from the loads that have been factored, whereas the flexural strength M_n . For any assumed depth to the neutral axis c , the strain level in the CFRP reinforcement can be computed as equations [18, 19]. The CFRP strain and stress calculation in Eqs. (7), (8), and (9).

$$\varepsilon_{fd} = 0.41 \sqrt{\frac{f'_c}{n E_f t_f}} \leq 0.9 \varepsilon_{fu} \quad (7)$$

$$\varepsilon_{fe} = \varepsilon_{cu} \left(\frac{d_f - c}{c} \right) - \varepsilon_{bi} \leq \varepsilon_{fd} \quad (8)$$

$$f_{fe} = E_f \varepsilon_{fe} \quad (9)$$

An additional reduction factor, ψ_f , reduces the CFRP reinforcement's flexural-strength contribution. The suggested value for ψ_f is 0.85 as per ACI 318-05 Section (10.2.10) as shown in Eq. (1.10).

$$M_n = A_s f_s \left(d \left(\frac{\beta_1 c}{2} \right) \right) + \Psi_f A_f f_{fe} \left(h \frac{\beta_1 c}{2} \right) \quad (10)$$

In the case of CFRP beams under shear, it was used by Eqs. (11) and (12). The load factors ACI 318-05 required calculating the required shear strength of a CFRP-reinforced concrete [18, 19]. As ACI 318-05, the design shear strength is derived by multiplying the nominal shear strength by the strength reduction factor. Equation (13) might compute the nominal shear strength of a fibre-reinforced concrete element by combining the FRP external shear reinforcement contribution to the reinforcing steel and concrete contributions. An additional factor ψ_f can reduce the contribution of the CFRP specimens.

$$V_u = \phi V_c + \phi V_s \quad (11)$$

$$V_f = \frac{A_{fv} f_{fe} (\sin \theta + \cos \theta) d_{fv}}{S_f} \quad (12)$$

V_f Shear strength of CFRP

A_{fv} Area of CFRP laminate

$$V_s + V_f \leq 0.66 \sqrt{f'_c} b_w d \quad (13)$$

4 Results

Twelve beams were tested to present the CFRP laminate strengthened beams effect compared to the control beam. These beams were subjected to load testing in both flexural and shear failure modes. The four control beams were compared to the strength of specimens before the strengthened approach using eight CFRP laminate beams in terms of loading capacity by four beams at flexural and four beams at shear cases. In Fig. 4, it has illustrated the differences in values between control beams and CFRP ones in both cases, flexural and shear. The first case of comparison between four control M20 concrete control beams and four strengthened beams by CFRP presents the increase of deflection of CFRP beams compared with control beams at flexural and shear, respectively. In terms of the flexural case, CFRP beams showed

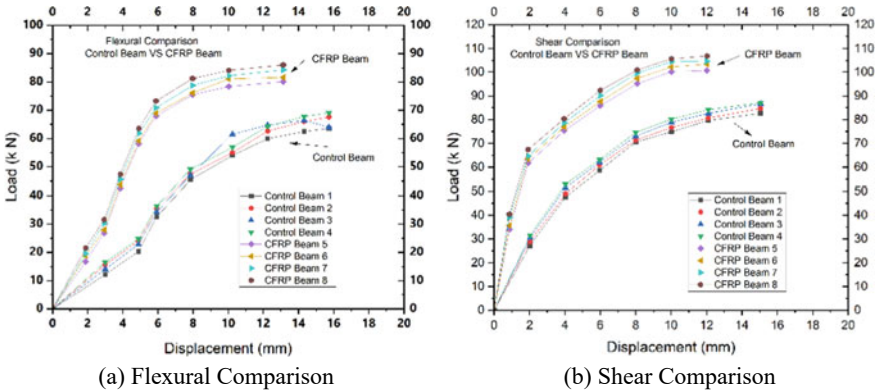


Fig. 4 Load-carrying and displacement capacity of control and CFRP beams

higher load capacity values than control beams. As the damaged average values of the four control beam increased by 23.84% in the case of using CFRP beams, the ultimate average values of CFRP increased by 25.69% compared to the control ones. The same investigation repeated in the shear case increased the damaged average and ultimate values of CFRP beams by 27.22% and 26.04%, respectively. In the summary of the first investigation related to Fig. 4, the CFRP beams have shown a significant performance compared to control beams in terms of damaged load and ultimate ones; it has performed fewer deformations in both shear and flexural effects. The maximum crack width of control beams was 1.19 mm, and for CFRP beams, it was 0.71 mm.

In Fig. 5, it was compared the experimental beam values with the American code predicted as illustrated in equations for the loading capacity in both flexural and shear effects. Figure 5a shows the varying flexural control beams to be increased in the ACI code calculation by 14.4% at the damaged load and 12.7% at the ultimate load, respectively. Figure 5b presents the varying flexural CFRP beams to be increased in the ACI code by 13.0% at the damaged load and 10.9% at the ultimate load, respectively. Figure 5c presents the varying shear control beams to be increased in the ACI code by 6.5% at the damaged load and 13% at the ultimate load, respectively. Figure 5d shows the varying of shear CFRP beams to be increased in the ACI code by 28.0% at damaged load and 40.2% at ultimate load, respectively.

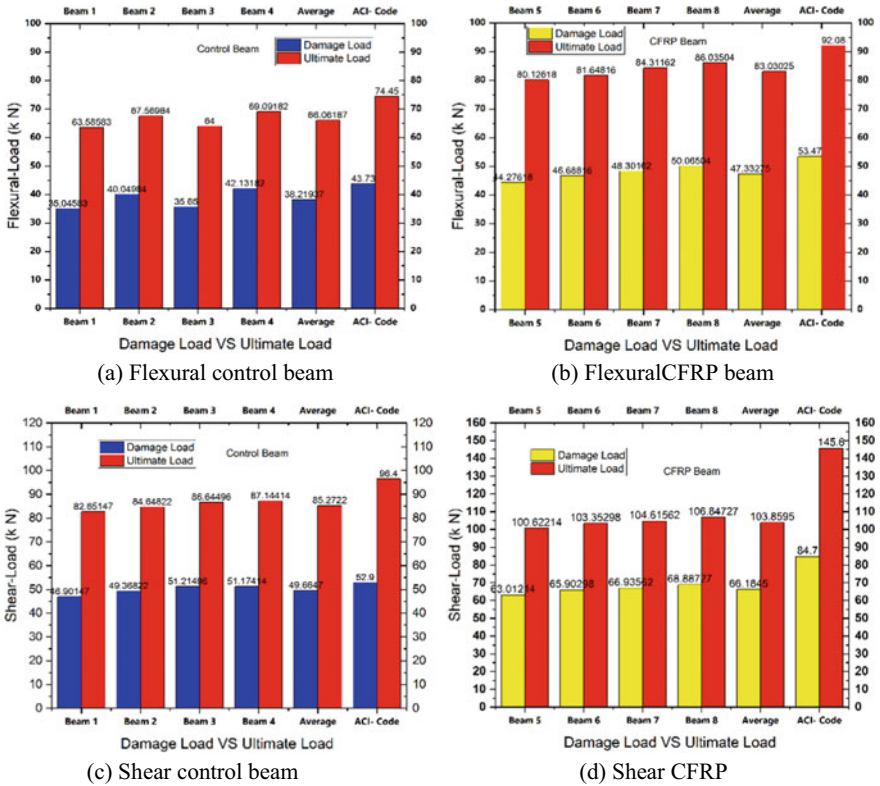


Fig. 5 Comparison between damage and ultimate load to experiment and ACI code

5 Conclusion

In this study, 12 concrete beams measuring $700 \times 150 \times 160$ mm were built and subjected to load testing in flexural and shear. Beams have been selected to ensure enhancement of yield point before using CFRP on the concrete undergoing a failure. The beams used M20 grade concrete. The output concludes as follows,

- CFRP material has improved the deflection behaviour of the beam, as demonstrated by a reduction in the initial deflection during both the damaged and ultimate stages of a flexural analysis.
- The effectiveness of CFRP laminates in beams that have undergone shear loads and strengthening has decreased the initial deflection observed during both the damaged and ultimate stages.
- The experimental samples demonstrated a reduction in crack widths, considerable deflection at the location of damage and ultimate load, a significant improvement in the ductility ratio, and a rise in energy absorption following reinforcement.

- In terms of shear loading, the utilisation of CFRP laminates compared to control beams resulted in a significant load capacity enhancement, as evidenced during both the damaged and ultimate stages.
- The findings from the experimental samples indicate a decrease in crack widths, notable deflection at the point of maximum load, essential enhancements in the ductility ratio, and an increase in energy absorption following reinforcement. The findings indicate that the constituents exhibited greater proficiency in enduring their maximum capacity in CFRP flexural and shear scenarios.
- The results of shear and flexural studies conducted on control and CFRP beams indicated that the American code predicted higher values at the damaged and ultimate stages.

Acknowledgements The authors would like to express appreciation to the Indian Council for Cultural Relations, India, and the INPS's social security contribution under separate management (CHIETI, IT), Italy.

References

1. Ravi K, Al Agha W, Thakur MS, Umamaheswari N (2021) Impact of the lead rubber base isolators on reinforced concrete building. *IOP Conf Ser Mater Sci Eng* 1026(1): 012004. <https://doi.org/10.1088/1757-899X/1026/1/012004>
2. Orsatelli JB, Paroissien E, Lachaud F, Schwartz S (2023) Bonded flush repairs for aerospace composite structures: a review on modelling strategies and application to repairs optimization, reliability and durability. *Compos Struct* 304:116338. <https://doi.org/10.1016/J.COMPSTRUC.2022.116338>
3. Sandeep MS, Tiprak K, Kaewunruen S, Pheinsusom P, Pansuk W (2023) Shear strength prediction of reinforced concrete beams using machine learning. *Structures* 47:1196–1211. <https://doi.org/10.1016/J.ISTRUC.2022.11.140>
4. Zhang Y, Duan L, Liu H, Lu J, Huo Y (2023) Experimental and numerical study on multi-impact performance of pre-damaged beams strengthened with CFRP. *Eng Struct* 285:116034. <https://doi.org/10.1016/J.ENGSTRUCT.2023.116034>
5. Prashanth MH, Manjunath R, Koppad A, Umesh B, Kuttigola I (2023) Experimental study on shear reinforced and shear deficient RC beams subjected to preloading and wrapping with CFRP sheets. *Mater Today Proc.* <https://doi.org/10.1016/J.MATPR.2023.01.299>
6. Wang Y, Li X, Li J, Wang Q, Xu B, Deng J (2019) Debonding damage detection of the CFRP-concrete interface based on piezoelectric ceramics by the wave-based method. *Constr Build Mater* 210:514–524. <https://doi.org/10.1016/j.conbuildmat.2019.03.042>
7. Huang Y, Lee MG, Kan YC, Wang WC, Wang YC, Pan WB (2022) Reinforced concrete beams retrofitted with UHPC or CFRP. *Case Stud Constr Mater* 17:e01507. <https://doi.org/10.1016/J.CSCM.2022.E01507>
8. Yu XY, Jiang C, Zhang WP (2022) Failure mode-based calculation method for bending bearing capacities of corroded RC beams strengthened with CFRP sheets. *Eng Struct* 271:114946. <https://doi.org/10.1016/J.ENGSTRUCT.2022.114946>
9. Qiang X, Chen L, Jiang X (2023) Experimental and theoretical study on flexural behavior of steel–concrete composite beams strengthened by CFRP plates with unbonded retrofit systems. *Compos Struct* 309:116763. <https://doi.org/10.1016/J.COMPSTRUCT.2023.116763>

10. Jiang X, Jin L, Lu K, Du X (2023) Experimental and numerical tests on shear failure and size effect of CFRP-wrapped RC beams without stirrups: Influence of the shear-span ratio. *Eng Struct* 288:116219. <https://doi.org/10.1016/J.ENGSTRUCT.2023.116219>
11. Yuan K, Liu K, Wang Z, Yang M (2021) An investigation on the perforation resistance of laminated CFRP beam and square plate. *Int J Impact Eng* 157:103967. <https://doi.org/10.1016/J.IJIMPENG.2021.103967>
12. Alabdulhady MY, Ojaimi MF, Chkheiwier AH (2022) The efficiency of CFRP strengthening and repair system on the flexural behavior of RC beams constructed with different concrete compressive strength. *Results Eng* 16:100763. <https://doi.org/10.1016/J.RINENG.2022.100763>
13. Bureau of Indian Standards, New Delhi, Indian Standard Plain and Reinforced Concrete -IS 456, 2000
14. IS 269: 2015, Ordinary Portland cement 43 Grade-Specification. Bureau of Indian Standards, New Delhi
15. IS 10262: 2009, Concrete mix proportioning-guidelines, Bureau of Indian Standards, New Delhi
16. Bureau of Indian Standards, New Delhi, Indian Standard Recommended Guidelines for Concrete Mix Design, IS10262, 2009
17. ACI 318M-11, Building Code Requirements for Structural Concrete and Commentary. American Concrete Institute, 2011
18. ACI Committee 549, 1993 State of the art report on Ferrocement. Report by ACI Committee 549, American Concrete Institute, Detroit
19. ACI 440.2 R-08, Guide for the design and construction of externally FRP

Comparative Study on Structural Performance Between Reinforced Concrete Beam and Ferro-Cement Laminate Strengthening



Mohanad Ali Ishaq Najajra , Taha Ahmed Ghaleb Mohammed ,
and Wesam Al Agha 

1 Introduction

It is vital to use concrete as the main construction material available in the industry due to its durability. However, concrete might sustain compression force and resist a low tension force accrued, which is neglected primarily in the practical design. Therefore, concrete needs more strength to resist the tension forces [1, 2]. Damage is described as a change in structural performance to be seen as discrete cracks and the appearance of a weak part of structural specimens, resulting in decreased stiffness [3, 4]. The relevant research on damaged structures involves acquiring information through observation, examining previous experiments, conducting preliminary testing, and validating the outputs [5, 6]. A systematic investigation of concrete structures is critical in determining the cause of damage, assessing the status of the structures in their damaged state, and formulating recovery suggestions [7]. Damage might occur due to overloading when the load on structural members exceeds the design loads, causing started cracking signs [8, 9]. A variety of material factors lead to the collapse of reinforced concrete structures. The environment causes chemical attacks and material lower serviceability [10]. Fire damage, explosion damage, impact damage, and damage from natural disasters are the leading causes, such as

M. A. I. Najajra · T. A. G. Mohammed
Department of Civil Engineering, Cyprus International University, via Mersin 10 Haspolat, North Cyprus, Turkey

W. Al Agha (✉)
Department of Civil Engineering, Delhi Technological University, Delhi 110042, India
e-mail: wesamalagha1@gmail.com; wesamalagha_2k21phdce16@dtu.ac.in;
wesam.alagha@unich.it

Present Address:

Department of Engineering and Geology, University G. d'Annunzio of Chieti-Pescara, Viale Pindaro 42, Pescara 65127, Italy

floods, cyclones, and earthquakes. Alkali-silica reaction, alkali-carbonate reaction, carbonation, sulphate attack, and steel corrosion are chemical causes of concrete deterioration [1, 11]. High structural stress, heat stress, shrinkage, and poor material quality are some additional elements contributing to concrete degradation [1, 12]. Therefore, selecting a suitable strengthening material is among the most crucial techniques in assuring long-lasting and reliable repair [1, 3]. A critical study of the actual cause is required for the repair system, widely exploring the deterioration process of materials like concrete and other supplementary materials such as plastics and epoxy under service conditions [11]. Before settling on a repair material, it should be checked if the selected material for the repair has a chemical component; the availability of relevant materials, equipment, and skilled labour must be checked [12]. In addition, the literature frequently emphasises the material's composition rather than its performance feature [8]. A variety of approaches are available for strengthening and rehabilitating structural damage. The corroded steel bars and damaged concrete are removed and replaced with new materials of the same type [12]. Epoxy mortar might be used alone or in conjunction with the two processes indicated. In summary, ferro-cement in the damaged area is used to restore the structure's performance.

1.1 Ferro-Cement Rehabilitation and Retrofitting Technology

Ferro-cement is defined by the ACI committee 549 (1993) as a thin-walled reinforced concrete structure in which a cement mortar is reinforced throughout the matrix with continuous and relatively small diameter mesh layers [7, 11]. The important part of ferro-cement that gives it a significant advantage over reinforced concrete in certain situations is that the ferro-cement components go through under stress functioning nearly as a relatively homogenous [13]. It has greater crack resistance because of its closely spaced tiny diameter reinforcements [6]. Due to its exceptional crack resistance, high strength, durability, ability to cast into any shape, quick constructions without heavy equipment, small extra self-weight imposed, and considering the economic aspects of rehabilitation, ferro-cement is a low-cost solution for repair that might be made into thin structural sections by the varied thickness from 15 to 25 mm. Over the top layers of reinforcement, only a thin mortar cover was used. Unlike typical concrete, ferro-cement might be constructed into the desired shape, as shown in Fig. 1. Ferro-cement has a very high tensile strength-to-weight ratio and superior cracking behaviour when compared to traditional reinforced concrete [3].

1.2 Applications of Ferro-Cement

Ferro cement is a composite material that combines ferro (iron) and cement (cement mortar). Ferro-cement is a reinforced concrete structure that employs a wire mesh with small diameters that is uniformly distributed across the cross-section instead of

Fig. 1 Ferro-cement specimens



individually placed reinforcing bars. Additionally, Portland cement mortar is used instead of traditional concrete [7, 8]. Ferro-cement set-up involves pasting cement mortar into wire meshes [14]. Ferro cement is a composite material composed of a highly compressed wire mesh tightly wrapped around a rigid steel structure and subsequently treated with a high-quality cement mortar [13]. Ferro-cement might be served as a viable construction material for various structural components, not limited to foundations, walls, floors, roofs, shells, and other load-bearing elements [1]. The referenced objects demonstrate a slender partition, exhibit a low mass, are resilient, and demonstrate an outstanding resistance to permeation. This particular material integrates the advantageous properties of slender cross-sections with the strength of steel. Formwork or shuttering is not necessary during the casting process [3]. Ferro-cement has a wide range of applications, including but not limited to water and soil retaining structures, building components, large-scale space constructions, bridges, domes, dams, boats, conduits, bunkers, silos, and water and sewage treatment plants.

1.3 Ferro-Cement Material Components

Compared to other complex engineering materials, ferro-cement employs easy-to-find resources and necessitates minimal specialised labour. The fundamental constituents necessary for ferro-cement constructions include wire mesh, sand, cement, water, and mild steel rod utilised as framework reinforcement [1]. It is presented in Fig. 2 as a brief description of the elemental components and procedural methodology utilised in the construction process [7].

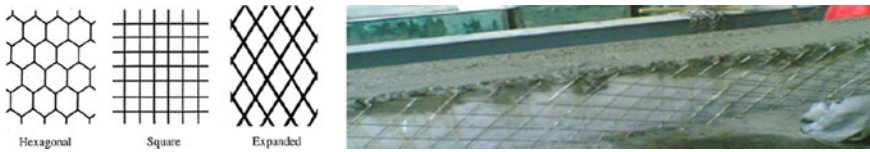


Fig. 2 Ferro-cement elemental components

1.3.1 Cement

Multiple types of cement are commercially available, with the most dominant being standard or ordinary portland cement [15]. This particular variety of cement is deemed appropriate for utilisation in conditions without specifications or demands. The study utilised ordinary Portland cement with a grade of 43, and sand was also employed. It is a well-graded coarse and fine aggregate, commonly used in concrete, and is used to prepare mortar for ferro-cement construction [1]. The installation of an excessive quantity of fine particles and the use of porous sand particles are not recommended due to their adverse effects on the durability and structural efficacy of the mortar. The mortar was composed of well-graded coarse sand transported by a river and possessed a fineness modulus.

1.3.2 Water

The water mixing for blending mortar must be devoid of any acidic, soluble salt, or organic constituents that may adversely impact the cement's setting duration and, consequently, the structural robustness. Using seawater as a mixing agent for mortar is not recommended due to its propensity to increase the risk of corrosion in the mesh and reinforcement [9]. It is vital to explore the process of preparing mortar. Ensuring consistent attainment of the required strength is of utmost importance when mixing mortar [13, 16]. The used ratio of cement to sand is commonly 1:2 by weight. The weight ratio of cement to sand employed in the mixture was 1:2. The water–cement ratio ranged from 0.4, depending on the level of dryness exhibited by the sand. The initial step in the mixing process involved the homogeneous combination of sand and cement. In order to attain the intended workability of the mortar mixture, water was incorporated gradually in small increments [1, 3].

1.3.3 Plastering

The quality of a ferro-cement structure is determined by the durability of its plastering. Before applying plaster to a building, the wire meshes were inspected to ensure proper placement on the beam surface was removed through brushing [2]. Manual plastering using a trowel has been demonstrated to be the most productive technique. The method of plastering employed in this context involved a singular,

integrated process whereby a cohesive layer of mortar was applied to fill the wire mesh and achieve a uniform finish across the interior and exterior surfaces, as shown in Fig. 2. It was accomplished before the initial cement setting, implementing a one-stage procedure. Typically, the mortar is applied to strengthened ferro-compositions to be exhibited the serviceability of structural elements.

2 Materials and Experimental Set-Up

The primary aim of this investigation is to examine the structural performance of reinforced concrete beams, both pre-and post-strengthening, in terms of, respectively, their flexural and shear behaviour. Furthermore, the study demands obtaining load–deflection curves before and after strengthening. This study aims to evaluate ferro-cement laminates' efficacy in enhancing the load-bearing capacity in both flexural and shear modes. The efficacy of ferro-cement laminates has been in mitigating crack propagation and reducing crack width. The 12 RC beams were cast to investigate ferro-cement strengthened. The materials used in RC concrete for the study include cement, aggregate, and water [15]. Therefore, it is vital to accomplish the necessary properties mix design at a strength age. The workability of fresh concrete and durability requirements of these materials are tested and presented using ordinary Portland cement of grade 43 of a specific gravity equal to 3.15. It has been tested where the cement's fines properties, compressive strength, and setting time were checked [16]. Even though RCC constructions are esteemed for their extended lifespan, it is vulnerable to deterioration caused by external factors. It might result in a reduction in load-bearing capacity and significant obvious cracks. The maintenance of safety and stability of reinforced concrete structures is determined depending on the critical task of repairing and strengthening them [16, 17]. Using retrofitting techniques presents an efficient and economically feasible solution for replacing RC structural elements. Therefore, the primary objective of this study is to devise a practical approach to enhancing structural integrity. In this study, 12 beams with $700 \times 150 \times 160$ mm dimensions were built using M20 grade concrete [16, 18]. These beams were subjected to load testing in both flexural and shear failure modes. The four control beams were casted to compare the strength of specimens before the strengthened approach using ferro-cement. The loading capacity in flexural and shear cases illustrates the outputs. The flexural failure mode was evaluated using a one-point loading test, while the shear failure mode was assessed using a two-point loading test. Then, it was compared to the four ferro-cement beams in the flexural case with the outputs of control specimens. The final group of experimental setup demonstrated four ferro-cement beams under shear loads to study the structural performance of reinforced concrete beams reinforced with ferro-cement laminate, as shown in Fig. 3a. The experiment was vital utilising a 1000 kN universal testing machine (UTM) to apply a load at a regular rate until failure progressively. The initial findings suggested that there is an enhancement in load-carrying capacity. The beam specimens' flexural failure testing was at the beams' centre, as illustrated in

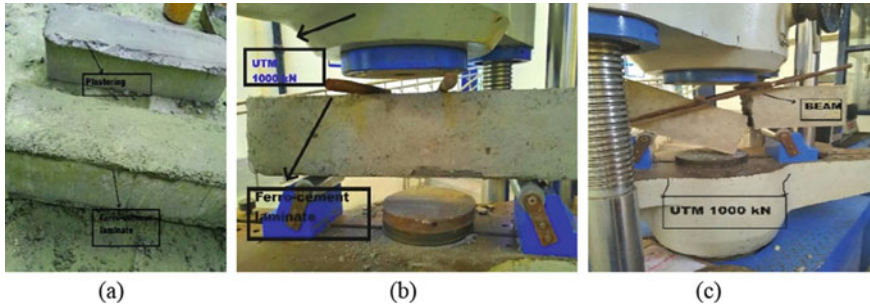


Fig. 3 Ferro-cement materials and experiments

Fig. 3c. The shear failure has been assessed through a two-point loading test, with a distance of 400 mm between the loading points and 600 mm between the supports, as presented in Fig. 3b.

3 Numerical Predictions of Beams as Per American Codes

This validation's primary objective is to determine whether the examined beam matches the minimum structural requirements defined by the ACI code in the two cases; control and ferro-cement laminate beam [14]. The primary advantage of this validation represents its potential effectiveness in designing conditions where experimentation is not workable. However, this is predicated entirely on the ACI code-based equations of the beam's structural behaviour integrating to a specific extent with the identified structural performance of the beam during testing [19].

3.1 Numerical Prediction of Control Beam as Per ACI-318-11

The utilisation of a control beam as a point of reference is aimed at evaluating the enhancement in structural performance subsequent to the application of ferro-cement as external retrofitting in the comparison terms of the structural load-bearing capacity of the beams. The section's moment resistance measurement will be conducted by utilising the criteria and formulas outlined in ACI-318M-11. Subsequently, a comparison will be made between the calculated results and the ultimate load and flexural resistance of the section obtained from the laboratory tests. The numerical prediction will ensure that the mathematical computations, following ACI-318-14, integrate with the experimental test outcomes regarding ultimate strength. Subsequently, these listed equations might be resolved to obtain the number "a" and moment " M_n " values. The abbreviation M_n represents the theoretical or nominal resistance of the section [17]. The concrete strength of a structural element, identified as ϕM_n , is assessed

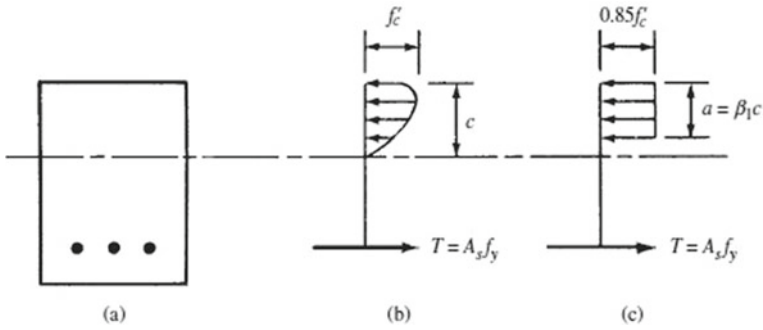


Fig. 4 Stress distribution at ultimate condition [19]

by multiplying its theoretical strength by a number known as the strength reduction factor. The minimum requirement for a member’s flexural strength, represented as φM_n , should be equivalent to the computed factored moment, M_u , resulting from applying a factored load, as shown in Fig. 4 in the equation lists [19].

$$\varphi M_n \geq M_u \tag{1}$$

The uniform distribution of concrete stress at 0.85 times the compressive strength of concrete needs to be considered over a compression zone equivalent to the cross-section limits. This zone is defined by a straight line parallel to the neutral axis and centred around a distance of 1 times the effective depth of the section from the fibre of maximum compressive strain [19].

The code presented in Section 10.2.7.3 lists the β_1 values, indicating that an index of 0.85 ought to be used for f_c' ranging from 17 to 28 MPa. The calculation method presented in Section 10.2.7.3 delivers the β_1 values, indicating that a value of 0.85 is required to be used for f_c' ranging from 17 to 28 MPa. In order to achieve an f_c' value exceeding 28 MPa, it is necessary to decrease β_1 linearly at a rate of 0.05 for every 7 MPa increase in strength beyond 28 MPa. However, the resulting value of β_1 must remain below 0.65. In the case of concretes possessing a compressive strength (f_c) greater than 30 MPa, the value of 1 might be determined by applying the following mathematical expression [13, 14].

$$\beta_1 = 0.85 * 0.008(f_c) + 0.65 \tag{2}$$

It is vital to calculate the horizontal forces C and T and calculation for the flexural effect as the equations.

$$0.85 f_c' a b = A_s f_y \tag{3}$$

$$a = A_s f_y / (0.85 f_c' b) = \rho f_y d / (0.85 f_c) \tag{4}$$

$$\rho = A_s/bd \quad (5)$$

The moment, M_n , can also be calculated since the yield stage reaches its full strength before the concrete, as in the equation.

$$M_n = T(d-a/2) = A_s f_y (d-a/2) \quad (6)$$

$$\varphi M_n = \varphi A_s f_y (d-a/2) \quad (7)$$

$$\varphi M_n = M_u = \varphi b d^2 f_y \rho (1 - \rho f_y / 1.7 f_c) \quad (8)$$

Values obtained for “ a ” into this formula and replace A_s with $\rho b d$, and equate φM_n to M_u to be obtained as the following equation.

$$\varphi M_n = M_u = \varphi b d^2 f_y \rho (1 - \rho f_y / 1.7 f_c) \quad (9)$$

- ρ ratio of steel to section area
- F_y yielding strength of steel
- M_n nominal resistance of the section
- M_u moment applied on the section

The shear resistance of RC control beam section, as per ACI-318M-11, is presented in terms of shear forces rather than shear stresses. Total shear forces are calculated by multiplying the average shear stresses mentioned in the equations below by the effective beam area.

$$V_n = V_c + V_s \quad (10)$$

- V_n member's theoretical shear strength
- V_c shear strength of concrete

$$\xi v = V_u/bd \quad (10)$$

$$V_u = \varphi V_c + \varphi V_s \quad (12)$$

$$V_c = (\lambda \sqrt{f_c} / 6) b w d \quad (13)$$

The validation of control beams calculation with the ferro-cement section's flexural strength might be calculated using an approach similar to that used for a reinforced concrete area, employing the ACI 318M-11 strength analysis procedure and

ACI 549 used to follow up on mesh effectiveness factor, elasticity modulus, and yield strengths as equation below [19].

$$M_n = \sum C_{si} \text{ or } T_{si}(d_i - \beta_1 C/2) \quad (14)$$

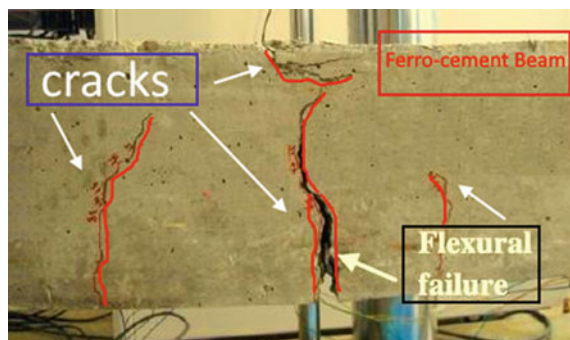
T_{si} force resisted by the section reinforced with ferrocement
 C depth of neutral axis

4 Results

Twelve beams were tested to present the ferro-cement strengthened beams effect compared to the control beam. These beams were subjected to load testing in both flexural and shear failure modes. The four control beams were compared to the strength of specimens before the strengthened approach using eight ferro-cement beams in terms of loading capacity by four beams at flexural and four beams at shear cases. The cracks are shown in ferro-cement beams, as in Fig. 5. Flexural cracks were created vertically towards the top from the bottom of the beam at mid-span during flexural failure loading. In contrast, shear cracks expand irregularly during shear failure loading, starting from the supports and increasing towards the loading point. Additionally, it has been observed that the width of the cracks and the deflection also vary.

As Fig. 6, it has illustrated the differences in values between control beams and ferro-cement ones in both cases, flexural and shear. The first case of comparison between four control M20 concrete control beams and four strengthened beams by ferro-cement presents the increase of deflection of ferro-beams compared with control beams at flexural and shear, respectively. In terms of the flexural case, ferro-cement beams showed higher load capacity values than control beams. As the damaged average values of the four control beam increased by 44.15% in the case of using ferro-cement beams, the ultimate average values of ferro-cement increased by 11.43% compared to control ones. The same investigation repeated in the shear case

Fig. 5 Ferro-cement beam cracks



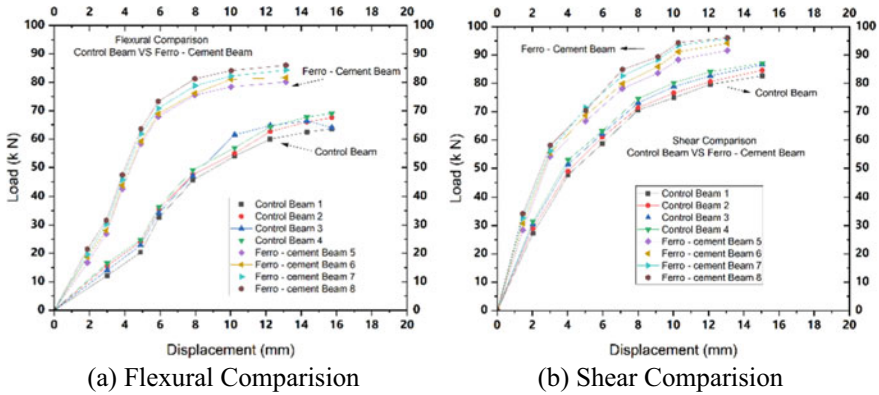


Fig. 6 Load-carrying and displacement capacity of control and ferro-cement beams

increased the damaged average values and ultimate average values of ferro-cement beams by 10.75 and 10.89%, respectively. In the summary of the first investigation related to Fig. 6, the ferro-cement beams have shown a significant performance compared to control beams in terms of damaged load and ultimate ones; it has performed fewer deformations also in both shear and flexural effect. The maximum crack width of control beams was 1.3 mm, and for ferro-cement beams, it was 0.73 mm.

In Fig. 7, it was compared the experimental beam values with the American code predicted as illustrated in equations for the loading capacity in both flexural and shear effects. Figure 7a shows the varying flexural control beams to be increased in the ACI code calculation by 14.4% at the damaged load and 12.7% at the ultimate load, respectively. Figure 7b presents the varying flexural ferro-cement beams to be increased in the ACI code by 15.2% at the damaged load and 8.8% at the ultimate load, respectively. Figure 7c presents the varying shear control beams to be increased in the ACI code by 6.5% at the damaged load and 13% at the ultimate load, respectively. Figure 7d shows the varying of shear ferro-cement beams which is to be increased in the ACI code by 46.5% at damaged load and 28.7% at ultimate load, respectively.

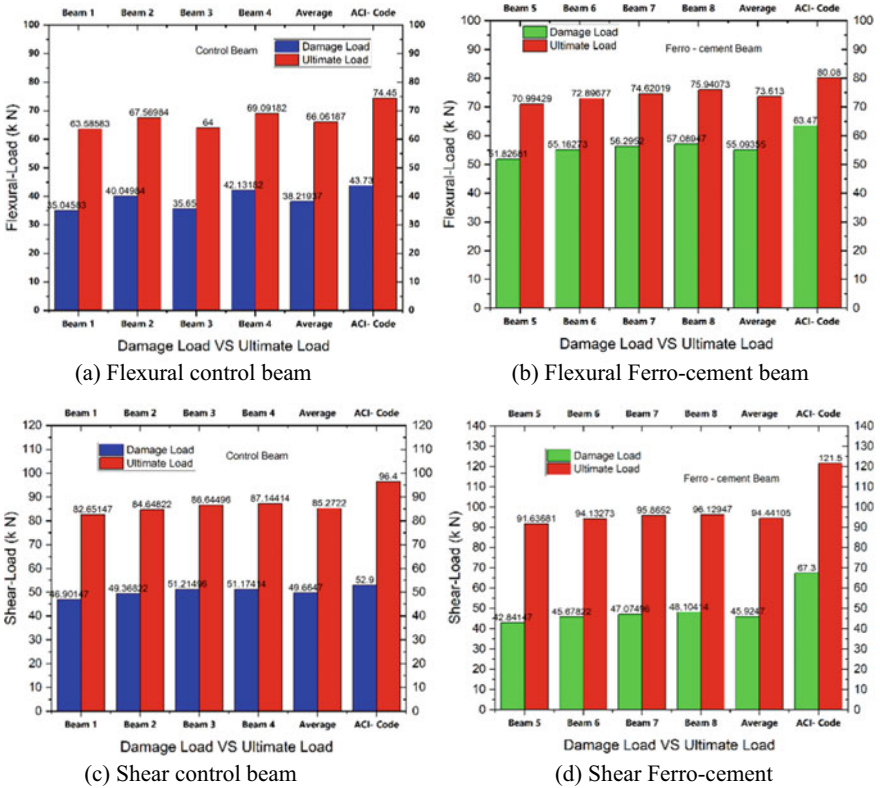


Fig. 7 Comparison between beam damage and ultimate load to experiment and ACI code

5 Conclusion

In this study, 12 concrete beams measuring $700 \times 150 \times 160$ mm were built and subjected to load testing in flexural and shear. Beams have been selected to ensure enhancement of yield point before using ferro-cement to the concrete undergoing a failure. The beams used M20 grade concrete. The output concludes as follows,

- Ferro-cement material has enhanced the beam’s deflection behaviour, as evidenced by a decrease in the initial deflection at the damaged and ultimate stage of a flexural investigation.
- The use of ferro-cement laminates in shear-strengthened beams resulted in a reduction of initial deflection during the damaged and ultimate stage.
- The test specimens exhibited a decrease in crack widths, substantial deflection at the point of damaged and ultimate load, a significant rise in the ductility ratio, and an increase in energy absorption subsequent to reinforcement.

- The application of ferro-cement laminates compared to control beams, as installing shear loading, led to increased load capacity, which was observed during the damaged and ultimate stages.
- The experimental samples demonstrated a reduction in crack widths, considerable deflection at the maximum load point, significant improvements in the ductility ratio, and a rise in energy absorption after being reinforced.
- These results suggest that the components were more adept at withstanding their ultimate capacity in ferro-cement flexural and shear cases.
- American code predicted higher values illustrated in shear and flexural studies at the damaged and ultimate stage of control ferro-cement beams.

Acknowledgements The authors would like to express appreciation to the Indian Council for Cultural Relations, India, and the INPS's social security contribution under separate management (CHIETI, IT), Italy.

References

1. Minde P, Bhagat D, Patil M, Kulkarni M (2023) A state-of-the-art review of ferrocement as a sustainable construction material in the Indian context. *Mater Today Proc*. <https://doi.org/10.1016/J.MATPR.2023.03.250>
2. Dawood ET, Shawkat AS, Abdullah MH (2021) Flexural performance of ferrocement based on sustainable high-performance mortar. *Case Stud Constr Mater* 15:e00566. <https://doi.org/10.1016/J.CSCM.2021.E00566>
3. Patil D, Aqeel Bukhari S, Minde PR, Kulkarni MS (2023) Review on comparative study of diverse wall materials for affordable housing. *Mater Today Proc* 77:823–831. <https://doi.org/10.1016/J.MATPR.2022.11.489>
4. Al Agha W, Alozzo Almorad W, Umamaheswari N, Alhelwani A (2021) Study the seismic response of reinforced concrete high-rise building with dual framed-shear wall system considering the effect of soil structure interaction. *Mater Today Proc* 43:2182–2188. <https://doi.org/10.1016/J.MATPR.2020.12.111>
5. Kant R, Al Agha W, Alozzo Almorad W, Thakur MS, Umamaheswari N (2021) Study on seismic performance of reinforced concrete multi-storey building considering soil-structure interaction effect. *Mater Today Proc*. <https://doi.org/10.1016/J.MATPR.2021.11.475>
6. El-Sayed TA, Shaheen YB, AbouBakr MM, Abdelnaby RM (2023) Behavior of ferrocement water pipes as an alternative solution for steel water pipes. *Case Stud Constr Mater* 18:e01806. <https://doi.org/10.1016/J.CSCM.2022.E01806>
7. Amala M, Dhal L, Gokul V, Christi S, Dhanasekar K (2021) Strengthening of compression member by ferrocement with high performance mortar—jacketing technique. *Mater Today Proc* 43:1810–1818. <https://doi.org/10.1016/J.MATPR.2020.10.495>
8. Aules WA, Saeed YM, Al-Azzawi H, Rad FN (2022) Experimental investigation on short concrete columns laterally strengthened with ferrocement and CFRP. *Case Stud Constr Mater* 16:e01130. <https://doi.org/10.1016/J.CSCM.2022.E01130>
9. Jarallah MN, Dawood ET, Abdullah MH (2022) Static and impact mechanical properties of ferrocement slabs produced from green mortar. *Case Stud Constr Mater* 16:e00995. <https://doi.org/10.1016/J.CSCM.2022.E00995>
10. Al Agha W, Umamaheswari N (2021) Analytical study of irregular reinforced concrete building with shear wall and dual Framed-Shear wall system by using equivalent static and response

- spectrum method. *Mater Today Proc* 43:2232–2241. <https://doi.org/10.1016/J.MATPR.2020.12.525>
11. Mariam Boban J, Susan John A (2021) A review on the use of ferro-cement with stainless steel mesh as a rehabilitation technique. *Mater Today Proc* 42:1100–1105. <https://doi.org/10.1016/J.MATPR.2020.12.490>
 12. Mohana R, Prabavathy S, Leela Bharathi SM (2021) Sustainable utilization of industrial wastes for the cleaner production of ferro-cement structures: a comprehensive review. *J Clean Prod* 291:125916. <https://doi.org/10.1016/J.JCLEPRO.2021.125916>
 13. ACI committee 549, (1993), “State of the art report on Ferro-cement”, Report by ACI committee 549, American Concrete Institute, Detroit
 14. ACI 318M-11, Building Code Requirements for Structural Concrete and Commentary, American Concrete Institute, 2011.
 15. Bureau of Indian Standards, New Delhi, Indian Standard Recommended Guidelines for Concrete Mix Design, IS10262, 2009
 16. IS 10262:2009, Concrete Mix Proportioning-Guidelines, Bureau of Indian Standards, New Delhi
 17. IS 269: 2015, Ordinary Portland cement 43 Grade-Specification, Bureau of Indian Standards, New Delhi
 18. Bureau of Indian Standards, New Delhi, Indian Standard Plain and Reinforced Concrete -IS 456, 2000
 19. ACI 440.2 R-08, Guide for the Design and Construction of Externally Bonded FRP Systems for Strengthening Concrete Structures, American Concrete Institute, 2008

Experimental Investigation on Chemically Treated Hooked End Steel Fiber Embedded in Rubberized Concrete



K. Thiagarajan  and N. Umamaheswari 

1 Introduction

Concrete is a primary material that is widely used in the construction field. It is evident from previous research that it is poor in tension compared to in compression which makes it brittle with low ductility. To escalate this property, fibers are being introduced that are randomly dispersed in concrete, which is called as fiber-reinforced concrete (FRC). Extensive research is being conducted worldwide on FRC to determine the influence of fibers on tension, flexure, compression, fatigue, etc. [1]. Research on microstructure of steel fiber with the cement mortar paste showed delayed cracking and failure, since the fiber arrests crack deviation [2]. Experimental research on steel fiber at various percentages in concrete shows improving results in terms of split tensile strength, modulus of rupture, and flexural strength of concrete as the percentage increases to certain extent [3, 4]. Studies on undulated steel fiber and larger diameter show enhancement in flexural toughness of FRC due to its cross-sectional area [5]. Strength of steel fiber-reinforced concrete (SFRC) is enhanced predominantly due to its interfacial bond and friction between the fiber/matrix that controls the pull-out of fiber, whereas weak bond does not contribute much to resisting the propagation of crack. Therefore, it is essential to identify the bond between fiber/matrix and its failure mechanism which is experimented in research by correlating analytical results [6]. Bond mechanism also varies with fiber orientation and embedment length with various concrete matrices [7]. Hooked end fibers are usually considered for construction, due to the response of the fiber hook that induces pull-out behavior, friction, plastic deformation of hook, and pull-out force in both normal and special concrete [8–10]. Research on pull-out behavior at elevated temperature shows that significant deterioration of bond properties occurs in case of

K. Thiagarajan · N. Umamaheswari (✉)

Department of Civil Engineering, Faculty of Engineering and Technology, SRM Institute of Science and Technology, Kattankulathur, Tamil Nadu 603203, India
e-mail: umamahen@srmist.edu.in

normal concrete [11]. Bond mechanism of deformed and spiral shaped fiber gives assured influence in terms of peak load and interfacial strength since multiple peaks are observed [12, 13] and in some cases deformed fiber of higher embedment length failed due to fiber rupture [14].

The research on fiber embedment for various strength of concrete matrix possessed elevated bond properties with higher peak load, e.g., in case of pull-out characteristics of steel fiber embedded in concrete with lesser water/binder ratio showed better peak loads [15, 16]. Few studies have focused on developing the interfacial transition zone between fiber and concrete, causing enhanced pull-out load and bond properties [17, 18]. Enhancing the bond characteristics and resistance to load depends on the interfacial transition zone between fiber and matrix, and the previous researches evidenced that use of HSC and material with enhanced physical properties to improve compressive strength can escalate those properties. An effective method is attempted by few researchers to create a transition zone between fiber and matrix by treating steel fiber with zinc phosphate (ZnPh). This method results in virtuous development of bond strength by 40–50% [19, 20] that is endorsed with the scanning electron microscope (SEM) analysis. Research proved that ZnPh performs better not only due to its delayed corrosion rate but also it roughens and alters the outer surface of the fiber that causes additional mechanical interlocking for straight and hooked end fibers [21–23].

There are several effective methods to enhance toughness, energy absorption, and impact resistance of concrete in construction. Since energy saving and reduction of carbon in the environment has become global movement, it is required to reuse the waste materials effectively. It is observed from earlier researches that waste tire rubber is one of the significant waste materials that have been of global concern [24]. Usage of waste tire rubber as crumb rubber in the production of concrete by replacing fine and coarse aggregate is being practiced since the last decade [25]. Earlier researches also proved to have a positive effect on the replacement of fine aggregate at a particular percentage (5–10%) [26], the mechanical properties have seen a trivial improvement if the fine aggregate is replaced by up to 5.5% and perceives a drastic decrease in compressive strength beyond this level [27]. Therefore, it is advised to add other strength increasing materials to enhance the properties [28]. Since silica fume has a rich content of SiO_2 [29], these materials utilized in the production of concrete readily improves the mechanical strength when replaced with cement [30, 31]. The addition of silica fume [32] and steel fiber [33] to increase the strength of rubber powder concrete [34] has been under research for some years. It reacts perfectly with other materials in counteracting the reduction of strength of concrete [35, 36].

Recycling of waste tire rubber is tried globally to enhance mechanical properties of crumb rubber through various reclamation processes [37, 38], done by breaking 3D link of the rubber that causes discerning disintegration of the sulfur-sulfur (ss) and carbon-sulfur (cs) bond without disturbing the backbone of the material and altering the properties; this treatment is called devulcanization [39, 40]. Of the various types of devulcanization processes [41], thermomechanical devulcanization is found to be effective and free from chemicals, which is considered for further usage in concrete. Using a rotating twin screw extruder, samples are subjected to a different temperature

that confirmed increment of mechanical properties at lowest temperature [42], after a certain temperature, tensile strength of rubber decreases which is established through crosslink density [43]. Therefore, it is evident that devulcanized rubber could further be used as normal rubber. As rubber powder is being used with steel fiber in the previous studies, it is important to identify the bond between these materials.

The novel aspect of the current study is to enhance the bond mechanism of hooked end steel fiber embedded in rubberized concrete after pre-treatment of fiber and recycling of the waste tire rubber. The research scope is to achieve better transition zone between fiber and concrete matrix assessed with single-fiber pull-out test for hooked end steel fiber inserted in various concrete matrix and identifying the matrix with higher pull-out load. In the current study, an experimental investigation was conceded on hooked end steel fiber embedded in concrete of varying strengths (30 and 60 MPa) by means of fiber pull-out from concrete. Steel fiber is pre-treated with the chemicals and evaluated along with the fibers without treatment to assess the encroachment of transition layer in fiber and matrix. Addition of silica fume in the concrete matrix stabilized the strength deficit caused by adding devulcanized rubber. Pull-out tests of fiber on these permutations of materials evidenced to deliver upstanding results with pre-treated fiber and concrete strength under consideration.

2 Experimental Program

The transition zone between the fiber/concrete matrix contributes in deciding the tensile strength and the failure pattern while evaluating the fiber/matrix interfacial strength. Pull-out tests were accomplished on steel fiber embedded in concrete matrix wideband due to the applied tensile force [8]. Pull-out test is classified into single-sided/double-sided pull-out with concrete matrix. In the current investigation, pull-out testing was done for fiber embedded at one end [21] where the fiber is placed at top of concrete matrix. The effect of concrete strength, fiber treatment, and replacement of fine aggregate by devulcanized rubber in the preparation of concrete is studied.

2.1 *Materials and Mix Proportions*

Hooked end steel fibers are used to perform a single-fiber pull-out test. Commercially available hooked end steel fiber aspect ratio (l/d) 50 and 100 is used in this study. The hooked end fibers pre-treated with the ZnPh by following the procedure proposed in the previous study [19]. The fibers are immersed in ZnPh conversion at 90 °C and then rinsed with water followed by drying the fiber for 10 min at 150 °C. It is evident from the treatment that ZnPh alters the exterior face of the steel fiber into a coarse texture, which helps in delaying slippage of the fiber from the matrix. The tensile strength properties of the steel fiber used are given in Table 1.

Table 1 Properties of steel fiber (from manufacturer's data)

Fiber	Aspect ratio	Tensile strength (N/mm ²)
Hooked end fiber (H50)	50	> 400
Hooked end fiber (H100)	100	> 500

Table 2 Mix proportions of concrete specimens

Type of concrete	Cement kg/m ³	w/C ratio	Fine aggregate kg/m ³	Coarse aggregate kg/m ³	Super plasticizer	Silica fume kg/m ³	Rubber powder kg/m ³	Slump (mm)
CC30	432.8	0.40	910.3	784.3	–	–	–	137
RC30	432.8	0.40	846.6	784.3	–	–	63.7	119
CC60	522.8	0.31	554.8	1099.3	4.64	58.1	–	105
RC60	522.8	0.31	515.9	1099.3	4.64	58.1	38.3	91

CC Conventional concrete, RC, Rubber concrete, w/C water/cement ratio

Two types of concrete are adopted in the present experimental investigation with the average compressive strength of 30 MPa [44] and 60 MPa. Normal strength concrete (NSC) was equipped by ordinary portland cement, river sand of specific gravity 2.62, coarse aggregate of 10 mm downsizes with a specific gravity of 2.65, and a water/cement ratio of 0.4.

In the case of HSC, silica fume containing a 0.11 μ m particle size of 0.11 μ m to improve the stuffing thickness and mechanical properties with the materials used for NSC. For HSC, super plasticizer named Conplast 400 was added to improve the flow and slump of fresh concrete. In the present experimental study, devulcanized rubber was used as a partial replacement for fine aggregate in concrete preparation and the crosslink density of normal and devulcanized rubber confirms that recycled waste rubber exhibits properties better than normal waste rubber. The mix proportion of NSC (grade M30) and HSC (gradeM60) along with the slack values obtained of fresh concrete is given in Table 2.

2.2 Preparation of Specimen

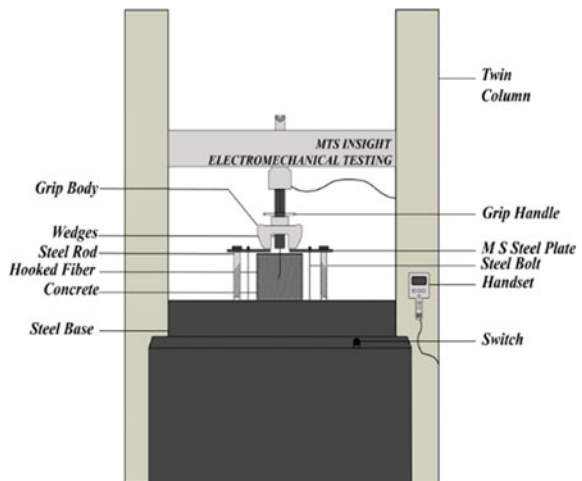
The present research includes experimental investigation on pull-out strength of hooked end fibers, with varying parameters such as type of concrete (normal and rubber concrete), concrete strength, embedment length and aspect ratio of fiber, and chemical treatment of fiber. Concrete was prepared with different material compositions such as conventional concrete, NSC and HSC, by replacing devulcanized rubber powder with fine aggregate. These combinations of materials follow different batching and mixing procedure. The super plasticizer was included at the prescribed level. Cube specimen of size 100 mm was used for single-fiber pull-out testing. The

average compressive strength was identified for each batch of concrete. Fiber was entrenched during the casting of cube at the top center face of concrete centrally at a desired embedment length (half-length of fiber/10 mm), and vibration was applied at a lower rate in order to confirm better compaction of concrete after placing the fiber. The current experimental plan includes a total of thirty-two specimens. A similar casting procedure was followed, considering the parameters such as aspect ratio of hooked end steel (50 and 100), concrete type (CC or RC), concrete strength (30 or 60 MPa), and fiber type (untreated or treated). The specimens were tested after 28 days of casting for pull-out strength as well as compressive strength of the samples.

2.3 Test Setup and Procedure

Bond characteristics of fiber/matrix is determined by performing single-fiber pull-out test [7]. The experimental setup is shown in Fig. 1. The pull-out test setup used in the present experimental investigation consists of a tensile testing machine of capacity 100 kN, with specimen grip, control unit for load cell, and fiber clutch. Rate of pull-out loading adopted was 1 mm/min. Earlier, concrete cubes were tested according to the specifications of IS to determine the compressive strength of concrete. The materials used fiber, silica fume, and rubber, and failure pattern of fibers is shown in Fig. 2a–d, respectively.

Fig. 1 Experimental setup



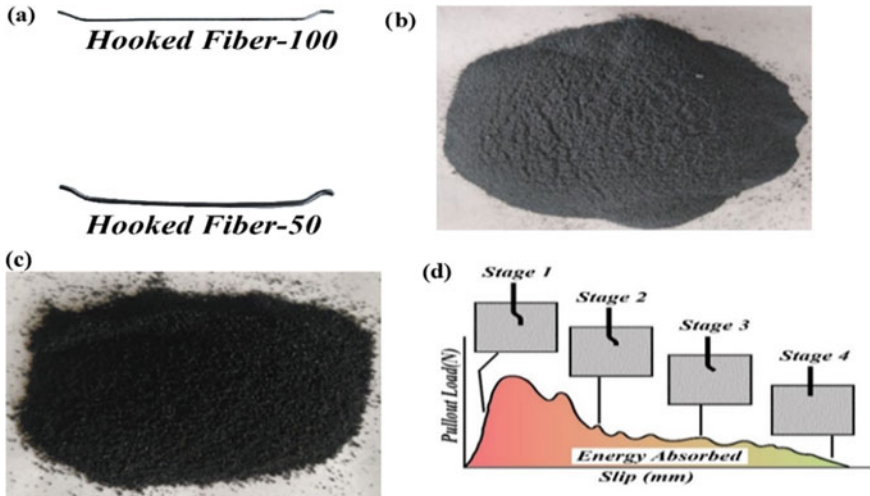


Fig. 2 Type of fiber and failure pattern, **a** fibers, **b** silica fume, **c** rubber, **d** failure pattern

3 Results and Discussion

The parameters that were investigated are the pull-out load (P) versus slip (s), the maximum pull-out load (P_{\max}), average bond strength (τ_{av}), and pull-out energy (Wp) and the equivalent bond strength (τ_{eq}) [17] for varying fiber aspect ratio, effect of pre-treatment of fiber, concrete compressive strength, and use of rubber concrete under static pull-out load.

3.1 Compressive Strength of Concrete

Compressive strength of NSC and HSC were identified for four concrete mixes after 28 days of casting. Devulcanized crumb rubber was added in both the concrete mixes as partial replacement (7%) of fine aggregate.

Average compressive strength achieved at 28 days was 35.1 and 69.3 N/mm² for NSC and HSC grades. The standard deviation is 3.88 and 7.91 for NSC and HSC, respectively. The coefficient of variation does not exceed 11.9 and 12.4% for NSC and HSC, respectively, which means that the results are agreeable. Addition of rubber powder relatively reduces the compressive strength due to the delayed hydration characteristic at early age of concrete and generation of voids, but when compared to normal rubber concrete, devulcanized rubber concrete possesses better strength, similar to [26]. The reduction in compressive strength of rubber concrete compared to conventional concrete was found to be 27 and 16% for grade M30 and M60, respectively.

3.2 Fiber Pull-Out Characteristics

In order to determine the bond characteristics of fiber and concrete, a single-fiber pull-out test was experimented which portrays P versus s curve, P_{\max} that is obtained from the curve and average bond strength (τ_{av}) between concrete and fiber (which can be obtained from Eq. 1)

$$\tau_{av} = \frac{P_{\max}}{\pi d_f L_E} \quad (1)$$

where d_f —diameter of the fiber and L_E is the initial embedded length of fiber.

The pull-out energy (W_P) presented is calculated from the area under P versus s curve until the fiber slips to the final load. Based on the pull out energy gained, the equivalent bond strength (τ_{eq}) is calculated using Eq. 2.

$$\tau_{eq} = \frac{2W_P}{\pi d_f L_E^2} \quad (2)$$

3.2.1 Effect of Using Hooked End Steel Fiber

The outcome of the hook geometry of hooked end steel fiber on pull-out behavior was assessed by relating pull-out test results obtained for different aspect ratio. The load versus slip behavior of the hooked end steel fiber of half the embedment length is shown in Fig. 3a–d for conventional concrete and rubber concrete for fiber aspect ratio, 50 and 100, respectively. The results of fibers with lesser aspect ratio were found to perform better than the fiber of larger aspect ratio. Due to the reduced cross-sectional area of fiber of larger aspect ratio, the effect of pull was less. The load slip characteristics in various other cases also show that the hooked end fiber with a lower aspect ratio / bigger diameter performed better, increasing the pull-out performance from the fiber/ concrete matrix. It was also confirmed that the usage of fiber of larger aspect ratio could not provide any positive impact in terms of pull-out load, and similar results were obtained by other researchers as the end fiber with a lower diameter had lesser peak load [10]. P_{\max} is always achieved during the initial stage of loading (slip-0.5 to 2 mm). The fiber showed plastic deformation at this stage to attain P_{\max} and to get straightened form in a matrix as perceived in a similar study where developed pull-out force could be achieved due to mechanical anchorage [8]. After undergoing initial deformation, a decrease in pull-out load was observed due to the reduced friction after the slip. It was observed that a certain amount of tensile force was observed by plastic deformation of the fiber at the end of curve that is caused by the friction resistance of fiber that results in higher pulling load [18].

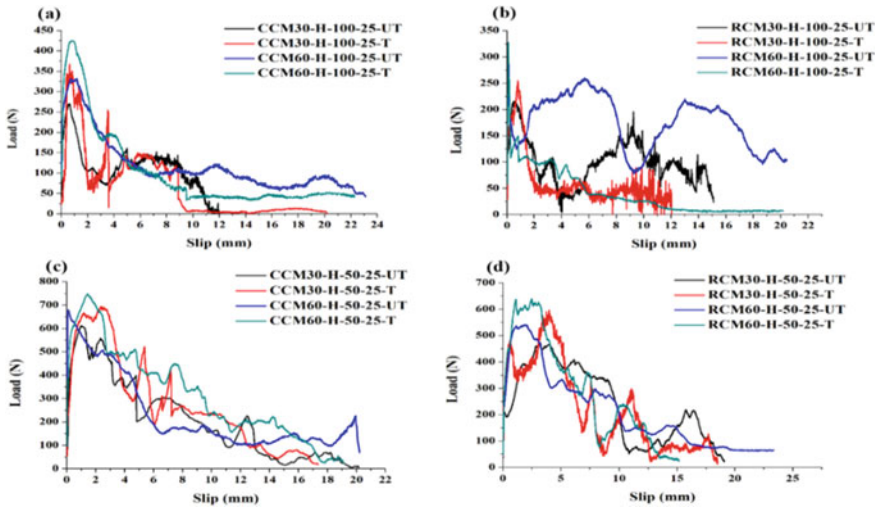


Fig. 3 Pull-out load vs slip curve-half embedment a CC – $l/d = 100$, b RC – $l/d = 100$, c CC- $l/d = 50$, d RC – $l/d = 50$

3.2.2 Effect of Embedment Length of Fiber

The P_{max} of the hooked end fiber showed that a reduction in peak load occurs when length of fiber in matrix decreased. The effects of the length on P_{max} were considered as major aspect as it helps in identifying performance of steel fiber from top surface of SFRC. The load versus slip behavior of the end steel fiber of 10 mm embedment length is shown in Fig. 4a–d for conventional concrete and rubber concrete for fiber aspect ratio, 50 and 100, respectively. The values of τ_{av} and τ_{eq} replicated that fiber with half embedment shows that higher contact with the concrete matrix provided improved resistance to pull-out. The increased fiber interaction in the concrete surface tends to delay fiber failure and requires further tensile energy to depart in concrete. Embedment of steel fiber of 10 mm path in concrete surface is lesser and requires very less pull-out energy to fiber slip [18]. This reduced pull-out energy is in parallel with the lower τ_{eq} and τ_{av} . Since the embedment length is smaller, the curve possesses multiple peak loads due to its deformed texture. Increasing the diameter of hooked end fiber and embedment length can cause increase in peak load which had close agreement with the previous results as the fiber embedded in half embedment provide better results [7]. There was only a trivial amount of deformation in fiber when embedded in 10 mm which can be confirmed with the available literature, and the fiber loses its grip from the matrix at a reduced embedment length in most cases [14] due to reduced contact surface of fiber from matrix, thus reducing P_{max} and τ_{eq} due to reduced frictional resistance.

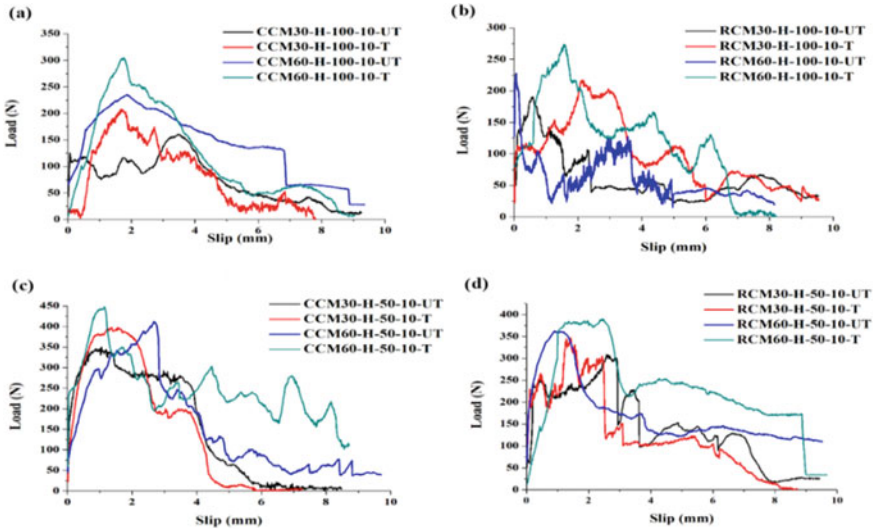


Fig. 4 Pull-out load vs curve-10 mm embedment **a** CC – $l/d = 100$, **b** RC – $l/d = 100$, **c** CC- $l/d = 50$, **d** RC – $l/d = 50$

3.2.3 Effect of Chemical Treatment on Fiber

Treatment of steel fiber was found to have a predominant effect, thus creating a strong layer between concrete and fiber. The fiber will fail due to deformation caused by slippage of fiber and reduced frictional resistance. To overcome the problem, Suguma et al. [19] effectively proposed a chemical treatment on fiber prior to concreting. Interfacial adhesion between fiber/concrete improved P_{max} and τ_{eq} of steel fiber [21].

The hooked end fiber of larger aspect ratio showed only a lesser difference in peak load for both untreated and treated cases while the fiber of smaller aspect ratio encountered an approximately 10% increase in peak load due to treatment of fiber. The rough topography of treated fiber influences P_{max} and W_p which is being similar to results proposed by Soulioti et al. [21]. Coarse pattern of fiber due to treatment increases the slipping period of fiber from the matrix, thus increasing the bond strength as reported in the previous literature [22]. The current test results also prove the same.

3.2.4 Effect of Concrete Compressive Strength

The effect of using NSC and HSC was evaluated by comparing the test results obtained for varying aspect ratio and length of fiber. The effect of concrete strength in the hooked end fiber of larger aspect ratio has a negligible effect in terms of P_{max} because the area of contact between fiber and concrete is less. The hook in this fiber

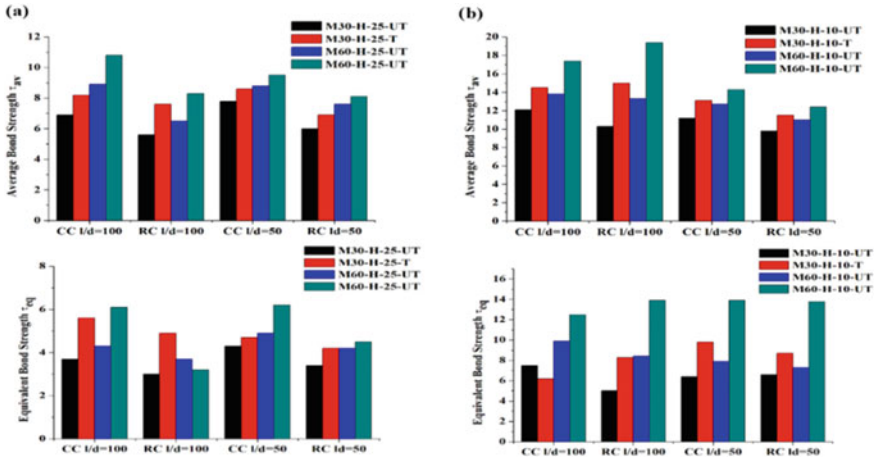


Fig. 5 Average bond strength of **a** half embedded fiber **b** 10 mm embedded fiber, equivalent bond strength of **a** half embedded fiber **b** 10 mm embedded fiber

will not favor any interfacial bonding between the fiber/matrix, resulting in a reduced average and τ_{eq} as compared to other fibers closely related to the behavior of higher concrete strength [17] as shown in Fig. 5. The hook end fiber had a better peak load behavior, obviously peak load, about 1.11 times more in the case of HSC under consideration when compared to the NSC as shown in the results [18].

3.2.5 Effect of Using Rubber Concrete

Pull-out characteristics of steel fiber in devulcanized rubber concrete (both normal and high strength) proved to have adverse effect in terms of P_{max} and W_p . Peak pull-out load and the level of bond are significantly lower in case of rubber concrete for all fibers under consideration. This difference in mechanism occurs due to the reduction in concrete strength which was caused due to addition of rubber waste as partial replacement of fine aggregate [24]. But when compared to normal crumb rubber concrete, devulcanized rubber concrete tends have positive impact on compressive strength of both the concrete grades. Hooked end fiber possesses lesser peak load of 19.25 and 22.2% at normal strength rubber concrete and 8.04 and 20.3% at high strength rubber concrete when compared to conventional concrete. The peak load gradually as the fiber could not undergo mechanical interlocking with the concrete matrix. Loss in P_{max} is more gradual in fiber of higher aspect ratio than in the lower one. The fiber in the concrete matrix slips away with the residual resistance that is produced only by the frictional force in the absence of plastic deformation where the fiber completely slips from concrete. It can be observed that initial pull-out response of these fiber is governed by several mechanism such as mechanical anchorage in fiber, interfacial strength, and frictional slip behavior and bond characteristics. It is

observed that these factors do not contribute much in adding pull-out resistance when the concrete mix possesses reduced strength.

3.2.6 Pull-Out Energy Dissipation

Fiber pull-out energy dissipation is determined from the region covered below the P versus s curve for all cases. τ_{av} and τ_{eq} of various types of fiber with different combinations are shown in Fig. 5. It is evident that an increase in peak load increases the energy dissipation. Hooked end fiber of higher aspect ratio is found to have higher influence on peak load that increased the energy dissipation by up to 25% for HSC compared to NSC, in case of higher embedment length as the pull-out curve tends to experience higher load with the slip of fiber, thus resulting the higher pull-out energy where the fiber in smaller embedment roughly influences the curve as the energy depends on the fiber slip [18].

4 Conclusion

The current experimental study involves investigation of chemically treated fiber at normal loading rate in various type of concrete, w.r. to aspect ratio of fiber embedded in NSC and HSC. The objective of this findings was to test a steel fiber to enhance its bond strength in rubberized concrete. An increased aspect ratio resulted in reduced energy absorption and equivalent bond strength. The embedment of chemically treated fibers in various concrete matrixes made the fiber to withstand the applied pull-out load due to the additional frictional resistance caused by the treatment. The influence of embedment length and concrete strength on fiber pull-out in HSC was found to have similar effect to that in NSC. The addition of devulcanized waste tire rubber is found to have influence to a considerable extent in the case of HSC when the fibers are treated. The usage of devulcanized rubber powder in the current study indicates that it will be a reasonable replacement material when compared to normal crumb rubber.

References

1. ACI 544.1R-96 Report on fiber reinforced concrete: American Concrete Institute; 1996 (Reapproved 2002)
2. Bentur A, Diamond S (1985) The microstructure of the steel fiber-cement interface. *J Mater Sci* 20:3610–3620
3. Song PS, Hwang S (2004) Mechanical Properties of high-strength steel fiber-reinforced concrete. *Constr Build Mater* 18:669–673
4. Abbas W, Khan I, Mourad S (2018) Evaluation of mechanical properties of steel fiber reinforced concrete with different strengths of concrete. *Constr Build Mater* 168:556–569

5. Banthia N, Sappakittipakorn M (2007) Toughness enhancement in steel fiber reinforced concrete through fiber hybridization. *Cem Concr Res* 37:1366–1372
6. Naaman AE, Namur GG, Ahwan JM, Najm HM (1991) Fiber pull-out and bond slip. II: experimental validation. *J Struct Eng* 117:2791–2800
7. Cunha VMCF, Barros JAO, Sena-Cruz JM (2010) Pull-out behavior of steel fibers in self-compacting concrete. *J Master Civ Eng* 22:1–9
8. Soetens T, Gysel AV, Matthys S, Taerwe L (2013) A semi-analytical model to predict the pull-out behavior of inclined hooked-end steel fibres. *Constr Build Mater* 43:253–265
9. Beglarigale A, Yazici H (2015) Pull-Out behavior of steel fiber embedded in flow able RPC and ordinary mortar. *Constr Build Mater* 75:255–265
10. Abbas MY, Khan I (2016) Fiber-Matrix Interfacial Behavior of hooked-end steel fiber-reinforced concrete. *J Master Civ Eng* 28:1–10
11. Abdallah S, Fan M, Cashell K (2017) Pull-Out Behavior of straight and hooked-end steel fibers under elevated temperatures. *Cem Concr Res* 95:132–140
12. Hao Y, Hao H (2017) Pull-Out behavior of spiral-shaped steel fibers from normal-strength concrete matrix. *Constr Build Mater* 139:34–44
13. Chin CS (2019) An approach to investigate the fiber- cementations composites bond-slip mechanisms. *Adv Civ Eng Mater*
14. Zile E, Zile O (2013) Effect of the fiber geometry on the pull-out response of mechanically deformed steel fibers. *Cem Concr Res* 44:18–24
15. Abdallah S, Fan M, Zhou X (2017) Pull-Out behavior of hooked end steel fibers embedded in ultrahigh performance mortar with various w/b ratios. *Int J Concr Struct Mater* 11:301–313
16. Abdallah S, Rees D, Ghaffar SH, Fan M (2018) Understanding the effects of hooked-end steel fiber geometry on the uniaxial tensile behavior of self-compacting concrete. *Constr Build Mater* 178:484–494
17. Yoo DY, Park JJ, Kim WS (2017) Fiber pull-out behavior of HPCFRCC: effects of matrix strength and fiber type. *Compos Struct* 174:263–276
18. Deng F, Ding X, Chi Y, Xu L, Wang L (2018) The pull-out behavior of straight and hooked-end steel fiber from hybrid fiber reinforced cementations composite: experimental study and analytical modelling. *Compos Struct* 206:693–712
19. Sugama T, Carciello N, Kukacka LE (1992) Interface between zinc phosphate-deposited steel fibers and cement paste. *J Mater Sci* 27:2863–2872
20. Yue CY, Cheung WL (1992) Interfacial properties of fiber-reinforced composites. *J Mater Sci* 27:3843–3855
21. Soulioti DV, Barkoula NM, Koutsianopoulos F, Charalambakis N, Matikas TE (2013) The effect of fiber chemical treatment on the steel fiber/cementations matrix interface. *Constr Build Mater* 40:77–83
22. Sun M, Wen DJ, Wang HW (2012) Influence of corrosion on the interface between zinc phosphate steel fiber and cement. *Mater Corros* 63:67–72
23. Aggelis DG, Soulioti DV, Gatselou EA, Barkoula NM, Matikas TE (2013) Monitoring of the mechanical behavior of concrete with chemically treated steel fibers by acoustic emission. *Constr Build Mater* 48:1255–1260
24. Rashad MAA (2016) Comprehensive overview of rubber recycling as fine aggregate replacement in traditional cementations materials. *Int J Sustain Built Environ* 5:46–82
25. Sofi A (2017) Effect of waste tyre rubber on mechanical and durability properties of concrete—a review. *Ain Shams Eng J* (2017)
26. Yung WH, Yung LC, Hua LH (2013) A study of the durability properties of waste tyre rubber applied to self-compacting concrete. *Constr Build Mater* 41:665–672
27. Bisht K, Ramana PV (2017) Evaluation of mechanical and durability properties of crumb rubber concrete. *Constr Build Mater* 115:811–817
28. Azevedo F, Torgal FP, Jesus C, Aguiar BGJL, Camoes AF (2012) Properties and durability of HPC with rubber tyre residues. *Constr Build Mater* 34:186–191
29. Saridemir M (2013) Effect of silica fume and ground pumice on compressive strength and modulus of elasticity of high strength concrete. *Constr Build Mater* 49:484–489

30. Siddique R (2011) Utilization of silica fume in concrete: review of hardened properties. *Resour Conserv Recycl* 55:923–932
31. Bhanja S, Sengupta B (2005) Influence of silica fume on the tensile strength of concrete. *Cem Concr Res* 35:743–747
32. Mohammed MS, Adamu M (2018) Mechanical performance of roller compacted concrete pavement containing crumb rubber and nano silica. *Constr Build Mater* 159:234–251
33. Ismail MK, Hassan AAA, Ridgley KEE, Colbourne B (2018) Steel-Fiber self-consolidating rubberized concrete subjected to impact loading. *Int Congr Polym Concr* 50:397–403
34. Li W, Huang Z, Wang X, Zang Z (2014) Experimental study on the mechanical properties of the crumb rubber concrete modified by silica fume. *Appl Mech Mater* 543:4031–4034
35. Wang X, Xia J, Nanayakkar O, Xi Y (2017) Properties of high-performance cementations composites containing recycled rubber crumb. *Constr Build Mater* 156:1127–1136
36. Li Y, Li Y (2017) Experimental study on performance of rubber particle and steel fiber composite toughening concrete. *Constr Build Mater* 146:267–275
37. Adhikari B, Maiti DDS (2000) Reclamation and recycling of waste rubber. *Prog Polym Sci* 25:909–948
38. Maridass B, Gupta BR (2003) Recycling of rubber powder from waste tires. *Mach Equipment's* 231–236
39. Asaro L, Gratton M, Seghar S, Hocine NA (2018) Recycling of rubber waste by devulcanization. *Resour Conserv Recycl* 133:250–262
40. Zhao F, Bi W, Zhao S (2011) Influence of crosslink density on mechanical properties of natural rubber vulcanizates. *J Macromol Sci Part: Phys* 50:1460–1469
41. Rooj S, Basak GC, Maji PK (2011) New route for devulcanization of natural rubber and the properties of devulcanized rubber. *J Polym Environ* 19:382–390
42. Formela K, Cysewska M, Haponiuk J (2014) Thermomechanical reclaiming of ground tyre rubber via extrusion at low temperature: efficiency and limits. *J Vinyl Additive Technol* 1–9 (2014)
43. Tao G, He Q, Xia Y, Jia G, Yang H, Ma W (2013) The effect of devulcanization level on mechanical properties of reclaimed rubber by thermal-mechanical shearing devulcanization. *J Appl Polym Sci* 2598–2605 (2013)
44. IS (2009) 10262 Concrete mix proportioning; recommended—guidelines, bureau of Indian standards, New Delhi

Study on Mechanical Properties of Polymer Fiber-Reinforced Nano-Concrete Under Elevated Temperature



S. Hariharan and S. Karthiga

1 Introduction

Nowadays, normal concrete is usually used in constructions, but due to environmental disasters and environmental changes, the lifetime of a building is reduced. Thus, to increase the lifetime of the building and the strength of the building, new technology or a new method is to be introduced in constructions. As concrete plays a major role in constructing a building, a new method should be implemented to the concrete. Studies show that nano-silica, a fine material of nanoparticle, has been added to normal concrete to make nano-concrete. This nano-concrete is made by adding nano-silica to the percentage weight of the cement in the proportion of the concrete. The size of the nano-silica is no greater than $500\ \mu\text{m}$. This nanoparticle fills the space that occurs in normal concrete between aggregate and portland cement, thereby increasing the material strength. The chemical formula for nano-silica is NaSiO_2 . Also, nano-calcium carbonate, alumina, silica fume, steel slag, and titanium oxide are used in nano-concrete. But compared to these materials, NaSiO_2 has more compactness and durability than the others. Nano-silica is also costlier than the other materials. This represents nano-technology in future constructions [1]. The use of NaSiO_2 in concrete enhances the durability and strength. Addition of nano-silica decreases the cement content, as cement increases carbon dioxide emissions. The grade of concrete used in this experiment is M40 grade [2]. It is said that by adding 0–2% of NaSiO_2 to the concrete, strength of the concrete increases by 9%, but 5% of nano-silica is used in this experiment to increase the strength by 12–15% which is greater than the normal concrete [3]. A 99.9% purity of nano-silica and materials like cement, M sand, and coarse aggregate were used. For extra support to the concrete, admixtures like structuro203, a superplasticizer, were also used in

S. Hariharan · S. Karthiga (✉)

Department of Civil Engineering, Faculty of Engineering and Technology, SRM Institute of Science and Technology, Kattankulathur, Tamil Nadu 603203, India

e-mail: karthigs@srmist.edu.in

this study. These materials were mixed using vertex mix design. The mix design was calculated by using the material properties. The nano-silica not only fills the material but also increases the high specific surface area of the concrete. It also reduces the setting time of concrete [4]. Nano-concrete requires only less amount of water in preparing the mixture of the concrete. Nano-concrete is proven to have more strength and durability than normal concrete. Nano-silica greatly increases the reliability and reduces the crack in concrete when the concentration enhances above 3% [5]. Further experiments and testing have been done to identify the physical properties, chemical properties, and mechanical properties of the nano-concrete. The qualities of nano-concrete are determined using compression, split tensile, and flexural testing. These mechanical properties have been identified, so that it improves the civil engineering infrastructures, including residential buildings as well as commercial buildings [6]. Different types of specimens like cubes, cylinders, and prisms were casted. A total of 27 cubes and 18 cylinders were casted in this experiment. These specimens were heated under different conditions of temperature, whereas only six prisms were initiated as they were not heated under elevated temperature. The prisms were tested only under the normal room temperature. Studies show that compressive strength and split tensile strength both decrease as temperature rises. But it is proven that NaSiO_2 has an advantage to improve the compressive strength and split tensile at various temperatures [7]. The fracture energy of the concrete is tested by a flexural test. Nano-silica plays a major role in the improvement of the flexural strength. For further development, polypropylene fiber is added. Polypropylene is a thermoplastic polymer. They are good chemical resistance of bases and acids. They also possess great fatigue resistance, impact strength, and electrical insulator. Thus, to increase the strength, nano-silica and polypropylene fiber are mixed together. The mixture of nano-silica and polypropylene in concrete makes the physical properties and mechanical properties stronger. Properties such as workability, elasticity modulus, compression, flexural, and split tensile strength of the concrete are made to increase [8]. The polypropylene fiber was added in different percentages of 1 and 2% in this experiment. The specimens with 1% of polypropylene have resulted in having more strength [9]. Thus, the compressive strength, split tensile strength, and flexural strength are improved by adding 1% of polypropylene to the nano-concrete [10]. Further the experiment is carried to cast reinforcement beams. A total of nine reinforced beams were casted. Each proportion consists of three reinforced beams. The reinforced beams were tested by applying two-point loading [11]. Before testing, the beams were heated by different temperatures in an oven. Temperatures were from 0 to 600 °C. In this study, the beams were kept under the elevated temperature of 50 and 100 °C only [12]. The deflection of the beams was noted by the cracking patterns, and mode of failure once the load is applied. The beam with 1% polypropylene under room temperature has taken the maximum load of 110 kN with least deflection of 9.66 mm [13].

Study has shown that concrete gets weak in its properties at high temperatures. Thus, the nano-concrete with polypropylene fiber is exposed to a particular degree of temperature to identify whether the concrete can withstand high heat pressure as polypropylene is a lightweight material that gives extra strength when it is heated.

From this study, it is proven that the mixture of 5% nano-silica and 1% polypropylene in a concrete has improved its strength even when it is subjected to high temperatures.

2 Materials and Methodology

2.1 Materials Properties

In the research, the materials and the methodology of the project are given in detail. The materials are selected by their unique properties. OPC 53 grade cement is used as it has high strength and durability because of its particle size and superior crystal structure. The properties of the cement are given in Table 1. Coarse aggregate was 20 mm in size. As the study is based on M40 grade, the specific gravity of the aggregate after the calculation is given as 2.67. M sand is a crushed fine aggregate with similar strength and durability to normal sand. The specific gravity of M sand is calculated by the pycnometer method and is given as 2.65. The use of nano-silica, a supernatural substance with new and interesting properties, gives more strength and durability when they are mixed with other substances. Nano-silica also increases the workability. The purity and the specific gravity of the nano-silica are given in Table 2. Polypropylene is a polymer fiber which is lightweight in nature, provides high strength, and corrosion resistance to the structure. The crack found in concrete can be minimized by adding polypropylene. The durability of the concrete will improve as polypropylene blocks the need for water in it. The properties of the polypropylene are given in Table 3.

Table 1 Physical properties of cement

Properties	Description
Specific gravity	3.15
Specific surface area (m ² /Kg)	340
Normal consistency (%)	28.9
Setting time (min)	180

Table 2 Physical properties of nano-silica

Properties	Description
Specific gravity	1.03
Purity (%)	99.9
Viscosity (cP)	0.8872
Count rate (kcps)	94.3

Table 3 Physical properties of polypropylene fibers

Properties	Description
Specific gravity	0.91
Fiber length (mm)	6
Fiber diameter (micron)	Approx 15–30
Water absorption (%)	< 0.1
Softening point (°C)	160–170
Melting point (°C)	165
Specific surface area (m ² /Kg)	Approx 200

**Fig. 1** Methodology of the study

2.2 Methodology

The methodology of this project only involves an experimental process as nano-concrete deals with strength and workability. The methodology gives the overall perspective of the project. The methodology of the study is shown in Fig. 1.

3 Results and Discussions

When polypropylene fibers were added, it was discovered that a specific dosage of 1 and 2% of fiber increased the strength. To identify the properties of nano-concrete and fiber-reinforced concrete, various tests (compression test, split tensile test, flexural test, and two-point loading deflection test) were carried out.

3.1 Effects on Compressive Strength

In order to identify the compressive strength, different specimens were casted with varying dosage of 1% and 2% of polypropylene fibers. The size of the cube is 150 mm × 150 mm × 150 mm. The specimens were cured for 28 days in the water. A total number of 27 specimens were heated under room temperature, 50 and 100 °C. Figure 2 shows the test of specimens. From Table 4, the maximum compressive strength is 53.3 MPa, i.e., the nano-concrete with 1% polypropylene

Fig. 2 Comparison of compressive strength

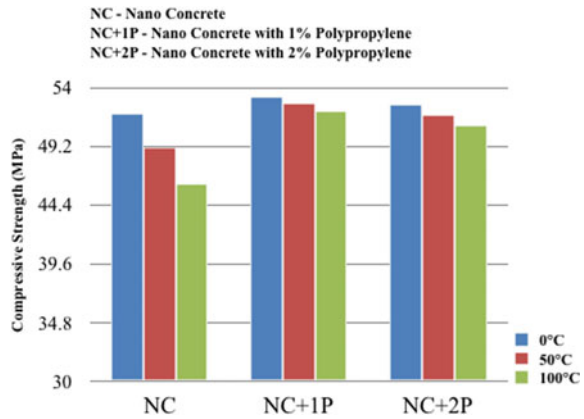


Table 4 Compressive strength of the specimens

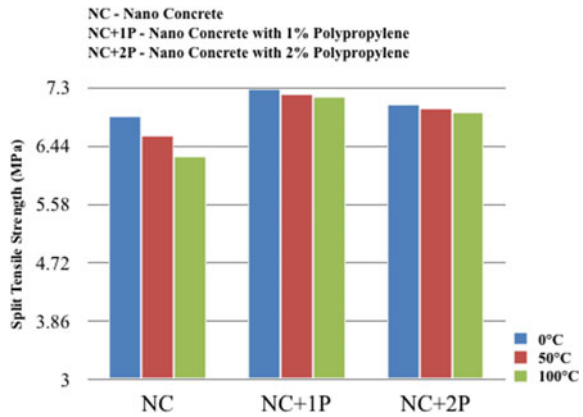
Specimens	Load (kN)	Strength (MPa)
NC 0 °C	1150	51.1
NC 50 °C	1106	49.1
NC 100 °C	1037	46.1
NC + 1P 0 °C	1199	53.3
NC + 1P 50 °C	1186	52.7
NC + 1P 100 °C	1179	52.1
NC + 2P 0 °C	1184	52.6
NC + 2P 50 °C	1166	51.8
NC + 2P 100 °C	1145	50.9

under room temperature. The least compressive strength is 46.1 MPa, i.e., the nano-concrete without polypropylene fiber under 100 °C. Figure 3 shows the comparison between the different specimens for compressive strength. Compared to nano-concrete without fiber, the compressive strength of the nano-concrete with 1% and 2% polypropylene fiber is increased up to 7.88% and 5.78%, whereas the strength of the nano-concrete with 1% polypropylene fiber is increased by 2.10% compared to the nano-concrete with 2% polypropylene fiber.

3.2 Effects on Split Tensile Strength

Different specimens were cast with variable dosages of 1% and 2% polypropylene fibers to the concrete in order to determine the split tensile strength. The cylinder is 300 mm × 150 mm × 150 mm in size. The specimens were cured for 28 days. A total of six specimens were heated at 50 °C, and six more specimens were heated at 100 °C.

Fig. 3 Comparison of split tensile strength



While the remaining six specimens were kept under normal room temperature. From Table 5, the highest strength of split tensile of the nano-concrete with 1% polypropylene under room temperature was 7.28 MPa. The nano-concrete without polypropylene fiber heated at 100 °C has the lowest strength of split tensile of 6.29 MPa. Figure 3 compares the split tensile strength of the various specimens. The split tensile strength of nano-concrete containing 1% and 2% polypropylene fiber is enhanced to 8.98% and 5.89%, respectively, as compared to nano-concrete without fiber. In comparison with nano-concrete with 2% polypropylene fiber, the strength of nano-concrete with 1% polypropylene fiber increases by 3.09%. As a result of the addition of 2% polypropylene fiber, the specimens strength is somewhat reduced.

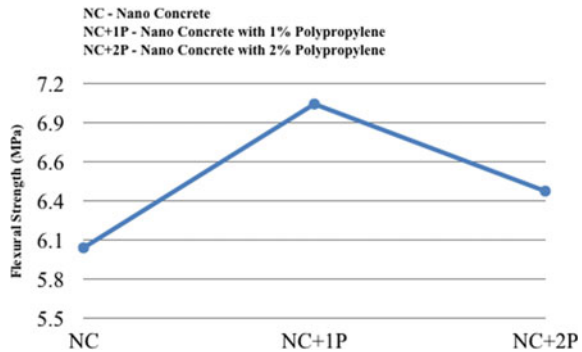
Table 5 Split tensile strength of the specimens

Specimens	Load (kN)	Strength (MPa)
NC 0 °C	487	6.89
NC 50 °C	466	6.59
NC 100 °C	445	6.29
NC + 1P 0 °C	514	7.28
NC + 1P 50 °C	509	7.20
NC + 1P 100 °C	506	7.16
NC + 2P 0 °C	499	7.06
NC + 2P 50 °C	494	6.99
NC + 2P 100 °C	490	6.93

Table 6 Flexural strength of the specimens

Specimens	Load (kN)	Strength (MPa)
NC	29	6.01
NC + 1P	34	7.05
NC + 2P	31	6.42

Fig. 4 Comparison of flexural strength



3.3 Effects on Flexural Strength

To assess flexural strength, three different specimens were casted without fiber and with varying amounts of 1% and 2% polypropylene fibers. The prism is 700 mm × 150 mm × 150 mm. The specimens were cured for 28 days. The test is done by applying two-point loading. Thus, the load equally spread into two halves and applied on the prism. From Table 6, the greatest flexural strength of the nano-concrete with 1% polypropylene was 7.05 MPa, and the nano-concrete without polypropylene fiber has the lowest flexural strength of 6.01 MPa at room temperature. Figure 4 compares the flexural strength of the various specimens. The specimens with fiber did not break but just produced a crack, whereas the specimens without fiber broke and split into two halves. The testing of the specimens with fiber and without fiber are shown in Figs. 5 and 6. In comparison with nano-concrete without fiber, the strength of nano-concrete including 1% and 2% polypropylene fiber is increased to 15.92% and 6.59%, respectively. The flexural strength of nano-concrete with 1% polypropylene fiber increased by 9.35% when compared to nano-concrete with 2% polypropylene fiber. The specimen strength is somewhat lowered as a result of the inclusion of 2% polypropylene fiber.

3.4 Effects on Deflection of Beams

According to the results of the beam deflection test, increasing the number of polypropylene fibers reduces beam deflection. A total of nine distinct reinforced

Fig. 5 Testing of flexural strength with fiber



Fig. 6 Testing of flexural strength without fiber



beams were casted without fiber and with variable amounts of 1% and 2% polypropylene fibers to determine the deflection. The beam is 1000 mm × 150 mm × 100 mm in size. The beams were cured for 28 days. A total number of three reinforcement beams were heated under 50 °C and three more reinforcement beams were heated under 100 °C. The remaining three reinforcement beams were kept under the normal room temperature. By applying two-point loading, the load eventually spread and acted on the reinforcement beams. The deflection (mm) of the beam is noted for every

5 kN. Figure 7 shows the testing of beams. The comparison of three reinforcement beams of nano-concrete without polypropylene fiber under different temperatures are given in Fig. 8. The difference between the reinforced beams of nano-concrete with 1 and 2% polypropylene fiber under normal room temperature and the temperature of 50 °C and 100 °C are shown in Figs. 9 and 10. The reinforcement beam of nano-concrete with 1% polypropylene under room temperature has a maximum load of 110 kN with a deflection of 9.66 mm. The reinforcement beam of nano-concrete without polypropylene fiber under 100 °C has the least load of 75 kN with a deflection of 11.26 mm.



Fig. 7 Testing of the reinforcement beam

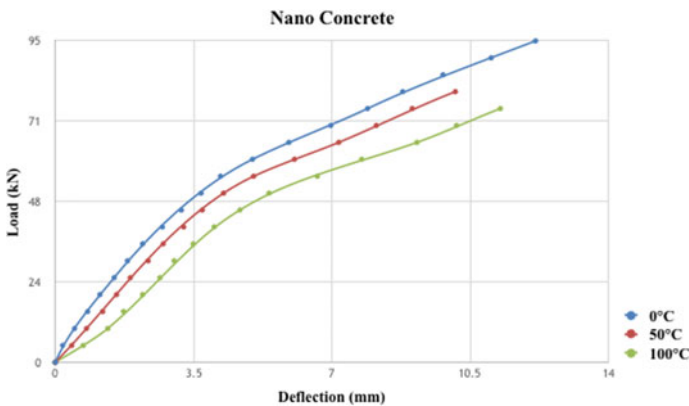


Fig. 8 Comparison of reinforcement beams of nano-concrete without fibers

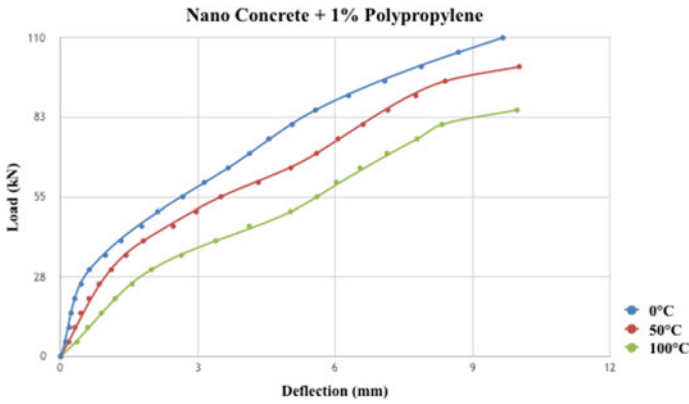


Fig. 9 Comparison of reinforcement beams of nano-concrete with 1% polypropylene fibers

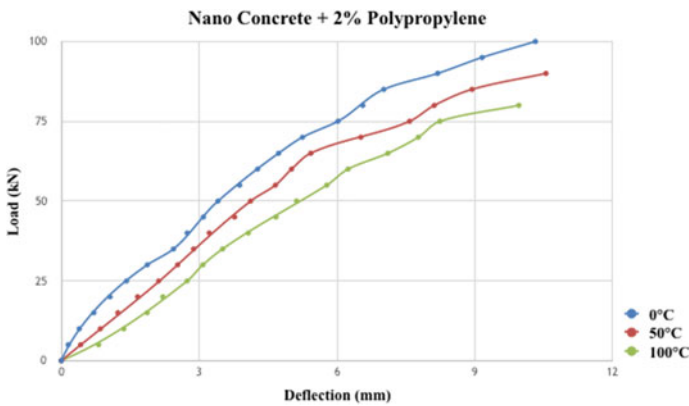


Fig. 10 Comparison of reinforcement beams of nano-concrete with 2% polypropylene fibers

4 Conclusion

Based on the test results, the experimental conclusions are listed below:

- At 1% polypropylene dose, compressive strength and split tensile strength were at its peak. At 1% polypropylene fiber dosage, the compressive strength and split tensile strength of nano-concrete with polypropylene fiber increased by 7.88 and 8.98% as compared to nano-concrete without polypropylene fiber.
- The greatest flexural strength was achieved with a 1% polypropylene dose. At 1% polypropylene fiber dosage, the improvement in flexure strength of nano-concrete with polypropylene fiber was determined to be 15.92% when compared to nano-concrete without polypropylene fiber.

- Under normal room temperature, the nano-concrete reinforcement beam with 1% polypropylene has a maximum load of 110 kN with a deflection of 9.66 mm.
- The nano-concrete increases with 1% of polypropylene fiber because the polypropylene fiber transforms the brittleness of the concrete to ductile material as they can arrest the micro cracks and as well as the nano-silica fills the void space in the material and increases the strength due to high specific surface area.
- It is proven that the addition of nano-silica and polypropylene fiber will improve the mechanical properties of the specimens. The NaSiO_2 and polypropylene fiber as increasing chemical properties which improves the strength of the specimens. Thus, the nano-concrete with 1% polypropylene has an accurate rate of proportion of mixture that increases the specimen's strength.
- The strength in 2% polypropylene is reduced compared to 1% polypropylene because under certain amount of addition of fibers the strength will decrease. As the polypropylene fiber is increased in the proportion, the strength started to decrease. It is clearly explained that with increase in temperature, the strength of the specimens decreases. Thus, by adding nano-silica and polypropylene to the concrete, the strength of the specimens manage to be stronger than the normal concrete.

References

1. Kansal CM, Goyal R (2021) Analyzing mechanical properties of concrete with nano silica, silica fume and steel slag. *Mater Today Proc* 45(6):4520–4525
2. Chekravarty D, Mallika A, Sravana P, Rao S (2022) Effect of using nano silica on mechanical properties of normal strength concrete. *Mater Today Proc* 51(8):2573–2578
3. Danielraj RC, Aniruddha DN, Parvati TS, Joanna PS (2021) Mechanical properties of sustainable nano concrete using optimized admixture. *Mater Today Proc* 45(7):5953–5959
4. Jo BW, Kim CH, Lim JH (2007) Investigations on the development of powder concrete with Nano- SiO_2 particles. *KSCE J Civ Eng* 11:37–42
5. Rao MV, Sivagamasundari R, Raju AS (2011) Study on reliability of concrete nano-mixture containing nano-silica. *Mater Today Proc* 62(4):1834–1838
6. Keshavarzian F, Saberian M, Li J (2021) Investigation on mechanical properties of steel fiber reinforced reactive powder concrete containing nano- SiO_2 : an experimental and analytical study. *J Build Eng* 44:102601
7. Yonggui W, Shuai peng L, Hughes P, Yuhui F (2020) Mechanical properties and microstructure of basalt fiber and nano-silica reinforced recycled concrete after exposure to elevated temperatures. *Constr Build Mater* 247:118561
8. Abna A, Mazloom M (2022) Flexural properties of fiber reinforced concrete containing silica fume and nano-silica. *Mater Lett* 316:132003
9. Orouji M, Zahrai SM, Najaf E (2021) Effect of glass powder and polypropylene fibers on compressive and flexural strength, toughness and ductility of concrete: an environmental approach. *Structures* 33:4616–4628
10. Bahar E, Ucar N, Onen A, Wang Y, Oksuz M, Ayaz O, Ucar M, Demir A (2012) Thermal and mechanical properties of polypropylene nanocomposite materials reinforced with cellulose nano whiskers. *J Appl Polym Sci* 125(4):2882–2889

11. Jameran A, Ibrahim IS, Yazan SHS, Rahim SNAA (2015) Mechanical properties of steel-polypropylene fiber reinforced concrete under elevated temperature. *Procedia Eng* 125:818–824
12. Meena A, Ramana PV (2022) Evaluation of mechanical characteristics of polypropylene fiber reinforced concrete at elevated temperature. *Mater Today Proc* 65(8):3328–3332
13. Rashmi R, Padmapriya R (2022) Experimental and analytical study on flexural behavior of reinforced concrete beams using nano silica. *Mater Today Proc* 50(1):57–69

Planning, Analysis and Design of Vented Drainage Canal Across River Ganga in Falta, West Bengal



Vishnu Vardhan Reddy, Avinash Pandey, Siddharatha Sarkar, Balasubramanian Murugesan, and Monisha Ravi

1 Introduction

Canals carry water from one place to another. Canals supply water to farms and sometimes prevent excess water from flowing into fields. In irrigation and drainage canals, the shape is typically trapezoidal to ensure structural stability and prevent silting and scouring [1–4]. A sluice gate, which is typically a metal barrier, controls and regulates the flow of water through a canal. Canals carry water from one place to another. In most cases, canals supply water to one or more farms and stop excess water from flowing into them [5, 6]. Usually, an irrigation and drainage canal is trapezoidal to maintain structural stability and avoid 'no silting, no scouring' situations. Sluice gates are metal barriers used to control and regulate the flow of water through canals. Canal construction is in an area with very weak soil and low bearing capacity. A proper pile foundation is needed to support the structure [7–11]. As part of scheduling, which means allocating time for the different tasks required to complete the project, the critical time is calculated. Including the contractor's profit and other additional charges, the rate analysis determines the total project cost. The cost-benefit ratio can be calculated from this. The higher the cost-benefit ratio, the more socially feasible the project [12–15].

V. V. Reddy · A. Pandey · S. Sarkar · B. Murugesan (✉) · M. Ravi
Department of Civil Engineering, Faculty of Engineering and Technology, SRM Institute of Science and Technology, Kattankulathur, Tamil Nadu 603203, India
e-mail: balasubm1@srmist.edu.in

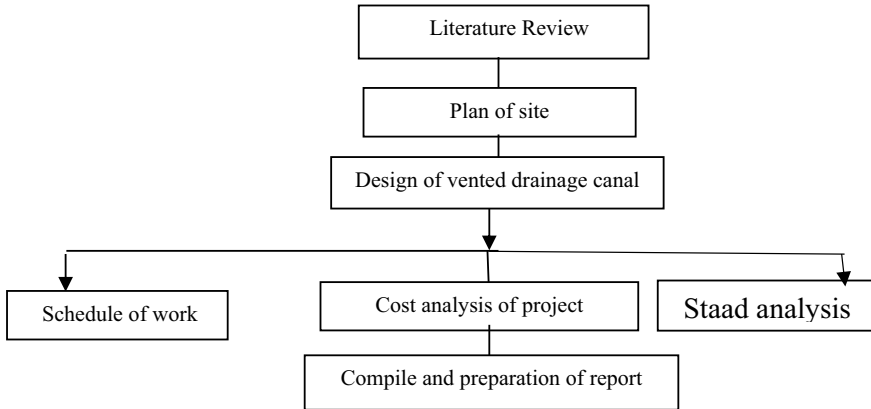


Fig. 1 Flow chart of the methodology

2 Methodology

During the project's duration, a regular series of activities were completed. Order and sequence of occurrences are specified. The project should be completed on time with this clear picture of how the work should go. A diagram of the project's methodology is presented in Fig. 1.

3 Planning of Model

The technical data collected from the irrigation department are as follows:

- Effective length = 5 m
- Net loss due to erosion per year = Rs 169.30 lac
- Net loss after completion of work = NIL
- No. of vents-Two-vented sluice
- Design discharge = 350 cumec
- Full supply level = 4.30 M
- L.W.L = 0.89 M
- H.F.L = 5.40 M
- Crest width of bank= 6 m

where,

L.W.L = Low flood level

H.W.L = High flood level

AutoCAD software was used to prepare a complete site plan based on the site visit data. The site plan shows the flow direction of the river (blue lines) and the

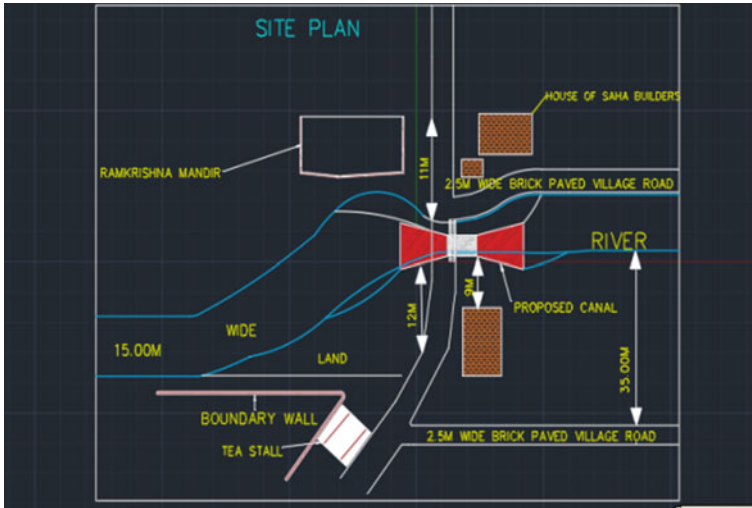


Fig. 2 Site plan of the vented drainage canal

proposed sluice. Sluice gate perimeter structures are also shown on the plan [16, 17]. In addition to the sluice gate, there is a 2.5-m thick brick village road. Figure 2 shows the site plan for the vented drainage canal.

4 Analysis

A STAAD.Pro model was created with the appropriate loads and supports. Figure 3 depicts the 3D model that was created.

4.1 Load Calculations

The type of loads acting on the structure is mentioned below:

- dead load
- soil load
- water load.

Load combinations used are:

- $1.5(D.L + S.L + W.L)$

The load combinations adopted in the project are shown with the help of Table 1.

Fig. 3 STAAD.Pro model

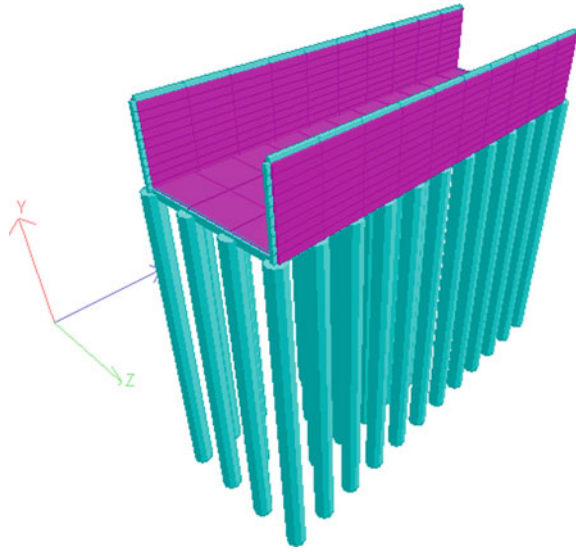


Table 1 Load calculations

Description	Load values (kN/m ²)
Plate load	125
Self-weight	25
Water load	0–50
Soil load	27

4.2 Bending Moment, Shear Force and Deflection

The maximum bending moment, shear force and deflection of the drainage canal obtained with help of analysis are shown with the help of Table 2.

The deflection of the structure under the application of the soil load water load and dead load is shown with the help of Fig. 4.

The bending moment of the vented drainage canal in Y and Z axis is shown with the help of Fig. 5. The green line shows the bending moment in Y direction, and the red line shows the bending moment in Z direction.

Table 2 Maximum bending moment, shear force and deflection

Description	Value
Maximum bending moment	39.185 kN m
Maximum shear force	85.669 Kn
Maximum deflection	18.7 mm

Fig. 4 Deflection diagram of the structure

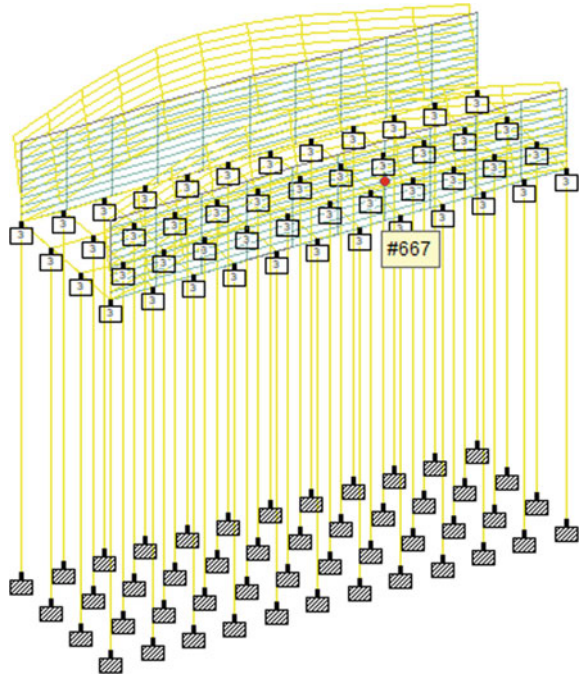


Fig. 5 Bending moment in Y and Z axis

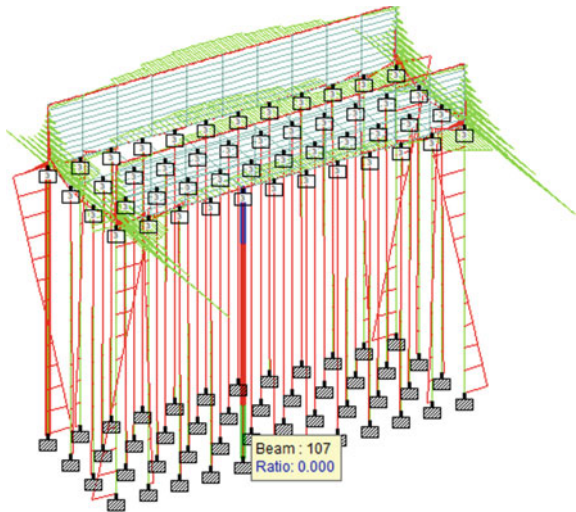
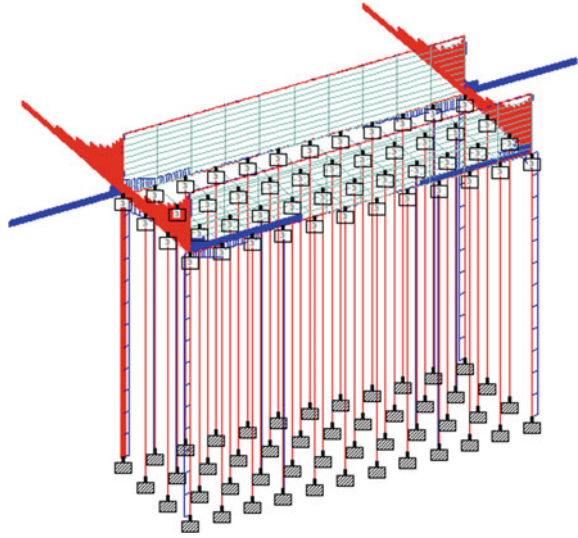


Fig. 6 Shear force diagram of the structure



The shear force marked with the help of the red and blue lines is shown with the help of Fig. 6.

4.3 Scheduling

In order to determine the critical time, we followed these steps:

- The process was broken down into steps.
- Using Primavera software, a proper work calendar was made with eight hours of working per day.
- The enterprise project structure was followed for the creation of the company profile.
- Object breakdown structure was used to divide the main work into several parts.
- Under subworks, the activities involved in each work were listed, followed by the number of days required to complete it.
- Each work had a predecessor and successor, along with a float time. Finally, the Gantt chart was obtained. Gantt charts show the completed work with a blue line and the remaining work with a red line [18].
- Project updates and up-to-date schedules can be obtained using schedule commands. In the following figures, you can see the results of Primavera software. Surveying, excavation and foundation WBSs are shown in Fig. 7, along with total time required for each [19].

Activity ID	Activity Name	Original Duration	Remaining Duration	Schedule % Complete	Start	Finish	Total Float
Project: SS01 VENTED DRAINAGE CAN		133	85	0%	01-Mar-21 A	12-Aug-21	0
WBS: SS01.4 Surveying		3	0	0%	01-Mar-21 A	03-Mar-21 A	
A1000	Project start	0	0	100%	01-Mar-21 A	01-Mar-21 A	
A1010	marking of points	1	0	100%	01-Mar-21 A	01-Mar-21 A	
A1020	Laying of co-ordinates using total station	1	0	100%	03-Mar-21 A	03-Mar-21 A	
WBS: SS01.3 Excavation		14	0	0%	04-Mar-21 A	19-Mar-21 A	
A1025	pumping out of water	2	0	100%	04-Mar-21 A	05-Mar-21 A	
A1030	removal of earthwork as per specification	3	0	100%	06-Mar-21 A	09-Mar-21 A	
A1040	stacking of the spoils	3	0	100%	06-Mar-21 A	09-Mar-21 A	
A1050	Cutting of desired slope for side trenches	2	0	100%	10-Mar-21 A	11-Mar-21 A	
A1060	levelling of ground	1	0	100%	12-Mar-21 A	12-Mar-21 A	
A1070	ramming of earth	2	0	100%	13-Mar-21 A	15-Mar-21 A	
A1080	backfilling as per specification	2	0	100%	18-Mar-21 A	19-Mar-21 A	
WBS: SS01.2 sheet pile foundation		58	10	0%	01-Mar-21 A	13-May-21	0
A1090	casting of in-situ sheet pile along with reinfo	10	0	100%	01-Mar-21 A	11-Mar-21 A	
A1100	loading/unloading and transporting sheet pile	3	0	100%	20-Mar-21 A	23-Mar-21 A	
A1110	Driving of piles with help of casing	15	0	100%	24-Mar-21 A	10-Apr-21 A	
A1120	Breaking of pile heads to resurface	1	0	100%	12-Apr-21 A	12-Apr-21 A	
A1130	shoring of the area	2	0	100%	13-Apr-21 A	16-Apr-21 A	
A1140	Placing of sheet pile along the area	3	0	100%	17-Apr-21 A	20-Apr-21 A	
A1150	Reinforcement for sheet pile cap	5	0	100%	21-Apr-21 A	27-Apr-21 A	
A1160	Provide shuttering	2	2	0%	30-Apr-21	03-May-21	0
A1170	Laying RCC of sheet pile caps	1	1	0%	05-May-21	05-May-21	0
A1180	Curing of the base	7	7	0%	06-May-21	13-May-21	0

Fig. 7 WBS structure of surveying, excavation and foundation

Figure 8 shows the WBS for the superstructure, which includes the abutment wall, wing walls and deck slab. This figure also shows several activities required to complete a WBS.

Figure 9 shows the WBS structure for the draw shutters and the approach road.

Figure 10 shows the Gantt chart from March to April. The blue line shows the completed work, and the red line shows the work left to do. Using thin line arrows, we can show the relationships between works.

#	Activity ID	Activity Name	Original Duration	Remaining Duration	Schedule % Complete	Start	Finish	Total Float
25	WBS: SS01.1 superstructure		75	75	0%	14-May-21	12-Aug-21	0
26	WBS: SS01.1.5 abutment wall		17	17	0%	14-May-21	03-Jun-21	0
27	A1190	cutting of bars for reinforcement as per spec	2	2	0%	14-May-21	15-May-21	0
28	A1200	placing of rebars for the abutment wall/both	5	5	0%	17-May-21	21-May-21	0
29	A1210	Provide shuttering for RCC	2	2	0%	22-May-21	24-May-21	0
30	A1220	RCC for the abutment wall	1	1	0%	25-May-21	25-May-21	0
31	A1230	curing of abutment wall	7	7	0%	27-May-21	03-Jun-21	0
32	WBS: SS01.1.4 flared wing wall		20	20	0%	04-Jun-21	28-Jun-21	0
33	A1240	cutting of reinforcement as per specificatio	2	2	0%	04-Jun-21	05-Jun-21	0
34	A1250	Placing rebars at a desired slope for wing w	7	7	0%	07-Jun-21	14-Jun-21	0
35	A1260	Provide formwork	2	2	0%	15-Jun-21	16-Jun-21	0
36	A1270	RCC for wing wall	1	1	0%	17-Jun-21	17-Jun-21	0
37	A1280	curing	7	7	0%	18-Jun-21	26-Jun-21	0
38	A1290	Removal of shuttering	1	1	0%	28-Jun-21	28-Jun-21	0
39	WBS: SS01.1.3 draw shutters		7	7	0%	29-Jun-21	06-Jul-21	0
40	A1300	making of draw shutters as per ISA specific	4	4	0%	29-Jun-21	02-Jul-21	0
41	A1310	creating channel for shutters	2	2	0%	03-Jul-21	05-Jul-21	0
42	A1320	creating lever mechanism for shutters	1	1	0%	06-Jul-21	06-Jul-21	0
43	WBS: SS01.1.2 deck slab		22	22	0%	07-Jul-21	02-Aug-21	0
44	A1330	cutting of reinforcement as per specification	2	2	0%	07-Jul-21	08-Jul-21	0
45	A1340	placing of bottom and side reinforcement	5	5	0%	09-Jul-21	14-Jul-21	0
46	A1345	provide formwork	2	2	0%	15-Jul-21	16-Jul-21	0
47	A1346	RCC for deck slab	1	1	0%	17-Jul-21	17-Jul-21	0
48	A1347	curing	5	5	0%	20-Jul-21	24-Jul-21	0
49	A1350	providing hand rails on both sides	2	2	0%	26-Jul-21	27-Jul-21	0

Fig. 8 WBS for the superstructure

Basic Schedule Layout		Filter: All Activities						
Activity Name	Original Duration	Remaining Duration	Schedule % Complete	Start	Finish	Total Float		
A1250 Placing rebars at a desired slope for wing w...	7	7	0%	07-Jun-21	14-Jun-21	0		
A1260 Provide formwork.	2	2	0%	15-Jun-21	16-Jun-21	0		
A1270 RCC for wing wall	1	1	0%	17-Jun-21	17-Jun-21	0		
A1280 curing	7	7	0%	18-Jun-21	26-Jun-21	0		
A1290 Removal of shuttering	1	1	0%	28-Jun-21	28-Jun-21	0		
WBS: S501.1.3 draw shutters	7	7	0%	29-Jun-21	06-Jul-21	0		
A1300 making of draw shutters as per ISA specific...	4	4	0%	29-Jun-21	02-Jul-21	0		
A1310 creating channel for shutters	2	2	0%	03-Jul-21	05-Jul-21	0		
A1320 creating lever mechanism for shutters	1	1	0%	06-Jul-21	06-Jul-21	0		
WBS: S501.1.2 deck slab	22	22	0%	07-Jul-21	02-Aug-21	0		
A1330 cutting of reinforcement as per specification	2	2	0%	07-Jul-21	08-Jul-21	0		
A1340 placing of bottom and side reinforcement	5	5	0%	09-Jul-21	14-Jul-21	0		
A1345 provide formwork	2	2	0%	15-Jul-21	16-Jul-21	0		
A1346 RCC for deck slab	1	1	0%	17-Jul-21	17-Jul-21	0		
A1347 curing	5	5	0%	20-Jul-21	24-Jul-21	0		
A1350 providing hand rails on both sides	2	2	0%	26-Jul-21	27-Jul-21	0		
A1360 provide paint on the hand rails	5	5	0%	28-Jul-21	02-Aug-21	0		
WBS: S501.1.1 approach slabroad	9	9	0%	03-Aug-21	12-Aug-21	0		
A1370 placing of moorum upto desired height	2	2	0%	03-Aug-21	04-Aug-21	0		
A1380 provide brick bats layer on both sides	2	2	0%	05-Aug-21	06-Aug-21	0		
A1390 laying of pcc concrete	2	2	0%	07-Aug-21	09-Aug-21	0		
A1400 levelling of pcc concrete	1	1	0%	10-Aug-21	10-Aug-21	0		
A1410 proving marking on the slab	2	2	0%	11-Aug-21	12-Aug-21	0		

Fig. 9 WBS for the shutters, deck slab and approach road

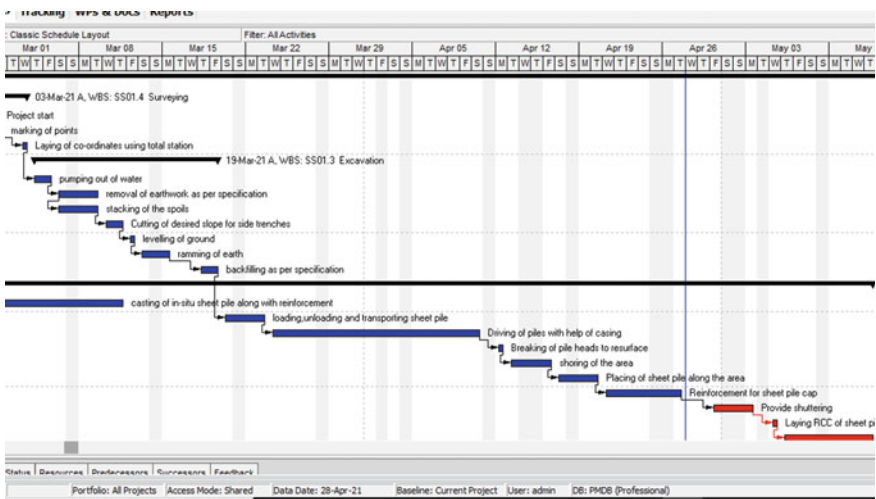


Fig. 10 Gantt chart output for the first half

The Gantt chart from May to August is shown with the help of Figs. 11 and 12.

4.4 Project Cost Estimation

Calculation of the cost-benefit ratio and total project estimate followed these steps:

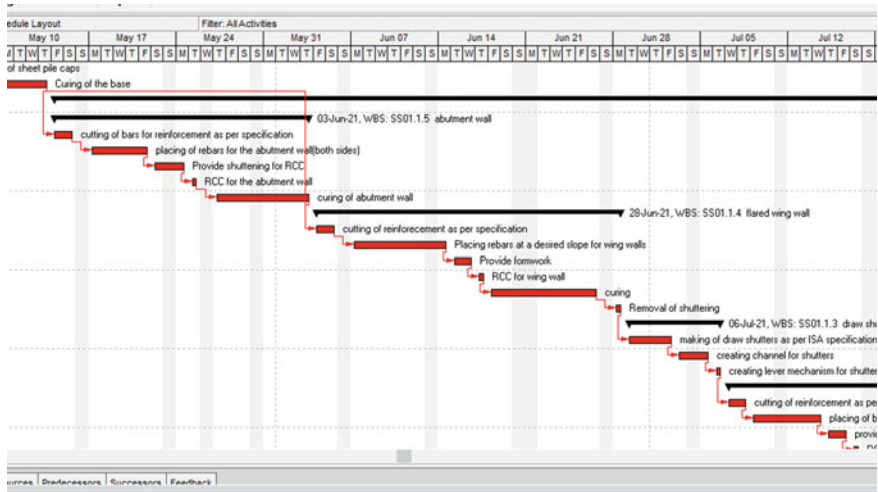


Fig. 11 Gantt chart output from May to July

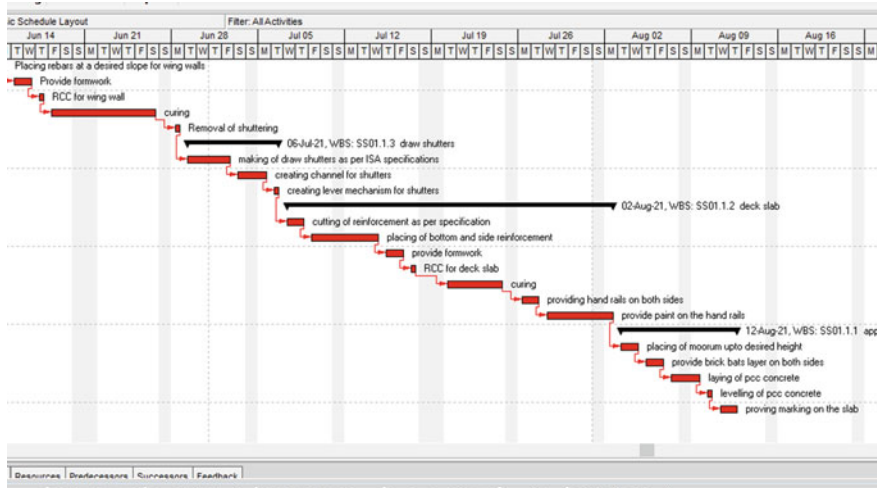


Fig. 12 Gantt chart output from July to August

- A design diagram and survey were used to divide the entire structure into its main components, including excavation, piles, pile foundations, sheet piles, bottom slabs, deck slabs, side walls and flared wings.
- Materials were calculated according to the desired specification.
- PWD rate schedule was used to calculate each material’s rate
- A spreadsheet was created, and using appropriate formulas, a total project cost was calculated.

- Estimated rates are accompanied by the calculation.
- Using the estimate, we calculated operational costs and cost–benefit ratios.
- Construction of the vented drainage canal costs Indian rupees 1.44 lakhs.
- Calculate using the formula [20]:-

$$\text{Cost - benefit ratio} = \frac{\text{Net loss per year due to erosion}}{17\% \text{ of the operational maintenance cost}} \quad (1)$$

- A high cost–benefit ratio makes the project feasible.
- This project has a cost–benefit ratio of 3, which means it is socially feasible.
- These figures show the total project rate estimated.
- The detailed estimate is shown in Fig. 13. Calculations are included for each work, as well as the quantity and rate.

The Fig. 14 shows the final part of the rate estimate along with the contractor’s profit and other contingencies.

SL NO	DESCRIPTION OF ITEM	QUANTITY	UNIT	RATE	AMOUNT	EXPLANATION
1	Excavation of earthwork as per technical specification (including pumping out water and shoring)	5668	cum	166.65	944572.2	
2	Earth filling in the foundation trenches and in back of abutments along with watering and ramming	2834	cum	162.61	460836.74	50% of 5668=2834
3	supplying, spreading and compacting sand to required thickness in order to make earthen bund with desired slope	467	cum	1347.07	629081.69	
4	Supplying M.S Sheet pile of all section including carriage, loading, unloading and stacking	65	M.Ton	79579	5172635	M.S SHEET PILE(size:-400mm×185mm×7.5 Length of work=2×[(28.55×0.75)+(5.70-0.75)]+65.50M for corner piles=4 × 0.40 = 1.60M No of piles = 167 total length = 167.75 × 7.64 = 1281M total=1320×49.25=65012=65MT
5	Painting of M.S sheet pile with anti-corrosive bituminous paint	1025	Sqm	69	70725	67.50 × 7.4 × 2= 1025
6	Driving of sheet pile including drilling holes and welding of piles	512	Sqm	765	392170	67.50 × 7.4 = 512
7	Cement concrete in foundation including dewatering, shuttering and curing(FOR M 15)	7.368	cum	4852	35749.536	for pile cap=2×28.55+2×4.20×0.75×0.15=7.368
8	Providing sand laying mix design for reinforced concrete work	13.68	cum	6610	90424.8	for pile cap=2× 5.70 × 0.75× 1.60= 13.680
9	Total Reinforcements	65.34	MT	64122	4189731.48	Assuming 2% of total RCC
10	formwork for the base slab	20.76	sqm	357	7411.32	2×2×(9.40-0.75)=0.60
11	formwork for the abutment wall	29.28	sqm	357	10452.96	2×2×9.15=0.80=29.28
12	formwork for the wing wall	165.37	sqm	357	59037.09	2×2×10.70+10.89×2×3.56+4.10×2=165.37
13	formwork for deck slab	18.37	sqm	357	6558.09	5.25×(2×1.75)=18.37

Fig. 13 Total rate estimate (initial part)

13 formwork for deck slab	18.37 sqm	357	6558.09	$5.25 \times (2 \times 1.75) = 18.37$
14 formwork for approach slab	2.1 sqm	357	749.7	$2 \times 2 \times 0.35 = 2.10$
15 RCC concrete for base slab	24 cum	6610	158640	$2 \times 10 \times 2 \times 0.60 = 24$
16 RCC concrete for abutment wall	56.708 cum	6610	374839.88	$2 \times (6.95 + 0.90) \times 0.70 \times 5.16 = 56.708$
17 RCC concrete for wing wall	16.608 cum	6610	109778.88	$(9.40 - 0.75) \times (2 \times 1.60) \times 0.60 = 16.608$
18 RCC concrete for deck slab	11.76 cum	6610	77733.6	$5.60 \times 5.25 \times 0.40 = 11.760$
19 RCC concrete for approach slab	7.35 cum	6610	48583.5	$2 \times 2 \times 5.25 \times 0.35 = 7.350$
			TOTAL	1289734.81
			CONTINGENCY(3%)	386918
			CONTRACTORS PROFIT(10%)	128973.48
			GRAND TOTAL	14573075.62

Fig. 14 Total rate estimate (final part)

5 Conclusion

According to the scheduling part, 133 days are required for the project to be completed. The schedule helps to track the project progress and complete the project on time. Due to the high cost-benefit ratio, this project will benefit many people. The 3D model shows the vented drainage canal of trapezoidal section in detail. The graphs obtained from the analysis part give the values of the shear force, bending moment and deflection. The trapezoidal shape is the most economical. In addition, this section reduces scouring and silting. The project has been designed to give maximum support to the structure despite the high erosion zone in the zone of construction. Scheduling and rate analysis will reduce the project delay and keep the resources allocated. To maintain a proper cost-benefit ratio, we have done a rate analysis.

References

1. IS 456: 2000, Plain and reinforced concrete—code of practice, Bureau of Indian Standards, New Delhi, 110002
2. Swamee PK (2017) Optimal irrigation canal sections, journal of irrigation and drainage engineering. ASCE 121(6):467–469
3. Arunkumar R, Ambujam NK (2010) Performance assessment of canal irrigation system. Indian Soc Hydraulics J Hydraul Eng 16(1):146–155
4. Jebelli J, Meguid, M.A., soil stability analysis in irrigation canal—a case study. Electron J Geotech Eng 18:4154–4168
5. Schedule of Rates (2010) Volume-III Public Works Department
6. IS2911:2010-Design and construction of Pile foundation-Code of practice, Bureau of Indian Standards, New Delhi
7. IRC 6: 2000, Standard specifications and code of practice for road bridges, Section II, Loads and Stresses, The Indian Roads Congress, New Delhi

8. Rodríguez E, Cunha RP (2018) Behavior of piled raft foundation systems in soft soil with consolidation process. *Electron J Geotech Eng* 15
9. Ambarish Ghosh A, Rituparna Dey B (2016) Study on the behaviour of Pile-Raft foundation in cohesive soil. *AGSSEA* 10:2341–2360
10. Lu JS, Zhang E, Li K (2018) Enhancing the ventilation of sewers by using inhaled air in the vertical stack of a building. *Water Pract Technol* 13:555–565
11. Tait SJ, Ashley RM, Cashman A, Blanksby J, Saul AJ (2008) Sewer system operation into the 21st century, study of selected responses from a UK perspective. *Urban Water J* 5:79–88
12. Akkuzu E, Nal HB, Karatafi B (2007) Determination of water conveyance loss in the Menemen open canal irrigation network. *Turk J Agric For* 11–22
13. Bos MG, Salatino SE, Billoud CG (2001) The water delivery performance within the Chivilcoy Tertiary Unit, Mendoza, Argentina. *Irrig Drainage Syst* 15:311–325
14. Gideon C, Saeed AB, Mohammed HI (2007) Evaluation of hydraulic performance of major canals in the Rahad agricultural scheme-Sudan. *Sudan J Sci Technol* 8(1):1–11
15. Jahromi SS, Depeweg H, Feyen J (2000) Water delivery performance in the Doroodzan I"igation Scheme, Iran. *Irrig Drainage Syst* 14:207–222
16. Javan M, Jahromi SS, Fiuzat AA (2002) Quantifying management of irrigation and drainage systems. *J Irrig Drainage Eng* 128(1):19–25
17. Krishnamurthy K, Rao SM (1969) Theory and experiment in canal seepage estimation using radioisotopes. *J Hydrol* 9:277–293
18. Tariq JA, Khan MJ, Kakar MJ (2004) Irrigation system performance monitoring as diagnostic tool to operation: case study of Shahibala minor of Warsak Gravity Canal. *Pak J Water Res* 8(1):13–22
19. Unal HB, Asik S, Avci M, Yasar S, Akkuzu E (2004) Performance of water delivery system at tertiary canal level : a case study of the Menemen left bank irrigation system, Gediz basin, Turkey. *Agric Water Manage* 65:155–171
20. Arya CK, Purohit RC, Dashora LK, Singh PK, Kothari, Mahesh, Performance evaluation of drip irrigation systems. *Int J Curr Microbiol App Sci* 6(4):2287–2292

Study on the Improvement of Properties of Expansive Soil Using Seashell Powder



V. Janani, Jigisha Yadav, and P. T. Ravichandran

1 Introduction

Most expansive soils found in arid and semiarid areas show excessive swelling and shrinkage properties when it is exposed to moisture [1, 2]. Black cotton soil makes up the majority of the expansive soil in India [3]. The formation of black cotton soil is either by igneous rocks or by rapid cooling and consolidation of lava erupted from volcanoes, forming lava basalt rocks which followed by weathering of rocks. This soil extends over roughly 20% of the total land cover in India [3].

Expansive soils show drastic changes in their volume with change in their water content [4]. They have a small particle size and a large surface area. The properties of expansive soils include less residual strength, high compressibility, and low bearing capacity [5]. These soils contain the mineral montmorillonite in very high percentages which results in their excessive shrinking–swelling behavior [6]. Due to this, expansive soils pose a great danger to structures constructed on them. The formation of black cotton soil is either by igneous rocks or by rapid cooling and consolidation of lava erupted from volcanoes, forming lava basalt rocks which followed by weathering of rocks [7].

In order to make the soil suitable for construction purpose, many soil improvement techniques are executed. The most common and effective ground improvement technique is soil stabilization. Soil stabilization includes any physical or chemical treatments which help in the increment or maintenance of soil stability or improve its engineering properties [8]. Most of the studies have been conducted on commonly used admixtures for soil stabilization such as lime [9–12] and cement [10, 13], fly ash [14–16] to name a few. But extracting and using these admixtures lead to depletion of raw sources and also harm the environment. While extracting or manufacturing

V. Janani (✉) · J. Yadav · P. T. Ravichandran
Civil Engineering Department, SRM Institute of Science and Technology, Chennai, Tamil Nadu, India
e-mail: jananiv@srmist.edu.in

these admixtures, a large amount of greenhouse gas emission is noted [17]. In order to overcome this disadvantage, waste materials can be used as an additive for stabilizing the soil. Several agricultural wastes such as rice husk ash [18, 19], egg shell powder [20, 21], coconut shell powder [22], coffee husk ash [5], and bagasse ash [23] have been used for study on soil stabilization. Industrial wastes like ground granulated blast furnace slag [17], stone dust [24], and marble dust [25, 26] have been proven to be a sufficient stabilizing agent.

In this study, seashell powder is being used as a soil stabilizing agent. Seashell powder has a high calcium content just like lime and hence can be used for soil stabilization [27]. Seashell powder is obtained after grinding the seashells which are the exoskeletons of mollusks [28]. Seashells are waste products that are produced from the fishery industry and are dumped in large amounts in landfills. This makes seashell powder a renewable and cheap alternative to other additives. It does not contain any toxic substances and is not harmful to the environment.

2 Materials and Methodology

2.1 Materials

The materials used for the tests were soil and seashell powder.

2.1.1 Soil

Black cotton soil was utilized for this project. It was found in Tharamani at a depth of 2 m after the top layer was stripped off. The soil has a high montmorillonite concentration, which contributes to its significant swelling and shrinking properties in response to temperature changes. The collected soil was dried and pulverized is shown in Fig 1. It was then passed through an IS475-micron sieve before using it for experiments. The classification of the collected soil is highly compressible clayey soil (CH) (Table 1).

2.1.2 Seashell Powder

The seashell powder was obtained from grinding the seashells which are the exoskeletons of mollusks. They are waste products that are produced from the fishery industry. Seashells are naturally a rich source of calcium as they are mainly composed of calcium carbonate. Seashell powder has a binding property which makes it a good soil stabilizing admixture. It is an eco-friendly and cost-effective additive. The extraction of other raw materials causes their depletion and also causes a lot of pollution. This can overcome by using seashell powder as an additive, as it is a waste product

Table 1 Properties of virgin soil

Properties	Results
Free swell index	90
Specific gravity	2.352
Liquid limit	61%
Plastic limit	24.64%
Plasticity index	36.36%
Shrinkage limit	15.77
Optimum moisture content (OMC)	23%
Maximum dry density (MDD)	1.565 g/cc
Unconfined compressive strength	100.36 kPa
California bearing ratio	3.26%

and also does not cause any damage to the environment. The seashell powder was passed through a IS475-micron sieve before using it for experiments. It was varied by 0% to 15% by soil's dry weight for this study.

2.2 Methodology

The tests were executed on soil with admixture in varying percentages such as 6, 8, 10, 12%, and 15% to find the optimum value of admixture at which greatest strength of soil could be attained. In order to find the geotechnical properties of untreated soil, several tests were conducted on it. The specific gravity test of the untreated soil was executed according to IS: 2720 (Part III/Sec 2)-1980. Atterberg's limit tests were executed on untreated soil as per IS: 2720 (Part V)-1985 and IS: 2720 (Part VI)-1972.

2.2.1 Standard Proctor Compaction Test

The standard Proctor compaction test was first used to measure the appropriate moisture content and maximum dry density of untreated soil. After the results had been evaluated, a compaction test was done on soil that included 6%, 8%, 10%, 12%, and 15% of seashell powder, respectively. According to IS: 2720 Part VII-1980, the test was carried out. The standard Proctor compaction was performed using a mold with a 10 cm diameter and a 12.7 cm height. A collar and a base plate made up the mold assembly. The hammer used was 2.6 kg in weight, and the fall was 30 cm high. The soil sample taken was mixed with a calculated amount of water and was filled into the mold assembly in 3 different layers, with the number of blows on each layer being 25 blows/layer. The compaction test was done to find the OMC and MDD of virgin soil and soil mixed with differing percentages of seashell powder. The determined

amount of water was added to the soil sample, which was then divided into three layers and placed into the mold assembly. Each layer received 25 blows. The purpose of the compaction test was to determine the ideal moisture content and MDD of both pure soil and soil that had been combined with varying amounts of seashell powder.

2.2.2 Unconfined Compression Test

The unconfined compression tests were executed on cylindrical soil specimens having 38 mm diameter and 76 mm height. The test was executed according to IS: 2720 (Part-X). The soil was passed through IS475-micron sieve for preparing the specimens. The amount of soil taken was calculated using the maximum dry density, and the amount of water to be added was calculated using the OMC found from the Proctor test. The samples were prepared for untreated soil and tested to find the unconfined compressive strength of the soil. The samples were then prepared for varying percentages of seashell powder such as 6, 8, 10, 12, and 15% and were tested for different curing periods (3, 7, 14, and 28 days) to find the variation in the unconfined compressive strength of soil when mixed with seashell powder.

2.2.3 Free Swell Test

Free swell test was executed on soil mixed with differing amounts of seashell powder such as 6, 8, 10, 12, and 15% under different curing periods (3, 7, 14, and 28 days). The free swell index found from the test helps in finding the swell attributes of the soil. The treated soil for the test was taken after pulverizing the oven-dried soil samples that had undergone UCS. Two 10-g soil samples were taken and added to two separate graduated cylinders filled with water and kerosene to 100 ml mark. These cylinders were then kept for a duration of 24 h, and the final reading was then noted.

3 Results and Discussions

3.1 Standard Proctor Compaction Test

The standard Proctor compaction was carried out on soil treated with differing percentages of seashell powder ranging from 6, 8, 10, 12, and 15% to find the compaction attributes of soil. The compaction characteristic curve obtained from the **standard Proctor compaction** test is shown in Figs. 2 and 3 shows the effect of seashell powder on the optimum moisture content (OMC) and maximum dry density (MDD) of the soil. The maximum dry density increases as the amount of seashell powder increases from 6 to 15%, as seen in the moisture content vs. dry density

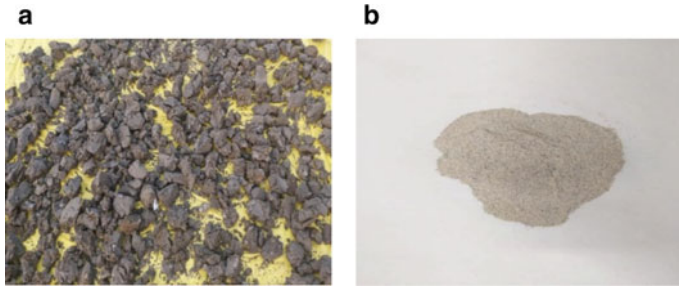


Fig. 1 a Black cotton soil, b seashell powder

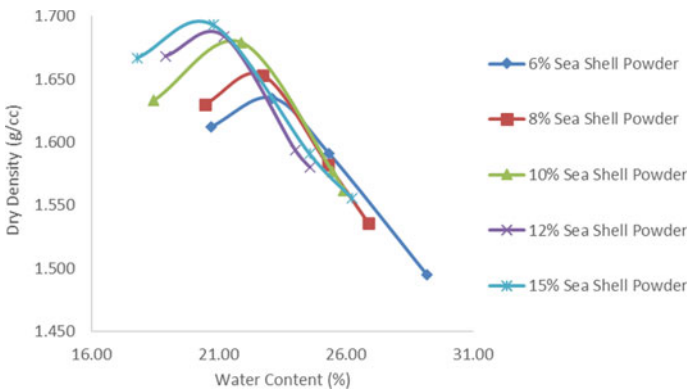


Fig. 2 Compaction characteristics of seashell powder-treated soil

graph. While the amount of seashell powder in the soil increases, the ideal moisture level drops. The seashell powder behaves as a filler material in the voids of the soil, increasing the total weight. As weight is directly proportional to density, the dry density of treated soil increases with an increase in percentage of seashell powder.

3.2 Unconfined Compression Test

This test was performed on soil treated with differing percentages of seashell powder such as 6, 8, 10, 12, and 15% under diverse curing days like 3, 7, 14, and 28 days. A plastic sheet was used to prepare and package the samples. These samples were then packed in airtight plastic packets and were cured by placing them over a wet sand base and covering with a wet gunny bag to prevent moisture loss. The soil samples treated with seashell powder were tested after curing on the unconfined compression testing machine.

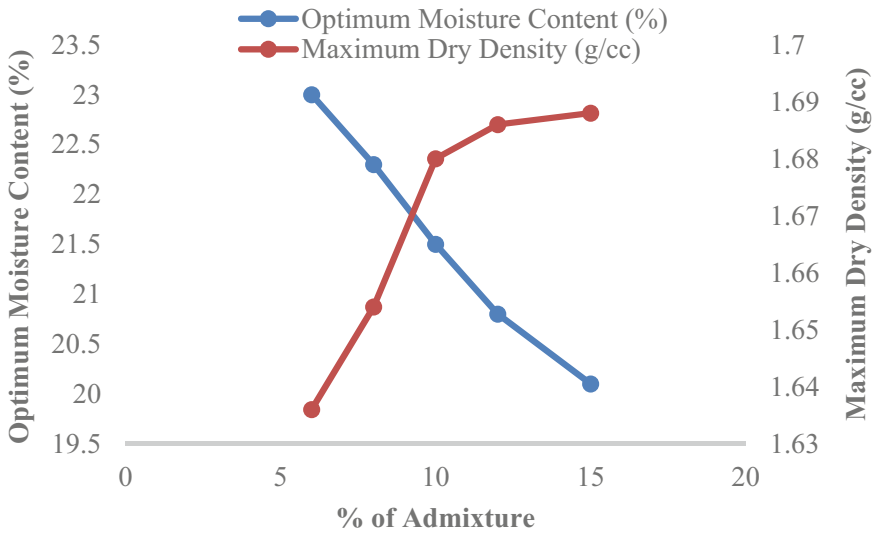


Fig. 3 Effect of admixture on optimum moisture content and dry density

The curing of treated samples was done to give time to the seashell powder to react with the soil and increase the soil strength.

The results obtained from the unconfined compression test for varying percentages of seashell powder for different curing periods and the stress versus strain graph plotted for different percentages of seashell powder under varying curing periods are shown in the Figs. 4, 5 and 6. From the graphs, it can be observed that the maximum strength is attained when the soil is mixed with 12% seashell powder. It can also be noted that with increment in the curing period of soil, an increase in the strength of soil is noticed. The seashell powder is rich in calcium. The calcium from the powder reacts with the soil to form CSH gel. A pozzolanic reaction takes place which increases the soil strength. On comparing the soil strength with 12% seashell powder to that of untreated soil, the strength increases by 88.87% under 28-day curing period. The influence of different seashell powder percentages on soil strength at various curing times can be seen in Fig. 7.

3.3 Free Swell Test

Free swell test was executed on soil mixed with differing amounts of seashell powder under different curing periods (3, 7, 14, and 28 days). The free swell index found from the test helps in finding the swell property of the soil. The treated soil for the test was taken after pulverizing the oven-dried soil samples that had undergone UCC test. Two 10-g soil samples were taken and added to two separate graduated cylinders

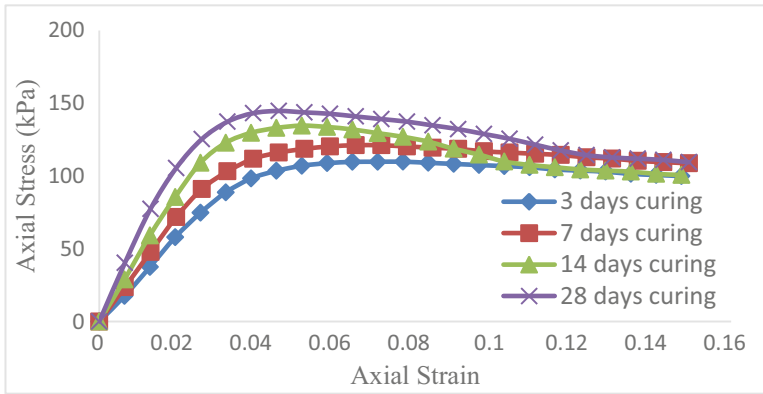


Fig. 4 Stress-strain characteristic curve for 6% seashell powder under varying curing periods

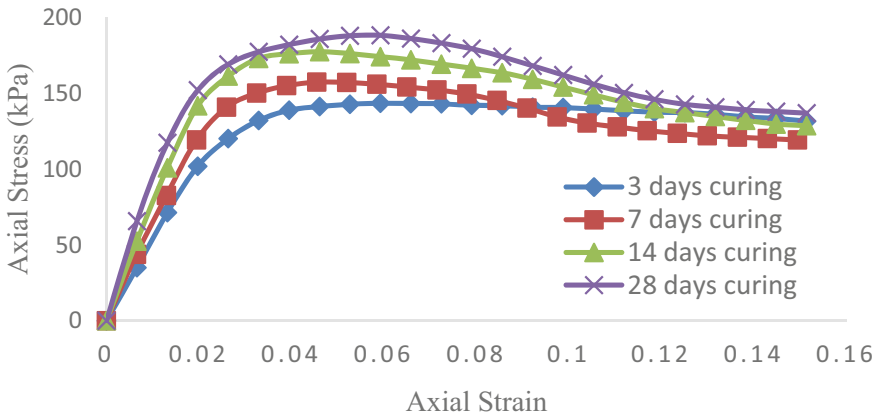


Fig. 5 Stress-strain characteristic curve for 12% seashell powder under varying curing periods

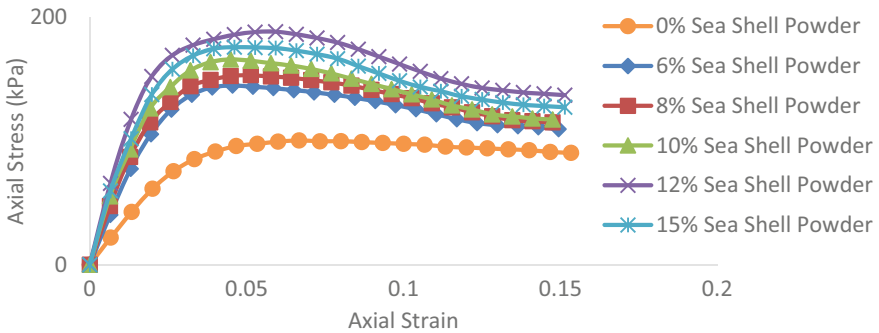


Fig. 6 Stress-strain characteristic curve for different percentage of seashell powder under 28 days of curing

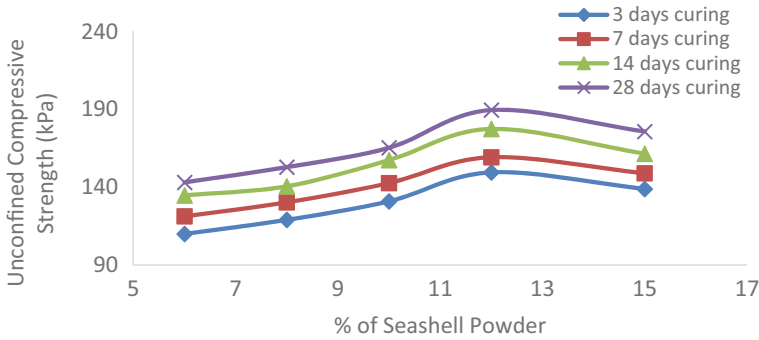


Fig. 7 Influence of different seashell powder percentages on soil strength at various curing times

filled with water and kerosene. These cylinders were then kept for a duration of 24 h, and the final reading was then noted. The free swell index results for treated soil containing different percentages of seashell powder under different curing days are plotted in Fig. 8.

The free swell test results are mentioned in the table, and it can be noted that the free swell index values for treated soil are lesser when comparing with virgin soil. This means that addition of seashell powder to the soil lowers the swelling capacity of the soil which reduces the expansive nature of the soil. This helps in stabilizing the soil. From the results obtained, it can be seen that the free swell index does not show any significant change after the 3-day curing period. However, the free swell index values for soil increase after 7 days, 14 days, and 28 days of curing. This means that the curing time also affects the swelling nature of treated soil. The least free swell index is given by soil mixed with seashell powder and kept for 28 days of curing.

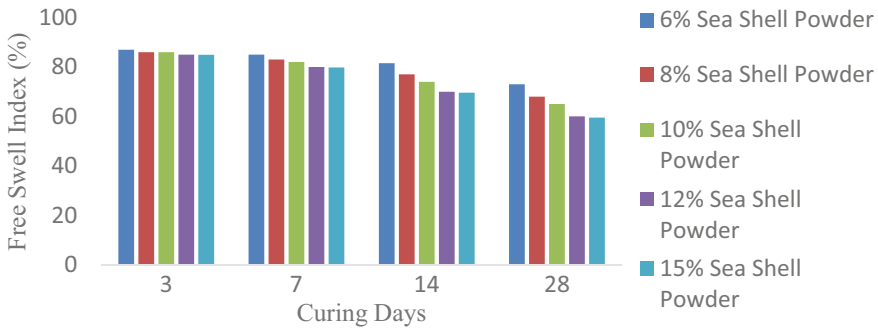


Fig. 8 Free swell index variation for different curing days

4 Conclusion

- The standard Proctor compaction test revealed the OMC and MDD. The OMC reduces and the MDD increases when the amount of seashell powder in the soil is increased, according to the findings of the standard Proctor compaction test on untreated and treated soil.
- The UCC test employed the OMC and MDD. The results show that applying the admixture enhances the soil's strength until a maximum strength is reached for various curing times. In this investigation, adding 12% seashell powder to soil results in the strongest material. Therefore, 12% of seashell powder is the ideal concentration for the soil.
- The unconfined compressive strength of the soil increases by 42.93, 54.63, 76.77, and 88.87% after curing the soil for different curing days at optimum percentage of seashell powder with respect to virgin soil.
- Different proportions of seashell were applied to the soil on various curing days for the free swell index experiment. The test findings demonstrate that adding seashell powder to the soil reduces its free swell index, which lessens the soil's tendency to expand, stabilizing the soil.
- From the above results, it is concluded that seashell powder can prove as an effective eco-friendly and cost-effective additive for soil stabilization thus overcoming the constraints faced while using other materials as additives.

References

1. Patel A (2019) Case examples of some geotechnical applications. In: Geotechnical investigations and improvement of ground conditions, pp 167–191. <https://doi.org/10.1016/B978-0-12-817048-9.00011-1>
2. Chaudhry L, Zulfiqar Z (2011) Construction on expansive soils in semi arid zone. In: Geotechnical special publication. ASCE, pp 256–263. [https://doi.org/10.1061/47633\(412\)34](https://doi.org/10.1061/47633(412)34)
3. Hagi S, Yabe T, Shiga T (2020) A study of swelling characteristics of expansive soils on high speed railway project area in India. In: Duc Long P, Dung N (eds) Geotechnics for sustainable infrastructure development. Lecture notes in civil engineering, vol 62. Springer, Singapore. https://doi.org/10.1007/978-981-15-2184-3_97
4. Jones L (2018) Expansive soils. In: Bobrowsky P, Marker B (eds) Encyclopedia of engineering geology. Encyclopedia of earth sciences series. Springer, Cham. https://doi.org/10.1007/978-3-319-12127-7_118-1
5. Atahu MK, Saathoff F, Gebissa A (2019) Strength and compressibility behaviors of expansive soil treated with coffee husk ash. *J Rock Mech Geotech Eng* 11(2):337–348. <https://doi.org/10.1016/j.jrmge.2018.11.004>
6. Liet Chi Dang, Hayder Hasan, Behzad Fatahi, Robert Jones, & Hadi Khabbaz (2021) Enhancing the engineering properties of expansive soil using bagasse ash and hydrated lime. *Geomate J* 11(25):2447–2454. Retrieved from <https://geomatejournal.com/geomate/article/view/2734>
7. Ponnada S et al (2021) In: IOP conference series: materials science and engineering, vol, 1025, p 012012

8. Selvakumar S, Soundara B (2020) Swelling behavior of expansive soils stabilized with expanded polystyrene geofoam inclusion. In: *New materials in civil engineering*, pp 745–776. <https://doi.org/10.1016/B978-0-12-818961-0.00024-7>
9. Bell FG (1996) Lime stabilization of clay minerals and soils. *Eng Geol* 42(4):223–237. ISSN 0013-7952. [https://doi.org/10.1016/0013-7952\(96\)00028-2](https://doi.org/10.1016/0013-7952(96)00028-2)
10. Saride S, Puppala AJ, Chikyala SR (2013) Swell-shrink and strength behaviors of lime and cement stabilized expansive organic clays. *Appl Clay Sci* 85:39–45. ISSN 0169-1317. <https://doi.org/10.1016/j.clay.2013.09.008>
11. Jha AK, Sivapullaiah PV (2015) Mechanism of improvement in the strength and volume change behavior of lime stabilized soil. *Eng Geol* 198:53–64. ISSN 0013-7952. <https://doi.org/10.1016/j.enggeo.2015.08.020>
12. Modarres A, Nosoudy YM (2015) Clay stabilization using coal waste and lime—technical and environmental impacts. *Appl Clay Sci* 116–117:281–288. ISSN 0169-1317. <https://doi.org/10.1016/j.clay.2015.03.026>
13. Cong M, Longzhu C, Bing C (2014) Analysis of strength development in soft clay stabilized with cement-based stabilizer. *Constr Build Mater* 71:354–362. ISSN 0950-0618. <https://doi.org/10.1016/j.conbuildmat.2014.08.087>
14. Mir BA, Sridharan A (2019) Mechanical behaviour of fly-ash-treated expansive soil. In: *Proceedings of the institution of civil engineers—ground improvement*, vol 172, no 1, pp 12–24. <https://doi.org/10.1680/jgrim.16.00024>
15. McCarthy MJ, Csetenyi LJ, Sachdeva A, Dhir RK (2014) Engineering and durability properties of fly ash treated lime-stabilised sulphate-bearing soils. *Eng Geol* 174:139–148. ISSN 0013-7952. <https://doi.org/10.1016/j.enggeo.2014.03.001>
16. Kumar AK, Thyagaraj T, Robinson RG (2022) Swell–shrink behaviour of fly ash-stabilised expansive soils. In: *Proceedings of the institution of civil engineers—ground improvement*, 2022. <https://doi.org/10.1680/jgrim.21.00024>
17. Yadu L, Tripathi RK (2013) Effects of granulated blast furnace slag in the engineering behaviour of stabilized soft soil. *Procedia Eng* 51:125–131. ISSN 1877-7058. <https://doi.org/10.1016/j.proeng.2013.01.019>
18. Basha EA, Hashim R, Mahmud HB, Muntohar AS (2005) Stabilization of residual soil with rice husk ash and cement. *Constr Build Mater* 19(6):448–453, ISSN 0950-0618. <https://doi.org/10.1016/j.conbuildmat.2004.08.001>
19. Raja K, Venkatachalam S, Vishnuvardhan K, Siva Rama Krishnan R, Tamil Selvan V, Vetriselvan N (2002) A review on soil stabilization using rice husk ash and lime sludge. *Mater Today: Proc.* ISSN 2214-7853. <https://doi.org/10.1016/j.matpr.2022.04.178>
20. Sathiparan N (2021) Utilization prospects of eggshell powder in sustainable construction material—a review. *Constr Build Mater* 293:123465. <https://doi.org/10.1016/j.conbuildmat.2021.123465>
21. Pauzi NIM, Aziz MAAMA, Ismail MS, Omar H (2019) Waste soil improvement using eggshell powder and lime at open dumping area. *Int J Civil Eng Technol (IJCIET)* 10(04):268–277. Article ID: IJCIET_10_04_028 Available online at <http://iaeme.com/Home/issue/IJCIET?Volume=10&Issue=4>
22. Prasanna S, Kumar P (2017) Soil reinforcement using coconut shell ash: a case study of Indian soil. *J Civ Eng Constr* 6(2). <https://www.xpublication.com/index.php/jcec/article/download/37/36>
23. Lal D, Kumar MJ, Kumar KN, Sindhu K, Kumar A (2020) Soil stabilization using bagasse ash. In: Saride S, Umashankar B, Avirneni D (eds) *Advances in geotechnical and transportation engineering. Lecture notes in civil engineering*, vol 71. Springer, Singapore. https://doi.org/10.1007/978-981-15-3662-5_3
24. Mishra S, Sachdeva SN, Manocha R (2019) Subgrade soil stabilization using stone dust and coarse aggregate: a cost-effective approach. *Int J Geosynth Ground Eng* 5:20. <https://doi.org/10.1007/s40891-019-0171-0>
25. Sreekumar. V. Babu, Mary Rebekah Sharmila. S, Soil stabilisation using marble dust. *Int J Civ Eng Technol (IJCIET)* 8(4):1706–1713. Article ID: IJCIET_08_04_192, Available online at <http://iaeme.com/Home/issue/IJCIET?Volume=8&Issue=4>

26. Debnath A, Saha S, Chattaraj R (2021) Stabilization of clayey soil with marble dust. In: Das B, Barbhuiya S, Gupta R, Saha P (eds) Recent developments in sustainable infrastructure. Lecture notes in civil engineering, vol 75. Springer, Singapore. https://doi.org/10.1007/978-981-15-4577-1_14
27. Kuzhali RK, Krishnan D (2017) Study on engineering behaviour of expansive soils treated with seashell powder. Int J Civ Eng Technol (IJCIET) 8(5):576–581. Article ID: IJCIET_08_05_065 Available online at <http://iaeme.com/Home/issue/IJCIET?Volume=8&Issue=5>
28. Vinod BR, Shobha R, Raghavendra AB, Rakesh M, Pallavi S (2020) Stabilization on expansive soil using seashell powder and rubber powder. In: ICSICME—2020, IOP conference series: materials science and engineering, vol 814, p 012028. <https://doi.org/10.1088/1757-899X/814/1/012028/pdf>